

Abstracts from the 11th American Conference on Pharmacometrics

ACoP11

ISSN 2688-3953

ACoP11, November 9 – 13, 2020

**Individual abstracts will be posted online post meeting.
For citation purposes please use the following**

Citation: Author names, Abstract title, ACoP11, ISSN:2688-3953, 2020, Vol 2

TUE- 001

Updated Review of Vancomycin Population Pharmacokinetic Analyses in Adults

Abdullah Aljutayli¹, Amélie Marsot^{2,3}, and Fahima Nekka^{1,4,5}

¹ Faculty of Pharmacy, Université de Montréal, Montréal, Canada

²Laboratoire de suivi thérapeutique pharmacologique et pharmacocinétique, Faculté de Pharmacie, Université de Montréal, Montréal, Québec, Canada.

³Centre de recherche, CHU Sainte-Justine, Montréal, Québec, Canada

⁴ Laboratoire de Pharmacométrie, Faculté de Pharmacie, Université de Montréal, Montréal, Québec, Canada.

⁵Centre de recherches mathématiques, Université de Montréal, Montréal, Québec, Canada.

Background: Vancomycin is a drug of choice in the management of methicillin-resistant *Staphylococcus aureus* (MRSA) infections. Nonetheless, vancomycin optimal dosage regimens have, long, been controversial owing to the large between- and within-subject variability in its population pharmacokinetic (PopPK) profile.

Objectives: Our primary aim was to better inform vancomycin dosing by providing a comprehensive synthesis of PopPK analyses of vancomycin to determine the most reported models, including the various sources of variability.

Methods: Systematic search for vancomycin PopPK studies was conducted on PubMed and EMBASE with a time limit from January of 2011 to May of 2019. In addition, we inspected all relevant lists of references.

Results: Thirty analyses met the research criteria and were included in this review. One-compartment and two-compartment models best-described vancomycin PopPK in thirteen and fourteen studies, respectively. Further, three-compartment models were implemented in three studies to account for an additional site of administration, i.e. in cerebrospinal fluids. Common reported covariates were creatinine clearance and bodyweight (Table 1). Estimated clearance (CL) and total volume of distribution (V_d) varied widely between the studies, ranging from 0.334 to 8.75 L/h (0.0054 to 0.1279 L/h/kg) and from 7.12 to 501.8 L (0.097-6.97 L/kg), respectively. An exponential interindividual variability model was used in almost all the studies, and the highest inter-individual variability on CL and V_d were 99.2% and 101%, respectively.

Conclusion: We outlined the wide range of vancomycin parameter estimates and the covariates retained in thirty different PopPK models developed in adults. This information might help guide the clinical dosing of vancomycin in different subpopulations.

Table 1. Summary of recurrent and significant covariates including their frequencies on CL and V_d

Covariate	PK Parameter	
	CL ¹	V_d ¹
Creatinine clearance	19	None
Bodyweight	3	12
Age	3	5
Hemodialysis	3	None
Fat free mass	None	1

¹Frequency

TUE-002

Pharmacokinetic Modeling and Simulation to Inform Dosing Regimen Selection for BIO 300 After Subcutaneous Administration in Irradiated and Non-Irradiated C57BL/6J Mice

Ahmed M. Salem¹, Isabel L. Jackson², Michael D. Kaytor³, Artur A. Serebrenik³, Zeljko Vujaskovic², Jogarao Gobburu¹, Mathangi Gopalakrishnan¹

¹Center for Translational Medicine, Department of Pharmacy Practice, University of Maryland School of Pharmacy, Baltimore, Maryland

²Division of Translational Radiation Sciences, Department of Radiation Oncology, University of Maryland School of Medicine, Baltimore, Maryland

³Humanetics Corporation, Edina, Minnesota

OBJECTIVES: BIO 300, a nanosuspension of genistein, is being developed in accordance to the FDA animal rule for the prevention and treatment of the delayed effects of acute radiation exposure (DEARE). A likely mechanism for radioprotection by BIO 300 is the activation of estrogen receptor beta (ER β). Previous research indicated that activation of ER β requires an EC₅₀ at least 24 ng/ml. The analysis objectives were to: (i) develop a pharmacokinetic (PK) model describing the disposition of BIO 300 in C57BL/6J mice following subcutaneous administration, (ii) perform PK simulations of multiple dosing to identify dose levels that are safe, therapeutic and do not cause significant drug accumulation. An optimistic EC₅₀ threshold of 24 ng/ml and a conservative EC₅₀ threshold of 240 ng/ml were explored as steady state C_{trough} targets.

METHODS: The PK analysis included 162 genistein serum concentrations from 162 sex-matched C57BL/6J mice following single subcutaneous administration of 100 or 200 mg/kg in non-irradiated mice or 200 mg/kg in 14.5 Gy total body irradiated mice with 2.5% bone marrow sparing. The data from irradiated and non-irradiated mice were pooled together as the radiation effect on PK was minimal to none from prior non-compartmental analysis (NCA). Each animal contributed to one of the PK sampling times between 0.5 to 72 hours' post-dose with triplicate measurements per time point. Hence, the naïve-pooled approach was used to estimate the mean PK parameters. The final PK model and the estimated mean parameters were used to simulate the following dosing scenarios: 25 mg/kg to 200 mg/kg every 12, 24, 48 or 72 hours at steady state. The analysis was performed using Pumas v0.10.0 (www.pumas.ai).

RESULTS: A two compartment PK model with first-order absorption and linear elimination adequately described the mean concentration time-profile of BIO 300. The maximum concentration occurred at 0.5 hours. The mean apparent volume of central and peripheral compartments was 40227 ml/kg and 107030 ml/kg, respectively indicating extensive distribution of genistein due to high lipophilicity. Consistent with a previous NCA, the mean value of apparent systemic clearance was 3873 ml/hr/kg. All the simulated dosing scenarios maintained steady state C_{trough} levels above the EC₅₀ target of 24 ng/ml. However, only the regimens of 200 mg/kg dose, twice daily and daily regimens of 50 mg/kg - 100 mg/kg were able to meet the C_{trough} levels above the EC₅₀ target of 240 ng/ml.

CONCLUSIONS: Assuming a conservative EC₅₀ target of 240 ng/ml and adequate safety, 50 mg/kg to 200 mg/kg daily subcutaneous doses would meet efficacy targets and avoid excessive fluctuation in concentrations. Given a possibility of dose disproportionality at 200 mg/kg or higher, possible dose levels that could effectively activate ER β and be administered consecutively for several weeks are 50 mg/kg – 150 mg/kg administered daily subcutaneously.

TUE-003

Stimulation of erythropoiesis with ESA or blood donation: QSP model.

Alexander Stepanov¹, Galina Lebedeva²

¹InSysBio, Moscow, Russia; ²InSysBio UK Ltd, Edinburgh, UK

Objectives: Erythropoiesis-stimulating agents (ESAs) enhance the red blood cells (RBC) formation by bone marrow. They are used to manage anemic states caused by chemotherapy, bleeding, bone marrow's malfunctions etc. To predict the effect of pharmacological intervention on hematopoiesis-related clinical endpoints we propose the QSP model of erythropoiesis.

Methods: Multi-compartment ODE model of erythropoiesis was constructed to comprehensively describe cell dynamics from hematopoietic stem cell to circulating red cells. The model includes variables corresponding to specific stages of cell development distinguished based on morphology and surface markers expression. Model processes are cell self-renewal, differentiation, proliferation, migration from bone marrow into circulation and cell death. Binding of erythropoietin (EPO) and stem cell factor (SCF) to cell-surface receptors regulates cell dynamics with feedback on the receptor expression modulated by interleukine-3 (IL-3). Regulation effects of EPO were implemented via explicit description of EPO binding to its receptor followed by internalization leading to acceleration of cell proliferation and differentiation, and inhibition of apoptosis. Hypoxia-Inducible Factor (HIF) stabilizers (Roxadustat, Desidustat, Daprodustat and Molidustat) included in the model prevent the degradation of HIF, thereby inducing synthesis of EPO mRNA. Upregulation of EPO contributes to a negative feedback on HIF degradation through increased hemoglobin production. The model was calibrated across published *in vitro/in vivo* data including cell expansion under growth factors exposure *in vitro*, flow cytometry cell counting of bone marrow aspirates and clinical data of ESAs' administration such as epoetins and HIF stabilizers. The QSP model was implemented in Heta language <https://hetalang.github.io>. Modeling files were transformed to SBML, DBSolveOptimum and Simbiology format using Heta-compiler [1].

Results: Data-driven model satisfactorily describes baseline levels of various cell precursors of erythroid branch in bone marrow and RBC in circulation of healthy subjects. The response of clinical outcomes such as reticulocytes count, erythropoietin and hemoglobin levels to administration of growth factors (epoetins, SCF and IL-3) as well as HIF stabilizers (Roxadustat, Desidustat, Daprodustat and Molidustat) were also well described by the model. The model was validated on the data for erythropoiesis recovery after blood donation.

Conclusions: The proposed comprehensive human erythropoiesis QSP model describes clinical data and could be seen as predictive tool for investigation of potential pharmacological interventions including epoetins and HIF stabilizers, and explanation of observed phenomena. The model is regarded as a branch of developing a general platform of human hematopoiesis.

[1] "Heta" is a New Declarative Language to Define the Large-Scale Systems Pharmacology and Systems Biology Models. ACoP10, Orlando, October 2019, DOI: 10.13140/RG.2.2.14881.35682.

TUE-004

Characterization of Drug-Drug Interactions on the Pharmacokinetic Disposition of Busulfan in the Pediatric Hematopoietic Stem Cell Transplantation Patient

Allison Dunn, Vijay Ivaturi, PhD, Hana Paek, PharmD, Amanda Gillespie, PharmD, Brady Moffett, PharmD, MPH, Joga Rao V.S. Gobburu, PhD, Robert Krance, MD

Center for Translational Medicine, Baltimore, Maryland, USA, Baylor College of Medicine, Houston, Texas, USA,
Texas Children's Hospital, Houston, Texas, USA
Gobburu is a co-founder of Pumas-AI that commercializes Pumas software

Background: Busulfan is an alkylating agent used as a pretreatment for hematopoietic progenitor cell transplantation in chronic myelogenous leukemia. Busulfan is highly cytotoxic and its narrow therapeutic index requires precise dosing.¹ Doses too low can lead to transplant failure, while doses too high cause hepatic veno-occlusive disease and seizures.² For this reason, accurate characterization of drug-drug interactions (DDIs) is pivotal to clinician. With what is currently understood about busulfan metabolism, there are a number of medications that theoretically impact busulfan clearance, but there is insufficient data to determine clinical relevance.

Objectives: The primary objective is to investigate whether routine comedications meaningfully interact with busulfan PK, using population analysis.

Methods: For this retrospective study patients were identified by querying the hospital electronic medical records from January 1, 2011 to December 31, 2018 to identify patients who received 16 doses of intravenous busulfan pretreatment with concentration monitoring after the 1st and 9th dose. A one compartment model with first order elimination was developed in Pumas program (Pumas-AI, Baltimore, MD). After adjusting for body size and maturation factors, the potential influence of DDIs, such as acetaminophen, phenytoin and azole anti-infective agents, were evaluated. The concomitant drugs were binned into strong, moderate or mild categories for the following enzyme systems: CYP3A4, CYP2C9, CYP2C19, CYP2D6, and GST depletion.

Results: Data used in the analysis was comprised of 250 patients, both males and females, ranging from 5 weeks to 18 years of age with a weight ranging from 3 kg to 117 kg. The final model incorporated covariates of weight and age in relation to their effect on both clearance and volume of distribution. None of the evaluated covariates for DDIs produced significant results.

Conclusions: No clinically relevant DDIs were identified, which is inconsistent with the theoretically assumed interactions based on the metabolism of busulfan. This is the first time the maturation of clearance and volume are quantified.

References:

1. Andersson, B. S., Thall, P. F., Madden, T., Couriel, D., Wang, X., Tran, H. T., ... Champlin, R. E. (2002). Busulfan systemic exposure relative to regimen-related toxicity and acute graft-versus-host disease: Defining a therapeutic window for i.v. BuCy2 in chronic myelogenous leukemia. *Biology of Blood and Marrow Transplantation*, 8(9), 477–485.
<https://doi.org/10.1053/bbmt.2002.v8.pm12374452>
2. Vassal, G., Deroussent, A., Hartmann, O., Challine, D., Benhamou, E., Valteau-Couanet, D., Brugières, L., Kalifa, C., Gouyette, A., & Lemerle, J. (1990). Dose-dependent neurotoxicity of high-dose busulfan in children: a clinical and pharmacological study. *Cancer research*, 50 19, 6203-7.

TUE-007

Advanced Organ Modeling and Computer-Assisted Assembly of Platform PBPK Models for the Early Evaluation of Target Druggability, Human Dose and Safety of Biologics

Armin Sepp¹, Paul Michalski², Dhaval K. Shah³

¹GlaxoSmithKline Plc., Stevenage, UK; ²GlaxoSmithKline, Upper Providence, PA, USA; ³University of Buffalo, Buffalo, NY 14260, USA.

Objectives: Two-pore physiologically-based pharmacokinetics (PBPK) provides a mechanistic predictive framework for assessing the tissue penetration, target engagement and elimination of biologics of any size according to Three Pillars paradigm (1). This requires detailed modeling of organ physiology and target-mediated interaction networks so that optimal modality, dosing and affinity requirements can be devised proactively, including flexible incorporation of large protein-protein interaction networks both for the fluid phase as well as cell surfaces, if required.

Methods: We evaluated the rodent data parameterized biologics PBPK framework (2) by comparing model predictions with the experimental observations for a ⁸⁹Zr-labeled albumin-binding domain antibody (AlbuAb) GSK3128349 tissue and plasma concentrations in healthy human volunteers, as measured by positron emission tomography-computed tomography (PET/CT) and mass-spectrometry respectively (3). In the case of CNS, cerebrospinal fluid (CSF) barrier was incorporated in addition to the blood brain barrier in order account for the flow of CSF and the turnover clearance of biologics in these immune privileged organs (4).

Results: Using a MatlabTM -assembled SimBiologyTM-compliant two-pore biologics PBPK model we demonstrate that the organ-specific fractional lymph flow rates estimated from rodent data (2) predict well the human tissue and plasma concentration time course of ⁸⁹Zr-GSK3128349 AlbuAbTM, thereby extending the modelling framework from mice to humans (5). In the case of CNS, the exposures predicted from the CSF barrier incorporating PBPK models were found to align well with brain PK of mAbs from rodents to humans (4).

Conclusions: We have demonstrated the reliability of cross-species/cross-modality platform PBPK modelling by extrapolating biologics tissue distribution and elimination PK directly from rodents to humans and the value of

dedicated organ-specific layouts which capture specific features of organs and tissues like CNS, kidneys, lungs and solid tumours.

References:

1. P. Morgan *et al.*, Can the flow of medicines be improved? Fundamental pharmacokinetic and pharmacological principles toward improving Phase II survival. *Drug Discovery Today* **17**, 419-424 (2012).
2. A. Sepp *et al.*, Computer-assembled cross-species/cross-modalities two-pore physiologically based pharmacokinetic model for biologics in mice and rats. *J Pharmacokinet Pharmacodyn* **46**, 339-359 (2019).
3. K. S. Thorneloe *et al.*, The biodistribution and clearance of AlbuAb, a novel biopharmaceutical medicine platform, assessed via PET imaging in humans. *EJNMMI Research* **9**, 45 (2019).
4. H.-Y. Chang, S. Wu, G. Meno-Tetang, D. K. Shah, A translational platform PBPK model for antibody disposition in the brain. *J Pharmacokinet Pharmacodyn* **46**, 319-338 (2019).
5. A. Sepp, M. Bergström, M. Davies, Cross-Species/Cross-Modality Physiologically Based Pharmacokinetics for Biologics: 89Zr-Labelled Albumin-Binding Domain Antibody GSK3128349 in Humans *Manuscript in preparation*.

TUE-009

Modeling Dynamics of White Blood Cells (WBC) in Patients With Relapsed or Refractory Acute Myeloid Leukemia (R/R AML) From a First-in-Human Study to Guide Dose and Schedule Exploration

Bishoy Hanna¹, S.Y. Amy Cheung², Eline M.T. van Maanen², Maria Luisa Sardu², Rik de Greef², Michael Pourdehnad³, Tonia J. Buchholz³, Simon Zhou¹, Manisha Lamba¹

¹Bristol Myers Squibb, Summit, NJ; ²Certara, Princeton, NJ; ³Bristol Myers Squibb, San Francisco, CA; USA.

Objectives: CC-90009 is a cereblon E3 ligase modulator and first-in-class small molecule that drives the binding of a novel target protein, G1 to S phase transition 1, to cereblon, leading to AML cell death. WBC count was analyzed as a surrogate marker of leukemic blasts and potential response. To provide quantitative metrics to guide the dose and schedule exploration in a first-in-human clinical study in patients with R/R AML (NCT02848001) through model-informed drug development, the objective of this analysis was to develop a semi-mechanistic model to link CC-90009 exposure to WBC count.

Methods: Data from the phase 1 dose-escalation study in patients with R/R AML were analyzed.¹ The study included 2 dosing schedules with CC-90009 administered intravenously on Days 1–5 or Days 1–3 and 8–10 of a 28-day cycle; the total dose intensities per cycle ranged from 1.5–21.6 mg. The pharmacokinetic (PK) model was a 3-compartment model with first-order elimination. A semi-mechanistic PK/pharmacodynamic (PD) model² that incorporated proliferation, maturation, and transit from bone marrow to peripheral blood was fitted. The inhibitory effect of CC-90009 on the proliferation rate was adequately described by an E_{max} model with system-specific parameters (baseline WBC levels, mean transit time [MTT], and feedback governing proliferation of WBCs [γ]) and drug-specific potency parameters (I_{max} and IC_{50}) were estimated. Simulations were performed to explore the effect of alternative dosing schedules on PK and WBC profiles.

Results: The PK model adequately described the observed PK profile; estimated central volume of distribution was 21.4 L; clearance was 5.6 L/hour. The PK–WBC model assumed that WBC data represented the total of mature WBC and leukemic blasts, and that both cell types follow the same dynamic trend. The model was deemed adequate based on goodness-of-fit plots and visual predictive checks, though a small bias remained at the population level that might be related to the nature of the total WBC data. Typical baseline WBC levels were estimated to be $4.68 \times$

$10^9/L$, MTT was 5.51 hours, and γ was 0.51. Model simulations indicated a stronger schedule effect; increasing treatment duration to 7 days (compared with 5 days) would result in prolonging leukemic blast suppression for approximately 3–4 additional days.

Conclusions: The series of PK and PK/PD models adequately described the observed PK and WBC data from a phase 1 study of CC-90009 in patients with R/R AML. These models were used to simulate the impact of different doses and schedules of CC-90009. The results support the exploration of extended consecutive dosing days in a 28-day cycle to prolong exposures, potentially leading to a prolonged drug effect on leukemic blasts.

References: ¹Uy GL, et al. *Blood* 2019;134(Suppl 1):232. ²Friberg LE, et al. *J Clin Oncol* 2002;20:4713-4721.

TUE-010

Title: Development and Verification of a Levonorgestrel PBPK Model for Enzyme- and Binding Partner-Mediated Drug Interaction Studies in Healthy and Obese Women

Authors: Brian Cicali¹, Karthik Lingineni¹, Rodrigo Cristofoletti¹, Thomas Wendl², Joachim Hoechel², Herbert Wiesinger², Ayyappa Chaturvedula³, Valvanera Vozmediano¹, Stephan Schmidt¹

Institutions:

1. Center for Pharmacometrics and Systems Pharmacology, Department of Pharmaceutics, College of Pharmacy, University of Florida, Orlando, FL, USA
2. Bayer AG, Leverkusen, Germany
3. Department of Pharmacotherapy, System College of Pharmacy, University of Northern Texas Health Science Center, Fort Worth, TX, USA

Objectives:

Levonorgestrel (LNG) is the active moiety in many hormonal contraceptive formulations. There is concern that LNG's widespread use in conjunction with its CYP3A4-mediated metabolism bares risk for drug-drug interactions (DDI) resulting in unintended pregnancy or breakthrough bleeding. LNG is also frequently administered with ethinyl estradiol (EE) to increase the contraceptive efficacy and decrease side-effects. Interactions between these two products both in terms of CYP3A4-mediated metabolism and protein binding changes have made modeling these combinations difficult. Further, there is evidence that risk of unintended pregnancy is exasperated in obese women due to changes in protein binding partner expressions and LNG exposure. Therefore, the objective of this study was to determine the plausibility and extent of DDIs for LNG and LNG+EE in healthy and obese women using a physiologically-based pharmacokinetic (PBPK) modeling and simulation approach.

Methods:

Model development was conducted in PK-Sim (v8.0) using a combination of bottom-up and top-down approaches via literature-reported and optimized parameter values. Parameters were optimized using patient-level data from Bayer AG following intravenous and oral administration of 0.03 mg LNG. The model was then subjected to multiple verification steps including sensitivity analysis, visual predictive checks at different doses with data not used for parameter fitting, and comparisons with clinical DDI data for combinations of EE as well as concomitant administration of three different CYP3A4 inducers (carbamazepine, rifampicin and efavirenz). The verified model was then applied to an obese population ($BMI \geq 30 \text{ kg/m}^2$) as well as two CYP3A4 inhibition DDI scenarios for investigation: clarithromycin to evaluate mechanism-based inhibition and itraconazole to evaluate competitive inhibition effects.

Results:

A whole-body PBPK model of LNG was verified for DDI studies both alone and in combination with EE. In combination with carbamazepine, the predicted and observed AUC ratios (AUCR) indicated good predictive performance. The simulated LNG AUCR, when administered with EE, decreased to 0.50 (unbound: 0.45) in the presence of rifampin, whereas it increased to 1.45 (unbound: 1.50) for itraconazole. These changes were further increased in obese populations, with AUCR of 0.38 (unbound: 0.40) and 1.60 (unbound: 1.25) in the presence of rifampin and itraconazole, respectively.

Conclusion:

Our results suggest that LNG shows moderate interactions with strong CYP3A4 inducers compared to weak interactions with strong CYP3A4 inhibitors. The results of this analysis will be linked to exposure-response models for unintended pregnancy and breakthrough bleeding events derived using a model-based meta-analysis approach to determine how the predicted changes in total LNG exposure effect clinical outcomes.

TUE-012

Illustrating improved confidence in Phase II decision making using longitudinal Item Response Theory analysis

Carolina Llanos-Paez¹, Claire Ambery², Shuying Yang², Maggie Tabberer³, Misba Beerahee², Elodie L. Plan¹, Mats O. Karlsson¹

1. Department of Pharmaceutical Biosciences, Uppsala University, Uppsala, Sweden

2. Clinical Pharmacology Modelling and Simulation, GlaxoSmithKline plc., London, UK

3. Patient Centred Outcomes: Value Evidence and Outcomes, GlaxoSmithKline plc., Stockley Park, UK.

Objectives: To develop and assess an alternative methodology to compare clinical trial outcome measures using a longitudinal model-based item response model (IRM) which could potentially replace a standard analysis (mixed model repeated measures - MMRM) of total score data as it may increase the statistical power and precision to detect a drug effect.

Methods: Patient reported outcome data collected using the EXACT (Exacerbation of Chronic Pulmonary Disease Tool) questionnaire in a randomized, placebo-controlled, phase II clinical trial [1] were analysed using an IRM. EXACT consists of 14 items related to chronic obstructive pulmonary disease (COPD). The E-RS:COPD (Evaluating Respiratory Symptoms in COPD) consists of 11 items from this EXACT instrument (sub-scales breathlessness, cough & sputum, and chest symptoms). The IRM was developed with a graded response model characterising item parameters. Functions describing symptom-time courses were assessed, while Markov elements handled correlated observations [2]. *EXACT total scores (logit score-transformed) and the sum of the E-RS:COPD scores and E-RS subscales were simulated at month 12 (N=2,000 with 5,000 subjects per arm) using the final parameter estimates with uncertainty. Specifically, the relationship between patient disease status and total score was derived and served as the basis for the simulations. The 50th (2.5th, 97.5th) percentiles of the resulting 2,000 differences in average total score between the trial arms at the end of the study were used to represent estimated drug effect (95%CI). These values were compared with published MMRM results at month 12 [1]. Further, a relative sample size (N_R) to MMRM CI (CI_{MMRM}) values was calculated considering the precision obtained from the IRM (CI_{IRM}) model as the desired margin of error ($N_R = (CI_{MMRM}/CI_{IRM})^2$).*

Results: Data from 93 patients who received either oral danirixin 75 mg twice daily (n=45) or placebo (n=48) on top of standard of care over 52 weeks were analysed. A step function best described the COPD symptoms-time course in both trial arms. From the IRM, typical value (SE) of maximum response and time of response was -0.12 (0.18) and 62.1 days (10.9) (danirixin arm) and 0.02 (0.13) and 98.6 days (14.6) (placebo), respectively. The IRM considerably improved precision of drug effect compared to MMRM (Figure). A sample size of 2.8 and 3.7 times larger would be required in the MMRM analysis to achieve the precision obtained with the IRM using EXACT and E-RS:COPD, respectively.

Conclusions: The IRM in this example provided a considerably more informed basis for assessing the drug effect. Thus, a longitudinal non-linear mixed-effect analysis based on item-level data may provide more precise estimates of drug effect than standard statistical analysis for the same endpoint, and thereby improving decision-making in Phase II.

References:

- [1] GlaxoSmithKline. U.S. <https://clinicaltrials.gov/ct2/show/NCT02130193?term=200163&draw=2&rank=1>
- [2] Germovsek E et al. AAPS J (2019) 21, 60.

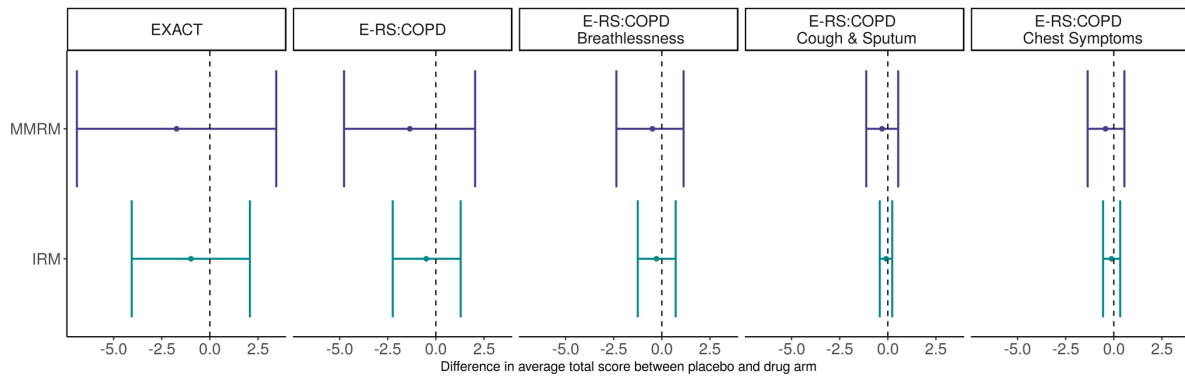


Figure. Mean (95%CI) difference in average total score between placebo and drug arm using a MMRM and IRM analysis for different scales.

Funding Information: GSK funded this research in the form of a Research payment to Uppsala University.

Conflict of Interest: CL-P, ELP and MOK declare that they have no conflict of interest. CA, SY, MT and MB are GSK employees and hold GSK shares.

TUE-013

Application of a dual PBPK-popPK model based approach across the age-population of adults using bilastine as a probe drug

Chaejin Kim¹⁺, Valentina Lo Re²⁺, Monica Rodriguez², John C. Lukas², Cristina Campo³, Aintzane Garcia³, Stephan Schmidt¹, Valvanera Vozmediano^{*1}

(1) Center for Pharmacometrics and Systems Pharmacology, Department of Pharmaceutics, University of Florida

(2) Drug Modeling & Consulting (DMC), Dynakin, SL, Bilbao, Spain

(3) Medical Department, FAES FARMA, S.A, 48940, Spain

* Correspondence: valva@cop.ufl.edu

⁺ Contributed equally to this study

Objective: Use of a dual physiologically-based pharmacokinetic model- population pharmacokinetic (PBPK-popPK) model-based approach to integrate bilastine physicochemical, *in vitro* and *in vivo* data in young adults to: 1) enhance the mechanistic understanding of intestinal transporters on drug PK, and 2) predict the PK in elderlys of different biological age (*i.e.*, young old (65~74 yrs), middle old (75~84 yrs) and oldest old (> 85 yrs)).

Methods: 1) *PBPK model:* Using GastroPlus 9.6® a PBPK model for young adults was developed considering apical efflux and apical and basolateral influx transporters in the enterocyte, using PK data from young adults after IV (10mg SD) and PO (20mg SOD)¹. Transporters' kinetics and colonic absorption parameters were optimized during the model development process (due to insufficient experimental data available to inform the model). The model was qualified using an external dataset containing data from 12 Phase-I studies with 13 different SOD and MOD². The model was then used to extrapolate the PK to young olds, which also served to verify the predictive capacity of the model. 2) *PopPK model:* A semi-mechanistic predictive popPK model for elderlys was developed in NONMEM version 7.2 using a previously developed popPK model² incorporating declining functions on different physiological systems (glomerular filtration, unbound fraction) and differences in body composition. Model predictive capacity was evaluated using observations from young olds. Both models were qualified by comparing the predicted *vs* observed PK parameters in elderlys, and by comparing the predicted concentration-time profiles to the clinical data. Both models were then applied to assess the suitability of the therapeutic dose in middle and oldest olds.

Results: Final PBPK model predictions showed AUC_{pred}/AUC_{obs} ratios within 0.5 and 2 for all the doses (5mg - 220mg). The final PBPK adequately predicted plasma concentrations in geriatrics (n=8 male; mean age= 69.75 yrs; n=8 female; mean age = 67.625 yrs). Similar results were also obtained for the semi-mechanistic popPK model where more than 90% of observations were within the 5~95% of simulated confidence intervals. The application of both models to middle and oldest old led to the conclusion that the 20 mg dose produces plasma concentrations of bilastine within the known therapeutic margin³.

Conclusions: The PBPK model supports the hypothesis that basolateral influx transporters are involved in bilastine PK (basolateral influx and apical efflux intestinal transporter were needed to adequately describe the PK) and of regional differences on P-gp's efflux capacity in the intestine. Both, PBPK and semi-mechanistic popPK models indicate that 20 mg QD dose is appropriate (safe and effective) for geriatrics of any age.

References:

- [1] Sádaba et al. *Clin Drug Investig*. 2013;33:375-381. doi:10.1007/s40261-013-0076-y
- [2] Jauregizar et al. *Clin Pharmacokinet*. 2009;48(8):543-554. doi:10.2165/11317180-00000000-00000
- [3] Vozmediano et al. *Eur J Pharm Sci*. 2019;128(November 2018):180-192. doi:10.1016/j.ejps.2018.11.016

TUE-015

TITLE: Using Mechanistic Quantitative Systems Pharmacology (QSP) Models To Connect Biomarkers To Clinical Disease Activity Scores – Examples In Atopic Dermatitis (AD) And Psoriasis (PsO).

AUTHORS: Christina Friedrich(1), Rebecca Baillie(1), Michael Weis(1), Meghan Pryor(1), Vincent Hurez(1), Katherine Kudrycki(1), Michael Reed(1)

INSTITUTIONS: (1) Rosa & Co. LLC, San Carlos, CA

OBJECTIVES: Many clinical trials use complex disease activity scores to assess patient response, and the connections between biological components and these scores are often unclear. We explore how QSP modeling supports elucidation of disease pathophysiology and better-informed extrapolation between biological components and disease scores to facilitate prediction of clinical outcomes.

METHODS: Mechanistically informed relationships were identified to connect biomarkers to the Eczema Area & Severity Index (EASI) in an AD model and to the Psoriasis Area & Severity Index (PASI) in a PsO model.

RESULTS: AD and PsO QSP models were developed and qualified. Changes in tissue biomarkers upon treatment, e.g., skin immune cell infiltration, were particularly helpful in establishing links between disease pathology and disease symptoms. The disease scores were modeled by (1) identifying the components of each disease activity score, (2) formulating a biological rationale for associating specific biomarkers with each score component, and (3) calibrating the proposed function using clinical data from existing therapies. EASI and PASI score improvement matched existing clinical trial data and the models were used to predict the clinical efficacy of novel interventions.

CONCLUSIONS: QSP models are valuable tools to integrate existing mechanistic and clinical data and generate plausible predictions of disease scores in response to novel interventions.

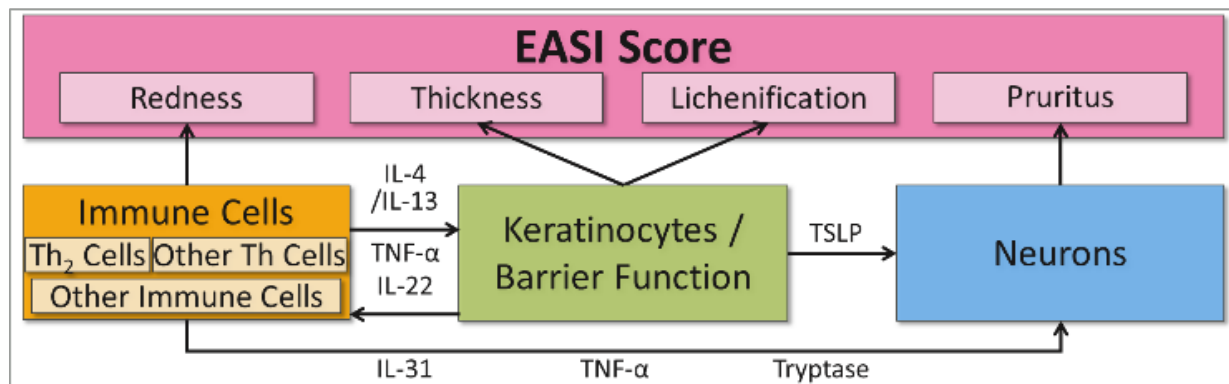


Figure 1. EASI score components linked to selected key biomarkers from an AD QSP model.

TUE-016

Title: Acceleration of Quantitative Systems Pharmacology Models Through Automatic Analysis of System Structure and Simulation on Graphics Processing Units

Authors: Christopher Rackauckas^{1,2}, Yingbo Ma⁴, Theodore R. Rieger³, Anna Sher³, Richard Allen³, Vijay Ivaturi², Viral Shah⁴, and C.J. Musante³

Affiliations:

¹Department of Mathematics, Massachusetts Institute of Technology, Cambridge, MA, USA

²College of Pharmacy, University of Maryland-Baltimore, Baltimore, MD USA

³Quantitative Systems Pharmacology, Pfizer Inc, Cambridge, MA USA

⁴Julia Computing, Cambridge, MA USA

Objectives:

Quantitative Systems Pharmacology (QSP) models often consist of stiff sets of ordinary differential equations (ODEs) and are traditionally slow to simulate and difficult to parallelize. The lack of high-throughput simulation limits the types of research questions amenable to analysis by a QSP approach. Here we addressed and improved some of the performance bottlenecks to extend the utility of QSP models.

Methods:

We approached acceleration of QSP model simulations by:

1. Optimization of the numerical solution of ODEs through automatic Jacobian generation, selection of solver, and stiffness detection.
2. Deployment of QSP models on Graphics Processing Units (GPUs) for high-throughput parallel simulations.

We tested that our approaches in three separate QSP models: a smaller (14 ODEs) model of leucine metabolism (unpublished), a model of cardiac metabolism and mechanics (54 ODEs) [1], and an ionic cardiac model (105 ODEs) [2]. The simulations were performed using the Julia Language [3] and the new methods have been incorporated into the relevant open-source packages. The performance of the simulations was compared to existing “baseline” code for all three models. The leucine and Tewari et al models were already fairly optimized as C-code using the SUNDIALS CVODE BDF solver. The Gong et al. model was implemented in Matlab using ode15s and had not necessarily been fully optimized for performance.

Results:

In the leucine model, application of automatic Jacobian generation resulted in a 7x, compared to the baseline code. These speed-ups extended to parallel computing, with a near-linear gain per Central Processing Unit (CPU) added (Figure 1). The time to perform global optimization of the model parameters was reduced from 16 hours to 1 hour with a comparable final objective function value. The Tewari et al. model accelerated 2x/CPU-used over the C-baseline code and the Gong et al. model gained 25x compared to simulations in Matlab.

We established a GPU acceleration strategy for parameter searches of small ODE systems (<200 equations). The approach involved specifying the stacked ODE system as single program multiple data over the parameters and specializing the implicit portion of the ODE solver to utilize a GPU-specialized (limited branching, partial pivoting) block LU factorization. The GPU kernel code is generated automatically by the compilation process, allowing users to write standard code and have the code GPU accelerated. Using a single GPU with 10,000 cores, the leucine model was accelerated 175x over the base code (Figure 1).

Conclusions:

The newly developed tools showed significant performance gains for the QSP models tested. This improved performance makes exploring uncertain parameter spaces of large QSP models that span multiple timescales much more practical.

References:

1. Tewari et al. 2017.
2. Gong et al. 2020.
3. The Julia Language. <https://julialang.org/>

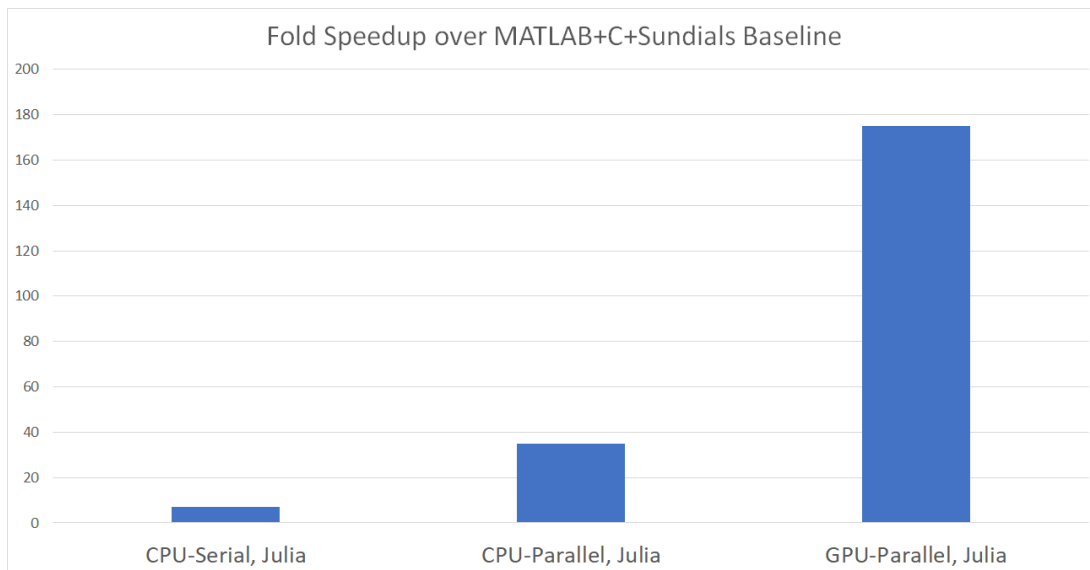


Figure 1. Relative speed-up of a simulation of the leucine QSP model vs. the base case. CPU-Serial- single set of parameters on a single CPU, CPU-Parallel- simulation of multiple parameter sets using 6 CPU cores, and GPU-Parallel-10,000 simultaneous runs across a GPU.

TUE-017

A target-mediated drug disposition-lymphocyte kinetics model simulates intricate interplay of immunocytokine drug pharmacokinetics and cellular dynamics in blood and lymphoid tissues

Dan Lu¹, Vittal Shivva¹, Rajbharan Yadav¹, John Desjarlais², Matt Bennett², Liz Bogaert², Irene Leung², Coco Liu², Pascal Chanu³, Saroja Ramanujan¹

¹ Genentech, Inc., South San Francisco, CA, USA

² Xencor, Inc. Monrovia, CA, USA

³ Genentech/Roche, France

Objectives

Immunocytokines such as engineered IL-2 and IL-15 are being developed as therapeutic agents to induce proliferation of lymphocytes, alone or in combination therapy with other cancer immunotherapy agents. XmAb24306 is an engineered IL15/IL15 R α -Fc that binds to IL2/IL15 R $\beta\gamma$ subunits on natural killer (NK) cell and T lymphocytes and leads to a durable expansion of target cells. XmAb24306 induced target cell expansion subsequently enhances the target-mediated drug disposition (TMDD) of XmAb24306. The objective of this work is to build a semi-mechanistic model to simulate these interactions, to delineate the mechanisms underlying observed PKPD, and to support translation and clinical development.

Methods

Serum concentration-time profiles of XmAb24306 and blood CD8+ T-cells and NK cells, were obtained from single and repeated dose studies in cynomolgus monkeys (0.1 to 0.6 mg/kg, intravenous administration). A semi-mechanistic model was developed with PK captured using a 3-compartment model with linear and receptor-mediated clearance. Drug-receptor binding and downstream PD is captured by modeling (i) dynamics of total cellular receptor levels as a function of receptor turnover and cellular dynamics (lymphocyte turnover and traffic); (ii) affinity-dependent drug-receptor binding and complex internalization; (iii) complex-stimulated lymphocyte margination (or exit from blood) and subsequent demargination (or re-entry); (iv) complex-stimulated lymphocyte proliferation in blood and tissue, and the resulted increases in free receptors, which in turn influences PK.

Results

Our model successfully describes the observed PK, CD8+ T-cells and NK cells dynamics, using the number of drug-bound receptors per cell in blood and tissue as the driver for cellular PD. Parameters were derived either from literature or were fit from cyno PKPD data; all parameter estimates were within physiologically reasonable ranges. Both blood and tissue cell dynamics appear to influence observed PK and PD in blood. The initial blood lymphopenia is resulted from margination. Drug-receptor binding leads to lymphocyte proliferation in both blood and tissue with an estimated maximum proliferation rate corresponding to a cellular doubling time of approximately 10 to 20 hours. The gradual demargination and trafficking of proliferated

lymphocytes from lymphoid tissues back into the blood explain the observed delay of maximal blood lymphocyte expansion at day 7-8 after dosing, without invoking empirical delays in the model. Furthermore, CD8+ T-cell and NK cell numbers alone, at physiological receptor expression levels and turnover rates, are insufficient to account for the observed drug clearance, suggesting a significant contribution of other IL2/IL15-R $\beta\gamma$ expressing cells (e.g., CD4+ T cells) to TMDD, which is also implemented in the model.

Conclusions

Based on the cynomolgus monkey data, a semi-mechanistic model was developed which can be leveraged for interpreting PK-PD in cancer patients and performing simulations to explore different dosing regimens. The model can also be used to explore the optimal combination with other lymphocyte-mediated therapies.

TUE-018

Efficient simulation of clinical target isoboles applied to drug combinations for malaria

Daniel Lill (1,3), Anne Kümmel (1), Nathalie Gobeau (2), Henning Schmidt (1), Jens Timmer (3)

1) IntiQuan GmbH, 2) Medicines for Malaria Venture, 3) University of Freiburg

Objectives: Dose selection in clinical trials is often based on the probability that the chosen dose achieves the desired clinical outcome. For combination therapies, clinical trial simulation for assessing this probability is impeded due to combinatorial complexity: Compared to one optimal dose for monotherapy, many dose combinations, i.e., isoboles, lead to the same desired effect. Calculating these isoboles is computationally demanding as many dose combinations must be simulated. The objectives of this work were two-fold: 1) to develop a fast algorithm able to calculate “isoboles” of the clinical target for combination treatments, i.e. all the possible dose combinations of two drugs that allow to reach the clinical efficacy target; 2) to obtain the statistics of the isoboles over a large population (e.g. median and its 95% confidence interval) at these doses. In these calculations, the time-dependent pharmacokinetics and pharmacodynamics of both compounds are predicted in a large number of individuals taking into account inter-individual variability and parameter uncertainty to calculate the clinical target.

Methods: A fast algorithm to calculate population-level isoboles was developed. Instead of simulating the model for all possible dose combinations, the algorithm iteratively refines the resolution of the dosing grid close to the actual isobole. To obtain statistical measures such as the median isobole and its 95% confidence bounds, an additional algorithm for two-dimensional quantile calculation was developed.

Results: We present properties of the algorithm and non-linear features of population isoboles by comparison of three different models from malaria research. For each model, the dose combinations yielding a 95% cure rate in the population, the target for antimalarial drug treatment, are determined. The isobole algorithm cuts down the required simulations by more than a hundred-fold. We find that population isoboles can differ remarkable from the isobole describing cure of a single subject, emphasizing the importance to consider population effects. Furthermore, the newly developed method to obtain confidence intervals for isoboles is a powerful way to quantify model uncertainty for combination therapies.

Conclusions: Population isoboles provide a visual, easy-to-communicate, as well as quantitative means to assess a combination and its potential to achieve the desired clinical outcome. The computational efficiency of the new algorithm allows its application to several anti-malarial combination therapies to select the most promising one to be tested in a clinical trial. Compared to isoboles of a single typical subject, they are better able to capture extremal behaviors in the population. Population isoboles also identify interesting dosing regimens which will help to prepare the design of the clinical trial.

TUE-019

Title: Literature review based modeling analyses to inform optimal clinical dose selection of chemotherapy

Authors: David J. Smith, Manash S. Chatterjee, Dinesh P. de Alwis, and Kapil Mayawala

Institutions: Quantitative Pharmacology and Pharmacometrics, PPDM, Merck & Co., Inc., Rahway, New Jersey

Objectives: While cytotoxic chemotherapy agents have traditionally been developed at their maximum tolerated dose (MTD), an alternative dose below the MTD may be sufficient to maximize efficacy. Additionally, the safety benefits at <MTD may return efficacy benefits through a reduction in patient dropouts.

A key challenge in the clinical investigation of chemotherapy <MTD is the possibility that such a dose may not maximize efficacy. Here, we seek to motivate the study of reduced chemotherapy doses based on clinical data using reverse translational principles.

Methods: We conducted a literature review to find studies reporting clinical efficacy and safety data at multiple chemotherapy doses. We also leveraged published clinical exposure-response and population PK/PD models to assess the impact of dose reductions on both efficacy and safety. Specifically, we quantitatively assessed the effect of solvent-based paclitaxel dose reduction using established models of paclitaxel PK and chemotherapy-induced myelosuppression (PD) [1], and gemcitabine dose reduction with and without infusion prolongation using an established PK model of the parent drug and active metabolite [2].

Results: Based on clinical studies of paclitaxel, we found that a 20-25% dose reduction on the q3w schedule improved dose-limiting toxicities, neutropenia and neuropathy, while preserving overall survival (OS) in metastatic breast cancer. Furthermore, our modeling analysis showed that the worst incidences of neutropenia are experienced in the top quartile of unbound plasma paclitaxel exposure and that these patients are most benefitted by 20-25% dose reduction.

Our investigation of gemcitabine clinical studies found that a 75% dose reduction improved myelosuppression while preserving OS in pancreatic adenocarcinoma. Our modeling analysis showed how infusion prolongation in tandem with dose reduction can offset the losses in active metabolite exposure in peripheral blood mononuclear cells, a possible surrogate for efficacy, upon dose reduction and optimize active metabolite exposure relative to parent drug exposure in plasma, a surrogate for toxicity.

We also identified agents such as carboplatin with rigorous exposure-response and dose optimization efforts that do not support dose reduction due to losses in efficacy.

Conclusions: We found that existing clinical evidence supplemented with population PK/PD analyses supports dose reduction of chemotherapy agents paclitaxel and gemcitabine. This work can be used to inform dose selection, improving safety and potentially efficacy, in future clinical investigations involving chemotherapy.

References:

1. Kloft C, et al. Clinical Cancer Research. 2006;12:5481–90.
2. Zhang L, et al. Journal of Pharmacokinetics and Pharmacodynamics. 2006;33:369–93.

TUE-020

Population pharmacokinetics of magrolimab (5F9, Hu5F9-G4) in patients with solid tumors and lymphomas

Denise Chao-Yu Jin¹, Bing Wang², Branimir Sikic³, Ranjana Advani³, Mark Chao¹, Chris Takimoto¹, Balaji Agoram¹

¹Forty Seven, Inc., Menlo Park, CA; ²Amador BioScience, Pleasanton, CA; ³Stanford University School of Medicine, Stanford, CA;

Objectives: Magrolimab (Hu5F9-G4) is a monoclonal IgG4 antibody that binds to CD47 and enables tumor cell phagocytosis and activates an anti-tumor T-cell response. Magrolimab is being evaluated as an anti-cancer therapy in multiple clinical trials both as a mono- and combination therapy. The objectives of this analysis were to develop a population pharmacokinetics (PK) model of magrolimab to quantitate the effect of patient/disease characteristics on PK.

Methods: Data were pooled from 2 studies: Study SCI-CD47-001 (Phase 1 monotherapy; solid tumors and lymphomas) and 5F9003 (Ph1/2; rituximab combination in lymphomas). A total of 3962 PK observations from 202 patients - dose range 0.1 to 45 mg/kg intravenous magrolimab - were used in this analysis. Population PK was performed using a non-linear mixed effects modeling approach (NONMEM v7.4). Stepwise covariate building approach was used to evaluate covariates.

Results: Magrolimab PK was described using a 2-compartment model with parallel first-order and Michaelis-Menten clearances. All PK parameters and their variabilities were precisely estimated and physiologically plausible for an antibody. The mean (standard error of estimate) estimates of linear clearance (CL) and central volume of distribution (V_1) were 0.273 L/day (0.012) and 3.70 L (0.06), respectively. Only body-weight was identified as a significant covariate. Other demographic covariates, anti-drug antibody formation, and coadministration of rituximab were not significant. In cancer patients with partial or complete tumor responses, a 28% decrease in CL was observed ($p<0.05$).

Conclusions: A population PK model of magrolimab was developed and validated. Model indicated no need for dose adjustments in any patient or disease sub-population.

Clinical trial information: [NCT02216409](#) and NCT02953509.

TUE-021

A Computational Model of Cerebral Metabolism during Cerebral Ischemia and Reperfusion

Donald E. Lee¹, Pawan Gupta¹, Emin Maltepe², Jogarao Gobburu¹

¹Center for Translational Medicine, School of Pharmacy, University of Maryland, Baltimore, Baltimore, MD, USA

²Department of Pediatrics, University of California, San Francisco, San Francisco, CA, USA

Objectives:

The brain consumes a disproportionate amount of total energy in the body and is particularly vulnerable to hypoxic-ischemic episodes. Currently, the only treatment for hypoxic-ischemic encephalopathy (HIE) is therapeutic hypothermia, which provides modest reductions in brain injury and mortality. Novel treatment approaches are therefore necessary. As metabolic and blood flow disturbances are fundamental to cerebral ischemia, we developed a computational model to study cerebral metabolism during cerebral ischemia and reperfusion.

Methods:

The computational model is adapted from Jolivet et al¹, with the neuron-glia-vascular functional unit, and was implemented in the Julia language. Hodgkin-Huxley modeling of neuronal excitability, Buxton-Wang modeling of vascular dynamics², and modeling of metabolic pathways were incorporated.

Results:

Several forms of cerebral ischemia are simulated, with alterations in blood flow conditions. The model predicted metabolic events consistent with experimental observations of cerebral ischemia, including lactate accumulation, buildup of extracellular potassium, and neuronal calcium influx.

Conclusions:

A computational model of cerebral metabolism was able to predict metabolic disturbances during cerebral ischemia and reperfusion. Future models will incorporate time-varying parameters to match the varying metabolic conditions during ischemia. Additionally, the cerebral metabolism model will be developed to include further pathophysiologic mechanisms, such as free radicals and inflammatory messengers. Such a model may be able to accelerate drug development for HIE by predicting responses to various treatments.

References:

¹Jolivet R, Coggan JS, Allaman I, Magistretti PJ (2015) Multi-timescale Modeling of Activity-Dependent Metabolic Coupling in the Neuron-Glia-Vasculature Ensemble. PLoS Comput Biol 11(2): e1004036. doi:10.1371/journal.pcbi.1004036

²Buxton, R. B., Wong, E. C., & Frank, L. R. (1998). Dynamics of blood flow and oxygenation changes during brain activation: The balloon model. Magnetic Resonance in Medicine, 39(6), 855-864. Doi:10.1002/mrm.1910390602

TUE-022

TITLE: Effect of URAT1 inhibition with verinurad on proximal tubule intracellular lactate: A mathematical modeling analysis and hypothesis for antiproteinuric effect¹

AUTHORS: Emily Nieves (1), Melissa Hallow, PhD (1), Peter Greasley (2), Joanna Parkinson (2)

AFFILIATIONS: (1) College of Engineering, University of Georgia, Ga, United States (2) AstraZeneca Gothenburg, Sweden

OBJECTIVES: Verinurad lowers serum uric acid by inhibiting URAT1, a urate/ carboxylate co-transporter in the proximal tubule (PT) of the kidney. Verinurad reduced proteinuria in a recent clinical trial, but the mechanism remains unknown. One proposed hypothesis is that the inhibition of URAT1 augments protein reabsorption by increasing intracellular lactate in proximal tubule cells. The increased availability of lactate may lead to a restoration of the reabsorption of protein by increasing ATP levels and/ or improving endocytosis of protein by lowering endosomal pH. The goal of this study was to mathematically evaluate the effect of URAT1 inhibition with verinurad on intracellular lactate concentration.

METHODS: A mathematical model of urate and lactate transport in the rat proximal tubule¹ of was adapted to simulate transport in humans. The transporter model was further adjusted to represent states of hyperuricemia and altered expression of uric acid transporters that likely occurs in hyperuricemia. The transporter model was linked to a systems description of plasma uric acid and the pharmacokinetics and pharmacodynamics of verinurad were incorporated into the model.

RESULTS: The model was able to reproduce observed verinurad pharmacokinetics, as well as the observed changes in plasma and urinary uric acid. The model predicted that URAT1 inhibition with verinurad increases intracellular lactate concentration in the human PT by 26% in normouricemic and 20% in hyperuricemic conditions.

CONCLUSIONS: Simulations indicate that verinurad may substantially increase the availability of lactate inside PT epithelial cells. Since lactate is used as a fuel by the PT, increased availability of lactate may help restore protein reabsorption capacity in fuel-deficient PT cells by increasing ATP levels. In addition, increased intracellular lactate could help maintain the low endosomal pH necessary for protein reabsorption.

REFERENCES:

1. Edwards, A., et al. A model of uric acid transport in the rat proximal tubule. *American Journal of Physiology-Renal Physiology*. 316(5), F934-F947 (2019).

¹ This abstract will be published under the same title in the FASEB journal but presentation at the annual Experimental Biology meeting was not given due to COVID-19.

TUE-025

Computational analysis of combination therapy of bispecific T cell engagers (BiTE®) with anti-programmed cell death-1 (PD1) inhibitor for the treatment of hematological malignancies

Florencio Serrano Castillo¹, Sameer Doshi¹, Hansen Wong², Vijay Upreti², Fiona Chandra¹, Khamir Mehta²

¹Clinical Pharmacology, Modeling and Simulations, Amgen Inc, Thousand Oaks, CA; ²Clinical Pharmacology, Modeling and Simulations, Amgen Inc, South San Francisco, CA

Objectives:

This work explores the development of a mechanistic systems model to explore possible therapeutic interactions between bispecific T cell-engaging antibodies and anti-PD1 mAb for potential application in the treatment of hematological malignancies. BiTE® molecules work by enhancing the immune response to the tumor by circumventing the need to be activated by antigen presenting cells, while anti-PD1 treatments suppress the tumor immune escape by blocking PD1 binding and decreasing the resistance to the cytotoxic activities of the immune cells. Furthermore, tumor upregulation of 26immune-regulating factors, including PD1, can potentially attenuate a BiTE® molecule's effectiveness and serve as a mechanism of tumor resistance. Both therapeutic modalities have demonstrated efficacy across various tumor types and have the potential to synergize. In this work, we combine proposed PK/PD models of BiTE® molecules and anti-PD1 mAbs, with prior knowledge about their respective methods of action and relevant biology to computationally explore possible efficacy/safety/PK/PD profiles following co-administration under different regimens.

Methods:

The proposed model consists of a system of nonlinear ordinary differential equations that incorporate the above-mentioned mechanisms and the PK based on published PK models. The model tracks the target-based dynamics and coverage for both compounds and includes regulatory feedbacks to explore the inhibitory effect of PD1 receptors both in the absence of a checkpoint inhibitor and following their addition at different dosing schemes. Other states include tumor growth, T-cell phenotypic dynamics, specifically, T-cell proliferation, and the transition between naïve T-cells, activated T-cells and PD1+ T-cells. Figure 1 shows a schema of the model structure.

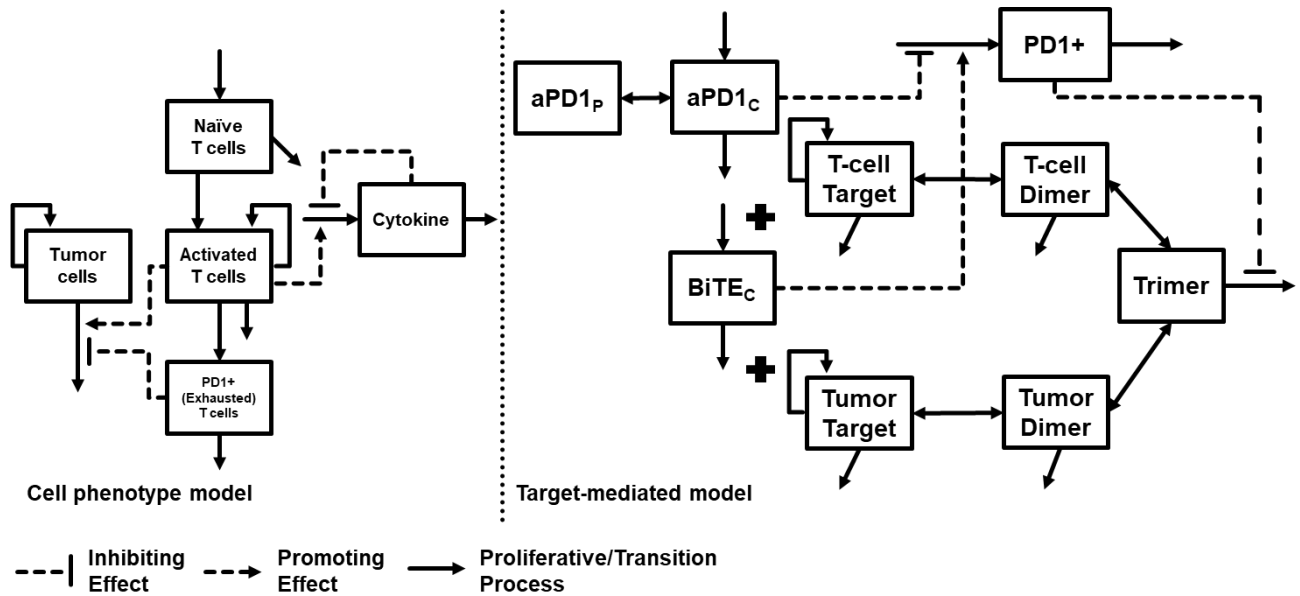


Figure 1. Schema of the multi-scale model structure implemented.

Results:

We explored model behavior using global sensitivity methods to understand the potential outcomes for different mathematical structures for the PD1 regulatory feedbacks on T-cell tumor killing activity. As expected, model simulations show a significant reduction of tumor burden with co-administration, compared to the monotherapy. Furthermore, the model suggests higher baseline levels of PD1+ T-cells lower a BiTE® molecule's cytotoxic activity, which is rescued through the co-administration. Model also suggested the magnitude of cytokine release may be influenced by two opposing elements: the suppression of T-cell regulation activity and the rapid decrease in tumor burden. Thus, an optimal treatment regimen should balance the two phenomena to ensure lower risk of cytokine storm but maintain the efficacy of tumor cell killing. We explore this idea through various simulated scenarios based on initial cell counts and dosing regimens.

Conclusions:

Our model explores the possible interactions and potential synergisms between a BiTE® and an anti-PD1 mAb. It proposes a mathematical framework to describe the underlying biology of the method of actions for these compounds and may provide valuable insight to facilitate the development of co-administration strategies for various hematological malignancies.

TUE-026

Population PBPK Modelling using the Quasi-Random Parametric EM Algorithm (QRPEM) and the Nonparametric Adaptive Grid Method (NPAG) of the Simcyp Simulator

Janak Wedagedera¹, Anthonia Afuape¹, Siri Kalyan Chirumamilla¹, Hiroshi Momiji¹, Robert Leary¹, Mike Dunlavey¹, Richard Matthews¹, Khaled Abduljalil¹, Masoud Jamei¹, Frederic Y. Bois¹.

¹CERTARA UK Limited, Simcyp division, Sheffield, UK.

Objectives: PBPK models usually include a large number of parameters because of their mechanistic nature. The best-practice workflow for PBPK modelling in clinical studies involves *in vitro* to *in vivo* extrapolation of parameter values. However, such extrapolations are uncertain and may benefit from inclusion of clinical observations. Yet, when clinical inter-individual variability is high, or the data sparse, it is essential to use a population pharmacokinetics framework. We compared the results obtained in such a case with parametric (QRPEM) and non-parametric (NPAG) asymptotic methods implemented in the Simcyp Simulator version 19 to those given by Bayesian numerical estimation.

Methods: The QRPEM and NPAG algorithms were used to analyse a canonical theophylline dataset (Trembath 1980; R-MEMSS package). A minimal PBPK model was used to describe theophylline pharmacokinetics after administration of an immediate-release (IR) formulation to 18 healthy subjects. We estimated the first-order absorption rate ka , the steady-state volume of distribution Vss , and the maximum rate of metabolism through liver CYP1A2 N3-demethylation $Vmax$ and their inter-individual variability (IIV). Renal clearance was set at 0.31 L/h. The same data were analysed in a parametric Bayesian framework using the same structural model using HMCMC (Stan software, Carpenter *et al.* 2017) and Metropolis-Hastings MCMC sampling (Bois 1997). We compared parameter estimates and model fits to the data.

Results: Simcyp version19 QRPEM and NPAG algorithms successfully fitted the PBPK model to observed data to estimate the key parameters. Overall, QRPEM and NPAG showed consistency in the estimates except that for ka was two to four higher with the NPAG method. Run-times were within the range of 45 minutes to 3 hr. The comparison with Bayesian MCMC and HMCMC shows good agreement in the estimates for Vss and $Vmax$ but ka was about 2-fold higher compared to the QRPEM estimates (HMCMC took about 60 minutes).

Conclusions: The QRPEM and NPAG methods implemented in the Simcyp Simulator version 19 gave consistent population and individual parameter estimates (including IIV) and were in reasonable agreement with Bayesian HMCMC or MCMC estimates in this study. Relatively higher estimate for absorption parameter ka with NPAG and MCMC or HMCMC seem to be due to sensitivity to prior information and measurement error, coupled with poor identifiability with this dataset. The run-times of both QRPEM and NPAG estimation methods were reasonable compared to the alternative Bayesian MCMC estimation methods.

References:

- Bois FY, Maszle D 1997. Journal of Statistical Software. 2, doi.org/10.18637/jss.v002.i09.
Carpenter B *et al.* 2017. Journal of Statistical Software. 76, doi.org/10.18637/jss.v076.i01.
Trembath PW, Boobis SW 1980. British Journal of Clinical Pharmacology 9:365-369.

TUE-027

Title: Simulation of first-in-human using an allometrically scaled population mechanistic TMDD model with preclinical monkey data

Authors: Géraldine Ayral (1), Pauline Traynard (1), Monika Twarogowska (1)

Affiliations: (1) Lixoft, Antony, France

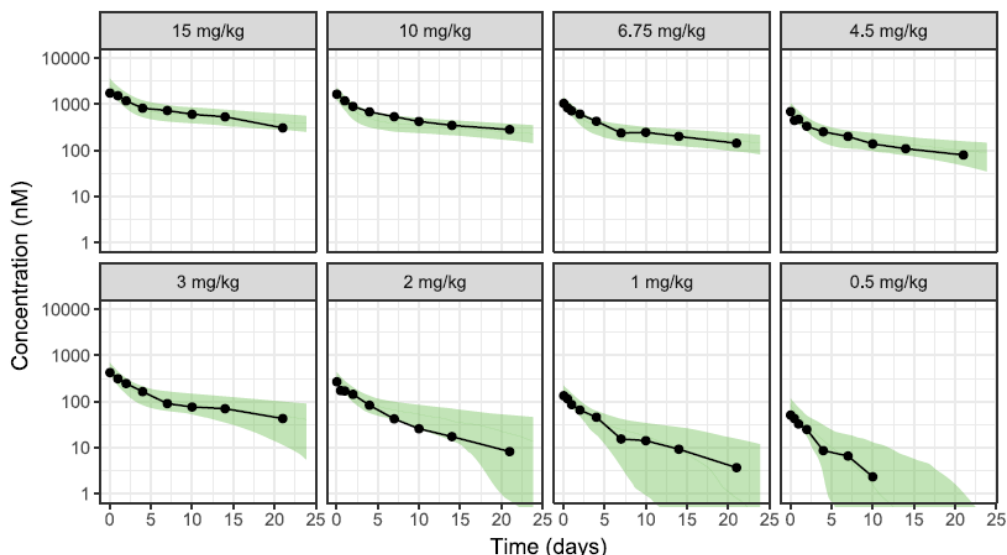
Objectives:

The design of first-in-human clinical trials relies on the extrapolation of preclinical animal data to human predictions. The ability to accurately predict the human pharmacokinetics (PK) of a drug candidate is therefore a key challenge in drug discovery and development. For small molecules, simple allometric scaling of clearance and volume is often sufficient. However, for many biologics, their nonlinear PK imposes the use of more advanced methods. In this poster, we compare several model-based approaches for the first-in-human dose selection for the fully human IgG2 monoclonal antibody PF-03446962, using cynomolgus monkey data and literature information.

Methods:

Drug concentration profiles after single and multiple doses of PF-03446962 for 14 monkeys are extracted from Luu et al [1]. Three different PK models are fitted on the data using a population approach in Monolix: (1) a linear 2-compartment model, (2) a simple target-mediated disposition (TMDD) model with linear and Michaelis-Menten elimination and (3) a more complex TMDD model, where the complex internalization rate and the binding affinity are fixed to literature values.

Each model is then used to simulate the human PK for a large range of doses using Simulx. Volumes and linear clearance parameters are scaled using classical allometric scaling. For model 2 (simple TMDD), Km and Vm are assumed identical in monkey and human. For model 3, the parameter values are replaced by the literature values for humans. The model predictions are finally compared with actual phase I human data.



First-in-human simulations using the complex TMDD model (green) and averaged phase I clinical data (black)

Results: The linear model is not able to capture the monkey PK profiles, but both the simple and more complex TMDD models provide satisfactory diagnostic plots and good confidence on all estimated parameters. According to the parsimony principle, one would favor the simpler TMDD model with linear and non-linear clearance. However, the estimated Km and Vm parameters have no clear biological meaning and it is therefore difficult to decipher how they scale to humans. On the opposite, the more complex TMDD model has parameters with clear physiological interpretation, which in addition have been experimentally measured both in monkey and humans. This greatly facilitates the choice of parameter values for the prediction of human PK. When compared to the actual PK profiles in human from the phase I study, the more complex TMDD model shows the most accurate prediction, within 1 to 2-fold of observations.

Conclusion: This example illustrates how the incorporation of mechanistic information from the literature into a model-based approach can help to obtain more accurate first-in-human predictions and thus inform the choice of the first-in-human doses.

References:

- [1] Luu et al. (2012). Journal of Pharmacology and Experimental Therapeutics, 341(3), 702–708.

TUE-029

Early prediction of response and survival using from a tumor growth inhibition (TGI) model in head and neck squamous-cell carcinoma (HNSCC) patients treated with immunotherapy

Ignacio González-García¹, Vadryn Pierre^{2,3}, Vincent F S Dubois¹, Nassim Morsli⁴, Stuart Spencer⁵, Paul G Baverel^{1,6}, Helen Moore⁷

¹Clinical Pharmacology Safety Sciences, AstraZeneca, Cambridge, United Kingdom

²Clinical Pharmacology Safety Sciences, AstraZeneca, Gaithersburg, MD, USA

³EMD Serono Research & Development Institute, Inc. Billerica, MA, USA (current address)

⁴Clinical Development, AstraZeneca, Cambridge, United Kingdom

⁵Clinical Statistics, AstraZeneca, Cambridge, United Kingdom

⁶Clinical Pharmacology, Roche Pharma Research and Early Development, Roche Innovation Center, Basel, Switzerland (current address)

⁷Applied Mathematics, Applied BioMath, Concord, MA, USA

Objectives

Predicting which cancer patients will respond to immuno-oncology (IO) therapy is of great interest for optimizing clinical trial design as well as for patients. We developed a novel method based on a tumor dynamics model^a coupled with machine learning to give early predictions of best overall response (BOR) and 6-month overall survival (OS6) in HNSCC patients treated with durvalumab (an anti-PD-L1 antibody). This work aims to evaluate the predictive performance of the method.

Methods

A training data set was formed with longitudinal tumor size data (sum of longest diameters, SLD) from four clinical trials with a total of 401 patients. A test data set with 482 patients from an additional clinical trial was designated for external validation. We fit the tumor dynamics model to the full training data set using nonlinear mixed-effects modeling to obtain patient-specific parameters. These were used with known patient outcomes to train a classification algorithm to predict BOR and OS6 categories. We finalized this classification model using five-fold cross-validation on the training data to select any informative covariates. We tested the method's predictive performance using test data truncated to 12, 18, and 24 weeks. The tumor dynamics model was fit to these truncated data, the resulting individual parameters were input to the classification model, and the resulting predictions were compared to the known eventual outcomes for each patient.

Results

During external validation, classification error rates were 9.75%, 7.05%, and 6.64% for BOR and 20.5%, 18.3%, and 18.0% for OS6, for data truncated at 12, 18, and 24 weeks, respectively. The area under the receiver operating characteristic curves was preserved for BOR (0.94, 0.97, and 0.97) and for OS6 (0.82, 0.84, and 0.85) at 12, 18, and 24 weeks, respectively. These results suggest that the algorithm predicts response accurately based on data \leq 12 weeks.

Conclusions

We developed and evaluated a method that predicts individual cancer patient response and survival based on early tumor size data and baseline characteristics. This method showed promising results using only twelve weeks of tumor size data for patients with HNSCC who received durvalumab. Further investigation for other cancers, and for treatment with other IO therapies and non-IO therapies, will help determine the usefulness of this method in the broader clinical setting.

The results in this abstract were previously accepted for an oral presentation at the Annual Meeting of the American Society for Clinical Pharmacology and Therapeutics (ASCPT) planned for March 17-21, 2020 in Houston, TX, and published in the conference proceedings as abstract OIV-003.

References

- ^a Moore H. A new tumor dynamics mathematical model. Poster presented at: American Conference on Pharmacometrics; Oct 23-26, 2016; Bellevue, WA.

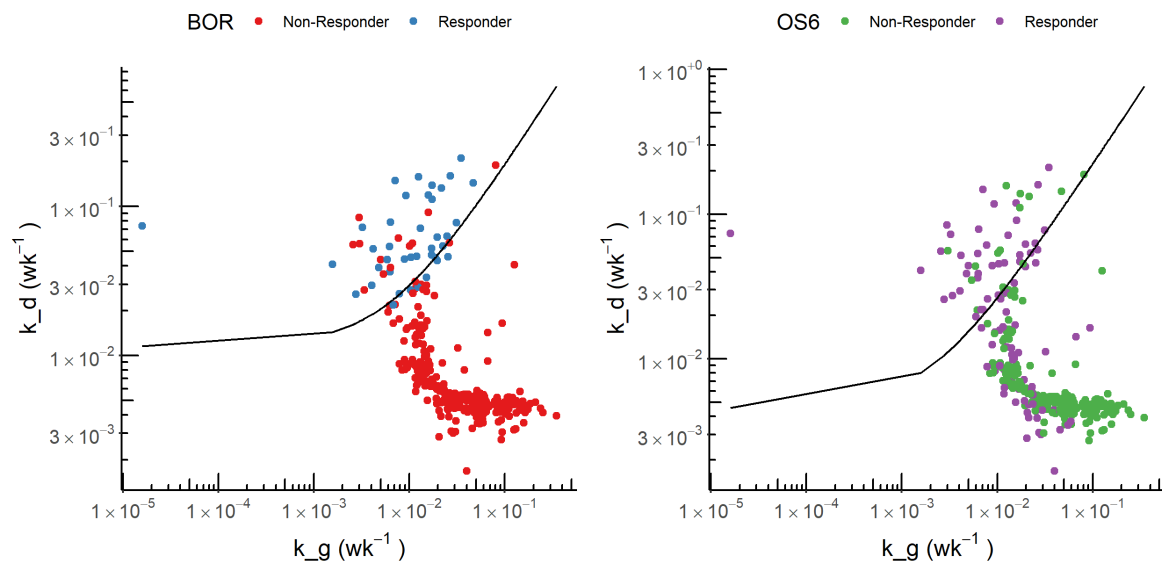


Figure 1 Classification of best overall response (BOR, left) and 6-month overall survival (OS6, right) categories using parameters k_d and k_g from the tumor dynamics model. The curves define the category predictions, and the colors represent the actual recorded patient response category.

Development of a QSP model for ADAMTS13 and von Willebrand factor interactions

Hoa Q. Nguyen¹, Steven Yu², Zhiwei Zhang³, Indranil Bhattacharya¹, Majid Vakilynejad¹, Andy Zhu¹

¹ Takeda, Cambridge, MA, US; ² LH Group, China; ³ RES Group Inc., Needham, MA, US

Objectives: Von Willebrand factor (VWF) is an adhesive and multimeric glycoprotein that plays an essential role in maintaining hemostatic balance. VWF promotes platelet aggregation and clot formation at the site of endothelial injury. In order to prevent unnecessary clotting, VWF is negatively regulated by a catalytic enzyme 'A Disintegrin and Metalloproteinase with Thrombospondin Type 1 Motifs 13' (ADAMTS13). In this study, we developed a quantitative system pharmacology (QSP) model to investigate the complex dynamics of VWF and ADAMTS13 under pathophysiological conditions of congenital thrombotic thrombocytopenic purpura (cTTP).

Methods: A biological process map was constructed to represent molecular interplay of critical components in ADAMTS13-VWF interactions, in which ADAMTS13 cleaves ultra-large VWF to smaller VWF fragments under the inhibition by extracellular hemoglobin (Hb) and thrombospondin-1 (TSP-1). Basal levels and kinetic parameters of VWF, ADAMTS13, Hb, and TSP-1 were extracted from the literature using *in vitro* and *in vivo* studies for the model parameterization. Model performance was evaluated using clinical data from first-in-human (FIH) study of recombinant ADAMTS13 (rADAMTS13) in cTTP patients^a.

Results: The molecular kinetics of ADAMTS13, VWF and Hb were established by comparing model simulations with basal levels in healthy and TTP patients without drug intervention. With rADAMTS13 treatment, the model was able to describe and recapitulate observed VWF fragment, total VWF and active VWF levels in cTTP patients.

Conclusions: A QSP model was built for ADAMTS13 and VWF interaction leveraging both biological data in literature and clinical observations from cTTP patients^a, providing an amenable framework to adapt and apply for other indications where rADAMTS13 could potentially influence the disease pathophysiology.

References

^a Scully, Marie, et al. "Recombinant ADAMTS-13: first-in-human pharmacokinetics and safety in congenital thrombotic thrombocytopenic purpura." *Blood, The Journal of the American Society of Hematology* 130.19 (2017): 2055-2063.

TUE-032

Mathematical Modeling of the Interactions between Radiation-Generated Reactive Oxidative Species and Thrombopoietic System in Animal Models

Ibrahim Mustafa¹, Allison Gibbs², Isabel Jackson², Joga Gobburu¹, Mathangi Gopalakrishnan¹

¹Center for Translational Medicine, School of Pharmacy, University of Maryland, Baltimore, USA

²The Department of Radiation Oncology, School of Medicine, University of Maryland, Baltimore, USA

Objectives: To build a systems biology model to investigate the effects of acute ionizing radiation (IR) doses on thrombopoietic system. The model aims to provide a mechanistic understanding of how IR generating reactive oxidative species (ROS) interacts and mediates damage to platelet counts and to predict the dynamic behavior of the thrombocytes in different animal models of radiation. The interaction between ROS and damage to the thrombopoietic system is a complex dynamic process that warrants a systems biological approach.

Methods: The systems biology model was built to elucidate key damage and dynamics of thrombopoiesis accompanied by ROS in response to acute IR. The thrombopoietic system was composed of three compartments: two were assumed to be radio-sensitive namely progenitors (proliferative cells) and megakaryocytes (non- proliferative cells) in bone marrow, while the third compartment was assumed to be radio resistant, i. e., platelets in blood stream. The ROS elucidating physiological changes was assumed to be radiation dose dependent. The model considered feedback effect for controlling the homeostasis in thrombocyte levels. The model was formulated in terms of ordinary differential equations (ODEs) and all optimization, sensitivity analysis, and simulations were conducted using Pumas v0.3.1 software. Dynamics of platelets as well as progenitors and megakaryocytes, in the presence of acute IR doses, were examined and compared to observed platelet count in irradiated mice and rabbits.

Results: The radiation dose is a variable input parameter of the model. It is found that at low radiation doses, the platelets count (as radio-resistance cells) can be recovered to the normal levels as both radio sensitive cells of bone marrow namely: progenitors and megakaryocyte can be repaired, and proliferation can occur. However, at high radiation doses, platelets are completely damaged and unable to recover as high ROS levels lead to damaged progenitors and megakaryocytes. Platelet counts reach nadir around 9000/ μ L on day 14 and 7200 / μ L on day 10 and did not recover at IR dose of 9.0 and 9.5 Gy in mice and rabbits respectively. The platelet counts in mice recovered after 20 and 25 days after the irradiation exposure of 6.75 and 8.25 Gy respectively. While rabbits started recovering after 11 and 17 days after exposure at 6.5 and 7.5 Gy respectively. The IR-ROS model adequately described the observed platelets counts in two animal models of radiation.

Conclusion: A novel systems biology model was developed to investigate the interaction between ROS-induced by acute IR and the thrombopoietic system. The model adequately explained the influence of ROS on the components of the thrombopoietic system and predicted the behavior of the system in the presence of a wide range of IR doses in mice and rabbits successfully.

TUE-033

Title: Computational Systems Pharmacology of Antibody-Drug Conjugates

Authors: Inez Lam¹, K. Phin Chooi², Conor S. Barry², Balakumar Vijayakrishnan², Thaïs Cailleau², Peter C. Tyrer², Philip W. Howard², Rosalin Arends³, Kathryn Ball³, Feilim Mac Gabhann¹

Affiliations:

¹ Institute for Computational Medicine and Department of Biomedical Engineering, Johns Hopkins University

² Spirogen (a member of the AstraZeneca group), AstraZeneca

³ Clinical Pharmacology and Safety Sciences, AstraZeneca

Objectives: Antibody-Drug Conjugates (ADCs) are engineered immunoconjugate drugs composed of 3 core components: (1) a monoclonal antibody and (2) one or more cytotoxic small molecules (known as warheads), attached via (3) a chemical linker. While ADCs have the potential to assist in the fight against cancer, clinical success has been hindered by a lack of understanding of the mechanisms driving ADC safety and efficacy, and difficulty in optimization of each subunit individually and within the context of the entire ADC. Here, we apply computational systems pharmacology approaches to study ADCs with pyrrolobenzodiazepine (PBD) as the cytotoxic drug entity, combining experimental data and mechanistic modeling to conduct simulations of ADCs in different experimental scenarios relevant to drug development. This work is critical to understanding how ADC design translates to ADC function, enabling the comparison of novel treatment scenarios and the development of better oncology therapies.

Methods: We have constructed a computational systems pharmacology model with cellular and intracellular mechanisms specific to ADCs with PBD warheads to understand the impact of ADC characteristics on in vitro efficacy and toxicity. The model is comprised of coupled, deterministic, nonlinear, ordinary differential equations (ODEs), outputting the concentrations of each molecule or molecular complex over time. Model parameters are calibrated and validated using in vitro experimental data provided by AstraZeneca for anti-HER2-PBD ADCs, which have antibodies targeting the HER2 antigen and carry PBD payloads with differing properties. The model describes ADC binding, internalization, recycling, intracellular trafficking and degradation, warhead binding, efflux and influx of warhead.

Results: We conduct sensitivity analyses to identify the most influential parameters in the system, and find that sensitivity changes with time after treatment and receptor expression levels. We also simulate different scenarios to understand the impact of key ADC characteristics, such as the Drug-to-Antibody Ratio (DAR), warhead potency, and linker design, and connect these to ADC efficacy and toxicity in vitro to investigate how key design characteristics can be manipulated to alter ADC performance. The computational model can also track populations of extracellular and intracellular warhead, revealing additional insights into warhead movement and mechanisms of action at the in vitro scale.

Conclusions: We have developed a computational systems pharmacology model of PBD ADCs at the in vitro scale. This model includes both cellular and intracellular mechanisms specific to ADCs with PBD warheads and contains parameters from literature or fit to AZ experimental data. Using the relevant experimental data, this in vitro model can be expanded to incorporate whole-body pharmacokinetics, to serve as the basis for in vivo and clinical models of PBD-ADCs. The resulting in models will describe whole-body pharmacology and can be further developed to create a human clinical model, which can be used to run virtual clinical trials.

TUE-034

RAS blockade and SARS-CoV-2 interaction through ACE2: QSP evaluation of pro- and anti-inflammatory pathway activity.

Authors: Ishaan Dave¹, Melissa Hallow, Ph.D.¹

Affiliations: University of Georgia, Athens, GA, USA

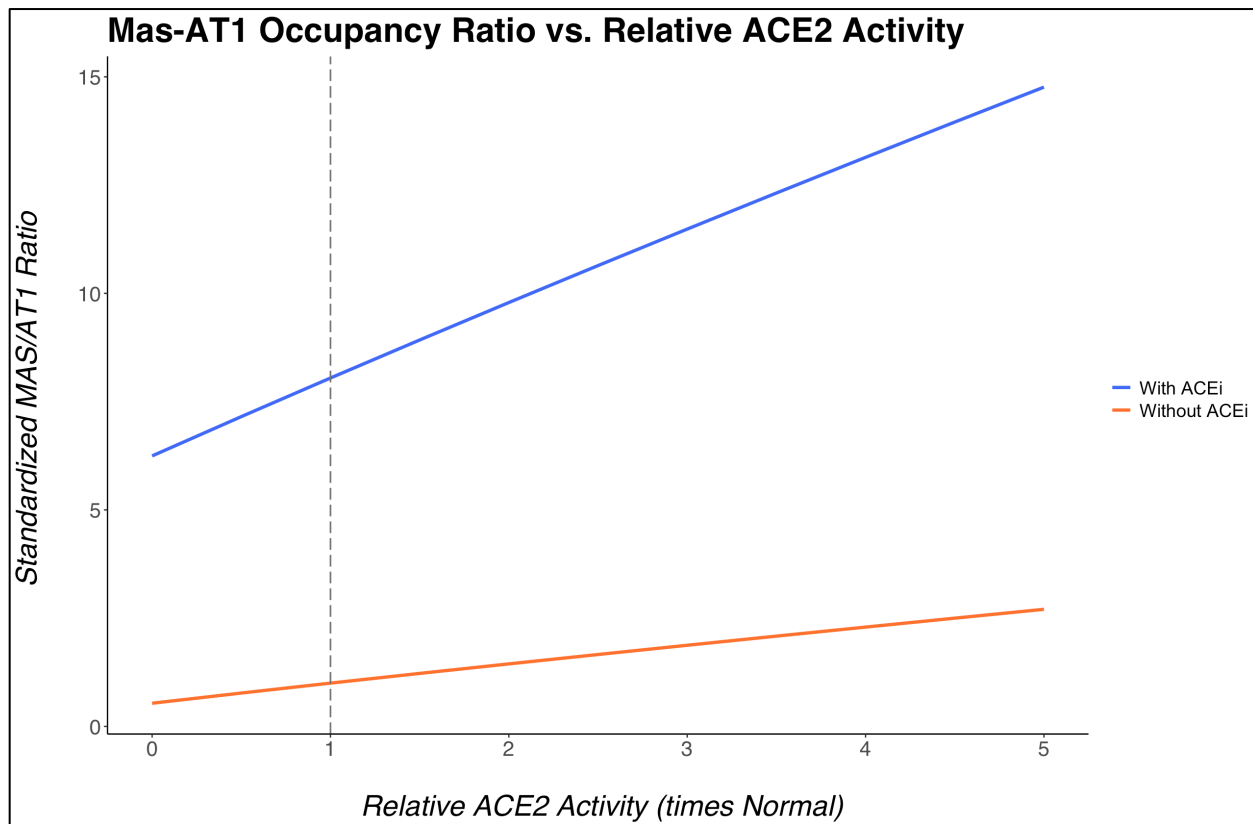
Objectives: The renin-angiotensin system (RAS) consists of two arms, one that promotes inflammation through the AT1 receptor and another that suppresses inflammation through the mas-receptor. ACE inhibitors (ACEi) and AT1 receptor blockers (ARBs) suppress the pro-inflammatory arm while promoting the anti-inflammatory arm. They may do this in part by upregulating angiotensin converting enzyme 2 (ACE2), the membrane-bound enzyme by which SARS-CoV-2 infects cells. ACE2 levels are also altered with age, diabetes, and hypertension. Further complicating things, SARS-CoV-2 may downregulate ACE2 after infection, promoting inflammation. Based on these qualitatively understood directional effects, it has been speculated that that RAS blockers may either increase or decrease risk of severe outcomes in COVID-19. This has introduced uncertainty in the management of diabetic and hypertensive patients, many who are already on RAS blockers. We aimed to develop a tool to quantify relative changes in pro- and anti-inflammatory pathways under different treatments (e.g. ACE inhibitor or Angiotensin Receptor Blocker (ARB)) and disease states (e.g. diabetes, hypertension, COVID-19).

Methods: A QSP model for the RAAS system was extended to account for the pathway involving conversion of Angiotensin I and II to Angiotensin-(1-7) via NEP and ACE2, respectively, as well as Ang(1-7) binding to the mas receptor. Literature data were used to inform model parameters, and the model was validated by simulating Ang(1-7) formation in response to labeled AngI infusion. A literature survey was used to define ranges for ACE2 upregulation or down-regulation under different conditions. The ratio between mas-receptor and AT1-receptor occupancy was used as a measure of relative activation of anti-inflammatory to pro-inflammatory arms, and was simulated over a range of ACE2 levels, with and without ACE inhibition.

Results: ACE2 activity is reported to be downregulated 65-75% with SARS-CoV-2 infection and with older age. As illustrated in Figure 1, simulations suggest that this degree of downregulation will suppress the mas-AT1 ratio 30-35%. In contrast, ACE inhibition alone, with normal ACE2 expression, increase this ratio 8-fold. ACE inhibition is reported to increase ACE2 activity 1 to 5 times normal. This would further increase the mas-AT1 ratio 1- to 3-fold.

Conclusions: These results indicate that the magnitude of the shift toward the anti-inflammatory RAS arm with ACEi is large relative to the pro-inflammatory shifts due to ACE2 downregulation with age or SARS-CoV-2 infection. Increased mas and decreased AT1 binding have been shown to be protective in animal models of acute respiratory distress syndrome. Future work will evaluate effects of parameter uncertainty, and will analyze differences between ACEi and ARBs, as well as combinations of RAS therapy, comorbidities, and timing of infection.

Figure 1. Effect of changes in ACE2 activity on the mas-receptor / AT1-receptor occupancy ratio.



TUE-035**Maribavir Dose Considerations for Treatment of Cytomegalovirus Infections During Co-administration of CYP3A4 Inducers and Inhibitors, Based on Physiologically Based Pharmacokinetic (PBPK) Modeling**

Manoranjenni Chetty^{1*}, Sibylle Neuhoff¹, Zoe Barter¹, Karen Yeo¹, Kefeng Sun², Haojing Rong³, Ivy H Song⁴

¹Certara UK Ltd, Sheffield, UK; ²Shire, a Takeda company, Cambridge, MA, USA; ³Kymera Therapeutics,

Cambridge, MA, USA; ⁴Shire, a Takeda company, Lexington, MA, USA

*Affiliation at time of research

Objectives: Maribavir is an oral antiviral drug in Phase 3 evaluation (NCT02927067, NCT02931539) for the treatment of transplant recipients with cytomegalovirus infections. Maribavir is primarily metabolized by the isozyme 3A4 of cytochrome P450 (CYP3A4) and has demonstrated linear pharmacokinetics (PK) at doses up to 1,200 mg twice daily (BID) [1]. The aims of this study were to develop a physiologically based pharmacokinetic (PBPK) model, predict the impact of co-administration of CYP3A4 modulators on maribavir PK, and to provide guidance on dose adjustments for maribavir.

Methods: A combination of in vitro and clinical PK data obtained from single oral doses of maribavir 400 mg was used to develop the PBPK model, using the Simcyp® Simulator (Certara UK Ltd, Simcyp Division, Sheffield, UK; Version 17 Release 1). Model verifications were performed against observed PK data following administration of single oral doses of maribavir 800 mg and 1,600 mg, following a single oral dose of maribavir 400 mg with and without ketoconazole (400-mg single dose), and multiple oral 400-mg doses of maribavir with and without rifampicin (600 mg once daily [QD]). The model was then applied prospectively to predict interactions with other CYP3A4 inducers and inhibitors. Simulations were used to predict doses of maribavir necessary to maintain mean area under the curve (AUC), maximum concentration (C_{max}), and concentration 12 hours after dosing (C_{12h}) in the desired range when maribavir was co-administered with CYP3A4 modulators.

Results: Predicted likely outcomes of interaction with rifampicin 600 mg QD, phenobarbital 100 mg QD, phenytoin 300 mg QD, carbamazepine 200–400 mg QD, and efavirenz 600 mg QD in a healthy population indicated mean maribavir C_{max} ratios, with and without an inducer, of 0.56, 0.73, 0.69, 0.77, and 0.75, respectively. Corresponding predicted maribavir AUC_{0-12h} ratios, with and without an inducer, were 0.37, 0.61, 0.58, 0.71, and 0.58, respectively. The predicted maribavir C_{12h} ratios, with and without an inducer, were 0.10, 0.37, 0.36, 0.54, and 0.27, respectively. CYP3A4 inhibitors such as ketoconazole, ritonavir, erythromycin, and diltiazem can increase maribavir exposure; however, the estimated magnitude of change in maribavir exposure is less than two-fold.

Conclusions: Based on the known exposure–response relationship for efficacy and safety, maribavir can be dosed with CYP3A4 inhibitors without dose adjustment. CYP3A4 inducers reduce maribavir exposure to a relevant extent; therefore, to ensure antiviral efficacy (correlated to C_{12h}), maribavir dose increase is necessary from 800 mg BID up to 1,600 mg BID for various inducers. These data suggest co-administration of maribavir with rifampicin should be avoided; potentially, alternative antibacterial therapies should be considered.

Funding:

This study was funded by Shire, a Takeda company.

References:

- [1] Lalezari JP, et al. Antimicrob Agents Chemother. 2002;46:2969–2976.

TUE-036

Characterization of Immunogenicity to a Monoclonal Antibody using a Mixed Hidden Markov Modeling Approach

Donald Irby¹, Camille Vong², Jatin Narula³, Timothy Nicholas⁴, Kevin Sweeney⁴, Ellen Wang⁵, Jae Eun Ahn³

¹Division of Pharmaceutics and Pharmacology, College of Pharmacy, The Ohio State University, Columbus, OH

²Novartis Pharma AG, Basel, Switzerland

³Pfizer Inc, Cambridge, MA

⁴Pfizer Inc, Groton, CT

⁵Pfizer Inc, New York, NY

Objectives: Anti-drug antibody (ADA) titers are often detected using semi-quantitative immunoassays.

Depending on the sensitivity of the assay, it may potentially detect low positive titers with no apparent clinical impact on PK, efficacy or safety. We aimed to characterize the ADA status of a subject using a previously described probabilistic framework^{1,2}, a two-state mixed hidden Markov model (MHMM) with data from a monoclonal antibody (mAb) clinical program.

Methods: Two sources of data - ADA titers and PK residuals derived from a PK model for the mAb that did not account for the impact of ADA - were used in tandem to inform the hidden state parameter estimation. Differential emission probabilities between states of ADA production (S_{ADA}) and no ADA production (S_{noADA}) were estimated. A bivariate normal probability density function (PDF) was used for the two data types and their correlation was characterized. However, when time-matched records were not available, the emission probabilities were calculated from the univariate normal PDF for whichever variable was present. The SAEM procedure in NONMEM 7.4.3 was used for the parameter estimation, and the individual, hidden-state sequences were determined through the Viterbi algorithm that was available as a post hoc subroutine in NONMEM³.

Results: A two-state, bivariate MHMM was developed, capable of producing individual ADA state sequence predictions over time. The parameter estimates from the base MHMM were aligned with expected values (see **Table 1**). The model predictions of the ADA incidence and the median time to first ADA positive record were also in relative agreement with the observed values.

Conclusions: A two-state, bivariate MHMM was implemented on immunogenicity data from a mAb clinical program, in which additional observations (PK residuals other than ADA titers only) were used to improve ADA identification. The final parameter estimates of the MHMM were aligned with prior expectations based on knowledge of the system, and the model performed reasonably well at recapitulating the observed ADA incidence and the median time to first ADA positive record. Though still to be determined, this approach may help to interpret ADA assay results and to identify possible covariate effects to inform clinical development strategies.

Table 1. Fixed and random effects parameter estimates of the MHMM.

Parameter	Description	Expectation	Estimate (RSE%)	IIV (RSE%)
ADA _{MES} in S _{ADA}	Mode of the ADA distribution in the two ADA states	> 6.23	8.47 (1)	0.0373 (7)
ADA _{MES} in S _{noADA}		3.12	3.12 FIX	0 FIX
PK _{RES} in S _{ADA}	Mode of the PK residuals distribution in the two ADA states	< 0	-0.744 (3)	0.001 FIX [†]
PK _{RES} in S _{noADA}		~ 0	0.05 (15)	0.001 FIX [†]
ρ in S _{ADA}	Correlation term of the bivariate normal distribution in the two ADA states	< 0	-0.0262 (79)	0.001 FIX [†]
ρ in S _{noADA}		0	0 FIX	0 FIX
φ_{Init} in S _{ADA}	Initialization probability for the ADA producing state	0	0 FIX	0 FIX
$\pi_{\text{ADA_noADA}}$	Transition probability from the ADA to non ADA producing states	~ 0%	-4.3* (1)	0.0259 (65)
$\pi_{\text{noADA_ADA}}$	Transition probability from the non ADA to ADA producing states	~ 36%	-1.37** (3)	0.0928 (38)
σ^2_{ADA} in S _{ADA}	Variance of the ADA distribution in the two ADA states	NA	2.12 (4)	0 FIX
σ^2_{ADA} in S _{noADA}		~ 0	1 FIX	0 FIX
σ^2_{RES}	Variance of the PK residuals distribution, shared between ADA states	NA	0.917 (1)	0 FIX
$\pi_{\text{noADA_ADA}}$ non-sero	Transition probabilities between the two ADA states for non-seroconverters	0	0 FIX	0 FIX
$\pi_{\text{ADA_noADA}}$ non-sero		1	1 FIX	0 FIX
PK _{RES} in S _{ADA} non-sero	Mode of the PK residuals distribution in the ADA producing state for non-seroconverters	~ 0	0 FIX	0 FIX

RSE, relative standard error; IIV, inter-individual variability; PK, pharmacokinetic

* transformed value ~ 1%

** transformed value ~ 20%

† omega was fixed to a small number to allow the SAEM algorithm to efficiently estimate parameters

References

- Brekkan A, Jonsson S, Karlsson MO, Plan EL. Handling underlying discrete variables with bivariate mixed hidden Markov models in NONMEM. *Journal of pharmacokinetics and pharmacodynamics* **46** 591-604. (2019)
- Brekkan AL, B.; Lledo-Garcia, R; Jonsson, S; Karlsson, M. O.; Plan, E.L. Characterization of Anti-Drug Antibodies Using a Bivariate Mixed Hidden-Markov Model. *PAGE* 27; 2018.
- ICON. hmm.f90. [file] 2019 [cited]Available from: <https://nonmem.iconplc.com/nonmem/hmm>

TUE-037

Statistical-mechanistic modeling of a myocyte population of models to study effects of cardiac inotropes via mapping pre-clinical data to parameters of myofilament contraction

Jaimit Parikh^{1*}, Xenia Butova², Tatiana Myachina², Anastasia Khokhlova², Tim Rumbell¹, Sushmita Allam¹, James Kozloski¹, Viatcheslav Gurev¹

¹IBM T.J. Watson Research Center., Yorktown Heights, NY, USA

²Ural Federal University, Yekaterinburg, Russia

Objectives: Biophysical models are increasingly explored to support clinical decision making, guide therapeutic design, and provide early predictions of intervention outcomes and risks. However, application of these models requires estimation of model parameter uncertainty and calibration to available pre-clinical and clinical observations, which are still open problems. The objective of our study is to design a robust method for construction of a population of models of cardiac myocytes that characterize variability of the pre-clinical and clinical data and identify differences in intrinsic contractile properties affected by drugs.

Methods: We employed a novel approach that integrates mechanistic models and machine learning methods to construct the population of cardiomyocyte models that captures variability in the pre-clinical data and thus provides a better understanding of the effects of Omecamtiv Mecarbil (OM), a cardiac inotropic currently in phase III of clinical trials. Resting myocyte length, time to peak contraction and amplitude of shortening features were extracted from the experimental unloaded shortening data traces measured in the presence and absence of OM, and the populations of models were constructed to match the joint density of these features. The core methodology used for parameter inference is based on the probability density mapping formulation proposed by Poole and Raftery (Poole D, Raftery AE, J. Am. Stat. Assoc, 2000). Model parameters are sampled from probability densities represented by Gaussian mixture models using an adaptive Markov chain Monte Carlo method and the surrogate AI model of the sarcomere.

Results: Using our approach, we matched the density of the unloaded shortening data features and generated corresponding coherent distribution of model parameters linked to contractile machinery of myocytes (Figure 1). The alterations in model parameters identified via calibration of the population of models by the unloaded shortening data allowed us to evaluate changes in calcium sensitivity and cooperativity induced by OM. The distribution of model parameters obtained not only captured the variability in the data but also highlighted a plausible mechanism of action of the drug, the cooperative activation of the thin filament.

Conclusions: We present a novel method for construction of a population of models coherent to the distribution of observed pre-clinical and/or clinical data. We demonstrate the application of the approach for improved understanding of OM mechanism of action from simple *in vitro* experimental measures. The developed methodology is highly suitable for enhanced analytics of multimodality data gathered across various phases of the drug-development pipeline. Another application of the proposed approach for the identification of candidate therapeutic regulation targets in Huntington's disease phenotypes is covered in detail in related reports of this method.

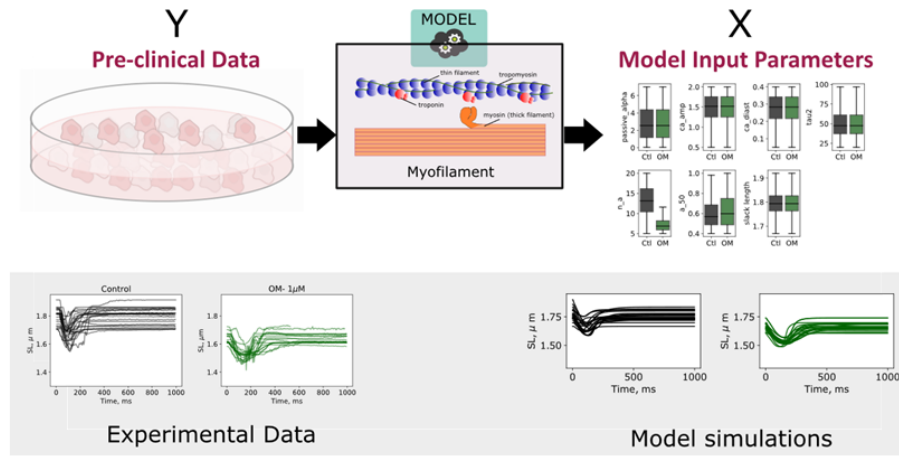


Figure 1: Estimation of mechanistic model parameters coherent to experimental unloaded shortening data under action of OM. (Black traces- Control condition, Green traces- OM)

TUE-038

Application of Physiologically-Based Pharmacokinetic Modeling to Evaluate the Potential Effect of Oxcarbazepine on Phenytoin Exposure During Concomitant Anti-Epileptic Drug Therapy in Adults

Jaydeep Sinha¹, Fernando Carreño¹, Andrea N. Edginton², Daniel Gonzalez¹

¹ UNC Eshelman School of Pharmacy, University of North Carolina, Chapel Hill, NC, United States

² School of Pharmacy, University of Waterloo, Waterloo, Ontario, Canada

Objectives: Oxcarbazepine (OXZ) and its pharmacologically active 10-monohydroxy derivative (MHD) are known to inhibit cytochrome P450 (CYP) 2C19 *in vitro*, which in addition to CYP2C9, metabolizes phenytoin (PHT). However, whether OXZ can lead to a clinically relevant drug-drug interaction (DDI) during adjunctive anti-epileptic therapy with PHT has remained inconclusive, primarily because of contradictory reports [1]. Therefore, the aim of this work was to systematically assess the clinical DDI potential of OXZ while concomitantly administered with PHT using a physiologically-based pharmacokinetic (PBPK) modeling framework.

Methods: PBPK models of OXZ (including MHD) and PHT were developed for adults using the software PK-Sim® (v. 8.0). The literature derived initial values of specific clearance (K_{cat}) and lipophilicity (LogP) were first optimized using concentration vs. time (C-T) data and urinary excretion data following intravenous administration [2-3]. Next, the PK-Sim® calculated specific intestinal permeability values were optimized using observed C-T data following oral administration, where empirical Weibull models were applied for oral absorption. Predicted C-T profiles and the respective area under the curve (AUC) values were compared with the observed data. The reversible CYP2C19 inhibition constants of OXZ and MHD ($K_i \sim 15 \mu M$) were used to develop the DDI model [4]. The ratio of AUC (AUCR) of PHT between the OXZ treated group (i.e., 1200 mg twice daily) and the control groups (300 mg and 600 mg single dose) were predicted for CYP2C9 wild type (WT: *1/*1) subjects and poor metabolizers (PM: *2/*2, *2/*3).

Results: The predicted C-T profiles captured the observed data well, and the predicted AUC values were mostly within 1.2-fold of the observed values. For the PHT model, 83% of the dose was metabolized by CYP2C9 and CYP2C19, and their relative contributions were $f_{m,2C9} = 95\%$ and $f_{m,2C19} = 5\%$, respectively. In addition, a 4-fold increase in PHT dose from 300 to 1200 mg resulted in a 6.7-fold increase in AUC. Overall, these PHT model predictions were in agreement with the literature information. The predicted AUCR values at the highest PHT dose (i.e., 600 mg) were 1.04 and 1.16 for the CYP2C9 WT and PM groups, respectively.

Conclusions: The PBPK modeling results suggest that OXZ (at a maximum daily dose) is not likely to cause a clinically relevant elevation of PHT exposure that would warrant dose adjustment in both CYP2C9 WT (lower $f_{m,2C19}$) and PM (higher $f_{m,2C19}$) groups. Therefore, the reported elevation of PHT exposure in a few previous studies might have been caused by other concomitantly administered drugs and/or patient related factors (e.g., pathology), which necessitates further investigation.

References:

1. Soskin et al., *Psychosomatics*, 51(6), 2010
2. Flesch et al., *Drug Metabolism and Disposition*, 39(6), 2011
3. Glazko et al., *Clinical Pharmacology & Therapeutics*, 10(4), 1969
4. Lakehal et al., *Epilepsy Research*, 52, 2002

TUE-039**Exceeding the Gastrointestinal Solubility of Abrocitinib:
An Example for Parallel First- and Zero-Order Absorption**

Authors: Jessica Wojciechowski,¹ Bimal K Malhotra,² Xiaoxing Wang,¹ Luke Fostvedt,³ Hernan Valdez,² Timothy Nicholas¹

Institutions: ¹Pfizer Inc., Groton, CT, USA; ²Pfizer Inc., New York, NY, USA; ³Pfizer Inc., Cambridge, MA, USA

Objectives: Abrocitinib is a selective Janus kinase 1 enzyme inhibitor being developed for the treatment of moderate-to-severe atopic dermatitis (AD). It is an orally bioavailable, Biopharmaceutics Classification System (BCS) Class II drug with apparent dissolution rate limited absorption after oral administration. Results of densely sampled, healthy volunteer (HV) studies with abrocitinib suggested high intra- and interindividual variability in the maximum concentration (C_{max}), lack of proportionality at high doses, and accumulation somewhat higher than that predicted from superposition. The objective of this analysis was to develop a population pharmacokinetic (PK) model of abrocitinib in HVs, patients with psoriasis, and patients with AD.

Methods: The analysis data set was pooled from 7 phase 1 studies, 2 phase 2 studies, and 2 phase 3 studies. Doses ranged from 3 mg to 800 mg administered as 4 formulations (suspension and 3 tablets) during clinical development. A nonlinear mixed-effects model was developed using NONMEM. Simulations of dose proportionality and steady state accumulation of C_{max} and AUC were conducted using the final model, with reference to a 200-mg once-daily regimen (highest dose in phase 3 program).

Results: A 2-compartment model with parallel first- and zero-order absorption, time-dependent bioavailability, and dose- and time-dependent clearance (CL) was developed. The parallel absorption model accounted for dissolution rate limited absorption by implementing a parameter—AK₁—that estimated the maximum amount absorbed by first-order processes (the remainder of which is absorbed by zero-order). The estimate for AK₁ was 121 mg, such that for a 200-mg phase 3 tablet dose (highest effective dose assessed in phase 3 studies), 60.5% was absorbed rapidly via first-order processes (k_a ; 4.01 hour⁻¹) and the remaining 39.5% was absorbed by zero-order processes (k_0 ; 75.3 mg/h). First- and zero-order absorption processes were predominant at lower (3-100 mg; assumed solubilized state) and higher doses (400-800 mg; assumed supersaturated or precipitated states), respectively. AK₁ was dependent on

different formulations (suspension increased AK_1 by 117%) and the patient's having eaten a high-fat meal (entirely zero-order). Abrocitinib exposure increased in proportion with dose over the range of 3-400 mg for C_{max} , and 100-800 mg for AUC at steady state.

Conclusions: A semimechanistic approach to handling absorption was applied to describing the PK of abrocitinib. Conditions altering the gastrointestinal pH (increased pH with high-fat meal) or particle size (formulations) or exceeding its intrinsic gastrointestinal solubility (doses sufficient for saturation or precipitation) significantly altered the rate of abrocitinib absorption. Understanding dose- and time-dependent absorption was imperative before evaluation of CL and impact of intrinsic patient factors on abrocitinib PK.

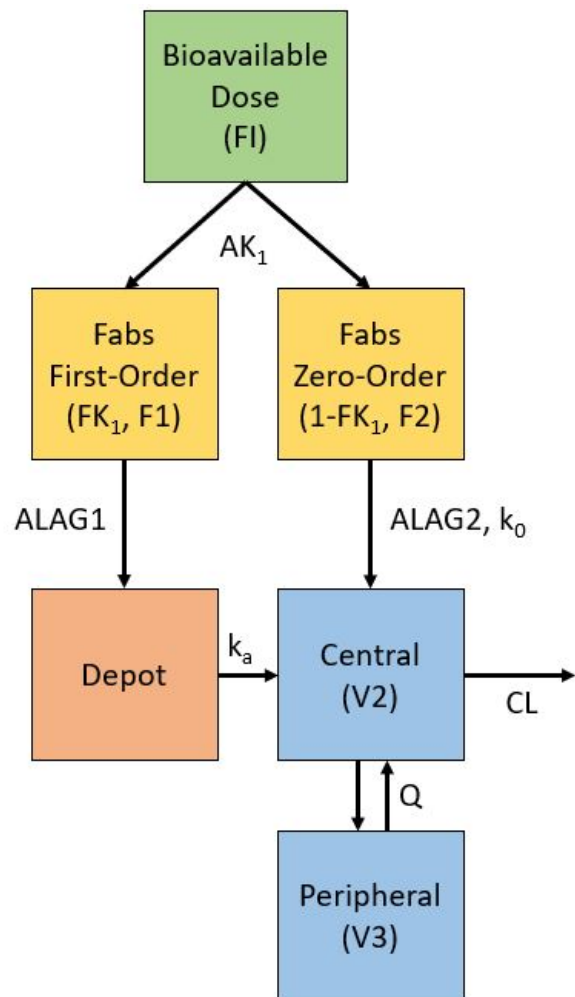


Figure 1. Schematic of Parallel First- and Zero-Order Absorption Model

TUE-040**Population pharmacokinetics modeling of Brincidofovir and the active metabolite cidofovir diphosphate in healthy volunteers**

Jie (Janet) Zhao¹, Camila de Almeida¹, Nathan Teuscher¹, Tim Tippin², John Dunn², Tom Brundage², Marion Morrison², Odin Naderer², Virna Schuck¹

¹Certara USA, Inc., Princeton, NJ, USA

²Chimerix, Inc

Objectives: Brincidofovir (BCV) is an orally available lipid conjugate of cidofovir (CDV), which is active against orthopoxviruses in vitro and is under development for the treatment of smallpox infections, one of the deadliest infectious diseases in human history and a national security threat. Inside peripheral blood mononuclear cells (PBMCs), BCV is hydrolyzed to CDV and then converted via anabolic kinases to the active metabolite cidofovir diphosphate (CDV-PP). Our aim was to develop an integrated parent-metabolite population pharmacokinetic (PK) model to describe the plasma BCV and intracellular (PBMC) CDV-PP concentration versus time profiles in healthy subjects after oral and intravenous (IV) administration, and to evaluate the effect of intrinsic and extrinsic factors on BCV PK. This model will contribute to the understanding of critical covariates and provide bases for BCV dose selection in the smallpox indication.

Methods: This population PK model utilized data from 7 Phase I studies, with BCV doses of 100 mg and 200 mg after oral administration and 10 to 50 mg after IV infusion. Plasma BCV and intracellular (PBMC) CDV-PP concentration data were obtained from 224 healthy subjects. A sequential modeling approach from BCV to the metabolite CDV-PP was developed with NONMEM VII (v7.3). A broad range of covariates including weight, age, sex, and food status were selected for evaluation based on scientific and clinical relevance. Precision of estimation and the predictive performance of the model were assessed by visual predictive checks. Some data used in this modeling was funded under BARDA contract HHSO100201100013C.

Results: Plasma BCV PK profiles were adequately described by a linear two-compartment model with a sequential absorption process: zero-order appearance in depot compartment followed by a first order absorption into central compartment. Weight, formulation (tablet and suspension), sex, food, and route of administration were identified as significant covariates. Bioavailability was estimated to be lower for tablets and fed state, and females were estimated to have lower clearance than males. Distribution appears different for IV and oral administration, with V_p being 27% lower after IV administration. The transit model (3 transits) was used to link and account for the delay between plasma BCV to intracellular (PBMC) CDV-PP PK. The PK profiles of CDV-PP were described by a linear one-compartment model, with sex as an important covariate on CDV-PP clearance.

Conclusions: The population PK model jointly described the plasma BCV and intracellular (PBMC) CDV-PP profiles in healthy subjects after oral and IV administration. The developed model was applied to simulate BCV and CDV-PP exposures at different clinical dosing scenarios, providing bases for BCV dose selection in smallpox patients.

TUE-041

Assessment of Cytochrome P450 3A4-Mediated Drug–Drug Interaction for Ipatasertib Using Physiologically Based Pharmacokinetic (PBPK) Model

Jing Jing¹, Rucha Sane¹, Yuan Chen¹, Kenta Yoshida¹

¹Genentech, Inc., South San Francisco, CA, USA

Objectives: Ipatasertib is a potent and highly selective small-molecule inhibitor of AKT and it is primarily metabolized by CYP3A4 in humans. The drug-drug interaction (DDI) risks for ipatasertib, as the victim or perpetrator, have not been assessed at the proposed clinical dose of 400 mg. The aim of the study is to develop a PBPK model for ipatasertib to evaluate the effect of CYP3A4 inhibitors (strong, moderate and weak) and inducers (strong, moderate) on ipatasertib PK and the impact of ipatasertib on midazolam PK at the proposed clinical dose.

Methods: A PBPK model was developed for ipatasertib using in silico, in vitro, and clinical data in Simcyp. The model was optimized and verified using DDI data [itraconazole-ipatasertib (100 mg single dose) and midazolam-ipatasertib (600 mg multiple dose)] and clinical PK data of ipatasertib which exhibited nonlinear PK at subclinical doses. The verified PBPK model was then used to predict the effect of CYP3A4 inhibitors and inducers on the PK profile of ipatasertib and the impact of ipatasertib (400 mg) on midazolam exposures.

Results: The developed PBPK model reasonably captured observed DDIs and nonlinearity in ipatasertib PK. As the victim of DDI, simulations showed that strong CYP3A4 inhibitors could increase ipatasertib AUC and C_{max} by 3.3- and 2.0-fold respectively and moderate inhibitors of CYP3A could increase ipatasertib AUC by ~2–2.5 fold and C_{max} by ~1.5~1.7-fold. Simulated exposures of ipatasertib at a reduced dose of 200 mg administered concurrently with moderate CYP3A4 inhibitors were similar to the observed exposures of ipatasertib at the 400 mg dose alone. Based on PBPK model simulation, strong and moderate inducers of CYP3A4 could decrease ipatasertib AUC by 86% and 74% and C_{max} by 68% and 51%, respectively. As a perpetrator of DDI, the simulation showed a mild inhibitory effect of ipatasertib on midazolam (predicted AUC and C_{max} ratios of 1.69 and 1.49) at the steady-state of the clinical dose of 400mg.

Conclusions: This study demonstrates the value of using PBPK model to assess the clinical DDI risks for ipatasertib and to provide dosing strategy for the concurrent use of other CYP3A4 perpetrators or victims.

TUE-042**Pharmacokinetically-Guided Dosing of Oral Sorafenib in Pediatric Hepatocellular Carcinoma:
A Simulation Study**

John C Panetta¹, Olivia Campagne¹, Jessica Gartrell², Wayne Furman², Clinton Stewart¹

¹Department of Pharmaceutical Sciences, St. Jude Children's Research Hospital, Memphis, TN; ²Department of Oncology, St. Jude Children's Research Hospital, Memphis, TN

Objectives: Pediatric hepatocellular carcinoma (pHCC), a rare malignancy accounting for 0.5% of all pediatric malignancies, is treated with sorafenib, which improves outcomes in adult HCC. We have previously treated pediatric refractory or recurrent solid tumors, including HCC, with a combination of sorafenib, bevacizumab, and cyclophosphamide and propose a prospective protocol in rare solid malignancies including HCC to evaluate the addition of atezolizumab to this regimen. Two objectives of this protocol are to, a) test the ability of targeting sorafenib exposure using pharmacokinetically-guided dosing and b) test the ability of pharmacokinetically-guided dosing to reduce the rate of hand foot skin reaction (HFSR), a dose limiting toxicity of sorafenib. Due to the rare nature of HCC, simulations were used to evaluate these objectives.

Methods: All pharmacokinetic simulations were based on the sorafenib pharmacokinetic and HFSR data from the St. Jude ANGIO1 study (n=35; Inaba, H., Clin Cancer Res, 25:2019). Population pharmacokinetics (Monolix 5.1.0) along with individual post-hoc estimates (sampled from the conditional distribution) were used to simulate AUC_{0-12hr} and C_{min} at steady-state given BID dosing of oral sorafenib at either a fixed dose ($90 \text{ mg/m}^2/\text{dose}$) or a pharmacokinetically-guided dose (adjusted to target a steady-state AUC_{0-12hr} between 20 and $55 \text{ hr}\cdot\mu\text{g/mL}$). The pharmacokinetically-guided dose was determined by adjusting the dose on day 4, based on day 1 pharmacokinetics, to obtain an exposure by day 7 within the target range. The probability of HFSR toxicity as a function of sorafenib exposure was based on a Cox proportional hazard model. The percentage of simulated studies within the target range was assessed and the 95% confidence intervals were determined using bootstraps (n=1000). The power to detect the probability of success of the study objectives given a fixed number of patients (n=6 to 24) was assessed using study re-sampling with replacement (n=1000).

Results: Simulations showed that 67% (95% CI: 62%-72%) of the pharmacokinetically-guided studies vs 50% (95% CI: 45%-55%) of the fixed dose studies could be expected in the target range. The power to observe at least 4 of 6 patients in the target range was 72% vs 33% using pharmacokinetically-guided vs fixed dosing. Next, we compared the probability of observing a grade 2/3 HFSR given either pharmacokinetically-guided or fixed dosing. These simulations showed an expected grade 2/3 HFSR toxicity rate of 17% (95% CI: 15%-20%) given pharmacokinetically-guided dosing vs 22% (95% CI: 21%-26%) given fixed dosing. The power to observe less than 6 of 24 studies with a grade 2/3 HFSR toxicity was 80% vs 52% using pharmacokinetically-guided dosing vs fixed dosing.

Conclusions: Our simulation studies have helped guide a study design for our proposed pHCC protocol where pharmacokinetically-guided dosing will both increase the percentage of studies in the target range and potentially reduce HFSR rates.

TUE-043**(Found in) Translation – Cotton Rat Modelling and Validation with Model Based Meta-Analysis (MBMA) for RSV**

Jos Lommers¹, Michelle Green¹, Amy Espeseth², Kalpit A. Vora², Antonios Aliprantis², Lynn Finelli², Radha Railka², Nele Mueller-Plock¹, Brian M. Maas², Luzelena Caro², Li Qin¹, Gerly van der Vleuten¹, Marianne van Vugt¹, Anna Largajolli¹, S. Y. Amy Cheung¹, Jeffrey R. Sachs²

¹Certara Strategic Consulting, Princeton, NJ, USA. ²Merck Research Laboratories, Merck & Co., Inc., Kenilworth, NJ, USA

Objectives: The cotton rat has enabled successful prediction of (passive) immunogenicity, safety, and efficacy in the clinic [1], and is therefore the preferred animal model for the development of novel vaccines and monoclonal antibodies (mAb) for prophylaxis against respiratory syncytial virus (RSV) infections. This motivates development of a translational model framework to demonstrate the applicability of cotton rat pharmacokinetic targets and biomarker readouts to the clinical setting for other mAbs.

Methods: We focused on mAbs that target the pre-fusion antigenic sites [2]. Protocols for testing RSV mAbs (and vaccines) in cotton rat studies have become relatively standard [3]. Blood samples are taken shortly after passive immunization to assess pharmacokinetics (mAb concentration). Efficacy data are obtained 4-6 days after inoculation (challenge infection) with RSV, which is the time of maximal viral replication (e.g. lung viral loads (VL)). Such non-clinical data were collected internally and from literature [4,5]. Data from RSV clinical trials were extracted from literature reports, in particular for pediatric populations.

The non-clinical data were modeled using a sigmoidal relationship between mAb concentration and lung VL:

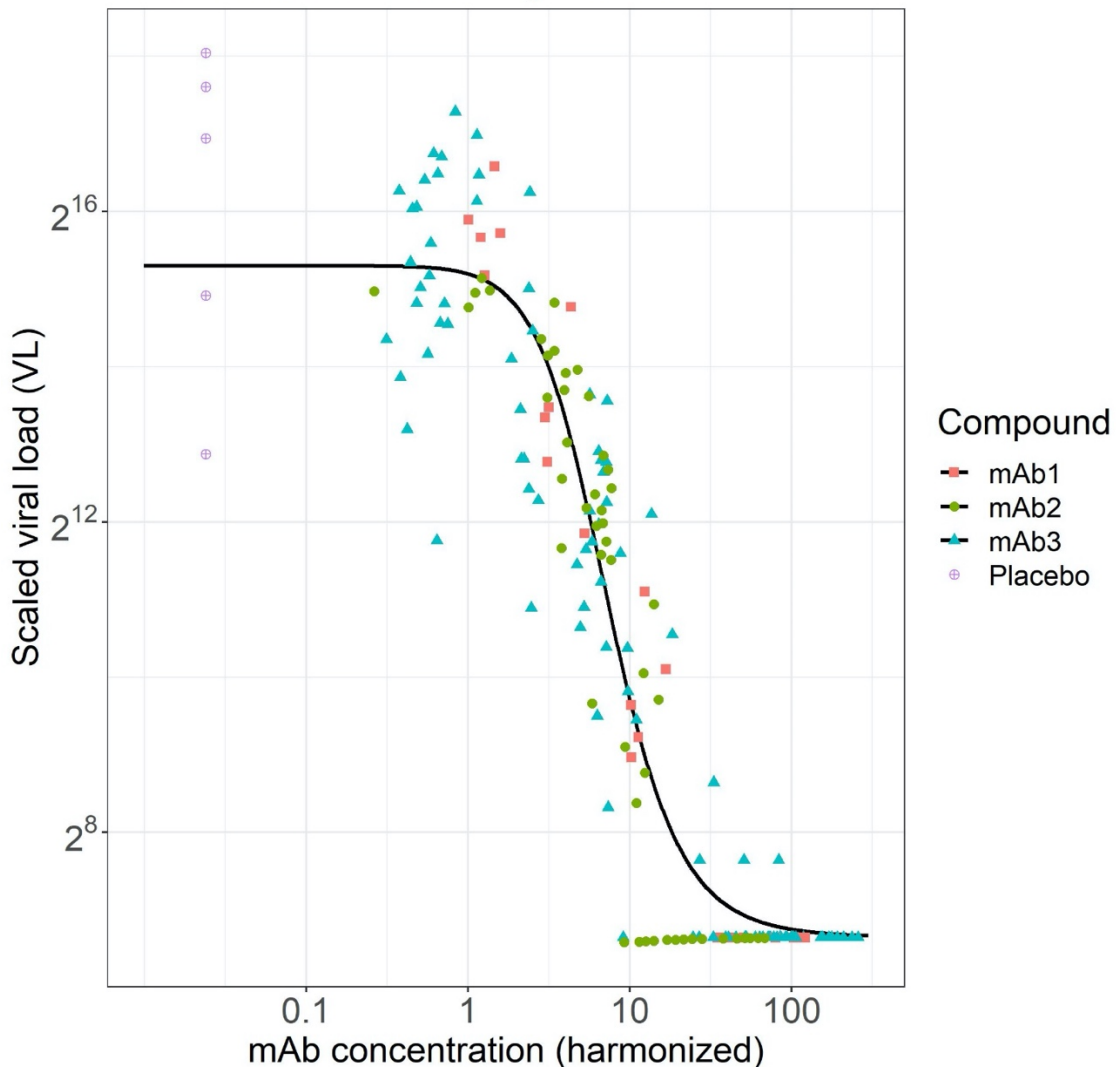
$$\log_{2}VL = \log_{2}VL_{max} \cdot e^{\log(\frac{\log_{2}VL_{min}}{\log_{2}VL_{max}}) \cdot suppr}$$

$$suppr = \frac{\log_{2}conc^{\gamma}}{\log_{2}conc^{\gamma} + \log_{2}IC_{50}^{\gamma}}$$

Where $\log_{2}VL=\log_{2}(\text{viral load})$ in cotton rat lungs and $\log_{2}conc=\log_{2}(\text{mAb concentration})$. Data were modeled using R.3.6.3 using package nlme. In order to compare with human data, mAb concentrations were transformed into human serum neutralizing titers (SN) and the lung viral load were scaled to RSV incidence rate in human.

Results: The cotton rat dataset had 179 data points. We obtained a robust relationship between mAb concentration and lung VL, enabling prediction of efficacious doses or concentrations (Figure, accounting for covariate effects [6])

Cotton rat RSV efficacy model



The cotton rat efficacy curve was translated to a pediatric RSV-A SN versus incidence rate curve using an internally developed clinical relationship between mAb concentrations and RSV-A SN. Furthermore, the maximum and minimum cotton rat lung viral loads were scaled to maximum and minimum clinical incidence rates for infections, respectively. This provided a quantitative means to predict clinical incidence rates based on pre-clinical study outcomes. The cotton rat curves agreed with previously reported clinical incidence rates at various concentrations.

Conclusions: Our analysis has shown that the cotton rat model can quantitatively predict clinical trial outcomes, by assuming that the RSV-A SN in human is predictive for RSV incidence rate. We aim to expand our non-clinical model to include mAbs that target other RSV-A pre-fusion sites and to build a translational model to assess RSV F vaccine candidates.

References:

- [1] The IMPact-RSV Study Group, Pediatrics. 1998 102(3 Pt 1):531-7 PMID:9738173
- [2] Graham BS, et al. Curr.Opin.Immunol. 2015 Aug;35:30-8. doi:10.1016/j.co.2015.04.005.
- [3] Boukhvalova, MS, et al. Antivir.Chem.Chemother. 2018;. doi:10.1177/2040206618770518
- [4] Zhu Q, et al. Sci.Transl.Med. 2017. doi: 10.1126/scitranslmed.aaj1928.
- [5] Tang A, et al. 2019 Sep;12;10(1):4153. doi:10.1038/s41467-019-12137-1.
- [6] Lommerse J, et al. ACoP2018

TUE-045**Integration of Pharmacodynamic Biomarker with Modeling & Simulation for Eculizumab Precision Dosing in Pediatric Patients with Hematopoietic Stem Cell Transplant Associated-Thrombotic Microangiopathy**

Kana Mizuno¹, Alexander A Vinks^{1,4}, Christopher E. Dandoy^{2,4}, Ashley Teusink-Cross³, Stella M. Davies^{2,4}, and Sonata Jodele^{2,4}

¹Division of Clinical Pharmacology, ²Division of Bone Marrow Transplantation and Immune Deficiency, Cancer and Blood Disease Institute, ³Department of Pharmacy, Cincinnati Children's Hospital Medical Center, Cincinnati, OH; ⁴Department of Pediatrics, University of Cincinnati College of Medicine, Cincinnati, OH

Objectives: Eculizumab, an anti-complement C5 antibody, is an effective therapeutic for the treatment of transplant associated-thrombotic microangiopathy (TA-TMA) which is associated with poor survival after hematopoietic stem cell transplantation (HSCT). We previously developed an eculizumab PK model and demonstrated the significant benefit of PK/PD-guided dosing for survival improvement [1]. However, the current model only takes into account elevated complement activation biomarker (sC5b-9) at start of therapy and has no capability to reflect contextual changes in disease progression and improvement. This study aimed to refine the PK model using an enriched PK/PD data set collected during the course of treatment by integrating time-varying sC5b-9 as a covariate on clearance. In addition, optimal dosing strategies were explored using Monte Carlo Simulation (MCS).

Methods: Eculizumab and biomarker of response data (sC5b-9) were collected from 64 pediatric TA-TMA patients with a median age of 6 years and until at least 100 days after transplant or until TA-TMA resolution [2]. Since disease profiles are different in patients with bleeding complications, those patients (n=26) were excluded from the analysis (to be analyzed in a separate study). Consequently, 38 non-bleeding patients were included in the current population PK model development using NONMEM 7.4. Potential covariates predictive of eculizumab PK were assessed including age, sex, body weight, albumin, GFR, dose courses and sC5b-9 levels. PK target attainment ($\geq 100 \mu\text{g/mL}$) for the current weekly dosing regimen was determined using MCS. Pediatric induction dosing regimens to improve the target attainment was explored by shortening the time interval at a maximum dose of 900 mg.

Results: The mean eculizumab clearance was highest after the first dose (58.5 mL/h/70kg) among the treatment courses. The clearance decreased over time in parallel with sC5b-9 reduction. The PK change was described by incorporating body weight, time-varying sC5b-9, and courses of dosing in the model as a covariate on clearance. The MCS analysis showed that poor target attainment is achieved in patients with higher body weight and sC5b-9 levels. The current weekly induction dosing protocol showed target attainment in only up to 25% of pediatric patients with body weight $\geq 30\text{kg}$, which was increased to 60% for our identified intensifying dosing regimen with dosing interval ranging from 1-4 days depending on body weight.

Conclusions: We successfully refined the eculizumab PK model that captures the temporal changes in clearance by integrating sC5b-9 and number of treatment courses. The developed model could be used to improve target attainment by tailoring individual dosing regimens considering time-varying sC5b-9. This model-based optimized dosing algorithm will be evaluated in a prospective study and can be incorporated into drug dosing strategies in clinic.

References

1. Jodele S et al. Biol Blood Marrow Transplant. 2016; 22: 307-315.
2. Jodele S et al. Blood. 2020; 135(13):1049-1057.

TUE-046**A Streamlined Approach to a Fully Validated, Part 11 Compliant, Pharmacometric Suite with a Version Controlled Data Repository and FTP Server for Data Transfer**

Authors: Kevin J. McConnell, Ronish Desai, Sachin Sanduja, Stephen A. Greene, Ry R. Forseth, Laurent Vernillet

Affiliations:

- 1) Rudraya Corporation – KJM, RD, SS
- 2) SK Life Science, Inc. - SAG, JKL, RRF, LV

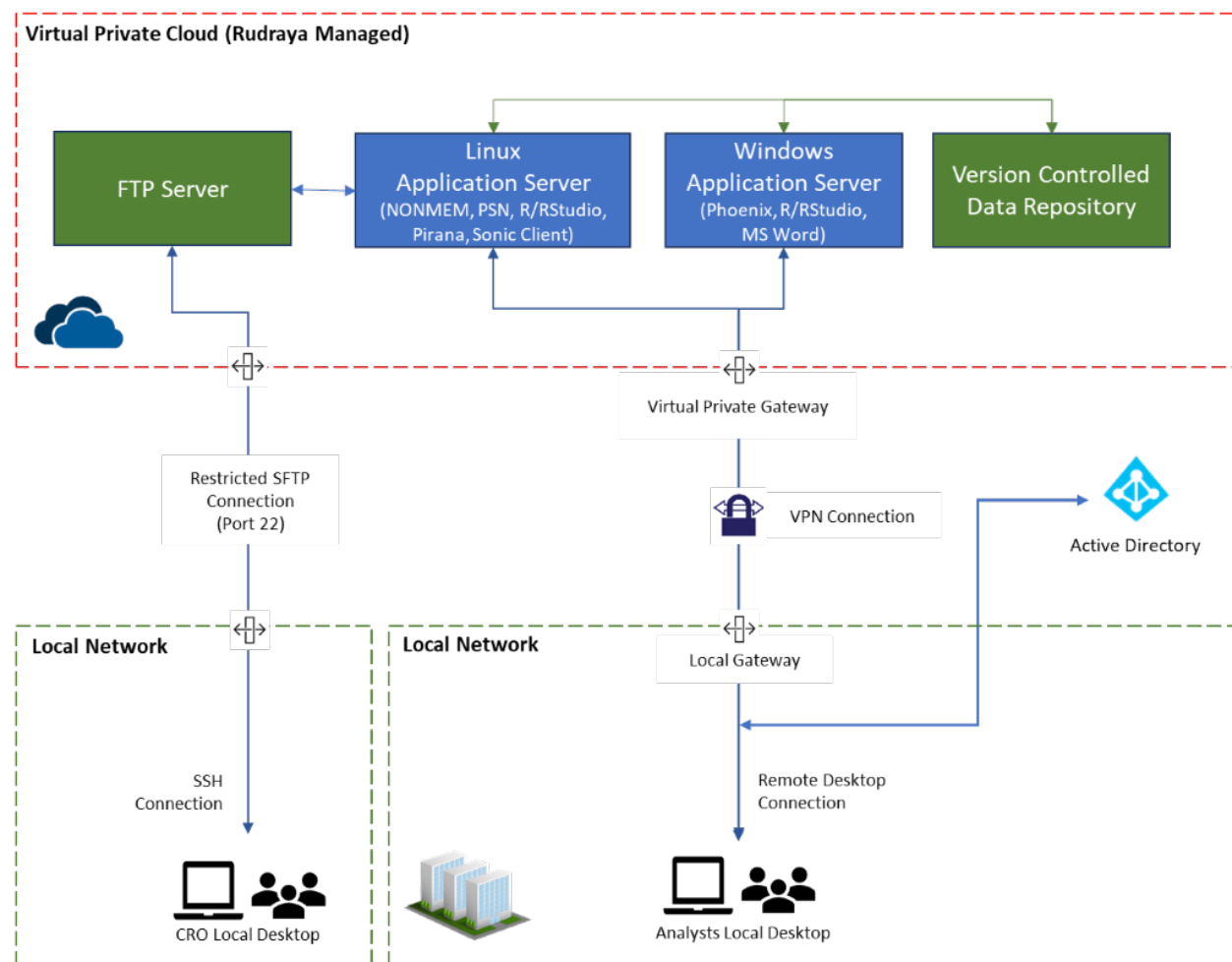
Objectives: Performing Pharmacokinetic (PK) and/or Pharmacodynamic (PD) analyses compliant with the regulatory expectations of many global health authorities presents several operational and technical challenges. Regulatory requirements mandate that all PK/PD analyses that support drug approval packages are conducted within a validated environment and with proper documentation to support the methodology used to validate said environment. With multiple software programs, data transfer mechanisms, and servers utilized across the majority of PK/PD analyses, the validation of an analysis environment requires assiduous planning and testing to meet regulatory expectations. As such, groups that carry the remit of validation often utilize systems that are inefficient and rate limiting in the drug development process. Herein is presented a streamlined approach to construct a fully validated clinical pharmacology (CP) computing platform (CPCP) to address the shortcomings of many validated environments.

Methods: The instigated CPCP system is centered around a Linux application server containing a version-controlled CP data repository (CPDR) called Sonic Projects®, for storage of all data and analysis files related to PK/PD analyses. The Linux server also houses commonly used PK/PD modeling software (NONMEM®, R/R studio, and Pirana®). A separate Windows application server was built for other commonly used PK/PD modeling software, GastroPlus®, Phoenix® WinNonlin/NLME, R/Rstudio, and Microsoft® Office. The CPDR housed on the Linux server is mounted on the Windows server to provide the ability to move files from the Windows server to the data repository housed on the Linux server, maintaining a centralized location for all PK/PD analysis files. Finally, an FTP server is integrated to allow for external vendors to place and obtain data. Access to the FTP server is restricted by IP address and a username and password. The FTP server also allows for transfer of data between external vendors and the CPDR via a single application (Sonic Client®) that's controlled from the Linux server. This approach restricts access to the CPDR from the FTP server to internal users.

Results: The fully validated CPCP system integrates many commonly used PK/PD analysis software programs, a version-controlled data repository, and a fluid means of data transfer between the validated environment and external sources. All servers are interconnected with appropriate security measures between servers that have access from external vendors.

Conclusions: The CPCP system provides a streamlined approach to PK/PD analyses from data transfer with the use of an FTP server to data analysis on a Windows application server and Linux application server and data management on a version controlled CPDR all while maintaining regulatory compliance (e.g, 21 CFR Part 11). The CPCP system provides a means to perform all necessary PK/PD analyses required throughout a drug development program without the potential shortcomings of more traditional systems.

Figure 1: Clinical Pharmacology Computing Platform Environment



TUE-047

A joint modeling workflow for the longitudinal and time-to-event data: tools, statistical methods and advanced diagnostics

Kirill Zhudenkov¹, Sergey Gavrilov¹, Alina Sofronova¹, Oleg Stepanov¹, Kirill Peskov^{1,2}

¹ M&S Decisions LLC, Moscow, Russia; ² Computational Oncology Group, I.M. Sechenov First Moscow State Medical University, Moscow, Russia.

Objectives: In the last decades the amount of clinical study results constantly grows, though the efficient treatment for many diseases is still being developed. Study biomarkers can be assessed both at baseline and longitudinal level. Particular biomarker value achievement can be an endpoint in studies, thus statistical methods of biomarker trend prediction may be useful. For late-phase studies, the analysis of event-type endpoints plays a crucial role (death, exacerbations, etc.), so study performance prediction and patient stratification, using interim data, is important for new medicines design. To address all these items, the methods of joint modeling of longitudinal and time-to-event data can be utilized [1]. The objectives of the current work were (1) to propose the generalized workflow for the development of joint models and (2) to compare existing tools able to cover it .

Methods: The workflow incorporates different statistical methods, that are controlled in R environment. Depending on the analysis aims, following tools can be utilized: JM, JMBayes, rstanarm, Monolix, NONMEM, Stan [5,6]. Model performance is initially assessed by means of statistical criteria (AIC, BIC). The workflow provides comprehensive graphical diagnostics for the models – observed vs. predicted and residuals plots. Prediction performance can be assessed for both time-to-event data and longitudinal biomarkers using external validation and involving survival discrimination by means of Receiver Operating Characteristics (ROC) curve and Brier Score. The workflow was tested using the datasets of oncology studies from the Project Data Sphere (NCT00312377, NCT00076388, NCT00364351, NCT00322452, NCT00988208, NCT00617669).

Results: The developed workflow was successfully applied to various clinical endpoints and longitudinal biomarkers [2-4]: tumor size, blood biomarkers and patient survival. We obtained an adequate description of the data on the diagnostic plots for all tested models. The long-term (12-24 months) validation performance of the models was tested

using interim (3-6 months) of longitudinal data. Each important longitudinal biomarker in multivariate models provided 0.05-0.1 gain in area under ROC curve (with a typical range of 0.65-0.85 dependent on the model complexity). Nonlinear multivariate models provided more efficient patient subgrouping and longitudinal biomarker trend prediction. Stan tool appeared to have the highest performance and flexibility, while being the most complex in implementation (Table 1).

Conclusions: Here we presented a workflow, incorporating the analysis of biomarkers and time-to-event data, that can be used in clinical study design and assessment. Utilizing the interim longitudinal biomarker data, the long-term patient cohort survival, patient stratification and biomarker trends can be efficiently predicted.

References:

1. Rizopoulos D. CRC press, 2012, ISBN 9781439872864.
2. Gavrilov S. StanCon 2019 Conference.
3. Gavrilov S. PAGE Meeting 2019.
4. Zhudenkov K. ACoP9 Conference 2018.
5. Brilleman S. 38th ISCB Conference 2017.
6. Riglet F. The AAPS Journal (2020) 22:50.

Table 1. Software and R packages for joint modeling

Tool name/ Feature	JM	JMbayes	Monolix	NONMEM	Rstanarm	Stan
Multivariate models	No	Yes	Yes	Yes	Yes	Yes
Linear models with splines	Yes	Yes	Coding	Coding	Yes	Coding
Nonlinear mixed-effects models	No	No	Yes	Yes	No	Yes
Survival function predictions	Embedded	Embedded	Random effects only	Partially implemented	Embedded	Coding
Calculation time	Fast	Fast	Slow	Slow	Fast	Slow
Overall Complexity	Low	Low	Medium	Medium	Low	High

TUE-048

Modeling of Tolerance to Opioid-induced Respiratory Depression in Chronic High-dose Opioid Users versus Opioid-naïve Individuals

Algera MH^{1*}, Olofsen E^{1*}, Moss L,³ Dobbins R,² Niesters M,¹ van Velzen M,¹ Groeneveld GJ,³ Laffont CM^{2#}, Dahan A^{1#}

* contributed equally; # contributed equally

¹ Department of Anesthesiology, Leiden University Medical Center, 2333 ZA Leiden, The Netherlands;

² Indivior Inc., North Chesterfield, VA 23235, USA.

³ Centre for Human Drug Research, 2333 CL Leiden, The Netherlands.

Objectives: Prolonged use of opioids is associated with addiction, physical dependence and development of tolerance. While there is indirect proof for the development of tolerance to respiratory effects of chronic opioid use in humans^{1,2}, such tolerance has not been formally assessed or quantified. The respiratory effects of fentanyl in chronic opioid users and opioid-naïve subjects were measured in an experimental medicine study³ and population pharmacokinetic/pharmacodynamic (PK/PD) modeling was conducted to quantify respiratory tolerance.

Methods: Fourteen opioid-naïve individuals (20-35 years) and 8 chronic opioid users (31-52 years, using ≥ 90 mg oral morphine equivalents daily) received escalating doses of intravenous fentanyl (opioid-naïve: 75-350 µg/70 kg; chronic users: 250-700 µg/70 kg). The study was conducted by anesthesiologists in a hospital setting and each subject had a facemask fitted to control inspiratory gases and to measure ventilation parameters under isohypercapnic conditions. Serial blood sampling was performed to measure fentanyl plasma concentrations. Pharmacokinetic and pharmacodynamic data (minute ventilation) were analyzed with NONMEM 7.4 using a sequential population PK/PD approach. Stimulated, nonspontaneous breathing data were set to zero (apnea). Censoring at zero (M3 methodology⁴) was used to describe prolonged apnea events.

Results: A three-compartment model best described the fentanyl PK data. The time course of the respiratory depressant effects of fentanyl was characterized using a biophase equilibration model in combination with an inhibitory E_{max} model. C_{50} , the effect-site concentration of fentanyl causing 50% ventilatory depression, was 0.42 ± 0.07 ng/mL in opioid-naïve subjects and 1.81 ± 0.38 ng/mL in chronic opioid users, indicative of a 4.3-fold sensitivity difference. For similar fentanyl exposure, the predicted probability of apnea in chronic opioid users was many fold lower than in the opioid-naïve population

Conclusion: Differences in tolerance between populations were well described by PK/PD modeling. Although chronic opioid users showed higher tolerance to the respiratory effects of fentanyl, model predictions indicate that fatal apneas may still occur at high doses reached during recreational use. The risk for these patients can be further increased after a drug holiday which may reduce tolerance towards levels observed in opioid-naïve subjects.

References:

- ¹Walsh TD, Rivera NJ, Kaiko R. Oral morphine and respiratory function amongst hospice in patients with advanced cancer. *Support Care Cancer* 11, 780-784 (2003).
- ²Santiago TV, Pugliese AC, Edelman NH. Control of breathing during methadone addiction. *Am. J. Med.* 62, 347-354 (1977).
- ³Wiest K, van Velzen M, Algera H, Moss L, Dobbins R (2019) High therapeutic buprenorphine levels reduce IV fentanyl respiratory depression. Annual Meeting of the American Society of Addiction Medicine, April 4-7, Orlando, FL.
- ⁴Ahn JE, Karlsson MO, Dunne A, Ludden TM. Likelihood based approaches to handling data below the quantification limit using NONMEM VI. *J Pharmacokinet Pharmacodyn.* 2008 Aug;35(4):401-21.

TUE-049

Quantitative mechanistic model for amyloid beta and tau protein role in synaptic plasticity

Stepan Lerner, Tatiana Karelina
InSyBio, Moscow, Russia

Objectives:

Current therapies for amyloid beta ($A\beta$) do not modify the progression of the Alzheimer's disease (AD). Amyloid hypothesis of AD is still debated. One of the most important property of neuron cells is its synaptic plasticity. Most of the physiological studies of synaptic plasticity investigate LTP (long-term potentiation) and LTD (long-term depression). The synaptic plasticity seems to underlie memory and learning formation. In animal models of AD, $A\beta$ inhibits LTP. An increased intracellular calcium level, mediated by NMDA and nACh receptors, is responsible for appearance of LTP, which is determined by increased AMPA receptor phosphorylation. These processes may contribute to tau hyperphosphorylation, further pathology progression. Understanding of these synaptic processes is particularly important for better prediction of cognitive outcomes in clinical trials. Quantitative systems pharmacology (QSP) model of synaptic plasticity was developed to investigate influence of amyloid beta on receptors governing LTP and state of tau protein.

Methods:

The model describes calcium influx in postsynapse through acetylcholine and glutamate receptors. Type of stimulation varies by changing the timing between cholinergic input and glutamatergic input. The model describes activation of kinase/phosphatase cascade, tau phosphorylation and level of AMPA receptors phosphorylation. The level determines the synaptic plasticity. $A\beta$ impairment of synaptic plasticity is modelled through impact on receptors and glial extracellular glutamate uptake. Potential $A\beta$ targeting therapy is represented as $A\beta$ washout. At the time of washout, $A\beta$ concentration is set to zero. Model is developed step by step by consecutive addition of new mechanistic details, using in vitro data and in vivo mouse data. In vitro data from the literature concerning synaptic plasticity (LTP) under various conditions are used for verification.

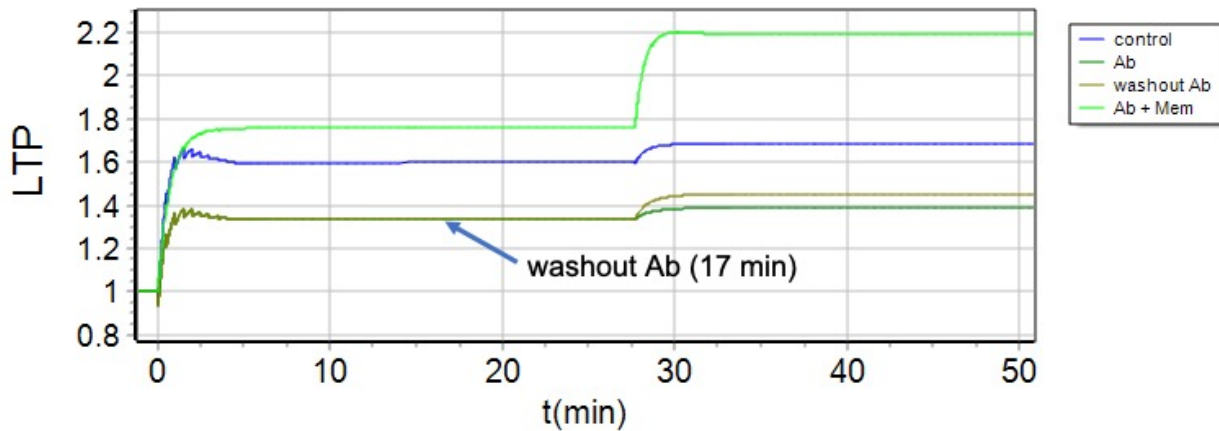
Results:

The model qualitatively describes LTP and its decrease in presence of $A\beta$ (Figure 1). It demonstrates that: 1) amyloid effect on LTP in such a system is partially irreversible, and amyloid washout does not lead to complete recovery of LTP 2) memantine protects from decrease of LTP 3) LTP recovers after exNMDAr blockers action, because memantine decreases binding glutamate with receptors and, thus, decreases calcineurin activity 4) at small concentration of amyloid beta ($<10nM$) with memantine, there is a complete rescue of LTP and decrease of tau phosphorylation; at medium concentration of $A\beta$ ($10nM < 50nM < 100nM$), with memantine recover LTP and decrease tau phosphorylation only after $A\beta$ washout; after influence of high $A\beta$ concentration ($>100nM$) memantine does not provide recovery of LTP even after amyloid washout, but tau phosphorylation may decrease.

Conclusions:

The model demonstrates a partial irreversibility effect of amyloid beta on LTP even on short times, which may partially explain failure of amyloid targeting and set up hypotheses for combinatorial treatments at different disease stages. This QSP model may connect models of proteinopathies with cognitive outcome.

Figure 1. Effect of synaptic plasticity (LTP) with Ab influence (green), washout amyloid beta (brown) and memantine blockade (light green)



TUE-050

An integrated glucose-insulin-cardiorenal QSP model of glucagon-like peptide-1 receptor agonist actions in the kidney

Lindsay E. Clegg¹, Robert C. Penland², David W. Boulton¹, K. Melissa Hallow³

¹Clinical Pharmacology & Quantitative Pharmacology, Clinical Pharmacology & Safety Sciences, R&D, AstraZeneca, Gaithersburg, USA

²Clinical Pharmacology & Quantitative Pharmacology, Clinical Pharmacology & Safety Sciences, R&D, AstraZeneca, Boston, USA

³School of Chemical, Materials, and Biomedical Engineering, University of Georgia, Athens, Georgia, USA

Objectives:

Glucagon-like peptide-1 receptor agonists (GLP-1 RA) improve glycemic control by slowing gastric emptying, increasing insulin secretion, and decreasing glucagon. GLP-1 RA also promote natriuresis over short time-scales and reduce urinary albumin excretion in clinical studies. However, the effects of GLP-1 RA on long-term renal outcomes remain unclear, as do the mechanisms through which GLP-1 RA exert their effects in the kidney. We built a QSP model to explore by which of many posited mechanisms of action GLP-1 RA may drive the observed renal effects, and what the implications of these mechanisms may be for long-term renal function.

Methods:

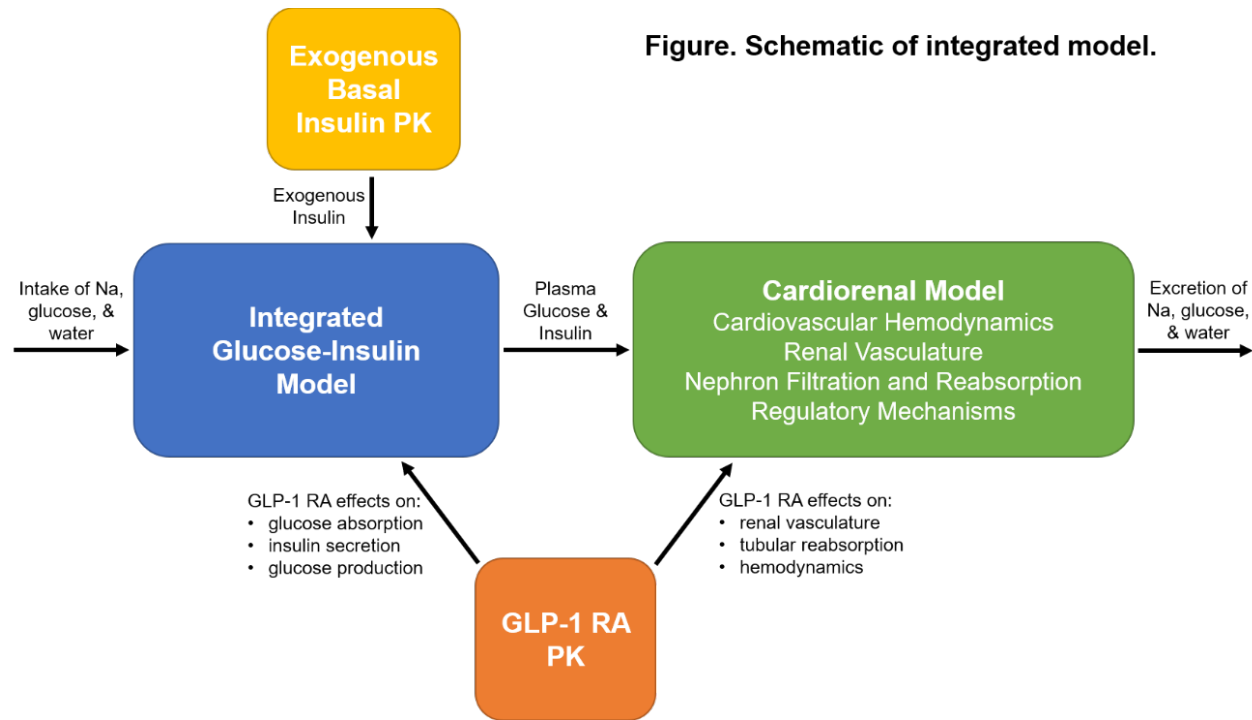
We integrated existing QSP and pharmacokinetic models of glucose-insulin dynamics[1], basal insulin pharmacokinetics[2], GLP-1 RA pharmacokinetics and pharmacodynamics[3, 4], and cardiorenal hemodynamics[5] (**Figure**) to study the effects of GLP-1 RA in acute renal studies performed under both fasting conditions[6] and following a standardized meal test[7, 8] in subjects with type 2 diabetes.

Results:

In the fasting state, the GLP-1 RA exenatide increased sodium excretion and moderately increased mean arterial pressure (MAP) without increasing glomerular filtration rate (GFR)[6]. The QSP model suggests a combination of decreased blood glucose, decreased proximal tubule sodium reabsorption, afferent arteriolar vasoconstriction, and a short-term increase in cardiac output are required to simultaneously match the observed changes in sodium excretion, MAP, and GFR. In the postprandial state, blood glucose increased less with the GLP-1 RA lixisenatide than without, and a larger increase in MAP was observed than in the fasting state[9]. The model suggests that slowing of glucose absorption from the gastrointestinal tract and decreased endogenous glucose production account for the observed effects on blood glucose, while similar mechanism appear to be acting in the kidney as in the fasting state.

Conclusions:

This model allows us to explore which of the hypothesized mechanisms of action of GLP-1 RA may drive the effects observed in the kidney. With further model development, we aim to provide key insight into these mechanisms, how they may complement treatment with SGLT2 inhibitors and renin-angiotensin-aldosterone system inhibitors, and what the implications of GLP-1 RA treatment on long-term renal outcomes in populations with varying levels of renal function may be.



References:

1. Jauslin P, et al. (2011) JCP. doi:10.1177/0091270010362536.
2. Tham LS, et al. (2017) JCP. doi: 10.1002/jcpb.899. PubMed PMID: 28394405.
3. Røge RM, et al. (2015) CPT: PSP. doi: 10.1002/psp4.11.
4. Frank T. (2013) J Pharm Drug Deliv Res. doi: 10.4172/2325-9604.1000112.
5. Hallow KM, et al. (2018) AJP-RP. doi: 10.1152/ajpregnol.00202.2018.
6. Tonneijck L, et al. (2016) Diabetologia. doi: 10.1007/s00125-016-3938-z. PubMed PMID: PMC4901099.
7. Tonneijck L, et al. (2018) AJP-RP. doi: 10.1152/ajpregnol.00432.2018.
8. Tonneijck L, et al. (2017) Diab. Obes, & Met. doi: doi:10.1111/dom.12985.

TUE-051

Zero-Inflated Beta Regression Exposure-Response Modeling of the Eczema Area and Severity Index for Patients Taking Abrocitinib

Authors: Luke Fostvedt¹, Jessica Wojciechowski², Bimal K. Malhotra³, Xiaoxing Wang², Hernan Valdez³, Ricardo Rojo², Timothy Nicholas²

Institutions: ¹Pfizer Inc., Cambridge, MA, USA; ²Pfizer Inc., Groton, CT, USA; ³Pfizer Inc., New York, NY, USA

Objectives: Abrocitinib is a selective Janus kinase-1 inhibitor being developed for the treatment of moderate-to-severe atopic dermatitis (AD). The objective of this analysis was to develop a pharmacokinetic-pharmacodynamic model to describe the time-course of the eczema area and severity index (EASI), one of the two primary efficacy measures for the abrocitinib program.

Methods: EASI is a validated measure of disease severity for AD using values from 0 (no disease) to 72 (severe lesions affecting the entire body) in increments of 0.1. Data from three randomized, double-blinded trials (one phase 2 and two phase 3 trials) and a non-randomized, open-label, run-in portion of an additional phase 3 trial were pooled for modeling. As a bounded measure, with many patients at 0, a zero-inflated beta regression model was developed with the EASI scores transformed to the (0,1) domain (beta distribution parameterized with a mean and precision parameter).¹ The mean parameter was modeled using an indirect response model with a maximum stimulatory effect (S_{max}) on k_{out} . S_{max} was modeled as the summation of a drug effect, using an Emax parameterization with C_{avg} , and a placebo effect. The zero-inflated probability was modeled using a logit transformation with the current mean from the beta distribution used as a predictor with a “cutpoint” parameter, estimated by the model, at which point the probability of 0 is 0.5. The expected decrease in EASI scores and the percentages of subjects achieving 75% decrease from baseline (EASI75) at Week 12 (the co-primary endpoint in the phase 3 registrational trials) were predicted.

Results: Doses of 10 mg, 30 mg, 100 mg, and 200 mg once daily (QD) and placebo arms were included in the model development. The EC₅₀ was estimated to be 312 ng/mL. The C_{avg} exposures were 104 ng/mL and 246 ng/mL for 100 mg and 200 mg QD doses after 12 weeks of treatment in a typical patient (white, male, 30 years old, 80 kg, with a baseline EASI score of 26). The response was rapid with the time to half of the maximal effect of 15.5 and 11.5 days for the 100 mg and 200 mg QD doses, respectively. The expected percent change from baseline of the EASI score after 12 weeks of treatment was 62.2% and 73.3% for 100 mg and 200 mg doses in a typical patient, respectively, resulting in a high proportion of patients achieving an EASI75 response of 38.6% and 55.9%, respectively.

Conclusions: A zero-inflated beta regression exposure-response model was developed using abrocitinib C_{avg} to characterize the time course of the EASI scores and predict the EASI75 response at Week 12.

References: 1. Ospina R, Ferrari SLP. A general class of zero-or-one inflated beta regression models. *Computat Stat Data Anal.* 2012;56(6):1609-1623.

TUE-052

Dynamic PBPK for Pharmacology in Intensive Care Medicine

Author: Marco Albrecht (1), Stephan Schaller (1)

Institutions: (1) esqLABS GmbH

Objectives: Fluid therapy is a standard treatment at intensive care units (ICU). It has implications on the absorption, distribution, metabolism, and excretion (ADME) properties in critically ill patients, leading to inadequate treatment decisions at intensive care units (1). While current PBPK software has a good representation of the steady-state in physiology, useful for most use-cases in drug development and regulatory authorization, the dynamic nature of rapidly changing physiology in intensive care patients requires a likewise dynamic PBPK software to assess the pharmacology of drugs in intensive care. Consequently, a modeling and simulation (M&S) framework is developed to predict the effects of fluid resuscitation on molecule levels to inform drug therapy decisions at the ICU.

Methods: Parameters, relevant for the volume distribution, are automatically extracted from the individual base physiology, as determined by the open-source and freely available PBPK software platform PK-Sim and MoBi. The parameters are then updated by both occasionally generated lab data and continuously monitored vital values. The quantitative shift in physiology is estimated by established equations for whole-body volume kinetics (2), endothelial transport considering the endothelial glycocalyx layer (EGL) via the two-pore model (3-5), and a model representing volume shifts between four compartments representing erythrocyte, plasma, interstitial, and cell volume (6).

Results: The implemented R-model of fluid resuscitation has been validated on data occurring in the series of papers of Matthew B Wolf as well as from publications on volume therapy and lymph-flow (2,5,6). The impact of volume shifts on dexamethasone PK has been assessed and quantified to provide a prototype for further qualification studies.

Conclusions: A dynamic PBPK modeling framework is possible in information-rich ICU settings and necessary to correct for the most common physiological disrupters of drug levels. The PBPK framework will integrate data as they occur at the bedside, extrapolate treatment consequences, and visualize both physiological and pharmacological key states for risk assessment. In the regulatory authorization perspective, the proposed framework might also be used as a physiological ICU stress test for refined and physiologically relevant safety margins.

446/450 Word

References:

- [1] Owen, Emily J, Gibson, Gabrielle A. and Buckman, Sara A. *Surg. Infect.* (2018) Pharmacokinetics and Pharmacodynamics of Antimicrobials in Critically Ill Patients.
- [2] Hahn, Robert. *Anesthesiology* (2010) Volume Kinetics for Infusion Fluids
- [3] **Rippe, Bengt and Haraldsson, Börje.** *Physiol. Rev.* (1994) Transport of Macromolecules Across Microvascular Walls: The Two-Pore Theory.
- [4] Niederalt, Christoph, et al. *J Pharmacokinet Pharmacodyn* (2018) A generic whole-body physiologically based pharmacokinetic model for therapeutic proteins in PK-Sims.
- [5] **Levick, J. Rodney and Michel, C. Charles.** *Cardiovasc. Res.* (2010) Microvascular fluid exchange and the revised Starling principle.
- [6] Wolf, Matthew B. *Am. J. Physiol. Renal Physiol.* (2013) Whole-body acid-base and fluid-electrolyte balance: a mathematical model.

TUE-053

Model-based Meta-analysis of Progression free survival in Pancreatic cancer with reconstructed individual patient data; application to drug-development decision making.

Marion Bouillon-Pichault, Li Li, Alex Azrilevitch, David Yao, Akintunde Bello, Tarek Leil

¹BMS, Princeton NJ, USA.

Objectives: Second Line adenocarcinoma of the pancreas is one on the most aggressive cancers with patients surviving a median of 6 months without treatment. Progression-free survival (PFS) is a widely used endpoint to assess the potential efficacy of a new therapy for pancreatic cancer. The current standard of care treatments for advanced pancreatic cancer are based on several chemotherapy combinations and have been extensively described in the literature. However, there has not been a systematic assessment of the current therapeutic landscape. A modeling framework to evaluate the PFS of chemotherapy in advanced pancreatic cancer was developed; potential predictors were identified, and the efficacies of different treatment options were quantified.

Methods: A database of randomized and non-randomized clinical trials of chemotherapy in Pancreatic cancer published between 2000 and 2017 was used. Individual Patient Data (with events and censored) were reconstructed from digitized PFS curves from these trials using Guyot's et al. algorithm (1). Fully parametric time-to-event (TTE) models were developed to describe the drop-out and the PFS survival curves and used to run clinical trial simulations using Monolix Suite 2019.

Results: Data used in the analysis came from 97 trials (138 trial arms), representing over 13,000 reconstructed patients. This model demonstrated that median PFS increased in later trial years and decreased with line of therapy. The efficacy of different chemotherapy groups was quantified and ranked with mPFS and 6mo-PFS ranging from 27 weeks and 52% for Capecitabine-based combination chemotherapy to 22 weeks and 43% for 5-FU-based combination chemotherapy for 1st line population.

$\Delta mPFS$ and $\Delta 6\text{moPFS}$ were simulated for different clinical trial scenarios (different control arms, number of patients per arms and assumptions for the efficacy of investigational treatment arms), to quantify the clinical probability of success and the false negative/false positive risks for those trial designs.

Conclusions: A model based meta-analysis was performed to describe the drop out and PFS for chemotherapy in pancreatic cancer on more than 13,000 reconstructed patients providing a quantification of the chemotherapy landscape. This analysis was used internally to support decision-making for clinical development of assets in pancreatic cancer by quantifying the clinical probability of success vs. potential standards of care.

References:

- (1) Guyot P1, Ades AE, Ouwens MJ, Welton NJ., Enhanced secondary analysis of survival data: reconstructing the data from published Kaplan-Meier survival curves. BMC Med Res Methodol. 2012 Feb 1;12:9. doi: 10.1186/1471-2288-12-9.

TUE-054**A Quantitative Systems Pharmacology Modeling Framework for Evaluation of Cytokine Release Mediated by REGN1979/Cemiplimab Combination Therapies in Patients with B-cell Non-Hodgkin Lymphoma (B-NHL)**

Masood Khaksar Toroghi, Min Zhu, Feng Yang, Nidal Huniti, John D. Davis, A. Thomas DiCioccio
Regeneron Pharmaceuticals, Inc., Tarrytown, NY, USA

Objectives: REGN1979 is a human immunoglobulin G4-based bispecific antibody that binds to CD3⁺ T-cells and CD20⁺ B-cells, targeting CD20⁺ tumor cells via T-cell-mediated cytotoxicity. The engagement of CD3 on T-cells and CD20 on B-cells activates T-cells. During T-cell activation, inflammatory cytokines are secreted, which can result in significant but temporary increase in the circulating cytokine concentrations and may lead to a systemic inflammatory response; this is known as cytokine release syndrome. The objective of this work is to evaluate cytokine profiles, as represented by interleukin (IL)-6, under REGN1979 monotherapy and in combination with cemiplimab, an anti-programmed death (PD)-1 inhibitor blocking PD-1/PD-L1 interaction, in patients with B-NHL.

Methods: A quantitative systems pharmacology (QSP) model was developed integrating pharmacokinetics of REGN1979 and cemiplimab, dynamics of T-cells and B-cells, disease characteristics of NHL, and cytokine data from a REGN1979 monotherapy study (NCT02290951) and a REGN1979/cemiplimab combination study (NCT02651662). In the QSP model, mechanism of cytokine release was described as 1) the formation of trimolecular synapse when REGN1979 binds to both CD3 on T-cells and target CD20 on B-cells, and 2) regulation of T-cell activation by the PD-1 pathway. To describe cytokine profiles under the treatment of REGN1979/cemiplimab combination, we hypothesized that cemiplimab increased the stimulation of IL-6 production by activating more T-cells and reduced the inhibitory effect of the immune system to attenuate the cytokine release. Concentrations of IL-6, REGN1979, and cemiplimab from NHL patients under monotherapy and in combination, as well as *in vivo/in vitro* data (e.g. tumor growth rate, CD20/CD3 expression levels, T/B-cell baseline levels, and drug affinity data), were used to calibrate the model. For simulation, 300 virtual patients with aggressive NHL were created using a Monte Carlo sampling approach.

Results: The model-based simulations indicate that, under REGN1979 monotherapy, IL-6 concentrations mostly peaked on day 1 following an initial split dose of 1 mg in week 1. The cytokine concentrations reduced over time even with increased REGN1979 doses up to 10- and 100-fold in weeks 2 and 3, respectively. When REGN1979 and cemiplimab were dosed simultaneously on day 1 week 1, the mean peaks of IL-6 concentrations were higher than that of REGN1979 monotherapy due to the cemiplimab effect on PD-1/PD-L1 signaling pathway. The model predicts that, when delaying cemiplimab dose to a later time following dosing REGN1979 alone, reduced IL-6 release is expected, and the IL-6 levels would not be affected by cemiplimab dose levels from 3 to 350 mg.

Conclusions: The developed QSP model provides a learning opportunity to evaluate the cytokine profiles of REGN1979 and cemiplimab under different dosing sequences and dose levels, where REGN1979/cemiplimab combination is modulating both CD20/CD3 and PD-1/PD-L1 signaling pathways.

TUE-055

Development and evaluation of a predictive model of hyperphosphatemia induced by inhibition of FGFR by extending an existing multiscale systems pharmacology

Matthew M. Riggs¹, Howard A. Ball², Kanji Komatsu³, Akihiro Yamada³

¹ Metrum Research Group, Tariffville, CT USA; ² Ball Pharma Consulting, LLC, Hartland, WI USA; ³ Astellas Pharma Inc., Tokyo, Japan

Objectives: Fibroblast growth factor receptor (FGFR) inhibition has been investigated as a potential target for treating cancer. Hyperphosphatemia (HP) has been observed clinically following FGFR inhibition due to its role in regulating phosphate (P) balance through FGF23, which regulates urinary P excretion and indirectly impacts dietary P absorption and calcitriol (C) activation. An existing systems pharmacology model was leveraged to explore whether HP circumvention can be achieved via intermittent dosing and concomitant P binders following administration of ASP5878, an FGFR inhibitor investigated for treatment of solid tumors (NCT02038673).

Methods: A systems pharmacology model (Bone, 2010) was extended to describe changes in serum P, C, parathyroid hormone (PTH), and FGF23 following oral ASP5878 administration. The model evaluated concomitant P binder and impact of varied dosing regimens on exposure-related P changes. Analyses were conducted in R; simulation and estimation included mrgsolve and minqa. QD and BID ASP5878 dosing, total daily dose, and intermittent, 5 days on / 2 off, and 4 days on / 3 off, regimens were considered.

Results: ASP5878 PK followed a 1 compartment model (typical $t_{1/2} = 2.63\text{h}$). Added mathematical descriptions included: FGF23 control urinary P, PTH and C production, with feedback on FGF23 production from P and C. P binder was estimated to decrease its dietary bioavailability by up to 32%. The extended model described the time-course and magnitude of dose-related increases observed for P, C, FGF23 and PTH, including $P > 6 \text{ mg/dL}$ at doses $\geq 32 \text{ mg/day}$. P binder was predicted to mildly alleviate the increase at targeted doses. Efficacious response was not obtained by any simulated regimen that minimized to acceptable P.

Conclusions: Results from the extended systems model supported program termination.

References:

The results in this abstract were previously accepted though not presented at canceled ASCPT, Houston TX March 2021 (canceled) and published in the conference proceedings as abstract PWI-002.

TUE-057

Development of a Mechanistic Model of Keratinocyte Dynamics and Skin Barrier Function for Psoriasis Research

Authors: Michael Weis^{1,*}, Douglas Chung¹, Vincent Hurez¹, Rebecca Baillie¹, Katherine Kudrycki¹, Michael Reed¹

Affiliations: ¹ Rosa & Co. LLC, San Carlos, CA

Objectives: While no longer considered the predominant factor, keratinocytes (KCs) have a central role in the pathophysiology of psoriasis(1). KCs become activated in response to extrinsic or intrinsic factors, producing cytokines and chemokines that contribute to the inflammatory state in psoriasis. The psoriatic KCs undergo hyperproliferation, resulting in thickened skin; and their abnormal desquamation results in squamous scales on the skin and itching. Understanding KC behavior and response to interventions is critical to the development of new psoriasis therapies. We sought to develop a focused, mechanistic model of KC dynamics and their relation to skin barrier function, which could be integrated within larger quantitative systems pharmacology (QSP) models of inflammatory skin disorders such as psoriasis.

Methods: The model defines three distinct states of KCs representing the functional phenotypes observed in normal and psoriatic skin: basal proliferating KCs of the stratus basale; non-proliferative differentiating KCs of the spinous and granular layers; and cornified, terminally differentiated KCs of the cornified layer or corneocytes. Fluxes included proliferation and clearance of basal KCs, differentiation into suprabasal KCs, and final cornification into corneocytes. These rates are regulated by various pro- and anti-inflammatory cytokines.

Results: The model assumes that strong stimulation of differentiation and cornification worsens the overall quality of the resulting corneocytes and epidermal barrier function. To represent this, a calculation of corneocyte quality tracks the epidermal turnover rates. This quality metric influences the rate of corneocyte shedding, the degree of barrier function, and clinical outcomes such as the “scaliness” component of the common clinical outcome, the Psoriasis Area Severity Index (PASI). The increased turnover rates in psoriasis results in a lower corneocyte quality and reduced barrier function, further stimulating KC proliferation. The consequence of these effects is a net increase in the number of keratinocytes and corneocytes, but reduced quality, leading to thickened and scaling skin.

The model behavior was constrained using a variety of data types including: transepidermal water loss measured in healthy and psoriatic subjects; cell numbers; cell-type specific mediator production; mediator turnover; cell production, differentiation, cornification, and overall epidermal turnover rates in psoriasis vs. healthy subjects; the magnitude of effects of individual mediators on KC lifecycles; and the reversion to a quasi-homeostatic state following therapies.

Conclusions: A focused QSP model was developed to capture the behavior of KCs in response to anti- and pro-inflammatory mediators in healthy and psoriatic conditions. This model has been successfully integrated within several larger QSP models of psoriasis to facilitate evaluation of novel targets and standard of care therapies.

References:

1. Bata-Csörgő, Zsuzsanna, and Marta Szell. 2014. "The psoriatic keratinocytes." Expert Review of Dermatology 7 (5):473-481. doi: 10.1586/edm.12.48.

TUE-058

Implementation of the standard concentration - QTc study using MonolixSuite applications on the example of Dofetilide.

Monika Twarogowska¹, Géraldine Ayral¹, Pauline Traynard¹, Jonathan Chauvin¹

¹Lixoft, Antony, France,

Objectives: In 2015, the International Council for Harmonisation (ICH) E14 guidance agreed to use a model-based study of concentration-QT data as a primary analysis in the proarrhythmic risk assessment. Currently recommended guidelines follow the methodologies presented in the “Scientific white paper on concentration-QTc modelling” by Ch. Garnett et al.[1]. This work presents the implementation of the C-QT analysis in MonolixSuite following these recommendations. Results, obtained on data of a class III antiarrhythmic agent Dofetilide, show the modelling workflow and calculations of the standard criteria for a drug-induced QTc interval prolongation.

Methods:

- The dataset[2]: PK measurements and ECG recordings in a randomized, double-blind, 2-period crossover clinical trial; single dose of Dofetilide or placebo.
- Heart rate corrected QT (QTc) intervals were obtained with the Fridericia's formula (the standard adopted by the FDA). Derived baseline-adjusted QTc interval (ΔQTc) and baseline-adjusted placebo-corrected QTc interval ($\Delta\Delta QTc$) were used as model variables.
- The pre-specified linear mixed effect models, given in the FDA guidelines and in [1], depend on the concentration and include fixed effect parameters, influence of baseline, treatment and diurnal effects.
- Monolix was used to implement models and estimate the parameters.
- Risk assessment simulations - two-sided 90% confidence interval for $\Delta\Delta QTc$ - were performed in Simulx.

Results: Monolix was used to fit the Dofetilide PK data with a two-compartment model with a time delay for the absorption and the baseline-adjusted QTc with the pre-specified linear mixed effect model. A joint modelling approach, where both QTc and PK models parameters are estimated simultaneously, was compared with the FDA recommended approach, where the C-QTc model uses directly the observed time-matched PK data. Both methods yielded very close estimates. The estimated parameters and their standard errors were used to calculate the estimated mean QTc change from the baseline and the 90% confidence interval for a large range of Cmax concentrations. For Cmax concentrations above 0.5 ng/mL, the estimated mean QTc change from the baseline exceeded the 10 ms safety threshold. The advantage of the joint PK-QTc model is that the QT interval prolongation can be studied for different doses and designs (instead of different Cmax values). For instance, in case of a 125 mg q12h regimen, 88% of patients had the QT prolongation longer than 10 ms.

Conclusions: The presented work shows step-by-step how the FDA recommended workflow for C-QTc analysis can be implemented in Monolix. The procedure is generic and can be applied to other compounds in the same way.

References:

- [1] Garnett C. et al. Scientific white paper on concentration-QTc modeling. *J Pharmacokinet Pharmacodyn*. 2018 Jun; 45(3):383-397
- [2] Johannessen L. et al. Differentiating Drug-Induced Multichannel Block on the Electrocardiogram: Randomized Study of Dofetilide, Quinidine, Ranolazine, and Verapamil. *Clin Pharmacol Ther*. 2014 Nov; 96(5):549-58

TUE-059

A Bayesian Population Compartmental Absorption and Transit Modeling Approach to Support Generic Drug Development: Application to Bupropion Hydrochloride Oral Dosage Forms

Nan-Hung Hsieh¹, Frédéric Y. Bois², Eleftheria Tsakalozou³, Miyoung Yoon³, Brad Reisfeld⁴, Weihsueh A. Chiu¹

¹Department of Veterinary Integrative Biosciences, College of Veterinary Medicine and Biomedical Sciences, Texas A&M University, College Station, TX, USA

²Simcyp Division, Certara UK Limited, Sheffield, UK

³Division of Quantitative Methods and Modeling (DQMM), Office of Research and Standards (ORS), Office of Generic Drugs (OGD), Center for Drug Evaluation and Research (CDER), U.S. Food and Drug Administration (FDA), Silver Spring, MD, USA

⁴Chemical and Biological Engineering and School of Biomedical Engineering, Colorado State University, Fort Collins, CO, USA

Objectives: The study purpose was to develop and validate an open-source compartmental absorption and transit (openCAT) model and apply a Bayesian population modeling approach to support establishing dissolution specifications for oral dosage forms of bupropion hydrochloride.

Methods: The openCAT model included six gut segments (stomach, duodenum, jejunum, ileum, cecum, and colon) and the liver connected to a standard two-compartment model that empirically described systemic disposition and elimination. Prior information on model parameters for gut physiology, bupropion physicochemical properties and drug product properties were from literature. The release of bupropion hydrochloride from the immediate-, sustained- and extended-release oral dosage forms was described by a Weibull function. To conduct the Bayesian analysis, we used our previously developed global sensitivity analysis framework and determined influential parameters for the central compartment and the openCAT model¹. In-vitro dissolution data were used to assign priors to the in-vivo release properties of the three bupropion hydrochloride formulations. To identify the inter- and intra-individual variability, we used published bupropion datasets from healthy volunteers that included six plasma concentration-time profiles (2 dose levels for each of the three formulations) for each subject². One-third of subjects were used in model calibration, while the rest were used for external model validation. Markov Chain Monte Carlo samples from the joint posterior of the calibrated parameters were then used to simulate virtual crossover trials with multiple variant formulations. For the immediate-release formulation, C_{max} and AUC estimates from the virtual crossover studies for formulation variants were used to identify allowable variability in dissolution profiles in terms of a bioequivalence assessment (“safe space”). The study workflow is summarized on Figure 1.

Results: Parameters related to absorption (gut permeability, stomach transit time), distribution (distribution volume, intercompartmental rate constants and liver partition coefficient), elimination (clearance) and dissolution were chosen for calibration. The calibrated model was in good agreement with the in-vitro dissolution and in-vivo exposure data and was able to describe inter- and intra-individual variability². The identified dissolution “safe space” suggested that dissolution may be delayed by up to one and a half hour before impacting systemic exposure in a meaningful manner.

Conclusions: We demonstrated that a Bayesian population semi-physiological model can capture inter- and intra-individual variability observed following the administration of bupropion hydrochloride oral dosage forms, and thereby characterizes the underlying physiological and substance-specific parameters. The application of our population modeling framework provides a novel approach in supporting decision-making in generic drug product development.

References:

¹Hsieh NH et al., 2018. Applying a global sensitivity analysis workflow to improve the computational efficiencies in physiologically-based pharmacokinetic modeling. *Front Pharmacol.* 9:588.

²Connarn JN et al., 2017. Pharmacokinetics and pharmacogenomics of bupropion in three different formulations with different release kinetics in healthy human volunteers. *AAPS J.* 19(5):1513-1522.

Acknowledgements:

Funding for this work was made possible, in part, by the U.S Food and Drug Administration through Grant 1U01FD005838. Views expressed in written materials or publications do not necessarily reflect the official policies of the Department of Health and Human Services; nor does any mention of trade names, commercial practices, or organization imply endorsement by the United States Government.

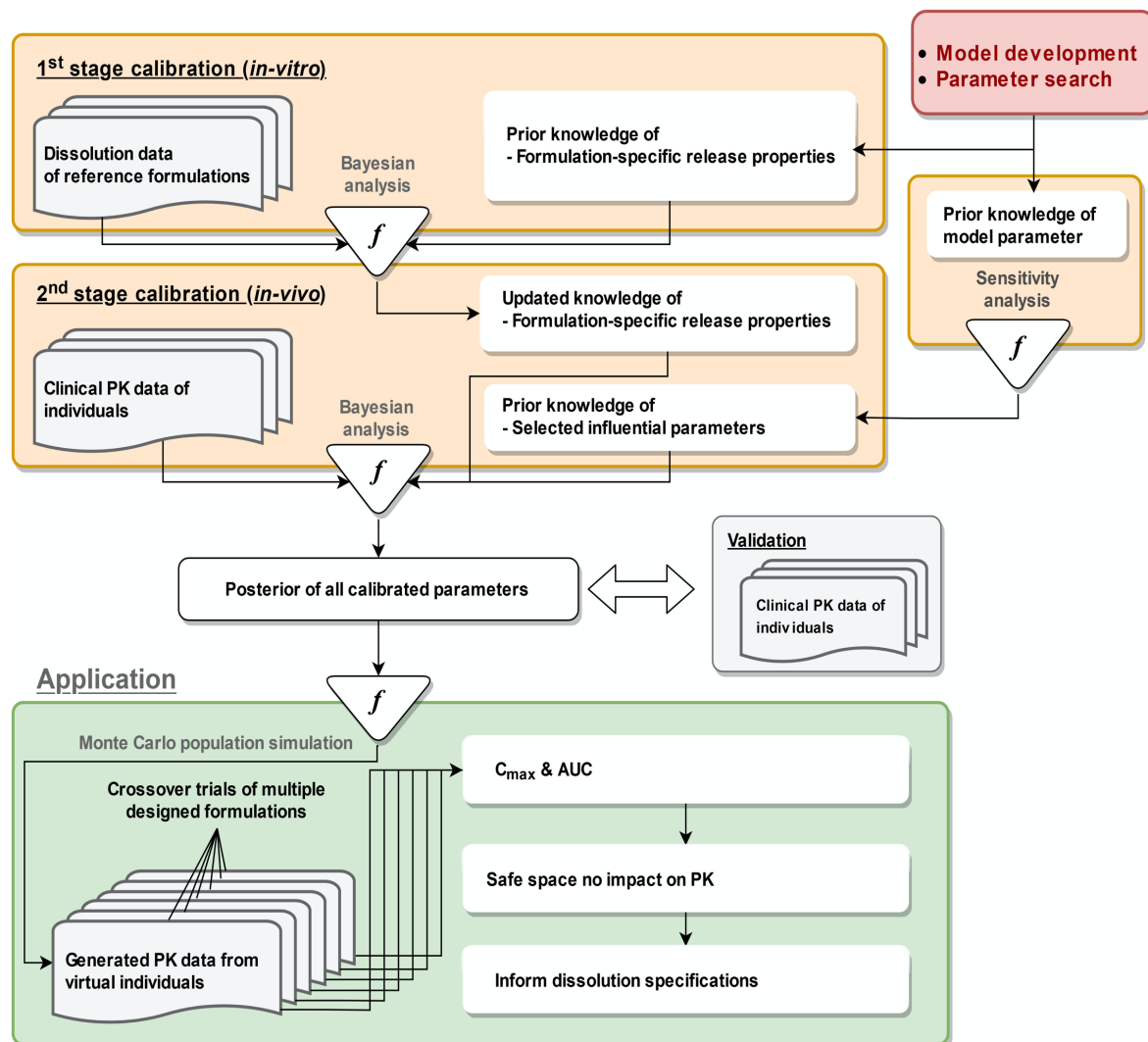


Figure 1. Schematic diagram of the overall study workflow.

TUE-060

Glofitamab, a T-cell-engaging Bispecific Antibody, in Relapsed or Refractory B-cell Non-Hodgkin Lymphoma: Population Pharmacokinetics and Exposure-response Analyses to Inform Optimal Biologic Dose Selection

Nassim Djebli¹, David Carlile², Felix Jamnion¹, Johann Laurent¹, Francois Mercier¹, Nicole A Kratochwil¹, Ann-Marie E Bröske³, Natalie Dimier², Cristiano Ferlini¹, Tom Moore¹, Martin Weisser³, Alexander Phipps², Nicolas Frey¹, Peter N Morcos⁴

¹Roche Innovation Center Basel, Roche Pharma Research and Early Development, Basel, Switzerland,

²Roche Products Ltd, Welwyn Garden City, United Kingdom, ³Roche Innovation Center Munich, Roche Pharma Research and Early Development, Penzberg, Germany, ⁴Roche Innovation Center New York, Roche Pharma Research and Early Development, New York, NY, USA

Category: General pharmacometrics

Objectives: Glofitamab (RG6026) is a novel T-cell-engaging bispecific antibody with a ‘2:1’ molecular format, comprising two binding regions for CD20 (on B cells) and one binding region for CD3 (on T cells). In NP30179 (NCT03075696), an ongoing Phase I dose-escalation study in relapsed/refractory (R/R) non-Hodgkin lymphoma (NHL) patients, glofitamab has shown promising activity and manageable safety.¹ Glofitamab population pharmacokinetics (PopPK) and exposure-response (E-R) relationships for efficacy/safety were investigated.

Methods: Indolent (i) and aggressive (a) R/R NHL patients received 1000mg obinutuzumab (G) as pre-treatment 7 days prior to first glofitamab administration on Cycle 1 to mitigate for cytokine release syndrome (CRS). Patients then received glofitamab 0.005–25mg Q2W or Q3W. A PopPK model was developed in NONMEM v7.4 using serial and spare PK data. To estimate glofitamab-receptor occupancy (RO%) in the presence of G concentrations competing for CD20 receptors over time, full G concentration-time profiles were constructed using the G PopPK model.² Using logistic regression, E-R relationships were investigated between glofitamab time-averaged RO% (AvgRO%) up to C3D1 and complete response rates (CRR – Lugano criteria³) in aNHL patients who reached C3D1; and between glofitamab AvgRO% over the first 24hours (majority of events occurred within 24hours of first glofitamab administration) and CRS (ASTCT criteria⁴) in iNHL and aNHL patients combined.

Results: As of December 18, 2019, PopPK were analyzed in 165 iNHL and aNHL patients with ≥ 1 PK sample. E-R relationships were analyzed in 87 aNHL patients with PK/efficacy data at C3D1, and in 139 iNHL and aNHL patients with PK/safety data. Glofitamab PK were best described using a two-compartment PK model with linear clearance and were comparable in patients with iNHL and aNHL. The effect of body weight on volumes and clearances was retained. Positive E-R relationships were observed between AvgRO% up to C3D1 and efficacy in aNHL patients ($p < 0.001$; Figure 1A), and between AvgRO% over the first 24 hours and Grade ≥ 2 CRS ($p < 0.001$; Figure 1B). Based on the exposure-response models, with an initial 10mg glofitamab dose at C1 (16mg thereafter), a CRR of 46.7% (41.5–58.1%), and a Grade ≥ 2 CRS rate of 32.6% (29.0–37.7%) were predicted. Step-up dosing starting at 2.5mg (followed by higher doses) might improve the benefit/risk profile of glofitamab. It would result in AvgRO% in the first 24hours of 0.160% (0.100%–0.290%), corresponding to a Gr ≥ 2 CRS rate of 22.1% (19.2%–26.3%).

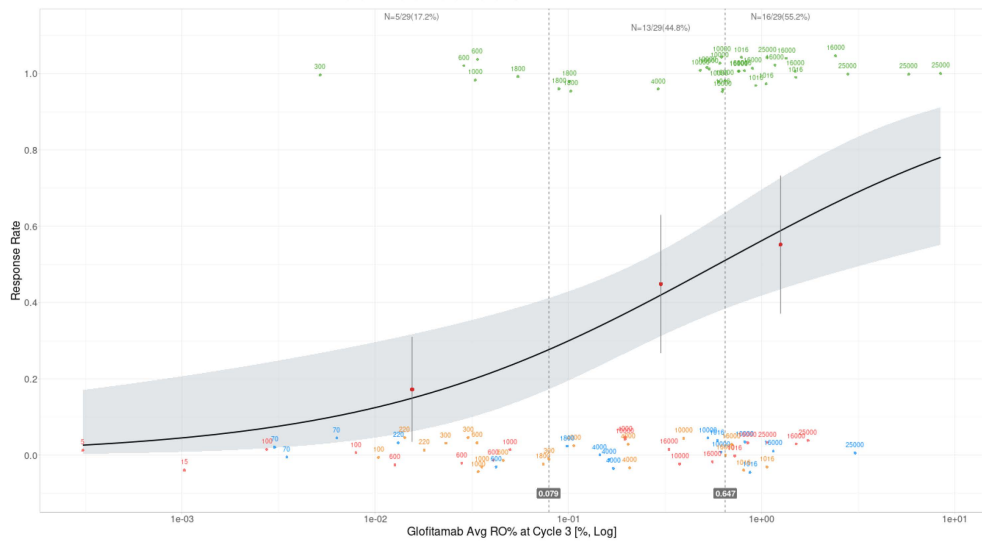
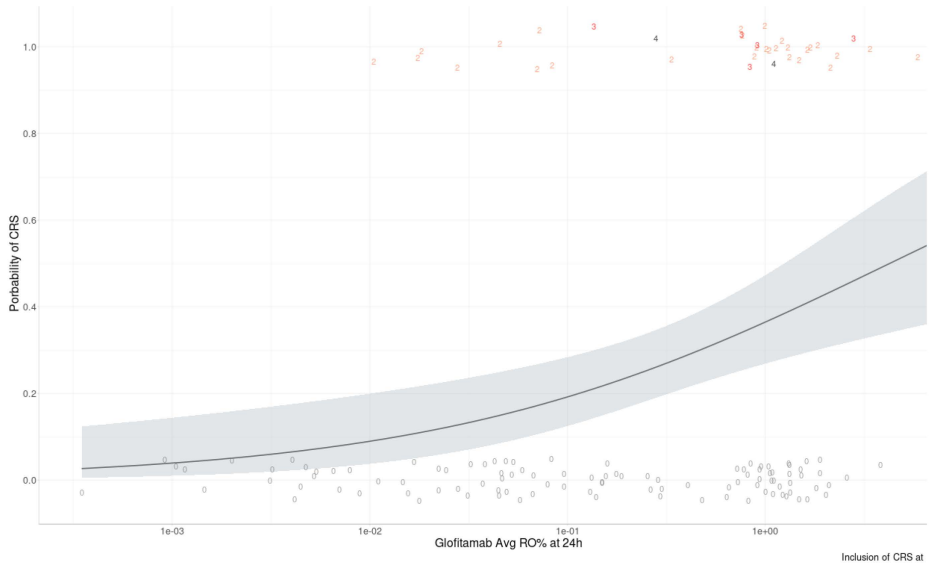
Conclusions: We characterized glofitamab PopPK and E-R relationships for efficacy/safety. These models are being used to identify optimal glofitamab dosing that maximizes efficacy and minimizes CRS risk.

References

1. Dickinson et al. Hematol Oncol 2019;37(S2):92–3.
2. Gibiansky et al. CPT Pharmacometrics Syst Pharmacol 2014;3:e144.
3. Cheson et al. J Clin Oncol 2014;32(27):3059–68.
4. Lee et al. Biol Blood Marrow Transplant 2019;25(4):625–38.

Acknowledgments: NP30179 is sponsored by F. Hoffmann-La Roche Ltd. Third party medical writing assistance, under the direction of Nassim Djebli, was provided by Stephanie Lacey and Khalida Rizi of Gardiner-Caldwell Communications and was funded by F. Hoffmann-La Roche Ltd.

Figure. Exposure-response analysis for: (A) the relationship between the probability of complete response versus glofitamab AvgRO% up to Cycle 3 in aNHL patients (N=87), and (B) the relationship between the probability of occurrence of Grade ≥ 2 CRS (ASTCT criteria⁴) versus glofitamab AvgRO% over the first 24 hrs in aNHL and iNHL patients (N=139). Q1–Q3 for AvgRO% up to Cycle 3 is 0.079%–0.647%. Dots in graph A illustrate the observed individual patient response coloured by achieved response. The proportion of responders (red circles) in panel A and associated 95% CIs (grey vertical solid lines) are provided in each tertile of AvgRO% (vertical dashed lines). Numbers in panel B illustrate the observed individual patient CRS event and associated grade. Black line=logistic regression; grey shaded regions=95% CI for the logistic regression. P-values are obtained from the Chi-squared test using ANOVA function of R, comparing the model to the null model. AIC, Akaike information criterion; aNHL, aggressive non-Hodgkin lymphoma; AvgRO%, time-averaged receptor occupancy; CI, confidence interval; CR, complete response; CRS, cytokine release syndrome; PD, progressive disease; PET CT, positron emission tomography – computed tomography; PR, partial response; SD, stable disease.

A**B**

TUE-061**A Single Platform that Accommodates the Ever Expanding Pharmacometrics Toolkit – Challenging But Achievable**

Navin Goyal¹, Lorenzo Ridolfi², Kevin McConnell³, Ronish Desai³, Sachin Sanduja³ and Stefano Zamuner²

¹ CPMS, GlaxoSmithKline USA, ² CPMS, GlaxoSmithKline UK, ³ Rudraya Corporation, USA

Objective: The current pharmacometric (PMx) toolkit has significantly expanded in recent years and continues to do so. The existing tools are not necessarily being replaced by the emerging technologies but are rather complemented in some cases. Based on the question that needs to be addressed, a user may want to employ several tools within a single analysis thereby harness advantages of individual tools rather than being limited to a single tool. Therein lies the necessity to have an infrastructure that allows utilizing multiple tools in a single environment while ensuring any regulatory requirements around validation and compliance. Additionally, the setup should allow elastic capacity, parallelization and grid support (e.g. slurm). Lastly, it has become increasingly critical to engage stakeholders i.e. non-PMx matrix team members and interact with the analyses in real time without getting deeply involved in model related technical details (e.g. RSHINY).

Methods: A list of must have software tools along with predefined constraints and variables (e.g. scalability, system flexibility and future proofing) was utilized as a starting point to develop the computational platform. A cloud-based solution that met most of the requirements was implemented. Newer tools and capabilities were introduced within the platform to allow their use within a single analysis.

Results: A customized enterprise platform hosted in the Amazon Web Services in a validated and encrypted environment was developed. The initial system included several open source and proprietary software tools such as PsN®, R, RStudio®, NONMEM®, Pirana® and PHOENIX®. Newer tools can be easily added on the Linux and Windows server system embedded within the system architecture. The system easily allows the user to run an analysis that calls several of the software tools while utilizing the grid capacity efficiently. Additional tools and capabilities are being continuously added to the system. The SONIC Visualize feature (under evaluation) allows users to load models wherein the user can create and share interactive and computationally intensive front ends (e.g. RSHINY) with non-PMx matrix team thereby leading to increased interactions with respect to analysis outcome. The system separates the model related technical details from the stakeholders while utilizing the platform capacity and capability behind the scenes.

Conclusions: Updating any PMx toolkit with emerging tools can often present challenges regarding integration of such tools and their use in tandem with existing tools. Adequate planning and domain expertise should allow setting up a custom cloud-hosted platform that integrates multiple tools commonly used by our discipline. We present such a system and share learnings with the community to implement such a comprehensive, high computing capacity and cost-effective platform solution.

Reference: Cloud-Based Computation Platform for Pharmacometrics – Challenges in Developing and Implementing an Integrated Solution, Navin Goyal, Des Buke, Lorenzo Ridolfi and Stefano Zamuner, Journal of Pharmacokinetics and Pharmacodynamics; 2018, 45

TUE-062

A library of tumor growth and tumor growth inhibition models for the MonolixSuite

Authors : Pauline Traynard (1), Geraldine Ayral (1), Monika Twaragowska (1)

Institution: (1) Lixoft, Antony, France

Objectives:

A wide range of ordinary differential equations (ODEs) models for tumour growth (TG) and tumour growth inhibition (TGI) is available in the literature and correspond to different hypotheses on the tumor or treatment dynamics. In the absence of detailed biological knowledge, selecting the most appropriate model is a challenge. Here, we present a modular TG/TGI model library that combines sets of frequently used basic models and possible additional features. This library permits to easily test and combine different hypotheses for the tumor growth kinetics and effect of a treatment, allowing to fit a large variety of tumor size data.

The use of the library is illustrated with the modeling of a published experimental dataset comparing different schedulings of bevacizumab and pemetrexed/cisplatin in non-small lung cancer xenografts in mice [1].

Methods:

The developed library allows to select:

- a basic tumor growth model,
- the use of the initial tumor size as a parameter to estimate or a regressor to read from the data set,
- additional features of angiogenesis or immune dynamics to combine to the basic tumor growth,
- the type of drug exposure to be considered for the treatment effect if any, such as a constant treatment or a standard PK model,
- the log-kill or Norton-Simon hypothesis for the treatment effect and its dynamics.

The flexible selection workflow allows to combine all the choices above, leading to a wide variety of models. In addition, the library includes a list of full pre-defined TGI models corresponding to common models used in the field. It is documented with figures and guidelines to help the selection of an appropriate model based on the characteristics of the data.

The library has been used to easily test different hypotheses and find the appropriate model for tumor growth and treatment effect for the non-small lung cancer cancer dataset with a stepwise approach.

Results:

First different growth models were compared on the control group and the Simeoni model was found to give the best fit. The effect of the chemotherapy was then considered and accounted for the modelling of pemetrexed and cisplatin's PK with parameters from the literature. The best model combined a log-kill linear effect with a delay induced by signal transduction. Further modification of the model allowed to include the increase in the drug's delivery brought by bevacizumab and implemented in [1].

The final model shows a good predictive power for each treatment group. Simulations of the model allow to test different schedules of treatment combinations.

Conclusions:

The MonolixSuite and the new TG/TGI library allow an efficient modeling and diagnosis of tumor size data.

References:

- [1] Schneider, B. K., et al. (2019). *CPT Pharmacometrics Syst Pharmacol*, 8: 577–586.

TUE-063

A minimal brain PBPK model to support the preclinical development of antibody therapeutics for neurological diseases.

Authors: Peter Bloomingdale^{1*}, Suruchi Bakshi^{2*}, Cesar Pichardo², Christian Maass², Eline van Maanen², Piet van der Graaf², Nitin Mehrotra¹

Affiliations: (1) Merck & Co. Inc, Kenilworth, New Jersey, US; (2) Certara UK Ltd.

* Authors have contributed equally to the work

Objectives: There are several antibody therapeutics in preclinical and clinical development, industry-wide, for the treatment of neurological diseases. Our goal was to develop a minimal physiologically-based pharmacokinetic model (PBPK) to enhance the quantitative understanding of antibody exposure in the brain of preclinical animal species and humans. Here we have reduced a full PBPK model to a minimal model with the goal of retaining physiological detail of the brain compartments without appreciably affecting model predictability.

Methods: An existing multi-species platform brain PBPK model¹ was reduced to a minimal PBPK model. All non-brain compartments were combined into a single tissue compartment. Fourteen tissue reflection coefficients were reduced to a single tissue-weighted value ($\sigma_{\text{Tissue}} = 0.92$). Brain reflection coefficients remain the same as in the full model. Tissue vasculature, endosomal, and interstitial volumes, besides brain, were combined into single parameter values for the tissue compartment. Tissue plasma flow was set to the difference between total cardiac output and brain plasma flow. The four cerebral spinal fluid compartments were combined into one. A local sensitivity analysis was performed on the full and minimal PBPK models. Percent error in the AUC between the full and minimal PBPK model predictions were determined for 1, 10, and 100 mg/kg IV doses in rats, monkey, and human.

Results: The minimal brain PBPK model contains 16 differential equations, compared to 100 in the full PBPK model. The run time for the reduced model was approximately 15 times faster. Brain reflection coefficients were identified as the most sensitive parameters on antibody exposure in the brain. The rank order, from most to least, of sensitive parameters were conserved between the original and reduced model. The percent error in predicted AUC between the full and minimal model was <2% for serum, 1-2% for ISF, and between -15% to 2% for CSF.

Conclusion: The minimal brain PBPK model retained detailed physiological processes of the brain while not significantly affecting model predictability. The minimal model can be expanded to include target information for evaluating target engagement to inform clinical dose selection and more easily implemented for population analysis.

References:

- 1 Chang, H.-Y., Wu, S., Meno-Tetang, G. & Shah, D. K. A translational platform PBPK model for antibody disposition in the brain. *Journal of pharmacokinetics and pharmacodynamics* **46**, 319-338 (2019).

TUE-064

Population PK of Rozibafusp alfa, a Bispecific IgG2 Peptide Antibody Conjugate Targeting T-cell and B-cell activity, Following SC Administration in Healthy Subjects and Rheumatoid Arthritis Patients

Po-Wei Chen¹, Lubna Abuqayyas², Sandeep Dutta¹, Brett Houk¹, Sameer Doshi¹

Amgen Inc. ¹Thousand Oaks. CA, ²Cambridge, MA

Objectives

Rozibafusp alfa is a bispecific IgG2 peptide antibody conjugate targeting both T-Cell and B-cell activity via neutralization of B-cell activating factor (BAFF) and inducible T-cell co-stimulator ligand (ICOSL) and currently in development for systemic lupus erythematosus (SLE). The objective of this analysis was to characterize the pharmacokinetics (PK) of rozibafusp alfa, including impact of target binding, after subcutaneous (SC) administration in healthy subjects (HS) and rheumatoid arthritis (RA) patients, and to develop a population PK model to guide future clinical development of rozibafusp alfa in SLE and other autoimmune diseases.

Methods

Rozibafusp alfa PK was characterized using data obtained from three Phase 1 studies (n= 80) after single or multiple (every 2 week) SC doses of rozibafusp alfa in HS (n= 54) or RA (n=26) patients (NCT02618967, NCT03156023). Serum concentrations of rozibafusp alfa were analyzed using first order conditional estimation with interaction in NONMEM® version 7.4.1 (ICON, Ellicott City, MD). Different structural PK models such as a two compartment population PK models with linear or nonlinear absorption and parallel linear plus nonlinear clearance including a target-mediated drug disposition (TMDD) model for a soluble target (BAFF) and a membrane bound target (ICOSL) (Gibiansky and Gibiansky 2010) were explored in parallel. Goodness of fit (GOF) and visual predictive checks (VPCs) were performed to compare structural models. Covariate analysis evaluated the effect of body weight, sex, race, disease, and immunogenicity on PK model parameters. Final PK model selection was based on improvement in objective function value using likelihood ratio test and diagnostics.

Results

Rozibafusp alfa PK after single or multiple SC doses was best described by a two-compartment popPK model with linear plus nonlinear (Michaelis Menten, or MM) eliminations based on GOF and VPCs. The model was superior to other model estimations, as nonlinear clearance mechanisms best described the greater than dose-proportional increases in exposure. The majority of conditional weighted residuals were between -4 to 4; normalized prediction distribution errors were within -3 to 3. Apparent linear clearance was 0.4 L/day and apparent volume of distribution was 4.5 L. No statistically significant difference in PK parameters was identified between HS and RA patients. Body weight was identified as the only significant covariate for linear clearance, volume and Vmax of MM clearance; no other covariates were identified as significant.

Conclusions

A population PK model of rozibafusp alfa in HS and RA patients was successfully developed. The semi-mechanistic nature of the model incorporates target related information and may be used to guide future dose selection for clinical development in SLE or other autoimmune diseases.

References

L. Gibiansky and E. Gibiansky. J Pharmacokinet Pharmacodyn (2010) 37:323-346.

TUE-065

A Multivariate Joint Model for Predicting Risk of End-Stage Renal Disease in Polycystic Kidney Disease

Authors: Rhoda Muse¹, Klaus Romero¹, Bob Stafford¹, Jane Larkindale¹, Jackson Burton¹

Affiliations: Critical Path Institute, Tucson, AZ;

Objectives

Autosomal Dominant Polycystic Kidney Disease (ADPKD) is a rare disease that results in kidney failure, currently with only one approved treatment that slows the progression to End Stage Renal Disease (ESRD). The objective of this work is to develop a bivariate joint model to predict individualized trajectories of time to ESRD using the simultaneous dynamic changes in mean Total Kidney Volume (TKV) and estimated Glomerular Filtration Rate (eGFR). To enable the effective development of treatments for ADPKD, understanding the progression of the disease as it relates to the timing of ESRD is critical for optimizing the design of clinical trials. The use the annual rate of change of eGFR, and changes in mean TKV as indicators of ADPKD progression have not been previously assessed simultaneously.

Methods

Patient level data from 5 registries was previously standardized, curated, and integrated. A subset of data was extracted comprising 587 individuals with 2392 longitudinal measurements for TKV, eGFR, and corresponding timing of diagnosis of ESRD or right-censored times. The longitudinal markers were best modeled using linear mixed effects, and the survival subcomponent was modelled using a Weibull baseline hazard. Covariates included were age at baseline, sex, race, baseline chronic kidney status and body mass index. Other covariates including PKD phenotype, anemia, hypertension, cholesterol levels, use of pain medication and smoking history were not tested due to missing information. The analysis was conducted using the Bayesian ‘rstarnarm’ package in R.

Results

Results showing factors associated with the risk of ESRD are presented in Table 1. Predicted TKV and rate of eGFR decline increased the risk of ESRD with log odds ratios of 1.0352 and 1.6903 respectively. The standard deviations of the intercepts and slopes show evidence of subject specific trends and baseline values (shrinkages for random intercept and slope respectively were 1.79%, 20.59% for TKV and 14.6%, 16.78% for eGFR). The correlations between the random slope and intercept in TKV and eGFR equations were significant. The cross-equation correlation between eGFR and TKV was due to significant correlation between the TKV intercept and the eGFR slope and intercept, hence the need for the multivariate model.

Conclusions

Modelling the eGFR and TKV jointly reduces bias in their effects on time to ESRD and quantifying the joint effects of these clinically relevant biomarkers helps to predict time to ESRD more accurately compared to the markers individually. The model developed, which allows for the prediction of individualized trajectories accounting for inter-subject variability, is intended to serve as the basis for a clinical trial simulation tool to help optimize efficacy studies for ADPKD.

Table 1. Weibull PH joint model results of end stage renal disease with eGFR and TKV as longitudinal markers

VARIABLE	POSTERIOR MEAN	STANDARD DEVIATION	95% CREDIBLE INTERVAL
STAGE3A	2.3041	0.5742	(1.2593, 3.489)
> STAGE 3A	6.0992	1.0708	(4.2737, 8.419)
BASELINE BMI	0.0771	0.0406	(-0.0021, 0.1576)
BASELINE AGE	0.0859	0.0307	(0.0317, 0.1551)
TKV: PREDICTED MEAN	1.0352	0.4041	(0.2749, 1.87)
EGFR: PREDICTED DECLINE	1.6903	0.3661	(1.0897, 2.5403)
RANDOM EFFECTS SD AND CORRELATIONS (COR)			
<u>TKV EQUATION</u>			
INTERCEPT	0.645	0.0199	(0.6065, 0.6867)
SLOPE	0.0422	0.0199	(0.0387, 0.0459)
COR	-0.1327	0.0585	(-0.2433, -0.0178)
<u>EGFR EQUATION</u>			
INTERCEPT	0.0547	0.0024	(0.0501, 0.0594)
SLOPE	0.01	0.0006	(0.0089, 0.0112)
COR	0.319	0.0739	(0.1726, 0.4653)
<u>CROSS EQUATION COR</u>			
TKV INT & EGFR INTERCEPT	-0.2448	0.051	(-0.3413, -0.1457)
TKV INTERCEPT & EGFR	-0.5767	0.0478	(-0.6666, -0.4771)
SLOPE			
TKV SLOPE & EGFR	-0.0221	0.07	(-0.1580, 0.1170)
INTERCEPT			
TKV SLOPE & EGFR SLOPE	-0.1272	0.0702	(-0.2584, 0.0180)

TUE-066

An *in silico* model of avadomide-induced neutropenia enables virtual clinical dose and schedule finding studies

Authors:

Roberto A. Abbiati¹, Michael Pourdehnad², Daniel W. Pierce², Shailaja Kasibhatla³, Mark McConnell⁴, Soraya Carrancio³, Alexander V. Ratushny⁴, Cristina C. Santini¹

Institutions:

¹Bristol Myers Squibb, Celgene Institute for Translational Research Europe, Seville, Spain

²Bristol Myers Squibb, San Francisco (CA), USA

³Bristol Myers Squibb, San Diego (CA), USA

⁴Bristol Myers Squibb, Seattle (WA), USA

Objectives:

Neutropenia is the most common adverse event experienced by clinical trial patients treated with avadomide, a modulator of the E3 ubiquitin ligase complex and a potent antitumor and immunomodulatory agent. Preclinical data from an *in vitro* assay of neutrophil differentiation has previously supported the introduction of an intermittent 5/7-day schedule which improved tolerability reducing frequency and severity of neutropenia (1-3). In this context, mathematical models are a convenient tool to explore schedules that maximize efficacy and minimize toxicity. Published models (4) of drug-induced neutropenia focus on chemotherapy and are inappropriate for avadomide given the different mechanism of neutropenia. Avadomide leads to cereblon-mediated degradation of the hematopoietic transcription factor Ikaros, leading to myeloid maturation arrest at a promyelocyte stage (3). Based on this understanding, we developed a mathematical model for avadomide-induced clinical neutropenia to enable exploration of dosing schedules for avadomide as monotherapy or in combination.

Methods:

The mathematical model has three components: (i) neutrophil life-cycle, (ii) avadomide pharmacokinetics (PK), and (iii) pharmacodynamics (PD). The neutrophil life-cycle component captures maturation stages of neutrophil within bone marrow, controlled cell retention/egress to systemic circulation, and cell death under both homeostatic and perturbed conditions. The PK/PD components determine avadomide concentration-dependent perturbations of neutrophil homeostasis. The model is determined by a system of ordinary differential equations and is informed by expert knowledge, literature, *in vitro* and clinical trial data (1-5). The model nominal parameter set for the homeostatic condition is based on literature data. Disease-specific models are obtained by fitting relevant parameters from the nominal set to the absolute neutrophil count (ANC)-time profiles for avadomide-induced neutropenia in glioblastoma (GBM) and Diffuse Large B-cell Lymphoma (DLBCL) patients. Parameter value distributions were generated by fitting disease-specific models to individual patients from actual GBM or DLBCL cohorts. Virtual patient cohorts were created by random sampling from these distributions.

Results:

The model was successfully fit to clinical data and quantitatively captured key characteristics of ANC-time profiles: (i) delayed ANC drop following avadomide administration, (ii) dose- and schedule-dependent changes of ANC-time profile patterns, (iii) ANC recovery following treatment interruption, and (iv) disease specific (GBM vs DLBCL) differences in neutrophil dynamics in blood. The model was validated by applying a Kolmogorov-Smirnov test to confirm that model-generated ANC-time profiles and validation clinical dataset belong to the same continuous distribution.

Conclusions:

We developed an *in silico* model of avadomide-induced neutropenia. The model was calibrated and validated on clinical data and applied to simulate a virtual patient cohort to explore avadomide dose/schedule regimens that minimize neutropenia.

References:

- [1] Chiu et al., Br J Haematol. 2019_Feb_14.
- [2] Santini et al., ISCB Comm. J:132(poster)_2019.
- [3] Carpio et al., Blood. 2020_Jan_23.
- [4] Friberg et al., J Clin Oncol. 2002_Dec_15.
- [5] Carpio et al., ASH abstract#1494. 2015.

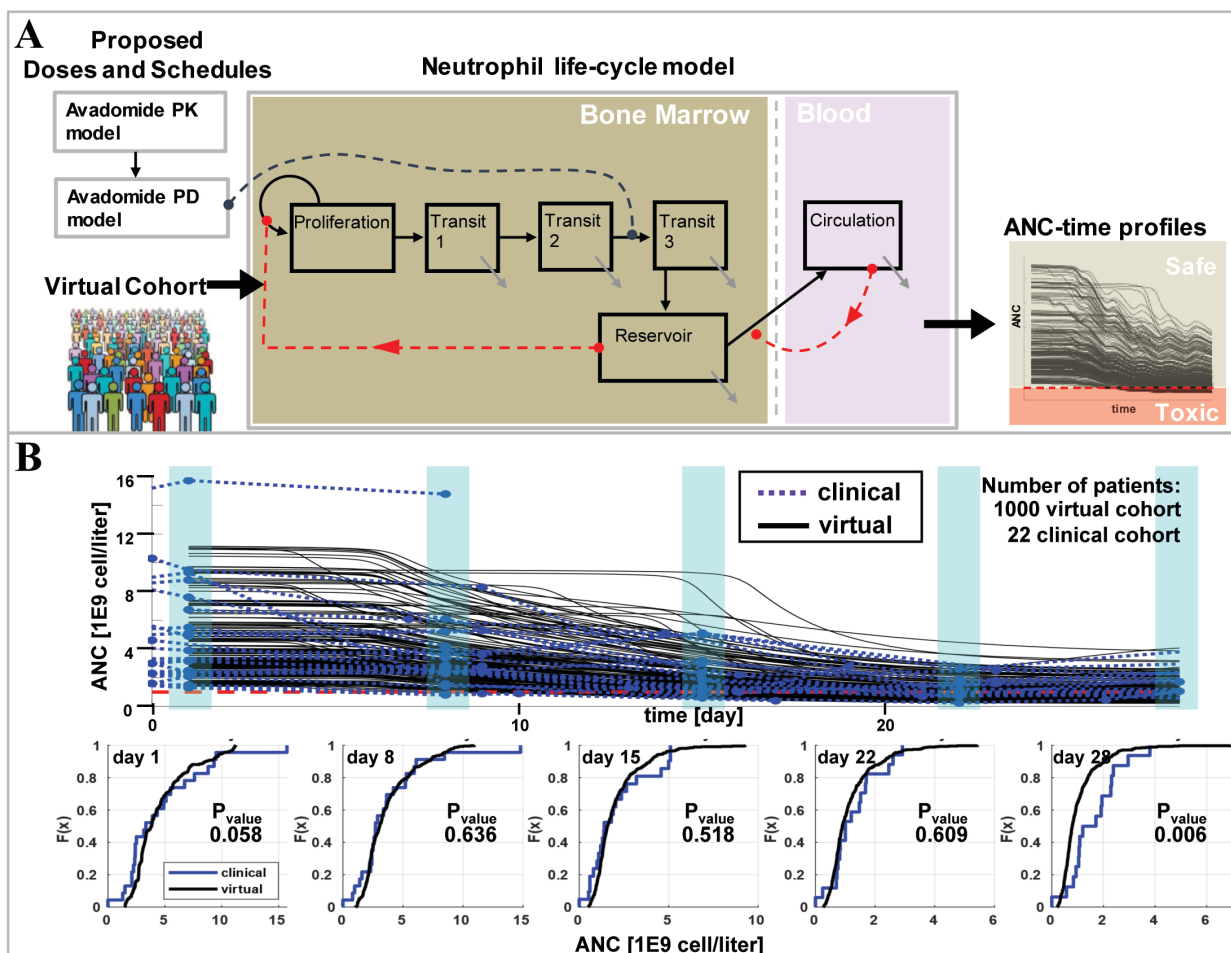


Figure 1. (A) Simulation framework: Model is simulated for cohorts of virtual patients and generates predictions of neutrophils dynamics. Results are post-processed for exploration of optimal schedules. **(B) Results for model validation:** Longitudinal ANC-time profiles (clinical cohort: dotted-blue, virtual cohort: solid-black) for avadomide, 4mg, QD for 28 days, in Non-Hodgkin's lymphoma patients. Two-sample Kolmogorov-Smirnov test compares clinical and virtual cohort confirming equivalence for 4 of 5 tested times (test significance 5%).

TUE-067

Exact solutions for the rapid expansion of blasting T cell populations

Authors: Ronny Straube & Brian J. Schmidt

Affiliation: Quantitative Clinical Pharmacology, Bristol Myers Squibb, Princeton, NJ, USA

Objectives: When lymphocytes encounter their cognate antigen in the thymus they become activated and undergo a finite number of cell divisions before they differentiate into memory or effector cells. We have previously proposed an age-structured model [1] together with preliminary solutions and fits to experimental data. Here, we provide new, time-dependent solutions for the case that the lymphocytes are activated from a pool of naïve cells undergoing a rapid expansion and subsequent contraction phase. We show that our model can describe T cell expansions for a wide range of input stimuli [2].

Methods: To describe the finite number of cell divisions of blasting lymphocytes we assume that their differentiation rate increases with the number of undergone divisions while their proliferation and death rate remains constant. As a result, we obtain an infinite dimensional (age-structured) system of ODEs which can be mapped to a partial differential equation for a generating function. The latter equation is solved for a linearly increasing differentiation function and different choices for the activation rate function.

Results: If the activation process is not explicitly modeled the total cell number can be described by a double exponential function. In the more realistic scenario, when T cell activation occurs from a pool of naïve (resting) cells, the total cell number can be expressed in terms of Γ -functions. Both solutions compare well with cell expansion experiments where mouse CD8 T cells were stimulated either with different levels of IL-2 or combinations of input stimuli [2]. The fits of our model to the data suggest that the initial propensity to differentiate into an effector cell decreases with increasing stimulus which is consistent with previous findings that the division destiny of a cell is set by the strength of the input signal [3]. Finally, we derive a solution for a constant (quasi-stationary) T cell activation rate which might be useful to parametrize QSP models.

Conclusions: Our model provides explicit time-dependent solutions for the rapid expansion and subsequent contraction phase observed in blasting T cell populations. These expressions can be used to extract rate constants for activation, proliferation, differentiation and apoptosis from *in vitro* proliferation assays using labeled lymphocytes. The theoretically rigorous lymphocyte proliferation model proposed here may give rise to new QSP model sensitivities and better predictive behavior than less rigorous approaches. We envision potential applicability for a variety of QSP models with an adaptive immune response component, including systems models of type 1 diabetes, immunogenicity, and immuno-oncology.

References:

[1] Straube R, Schmidt BJ, Thalhauser CJ. An age-structured model for blasting T cell populations. Poster presentation, ACoP 10, Orlando (FL)

[2] Marchingo JM et al. (2014) *Science* **346** 1123 – 1127.

[3] Heinzel S, et al. *Nat Immun* 2017; **18**, 96 – 104.

TUE-068

Comparative study of alternative models capturing Target Mediated Drug Disposition (TMDD) for CD40 agonists

PC Seshasai¹, Anuraag Saini¹, Mrittika Roy¹ and Rukmini Kumar¹

¹Vantage Research, India

Objectives:

1. Evaluate the trade-off between Target mediated drug disposition (TMDD) models versus simpler models such as Michaelis-Menten (MM) or Quasi steady-state (QSS) with fewer parameters, in the context of sparsely available clinical data.
2. Identify the most suitable model using available PK data from three CD40 agonist therapies to get predictions on tumour concentrations.

Methods: A full TMDD modelling approach captures mechanistic interactions between antibody and receptor and is standard for characterising the non-linear pharmacokinetic behaviour of a drug. However, TMDD models may be over-parameterized and difficult to converge when data is limited. In such cases, approximations of TMDD models such as QSS and MM models can be used to estimate model parameters [1]. In this work, we have used a two compartment TMDD model. The drug undergoes linear clearance from the plasma compartment and receptor-mediated endocytosis from both plasma and tumour compartment. We used plasma PK data of three CD40 agonists namely CDX1140, CP870, 893 and ChiLob7/6 from various clinical studies and evaluated the fit and performance based on the value of AIC from these alternative models. The model with the least AIC value was chosen as the best model. Further, we predicted the amount of drug reaching the tumour compartment. AUC (area under the concentration-time curve) analysis were done for the three CD40 agonists and they were ranked based on their exposure in the tumour compartment.

Results: Based on our analysis the exposure of various CD40 agonists in the tumour compartment was estimated and compared. CD40 agonists were ranked based on their exposure in the tumour tissue. The AUC for both plasma and tumour compartments is plotted against the doses for different model. The best model should have minimal number of parameters estimated from the model to describe the data with acceptable precision [2]. TMDD model is over-parameterized and some of the parameter estimates were not reliable. While MM model provides the most precise and unbiased parameter estimates and predictions for free drug concentration. Therefore, MM model is therefore the best among the 3 models for predictions given a sparse dataset.

Conclusions: After analyzing 3 types of models for capturing TMDD, we arrived at the following conclusions. MM model is a good option when PK data is sparse as it explains the data with acceptable precision using minimal number of parameters. QSS models, while having fewer parameters are often inconsistent with full TMDD model predictions.

References:

1. Gibiansky L, Gibiansky E, Kakkar T and Ma P (2008) Approximations of the target-mediated drug disposition model and identifiability of model parameters. *J Pharmacokinet Pharmacodyn* doi:10.1007/s10928-008-9102-8.
2. X. Yan, D. E. Mager, W. Krzyzanski (2010), Selection between Michaelis-Menten and target-mediated drug disposition pharmacokinetic models. *J Pharmacokinet Pharmacodyn* 37:25-48.

TUE-069

A pharmacometrics approach to assess feasibility of capillary microsampling to replace venous PK sampling in clinical studies

Authors: Sagar Bachhav¹, Max Taylor², Ana Martin², Justin Green², Stephan Duparc³, Katie Rolfe², Hema Sharma², Lionel Tan², Navin Goyal¹

¹GlaxoSmithKline, Collegeville, PA, USA; ²GlaxoSmithKline London, UK; ³Medicines for Malaria Venture, Geneva, Switzerland;

Objectives: Microsampling offers numerous advantages of being less invasive, requiring small blood volume (50-100 µL) and well suited in vulnerable populations, as compared with conventional venous sampling in clinical studies. Current regulatory guidance recommends bridging or correlative studies to enable microsampling as a PK sample collection technique. A population pharmacokinetic (POP PK) approach is employed to assess the feasibility of blood microsampling as an alternative to venous sampling. Interim data from a pediatric study evaluating tafenoquine (TQ), a new single-dose anti-malarial for the radical cure of *Plasmodium vivax* (*P. vivax*) malaria in adults was utilized in this analysis.

Methods: Pediatric subjects (bodyweight range 12-54 kg and age range 2-15 years) received TQ doses based on body weight. Sparse PK samples were collected using both venous and capillary microsampling around days 3, 15, 29 and 60. A direct comparison of TQ PK concentrations (venous and capillary microsampling data) was conducted using correlation and Bland-Altman analysis. Subsequently, two separate POPPK models were developed and qualified using bootstrap, goodness-of-fits and predictive checks. POPPK model *post-hoc* exposures (AUC, Cmax) were estimated for each individual based on venous and microsampling data. Simulations were conducted to predict TQ exposures and dose recommendations across pediatric weight bands and compared against each of the blood sampling methods.

Results: The correlation and Bland-Altman analysis did not meet the *a priori* established criteria - positive correlation ($\rho \geq 0.98$) and limits of agreement within 5% of the median concentration in each quartile across entire concentration range. This is potentially attributed to the underlying stochastic variability in the data. Each POPPK model adequately described TQ PK using a 2-compartment model with bodyweight based on allometric scaling of apparent clearance and volume of distribution. The two models were qualified based on results of bootstrap analysis, goodness-of-fit plots and visual predictive checks. TQ PK parameter estimates were very similar across the two models with slightly higher between-subject variability (BSV) in PK data from capillary microsampling. The median predicted AUC across different dose regimens and weight bands were comparable across the two models (Figure 1). Predicted exposure range across the body weight bands overlapped with slightly wider prediction intervals for capillary microsampling given the higher BSV (Figure[b]). The two models recommended the exact same dosing regimen.

Conclusions: The current analysis based on interim data demonstrated that a POPPK approach successfully evaluated the performance of an alternative PK sampling technique. The pharmacometric approach provides a robust solution in scenarios where random variability in PK data collected via venous and microsampling does not result in a 1:1 correlation. The findings establish that, when employed appropriately, microsampling techniques can potentially replace the conventional venous sampling method. Availability of such alternative PK sampling methods is highly useful across any drug development program.

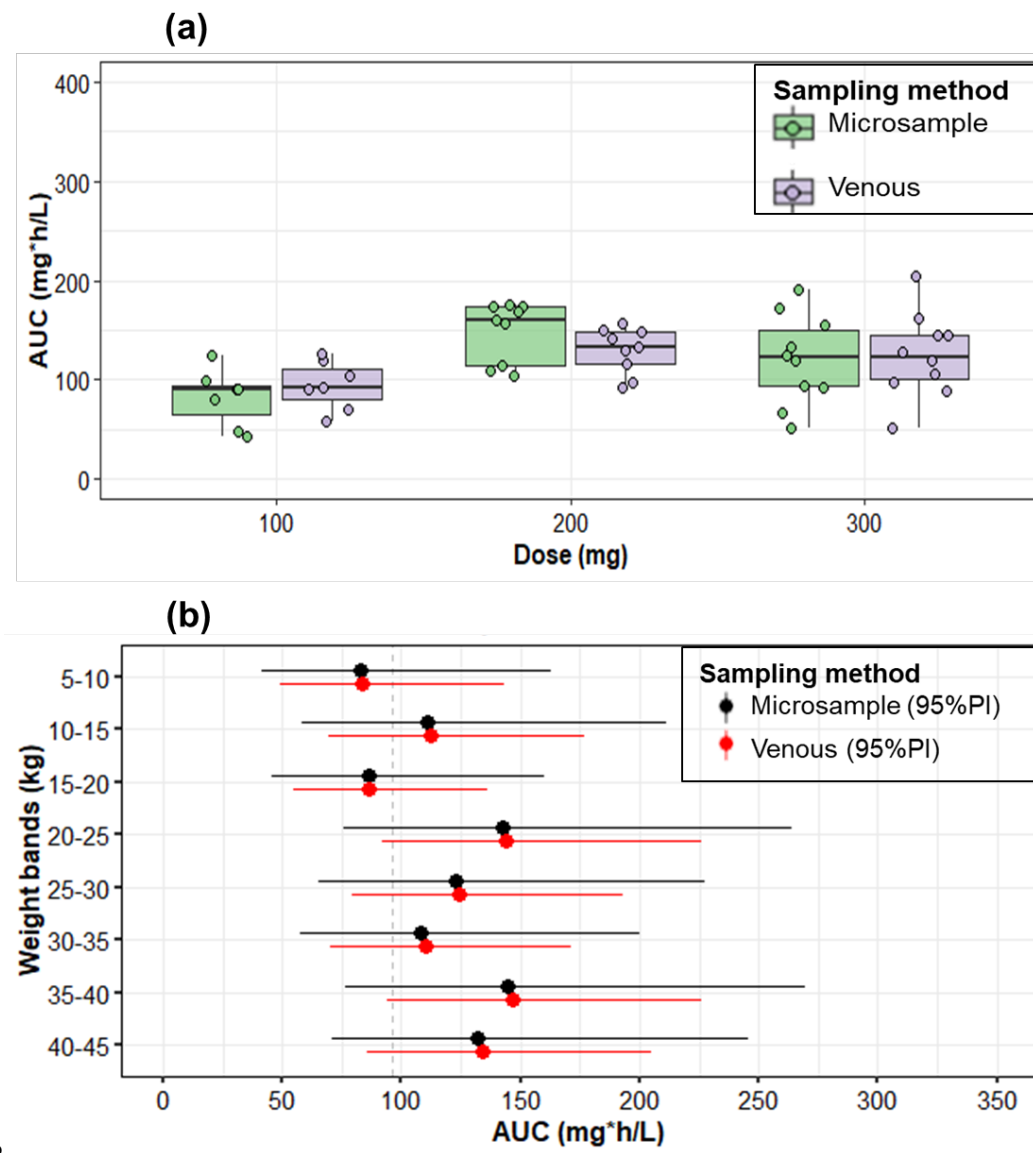


Figure 1: Comparisons of predicted exposure based on microsampling and venous sample model. Simulations (a) with *post hoc* individual estimates at different doses, (b) with population estimate vectors from bootstrap runs (the solid line in forest plot indicates 95% prediction interval [PI] and point ‘●’ or ‘●’ indicates median).

TUE-070

Mechanistic TK-TD Modeling of Agonist Anti-TrkB Therapeutic Antibody for Biomarker Rationalization and Safety Risk Assessment

Seung-Wook Chung, James Smith, Qihong Huang, Warren Ku

Nonclinical Drug Safety US, Boehringer Ingelheim, Ridgefield, Connecticut, United States

Objectives

Tyrosine receptor kinase-B (TrkB) signaling is known to play a vital role in the survival of neuronal tissues, and thus an agonist therapeutic antibody targeting TrkB is expected to protect neurons and glial cells in the retina of diabetic patients. However, it has also been reported that TrkB agonists (both endogenous ligands like brain-derived neurotrophic factor (BDNF) and therapeutic antibody) can increase food intake and body weight in non-human primates (NHPs) [1, 2]. In this study, we demonstrate how toxicokinetic-toxicodynamic (TK-TD) modeling and simulation (M&S) can inform preclinical safety evaluation decisions with regard to biomarker and assay selection, and risk assessment.

Methods

First, to determine whether BDNF can be an appropriate surrogate of systemic target engagement for toxicology studies, a mechanistic TK-TD model for intravenous (IV) injection was developed based on literature findings including reported PK-PD observations of TAM-163 (Pfizer) [1] and TrkB-BDNF biology (e.g., target expression/shedding/turnover, target-ligand/-drug binding, etc). Next, to assess a potential clinical risk of drug-mediated obesity in diabetic retinopathy patients, different TK-TD models for intravitreal (IVT) administration in monkeys and humans were developed with respect to body weight gain as a TD endpoint [1, 2].

Results

Key predictions obtained from the first model are as follows: (1) The systemic BDNF does not seem a sensitive target engagement marker due to its minimal post-dose elevations; (2) Free and total BDNF are almost identical due to the very minimal impact of soluble TrkB binding to BDNF; (3) Post-dose serum BDNF elevation can be sustained for long because of prolonged target engagement. The second model predicts that after monthly intravitreal administration of agonist TrkB mAb (e.g., TAM-163), body weight gain may be noticeable (~6-10%) in NHPs but almost negligible (~1%) in humans. The result implies a low obesity risk in diabetic retinopathy patients and thus, additional de-risking studies with regard to obesity are not recommended.

Conclusions

M&S can guide the design of preclinical toxicology studies by helping select right biomarkers, right assay, and right sample collection times. M&S can also serve as a safety de-risking tool.

References

- [1] Vugmeyster Y. et al. (2013) mAbs 5:3, 373–383
- [2] Perreault M. et al. (2013) PLoS One 8(5): e62616

TUE-071

A Population Pharmacokinetic and Pharmacodynamic Analysis of Anti-ADAMTS-5 Nanobody to Support the Phase II Trial Design

Lanke Shankar PhD¹, Girard Pascal PhD², Flavie Moreau¹, Christoph Ladel PhD³, Hans Guehring MD³, Goteti Kosalaram PhD¹

¹EMD Serono, Inc., Billerica, MA, USA, a business of Merck KGaA, Darmstadt, Germany; ²Merck Institute of Pharmacometrics, Lausanne, Switzerland, an affiliate of Merck KGaA, Darmstadt, Germany; ³Merck KGaA, Darmstadt, Germany

Objective: To develop a population pharmacokinetic (PK) and pharmacodynamic (PD) model of anti-ADAMTS-5 (M6495) nanobody and simulate phase II trial dosing scenarios.

Methods: Data from phase I single ascending dose (SAD) and phase Ib multiple ascending dose (MAD) studies were used for PK/PD model development. The SAD study included 54 healthy volunteers that received a single dose of subcutaneous M6495 (1, 5, 20, 75, 150 and 300 mg) or matching placebo (n=3 in the 6 dose groups). The MAD study included 32 patients with symptomatic knee osteoarthritis who received M6495 75, 150 and 300 mg every other week, 300 mg weekly, or matching placebo (n=2 in the 4 dose groups) for six weeks. PK (serum) and PD (Alanine-Arginine-Glycine-Serine [ARGS] biomarker) samples were assessed at prescheduled intervals. Nonlinear mixed effects modeling was performed using NONMEM (version 7.3.0) and R (version 3.5.1) for data manipulation, dataset simulation, and for plots. The First Order Conditional Estimation with Interaction (FOCEI) estimation method was used. Criteria for model selection were based on a likelihood ratio test with $p<0.01$ for inclusion in the model and $p<0.001$ for backward elimination. The PK/PD model was used to simulate phase II dosing scenarios.

Results: The M6495 concentration-time profiles were well captured by the two-compartmental base model, with a zero and first order absorption process and a linear plus non-linear drug elimination process observed. The model improved with inception of a lag in the absorption process (decrease in objective functional value by 21 points). No significant covariate effect was observed on any PK parameters. Interindividual variability (IIV) was tested on all parameters and were retained on clearance, volume of distribution of central compartment, and absorption rate constant. The target PD (ARGS level) was described effectively with an indirect response model in which

(predicted) M6495 concentrations inhibited ARGs production. IIV was tested on all parameters and were retained on baseline ARGs (E0). IIV was not retained on other PD parameters. The dose- and regimen-stratified VPCs showed that the observed PK/PD profiles were well within the respective model based on simulated 90% prediction intervals.

Dosing scenario simulations showed that greater than 70% ARGs suppression was observed with a dose of greater than 75 mg once a month. A dose of 25 mg M6495 was distinguishable from placebo. The dose that elicited two thirds of the effect compared to the top dose was 25 mg M6495. A monthly dosing injection scenario appears to be feasible.

Conclusions: Based on the totality of available data, a population PK/PD model was successfully developed to describe the M6495 PK and ARGs levels in healthy volunteers and patients. This preliminary PK/PD model predicted the emerging PK and ARGs profiles in osteoarthritis patients.

TUE-072

Comparison of pharmacokinetics and QTc effect of Quizartinib in Japanese and non-Japanese patients with Relapsed/Refractory (R/R) *FLT3*-ITD positive acute myeloid leukemia (AML) using population pharmacokinetic (PopPK) analyses

Shintaro Nakayama¹, Masaya Tachibana¹, Elizabeth Ludwig², David Jaworowicz², Hannah Huang², Jill Fiedler-Kelly², Dongwoo Kang³, Malaz Abutarif³, Ophelia Yin³, Hitoshi Ishizuka¹, Kazutaka Yoshihara¹

¹Daiichi Sankyo Co., Ltd. Tokyo, Japan; ² Cognigen Corporation, a Simulations Plus company, Buffalo, NY; ³ Daiichi Sankyo, Inc., Basking Ridge, NJ

Objectives: The PopPK and C-QTc analyses were conducted to compare the pharmacokinetic (PK) profiles and QTc effect of quizartinib in Japanese and non-Japanese patients.

Methods: Data for PopPK analysis were obtained from the participants in quizartinib treatment arms of the 7 global studies and 2 Japanese studies. The previously developed PopPK models for quizartinib and its metabolite AC886 were updated using the pooled data. The affect of Japanese population was then evaluated as a covariate on relevant clearance and volume parameters. A sensitivity analysis was performed with only Japanese studies. Mean of triplicate ECG measurement and observed time-matched concentrations of quizartinib and AC886, obtained from 1 Japanese study and 1 global study, were used for concentration-QT interval corrected using Fridericia's formula (C-QTcF) analysis. To establish the relationship between quizartinib and AC886 concentrations and QTcF, a previously developed C-QTcF model was used (Dongwoo Kang et. al., 2019). A full model was formed by inclusion of the affect of Japanese population on baseline QTcF and Emax for quizartinib and AC886.

Results: The PK of quizartinib in healthy volunteers and non-Japanese and Japanese patients with AML was well characterized by a 3-compartment model with sequential zero- and first-order absorption and linear elimination. The time course of quizartinib and AC886 concentrations in Japanese patients was adequately described using the same structural popPK model with updated parameter estimates. Japanese population was not found to be a statistically significant covariate on quizartinib and AC886 PK parameters. The estimate of quizartinib CL in the sensitivity analysis model was consistent with the CL estimate in the final PopPK model, suggesting that the model was robust enough to accurately characterize quizartinib disposition in the Japanese population alone. The C-QTcF relationship in Japanese patients was adequately described by the same structural model developed for the global study with parameters updated. Covariate of Japanese population was evaluated on baseline QTcF, Emax of quizartinib, and Emax of AC886 and were not statistically significant. The predicted median Δ QTcF at the geometric mean peak plasma quizartinib concentration (378 ng/mL) and corresponding AC886 concentration (205 ng/mL) on Cycle 1 Day 28 after once-daily dosing of quizartinib at 60 mg using actual dosing history in patients was 19.9 msec [90% CI: 17.8, 22.0 msec].

Conclusions: The PopPK analysis demonstrated similar PK profiles of quizartinib and AC886 in Japanese and non-Japanese AML patients. There were no significant differences in the C-QTcF relationships for quizartinib and AC886 between the Japanese and non-Japanese AML patients. These results support the same dosing regimen for quizartinib in Japanese and non-Japanese AML patients.

Reference: Dongwoo Kang et. al., (2019) 24th Congress of European Hematology Association. Population pharmacokinetics and concentration-QTc analysis of quizartinib in patients with *FLT3*-ITD positive relapsed/refractory acute myeloid leukemia.

TUE-073

Population Pharmacokinetics of Melphalan for Pediatric Patients Undergoing Allogenic Hematopoietic Cell Transplantation

Shuhui Li¹, Danna Chan², Christopher C. Dvorak³, Alexis Melton³, Elyes Dahamane¹, Joga Rao Gobburu^{1,2}, Vijay Ivaturi^{1*}, Janel Long-Boyle^{3,4}

¹School of Pharmacy, University of Maryland, Baltimore, MD, USA; ²ASTEX Pharmaceuticals, Pleasanton, CA, USA; ³Department of Pediatrics, Division of Allergy, Immunology, and Bone Marrow Transplantation, University of California San Francisco, San Francisco, CA, USA; ⁴Department of Clinical Pharmacy, University of California San Francisco, San Francisco, CA, USA.

Objectives: Melphalan is an alkylating chemotherapeutic agent widely used in combination pretransplant conditioning prior to hematopoietic stem-cell transplantation (HCT). The pharmacokinetics (PK) of melphalan exhibits significant interpatient variability. This study was the first to characterize the PK of melphalan in the pediatric allogenic HCT (alloHCT) patient population, including evaluation of potential patient-specific covariates impacting drug exposure.

Methods: Twenty-nine patients (1.4 -18 years old) who received melphalan as part of conditioning were recruited in a single center, prospective, open-label, non-interventional study. The most common dosing regimen (25/29) was 140 mg/m², given as either one single dose (140 mg/m² x 1) or two equal doses on two consecutive days (70 mg/m² x 2). Five samples per patient were taken up to 3 hours after infusion. Non-linear mixed effects modelling was utilized to characterize the 145 observations, using Pumas v0.10.0 (Pumas-AI Inc., Baltimore, MD, USA). Patient-specific covariates were tested to explain the variability in PK parameters, including actual body weight, lean body mass, and markers for renal function. The final covariate model was used to evaluate the doses of melphalan over a wide range of ages as compared to the conventional dosing of 70mg/m² x 2 doses.

Results: A 2-compartment model with proportional residual error model best fitted the data with the final estimation in agreement with the previously reported values: clearance 18.3 L/hr/25 kg, volume of the central compartment 7.7 L/25 kg, volume of the peripheral compartment 5.7 L/25 kg, intercompartmental clearance 12.1 L/hr/25/kg, and 12.3%

² Gobburu and Ivaturi are co-founders of Pumas-AI that commercializes Pumas software.

residual unexplained variability. Actual body weight was found to explain a significant portion of the variability in the parameters with the reduction of the between-subject variability up to 62% (CV%); thus, was retained in the final model. Variability for all the PK parameters was less than 30% in the final covariate model. The median daily AUC for 70mg/m² cohort was estimated to be 3.3 mg·hr/L that was used as the therapeutic target to project the doses for pediatric patients with body weight range of 10.0 kg to 64.7 kg (age: 2 – 17 years old). The model-informed dose was shown to be slightly lower than typical body surface area dosing.

Conclusions: In summary, a population PK model was developed to describe the PK of melphalan in a pediatric alloHCT population. Among all covariates tested, actual body weight was the most significant covariate to explain the variability in the PK parameters. These results suggested that individualized, model-based dosing of melphalan can optimize melphalan exposure, reduce the variability in exposure, and have the potential to improve clinical efficacy while minimizing the regimen related toxicity.

TUE-074

Development of a PK/Efficacy model supplemented with mixture and logistic regression models for describing the heterogeneity of tumor growth inhibition in tumor-bearing mice in immuno-oncology

Siak-Leng Choi¹, Xavier Boulenc¹, Christine Mauriac¹, Delphine Valente¹

¹ Sanofi, R&D DMPK France, Alfortville, France

Objectives: Heterogenous distribution in responding to tumor growth inhibition (TGI) can lead to different subpopulations exhibiting distinct TGI responses after receiving repeated dosing in immuno-oncology (IO). Although the underlying mechanism of action is unclear, developing a semi-mechanistic population PK/TGI model supplemented with both mixture and logistic regression models is necessary to predict the population TGI response being impacted by the heterogeneity for exploring different dosing schemes.

Methods: Plasma PK and longitudinal TGI data following oral and intravenous (IV) dosing in mice were collected. The semi-mechanistic PK/TGI model adopts a TGI model described by Simeoni et al.[1], incorporating with a mixture model [2] to estimate the proportion of subpopulations (i.e., responders and non-responders). Subsequently, the discrete data of subpopulation grouping assigned by mixture model was analyzed by logistic regression model for its correlation with PK metrics (C_{max} and AUC). Thereafter, the resultant logistic regression model was combined with the semi-mechanistic population TGI model for the simulations. These analyses were performed using NONMEM® version 7.3 (ICON Development Solutions, Ellicott City, MD, USA).

Results: PK observations from 79 mice following single- and repeated dosing were collected. Whereas, TGI observations collected from days 7 to 36 from 146 MC-38 tumor bearing mice, receiving different dosing schemes of oral and IV repeated dosing, from three efficacy studies were pooled. A two-compartment PK model links with a semi-mechanistic TGI model, incorporating with a mixture model to estimate the second-order tumor killing parameter (k_{kill}) for each subpopulation by assuming 50% population probability of being responder, successfully distinguishes responders' TGI profiles from non-responders. This model estimates typical k_{kill} in responders is about 60-fold higher than non-responders. Based on the logistic regression model, total C_{max} ($C_{max} \cdot$ Number of doses) correlates significantly with the proportion of responders. Combining with the resultant logistic regression model, the semi-mechanistic TGI model allows an adequate prediction of the partial- and complete tumor responder rates, the population median regression rate in relative to vehicle group (dT/dC), and the probability of a dosing scheme to be efficacious.

Conclusions: The model adequately predicts the heterogeneity of population TGI and is warranted to be utilized for informing the active dose selection in IO at the preclinical setting.

References :

- [1] Simeoni M et al. (2004) Predictive pharmacokinetic-pharmacodynamic modeling of tumor growth kinetics in xenograft models after administration of anticancer agents. *Cancer Res.* 64(3):1094-101.
- [2] Carlsson KC et al. (2009) Modeling subpopulations with the \$MIXTURE subroutine in NONMEM: finding the individual probability of belonging to a subpopulation for the use in model analysis and improved decision making. *AAPS J*;11(1):148-54.

TUE-075

**PK/PD Model Prediction of Platelet Reduction as a Guide for Dose-Escalation Design of Navitoclax
Added on to Ruxolitinib in a Phase 2 Study**

Silpa Nuthalapati¹, John Hayslip³, Rajeev Menon¹, Sven Mensing²

¹Clinical Pharmacology and Pharmacometrics, AbbVie, North Chicago, IL, USA; ²Clinical Pharmacology and Pharmacometrics, AbbVie, Ludwigshafen, Germany; ³Clinical Development, AbbVie, North Chicago, IL, USA

Objectives: Navitoclax, a first-in-class BCL-2/BCL-XL inhibitor is being investigated in combination with the current standard of care for myelofibrosis, ruxolitinib (Jakafi™, JAK1/2 inhibitor) in primary and secondary myelofibrosis. Both navitoclax and ruxolitinib cause thrombocytopenia via different mechanisms: navitoclax by peripheral platelet apoptosis and ruxolitinib by slowing platelet production. We report a model-based approach to quantitate the magnitude of thrombocytopenia for the navitoclax and ruxolitinib combination to recommend navitoclax starting dose and ramp up doses.

Methods: A single arm, open-label Phase 2 proof-of-concept study was designed to evaluate safety and efficacy of navitoclax added to ruxolitinib in patients with primary or secondary myelofibrosis (NCT03222609). Subjects must be currently on a stable dose of ≥ 10 mg BID of ruxolitinib without achieving an adequate clinical response to ruxolitinib. A mechanistic model modifying the literature reported Friberg model for neutrophils was developed to evaluate the effect of navitoclax and ruxolitinib on platelets count based on navitoclax data from previous studies and literature data for mean platelet profiles with ruxolitinib. Navitoclax effect was modeled to increase the elimination of circulating platelets while ruxolitinib inhibitory effect was on platelet proliferation. The combined PK/PD parameters were used to perform simulations of the add-on effects of navitoclax at steady dose of ruxolitinib (10 mg BID) to aid in navitoclax dose escalation planning for different dosing scenarios of navitoclax

Results: The mechanistic PK/PD model was fitted to individual navitoclax platelet count data from 256 subjects receiving oral navitoclax (dose range 10–475 mg) as a 14/21-day schedule or a continuous once daily (QD) schedule and literature data for mean platelet profiles for ruxolitinib.

Simulations conducted using the combined PK/PD model to evaluate weekly or bi-weekly dose escalations of navitoclax from 50 mg QD to 300 mg QD added on to 10 mg BID of ruxolitinib showed that:

- The maximum decrease in platelet count was predicted to be comparable between weekly dose escalation versus biweekly dose escalation.
- Dose escalating weekly achieved target dosing of 300 mg 4 weeks earlier.
- A starting dose of 25 mg showed only a minor median difference in platelet counts when compared to 50 mg dose.

The recommendation was to start with 50 mg navitoclax QD co-administered with a stable dose of ruxolitinib BID and weekly escalation of navitoclax, with careful platelet monitoring in the Phase 2 study.

Conclusions: A mechanistic PK/PD model was developed to predict the effect on platelets for combination drugs causing thrombocytopenia by different mechanisms. Based on the model-based approach, a navitoclax starting dose of 50 mg QD followed by weekly dose ramp up to 300 mg QD at a steady dose of ruxolitinib was chosen in the proof-of-concept study to manage thrombocytopenia and maximize exposures to navitoclax.

Clinical trial information: NCT03222609

Author disclosures:

All authors are AbbVie employees and may hold stock or options

AbbVie disclosures:

AbbVie provided financial support for the study and participated in the design, study conduct, analysis and interpretation of data as well as the writing, review and approval of the abstract.

TUE-076

In vitro–In vivo Relationship and Bioequivalence Prediction of ziprasidone Capsules based on a PBPK Model.

Authors: Frederico S. Martins (1), Fabricia Ré (2), Fábio P. de Souza (2), Francine A. de Castro (3), Stephan Schaller (1), Rodrigo Cristofoletti (4), Marli M. Lima (2), Andrea Diniz (2)

Affiliations: (1) esqLABS GmbH, Saterland, Germany; (2) State University of Maringá, Paraná, Brazil, (3) University of São Paulo, São Paulo, Brazil; (4) Center for Pharmacometrics & Systems Pharmacology ,University of Florida, FL, US;

Objectives: The aim of this study is the comparison of two immediate release formulations containing ziprasidone (ZIP) using PBPK-based virtual bioequivalence (BE) trials.

Methods: The in-vitro dissolution assessment was performed in flow-through cell dissolution apparatus (USP apparatus-4) Sotax CE 7 Smart and the obtained dissolution profiles were incorporated into a validated ZIP-PBPK model, which was previously developed in PK-Sim/MoBi [1]. The comparison of dissolution profiles was conducted by calculating the difference factor (f_1), and the similarity factor (f_2). To perform the virtual BE assessment, a population of 1000 healthy adults, representative of the gender ratio and demographics of the sampled cohort recruited for the in vivo study were simulated. The *in vivo* BE study was an open-label, 2-period, randomized, single dose, crossover study in 40 healthy adults from both sexes with 21-50 years old. In each period, subjects received either the Brazilian reference listed drug, Geodon® (40 mg of ZIP hard capsule) or the test formulation (40 mg ZIP capsule). For each subject and formulation, C_{max} and AUC of the study data were computed by NCA, and the geometric mean and CI-90% were derived for each formulation.

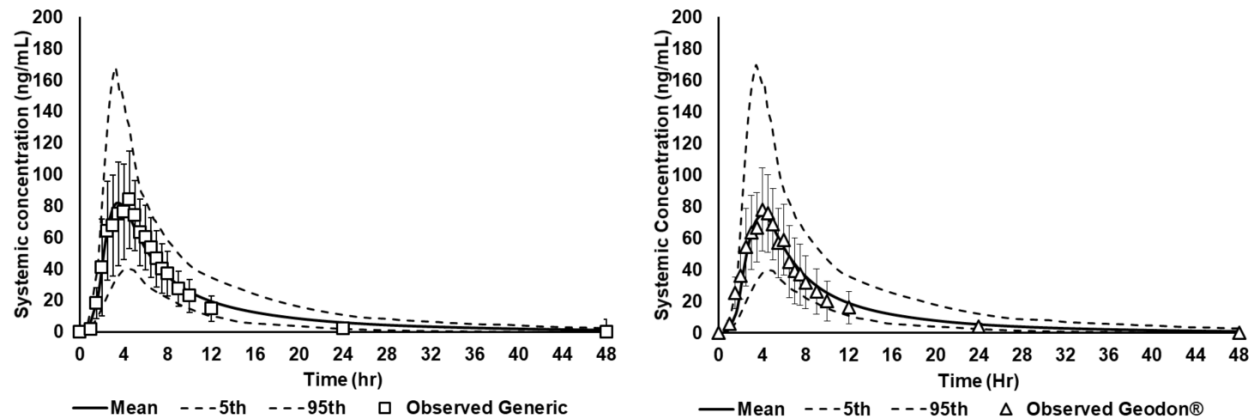
Results: The PBPK model was qualified with i.v and oral dose data within single and multiple dose regimens. The simulated PK parameters were consistent with the observed values; the minimum folder error (MFE) values for the AUC and C_{max} ranged from 0.7-1.2 0.8-1.2, respectively (Figure1). A model is considered robust when MFE values are well within a range of 0.5 - 2.0. The similarity factors between both formulations were $f_1=12.4$ and $f_2=65.2$, values of $f_1 \leq 15$ and $f_2 \geq 50$ are considered within the similarity range defined by the guidelines[2]. Two formulations are considered bioequivalent when the CI-90 of AUC and C_{max} are within 80-125% [2] .For the present study, the CI of C_{max} lies within 112-128% for the clinical data and within 122-129% for the virtual population, which indicates non-bioequivalence.

Conclusions: The confirmation of the observed CI for C_{max} by the PBPK analysis through the performed analysis demonstrates, that a validated PBPK absorption model is an appropriate tool for the translational evaluation of *in vitro* dissolution properties to *in vivo* product pharmacokinetic performance.

References:

- 1 Biesdorf C, Martins FS, Sy SKB, Diniz A. Physiologically-based pharmacokinetics of ziprasidone in pregnant women. Br J Clin Pharmacol 2019; 85: 914–923
- 2 Fda, Cder, Purdie. Guidance for Industry Bioavailability and Bioequivalence Studies Submitted in NDAs or I<http://www.fda.gov/Drugs/GuidanceComplianceRegulatoryInformation/Guidances/default.htm>

Figure 1: Simulated and observed plasma concentration profiles for oral administration of Geodon and generic formulation.



TUE-077

Meta-analysis of dapagliflozin dosing to assess influence on low density lipoprotein (LDL) cholesterol in type 2 diabetes mellitus (T2DM)

Srinivas Martha, Preethi Hepzibah Jangam, Suraj G. Bhansali

ClinPharm, Excelra Knowledge Solutions, 6th & 7th Floor, Wing B NSL SEZ ARENA, IDA Uppal, Habsiguda, Hyderabad, Telangana State 500039, India.

Objectives:

Dapagliflozin is widely used novel oral anti-diabetic drug for type-2 diabetes mellitus (T2DM) patients whose glucose levels are inadequately controlled by metformin along with diet and exercise. A systematic literature review (SLR) was performed and meta-analysis was done to evaluate the effects of dapagliflozin on LDL cholesterol in T2DM.

Methods:

SLR was conducted using MEDLINE, EMBASE, and the Cochrane Library from 1950 to January 2020 for trials of at least 12 weeks duration in which diabetic patients were treated with either dapagliflozin monotherapy or as an add-on therapy. Data on change in LDL cholesterol levels were pooled in a meta-analysis. Data from dose-comparison trials were separately pooled.

Results:

A total of 44 trials were identified for the analysis and 6 trials for the dose comparison analysis. Dapagliflozin monotherapy (1, 2.5, 5, 10, 20 mg) increased LDL cholesterol by 2.5 mg/dL (95% CI 1.17 to 3.81; $I^2 = 0\%$) versus placebo or active comparator; dapagliflozin added to oral therapy increased LDL cholesterol by 2.59 mg/dL (-1.53 to 6.72; $I^2 = 74\%$) versus placebo or active comparator. Dapagliflozin monotherapy (10 mg) increased LDL cholesterol by 3.67 mg/dL (1.61 to 5.73; $I^2 = 6\%$) versus placebo or active comparator. There was a slight increase in LDL cholesterol by 0.91 mg/dL (-4.34 to 6.17; $I^2 = 68\%$) with 10 mg dapagliflozin compared with 5mg dapagliflozin.

Conclusions:

Dapagliflozin therapy increases LDL cholesterol when used as monotherapy and in combination with other therapeutic agents. Increase in LDL cholesterol levels are higher with 10 mg as compared to 5 mg of dapagliflozin.

TUE-078**Using longitudinal tumor size (TS) modeling to power phase 1b oncology dose finding trials**

Tarjinder Sahota¹, Vincent Haddad² and Ghada F. Ahmed³

¹ Clinical Pharmacology and Safety Sciences, BioPharmaceuticals R&D, AstraZeneca, Cambridge, UK.

² Oncology Biometrics R&D, AstraZeneca, Cambridge, UK

³ Formerly Clinical Pharmacology and Safety Sciences, BioPharmaceuticals R&D, AstraZeneca, Cambridge, UK.

Objectives: Dose optimization for targeted anti-cancer agents requires exploring several dose levels early in development. Typically, large sample sizes are needed for adequate dose differentiation power making the consequent delay to phase 3 a challenge. To address this, we demonstrate how exposure-TS modeling for savolitinib (AZD6094, HMPL-504, volitinib), a potent and selective cMET inhibitor can maximize dose selection power without inflating the sample size for the dose finding trial.

Methods: TATTON was a multi-part phase 1b study that included savolitinib+osimertinib arms in patients with NSCLC¹. Initial expansion arms (N~40/arm) explored savolitinib 600 mg QD. One subsequent expansion sought to explore 300 mg QD for alternate dose finding. However, 80% power to detect a 20% drop in objective response rate (ORR) with 300 mg, assuming 10% 1-sided α , required 150 subjects/arm, a study deemed unfeasible. TS change from baseline (Δ TS) was used as a surrogate biomarker for ORR. To explore power using exposure-TS, subjects were sampled with replacement from the 600 mg pharmacokinetic and TS profiles. Trials (600 vs 300) were simulated (300/scenario) with 10, 25 and 80 patients/arm and 0-50% Δ TS loss applied for the 300 mg profiles. An E-TS model (exponential function with first-order shrinkage rate, K_{eff}) was fitted to the trials and a likelihood ratio test was used to conclude significance of exposure on K_{eff} ($\Delta OFV = 3.84, \chi^2_{df=1}$). The power function was calculated as percentage of times statistical significance was achieved. A threshold of acceptable Δ TS loss with 300 mg was set at <20% after clinical team consultation. The procedure was repeated using the dose-RR model. Resampling/re-estimation was conducted in NONMEM 7.3.1 and automated via the NMproject interface².

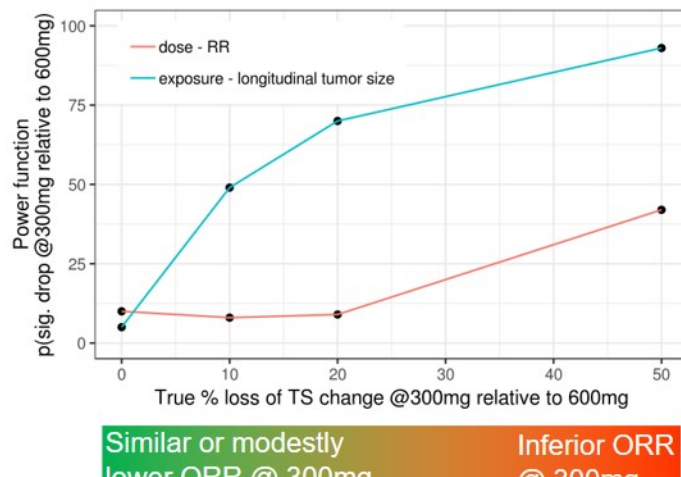
Results: A total of 51 TS profiles were available from the 600 mg cohort. Seventy-eight and fifty-three percent of subjects had at least 6 and 12 weeks follow up, respectively, thus the data reflected early change in target lesion size. E-TS provided ~70% power to detect 20% loss in Δ TS (N=25/arm) (Figure 1). In collaboration with statistics, a dose selection framework based on the widely-utilized ORR and biomarker-based Exposure-TS analyses is proposed (Figure 1).

Conclusions: Longitudinal TS modeling offered meaningful power to detect modest but relevant drops in efficacy with 300 mg. This provided assurance for a robust dose decision where ORR would have been inconclusive for small but relevant effect sizes and justified an expansion arm of at least 25 subjects for 300 mg¹. The E-TS model is limited by exclusion of non-target and new tumor lesions. However, the composite dose selection framework combined multiple analyses to guide dose decision and was enabled by effective cross-functional collaboration between clinical pharmacology-pharmacometrics and statistics.

References:

1. Sequist LV, et al. Lancet Oncol.2020 Mar;21(3):373-386.
2. PAGE26 (2017) [www.page-meeting.org/?abstract=7357], <https://github.com/tsahota/NMproject>

Figure 1. Power function (N=25) using exposure-TS and dose-RR models and a framework for a composite dose selection criteria



Decision basis	Similar or modestly lower ORR @ 300mg	Inferior ORR @ 300mg
	Supplement ORR with exposure – biomarker (e.g. longitudinal TS) modeling	Use dose-ORR. Exposure-response modeling not needed

TUE-079

Characterisation of dapagliflozin efficacy as an adjunct-to-insulin therapy in patients with type 1 diabetes mellitus: a semi-mechanistic exposure-response analysis

Tatiana Yakovleva¹, Joanna Parkinson², Robert C. Penland³, David W. Boulton⁴, Kirill Peskov^{1,5}, Victor Sokolov¹, Weifeng Tang⁴

1 – M&S Decisions LLC, Moscow, Russian Federation

2 – Clinical Pharmacology & Quantitative Pharmacology, Clinical Pharmacology and Safety Sciences, R&D, AstraZeneca, Gothenburg, Sweden

3 – Clinical Pharmacology & Quantitative Pharmacology, Clinical Pharmacology and Safety Sciences, R&D, AstraZeneca, Boston, USA

4 – Clinical Pharmacology & Quantitative Pharmacology, Clinical Pharmacology and Safety Sciences, R&D, AstraZeneca, Gaithersburg, USA

5 – I.M. Sechenov First Moscow State Medical University, Moscow, Russian Federation

Objectives: Dapagliflozin is a highly potent, selective inhibitor of sodium-glucose cotransporter 2 that was approved in Europe and Japan for the treatment of type 1 diabetes mellitus (T1DM) as an adjunct to insulin therapy based on the results of Phase 3 DEPICT programme [1, 2]. The aim of this work was to characterize the joint effect of dapagliflozin and total daily insulin dose (TDID) on daily glucose and HbA1c using a semi-mechanistic exposure-response model.

Methods: Data from Phase 2 (MB102-072, NCT01498185) and Phase 3 (DEPICT-2, NCT02460978) studies were used to develop a non-linear mixed effects (NLME) model. External model qualification was performed on the data from Phase 3 (DEPICT-1, NCT02268214) trial. The following baseline covariates were evaluated: age, sex, diabetes duration, body weight, BMI, fasting plasma glucose, haemoglobin, HbA1c.

The model was developed in a stepwise fashion to consecutively characterize TDID as a function of dapagliflozin exposure (1), continuous glucose measurements (CGM) response to TDID changes (2), dapagliflozin effect on CGM (3), and the link between CGM and HbA1c (4). The forward covariate search as well as the mixture of distributions

based on a categorical covariate were performed at the last stage of model development. The models were evaluated by convergence, precision/stability of estimates, improvements in objective functions, and visual predictive checks.

The Monolix software (version 2018R2) was used for NLME modelling. Data visualization and forward simulations were performed in R software (version 3.5.1).

Results: The decrease of TDID with dapagliflozin treatment was successfully characterized by an Imax equation ($I_{max} = 0.0813$, $IAUC_{50} = 19 \text{ ng/mL}^*\text{h}$). The gradual increase of CGM with time (0.139 mg/dL/week) and the TDID impact on CGM were calibrated using placebo data, while the effect of dapagliflozin exposure was estimated using the data from the active arms. Due to poor convergence of the model, $IAUC_{50}$ was fixed at the previously defined value for CGM. The changes in CGM alone were insufficient explain the HbA1c response. The adequate description of HbA1c response and successful model validation was achieved when glucose-independent impact of dapagliflozin was introduced to the model structure.

Conclusion: We have successfully established a quantitative link between the dapagliflozin exposure, TDID, plasma glucose and HbA1c in patients with T1DM. An additional glucose-independent dapagliflozin impact on HbA1c decrease was identified during model development.

References:

1. Dandona P et al. Efficacy and safety of dapagliflozin in patients with inadequately controlled type 1 diabetes (DEPICT-1): 24-week results from a randomised controlled trial. Lancet Diabetes and Endocrinol. 2017;5:846–17
2. Mathieu C et al. Efficacy and Safety of Dapagliflozin in Patients With Inadequately Controlled Type 1 Diabetes (the DEPICT-2 Study): 24-Week Results From a Randomized Controlled Trial. Diabetes Care 2018;41:1938–1946

TUE-081

Population Pharmacokinetics (PopPK) and Exposure-response (ER) Analysis of Nirsevimab in Healthy Preterm Infants

Vadry Pierre¹, M Pamela Griffin², Yuan Yuan², Therese Takas², Mark T Esser³, Tonya

Villafana², Lorin Roskos¹, Rajesh Narwal¹, Anis A Khan¹

¹Clinical Pharmacology and Safety Sciences, AstraZeneca, Gaithersburg, MD

²Late RIA, AstraZeneca, Gaithersburg, MD

³Microbial Sciences, AstraZeneca, Gaithersburg, MD

Objectives: Nirsevimab is a human IgG1κ monoclonal antibody with YTE-extended half-life properties, which binds with nanomolar affinity to antigenic site Ø on the prefusion conformation of the RSV-F protein. In a recent placebo-controlled Phase 2b study (NCT02878330), a single, fixed 50 mg nirsevimab intramuscular dose demonstrated clinical efficacy as RSV prophylaxis in healthy preterm infants against MA-LRTI (Medically-attended Lower Respiratory Tract Infection)¹. In this work, we aim to characterize the popPK and ER properties of nirsevimab in healthy preterm infants in order to optimize the dosing across a wider age and weight groups of infants.

Methods: The popPK and ER characterization of nirsevimab was conducted in a pooled dataset consisting of serum PK, ADA and demographic information from the Phase 1 study (NCT02114268; n=137) in healthy adults, the Phase 1b/2a (NCT02290340; n=71) and Phase 2b (NCT02878330; n=968) studies in infants. The median (range) baseline postnatal and postmenstrual age ranged from 3 months (0.1 – 11.9 months) and 13.9 months (7.4 – 19.7 months), respectively. Baseline bodyweight ranged from 1.6 kg to 11.1 kg with a median of 6.8 kg. The ER properties of nirsevimab were explored using a multivariate hazard model with popPK-derived continuous and ordered categorical quartiles of exposure metrics such as, serum

concentration $C_{(t)}$, C_{\max} , and AUC implemented as linear or sigmoidal relationships along with clinically pertinent covariates.

Results:

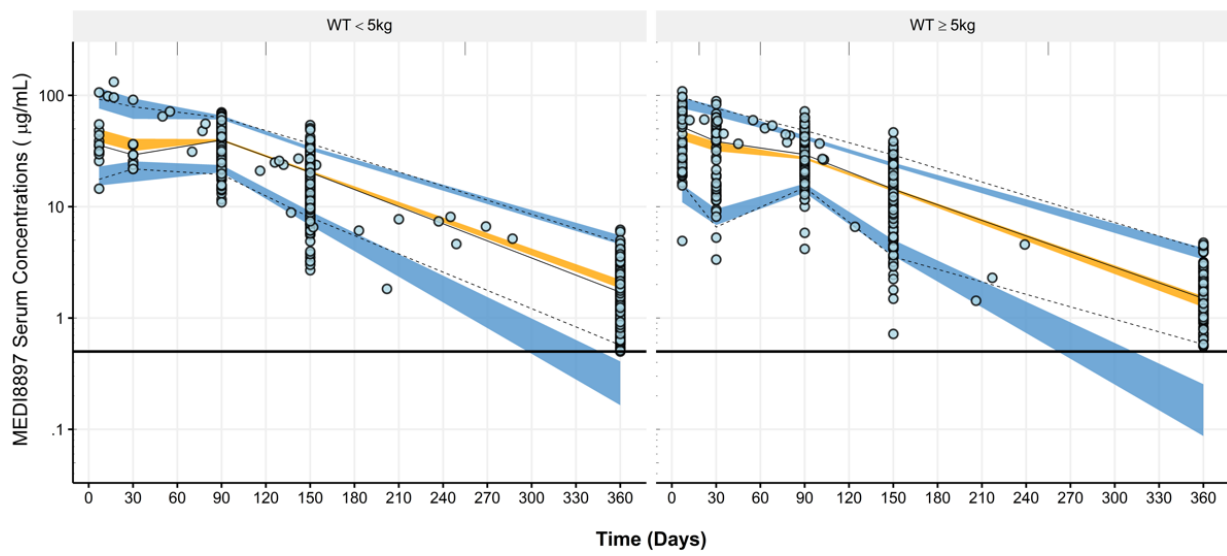
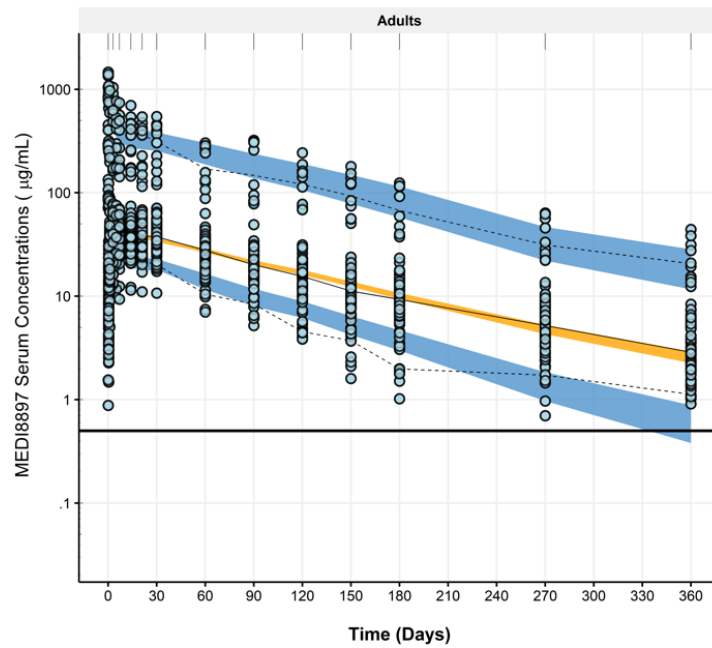
The popPK covariate model accounted for the impact of allometrically-scaled bodyweight on clearance and volume parameters as well as the effects of maturation on systemic clearance². The model was internally qualified using goodness of fit and visual predictive check plots (Fig 1).

The hazard analysis demonstrated that infants with serum AUC>Q1 have a lower risk of MALRTI with an instantaneous hazard ratio (HR) and 95% confidence interval (CI) of 0.17 (0.09, 0.32) compared to those with lower exposure or placebo. Notably, only 40% of the infants weighing ≥ 5 kg had serum AUC>Q1 compared to 97% of those weighing < 5 kg. Although the ordered categorical quartiles AUC model resulted in the lowest objective function value, the sigmoidal model with continuous C_{\max} further corroborated the protective effect of higher exposure. Hence, a fixed weight-band dosing strategy is proposed, which results in a geometric mean ratio (GMR) of nirsevimab serum AUC 0.985[0.948, 1.02] for infants weighing < 5 kg versus those weighing ≥ 5 kg. Additionally, simulated profiles indicated that the proposed dosing will result in over 90% of infants achieving serum AUC>Q1 and a $C_{\max} > EC_{80}$ using the weight-band dosing scheme.

Conclusion: Model-based approaches resulted in identifying an optimal weight-band dosing strategy to ensure protective exposures across a wide range of age and body weights in late stage trials.

References: 1. Griffin P. ID week 2019, 2. Robbie G AAC. 2012

Figure 1: Visual Predictive Check of Adults (a) and Infants (b) PK Data by Scheduled Visit



TUE-083

Model-informed optimization of titration regimens to reduce nausea incidence under treatment with GLP-1 analogues

Veronika Voronova¹, Victor Sokolov¹, Binbing Yu², Holly Kimko³, Jing Li³, Marcella Petrone³, Gabriel Helmlinger³, Kirill Peskov¹, Rosalin Arends³

1 – M&S Decisions LLC, Moscow, Russia

2 – Oncology Biometrics, Oncology R&D, AstraZeneca, Gaithersburg, USA

3 – Clinical Pharmacology and Quantitative Pharmacology, Clinical Pharmacology & Safety Sciences, BioPharmaceuticals R&D, AstraZeneca

4 – Sechenov University, Moscow, Russia

Objectives:

The administration of glucagon-like peptide-1 receptor agonists (GLP-1 RA) is associated with nausea as the most common treatment-related adverse event [1]. Nausea incidence decreases over time as a result of tolerance development over time. Therefore, dose titration is used as an effective measure to mitigate nausea risk [1]. In this work, we aimed to quantify the relationship between GLP-1 receptor occupancy and nausea incidence dynamics when treating with various GLP-1 RA and explore optimal titration scheme for a novel dual glucagon-GLP-1 RA - cotadutide.

Methods:

The model is based on aggregated data from 17 randomized clinical trials in healthy subjects and T2DM patients receiving placebo, exenatide immediate or extended release (IR, ER) formulations, oral or subcutaneous semaglutide formulations, liraglutide, or cotadutide and is represented by a system of ordinary differential equations reflecting the change over time in plasma drug concentration, GLP-1 receptor occupancy and nausea incidence. Tolerance development was captured by a time-dependent Emax equation. PK parameters were taken from the literature or estimated based on publicly available data. Pharmacodynamic (PD) parameters were estimated using the data on nausea incidence dynamics. The model compilation was done using R-based mrgsolve package.

Results:

The model diagnostics were adequate, though significant variability was observed in nausea incidence even in the framework of a single compound. The estimated adaptation rate was different across the drugs with rates ranging from fast to slower for exenatide ER, followed by cotadutide, liraglutide, exenatide IR, and both subcutaneous and oral formulations of semaglutide.

Different titration schemes were simulated for cotadutide, starting with daily administration of 50 or 100 ug dose and subsequent weekly or bi-monthly increase in dose with an increment of 50 to 100 ug until the maximum dose level of 600 ug. Starting dose was found to significantly impact maximum nausea incidence (15% and 20% of patients for 50 and 100 ug respectively), while the titration schedule mostly affected the nausea during the first 2-3 weeks of the treatment (Figure 1).

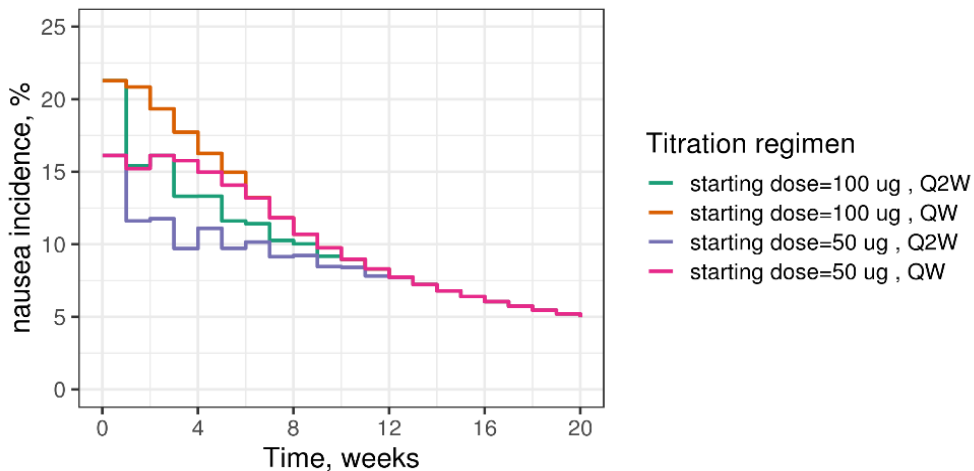


Figure 1. Predicted nausea incidence dynamics for various cotadutide titration schemes. Dose escalation was done every week (QW) or every two weeks (Q2W)

Conclusion: We have successfully established a quantitative link between change over time in GLP-1 receptor occupancy and nausea incidence for six GLP-1 receptor agonists. The resulting PK-PD model was used to explore dynamics of tolerance development with different treatment regimens to inform titration strategies for cotadutide.

References:

1. Aroda VR, Ratner R. The safety and tolerability of GLP-1 receptor agonists in the treatment of type 2 diabetes: a review. *Diabetes Metab Res Rev.* 2011;27(6):528–542.

TUE-084**Mechanistic PK/PD Modeling in Support of a Patient Convenient Once-Weekly Dosing Regimen of KYPROLIS (carfilzomib)**

Authors: Yago MR¹, Bhagwat S¹, Mehta K¹, Klipper Z², Obreja M³, Chopra VS⁴, Dutta S¹, Upreti VV¹

Institutions: ¹ Amgen, Inc., Clinical Pharmacology, Modeling & Simulation; ² Amgen, Inc., Global Development; ³ Amgen, Inc., Global Biostatistical Science; ⁴ Amgen, Inc., Clinical Biomarkers & Diagnostics

Objectives: Carfilzomib (CFZ) is an irreversible proteasome inhibitor approved for treatment of relapsed or refractory multiple myeloma. Demonstrating exposure-response for once-weekly (QW) and twice-weekly (BIW) regimens with typical modeling and simulation approaches is challenging due to CFZ's unconventional PK properties. A mechanistic PK/PD model was developed to evaluate the feasibility of less frequent CFZ dosing regimens based on its mechanism of action.

Methods: The model, based on mechanism of action, drug binding kinetics, and proteasome turnover, used a compartmental population PK model to drive irreversible binding kinetics (synthesis, recovery, homeostasis) of proteasome inhibition (PI). The model predictions were compared with observed PI data of CFZ and bortezomib (BTZ; reversible PI) from the phase 3 ENDEAVOR study and their correlation with observed efficacy metrics was evaluated for QW and BIW CFZ regimens.

Results: Observed CFZ and BTZ PI was in agreement with model predictions. Deeper and longer lasting PI was predicted for CFZ versus BTZ, consistent with superior efficacy of CFZ in the ENDEAVOR trial. PI simulations for 70 mg/m² QW and 56 mg/m² BIW at steady-state were comparable (>98%), and consistent with cross-study efficacy comparisons between 70 mg/m² QW from the phase 3 ARROW trial and 56 mg/m² BIW from ENDEAVOR (ORR and PFS). Expectedly, based on the irreversible mechanism of action of CFZ, higher C_{max} of CFZ with 70 mg/m² QW (approximately 25%) compensates for the approximately 40% lower AUC with 56 mg/m² BIW.

Conclusions: The mechanistic model demonstrated comparable PI between CFZ 70 mg/m² QW and 56 mg/m² BIW, which correlated well with comparable clinical efficacy between the regimens. Overall the results of the mechanistic model indicate CFZ is amenable to less frequent dosing.

TUE-085

Usage of a validated environment to support modeling and simulation activities

Vincent Buchheit¹, Michael Hackl³, Katja Kuldszun², Guillaume Schmitt², Christian Flandorfer³

(1) Roche Pharma Research and Early Development, Pharmaceutical Sciences, Roche Innovation Center Basel, Switzerland

(2) Roche Pharma Research and Early Development, Pharmaceutical Informatics, Roche Innovation Center Basel, Switzerland

(3) scinteco gmbh, pharma IT company, Vienna, Austria

Objective: Given the importance and impacts of quantitative clinical pharmacology contribution to drug development, it has become crucial to move from an open shared drive to a more robust and validated platform.

The objective of this abstract is to highlight the user's perspectives on using a validated environment to support modeling and simulation activities and how it further improves efficiency and quality of the quantitative clinical pharmacology analyses.

Methods: Together with our IT colleagues, we defined user requirements and explored several solutions. Quickly we noticed that **improve** had the potential to fulfill our needs. **improve** was designed to support PKPD analysis and provides a valuable and convenient interface with modeling software.

Results: **improve** is a repository allowing scientists to perform their daily work, in a secured validated and versioning control environment. **improve** combines a global, secure file repository with a robust and versatile modeling management interface for 3rd party tools like NONMEM®, Monolix®, Pumas, SAS®, R, PsN, Rstudio....No matter which analysis you choose, **improve** will keep track of the "who, what, when, where and why" of your data.

improve automatically extracts key information from the users NONMEM® run, such as objective function value, thetas, omegas, and sigmas. **improve** provides also a graphical representation of your analysis flow using steps. You can flag steps to easily identify your base, full or final models.

At any time, you can go back to a previous version of your script, input data or output files. You can also compare versions of files, or versions of outputs. This also works for entire runs, so you can compare inputs, outputs and estimates of specific versions of a run or other runs.

Current Limitations: Besides the client, there is the **improve.office** Module that enables easy access to the client repository without having to use the client itself. This is particularly useful for code development in SAS® for example. We are also using this module to save Phoenix Project Files via **improve.office** into the client. A loose integration of the **improve.client** and **improve.office** led to high disc space usage and conflicts due to the manual synchronisation process. A new version is currently developed to allow a more fine-grained control which files actually are needed on the user hard drive and gives direct feedback if data in the repository has been changed.

Conclusions: **improve** is currently used to support modeling and simulation activities, as well as Non-Compartmental Analysis (NCA). During the course of the year, we are planning to use **improve** to store all Clinical Pharmacology documents, making this new platform the single source of data and analysis for all Quantitative Clinical Pharmacology activities.

References:

www.scinteco.com

TUE-086

Development of a PBPK Model for TAK-018 (EB8018/Sibofimloc), a Bi-mannoside Compound Targeting FimH Expressing Bacteria in Intestinal Lumen to Inform Dose Selection for the Treatment of Crohn's Disease

Wan Sun¹, Abdul Naveed Shaik^{2*}, Grace Fraczkiewicz², Suresh K. Balani¹, Scott Butler¹, Ajit Suri¹, Jean-Michel Paillarse³, Vijay Yajnik¹, Maria Rosario^{1†}

¹Takeda Pharmaceuticals, Cambridge, MA, USA; ²Simulations Plus, Inc., Lancaster, CA, USA, ³Enterome, Paris, France

*Employee of Simulations Plus at the time work was conducted

†Employee of Takeda at the time work was conducted

Objectives:

TAK-018 is an oral FimH blocker being developed for Crohn's disease (CD) treatment. Since the therapeutic site of action is gut mucosa, local gut exposure is more relevant for efficacy than systemic, but more difficult to measure. Physiologically-based pharmacokinetic (PBPK) model enables predicting drug exposure at different gut regions in order to inform the dose selection for a phase 2 study.

Methods:

The model input parameters were combination of in vitro measurements, structure-based predictions, and fitted to in vivo data. The model was calibrated using single and multiple dose (50-3000 mg daily) PK data from a first-in-human study conducted in healthy subjects. Nonlinear PK was captured through saturable absorption via an active transporter. To account for binding of TAK-018 to mucosal lining of the gut wall as well as bacteria in the gut lumen, enterocyte binding was used as a surrogate and fraction unbound in enterocytes was fitted to match the observed plasma concentrations. Biliary secretion was modeled as linear flux of TAK-018 from hepatocytes to bile with excretion rate defined through permeability-surface area product and fitted against in vivo data. Renal secretion was estimated as product of glomerular filtration rate and fraction unbound in plasma. Enterohepatic circulation of TAK-018 was used to describe the prolonged terminal phase of PK profiles. Human gut concentrations were calculated from the simulated amount of TAK-018 in gut lumen (accounting for the volume of liquid in each compartment) and the bound amount to enterocytes. Based on published data showing increased permeability of gut in CD patients, both plasma and gut exposure of TAK-018 were predicted in CD patients with adjustment on the intestinal permeability. The target efficacious concentration was based on the IC₉₉ from in vitro pharmacology studies and compared with predicted gut concentration profiles of TAK-018 to evaluate different dose regimens.

Results:

The final model reasonably described the available plasma concentrations across a wide range of doses, and provided predicted segmental and total lumen concentrations of TAK-018 in human. Projected permeability increase by 4- or 10-fold for patients resulted in higher plasma concentrations and lower gut concentrations. The gut concentrations after 300 mg BID dosing appeared to be consistently well above IC₉₉ including trough level. Therefore, dose levels of 1500 and 300 mg will be evaluated in the phase 2 study to explore the efficacious dose range of TAK-018.

Conclusions:

PBPK model with mechanistic absorption provided prediction of local drug exposure in the absence of observed data in gut. The model developed with healthy subjects data allows PK projections of patient population based on known physiological changes caused by a disease. Such projections are of great value at early stage of development, when clinical data is limited, providing aid in dose selection.

Novel Mechanistic PBPK Model to Predict Renal Clearance in Varying Stages of CKD by Incorporating Tubular Adaptation and Dynamic Passive Reabsorption

Weize Huang and Nina Isoherranen

Department of Pharmaceutics, University of Washington, Seattle, WA, USA.

Objectives: Chronic kidney disease (CKD) has a multiplicity of effects on renal clearance (CL_r) of drugs. Empirically, CL_r is considered to decrease proportionally with GFR, assuming all renal drug handling pathways decline with renal function in parallel. However, CL_r was shown to decrease more than proportionally with GFR in stage 4/5 CKD for highly secreted drugs via OAT1/3,¹ and to decrease much less than proportionally with GFR in stage 4/5 CKD for permeable and renally reabsorbed drugs.² To predict the complicated CKD effects, physiologically-based pharmacokinetic (PBPK) models have been recently used to specifically address active secretion and CL_r for hydrophilic nonpermeable compounds. However, no studies have shown systematic PBPK modeling of renal passive reabsorption or CL_r for hydrophobic permeable drugs in CKD. The objective of this study was to develop a novel adaptive kidney model to universally predict changes in CL_r in CKD for permeable and nonpermeable drugs that accounts for the dramatic nonlinear effect of CKD on renal passive reabsorption.

Methods: To simulate the CKD effect on passive reabsorption, we expand our previously developed and verified mechanistic kidney model³ to incorporate the physiologically-based tubular changes of reduced water reabsorption/increased tubular filtrate flow per remaining functional nephron for each renal subsegment across varying CKD stages. The final adaptive kidney model enables the translation from *in vitro* drug permeability into degree of passive reabsorption and renal clearance value and was validated using a set of 20 compounds with differing properties without any optimization or empirical scaling throughout the progression of CKD from healthy to the end stage.

Results: The final adaptive kidney model successfully captures the physiological changes in renal tubular filtrate flows of remaining functional nephrons in CKD patients, resulting in a predicted urine flow of 0.6 mL/min that matches with observed data in CKD patients with GFR of 10 mL/min.⁴ The simulation results showed successful (absolute-fold-error (AFE_A) all<2) prediction of renal passive reabsorption and CL_r for 20 permeable and nonpermeable test compounds across the stages of CKD. In contrast, the proportional GFR reduction approach without addressing tubular compensation processes in CKD generated unacceptable CL_r predictions (AFE_P=2.61-7.35) in severe CKD. Finally, the adaptive kidney model accurately predicted CL_r of PAH and memantine, two secreted compounds, in CKD, suggesting successful integration of active secretion into the model, along with passive reabsorption.

Conclusions: The final adaptive kidney model enables mechanistic predictions of *in vivo* CL_r for secreted, non-secreted, permeable, and non-permeable drugs and metabolites throughout CKD progression from *in vitro* data without any empirical scaling factors, facilitating dosing regimen optimization and clinical trial design prior to renal impairment studies.

References:

1. Hsueh, *et al.* (2016).
2. Houghton, *et al.* (1985).
3. Huang and Isoherranen. (2018).
4. Nechita, *et al.* (2015).

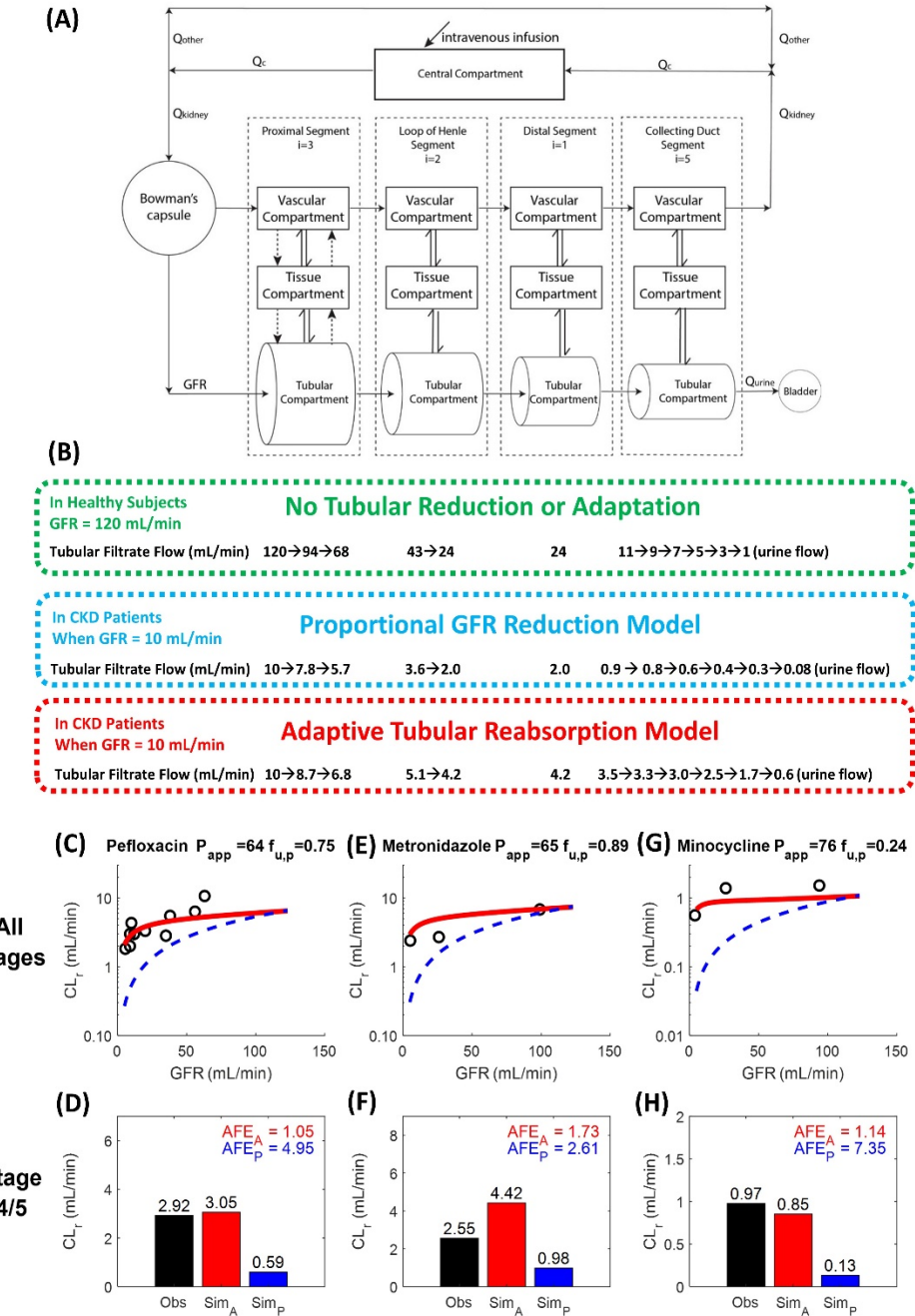


Figure 1: **(Panel A)** Schematic presentation of the mechanistic kidney model structure. **(Panel B)** The renal tubular filtrate flow (TFF, in mL/min) for each individual subsegment of the kidney model (a total of 12). Three sets of physiologically-based TFF shown here are for healthy subjects (GFR 120 mL/min, in green) and for the representative CKD patients who have residual GFR of 10 mL/min using the proportional model (in blue) and the adaptive model (in red). **(Panel C-H)** Simulation and verification of renal drug clearance (CL_r) of 3 representative test compounds that are permeable and highly renally reabsorbed: pefloxacin (C and D), metronidazole (E and F), and minocycline (G and H), across multiple stages of CKD (Panel C, E, and G). Model performance was quantitatively evaluated at CKD stage 4/5 (GFR ≤ 30 mL/min) using calculated AFE_A (shown in red) and AFE_P (shown in blue). The observed CL_r are shown in black, the simulated CL_r values using adaptive and proportional model are shown in red and blue, respectively.

TUE-088

Exposure–Response of TAK-906 in Patients with Diabetic or Idiopathic Gastroparesis and Healthy Subjects

Chunlin Chen¹, Cecilia Scimia^{1*}, George Dukes¹, Saurabh Gupta^{1*}; Wenwen Zhang¹, Mukker, Jatinder¹, Cristina Almansa¹, William S. Denney²

¹ Takeda Pharmaceuticals International Co., Cambridge, MA, USA; ² Human Predictions, Cambridge, MA, USA;

*At the time of the study

Objectives: TAK-906 is a novel oral D₂/D₃ receptor antagonist currently under development for chronic treatment of moderate to severe diabetic and idiopathic gastroparesis (GP). The objective of this analysis was to characterize exposure–response (E-R) relationships for prolactin (pharmacodynamic engagement marker) and relevant exploratory endpoints (gastroparesis symptoms) assessed via American Neurogastroenterology and Motility Society Gastroparesis Cardinal Symptom Index-Daily Diary (ANMS-GCSI-DD).

Methods: This analysis was based on data from first-in-human (FIH) study in healthy volunteers (N=72) and proof of concept (POC) study in subjects with GP (N=51). In the FIH study, participants received doses between 5-300 mg or placebo in single-ascending dose phase, and b.i.d dosing of (50 or 100 mg) or placebo on Days 1-4 followed by single dose on Day 5 in multiple-ascending dose phase. In the POC study, participants (N=12-14/cohort) received TAK-906 (5, 25 or 100 mg) or placebo for 9 consecutive days. Prolactin was assessed at baseline, following a single dose, and after 7 days dosing in subjects with GP. Effect of TAK-906 on GP symptoms (nausea, postprandial fullness, early satiety and abdominal pain) was assessed via ANMS-GCSI-DD prior to Day 1 and continued daily throughout the trial.

Exposure-prolactin model was based on combined data from FIH and POC studies without placebo arm and using ‘nlme’ package (version 3.1-137) in R (version 3.5.1). Exposure-nausea model was based on data from subjects with GP including placebo arm and using ‘rstan’ package (version 2.18.2) in R (version 3.5.1). Nausea was exploratory endpoint with most relevant effect and therefore selected for the E-R analysis. Models were selected by a combination of biological plausibility and goodness of fit.

Results: Exposure-prolactin model was a mixed-effects E_{max} model with hill slope, a different E₀ by disease, diurnal variation in baseline, a different E_{max} by sex, and a different residual error by disease. Residual error was log-normally distributed. Indirect effect models with and without a precursor pool were also tested. Female prolactin E_{max} was 117.1 ng/mL and male prolactin E_{max} was 59.32 ng/mL, respectively.

ANMS-GCSI-DD nausea model was an ordered logistic model with linear effect of baseline, linear placebo effect by time after dose, and baseline-adjusted E_{max} effect of PopPK estimated AUC on nausea score (0 to 4 scale). The maximum effect depended on baseline severity, and from a baseline of 3.5 points, the estimated placebo-adjusted change from baseline in the ANMS-GCSI-DD nausea score was approximately 1 point. Visual predictive checks suggest very severe category is underpredicted in favor of less severe categories, but E-R profile appears to be reasonably captured.

Conclusions: TAK-906 increases prolactin levels with an E_{max} trend, suggesting maximal receptor antagonism had been achieved. The analyses indicate TAK-906 appears to improve ANMS-GCSI-DD nausea symptom score more than placebo over time.

TUE-089

Population Exposure Response Analysis of Evinacumab in Patient with Homozygous Familial Hypercholesterolemia Using an Indirect Response Model to Predict Low-Density Lipoprotein Cholesterol Lowering

Xia Pu, Feng Yang, Yi Zhang, Hong Yan, John D. Davis, Nidal Huniti

Regeneron Pharmaceuticals, Inc., Tarrytown, NY, USA

Objectives:

Evinacumab, a human monoclonal antibody against Angiopoietin-like protein 3 (AngPTL3), significantly lowers low-density lipoprotein cholesterol (LDL-C) levels. This analysis aimed to develop and qualify a population exposure response model for evinacumab in patient with homozygous familial hypercholesterolemia(HoFH), using pooled patient data obtained from three phase II/III clinical trials. This model was used to provide supporting evidence for dose selection.

Methods:

The exposure response (ER) analysis was performed sequentially where individual evinacumab concentrations were predicted using a population pharmacokinetic model. Data from one phase-II and two phase-III studies ($n=95$ HoFH patients) were used to develop indirect response model, parameterized with decreasing LDL-C production, to relate evinacumab concentrations to LDL-C values. The model was parameterized with a zero-order rate constant for production of LDL-C (K_{in}), the maximum drug-induced inhibitory effect (I_{max}), and the evinacumab concentration inducing 50% of I_{max} (IC_{50}). Covariates were selected based on clinical relevance and biological plausibility and tested using a stepwise approach. Post-hoc prediction was performed to calculate the LDL-C reduction on week 24 of the patients included in the analysis.

Results:

The population ER analysis allowed the characterization of the time course of LDL-C levels in HoFH and estimation of individual LDL-C levels and derived pharmacodynamic parameters (the percentage change of LDL-C from baseline at week 24). The final PopPK/PD model included two covariates on I_{max} , one on IC_{50} . A smaller IC_{50} was observed in patients with a higher baseline LDL-C, suggesting greater sensitivity to treatment. An increase in potential maximum effect (I_{max}) was observed in patients who are white and/or have a lower baseline weight. Compared to the base model, the inclusion of the covariates reduced parameter variability (CV%) of I_{max} and IC_{50} by 0.3% and 14.4%, respectively. The predicted percentage of patients reaching LDL-C reduction are close to the observed values reported in pivotal trial, confirming the model performance.

Conclusions:

This model adequately characterized of the population pharmacokinetic/pharmacodynamic properties of evinacumab in its target population and the estimation of individual LDL-C levels, to assist in dose selections of evinacumab.

TUE-090

Population Pharmacokinetic/Pharmacodynamic (PK/PD) Modeling of the Effect of Abrocitinib on QT Intervals in Healthy Volunteers

Authors: Xiaoxing Wang¹, Pankaj Gupta², Saleem Ashley Farooqui³, Vu H. Le¹, Jessica Wojciechowski¹, Bimal K. Malhotra², Timothy Nicholas¹

Institutions: ¹Pfizer Inc., Groton, CT, USA; ²Pfizer Inc., New York, NY, USA; ³Pfizer R & D UK Ltd., Sandwich, UK

Objectives: Abrocitinib is a selective Janus kinase-1 enzyme inhibitor in development for the treatment of moderate-to-severe atopic dermatitis (AD). The objectives of this study were to assess the relationship between plasma concentrations of abrocitinib and two electrocardiogram-related measures: heart rate-corrected QT (QTc) and heart rate (HR); and to investigate the effect of abrocitinib on QTc and HR at the supra-therapeutic concentration in atopic dermatitis (AD) patients.

Methods: The study enrolled 36 healthy volunteers into 3 crossover treatments: single doses of abrocitinib 600 mg, placebo, and moxifloxacin 400 mg. The relationship between change from baseline in Fridericia-corrected QTc (ΔQTcF) values and abrocitinib plasma concentrations was explored graphically and modeled using a pre-specified linear mixed effects model.¹ The two-sided 90% confidence interval (CI) for time-matched placebo-corrected ΔQTcF ($\Delta\Delta\text{QTcF}$) was calculated from the model parameter estimates. The upper end of the 90% CI at the supra-therapeutic concentration in AD patients was used to assess whether the QTc prolongation exceeded the regulatory threshold level (10 milliseconds [ms]).¹ As abrocitinib is eliminated primarily by CYP2C19/2C9/3A4 metabolism, the supra-therapeutic concentration was estimated from the predicted maximum plasma concentration (C_{\max}) for AD patients using a population PK model, multiplied by the increase in C_{\max} observed in the drug-drug interaction study with fluconazole (a potent CYP2C19, moderate CYP2C9, and CYP3A inhibitor). The same procedure was followed to derive predictions of time-matched placebo-corrected change from baseline in HR ($\Delta\Delta\text{HR}$) with 90% CI at this concentration.

Results: The model-predicted 90% CI of the mean $\Delta\Delta\text{QTcF}$ for the supra-therapeutic concentration in AD patients (2156 ng/mL) was 6.00 (4.52, 7.49) ms. The mean $\Delta\Delta\text{HR}$ (90% CI) at the supra-therapeutic concentration in AD patients was 6.51 (5.23, 7.80) beats per minute (bpm). Graphical assessments showed no apparent hysteresis and no apparent nonlinear relationship between the PK profile and QTcF. In the concentration-QTc analysis, a statistically significant slope (90% CI) was estimated (0.0026 [0.0018, 0.0035] ms/[ng/mL]) indicating an effect of abrocitinib concentrations on ΔQTcF . Similarly, abrocitinib was found to have a positive effect on ΔHR with statistically significant slope (0.0031 bpm/[ng/mL] with 90% CI of [0.0024, 0.0038]).

Conclusions: At the predicted supra-therapeutic concentration of abrocitinib in AD patients, there was no clinically relevant effect on QTc interval; the upper bound of the 90% CI of predicted $\Delta\Delta\text{QTcF}$ was less than 10 ms. In addition, there was no clinically relevant effect of abrocitinib on $\Delta\Delta\text{HR}$. The concentration-QTc/HR modeling demonstrated that QTc interval and HR increased with increasing abrocitinib concentration after administration of a single dose of abrocitinib 600 mg.

References:

1. Food and Drug Administration. Guidance for Industry: E14 Clinical Evaluation of QT/QTc Interval Prolongation and Proarrhythmic Potential for Non-Antiarrhythmic Drugs. <https://www.fda.gov/media/71372/download>. Published October 2005.

TUE-091

Model Based Pharmacometric Analyses of Nivolumab and Ipilimumab Combination in Chinese Patients with Previously Treated Advanced Solid Tumors including Microsatellite Instability-High Colorectal Cancer

Yali Liang^{1*}, Pradeep Vuppala^{1*}, Amol Tendolkar^{1*}, Sunney Li¹, Heidi Wang¹, Joyce Xu², Akintunde Bello¹, Amit Roy¹, and Jennifer Sheng¹

¹Bristol-Myers Squibb, Princeton, NJ, USA; ²Bristol-Myers Squibb China, Shanghai, China

*Co-leading authors

Objectives: Nivolumab, in combination with ipilimumab, is indicated for the treatment of multiple tumor types in the US, EU, and other countries, but combination therapy is not yet approved in China. With ongoing regulatory reforms, the China National Medical Products Administration requires the assessment of a product's "ethnic sensitivity", through evaluating pharmacokinetics (PK), pharmacodynamics, safety and efficacy outcomes that can be potentially influenced by ethnic factors following the principles of ICH E5 and E17. Nivolumab, as a single agent, is not ethnically sensitive in Chinese, non-Chinese Asian and non-Asian patients¹. This work presents the pharmacometric analyses of ipilimumab monotherapy and nivolumab and ipilimumab combination therapy in Chinese patients including colorectal cancer (MSI-H CRC).

Methods: Non-compartmental analysis (NCA) was performed using data from a Chinese Phase 1 safety/PK study for nivolumab and ipilimumab combination treatment in solid tumors including MSI-H CRC. Population PK (PPK) analyses were conducted using data from 12 and 15 clinical studies of nivolumab and ipilimumab, respectively. The PPK models were developed by re-estimating parameters of previously developed models and then incorporation of additional covariates to assess the magnitude of covariate effects on model parameters. PPK model evaluation was performed using prediction corrected visual predictive checks.

Results: The PK parameters Cmax and AUC(TAU) derived by NCA exhibited a logical rank order in terms of magnitude for nivolumab and ipilimumab (Nivolumab 3 mg/kg Q2W > 3 mg/kg Q3W > 1 mg/kg Q2W and ipilimumab 3 mg/kg Q3W > 1 mg/kg Q3W > 1 mg/kg Q6W). The PK of nivolumab or ipilimumab was well described by a linear two-compartment model with time-varying clearance (CL) that decreased with time. The PK of nivolumab and ipilimumab when administered in combination were similar to that seen with monotherapy in Chinese subjects. Nivolumab exposures in Asian subjects were similar to those in non-Asian subjects with MSI-H CRC treated with combination therapy. Nivolumab exposures with 3 mg/kg Q2W, 240 mg Q2W or 480 mg Q4W dose, during the maintenance phase of combination treatment for CRC, were maintained below the corresponding exposures observed with the well tolerated 10 mg/kg Q2W dosage. Ipilimumab exposures were marginally ($\leq 22\%$) lower in Chinese subjects as compared to non-Asian subjects for combination therapy, which is not expected to be clinically relevant.

Conclusions: Neither nivolumab nor ipilimumab showed ethnic sensitivity with regards to PK when administered in combination, between Chinese, non-Chinese Asian and non-Asian MSI-H CRC patients. Ipilimumab, as monotherapy, is ethnically insensitive in Chinese, non-Chinese Asian and non-Asian patients.

References:

1. Zhang J, Cai J, Bello A, Roy A, Sheng J. Model-Based Population Pharmacokinetic Analysis of Nivolumab in Chinese Patients With Previously Treated Advanced Solid Tumors, Including Non-Small Cell Lung Cancer. *J Clin Pharmacol*. 2019 Oct;59(10):1415-1424.

TUE-092

Model-based Cellular Kinetic Analysis of Chimeric Antigen Receptor-T Cells in Humans

Can Liu¹, Vivaswath S. Ayyar², Xirong Zheng², Wenbo Chen², Songmao Zheng², Hardik Mody², Weirong Wang³, Donald Heald², Aman P. Singh^{2*}, Yanguang Cao^{1,4*}

¹Division of Pharmacotherapy and Experimental Therapeutics, School of Pharmacy, University of North Carolina at Chapel Hill, NC 27599, USA; ²Discovery and Translational Research, Biologics Development Sciences, Janssen Biotherapeutics, Spring House, PA, USA; ³Clinical Pharmacology and Pharmacometrics, Janssen Research & Development, Spring House, PA, USA; ⁴Lineberger Comprehensive Cancer Center, School of Medicine, University of North Carolina at Chapel Hill, Chapel Hill, NC 27599, USA

Objectives: Chimeric antigen receptor (CAR)-T cell therapy has achieved considerable success in treating B-cell hematologic malignancies. However, the challenges of extending CAR-T therapy to other tumor types, particularly solid tumors, remain appreciable. The cellular kinetics of CAR-T may correlate with patient responses, but which factors determine CAR-T cellular kinetics remain poorly defined. Herein, we developed a cellular kinetic model to retrospectively characterize CAR-T kinetics and systematically compared CAR-T kinetics across patient populations and tumor types.

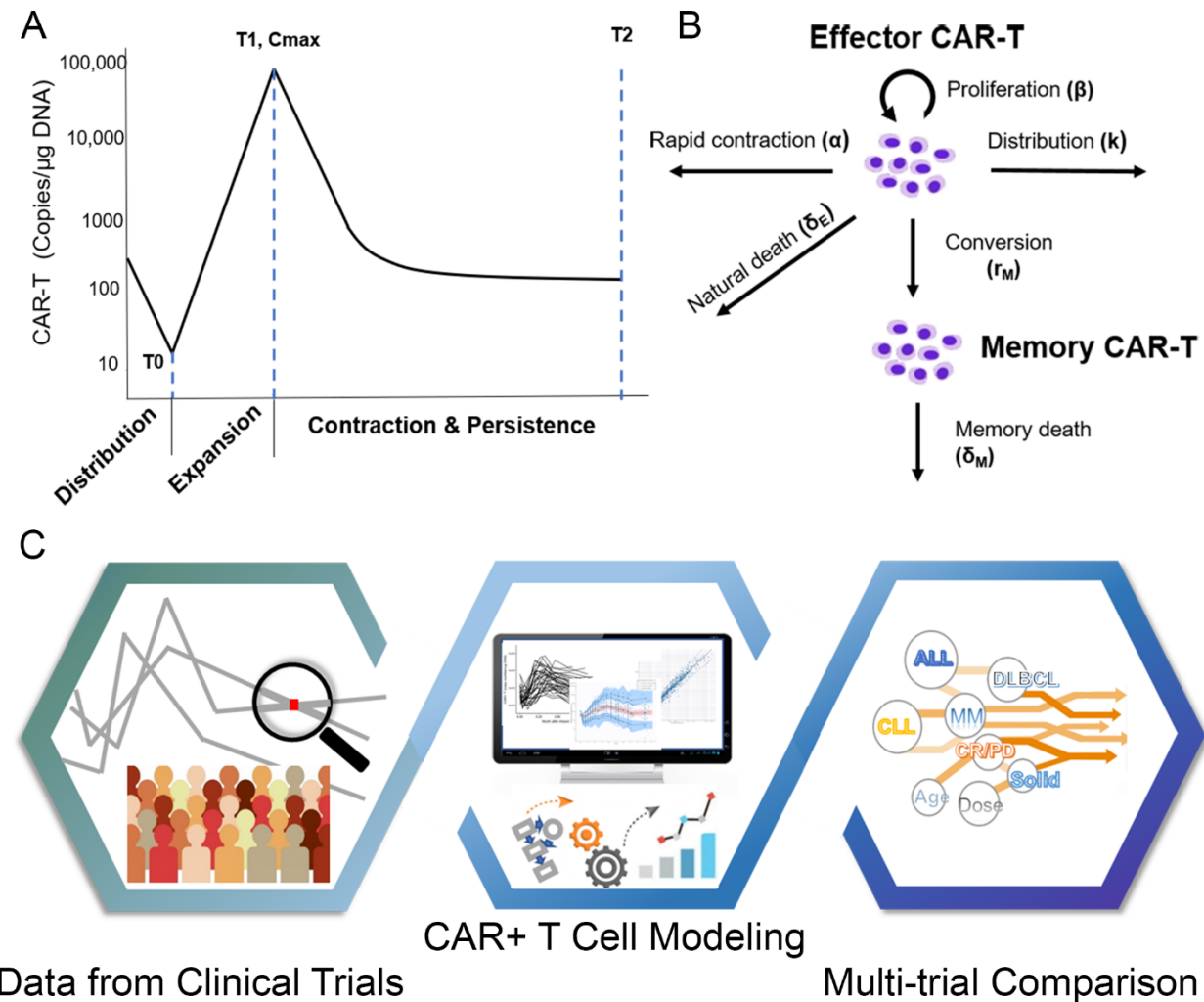
Methods: An empirical cellular kinetics model was developed to capture multiphasic CAR-T cellular kinetics (distribution, expansion, contraction, and persistence) in 218 patients from 7 trials. Cellular kinetic parameters were further taken to evaluate substantial variabilities in CAR-T cellular kinetics across CAR-T products, dosing regimens, patient responses, disease types, tumor burdens, and lymphodepletion conditions.

Results: Based on our analysis, CAR-T cells exhibited a significantly higher cell proliferation rate constant and capacity but a lower contraction rate constant in patients who responded to treatment. CAR-T cells showed higher proliferate potential and lower contraction rate constant in hematologic malignancies than in solid tumors. The pre-infusion CD4:CD8 ratio in CAR-T product and lymphodepletion conditions showed a certain degree of influence on CAR-T cellular kinetics and patient response. Within the assessed dose ranges (10^7 – 10^9 cells), CAR-T doses were weakly correlated with CAR-T cellular kinetics and patient response status, suggesting steep dose-response curves.

Conclusions: The developed CAR-T cellular kinetic model adequately characterized the multiphasic CAR-T cellular kinetics and supported systematic evaluations of the potentially influencing factors, which can have significant implications for the development of more effective CAR-T therapies.

Figure 1.

Model structure for CAR-T cellular kinetics and schematic diagram of three-step workflow for modeling and analysis.



TUE-094

Population Pharmacokinetic/Pharmacodynamic (Pop PK/PD) Modeling of Dupilumab on Nasal Polyps Score (NPS) in Patients with Chronic Rhinosinusitis with Nasal Polypsis (CRSwNP)

Yue Gao¹, Zhicheng Qian^{1*}, Christine Xu¹, John D. Davis², Vanaja Kanamaluru¹, Qiang Lu¹

¹Sanofi, Bridgewater, NJ; ²Regeneron Pharmaceuticals, Inc., Tarrytown, NY; USA

*Affiliation at time of study

Objectives: Dupilumab is a fully human, VelocImmune-derived monoclonal antibody, that binds to the shared receptor component for interleukin (IL)-4 and IL-13, cytokines that are key drivers of type 2 inflammatory diseases. The binding of dupilumab to human IL-4 receptor alpha (IL-4R α) results in blockade of the functions of IL-4 and IL-13 signal transduction. Dupilumab is approved for subcutaneous (SC) treatment of adult patients with CRSwNP as well as patients aged 12 years and older with moderate-to-severe atopic dermatitis or with moderate-to-severe asthma. This analysis aimed to develop a Pop PK/PD model to characterize the relationship between dupilumab exposure and time course of NPS response, and to identify intrinsic and/or extrinsic factors significantly contributing to NPS response variability in CRSwNP patients.

Methods: The Pop PK/PD model was developed using data pooled from one phase 2 study (NCT01920893) and two phase 3 studies (NCT02912468 and NCT02898454) in CRSwNP patients who received SC dupilumab 300 mg every week, 300 mg every two weeks, or 300 mg every two weeks for 24 weeks followed by 300 mg every four weeks. Estimated individual PK parameters from a previously published Pop PK model^[1] were used to simulate PK exposure to drive NPS inhibition in an indirect response model. Demographic variables, baseline disease characteristics, type 2 inflammation biomarkers, immunogenicity and asthma history were tested as covariates by forward selection and backward elimination. The model was validated with visual predictive check and bootstrap.

Results: The Pop PK/PD dataset included 5357 NPS observations from 777 CRSwNP patients (N=312 treated with placebo, N=465 treated with dupilumab). The placebo effect for NPS was found to be minimal (mean observed NPS change from baseline at end of treatment was < \pm 5%) and was not included in this Pop PK/PD model. Baseline age and nasal congestion (NC) were identified to have statistically significant influence on NPS response variability in covariate analysis, but not deemed to be clinically relevant based on simulations. None of the other tested covariates, including body weight, gender, race, region, baseline type 2 inflammation biomarkers and anti-drug antibodies, were statistically significant. Concomitant use of common nasal polypsis medication (systemic corticosteroids) and other comorbidities (asthma history, exacerbated respiratory disease history and allergic rhinitis history) did not show effect on NPS response based on covariate or post-hoc analysis.

Conclusions: The NPS response over time in CRSwNP patients treated with dupilumab was well characterized by an indirect response model. Baseline age and NC were identified as statistically significant, but not clinically relevant, covariates on dupilumab treatment effect in CRSwNP patients.

References:

- [1] Gao Y, Xu C, Davis JD, Kanamaluru V, Lu Q. Population pharmacokinetic analysis of dupilumab in adult patients with chronic rhinosinusitis with nasal polypsis. ACOP10, Orlando, FL, ISSN:2688-3953, 2019, Vol 1.

Acknowledgments:

Research sponsored by Sanofi and Regeneron Pharmaceuticals, Inc. ClinicalTrials.gov Identifiers: NCT01920893, NCT02912468 and NCT02898454.

Disclosures:

Gao Y, Xu C, Kanamaluru V, and Lu Q: Sanofi - employees. may hold stock and/or stock options in the company of Sanofi.

Qian Z: Sanofi - employees at time of study. have nothing to disclose.

Davis JD: Regeneron Pharmaceuticals. Inc. - employee and shareholder.

TUE-095

A novel webtool, MTXPK.org, uses a three-compartment high-dose methotrexate population pharmacokinetic model to inform glucarpidase use

Authors:

Zachary L. Taylor^{1,2,3}, Tomoyuki Mizuno^{3,4}, Nieko C. Punt⁵, Balaji Baskaran⁶, Adriana Navarro Sainz⁶, William Shuman⁶, Nicholas Felicelli⁶, Alexander A. Vinks^{2,3,4}, Jesper Heldrup⁷, Laura B. Ramsey^{2,3,4}

Affiliations:

¹ Department of Molecular, Cellular, and Biochemical Pharmacology, University of Cincinnati, Cincinnati, OH

² Division of Research in Patient Services, Cincinnati Children's Hospital Medical Center, Cincinnati, OH

³ Division of Clinical Pharmacology, Cincinnati Children's Hospital Medical Center, Cincinnati, OH

⁴ Department of Pediatrics, University of Cincinnati, Cincinnati, OH

⁵ Medimatics, Maastricht, The Netherlands

⁶ Division of Biomedical Informatics, Cincinnati Children's Hospital Medical Center, Cincinnati, OH

⁷ Department of Pediatrics Oncology, Lund University Hospital, Lund, Sweden

Objective:

There is significant inter-patient pharmacokinetic (PK) variability associated with high-dose methotrexate (MTX). Patients who experience delayed renal elimination are at an increased risk for severe nephrotoxicity. Glucarpidase is a lifesaving rescue agent for these patients, but determining the appropriate administration is difficult due to challenges interpreting the labeled indication and consensus guideline. The objective of our study was to create a web-based clinical decision support tool, MTXPK.org, that uses real-time drug concentrations and Bayesian estimation to facilitate model-informed post-infusion care and use of glucarpidase for patients receiving HD MTX.

Methods:

A population pharmacokinetic (PK) model was developed using 31,717 MTX plasma concentrations obtained from 772 pediatric patients with acute lymphoblastic leukemia receiving HD MTX on Nordic Society of Hematology and Oncology protocols. Two- and three-compartment structural models with first-order conditional estimation were explored with demographic and laboratory data being evaluated as potential covariates to predict clearance. Model preference and covariate inclusion were based off a change in objective function value (OFV) > 3.54. The final population PK model was validated on two external datasets with diverse age range, indication, and dosing schedules prior to its integration into MTXPK.org. A module for Bayesian estimation is included in the MTXPK.org platform. The Edsim++ model designer compatible PK-engine runtime enables the Bayesian estimation of individual PK parameters.

Results:

The default population PK model for MTXPK.org is a three-compartment structural model since it significantly improved the description of the data ($\Delta OFV = -6,136.43$, $p < 0.001$) and the population prediction performance compared to the two-compartment structural model (R^2 : 0.83 vs. 0.63, respectively, $p < 0.001$). Body surface area and serum creatinine were significant covariates and included in the final model. MTXPK.org uses these model parameters as prior knowledge for a posteriori Bayesian estimation of a patient's elimination profile, which is generated once the user enters the patient's demographics, dose administered, infusion duration, MTX concentrations, and serum creatinine levels into the tool. Then, MTXPK.org plots the profile along with the population's average concentration-time curve and associated ± 2 standard deviation, which illustrates the labeled indication of glucarpidase, and glucarpidase guideline thresholds at 24, 36, 42, and 48 hours. The visual and numerical information generated by the tool provides feedback of a patient's MTX clearance and can be used to inform post-infusion care and use of glucarpidase. MTXPK.org went live in December 2019; since then, the webtool has been used by >900 unique users in at least 35 countries.

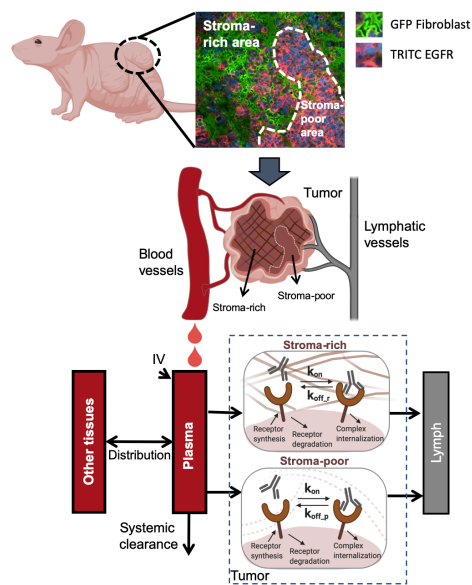
Conclusions:

MTXPK.org is a free, web-based clinical decision support tool that uses a patient's demographics and real-time drug concentrations to provide model-informed post-infusion care and use of glucarpidase. This tool has the capability to improve patient outcomes for all patients receiving high-dose MTX treatment.

Modeling the dynamics of antibody-target binding in living tumors

Yu Tang¹, Yanguang Cao¹ #

Division of Pharmacotherapy and Experimental Therapeutics, UNC Eshelman School of Pharmacy, University of North Carolina at Chapel Hill, Chapel Hill, North Carolina. 27599, United States



Objectives: Antibody binding to its target is the first and most critical step for the treatment efficacy. However, our understanding of their binding dynamics in living tumors remained limited. We had developed a bioluminescence resonance energy transfer (BRET) imaging approach that directly supports the measurement of the antibody-target engagement in the native tumor environment. In the present study, we developed a spatially resolved computational model to analyze the BRET imaging data and then explore the mechanisms of a biphasic binding dynamics between a model antibody cetuximab and its target epidermal growth factor receptor (EGFR) in living xenograft tumors.

Methods: A sequential modeling strategy was implemented in which the pharmacokinetic model was first optimized against plasma data and then fixed during the second step of tumor binding characterization. In the spatially resolved mathematical model, the tumor was conceptually dissected into two anatomical compartments: a stroma-rich and a stroma-poor area, to account for the spatial histological heterogeneity. Two competing hypotheses were tested to evaluate which one makes more consistent predictions to the observed binding data: (1) the antibodies bind to the targets differentially across two tumor areas (the heterogeneous binding model, HBM) and (2) the antibodies are distributed differentially into two tumor areas, but with the same binding profile (the heterogeneous distribution model, HDM).

Results: Compared to the heterogeneous antibody distribution model (HDM), the heterogeneous binding (HBM) better explained the biphasic and dose-shifted binding dynamics of cetuximab-EGFR in the living tumors. The antibody bound differently to its target in the stroma-rich areas than in the stroma-poor regions. Antibodies had a much slower dissociation rate in the stroma-rich areas, which was confirmed by immunofluorescence staining. We also observed that cetuximab bound to EGFR to a “slower-but-tighter” degree in living tumors in comparison to *in vitro*, demonstrated by a significantly slower association rate (k_{on}) and a disassociation rate (k_{off}) compared to the surface plasma resonance measurements.

Conclusions: We demonstrated the spatial heterogeneity in antibody-binding dynamics in living tumors. These findings improve our understanding of the complex antibody targeting process and should aid in the design of antibodies that show more favorable targeting properties (NIH: GM119661).

WED-001

Mechanistic mathematical model to optimize drug delivery via intratumoral injection

Abed E. Alnaif¹, Frederic J. Reu¹, Craig J. Thalhauser^{1,2}, Brian J. Schmidt¹, Yash Gandhi¹, George T. Currier³, Mark S. Howansky³, Tarek A. Leil¹

¹Bristol-Myers Squibb, Princeton, NJ, USA. ²Genmab U.S., Princeton, NJ, USA. ³Bristol-Myers Squibb, Princeton, NJ, USA.

Objectives: Intratumoral (I-TUMOR) injection is thought to enable effective delivery of drug to the site of action while limiting risk related to systemic exposure. However, although I-TUMOR injection is currently being employed in several clinical trials [1], and even in an approved therapy [2], little experimental work has been done to optimize the parameters of I-TUMOR injection in terms of amount of drug delivered to the tumor. Furthermore, commonly used mouse experimental models are of questionable relevance to addressing this problem given the substantial differences in biomechanical properties of tumors, and examination of tumor pharmacokinetics in humans is technically highly challenging and therefore not part of standard clinical development in studies that administer small molecules intratumorally. Given these obstacles to characterizing I-TUMOR injection experimentally, we developed a mechanistic mathematical model in an effort to understand and predict how various I-TUMOR injection parameters may affect the success of drug delivery.

Methods: Unsuccessful I-TUMOR injections provide minimal tumor drug exposure due to the drug flowing out from the tumor along the injection tract. Thus, we modeled this as an expandable, leaky annular “pipe”, whereby the loss of drug occurs by flowing out along the annular space between the needle and tumor (the injection tract; Figure 1). This was modeled according to a partial differential equation (PDE) model in which the pressure of the drug can expand the annular space (by compressing the tumor), and in which leakage of the drug into the tumor can happen across the outer surface of the injection tract. This leakage of the drug into the tumor is what we sought to maximize, as it represents delivery of the drug into the tumor.

Results: We used the model to understand and predict the effects of various injection parameters on the efficacy of drug delivery. Specifically, the model was used to predict the impacts on drug delivery of varying both tumor-specific

(tumor malleability, tumor hydraulic conductivity, and intratumoral pressure) and needle/drug-specific (injection speed, needle penetration depth, needle diameter, needle opening configuration, and drug viscosity) parameters.

Conclusions: Using this platform, we predicted the influence of various parameters on the efficacy of drug delivery via I-TUMOR injection. Several of the model's predictions went against the intuition we had at the start of this exercise, which has prompted the development of experiments to validate the model. If experiments validate the model, it may allow tailoring I-TUMOR injection methods to achieve maximum drug delivery in human tumors.

References:

1. Marabelle, A et al. Ann Oncol. 2018 Nov; 29(11): 2163–2174.
2. Conry, RM er al. Hum Vaccin Immunother. 2018; 14(4): 839–846.

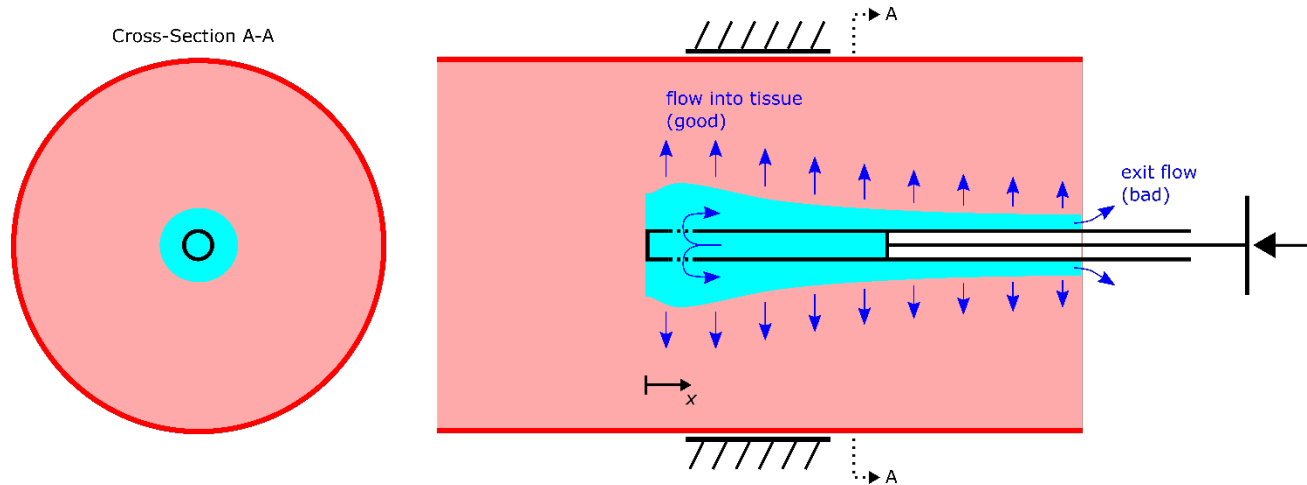


Figure 1: Diagram of the model of drug delivery via I-TUMOR injection, illustrating the undesirable loss of injectate along the annular space formed by the injection tract.

WED-003

PKPD Exploratory Graphics (xGx) Cheat Sheet

Alison Margolskee¹, Fariba Khanshan¹, Andrew Stein¹, Camille Vong², Yu-Yun Ho³ and Michael Looby²

¹Novartis Institutes for Biomedical Research, Cambridge, MA, USA; ²Novartis Pharmaceutical Company, Basel, Switzerland; ³Novartis Pharmaceutical Company, East Hanover, NJ, USA

Objectives:

Checklists are useful tools not only for beginners, but also for experts in any field. As John D. Cook stated: “We resist checklists because they insult our intelligence, and yet they greatly reduce errors. Experienced people in every field can skip a step, most likely a simple step, without some structure to help them keep track.”

(<https://www.johndcook.com/blog/2019/12/03/distracted/>)

As pharmacometrists, we sometimes jump into complex modeling before thoroughly exploring our data. Exploratory plots help uncover issues with data, useful insights, or aspects to explore further, and can sometimes answer questions without the need for complex models.

To help pharmacometrists remember the key steps in exploring PKPD data, we created the PKPD Exploratory Graphics (xGx) Cheat Sheet

([https://opensource.nibr.com/xgx/Resources/PKPD_Exploratory_Graphics_\(xGx\)_Cheat_Sheet.pdf](https://opensource.nibr.com/xgx/Resources/PKPD_Exploratory_Graphics_(xGx)_Cheat_Sheet.pdf)) a 1-page (front and back) question-based reference sheet, designed around the principles from the Exploratory Graphics (xGx) tool, an open-source R-based tool available on GitHub (<https://opensource.nibr.com/xgx/>)

Methods: The key steps in dose-exposure-response exploration were organized by structured PK, PD, and PKPD exploration. Key questions and example graphs were created to accompany each step. Guiding Principles from xGx were simplified and organized into Technical Considerations. Commonly used functions from the xgxr package were compiled along with brief descriptions of their usage. Finally, a high-level checklist was written to summarize the key steps in PKPD data exploration. All of these components were streamlined and optimized to fit into a 1-page cheat sheet.

Results:

Key steps in PKPD exploration include:

- Identify data type and choose appropriate graph types (PD)
- Identify axis scale that reflects distribution of data (PK, PD)
- Provide an overview of the data (PK, PD)
- Determine whether data corrections are needed (PD)
- Assess trends over time (PK, PD)
- Assess trends by dose (PD)
- Assess PK linearity (PK)
- Assess extent and sources of variability (PK, PD)
- Get an overview of the relationship between exposure and response (PKPD)
- Explore delays between exposure and response (PKPD)

Technical Considerations include: extent and sources of variability (between vs. within subject, explained vs. unexplained), PD data corrections (e.g. baseline correction), and effective use of scales.

Useful functions include: `xgx_theme()`, `xgx_check_data()`, `xgx_summarize_covariates()`, `xgx_geom_ci()`, `xgx_geom_pi()`, `xgx_scale_y_log10()`, `xgx_scale_y_reverselog10()`, `xgx_scale_y_percentchangelog10()`, `xgx_annotate_status()`, `xgx_annotate_filenames()`, and `xgx_save_table()`.

PKPD Exploratory Graphics (xGx) Cheat Sheet v1.0

<http://opensource.nibr.com/xgx>

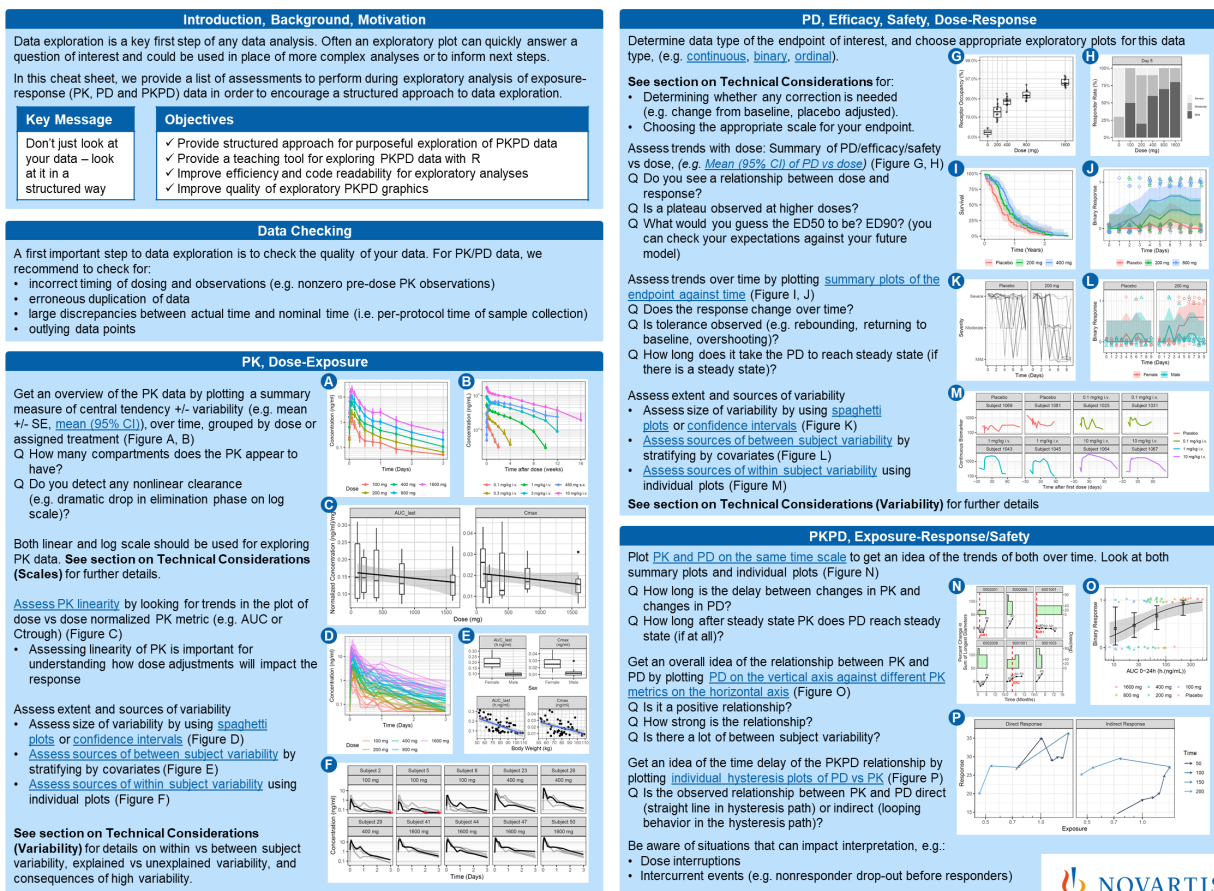


Figure 1: Front page of PKPD Exploratory Graphics (xGx) Cheat Sheet

([https://opensource.nibr.com/xgx/Resources/PKPD_Exploratory_Graphics_\(xGx\)_Cheat_Sheet.pdf](https://opensource.nibr.com/xgx/Resources/PKPD_Exploratory_Graphics_(xGx)_Cheat_Sheet.pdf))

Conclusions: The PKPD Exploratory Graphics (xGx) Cheat Sheet was created to help pharmacometrists follow a structured approach to PKPD data exploration. The key steps to PKPD exploration along with questions and example graphs were compiled into a 1-page reference sheet. The cheat sheet also includes technical considerations, useful functions from the xgxr package, and a high-level checklist. Cheat sheets, similar to checklists, can be useful for people of all levels of experience, from beginners learning PKPD, to experts who can sometimes skip simple but important steps.

The use of PBPK modelling from clinical drug-drug interaction studies with inhibitors and inducers of CYP3A4, CYP2C9 and OATP1B1 for BIIB093 (IV glibenclamide) to support regulatory decision making

Anas M Fathallah¹, Alice Ke², Lilly East³, Himanshu Naik¹ and Eric Masson¹

¹Biogen, Inc., Cambridge, MA, USA. ²SimCYP LTD. Sheffield, UK. ³Previously with Biogen, Inc., Cambridge, MA, USA

Objectives: Construct and verify a PBPK model of BIIB093, an investigational product under development for the treatment and prevention of severe cerebral edema, using published clinical PK data with oral glibenclamide, in house clinical data with BIIB093 as well as *in vitro* data to evaluate DDI potential of BIIB093 *in-silico* with inhibitors/inducers of CYP3A4, CYP2C9 and OATP1B1.

Methods: Literature and inhouse clinical and *in-vitro* data were used in the PBPK model development. The model incorporated a first-order absorption model and hepatic OATP1B1 uptake followed by metabolism split between CYP3A4 and CYP2C9. Due to limitations of scaling of CYP2C9 mediated metabolism from *in vitro* data, the clinical data on the systemic exposure of oral glibenclamide in subjects with differing CYP2C9 polymorphic status was used to estimate fm_{CYP2C9}. A scalar (RAF) for the OATP1B1-mediated hepatic uptake was optimized based on matching the reported IV clearance for glibenclamide. The hepatic OATP1B1 component was subsequently verified against single-dose rifampicin DDI in the literature. The CYP3A4 component was verified against clarithromycin DDI data in the literature. The multiple-dose rifampicin DDI effects were assessed by incorporating the induction of CYP2C9, OATP1B1 and CYP3A4. An intestinal P-gp component was not considered in the model initially, due to reported high bioavailability of the oral formulation (≥ 0.89). The recovery of PK profiles for BIIB093 following various IV dosing regimens was also demonstrated.

The model was prospectively applied to predict the likely outcomes of interaction of BIIB093 with ketoconazole (strong CYP3A4 inhibitor), fluconazole (strong CYP2C9 inhibitor and moderate CYP3A4 inhibitor), rifampicin 600 mg SD (OATP1B1 inhibitor) and QD (CYP3A4/CYP2C9/OATP1B1 inducer) following IV infusion of BIIB093 (3 and 5 mg/day)

Results: The final PBPK model captured the mean AUC and C_{max} ratios of glibenclamide reported in several publication within the criteria described by Guest *et al*¹. The model recovered the PK profiles for BIIB093 from 2 phase I clinical studies in healthy subjects within 0.88 to 1.1-fold. The predicted changes in plasma exposure of BIIB093 during coadministration of single dose rifampicin (strong OATP1B1 inhibitor) and daily rifampicin (CYP3A4/CYP2C9/OATP1B1 inducer) are modest (AUC_r or $C_{max,r}$ $r > 2$ and < 5). Simulations with the strong CYP2C9 inhibitor fluconazole and with the strong CYP3A4 inhibitors predicted weak interactions ($AUC_r \geq 1.25$ and < 2) and ($AUC_r \geq 1.25$ and < 2) respectively.

Conclusions: A PBPK model constructed from literature and inhouse clinical and *in-vitro* data was developed and validated. The approach is supportive of regulatory decision-making and elimination of additional clinical DDI studies.

¹ Guest EJ, et al (2011) Critique of the two-fold measure of prediction success for ratios: application for the assessment of drug-drug interactions. *Drug Metab Dispos* **39**:170-173

WED-005

Population Pharmacokinetic Modeling of Belinostat and its Major Metabolite in Advanced Cancer Patients with varying degrees of Liver Dysfunction

Anitha Suram¹, Naoko Takebe², Alice Chen², Shivaani Kummar³, Richard Piekarz⁴, Brian Kiesel⁵, Nancy Moore¹, James Doroshow³, Jan Beumer⁵, Jogarao Gobburu¹

¹Center for Translational Medicine, School of Pharmacy, University of Maryland, Baltimore, MD, USA; ²Early Clinical Trials Development Program, National Cancer Institute, Bethesda, USA; ³Division of Cancer Treatment and Diagnosis, National Cancer Institute, Bethesda, USA; ⁴Cancer Therapy Evaluation Program, National Cancer Institute, Bethesda, USA; ⁵Cancer Therapeutics Program, UPMC Hillman Cancer Center, Pittsburgh, PA, USA.

Purpose

Belinostat, a second-generation histone deacetylase (HDAC) inhibitor, is an anticancer drug. Belinostat is extensively metabolized by the liver; and a recent phase I pharmacokinetic (PK) safety and tolerability study in patients with declining liver function demonstrated significant differences in belinostat clearance and exposure of its metabolites (Takebe et al., 2018). The aim of this study is to develop a simultaneous population PK model for belinostat and its major metabolite (glucuronide) to delineate the effect of liver dysfunction, and to investigate the sources of variability in the PK parameters.

Methods

Data consisted of 64 advanced cancer patients with normal, mild, moderate, and severe hepatic impairment. A single dose of 400 mg/m² belinostat was administered by IV infusion over 30 minutes. Nonlinear mixed effect modelling of belinostat and glucuronide PK data was conducted using Pumas (www.pumas.ai). FOCEI method was used for the maximum likelihood estimation (MLE). The point estimates, between subject (BSV), and residual variabilities of the PK parameters were estimated. The influence of declining liver dysfunction, body weight, and CRCL (creatinine clearance) on the PK parameters were determined.

Results

A two- compartment model for both belinostat and glucuronide with combined proportional and additive error model best described the data. Belinostat clearance (Cl) was parameterized to formation clearance of glucuronide ($Cl_{pm} = Cl * fm$) and rest clearance $Cl * fr$ ($fr = 1 - fm$). The fraction of parent converted to the metabolite (fm , 65%) was derived from the mass balance study.

Allometric scaling of clearance and volume parameters to body weight (75 kg) significantly improved the model fit ($\Delta OFV = -45$, $p < 0.05$). Liver dysfunction status on Cl_{pm} and CRCL on glucuronide clearance (Cl_{met}) further improved the model fit ($\Delta OFV = -52.4$ and -55.9 , respectively; $p < 0.05$). The cohorts with mild, moderate and severe liver dysfunction demonstrated 5%, 11 %, and 27 % reduction in Cl_{pm} respectively, relative to normal status. The coefficient for the effect of CRCL on Cl_{met} was estimated to be 0.35. Overall, covariates reduced 25% BSV in the clearance of belinostat, 6% BSV in central volume of belinostat and glucuronide, 2% BSV in Cl_{met} . The final parameter estimate of belinostat central volume is 8.6 L/75 kg, total clearance is 56.6 L/hr/75 kg in the normal cohort.

Conclusions

We characterized the PK of belinostat and its major glucuronide metabolite from the data collected in advanced cancer patients and evaluated the effect of liver dysfunction on the metabolic pathway and CRCL on the metabolite clearance. The population PK model proposed can be leveraged to facilitate dosing adjustment in patients with severe liver dysfunction.

Reference

Takebe et al., A phase 1 pharmacokinetic study of belinostat in patients with advanced cancers and varying degrees of liver dysfunction. *Br J Clin Pharmacol*. 2019, 85(11):2499-2511

A META EXPOSURE-RESPONSE ANALYSIS OF TAFENOQUINE IN PATIENTS WITH *PLASMODIUM VIVAX* MALARIA

Ashwin Karanam¹, Nilay Thakkar², Justin Green³, Stephan Duparc⁴, Lionel Tan³, Navin Goyal²

¹Department of Experimental and Clinical Pharmacology, University of Minnesota, MN, USA;

²GlaxoSmithKline, Collegeville, PA, USA; ³GlaxoSmithKline London, UK; ⁴Medicines for Malaria Venture, Geneva, Switzerland

Objectives:

Tafenoquine (TQ) is an anti-malarial for the radical cure (prevention of relapse) of *Plasmodium vivax* (*P. vivax*) malaria in combination with a blood stage antimalarial (chloroquine [CQ]). The goal of these analyses was to characterize the TQ exposure-response (recurrence-free at 6 months) in *P. vivax* malaria patients across 3 clinical trials.

Methods:

Subjects randomized to TQ + CQ and CQ-only arms from three trials (TAF112582 Parts I and II; TAF116564) were included in this analysis. TAF112582 Parts I and II (N = 613) were used as training datasets for model building and TAF116564 (N = 166) as test dataset for model evaluation. Multivariate logistic regression and time to event (TTE) analyses were performed in NONMEM using the Laplace method. Model evaluation was based on multiple criteria and included simulation-based visual predictive checks. A classification and regression tree (CART) analysis was performed to identify key determinants impacting *P. vivax* recurrence.

Results:

Logistic Regression and CART Analysis: TQ AUC and country (Thailand vs Others) were found to be statistically significant ($p < 0.01$) predictors of clinical response based on multivariate logistic regression analyses. After accounting for country, the odds of being recurrence-free at 6 months increased by approximately 44% (95% CI, 28 – 60%) for each 25-unit increase in AUC above the median value of 74 $\mu\text{g}\cdot\text{h}/\text{ml}$. Adequate model performance was established by comparing the predictions against test data outcome (Figure 1). CART analyses identified a breakpoint for AUC (48.35 $\mu\text{g}\cdot\text{h}/\text{ml}$) indicating higher likelihood of being recurrence-free at 6 months in subjects who achieved exposures $>$ the breakpoint AUC as compared to those who did not.

TTE Analysis:

A Weibull distribution hazard model with a delay function adequately described the data. TQ AUC (Emax model) and country (Thailand vs Others) were found to be statistically significant ($p < 0.01$) predictors of time to relapse with a potency estimate (EC50) of 65.3 $\mu\text{g}\cdot\text{h}/\text{ml}$. After accounting for region/country, the risk of relapse at 6 months decreased by 46% (95% CI, 37 – 54%) for every 25 $\mu\text{g}\cdot\text{h}/\text{ml}$ increase in TQ AUC compared to the CQ-only group.

Conclusions:

The results demonstrate that TQ + CQ therapy improves recurrence-free rates at 6 months compared with the subjects with CQ-only therapy. A clinically relevant exposure threshold of TQ AUC of 48.4 $\mu\text{g}\cdot\text{h}/\text{ml}$ was estimated impacting recurrence outcome and was comparable to the previous estimate (56.4 $\mu\text{g}\cdot\text{h}/\text{ml}$) based on analysis of TAF112582 Part I data only. The analyses also identified differences in recurrence rates in Thailand as compared to rest of the world. Tafenoquine exposure is directly related to an improved efficacy outcome and significantly influences the probability of preventing malaria relapse. The model can be employed to perform further clinical trial simulations and predict outcomes under different dosing regimen scenarios.

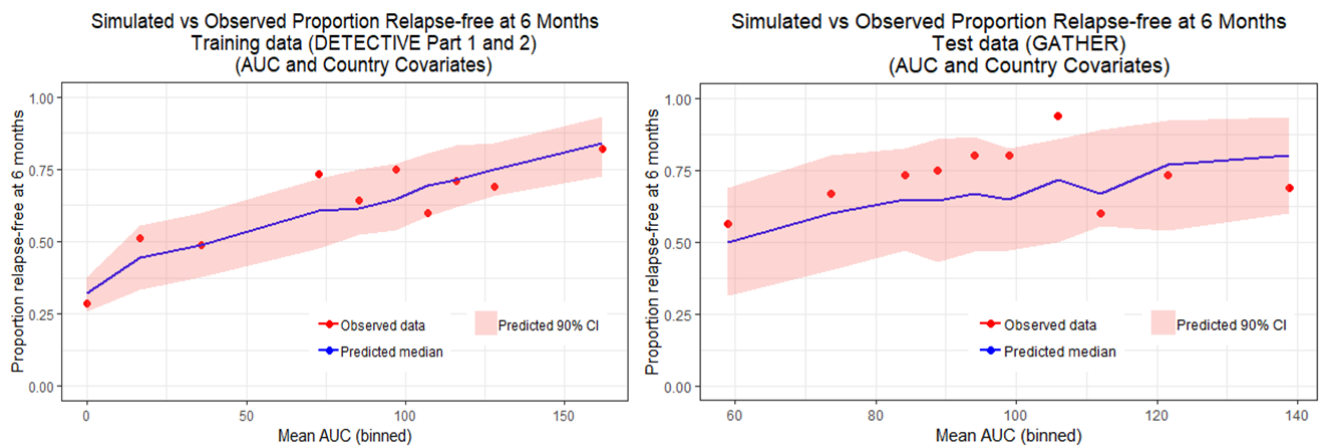


Figure 1: Simulated versus observed proportion of subjects for determining relapse-free status at 6 months

Population pharmacokinetics of R and S methadone in children undergoing major surgery

Authors:

Blessed W. Aruldas^{1,3}, Brian R. Overholser^{1,2}, Sara K. Quinney¹, Andrea R. Masters¹, Christine M. Bach¹, Senthil Sadhasivam¹

Author affiliations:

1. Indiana University School of Medicine, Indianapolis, IN, 2. Purdue University College of Pharmacy, Indianapolis, IN, 3. Christian Medical College, Vellore, India

Objectives:

Methadone is a racemic (50/50 of the R and S enantiomers) synthetic opioid used for postoperative analgesia in addition to its widespread use in opioid abuse disorder. The individual enantiomers vary in their pharmacokinetic and pharmacodynamic properties. The optimal dose required to achieve therapeutic concentrations for effective analgesia in children is not fully known. This study aims to develop pharmacokinetic models of R and S methadone in children undergoing surgery.

Methods:

The study was conducted at Riley Hospital for Children, Indianapolis, IN. A total of 38 children 8 to 17.9 years of age undergoing specific surgeries were recruited after obtaining informed consent. Methadone was given both intravenously in the operating room and orally at a dose of 0.05 to 0.1 mg/kg every 12 hours. Blood samples were collected 6 to 10 times over 3 to 5 inter-dose intervals for each child. R-methadone, S-methadone and AAG (acid alpha glycoprotein) concentrations were measured using liquid chromatography. The pharmacokinetic data were analyzed using a nonlinear mixed effect model approach in NONMEM(v7.4) using FOCE method with interactions. Covariates were graphically explored and were added by a stepwise process. Model qualification was performed using visual predictive check (VPC) and bootstrap.

Results:

The pharmacokinetics of both R and S-methadone were described by two-compartment disposition models with linear elimination and first order absorption. Bodyweight was added allometrically to clearance and volume parameters raised to a fixed exponent of 0.75 and 1 respectively. AAG (alpha-acid-glycoprotein) was identified as a covariate on central volume for both the enantiomers (Δ OFV = 11.5 and 12.4 respectively). The eta and epsilon shrinkages of the final models were low (Table 1). Visual predictive checks were done using 1000 samples generated from the final models showed a good fit with the observed data. A bootstrapping procedure generated with 1000 random samples from the data found parameter estimates to be reliable with acceptable relative standard errors (Table 1).

Table 1.

	R Methadone			S Methadone		
Parameters	Population estimates (%RSE)	%CV for BSV(% RSE)	Shrinkage	Population estimates (%RSE)	%CV for BSV(% RSE)	Shrinkage
KA (hr-1)	0.111 (26.6)	92.5 (0.277)	0.312	0.131 (25.7)	91.7 (0.25)	0.273
CL (L.hr-1)	29.8 (14.7)	60.3 (0.229)	0.2	29.4 (10.3)	54.3 (0.198)	0.148
Vc (L)	234 (18)	85 (0.18)	0.183	219 (16.6)	54.9 (0.328)	0.271
Q (L.hr-1)	110 (20)			74.1 (18.3)		
Vp (L)	348 (21.2)			138 (24.5)		
AAG on Vc	-0.0032 (19.7)			-0.00289 (35.9)		
BMI on Vc	-			-0.0454 (41.9)		
RUV	0.202 (0.122)		0.08	0.206 (16.5)		0.081

Conclusions:

Pharmacokinetic models were successfully created for both R and S methadone in children. AAG and BMI were important covariates describing the volume of central compartment in children. Additional pharmacokinetic/pharmacogenomic/pharmacodynamic modelling is required to personalize and further optimize dosing of methadone for each child.

References (if applicable): NA

WED-010**Simulations of Orally-Administered Ivermectin Utilizing A Minimal Physiologically-Based Pharmacokinetic (mPBPK) Model: Potential COVID-19 Therapeutic Option**

Brian Jermain¹, Patrick Hanafin¹, Carter Cao¹, Gauri Rao¹

¹ Division of Pharmaceutics and Experimental Therapeutics, Eshelman School of Pharmacy, University of North Carolina at Chapel Hill, Chapel Hill, NC 27599, USA

Objectives: Ivermectin has been shown to inhibit SARS-CoV-2 replication *in vitro* with an IC₅₀ value of 1750 ng/mL.¹ SARS-CoV-2 infects the lungs resulting in COVID-19. Hence, concentrations of ivermectin in the lungs help us understand the therapeutic potential of ivermectin against COVID-19. The only FDA-approved formulation of ivermectin for systemic use in humans is an oral tablet. The objective of the study was to utilize a developed mPBPK model to simulate a dosing regimen of oral ivermectin that would achieve lung concentrations above 1750 ng/mL for 50% of the 5-day treatment period.

Methods: Simulations of an orally-administered loading dose (LD) and maintenance dose (MD) were performed in Phoenix® (8.2, Certara) utilizing the mPBPK model developed based on a single-dose pharmacokinetics study of ivermectin.² The duration of time when ivermectin lung concentration were above 1750 ng/mL was assessed. Single dose simulations were performed using the FDA-approved dose for strongyloidiasis (12 mg) and the highest dose shown to be safe in clinical trials (120 mg) as references for assessing the finalized regimen. A 5-day course of treatment was selected to resemble the treatment duration of a clinical trial of remdesivir.³ The 50% time above IC₅₀ cutoff was selected in the absence of standardized pharmacodynamic endpoints for antiviral treatment.

Results:

FDA-approved single dose (12 mg): Lung C_{max} = 59.6 ng/mL, Plasma C_{max} = 29 ng/mL

Highest single dose proven safe in clinical trials (120 mg)⁴: Lung C_{max} = 596 ng/mL, Plasma C_{max} = 289.5 ng/mL

Simulations with a 480 mg LD followed by 180 mg MD every 12 hours resulted in ivermectin lung concentrations above 1,750 ng/mL for 53.2% of the 5-day treatment period. Lung and plasma C_{max} resulting were 2,384.5 ng/mL and 1,158.1 ng/mL respectively; the plasma C_{max} is 4-fold higher than that after a 120 mg single dose.

Conclusions: Orally-administered ivermectin as monotherapy is likely not ideal for COVID-19 treatment given the high plasma concentrations required to achieve sufficient lung concentrations. The 480 mg LD followed by 180 mg MD every 12 hours results in consistently high ivermectin plasma concentrations which may cause central nervous system toxicity.⁴ Additionally, ivermectin is a lipophilic drug with a long half-life (~24 hours) which may potentiate the risk of this adverse effect. Reformulating ivermectin for inhalational delivery should be considered as this may achieve adequate concentrations in the lung while minimizing its systemic uptake and related adverse effects.

References:

¹Caly et al. *Antiviral Res.* 2020.

²El-Tahtawy et al. *PLoS Neglected Tropical Diseases.* 2008

³ClinicalTrials.gov Identifier: NCT04292899

⁴Guzo et al. *J Clin Pharmacol.* 2002.

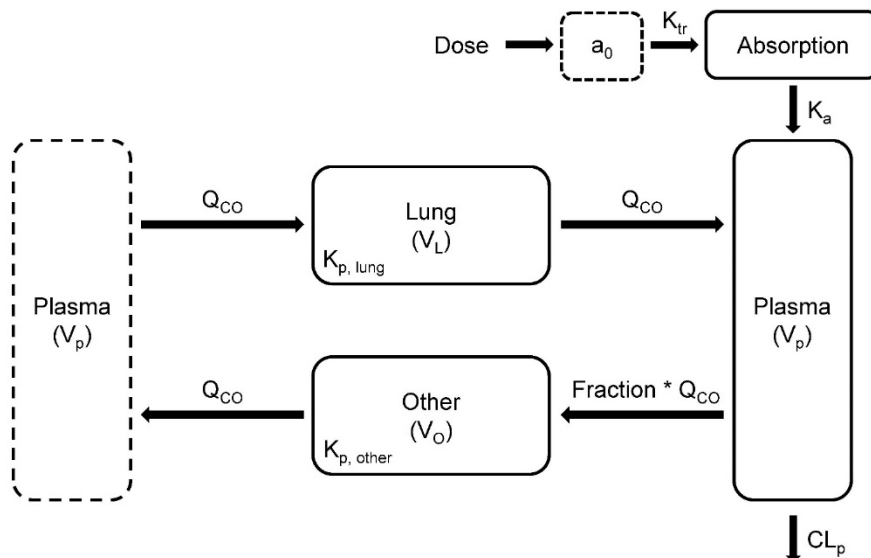


Figure 1: Schematic of the developed mPBPK model for ivermectin following oral dose administration in humans. The plasma compartment (dashed line) on the left is identical to the plasma compartment on the right. The mPBPK model comprises two tissue compartments that represent the entire body (lung and other) along with the plasma compartment. The delay following oral dosing is described by a transit compartment (a_0) with transit rate K_{tr} ; absorption rate K_a ; cardiac output, Q_{CO} ; lung partition coefficient, $K_{p,lung}$; fraction of cardiac output, Fraction; tissue partition coefficient, $K_{p,other}$; plasma clearance, CL_p

WED-011

**EXPOSURE-RESPONSE MODEL TO DESCRIBE THE RELATIONSHIP BETWEEN
BARICITINIB AND THE TEMPORAL RESPONSE PROFILES IN SYSTEMIC LUPUS
ERYTHEMATOSUS (SLE) PATIENTS FROM A PHASE 2 TRIAL**

C. Steven Ernest II, Rodney Decker, Robert Hoffman, and Maria Silk. Eli Lilly and Co, Indianapolis, IN

BACKGROUND/OBJECTIVE:

Baricitinib is an orally available, selective JAK inhibitor with excellent potency/selectivity for JAK1/2 and less potency for JAK3/Tyrosine kinase 2 that may inhibit cytokines implicated in SLE such as type I IFN, type II IFN- γ , IL-6, and IL-23 as well as others. A Phase 2 trial was conducted to evaluate the effect of baricitinib on efficacy measures in SLE patients. Two of the efficacy measures assessed in this trial were the proportion of patients achieving resolution of arthritis or rash as defined by the SLE Disease Activity Index 2000 (here after referred to as SLEDAI-2K response) and proportion of patients achieving SLE Responder Index-4 (SRI-4) response at Week 24 compared to baseline. The results presented characterize the exposure-response relationship of these efficacy measures for dose assessment for upcoming Phase 3 studies.

METHODS:

The database comprised 1 Phase 2 study in SLE patients receiving placebo, 2- or 4-mg baricitinib daily up to 24 weeks. The corresponding pharmacokinetics (PK) and SLEDAI-2K and SRI-4 response rates were analyzed using NONMEM. Models were developed to describe the time-course of SLEDAI-2K and SRI-4 responses following administration of baricitinib or placebo up to 24 weeks. Patient specific factors (age, body weight, etc.) affecting the response rates were explored.

RESULTS:

The observed response rates were 48.6%, 53.4% and 65.0% for SLEDAI-2K and 47.6%, 52.4%, and 65.0% SRI-4 at week 24 for placebo, 2-mg and 4-mg baricitinib QD dosing regimens, respectively. Compared to placebo, a statistically significant improvement in efficacy was observed at Week 24 for the baricitinib 4-mg group but not the baricitinib 2-mg group. The PK/PD models adequately characterized the exposure-response time course of SLEDAI-2K and SRI-4 responses. Both baricitinib and placebo exhibited an indirect inhibitory effect on a latent variable describing the disease progression of SLE with a 2-compartment model describing the plasma baricitinib concentrations. Model-estimated exposure-response analyses demonstrated the baricitinib 2-mg and 4-mg dosing regimen produce a higher predicted response than placebo at week 24 and predict a slight increase in responses between dose groups after 52 weeks of treatment.

CONCLUSIONS:

The exposure-response analyses support examination of both 2-mg and 4-mg baricitinib QD for the treatment of SLE in longer term Phase 3 studies and suggest that both doses could be efficacious.

WED-013

Exposure-Response (E-R) analyses for therapeutic dose selection of belantamab mafodotin in patients with relapsed/refractory multiple myeloma (RRMM)

Chetan Rathi¹, Jon Collins², Herbert Struemper², Joanna Opalinska¹, Roxanne C Jewell², and Geraldine Ferron-Brady¹

¹GlaxoSmithKline, Collegeville, PA; ²GlaxoSmithKline, Research Triangle Park, NC

Objectives:

Belantamab mafodotin (GSK2857916) is a first-in-class B-cell maturation antigen (BCMA)-targeting immunoconjugate with a humanized afucosylated anti-BCMA monoclonal antibody conjugated to a cytotoxic payload mafodotin (MMAF) by a protease-resistant maleimidocaproyl linker (mc). This antibody-drug conjugate (ADC) binds to BCMA and eliminates MM cells by a multimodal mechanism. It delivers MMAF to MM cells which inhibits microtubule polymerization, resulting in apoptosis, enhances antibody-dependent cellular cytotoxicity and phagocytosis, and induces immunogenic cell death. The objective was to determine the relationships between ADC and cys-mcMMAF exposure and key efficacy and safety endpoints in support of the monotherapy dose justification.

Methods:

Individual Cycle 1 exposure measures from population PK models of ADC and cys-mcMMAF [1] were used for E-R analysis. Data were included from heavily pretreated RRMM patients who received intravenous (IV) doses ranging from 0.03 to 4.6mg/kg Q3W in a phase 1 study (DREAMM-1; n=73) and doses of 2.5 or 3.4mg/kg Q3W in the pivotal phase 2 study (DREAMM-2; n=218). Exposure-efficacy analyses evaluated probability of response (PoR), progression-free survival (PFS), and time to response or best response (TTR, TTBR). Exposure-safety analyses evaluated probability of any grade or ≥ 2 keratopathy (KP), blurred vision (BV) and dry eye (DE), grade ≥ 3 thrombocytopenia (TCP) or neutropenia (NTP), and infusion-related reactions (IRR). Generalized linear models were used to assess event probabilities, while Cox proportional hazard models were used to assess time-to-event endpoints. Covariates were identified using a step-wise model building procedure.

Results:

In DREAMM-2, PoR and PFS were not related to exposure and inversely related to baseline disease factors including soluble BCMA (sBCMA) and β_2 -microglobulin being the most significant predictors, respectively. In DREAMM-1, PoR and PFS were significantly related to Cycle 1 ADC trough concentration (Ctau). After normalizing for baseline patient characteristics including sBCMA and IgG, model-predicted PoR increased from 38% at 2.5mg/kg to 40% at 3.4mg/kg for an increase in typical ADC Ctau from 2.2 μ g/mL (2.5mg/kg) to 3 μ g/mL (3.4mg/kg). TTR was significantly inversely related to ADC Ctau, whereas TTBR was exposure-independent. KP was strongly associated with exposure. Increasing dose from 2.5 to 3.4mg/kg increased the model predicted probability of any grade KP from 80% to 89% and grade ≥ 2 KP from 57% to 67% after normalizing for other significant covariates (history of dry eye and sBCMA). Time to any grade or grade ≥ 2 KP was inversely related to ADC Ctau. Probability of TCP was significantly related to cys-mcMMAF Cmax. BV, DE, NTP and IRR were independent of ADC or cys-mcMMAF exposure.

Conclusions:

Overall, E-R relationships for KP showed a greater increase with increasing exposure than the efficacy endpoints, which supported monotherapy dose selection of 2.5mg/kg.

References: [1] Collins et al., ACoP2020

Results in this abstract have been presented in part at AACR, 2020.

WED-014

Mathematically modeling CD8+ T cell-mediated drug-induced liver injury (DILI): from ovalbumin (OVA) to amodiaquine in mice

Christina Battista^a, Zackary R. Kenz^a, Lisl K.M. Shoda^a

^aDILIsym Services, Inc., a Simulations Plus Company, Research Triangle Park, NC

Objectives: Idiosyncratic drug-induced liver injury (iDILI) is poorly understood, but there is evidence to support that some iDILI events may be immune-mediated. Amodiaquine (AQ), a malaria medication, is thought to cause immune-mediated iDILI due its delay between treatment initiation and DILI onset and its ability to induce a more rapid injury upon drug re-challenge.¹ Previous work has been devoted to representing T cell-induced cytotoxicity in response to ovalbumin (OVA)-expressing hepatocytes in mice.² The current work aims to translate the OVA representation to recapitulate AQ-mediated hepatotoxicity in mice.

Methods: An existing quantitative systems toxicology (QST) model (DILIsym[®]) was previously expanded to characterize CD8+ T cell responses to hepatocyte-expressed OVA.² This model has further been expanded to incorporate exposure of AQ via a physiologically-based pharmacokinetic (PBPK) representation which includes AQ metabolism to reactive metabolites (RMs). AQ RMs induce hepatocellular ER stress³ as well as oxidative stress⁴. These mechanisms for intrinsic toxicity were evaluated for their potential to alter the hepatic microenvironment, making it more permissive for a CD8+ T cell response. The model representation of T cell interaction with hepatocyte-presented antigen was also updated to incorporate the putative lower T cell receptor affinity of AQ compared with OVA and to represent a function of cytokine/co-stimulation levels which modulate T cell activity. These modifications, along with the pathway for T cell exhaustion already built into the OVA model, allow for representing interference in pathways implicated by CTLA4 and PD-1 compared with a wild-type mouse. Simulations aimed to reproduce CD8+ T cell-mediated DILI in a PD-1^{-/-} mouse model (bred on a C57BL/6 background) exposed to AQ with anti-CTLA4 treatment.^{5,6}

Results: Simulations successfully captured differences in CD8+ T cell responses under different experimental conditions. No ALT elevations were predicted in simulated wild-type mice treated with AQ. Simulations designed to mimic inhibition of regulatory pathways, *i.e.*, PD-1^{-/-} mice treated with anti-CTLA4, predicted CD8+ T cell-mediated ALT elevations consistent with levels seen in experimental data.^{5,6} Variations in cytokine/co-stimulation levels were simulated to assess T cell response sensitivity and range of response. These abstract results have been previously presented in part at Immunology2020, Honolulu, HI, 5/2020 and published in the conference proceedings as abstract 2395.

Conclusions: The results provide confidence in the QST model translation of OVA hepatotoxicity to AQ-induced DILI in mice. Results provide a basis for exploring AQ-induced DILI in humans using QST modeling with the goal of investigating immune-mediated iDILI risk for future compounds.

References:

1. Larrey. Ann. Intern. Med. 1986. 104(6):801;803.
2. Kenz. ACoP9 Poster W-076. 2018.
3. Zhang. Front Pharmacol. 2018. 9:388.
4. Heidari. Res Pharm Sci. 2014. 9(2):97-105.
5. Mak. Chem Res Toxicol. 2015. 28(8):1567-1573.
6. Metushi. Hepatol. 2015. 61(4):1332-1342.

WED-015

Population Pharmacokinetic Simulations of Sarilumab to Support Dose Selection in a Pediatric Population with polyarticular-course juvenile arthritis (pcJIA)

Christine Xu¹, Qiang Lu¹, and Vanaja Kanamaluru¹

¹Sanofi, Bridgewater, NJ, USA

Objectives: To guide pediatric subcutaneous (SC) dose selection of sarilumab using simulations in pediatric patients with pcJIA using the allometrically-scaled population pharmacokinetic (PopPK) model developed in adult patients with rheumatoid arthritis (RA).

Methods: The pharmacokinetics of sarilumab in adult patients with RA were described previously using a 2-compartment, target-mediated drug disposition model with parallel linear and non-linear (ie., Michaelis-Menten) elimination and first order absorption (1). A virtual pediatric population based on typical weight and sex distribution in pediatric patients with pcJIA was created. The PopPK model in adult patients with RA was adapted to a pediatric population by allometrically scaling with body weight, using scaling exponents of 0.85 for clearance (CL/F) and 1 for volume of distribution. Sarilumab exposure following multiple doses was then simulated using the pediatric PopPK model to select the pediatric dose regimens achieving similar exposure as the dose regimens tested in phase 2/3 studies in adults with RA. A sensitivity analysis of the model was carried out by applying an allometric scaling exponent of 0.75 instead of 0.85 on CL/F.

Results: Based on steady-state exposure predictions ($AUC_{0-14\text{ days}}$, C_{max} , and C_{trough}) from PopPK simulations, pediatric patients with polyarticular-course JIA (pcJIA) were divided by body weight into 2 groups, A (30–60 kg) and B (10–<30 kg). Group A/B doses of 2.0/2.5 mg/kg every two weeks (q2w); 3.0/4.0 mg/kg q2w; and 2.0/2.5 mg/kg once weekly (qw) were predicted to achieve similar exposure to adult RA doses (150 mg q2w, 200 mg q2w, and 150 mg qw, respectively). Sensitivity analysis showed a small impact of the allometric scaling exponent (0.75 vs 0.85 for CL/F) on predicted pediatric exposure across the range of pediatric weights, but with no impact on the dose recommendations. Compared to flat SC dosing, individual body weight-based dosing (mg/kg) showed lower PK variability of simulated exposure in pediatric patients. The observed PK data in the phase 2 pediatric study subsequently confirmed that doses recommended using PopPK simulations had similar exposures in the two weight groups in pcJIA and achieved the targeted adult exposures.

Conclusions: Model-based simulations provided a quantitative approach to guide a sarilumab SC dose recommendation by body weight groups in pediatric patients with pcJIA.

Reference:

- (1) Population Pharmacokinetics of Sarilumab in Patients With Rheumatoid Arthritis. 26th Population Approach Group in Europe Meeting; Budapest, Hungary; June 6-9, 2017.

Disclosures: Christine Xu, Qiang Lu, and Vanaja Kanamaluru are employees of Sanofi and may hold stock and/or stock options in the company.

WED-016

Population pharmacokinetics of blonanserin, an atypical antipsychotic drug, in adolescent patients with schizophrenia.

Daisuke Nemoto, Takeshi Takagaki, Atsushi Kitamura, Yoshiko Tomita, Hiroyoshi Kakuyama, Katsunori Maruta
Sumitomo Dainippon Pharma Co., Ltd., Tokyo, Japan;

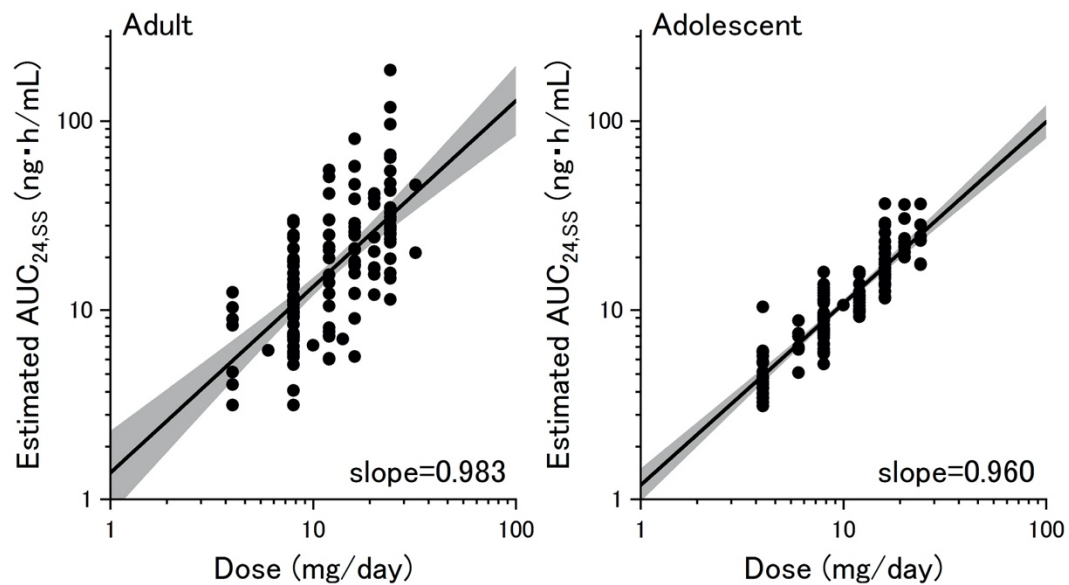
Objectives: Blonanserin is an atypical antipsychotic drug with high affinity, selective and full antagonisms for dopamine D₂, D₃ and 5-HT_{2A} receptors and was approved in Japan, Korea and China for treatment of adult patients with schizophrenia. Double-blind, placebo-controlled study (DB study) and open-label extension study (OLE study) were conducted to evaluate the efficacy, safety, and pharmacokinetics of blonanserin in adolescent patients with schizophrenia. The objectives of this population pharmacokinetic (PPK) analysis were to evaluate the characteristics of blonanserin pharmacokinetics in adolescent patients with schizophrenia and to compare their pharmacokinetic parameters with adults.

Methods: PPK analysis was conducted using 330 plasma concentration data from 131 adolescent patients (12 to 18 years) in two studies. DB study was a 6-week, randomized, three arm (placebo, 4 mg BID, 8 mg BID) study. OLE study was a 52-week, flexible dose (4 to 24 mg/day) study. For the structural model, one and two compartment models with first-order absorption were tested. The impact of age, weight, sex, dose, or concomitant drugs on apparent clearance (CL/F) and that of weight or BMI on apparent volume of distribution were tested by stepwise forward addition and backward elimination. Final model was validated by goodness of fit plots, visual predictive check (VPC) and bootstrap analysis. Area under the concentration-time curves during 24 hours at steady state (AUC_{24,ss}) in adolescents estimated by PPK analysis were compared with those in adult patients estimated in the previously conducted PPK analysis for adult patients with schizophrenia. PPK analysis was performed using NONMEM 7.3 with PDx-Pop 5.0.

Results: Blonanserin pharmacokinetics were described by a 2-compartment model with first-order absorption. Typical population estimates of CL/F, central (Vc/F) and peripheral (Vp/F) apparent volume of distribution, apparent inter compartmental clearance (Q/F) and absorption rate constant (Ka) were 0.916 kL/h, 10.5 kL, 91.0 kL, 0.494 kL/h, and 1.23 h⁻¹, respectively. Inter individual variability was 29.1% for CL/F. Shrinkage was reasonable for CL/F (11.2%). None of the tested variables was detected as covariate in the model, including age or weight, and the final model was well validated. There was no noticeable relationship between age and CL/F in adolescents. Most of estimated AUC_{24,ss} in adolescents were comparable with that in adults at the same dose.

Conclusions: A 2-compartment model with first-order absorption has been developed that can adequately describe the blonanserin plasma concentration profile in adolescent patients with schizophrenia. Age and weight were not identified as a covariate in the final model. The distribution of estimated AUC_{24,ss} in adolescent patients was comparable to that in adult patients with schizophrenia. This PPK model can be used to understand and predict pharmacokinetics of blonanserin in adolescent patients with schizophrenia.

Figure 1: Relationship between dose and AUC_{24,ss} (95% CI) in adult and adolescent patients of schizophrenia



Development of a Tumor Growth Inhibition Model for Dacomitinib in Patients with EGFR Mutant Non-Small Cell Lung Cancer

Authors: Dana Nickens², Luke Fostvedt¹, Weiwei Tan²

Institutions: ¹Global Product Development, Pfizer Inc., Cambridge, MA, USA; ²Global Product Development Pfizer Inc., La Jolla, CA, USA

Objectives:

Dacomitinib is a second-generation, irreversible EGFR tyrosine kinase inhibitor (TKI) for the first-line treatment of patients with metastatic non-small cell lung cancer (NSCLC) and EGFR-activating mutations. The recommended starting dose of dacomitinib is 45 mg QD with dose reductions of 30 mg QD and then 15 mg QD for adverse reactions. Due to a high rate of dose reduction or dosing interruption in the pivotal trials, a longitudinal tumor growth inhibition (TGI) model was developed to support the dacomitinib dosing regimen. This work supported the recent NDA approval by the FDA with a starting dose of 45 mg QD.

Methods:

Several TGI models were evaluated to characterize the change in tumor size over time in patients with NSCLC and EGFR-activating mutations taking dacomitinib at a starting dose of 45 mg (N=250) or 30 mg (N=16) QD. A time-varying exposure metric¹ (C_{avg}) was incorporated into the model using a power parameterization (i.e. C_{avg}^{θ}) calculated as the cumulative AUC up to the time of each tumor measurement divided by the length of time since the first dose based on post hoc estimates from the population PK model. The Claret model² was chosen for the final analysis, which best characterized changes in tumor size over time. Using the model, the effect of dose reductions and drug holidays on the tumor shrinkage over time was assessed.

Results:

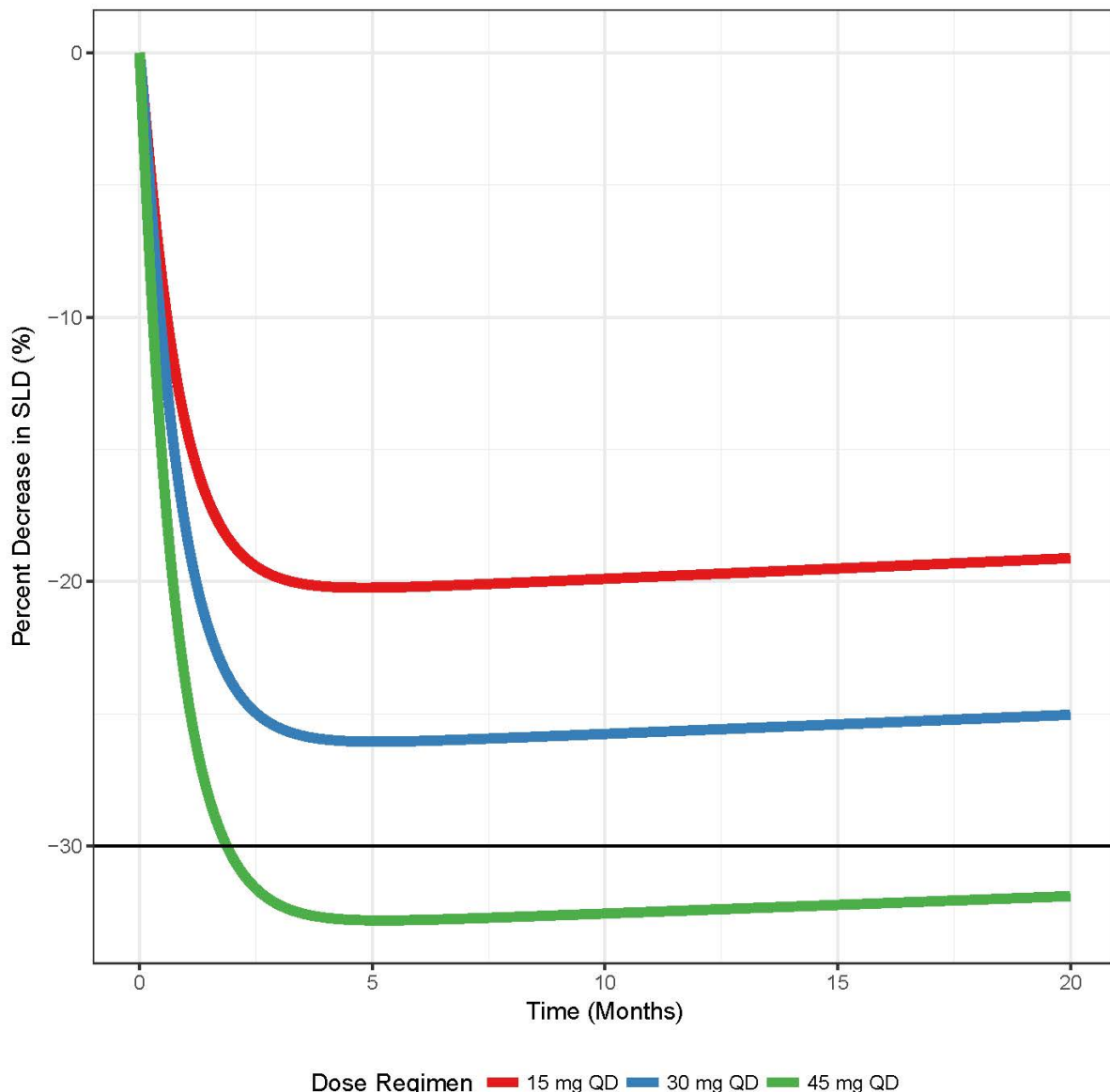
The exposure-response model for dacomitinib presents a fast kill rate ($K_D = 1.002 \text{ years}^{-1}$) with slow drug-resistance ($\lambda = 14.47 \text{ years}^{-1}$) which leads to a prolonged tumor shrinkage. The median time to maximum tumor shrinkage was estimated to be 5.27 months with 5th and 95th percentiles of 1.57 and 16.69 months, respectively. The estimated exposure effect was 0.454 (i.e. $C_{avg}^{0.454}$) indicating greater tumor shrinkage and longer duration of tumor growth inhibition associated with increased dacomitinib exposure (Figure 1). The effect of the 45 mg versus 30 mg QD starting dose on tumor shrinkage, with and without dose reductions, was simulated using the observed median times of the first and second dose reductions. The results reveal that a patient who receives 45 mg QD with 1 or 2 dose reductions has greater and prolonged tumor suppression, compared to a starting dose of 30 mg QD without dose reductions.

Conclusions: The tumor growth inhibition modelling and simulation played an important role in justifying the clinical dose regimen with a starting dose of 45 mg QD by showing a greater and more prolonged tumor shrinkage.

References:

1. Jingyu Yu, "Regulatory Perspectives on Quantitative Clinical Pharmacology in Oncology Drug Development", AAPS Meeting, 2017
2. Claret, L. *et al.* Model-based prediction of phase III overall survival in colorectal cancer on the basis of Phase II tumor dynamics. *J. Clin. Oncol.* **27**, 4103–4108 (2009).

Figure 1: Predicted Percent Change in Tumor Size by Regimen



WED-018

BCMA-CD3 Bispecific Antibodies - A Modeling Framework to Characterize Kinetics of Bispecific Antibody, T Cell, Cytokines, and Serum M-Protein.

Chandra Udata, David Dai, Sibo Jiang, Alison Forgie, Wenlian Qiao, Cynthia Musante, Donghua Yin

Institution: Pfizer Inc.

Objectives:

The B-cell maturation antigen (BCMA) is an attractive target in multiple myeloma (MM) since it is more selectively expressed on myeloma cells (1). T-cell-engaging BCMA-CD3 bispecific antibodies (BsAbs) simultaneously bind to CD3 on T-cells and BCMA on tumor cells, activate T-cells, and redirect T-cells' cytotoxicity against tumor cells (2). BCMA is shed from the surface of plasma cells by gamma-secretase-mediated cleavage, leading to detectable, soluble BCMA (sBCMA) in circulation. Higher concentrations of sBCMA in patients with myeloma are associated with lower objective response rate (3). Furthermore, sBCMA in circulation may potentially impact pharmacokinetics, target engagement on tumor cells, and efficacy when it is present in a relatively higher concentration compared to the drug concentration (4). Quantification of therapeutic response often relies on surrogate measurements such as serum M-protein and free light chains. The objective of this work is to develop a quantitative systems pharmacology (QSP) model to characterize the kinetics of BsAb, T-cell, cytokines and serum M-protein upon BsAb treatment based on the published Bispecific T cell Engager (BiTE) data (5).

Methods:

We developed a QSP model (Figure 1) to capture T cells engagement to malignant cells expressing BCMA that leads to selective cell death of MM cells, and cytokine release. To quantify the influence of sBCMA on efficacy of CD3-BCMA-bispecific therapies, we accounted for the formation of sBCMA-drug dimers that reduced the free drug concentration. The model was calibrated to published data of BiTE pharmacokinetic profiles, serum M-protein dynamics and efficacy across the clinically evaluated dose range.

Results:

The QSP model was able to capture the pharmacokinetic and serum M-protein profiles of the calibration data, across the clinical dose range. The simulations also predicted sBCMA dynamics of the responders treated with BiTE. We found that the absolute concentration of circulating sBCMA was associated with decreased efficacy, especially at lower doses. Despite the presence of sBCMA, we determined that higher BCMA binding affinity increased efficacy.

Conclusion:

The model serves as a foundation to better understand the impact of sBCMA, tumor burden, T-cell abundance and redistribution, trimer levels, and cytokine on efficacy and safety. This model could assist in the design of clinical dosing strategies for CD3-BCMA BsAb programs. In addition, the framework can be adopted as a platform for optimizing therapeutic outcome of other CD3-BsAb programs.

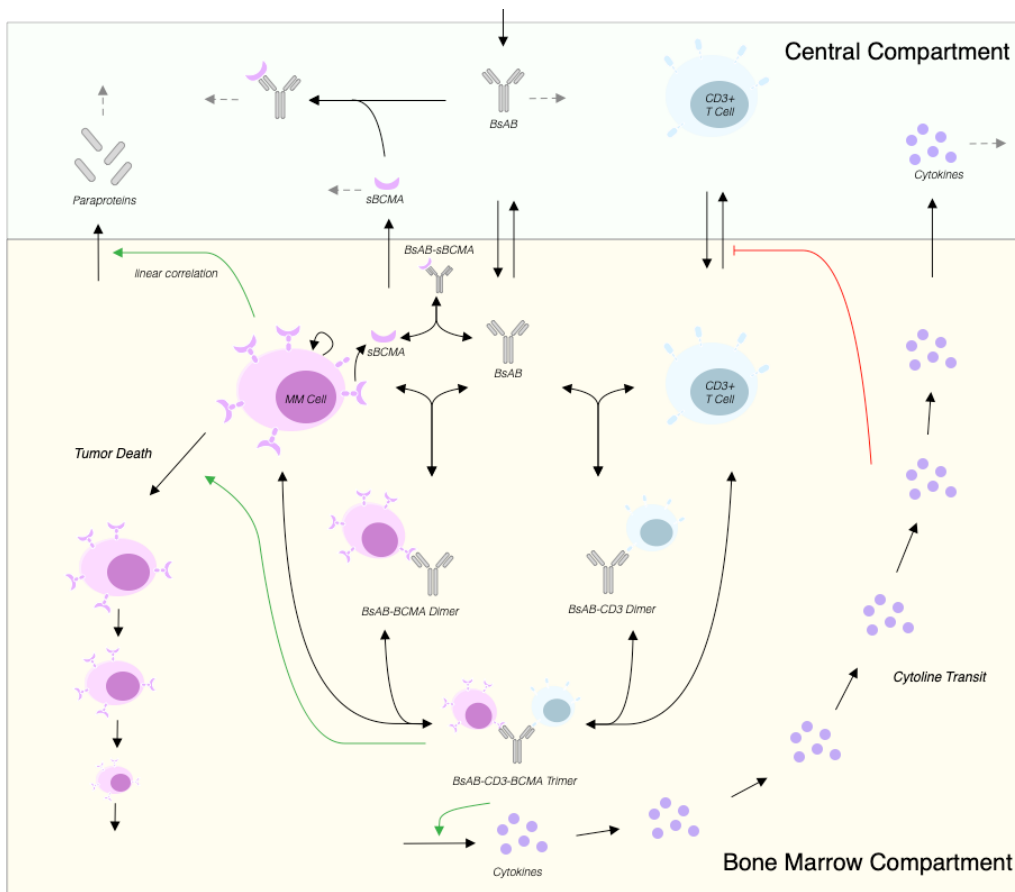


Figure 1. BCMA-CD3 QSP Model Schematic

References

1. Cho, S. F., Anderson, K. C., & Tai, Y. T. (2018). Targeting B cell maturation antigen (BCMA) in multiple myeloma: potential uses of BCMA-based immunotherapy. *Frontiers in immunology*, 9, 1821.
2. Shah, N., Chari, A., Scott, E., Mezzi, K., & Usmani, S. Z. (2020). B-cell maturation antigen (BCMA) in multiple myeloma: rationale for targeting and current therapeutic approaches. *Leukemia*, 1-21.
3. Ghermezi, M., Li, M., Vardanyan, S., Harutyunyan, N. M., Gottlieb, J., Berenson, A., ... & Udd, K. (2017). Serum B-cell maturation antigen: a novel biomarker to predict outcomes for multiple myeloma patients. *Haematologica*, 102(4), 785-795.
4. Chen H, Li M, Xu N, Ng N, Sanchez E, Soof CM, et al. Serum B-cell maturation antigen (BCMA) reduces binding of anti-BCMA antibody to multiple myeloma cells. *Leuk Res*. 2019;81:62–6.
5. Topp, M. S., Duell, J., Zugmaier, G., Attal, M., Moreau, P., Langer, C., ... & Beutner, K. (2019). Evaluation of AMG 420, an anti-BCMA bispecific T-cell engager (BiTE) immunotherapy, in R/R multiple myeloma (MM) patients: Updated results of a first-in-human (FIH) phase I dose escalation study.

Physiologically-Based Pharmacokinetics of Dexamethasone in Rats

Dawei Song^{1#}, Le Sun^{1#}, Debra C DuBois^{1,3}, Richard R Almon^{1,3}, Shengnan Meng², William J Jusko¹

¹ Department of Pharmaceutical Sciences, School of Pharmacy and Pharmaceutical Sciences, State University of New York at Buffalo, Buffalo, NY, 14214, USA; ² Department of Pharmaceutics, School of Pharmacy, China Medical University, Shenyang 110122, China; ³ Department of Biological Sciences, State University of New York at Buffalo, Buffalo, NY, 14260, USA; [#] Authors have contributed equally to these studies

Objectives: The tissue distribution of dexamethasone (DEX) in male and female rats was assessed in order to develop a physiologically-based pharmacokinetic (PBPK) model for the purposes of: 1. Thorough investigation of multi-organ PK profiles of DEX to gain better understanding of determinants for DEX whole-body PK. 2. Comparison of tissue partition coefficients between females and males to augment previous PK studies of DEX in relation to sex in rats. 3. Obtaining a data base for possible scaling the PBPK of DEX to other species.

Methods: Blood/plasma and 11 tissue samples were collected from groups of male and female Wistar rats after subcutaneous (SC) infusions to achieve steady-state (SS) and after a SC bolus of 2.25 mg/kg of DEX. In vitro and in vivo assessments were made of plasma protein binding and RBC partitioning. Quantitation of DEX was done by liquid chromatography-tandem mass spectrometry (LC-MS/MS). The observed plasma and tissue profiles were described by a traditional PBPK model using appropriate differential equations with the Adapt software. The tissue partition coefficients (K_p) of DEX were estimated by PBPK model fitting and compared to those obtained from SS infusion and published in silico methods (GastroPlus).

Results: The plasma clearance of DEX averaged 0.198 in males and 0.178 L/h/kg in female rats, consistent with hepatic CYP3A expectations. The blood-to-plasma ratio of DEX was 0.664 in males and 0.725 in females indicating limited entry of unbound (fraction unbound = 0.175) drug from plasma into RBC. Despite its expected high permeability (LogP=1.83), limited partitioning of DEX into brain (K_p = 0.06/0.10 males/females) was found and modeled based on known P-glycoprotein-mediated efflux. Distribution of moderately lipophilic DEX into adipose tissue was low (K_p = 0.16/0.10 males/females). The PBPK-fitted SC-dosed K_p values were close to those from SS infusion data. The PBPK-estimated liver K_p was 6.76, reflecting appreciable liver partitioning and binding similar to other corticosteroids. Various K_p values obtained from male and female rats were generally similar (within 1.6-fold). By using female K_p and clearance values and physiological parameters, DEX plasma PK profiles were well captured in female rats. Use of three in silico prediction methods for K_p produced a range of values that were in reasonable agreement with in vivo values for all tissues except brain, fat, and liver.

Conclusions: The tissue distribution and PK of DEX differed only modestly between male and female rats. Our PBPK model well describes the experimentally determined tissue and plasma DEX PK profiles in rats and can serve as the PK driving force for receptor-mediated pharmacodynamic effects in various tissues.

WED-020**Representation of Efavirenz-mediated Drug-Induced Liver Injury (DILI) Using Quantitative Systems Toxicology (QST)**

Diane M. Longo¹, Kyunghee Yang¹, Brett A. Howell¹, Jeffrey L. Woodhead¹

¹DILIsym Services Inc., Research Triangle Park, NC, USA.

Objectives: Efavirenz is a non-nucleoside reverse transcriptase inhibitor (NNRTI) used in combination with other agents to treat human immunodeficiency virus (HIV) infection. Efavirenz treatment is associated with a low frequency of serum enzyme elevations. To understand the hepatotoxicity mechanisms underlying clinically observed liver signals, efavirenz was represented in DILIsym®, a QST model of DILI.

Methods: The potential for efavirenz to inhibit bile acid transporters was assessed using transporter-overexpressing vesicles and cells. The potential for efavirenz to induce mitochondrial dysfunction or oxidative stress was assessed in HepG2 cells. These *in vitro* data were used to define DILIsym hepatotoxicity parameters for efavirenz. A previously constructed GastroPlus physiologically based pharmacokinetic (PBPK) representation was used to predict efavirenz exposure. Simulated populations (SimPops) that include variability in hepatotoxicity mechanisms and in efavirenz exposure were used to simulate the *in vivo* response in humans to efavirenz in DILIsym.

Results: Mechanistic *in vitro* assays indicated that efavirenz inhibits the mitochondrial electron transport chain (ETC), increases oxidative stress, and inhibits bile acid transporters (BSEP, NTCP, and MRP4). Combining *in vitro* hepatotoxicity data with predicted exposure, DILIsym predicted infrequent ALT elevations (1-2%) in SimPops following administration of efavirenz (600 mg QD) for 12 weeks.

Conclusions: Using *in vitro* mechanistic data to determine efavirenz toxicity parameters, DILIsym predicted infrequent hepatotoxicity, consistent with the low rate of ALT elevations seen clinically for efavirenz.

	Observed ALT >5X ULN	Simulated ALT >5X ULN
Efavirenz 600 mg QD oral	1% to 8% (LiverTox)	1% to 2%

Table 1. Comparison of observed vs. simulated hepatotoxicity for efavirenz.

WED-021

Using a QSP model of Rheumatoid Arthritis calibrated to capture clinical response to Adalimumab to perform population analysis

Tanvi Joshi, Prakash Packirisamy and Rukmini Kumar
Vantage Research, India

Objectives:

1. Develop a QSP model of Rheumatoid Arthritis (RA) capturing mechanistic pathways and clinical responses to Methotrexate, Adalimumab and Tocilizumab.
2. To derive insights from population analysis about differences between Adalimumab responders and non-responders.

Methods:

The Vantage RA QSP model [1] represents an inflamed RA joint at steady state. Modular design approaches used to set up common immunological subsystems (cell life cycles and cytokine effects), enable repurposing to other auto-immune diseases.

Using Ordinary Differential Equations (ODEs), the model captures lifecycle and cellular interactions of Fibroblast like Synoviocytes (FLS), B cells, T cells and macrophages and relevant pro and anti-inflammatory cytokines like IL-6, TNF- α , TGF- β . The model parameters are constrained by clinical trial data (top down constraints) and by bottom up data (cell proliferation rate, cytokine secretion rates). ACR and DAS-28 scores in Virtual Population are calibrated to match clinical trials for Methotrexate, Adalimumab (anti-TNF- α therapy) and Tocilizumab. Population analysis was performed on the calibrated virtual population to derive insights about differences between Adalimumab responders and non-responders.

Results:

The Vantage RA QSP model was developed to capture multiple physiological pathways in RA and post therapy effects on disease severity scores. The virtual population was calibrated to capture the clinical trial entry characteristics, such as DAS-28 ranging from 5 to 7 at baseline, and match the clinical trial readouts, such as remission and response percentages for three therapies studied in the Williams et al. 1985, OPTIMA and ROSE trials. [2, 3, 4]

Conclusions:

The Vantage RA QSP model captures the physiology of RA, the clinical outcomes, and the response to three standard therapies. Modular model design enables model repurposing to other auto-immune diseases with similar pathophysiology. Population analysis helps derive insights about Adalimumab responders and non-responders. Future efforts include determining differences between different responders of Adalimumab and Infliximab and exploring response to JAK inhibitors.

References:

1. Tamara Ray, Madhav Channavazzala, Dinesh Bedathuru, Maithreye Rengaswamy, Rukmini Kumar. QSP Model of Rheumatoid Arthritis, capturing range of clinical responses to Methotrexate and anti-TNF-a therapies. *PAGE 28 (2019) Abstr 9081 [www.page-meeting.org/?abstract=9081]*
2. Williams, H. J., et. al. (1985). Comparison of low-dose oral pulse methotrexate and placebo in the treatment of rheumatoid arthritis. A controlled clinical trial. *Arthritis & Rheumatism: Official Journal of the American College of Rheumatology.*
3. Kavanaugh, A., et. al. (2013). Clinical, functional, and radiographic consequences of achieving stable low disease activity and remission with adalimumab plus methotrexate or methotrexate alone in early rheumatoid arthritis: 26-week results from the randomised, controlled OPTIMA study. *Annals of the rheumatic diseases.*
4. Yazici Y, et. al. (2010). Efficacy of tocilizumab in patients with moderate to severe active rheumatoid arthritis and a previous inadequate response to disease-modifying antirheumatic drugs: the ROSE study. *Annals of the rheumatic diseases.*

WED-022

Pharmacometric Modeling with the Zero-Order Hold

Violeta Rodriguez-Romero^{1*}, Rudy Gunawan^{1*}, and Eric Haseltine¹

¹Vertex Pharmaceuticals Incorporated, Boston, MA, United States

*These authors contributed equally to this work.

Objectives:

Solving models of ordinary differential equations (ODEs) in NONMEM using ADVAN6 or ADVAN13 typically requires substantially longer run times than models with analytical solutions. Often the need to use these methods results from PK variations over the dosing interval preventing derivation of an analytical solution, as is the case for indirect-response models and enzyme induction models. As long run times hinder model development, it is desirable to derive suitable approximations to speed up model solutions.

Methods:

The zero-order hold¹, a concept used in the field of advanced process control to optimize control decisions, provides an attractive approximation for these situations. Consider as an example the indirect-response model shown in

Figure . The PK component of the model can be solved analytically using ADVAN2. The continuous PK profile is discretized over a pre-specified interval using a suitable metric, such as C_{avg} – this approximation is the zero-order hold (see

Figure , right). Subsequently, the nonlinear ODE for the indirect response model becomes a linear ODE over the interval as C_{avg} is constant. This linear ODE can be solved analytically by providing C_{avg} values in the NONMEM input file, which eliminates the need to solve for the PK in the PK/PD model. Note that this approach differs from the one reported by Petersson et al.², who applied a forward-difference approximation for the ODEs. In contrast, we exactly solve all ODEs but discretize the PK response over a pre-specified interval.

Results:

Two examples are considered: an indirect-response model and an enzyme induction model. Results are simulated from an ADVAN13 model, and then refit using either the same model or the zero-order hold approximation. It is shown that the zero-order hold approximation provides a substantial reduction in computational time without unduly biasing the parameter estimates. For the indirect-response model, the speed-up is ~50-fold with comparable estimated parameters.

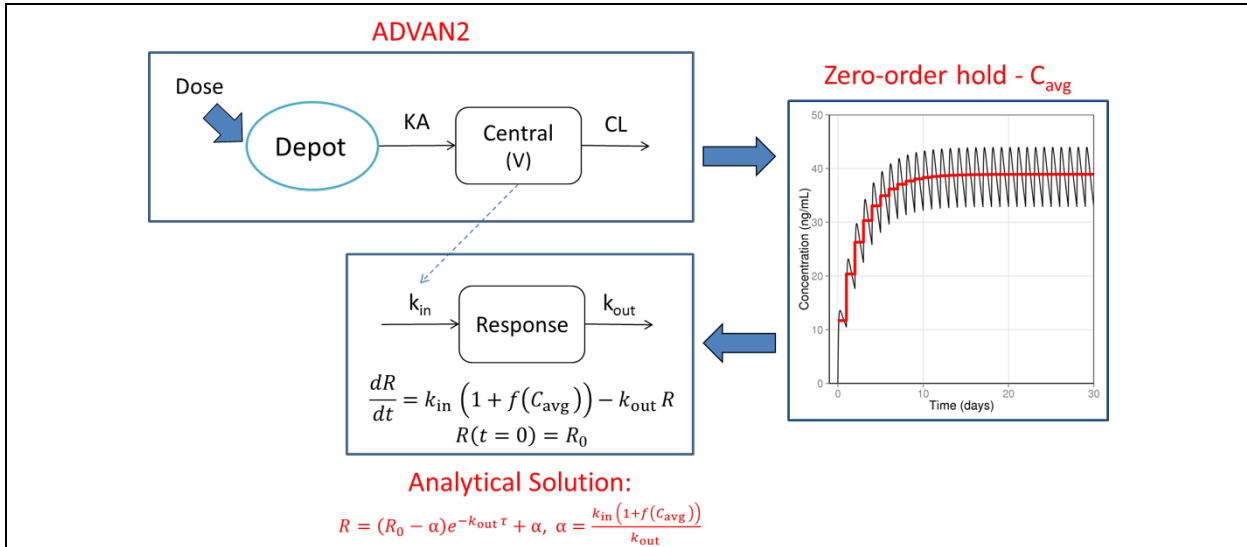
Conclusions:

Applying the zero-order hold is an attractive method for efficiently solving models where time-varying PK prevents an analytical solution. Although this approach ignores PK variation within the discretization interval, the results provide two examples where such an approximation does not adversely impact the estimated parameters. The approach does require thoughtful selection of the PK metric used to drive the response, and if the approximation is appropriate for the situation. If appropriate, computational expense can be substantially reduced for estimating models typically solved with ADVAN6 or ADVAN13.

References

1. Ogunnaike, B. A. & Ray, W. H. *Process Dynamics, Modeling, and Control*. (Oxford University Press, 1994).
2. Petersson, K. J. F., Friberg, L. E. & Karlsson, M. O. *J. Pharmacokinet. Pharmacodyn.* **37**, 493–506 (2010).

Figure 1: Indirect-Response Model with Zero-order Hold Approximation (C_{avg} - red line)



WED-023

Population Pharmacokinetic Analysis of JP-1366, a Novel Potassium-Competitive Blocker, in Healthy Subjects

Eunsol Yang¹, Inyoung Hwang, MD¹, SeungHwan Lee, MD, PhD¹

¹ Department of Clinical Pharmacology and Therapeutics, Seoul National University College of Medicine and Hospital, Seoul, Republic of Korea

Objectives: JP-1366 is a novel potassium-competitive acid blocker under clinical development for the treatment of acid-related disorders. This analysis aimed to establish a population pharmacokinetic (PK) model for JP-1366.

Methods: PK data from a first-in-human study of JP-1366 (single ascending dose part (n=38); multiple ascending dose part (n=30)) in healthy Korean subjects was used for the analysis. The dataset for model development included 1495 plasma concentrations from 68 subjects. Population PK modeling was carried out using NONMEM® version 7.4.4, and PK parameters were estimated by first-order conditional estimation method. Also, potential covariates such as body weight, albumin, alanine aminotransferase and aspartic acid transaminase were evaluated. Final population PK model was validated by goodness-of-fit (GOF) plots and Visual Predictive Check (VPC).

Results: A two-compartment model with Erlang-type absorption (n=6), first-order elimination and a proportional error model well described PK profile of JP-1366. The population parameter estimates for absorption rate constant (K_{tr}), apparent clearance (CL/F), apparent inter-compartmental clearance (Q/F), apparent central volume of distribution (V_c/F) and apparent peripheral volume of distribution (V_p/F) were 13.6 h^{-1} , 29.5 L/h , 29.4 L/h , 97 L and 147 L , respectively. None of the covariates had significant effects on CL/F and V_c/F . The GOF and VPC plots showed robustness and predictability of the developed final population PK model.

Conclusions: The population PK model for JP-1366 successfully described the observed PKs of JP-1366. This model will be utilized for designing further clinical studies and establishing dosing regimen.

WED-024

A Population Pharmacokinetic/Pharmacodynamic/Exposure Response Model to Relate Complement 4 Antigen Concentrations and Risk of Attacks in Hereditary Angioedema Patients

Authors: Fiona Glassman¹, Ziheng Hu¹, Theresa Yuraszeck¹, Ingo Pragst², Dipti Pawaskar¹

Affiliations: ¹CSL Behring, King of Prussia, PA, USA; ²CSL Behring GmbH, Marburg, Germany

Objectives: Hereditary angioedema (HAE) is a rare genetic disease caused by deficiency in functional C1 esterase inhibitor (C1-INH[f]). Uncontrolled activation of the classical complement pathway leads to low concentrations of complement 4 (C4), which is a less varying biomarker of HAE than C1-INH(f). While the relationship between HAE attack risk and C1-INH(f) is well established, its relation to C4 antigen is unknown. This analysis aims to explore the relationship between C4 antigen and risk of attack in HAE patients.

Methods: C1-INH(f) and C4 antigen were measured in COMPACT Phase 2, 3 and open-label long-term safety clinical studies. A population PK/PD model was developed to characterize the relationship between C1-INH(f) and C4 antigen, which was described using an indirect response model. An exposure-response (ER) model was also developed to relate C1-INH(f) and risk of HAE attack. The relationship between C4 antigen concentration and risk of HAE attack was evaluated based on combined simulation results of the PK/PD and ER models of C1-INH(f) and risk of HAE attack.

Results: The relationship between C4 antigen concentration and risk of HAE attack was investigated with a combined population PK/PD/ER model previously developed. A positive linear relationship was observed between C4 antigen concentrations and C1-INH(f) until C1-INH(f) of ~50%, at which point signs of saturation were apparent. In addition, an inverse relationship was observed between C1-INH(f) and risk of HAE attack. Similarly, HAE attack hazard decreased with the increase of C4 antigen concentrations.

Conclusions: The inverse relationship between the risk of HAE attack and C4 antigen concentrations in HAE patients can be described by a population PK/PD/ER model. This can provide a basis for the use of C4 antigen in addition to C1-INH(f) for assessing drug efficacy.

WED-027

Application of different approaches to generate virtual patient populations for QSP model of Erythropoiesis

Galina Kolesova¹, Oleg Demin¹, Alexander Stepanov¹

¹InSysBio, Moscow, Russia

Objectives: In the study we propose and compare four different techniques to generate virtual patient populations basing on experimentally measured mean data and statistics.

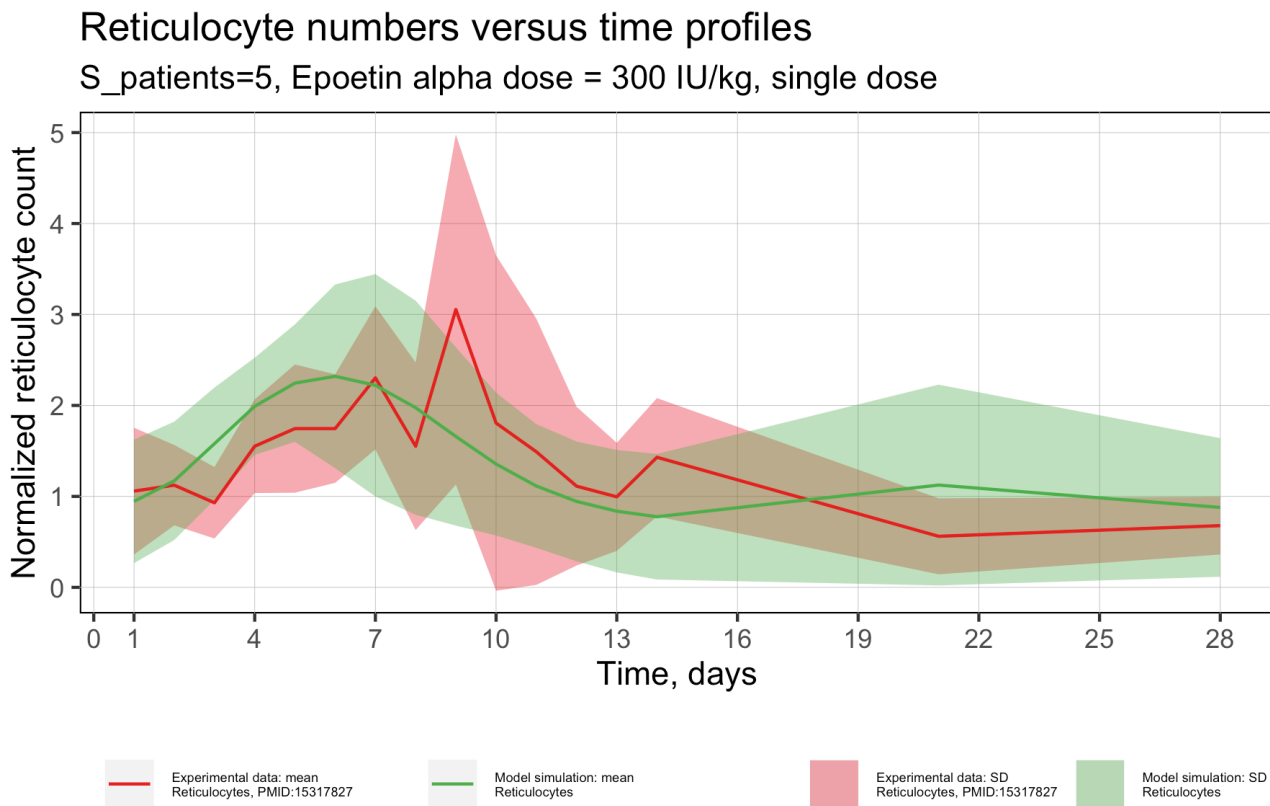
Methods: QSP model of erythropoiesis [1] was constructed to comprehensively describe cell dynamics from hematopoietic stem cell to circulating red cells. The model describes cell self-renewal, differentiation, proliferation, migration from bone marrow into circulation and cell death. Binding of growth factors such as stem cell factor (SCF) and erythropoietin (EPO) to cell-surface receptors regulates cell dynamics modulated by interleukin-3 (IL-3). The model was calibrated across published in vitro/in vivo data.

Data describing time series of plasma reticulocyte count in response to single dose erythropoietin administered to 5 healthy subjects is used to find out final population of virtual patients (VP). Experimental data are given in the form of mean and standard deviation (SD).

Four different approaches were applied to generate virtual patient populations (VPpop): (1) Monte-Carlo Markov Chain, (2) Model fitting to Monte-Carlo sample, (3) Population of clones, (4) Stochastically bounded selection. 36 parameters of the erythropoiesis model were chosen to be responsible for variability in observed clinical data. Initial VPpop was generated based on a priori distribution of the selected parameters. Number of VPs equal to that specified in clinical data and allowing to satisfactorily describe both mean and SD of reticulocyte values measured clinically were chosen from initial VPpop on the basis of each of the approaches.

Results: In addition to approaches (1), (2) and (3) presented earlier [2] we have developed an approach (4) entitled as “Stochastically bounded selection”. The approach includes (i) finding minimal (RETmin) and maximal (RETmax) values of reticulocyte count in particular time point among initial VPpop, (ii) building a truncated lognormal distribution for reticulocyte count, the distribution is concentrated at [RETmin, RETmax] and has mean and SD equal to those of experimental data, (iii) generation of S random values of the endpoint (in our case reticulocyte count and

$S=5$ equal to number of patients in experimental data), (iv) finding 5 VPs in initial VP_{pop} which reticulocyte values are closest to the 5 randomly selected values at step (iii). Fig 1 illustrates application of the approach (4). Similar results were obtained for other approaches.



References

- Alexander Stepanov, Galina Lebedeva, ACoP 10 (2019) From stem cell to erythrocyte and platelet: QSP model of erythropoiesis and thrombopoiesis for assessing the impact of pharmacological interventions. Poster.
- Galina Kolesova, Oleg Demin, PAGE 28 (2019) Abstr 9008 [www.page-meeting.org/?abstract=9008].
- Experimental data source: PMID:15317827

Conclusions: The approaches proposed are capable for reproducing the endpoint distribution characteristics. The choice of a specific technique is determined by characteristics of the particular problem. Namely, in case of distribution with relatively small SD all methods work similarly. However, to reproduce distributions with relatively large SD second, third and fourth methodologies are preferable. But for large models, the fourth method can preferentially be used. This method allows to include in generation of VP_{pop} any number of variable parameters.

WED-028

Novel Quantitative Approach for the First-in-human Dose in an Oncology Setting for the Anti-programmed Cell Death-1 Monoclonal Antibody, AMG 404

Hansen L. Wong¹, Khamir Mehta¹, Sandeep Dutta², Vijay V. Upreti¹.

¹Amgen Inc., South San Francisco, CA, USA; ²Amgen Inc., Thousand Oaks, CA, USA.

Objectives: AMG 404 is a novel monoclonal antibody (mAb) that blocks programmed cell death-1 (PD-1) from binding to its ligands, programmed death-ligand 1 and 2 (PD-L1 and PD-L2, respectively). We present here a strategy for first-in-human (FIH) starting dose selection that integrates preclinical assessments and human pharmacokinetic (PK) predictions of AMG 404 with existing literature data of anti-PD-1 mAbs.

Methods: The key motivation of this effort was to recommend a starting dose that provides similar pharmacological activity as the existing, generally well-tolerated and efficacious exposures of anti-PD-1 mAbs in patients. By this strategy as shown in Figure 1, the proposed dose was expected to be efficacious. AMG 404 exposure targets [steady-state average concentration ($C_{avg,ss}$)] were predicted by scaling the known clinical $C_{avg,ss}$ values of multiple approved anti-PD-1 mAbs (also referred to as anti-PD-1-drugs) to AMG 404 using corrections for molecular weight (MW) and PD-1/PD-L1 blockade activity from Jurkat T cell-based reporter gene and HEK293T cell-based assays (as assessed by concentrations for half-maximal effect [EC_{50}] and half-maximal inhibitory effect [IC_{50}], respectively) using the equation:

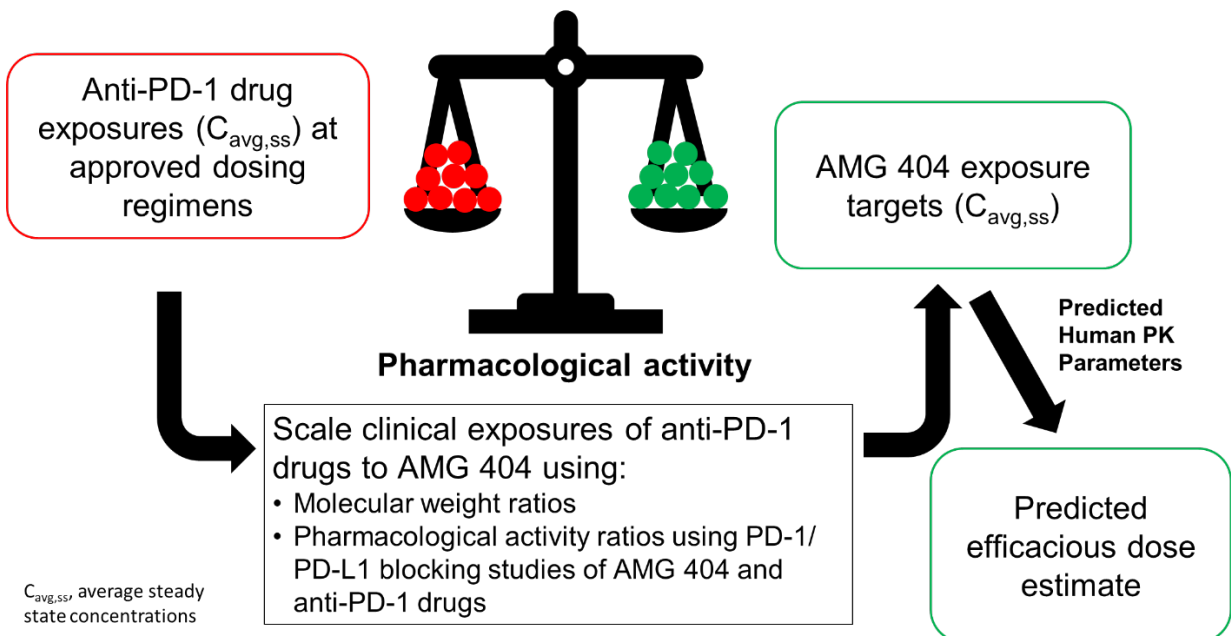
$$\text{Target } C_{avg,ss,AMG\ 404} = C_{avg,ss, \text{Anti-PD-1\ Drug}} \times \frac{\text{Average IC(EC)}_{50} \text{ ratio of AMG\ 404/Anti-PD-1\ Drug}}{\text{Average MW ratio of AMG\ 404/Anti-PD-1\ Drug}}$$

AMG 404 doses were predicted in conjunction with human PK parameters derived from allometric scaling of cynomolgus monkey PK using a 2-compartment model with linear elimination.

Results: Using derived human PK parameters, AMG 404 dose range for intravenous administration was estimated to achieve the predicted target $C_{avg,ss}$ exposures. A starting dose was proposed near the mean estimate that was expected to be well-tolerated and efficacious in light of the prior experience with anti-PD-1 mAbs, though potential regulatory feedback was fully expected. Favorable regulatory feedback was received: starting dose was reduced only 2-fold from proposed. The results in this abstract have been previously presented in part at the 2020 annual meeting of the American Society of Clinical Pharmacology and Therapeutics and published in the conference proceedings as abstract PII-059.

Conclusions: This work showcases a successful FIH dose selection strategy towards rapid evaluation of a new drug which considers literature results of other anti-PD-1 mAbs that was accepted by regulatory agencies and can be used for future programs.

Figure 1. Proposed Starting Dose of AMG 404 with Similar In Vitro Pharmacological Activity of Efficacious Doses of Other Anti-PD-1 mAbs



WED-029

pbpkme: A Flexible Fit Matrix-Based Framework for PK and PBPK Models in R

Authors: Hillary R. Husband and Eric A. Sherer

Institutions: College of Engineering and Science, Louisiana Tech University

Objectives: The pbpkme package is designed for solving classic compartmental or physiologically-based pharmacokinetic (PBPK) models. These models are often characterized by large systems of linear ordinary differential equations (ODEs), but the dimensionality of PBPK models can be burdensome and inefficient. The objectives of this work are to:

- Construct a matrix-based framework for efficiently solving large systems of differential equations as often used to define PBPK models
- Openly provide this framework in the form of an R package, pbpkme, which takes in rate coefficients, initial conditions, and dose information and returns drug concentrations in all compartments

Methods: This package uses the eigenvalue/eigenvector solution to a system of linear ODEs. Matrix manipulation is computationally fast, making it ideal for model fitting/parameter estimation, especially for large models. The equation for the analytical solution is

$$\mathbf{x}(t) = \Phi(t)\mathbf{x}^0 + \Phi(t) \int_{t_0}^t \Phi^{-1}(s)\mathbf{g}(s)ds,$$

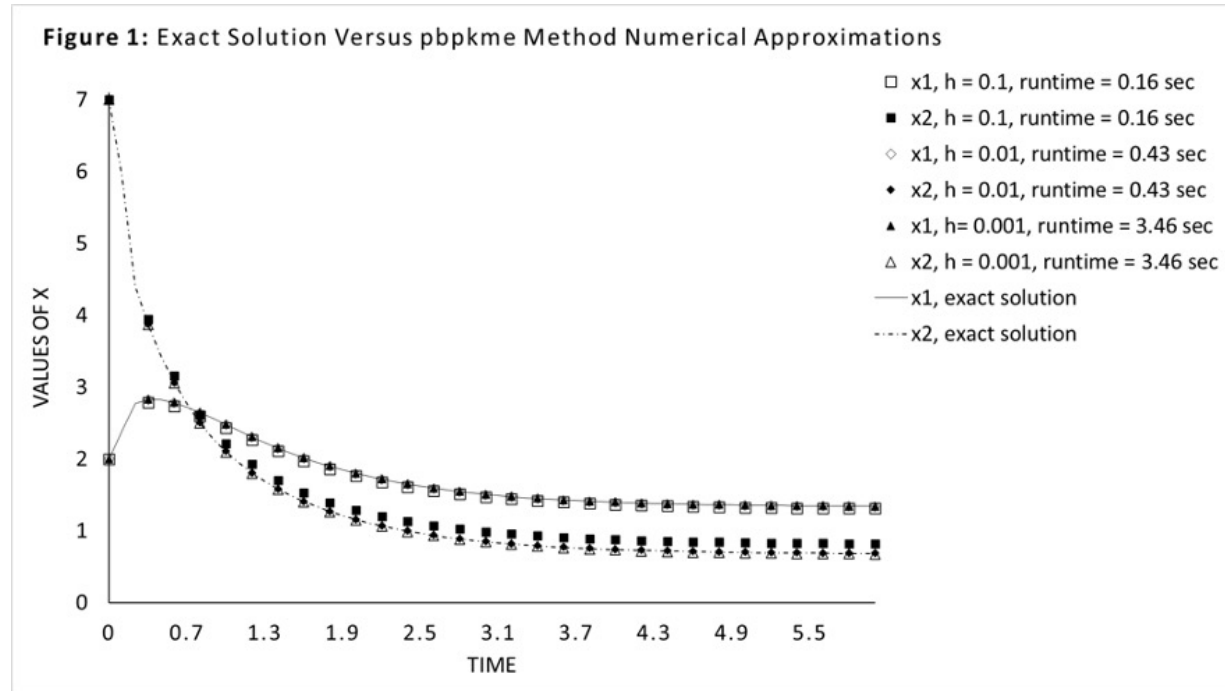
where \mathbf{x} is a vector of amounts or concentrations, $\Phi(t)$ is the fundamental matrix derived from the eigenvalues/eigenvectors of the linear ODEs, \mathbf{x}^0 is the vector of initial conditions, and $\mathbf{g}(s)$ is the non-homogenous portion of the system, if one exists, representing an infusion profile.¹ It is common for larger systems to produce complex conjugate pairs in their solutions, which pbpkme handles automatically. The method by itself solves for a solution to the model over the specified time; its limitation being it only produces a solution for the last time point. However, we are able to use that solution as the initial condition for the next iteration of the function. The method is computationally fast; therefore, the solution over a sufficiently small time interval t can be calculated many times very quickly (which reduces propagation of error – a common flaw of numerical time-stepping methods).²

Results: The method was validated against an example with a known solution. Results for varying time-steps illustrating the method's accuracy and speed are shown in Figure 1. To showcase pbpkme's computation speed compared to traditional approaches, a three-compartment PK model was computed in R using the fourth-order Runge-Kutta method (RK45) and the pbpkme function.¹ The pbpkme function was 43%-94% faster than RK45 at step-size 0.01 and 0.1, respectively. Finally, ODEs for a forty compartment PBPK model were converted into matrix form and its predictions were accurate compared to the original model's predictions, demonstrating the flexibility of this function.³

Conclusions: Using a matrix-based approach to model systems of first-order ODEs is a computationally efficient and accurate technique. The pbpkme package simplifies the use of this mathematical method for general use in the pharmacometrics community.

References

- [1] Boyce, WE and RC Prima. 1996. New York. John Wiley & Sons.
- [2] Hegarty, G and SB Duffull. 2012. School of Pharmacy, University of Otago.
- [3] Dubbelboer, et al. 2017. *Mol. Pharmaceutics*, 14(3):686-698.



Application of a QSP Model for Recombinant Human ADAMTS13 in Sickle Cell Disease

Hoa Q. Nguyen¹, Steven Yu², Zhiwei Zhang³, Andy Zhu¹, Indranil Bhattacharya¹

¹Takeda, Cambridge, MA, US; ²LH Group, China; ³RES Group Inc., Needham, MA, US

Objectives: Sickle cell disease (SCD) is an inherited blood disorder characterized by sickle hemoglobin formation, leading to rigid and deformed sickle shaped red blood cells. These sickle shaped blood cells cannot traverse the microcirculation, creating blockages (vaso-occlusion) leading to tissue hypoxia and excruciating pain (vaso-occlusive crisis, VOC). In VOC state, due to increased VWF multimers, it is hypothesized that administration of recombinant human ADAMTS13 (rADAMTS13) could regulate homeostasis in VOC state through improved VWF-ADAMTS13 interaction. A QSP approach was used to guide dose selection for SCD indication.

Methods: A previously developed QSP model for congenital thrombotic thrombocytopenic purpura was adapted for SCD pathophysiology. Basal levels of endogenous ADAMTS13, VWF and Hb were adjusted for SCD patients during steady state as well as in painful crisis accordingly. A combination of a pharmaco-statistical and QSP approach was used to generate a virtual patient population ($n = 1000$) accounting for inter-individual variability in drug exposure (PK) and basal level of VWF. The model was then used to simulate the reduction in active VWF for different dose levels of rADAMTS13 in SCD patients at steady state and those experiencing VOC.

Results: The model-predicted VWF, Hb levels were comparable to reported baseline estimates. Based on model simulation for virtual SCD patient population, 40 – 160 U/kg was predicted to result in 23-52 % reduction of active VWF compared to its VOC level without treatment in the first 5-15 hours after dosing. At 160 U/kg, active VWF is expected to stay under remission during 3-8 days. Active VWF and VWF fragment were shown to be sensitive to rADAMTS13 dosage and are potentially informative clinical biomarkers.

Conclusions: An ADAMTS13 QSP model adapted for SCD patients demonstrated the reduction of active VWF with drug intervention. The model supported a recommendation of rADAMTS13 40 – 160 U/kg dose for SCD patients in the currently ongoing phase 1/2 study.

WED-031

Measurement and Quantitative Characterization of Whole-Body Pharmacokinetics of MMAE in Mice

Hsuan-Ping Chang¹, Dhaval K. Shah¹

¹Department of Pharmaceutical Sciences, School of Pharmacy and Pharmaceutical Sciences, The State University of New York at Buffalo, Buffalo, NY, USA.

Objectives: The tubulin inhibitor, auristatins monomethyl auristatin E (MMAE) is one of the most studied payloads in antibody drug conjugates (ADCs). Although MMAE-conjugated ADCs significantly improves efficacy compared to naked antibodies, the highly potent payload can cause on-target off-tumor toxicities and target-independent toxicities. We therefore investigated whole-body pharmacokinetic (PK) of MMAE in mice and developed a physiological-based pharmacokinetic (PBPK) model to better understand the toxicity profiles of MMAE-conjugated ADCs.

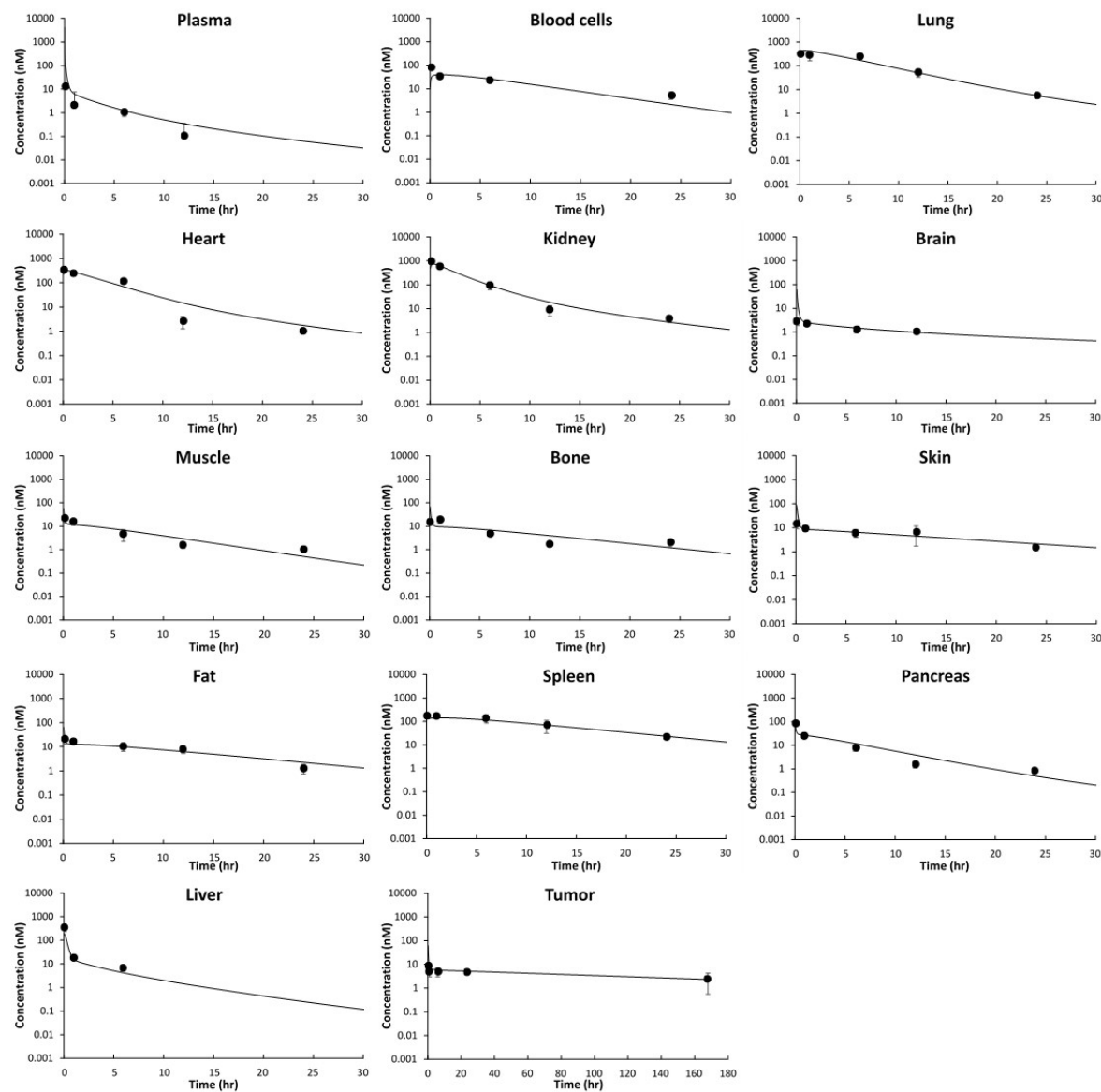
Methods: A total of fifteen N87 tumor-bearing nude mice were treated with single 0.1 mg/kg of MMAE intravenously. Blood, tumor, and tissue (heart, liver, lung, kidney, spleen, pancreas, fat, muscle, skin, bone, and brain) samples were collected at 5 min, 1, 6, 24, and 168 h post-dose. MMAE in plasma, blood cell, tissue, and tumor homogenates were analyzed by LC-MS/MS method. The PBPK model included 17 tissue compartments and a tumor compartment, with each of tissue divided into plasma, blood cells, endosomal, interstitial, and cellular sub-compartments. Tissue distribution of MMAE between plasma-blood or interstitial-cellular sub-compartments was assumed to be permeability-limited and connected via permeability-surface area product (PS) values. Partition of MMAE to tissue cellular space and blood cells were characterized via partition coefficient (K_p) calculated by ratio of tissue to plasma area-under-the curve (AUC_{0-t}). MMAE was mainly eliminated by CYP3-mediated metabolism and biliary excretion, and thus the PBPK model only included hepatic clearance (CL).

Results: Plasma concentration dropped rapidly with 0.3% of injected MMAE remaining after 5 minutes. Blood-to-plasma AUC ratio was 5.46, indicating MMAE distribution into blood cells. K_p values were greater than 18 (range from 17.9 to 35.3) in highly perfused tissues (lung, kidney, heart, and spleen), around 2 (range from 1.20 to 2.40) in muscle, skin, bone, adipose, pancreas, and liver, and 8.21 in tumor, indicating MMAE significantly distributes into tissues and binds to the tubulin. The PBPK model well captured the MMAE PK profiles in plasma, tissues, and tumor (**Figure 1**), with percent predictive error (%PE) less than 10% for all tissues except liver (%PE 38%). The estimated

hepatic CL (107 mL/h, CV% 8.92) corresponded to the calculated CL (109 mL/h) using IVIVE based on human liver microsome intrinsic CL. The PS values for individual tissues were estimated with good precision (%CV < 40%).

Conclusions: The whole-body distribution data indicated MMAE distributes into blood cell and supported MMAE binds to tubulins and thus retains in tissues for a prolonged period. The PBPK model well characterized PK data of MMAE, which can further be utilized to build MMAE-conjugated ADC model and to predict disposition of MMAE in higher species after scaling up.

Figure 1. Observed and PBPK model predicted MMAE concentration profiles in plasma, tissues, and tumor.



WED-032

Sub-Compartmental Systems Biology Modeling of Acute Radiation effects on the Thrombopoietic System in Animal Models

Ibrahim Mustafa¹, Allison Gibbs², Isabel Jackson², Joga Gobburu¹, Mathangi Gopalakrishnan¹

¹Center for Translational Medicine, School of Pharmacy, University of Maryland, Baltimore, USA

²The Department of Radiation Oncology, School of Medicine, University of Maryland, Baltimore, USA

Objectives: The nature of the interaction of ionizing radiation (IR) with biological systems is not well understood. The research objective was to develop a sub-compartmental systems biology model to describe the potential mechanism of the interaction between IR and thrombopoietic system in terms of reactive oxidative species (ROS). The model aims to investigate time delays of the system considering feedback mechanisms in two animal models of irradiation and compare with the experimental data.

Methods: The thrombopoietic mechanistic model considered three main compartments: progenitors, megakaryocytes (MKs), and platelets. The ROS are dose dependent and triggers alterations in the structure of the system. Both progenitors and MKs were assumed to be radiosensitive while platelets are radio resistant. The MKs compartment was divided into 10 sub-compartments while the platelets compartment was divided into 9 sub-compartments to investigate the time delay in response to different doses of acute IR. Parameters values were obtained by optimization procedures using dynamic platelet data or from literature. The model was externally validated using experimental data from mice and rabbits that was not used during the parameters estimation process. The model was formulated in terms of ordinary differential equations (ODEs). All numerical analysis, and simulations were conducted using Pumas v0.3.1 software

Results: The model showed that the thrombopoietic system is a complex multistage dynamic process with potential differences between the radio-sensitive stem cells and radio-resistant platelets. The model showed that the nadir times of progenitors and MKs in rabbits at IR dose of 2 Gy are reached on day 2 while platelets are reached on day 10 following acute IR exposure. Both progenitors and MKs recovered on day 7 while platelets recovered on day 10. The model allowed for comparison of the system's response across species and can simulate the average response in mice and rabbits following irradiation. At IR dose of 7.5 Gy in rabbits, platelet recovered on day 10, whereas in mice at IR dose of 7.5 Gy platelet did not recover, in agreement with the experimental results. Variation in platelet dynamics was due to the sensitivity of stem cells to ROS. The model was successfully validated with observed platelet count from mice and rabbits.

Conclusion: The sub-compartmental system biology model realistically predicted thrombocytes behavior following acute IR in a wide range of doses: 2.0-9.5 Gy and explained the variation of platelets response of rabbits and mice to radiation which is attributed to the sensitivity of stem cells to ROS. It is found that MKs could be the rate limiting components in the thrombopoiesis process to IR. The model could be useful in drug development of radiation medical countermeasures.

WED-033

A Quantitative Systems Pharmacology Model of Individualized NeoAntigen Specific Immunotherapy (iNeST)

Iraj Hosseini^{1,*}, Tom Snowden², Jaehak Oh¹, Yoko Oei¹, Sophie Lehar¹, Jill Schartner¹, Lelia Delamarre¹, Saroja Ramanujan¹

¹ Genentech Inc., South San Francisco, CA

² Certara QSP, Canterbury, UK

Objectives: To develop and apply a systems pharmacology model to support research and clinical development of individualized neoantigen specific immunotherapy (iNeST).

Methods: Cancer is characterized by an accumulation of somatic mutations, which can generate cancer-specific neoantigens. Preclinical and clinical studies have shown the feasibility of increasing the immune response to tumors by using a vaccination strategy that encodes cancer-specific neoantigens [1-2]. iNeST is an individualized therapeutic approach that consists of mRNA encoding patient-specific neoantigens, protected by a lipoplex nanoparticle formulation. The particles are designed for preferential uptake in the spleen to drive antigen presentation and anti-tumor immunity. We developed a systems model to describe the mechanism of action of iNeST and its interaction with the innate and immune response. The model includes three physiological compartments (peripheral blood (PB), spleen, and tumor), and the following processes: pharmacokinetics of RNA lipoplex in PB and spleen; RNA uptake by antigen presenting cells (APCs) in spleen; TLR7/TLR8 stimulation by RNA and release of cytokines by APCs; maturation of dendritic cells; antigen presentation on MHCI molecules; interaction of DCs with CD8+ T-cells; T cell priming, differentiation, activation and memory generation; and finally tumor killing by activated CD8+ T-cells. The model was developed in SimBiology and Matlab (MathWorks, Natick MA).

Results: The model was calibrated using preclinical data in mice treated with GFP-, OVA- or gp70-encoded RNA lipoplex [1]. The model successfully reproduced RNA uptake, translation, and antigen presentation at different dose levels, and replicated the effects of RNA-lipoplex on cell maturation and dynamics of DCs and macrophages. Additionally, the model captured the complex dynamics of antigen-specific T-cells in response to a wide range of dose levels, different regimens, and antigens. Importantly, the model also reproduced the behavior of antigen-specific T-cell response when only a fraction of RNA-lipoplex encodes meaningful antigen and the remaining RNA is irrelevant. The model has the potential to evaluate different dosing strategies in patients and to inform combinations of iNeST with other molecules.

Conclusions: The mechanism-based systems model of innate and adaptive immune response accurately reproduces the pharmacodynamics of iNeST in preclinical settings in response to different antigens at different dose levels and regimens. The model provides mechanistic insight into how iNeST works and has the potential to inform research and clinical questions.

References:

- [1] Kranz, L. M., et al. Nature (2016) 534.7607: 396.
- [2] Sahin, U., et al. Nature (2017) 547.7662: 222.

Practical Identifiability Analysis of QSP Models with LikelihoodProfiler

Ivan Borisov¹, Evgeny Metelkin¹

¹InSysBio, Moscow, Russia

Background: Identifiability analysis is a crucial step in improving reliability and predictability of QSP models. Various methods of practical identification have been proposed including Monte Carlo simulations, Fisher information matrix, Profiler Likelihood, etc. Profile Likelihood (PL) is a reliable though computationally expensive approach. Confidence Intervals by Constraint Optimization (CICO) algorithm based on Profile Likelihood was designed to reduce computational requirements and increase the accuracy of the estimated parameters confidence intervals.

Objectives: The software package LikelihoodProfiler implementing CICO algorithm was tested on real QSP models and compared to other approaches to identifiability analysis. The results of these analyses will be presented.

Methods: CICO algorithm has several advantages over original stepwise PL implementations. Stepwise approach implies visualizing parameters profiles and deriving confidence intervals endpoints as profiles intersections with the significance level threshold. This approach often produces inaccurate endpoint estimates and is computationally expensive. CICO algorithm tests parameters identifiability by estimating their confidence interval endpoints with some preset tolerance. The algorithm does not recover the whole profile to obtain confidence intervals endpoints (or to state non-identifiability), which results in less likelihood function evaluations and increased performance in comparison with stepwise PL approach. CICO translates confidence intervals estimation problem into an optimization problem and solves it by converging to confidence interval endpoint. The algorithm does not require likelihood function derivatives and enables modeler to choose derivative-free or gradient-based optimization algorithm.

Results: CICO algorithm is proposed for complex QSP models where each likelihood estimation can be computationally expensive and some parameters are non-identifiable. The algorithm was tested on SB (Systems Biology) and QSP models described in published studies, including Cancer taxol treatment model [1], TGF- β pathway model [2], etc. Confidence intervals endpoints estimated with CICO correspond with the values reported in the articles. It was shown, that on average the algorithm overperforms stepwise PL approach especially in case of non-identifiable parameters. Detailed analysis of each model can be found on github: <https://github.com/insysbio/likelihoodprofiler-cases>. The CICO algorithm is available in a free software package LikelihoodProfiler based on Julia (<https://github.com/insysbio/LikelihoodProfiler.jl>) and Python (<https://github.com/insysbio/LikelihoodProfiler.py>).

Conclusions: The proposed algorithm and software package can be used as a means of identifiability analysis and confidence intervals evaluation for SB and QSP models of different complexity.

References:

- [1] M. C. Eisenberg and H. V. Jain, "A confidence building exercise in data and identifiability: Modeling cancer chemotherapy as a case study," *J. Theor. Biol.*, vol. 431, pp. 63–78, Oct. 2017, doi: 10.1016/j.jtbi.2017.07.018.
- [2] A. Gábor, A. F. Villaverde, and J. R. Banga, "Parameter identifiability analysis and visualization in large-scale kinetic models of biosystems," *BMC Syst. Biol.*, vol. 11, no. 1, p. 54, Dec. 2017, doi: 10.1186/s12918-017-0428-y.

WED-035

Using Population Pharmacokinetic Modelling Methods in Hemophilia A to Guide Individualized Dosing for Clotting Factor Concentrates

Jacky K Yu¹, Alfonso Iorio^{2,3}, Andrea N Edginton¹

¹School of Pharmacy, University of Waterloo, Waterloo, ON, Canada; ²Department of Health Research Methods, Evidence, and Impact, McMaster University, Hamilton, ON, Canada; ³McMaster-Bayer Research Chair in Clinical Epidemiology of Congenital Bleeding Disorders, Department of Medicine, McMaster University, Hamilton, ON, Canada.

Objectives:

Hemophilia is a bleeding disorder caused by a lack of clotting factor. Due to the development of extended half-life (EHL) clotting factor concentrates (CFC), hemophilia A patients may switch their prophylactic treatment to another CFC that is dosed less frequently. When switching, CFCs are prophylactically dosed based on international units per weight, however this approach does not account for the large pharmacokinetic (PK) variability between individuals. Our goal is to develop and evaluate methods to predict individual PK on efmoroctocog alfa (Eloctate) using population PK (PopPK) models.

Methods:

PK data from subjects taking Eloctate as well as Adynovate or a standard half-life (SHL) CFC was collected from the Web-Accessible Population Pharmacokinetic Service – Hemophilia (WAPPS-Hemo.org) database. The PopPK models used were two-compartment models with fat-free mass and age as covariates, with between-subject variability terms (η , or η) on clearance and volume. Method 1 used a PopPK model for Eloctate based on covariates only (e.g. age, weight) while Method 2 included knowledge of η , the individual deviation from a population for any PK parameter, calculated from the prior CFC PopPK model (Adynovate or SHL CFC). Individual PK outcomes including half-life and time-to-2% were obtained. Percent differences of predicted individual PK outcomes of Eloctate compared to observed PK outcomes were derived for each method.

Results:

Data used in the analysis included 231 subjects. The half-life geometric mean absolute percent differences were lower by up to 4.1% for Method 2 compared to Method 1. Individuals with η_{CL} or η_{V1} below the 20th percentile and above the 80th percentile benefited the most from Method 2, with half-life and time-to-2% estimates up to 25% relative error lower than Method 1 when compared to observed.

Conclusions:

During the time of switching, PK-guided dosing using PK knowledge from prior CFC (η 's) may improve the ability of clinicians to target appropriate CFC activities in patients.

WED-036

POPULATION PHARMACOKINETICS OF THIOTEPA AND ITS ACTIVE METABOLITE, TEPA, IN PEDIATRIC PATIENTS UNDERGOING HEMATOPOIETIC CELL TRANSPLANTATION (HCT)

Jagan Parepally, PhD¹, Jayesh Patel, MS¹, Christopher C. Dvorak, MD², Alexis Melton, MD², Christine Highan, MD², Ying Lu, PhD², Beth Apsel Winger, MD, PhD³, Joga Gobburu, PhD^{1*}, Janel Long-Boyle, PharmD, PhD^{2,4}

¹Center for Translational Medicine, School of Pharmacy, University of Maryland, Baltimore, MD, USA;

²Department of Pediatrics, Division of Allergy, Immunology, and Bone Marrow Transplantation, University of California San Francisco, San Francisco, CA, USA

³Department of Pediatrics, Division of Hematology and Oncology, University of California San Francisco, San Francisco, CA, USA,

⁴Department of Clinical Pharmacy, University of California San Francisco, San Francisco, CA, USA.

Objectives: ThioTEPA is an alkylating agent used in pretransplant combination chemotherapy prior to hematopoietic cell transplantation (HCT) to support engraftment of donor stem cells. The primary aims of this study were 2-fold: (1) to develop a combined population PK model for thioTEPA and its active metabolite, TEPA and (2) to identify sources of variability that contribute to patient disposition including drug clearance and exposure. An exploratory objective was to estimate and compare PK parameters obtained from using nonlinear mixed effects (NLME) modeling via NONMEM and those obtained using the Pumas software.

Methods: Plasma time-concentration data for thioTEPA and TEPA were collected in 14 pediatric patients as part of a single center, prospective, open-label, non-interventional study. Multiple dosing strategies were evaluated depending on diagnosis and included 300 mg/m², 5 mg/kg or 10 mg/kg administered by a continuous IV infusion over 1 to 2 hours. Following a single dose of thioTEPA a total of 4 blood samples were collected were collected as determined through an optimal sampling strategy. The FOCEI maximum likelihood approximation (MLE) estimation method was used for the model-building process to estimate PK parameters, along with estimation of between-subject variability (BSV), and residual unexplained variability. Patient-specific covariates, including gender, age, actual body weight and laboratory markers for hepatic and renal function, were evaluated to quantify the contribution to variability in PK parameters.

Results: A two- compartment PK model for both thioTEPA and TEPA with proportional error model best described the data. An empirical allometric scaling of clearance and volume parameters significantly improved the model fit (Δ OFV = 8.964, $p < 0.05$). The population mean volume of distribution and clearance of thioTEPA from the final population PK model are 12.6 L/15 kg and 2.5 L/h/15 kg, respectively, and were in good agreement with those previously reported by TEPADINA prescribing information (18 L and 9 L/hr). Actual body weight was identified as the predictor of clearance and volume of distribution of thioTEPA and TEPA, which explained 33% and 161% of the BSV in central volume and clearance, 43% of intercompartmental clearance of thioTEPA in the final model. Most of the PK parameter estimates were comparable between the Pumas and NONMEM software.

Conclusions: A two-compartment combined population PK model for both thioTEPA and TEPA with proportional error with standard allometric scaling of all fixed parameters best described the data. The population PK model can be applied to evaluate and optimize dosing strategies within the pediatric autologous and allogeneic HCT patient population with future studies.

*Disclaimer: Dr. Gobburu is a co-founder of Pumas-AI that commercializes Pumas software.

WED-037

Exposure-Response Analyses of Idecabtagene Vicleucel (Ide-Cel; bb2121), a Novel Anti-BCMA CAR T Cell Therapy, in Patients With Relapsed/Refractory Multiple Myeloma

Jamie Connarn¹, Han Witjes², Benjamin Rich³, Marielle van Zutphen-van Geffen², Rik de Greef², Timothy Campbell¹, Liping Huang¹, Kristen Hege¹, Shari Kaiser¹, Maria Palmisano¹, Simon Zhou¹, Manisha Lamba¹

¹Bristol Myers Squibb, Princeton, NJ, USA

²Certara Strategic Consulting, Oss, The Netherlands

³Certara Strategic Consulting, Montreal, Quebec, Canada

Objectives: Ide-cel is an immunotherapy consisting of T cells transduced with an anti-BCMA chimeric antigen receptor (CAR) lentiviral vector. In the phase 2 KarMMA study (NCT03361748), ide-cel demonstrated an overall response rate (ORR) of 73%, and complete response rate (CRR) of 31%, in heavily pretreated patients with multiple myeloma who received ≥ 3 prior therapies, including an immunomodulatory agent, a proteasome inhibitor, and an anti-CD38 antibody [1]. The objective of this analysis was to evaluate exposure-response (ER) relationships of ide-cel efficacy endpoints and safety events in KarMMA.

Methods: Ide-cel exposure data were available from 127 treated subjects at target doses of 150, 300, and 450×10^6 CAR+ T cells in KarMMA. Key exposure metrics including area under the transgene curve from 0–28 days ($AUC_{0-28\text{days}}$), area under the transgene curve from 0–3 months ($AUC_{0-3\text{M}}$), and maximum transgene level (C_{\max}) were calculated via noncompartmental methods. ER evaluation analyzed multiple efficacy endpoints, including ORR, very good partial response rate or better, and CRR, as well as safety events, such as cytokine release syndrome (CRS), CRS that required concomitant medication with tocilizumab and corticosteroids, investigator-identified neurotoxicity, and cytopenias. ER trends were examined by evaluating the proportions of responders for quartiles of the exposure distribution across the dose range. Upon observation of an apparent ER trend, candidate models were developed with logistic regression, fitting either linear, maximum effect (E_{\max}), or sigmoid E_{\max} functional forms. Covariates were also evaluated for potential effects on the likelihood of response using stepwise forward selection followed by backward elimination, with significance levels of 0.05 and 0.01, respectively. Established ER models were finally used to simulate dose-response relationships and evaluate the impact of identified covariates.

Results: There was wide overlap of exposures across the target doses. ER relationships were observed for each of the efficacy endpoints, with higher response rates associated with higher exposure. Model-based evaluations identified statistically significant covariates and baseline demographics and disease characteristics for each of the efficacy endpoints, in addition to the impact of the exposure parameter. Specifically, female sex was predictive of a higher ORR ($p=0.003$) and baseline serum monoclonal-protein ≤ 10 g/L was predictive of a higher CRR ($p<0.001$). ER relationships were observed for safety events of CRS requiring tocilizumab or corticosteroids; however, no ER trends were observed for grade ≥ 3 CRS, investigator-identified neurotoxicity, or cytopenias.

Conclusions: The observed ER relationships were primarily driven by lower response rates being associated with the lowest quartiles of exposure. Established ER models were used to predict dose-response relationships, which showed a positive benefit-risk assessment across the range of ide-cel exposures associated with a dose range of $150-540 \times 10^6$ CAR+ T cells.

Reference: 1. Munshi et al. *J Clin Oncol* 38:2020 (suppl; abstr 8503).

**Quantitative Systems Toxicology Modeling Supports Safety Determination
for Ubrogepant, a Novel CGRP Inhibitor**

Jeffrey L. Woodhead*, Brett A. Howell*, Brenda Smith**, Josh M. Rowe**, Scott Q. Siler*

*DILIsym Services, Inc., a Simulations Plus company, RTP, NC, USA

**Allergan Plc, Irvine, CA, USA

Objectives: CGRP inhibitors are a class of drugs that meet a significant unmet medical need for migraine treatments. However, two CGRP inhibitors, telcagepant and MK-3207, failed in clinical trials due to liver toxicity (1,2). Telcagepant, MK-3207, and the next-in-class compound ubrogepant were represented in DILIsym, a quantitative systems toxicology (QST) model of drug-induced liver injury, in order to predict whether ubrogepant would be a safer alternative.

Methods: *In vitro* experiments were undertaken determining the potential for the three compounds to inhibit bile acid transporters, cause mitochondrial dysfunction, and produce oxidative stress. The results of the *in vitro* assays were used to produce a representation of each compound in DILIsym, along with a PBPK model of each compound. The clinical doses of telcagepant and MK-3207 at which liver toxicity was observed were simulated, as well as a range of potential ubrogepant clinical protocols.

Results: Each of the molecules tested displayed signals in the *in vitro* assays for bile acid transporter inhibition, oxidative stress generation, and mitochondrial dysfunction. DILIsym correctly predicted the liver toxicity of telcagepant and MK-3207, while ubrogepant was predicted to be safe at doses up to 10X the proposed clinical dose (Table 1). Subsequent clinical trials demonstrated that ubrogepant was indeed safe (3), and the drug was approved by the FDA for the acute treatment of migraine.

Conclusions: QST modeling can prospectively differentiate between toxic and non-toxic drugs within the same class and identify which drugs within a class carry less risk of toxicity. These applications can contribute to success in the clinic and regulatory approval of new drugs.

- References:**
1. Ho TW, Connor KM, Zhang Y, Pearlman E, Koppenhaver J, Fan X, et al. Randomized controlled trial of the CGRP receptor antagonist telcagepant for migraine prevention. *Neurology*. 2014 Sep 9;83(11):958–66.
 2. Holland PR, Goadsby PJ. Targeted CGRP Small Molecule Antagonists for Acute Migraine Therapy. *Neurotherapeutics*. 2018 Apr;15(2):304–12.
 3. Ailani J, Lipton RB, Hutchinson S, Knievel K, Lu K, Butler M, et al. Long-Term Safety Evaluation of Ubrogepant for the Acute Treatment of Migraine: Phase 3, Randomized, 52-Week Extension Trial. *Headache*. 2020 Jan;60(1):141–52.

Table 1. Simulated ALT elevation frequency in a 285-individual model population using DILIsym v7A.

Compound	Dosing Protocol	Simulated* ALT > 3X ULN**	Clinical ALT > 3X ULN***
MK-3207	200 mg q2h, 2 daily doses (400 mg daily dose), for 14 days	3.5% (10/285)	42% (5/12) amongst individuals dosed for more than 1 week; most responding were given 600 – 900 mg per day
	300 mg q2h, 2 daily doses (600 mg daily dose), for 14 days	7% (20/285)	
	450 mg q2h, 2 daily doses (900 mg daily dose), for 14 days	10.2% (29/285)	
Telcagepant	280 mg BID 12 weeks	12.6% (36/285)	3.2% (8/265)
	140 mg BID 12 weeks	0% 0/285	1.9% (5/263)
Ubrogepant	100 mg qd, 2 days on, 2 days off for 56 days, 28 total doses	0% (0/285)	No ALT elevations observed
	1000 mg qd, 2 days on, 2 days off for 56 days, 28 total doses	0% (0/285)	N/A

WED-039

Population Pharmacokinetic-Pharmacodynamic Modeling of Platelet Time Courses After Administration of Abrocitinib

Authors: Jessica Wojciechowski,¹ Bimal K. Malhotra,² Xiaoxing Wang,¹ Luke Fostvedt,³ Hernan Valdez,² Timothy Nicholas¹

Institutions: ¹Pfizer Inc., Groton, CT, USA; ²Pfizer Inc., New York, NY, USA; ³Pfizer Inc., Cambridge, MA, USA

Objectives:

Abrocitinib is a selective Janus kinase 1 inhibitor being developed for the treatment of moderate-to-severe atopic dermatitis (AD). Transient decreases in platelet counts were observed in phase 2 psoriasis and AD patient studies. The objectives of this analysis were to develop a population pharmacokinetic-pharmacodynamic (PK-PD) model to describe the time course of drug-induced platelet reduction after abrocitinib administration.

Methods:

The platelet analysis data set was pooled from 2 phase 2 studies and 3 phase 3 studies (duration; 12 weeks, dose range; 10 mg once daily [QD] up to 400 mg QD). Abrocitinib concentrations for time-matched platelet observations were predicted for analysis individuals based on empirical Bayes estimates of parameters from a population PK model or assumed the population-typical values for individuals when abrocitinib concentrations were not available (ie, placebo). The semimechanistic platelet model was based on the chemotherapy-induced myelosuppression model.¹ The effect of abrocitinib concentrations on platelet proliferation was described by an E_{max} relationship, and the implementation of tachyphylaxis (additional to inherent feedback mechanisms) was considered. Intrinsic patient factors on the platelet time course were assessed by stepwise covariate modeling procedures. The impact of baseline platelet count on the probability of thrombocytopenia at the nadir and week 12 after administration of the highest therapeutic dose of 200 mg QD in phase 3 was assessed by simulation.

Results:

The final estimate for the concentration at 50% of the maximum effect (EC_{50}) on platelet proliferation was 55.3 ng/mL. For the average AD patient administered 200 mg QD at steady state, the typical time above EC_{50} was 15.3 hours, and the time delay between dosing and a decrease in circulating platelets was 7.21 days, corresponding to a time of nadir of 24 days. Significant predictors of lower baseline platelets counts were disease-type (psoriasis, 12% lower), lower baseline white blood cell count (4300/ μ L [5th percentile], 9% lower), sex (male, 6% lower), older age (64 years [95th percentile], 5% lower), higher baseline hematocrit (49% [95th percentile], 3% lower). For example, an individual with a baseline platelet count of 170,000/ μ L was predicted to experience a net decrease in platelets after 12 weeks of 26.2%, and a probability of grade 1 (75,000-150,000/ μ L; 76.2%) and grade 2 thrombocytopenia (50,000-75,000/ μ L; 16.3%) at the nadir after administration of 200 mg QD. The probability of grade 3 (25,000-50,000/ μ L) and grade 4 (<25,000/ μ L) thrombocytopenia was <3%.

Conclusions:

For a typical AD patient given 200 mg QD for 12 weeks, the probability of grade 1 thrombocytopenia was <10% at the nadir and <1% at week 12. The probability of higher grades of thrombocytopenia was approximately 0%.

References: 1. Friberg LE et al. *J Clin Oncol*. 2002;20:4713-4721.

WED-040

Usage of In vitro Metabolism Data for Drug-drug Interaction Prediction in Physiologically-Based Pharmacokinetic (PBPK) Modeling Submissions

Jieon Lee^{1,2}, Yuching Yang¹, Xinyuan Zhang¹, Jianghong Fan¹, Manuela Grimstein¹, Hao Zhu¹, Yaning Wang¹

¹Office of Clinical Pharmacology, Office of Translational Sciences, Center for Drug Evaluation and Research, U.S. Food and Drug Administration

²Oak Ridge Institute for Science and Education

Objectives: The physiologically-based pharmacokinetic (PBPK) models are usually developed by combining information from *in vitro* and *in vivo* studies. Intrinsic clearance (CL_{int}) and fractional contribution of the metabolizing enzyme toward metabolism (f_m) are the key parameters for the prediction of DDI. We aimed to summarize the accumulated knowledge from new drug applications (NDAs) to understand the current usage of *in vitro* data in PBPK models used for DDI prediction.

Methods: We collected the *in vitro* data in approved NDAs containing PBPK models which were submitted to the Office of Clinical Pharmacology, U.S. Food and Drug Administration from 2016 to 2018. The collected information includes physicochemical properties, *in vitro* metabolic profiling methods and data, and the methods used in the final model for determining CL_{int} and f_m .

Results: We screened all approved 51 NDAs including PBPK models. 35 and 26 NDAs were included for evaluation of CL_{int} and f_m respectively. For CL_{int} , most of the PBPK model (86%) used modified value based on *in vivo* data. A limited number of the evaluated models used CL_{int} scaled from *in vitro* data without modification. For f_m , 38.5% of the models modified the values with modification ranging -65%-178.6% from *in vitro* test. When using *in vitro* CL_{int} and f_m , without modification or optimization, the model resulted in up to 12.1-fold, 2.9-fold underprediction in area under concentration of substrate (AUC%) or AUC of substrate with and without inhibitor/inducer administration (AUCR), respectively.

Conclusions: Our results can be used to leverage the accumulated knowledge from these applications to better understand current usage of *in vitro* data and in PBPK models. Alignment between industry, academia, and regulatory agencies in developing the best practices for usage of *in vitro* data in PBPK modeling is warranted.

Keywords: PBPK modeling, *in vitro* metabolism, drug-drug interaction

WED-041

Clinical Trial Simulation to Inform Phase 1b/2a Study Design in Infants to Accelerate Development of an RSV Monoclonal Antibody (MK-1654)

Authors: Jingxian Chen, Brian Maas, Wei Gao, Ferdous Gheyas, Luzelena Caro

Affiliation: Merck & Co., Inc., Kenilworth, NJ, USA

Objectives: MK-1654 is a monoclonal antibody being developed for the prevention for Respiratory Syncytial Virus (RSV) in infants. A Phase 1b/2a dose-ranging study in infants is currently ongoing. An interim analysis is planned for this study to facilitate a Go/No-Go to Phase 2b/3 decision. The Go decision criteria under consideration for the interim analysis requires adequate pharmacokinetic (PK) data to predict with high confidence that a typical infant will have a true geometric mean concentration 150 days after a single dose (C_{150}) above the pre-established PK target. Concentration on Day 150 was chosen as the PK endpoint since it covers the typical length of an RSV season. The current analysis aims to determine the minimum sample size required to enable an early interim analysis decision using clinical trial simulation (CTS).

Methods: An established adult population pharmacokinetic model describes MK-1654 PK using a two-compartment model with first-order absorption [1]. Infant PK was predicted from the adult model using allometric scaling. Time-varying PK resulting from infant growth was taken into account by predicting body weight over time using modified growth chart equations developed by U.S. Centers for Disease Control and Prevention (CDC). Clinical trials were simulated for scenarios with varying sample sizes. In addition, uncertainty in adult-infant PK extrapolation was explored through a sensitivity analysis by varying allometric scaling exponents on clearances and volumes of distribution (separately and jointly) and including a maturation function [2]. For each scenario, 200 clinical trials were created accounting for parameter uncertainty, and C_{150} for the total number of infants in each trial were simulated with inter-subject and residual variability. Study power was estimated as the percentage of simulated trials meeting the prespecified criteria, i.e. the geometric mean of simulated C_{150} within this trial exceeding the PK target.

Results: Clinical trial simulation (CTS) showed a >90% power to make a Go/No-Go decision for the all sample sizes under the most likely scenario. Sensitivity analyses indicated that study power based on the current Go/No-Go criteria is sensitive to allometric scaling parameters. In each allometric scaling scenario, only modest improvement in power (approximately 10%) was gained by increasing the sample size from the minimum to the maximum being considered. Therefore, delaying the interim analysis to enroll additional infants was considered unnecessary.

Conclusions: CTS analyses provide confidence that the interim analysis can be triggered with fewer subjects than originally planned. This analysis highlights the application of clinical trial simulation to help accelerate development timelines and provides a framework that can be leveraged in other pediatric drug development programs.

References:

- 1) Maas, BM, et al. Open Forum Infectious Diseases, 2018, Nov, Volume 5, Issue suppl_1, S424–S425.
- 2) Pierre V, et al. American Conference for Pharmacometrics. 2018. Abstract # W-082.

WED-042

Population pharmacokinetics of belantamab mafodotin, a BCMA targeting agent in patients with relapsed/refractory multiple myeloma (RRMM)

Authors: Jon Collins¹, Chetan Rathi², Herbert Struemper¹, Joanna Opalinska², Roxanne C Jewell¹, and Geraldine Ferron-Brady²

Institutions: ¹GlaxoSmithKline, Research Triangle Park, NC; ²GlaxoSmithKline, Collegeville, PA;

Objectives: Belantamab mafodotin (GSK2857916) is a first-in-class B-cell maturation antigen (BCMA)-targeting immunoconjugate with a humanized afucosylated anti-BCMA monoclonal antibody (mAb) conjugated to a cytotoxic payload mafodotin (MMAF) by a protease-resistant maleimidocaproyl linker (mc). This antibody-drug conjugate (ADC) binds to BCMA and eliminates MM cells by a multimodal mechanism. It delivers MMAF to MM cells which inhibits microtubule polymerization resulting in apoptosis, enhances antibody-dependent cellular cytotoxicity and phagocytosis, and induces immunogenic cell death. The objective was to develop a population PK model for belantamab mafodotin, to identify covariates of clinical relevance, and to estimate relevant exposure measures for E/R analysis^[1].

Methods: Nonlinear mixed-effects models were developed to characterize the PopPK of ADC, total mAb and cys-mcMMAF after intravenous infusion at 0.03 to 4.6 mg/kg Q3W in 291 heavily pretreated RRMM patients enrolled across a phase I (DREAMM-1, n=73) and the pivotal phase II study (DREAMM-2, n=218). Sequential modeling was performed, with individual *post hoc* parameter estimates from the final ADC model being used for model development of total mAb and cys-mcMMAF models. Covariates were assessed using forward inclusion ($p < 0.01$), backward elimination ($p < 0.001$) modelling procedures. Covariates evaluated included demographics, clinical chemistries, organ function, soluble BCMA (sBCMA) concentration, and drug configuration.

Results: A linear, two-compartment PopPK model with time-varying clearance described the PK of ADC. The sum of ADC and naked antibody formed via deconjugation of cys-mcMMAF using a first-order rate constant accounted for total mAb concentration. Cys-mcMMAF concentrations were described with a linear two-compartment model linked to ADC; the input rate was governed by deconjugation/intracellular proteolytic degradation of ADC modulated by an exponentially decreasing MMAF:mAb ratio (DAR) after each dose. Baseline sBCMA, IgG, albumin (inverse), and body weight were found to impact clearance, whereas baseline albumin (inverse), body weight, and gender affected central volume of ADC. Baseline sBCMA and IgG impacted the central volume of distribution of cys-mcMMAF. The initial geometric mean(%CV) ADC clearance in patients from DREAMM-2 was 0.924 L/day (42%) with a half-life of 11.8 days (31%). Over time, clearance was reduced to 0.725 L/day (50%), resulting in a longer half-life of 14.0 days (37%). The time to 50% of maximal change in clearance was ~50 days. The time to 50% reduction in DAR was 10.3 days after an administered dose.

Conclusions: ADC, total mAb, and cys-mcMMAF concentration–time profiles in RRMM patients were well described by their respective PK models, with disease-related characteristics the most significant factors associated with exposure. Mild to moderate renal impairment, mild hepatic impairment, age, African American race, prior treatments and drug configuration were not found to significantly impact ADC or cys-mcMMAF pharmacokinetics.

References: [1] Rathi et al., ACoP2020

Results in this abstract have been accepted in part for AACR, 2020.

WED-043

Leveraging Data from a Phase 1 Study of Loncastuximab Tesirine in Adults with Relapsed/Refractory Non-Hodgkin Lymphoma for Pediatric Dose Prediction

Xiaoyan Zhang¹, David Ungar¹, Yajuan Qin¹, Joseph Boni^{1*}

¹ADC Therapeutics America Inc., Murray Hill, NJ, USA

*Corresponding Author E-mail: joe.boni@adctherapeutics.com

Objectives: ADCT-402-101 is a first-in-human Phase 1 study of loncastuximab tesirine (Lonca; previously ADCT-402) in adult patients (≥ 18 years old) with relapsed or refractory B-cell non-Hodgkin lymphoma (NHL). Lonca is a novel antibody-drug conjugate comprising a humanized monoclonal antibody of immunoglobulin G1 (IgG1) directed against human CD19, stochastically conjugated with a potent pyrrolobenzodiazepine (PBD) dimer toxin. This analysis aims to use a pharmacostatistical model of Lonca in the adult population to determine a dosing regimen for the initial treatment of pediatric patients with NHL.

Methods: Serum concentrations of Lonca PBD-conjugated antibody from 183 adult patients were used to establish a linear two-compartment model with inter-occasion variability for pediatric dose estimation. The population pharmacokinetic (PK) model added body weight (WT) as a covariate on both clearance (linear elimination clearance [CL], distribution clearance [Q]), and volume of distribution (central compartmental [V1] and peripheral compartment [V2]). Allometric scaling constants of 0.75 on clearance and 1 on volume of distribution were employed to predict the exposure of conjugated antibodies in the simulated pediatric population. CDC NHANES datasets from 1999–2016 were used to derive and sample the distribution of WT for pediatric age groups from ages 6 months to 17 years. The model was used to stochastically simulate PK profiles for 2000 virtual pediatric patients in each age stratification group to determine the corresponding dose that matched the target exposure for the adult Lonca dosing regimen in NHL (150 $\mu\text{g}/\text{kg}$ every 3 weeks [Q3W] for 2 doses [x2], followed by dose reduction to 75 $\mu\text{g}/\text{kg}$ Q3W x4).

Results: The simulations provided reasonable comparability of the predicted area under the curve at steady state (AUC_{ss}) and peak concentration (C_{max}) values within the 90% prediction interval (PI) of the corresponding adult exposure range across the various pediatric age/WT bands. For the first 2 cycles of treatment, predictions from the exposure metrics indicate that Lonca doses required to achieve target exposure within the 90% PI of adult exposure following 150 $\mu\text{g}/\text{kg}$ Q3W x2 treatment are 170 $\mu\text{g}/\text{kg}$ Q3W x2 for children aged 6 months to <24 months and age 2 years to <6 years, and 150 $\mu\text{g}/\text{kg}$ Q3W x2 for children aged 6 years to <12 years and adolescents aged 12 to <17 years. For cycles 3–6, Lonca doses would be commensurately reduced by 50% for the respective subgroups.

Conclusion: Through pharmacostatistical modeling, rational dosing regimens for the initial treatment of pediatric patients with NHL are proposed.

Quantitative Systems Pharmacology Dissection of IL-4/IL-13 Contribution to Human Allergic IgE Production

Kamau Pierre¹, Randolph J. Leiser¹, Yui-Hsi Wang², Mengdi Tao¹, Christine Xu³, Haobin Luo⁴, John Pappas⁴, Zhiwei Zhang⁴, Susana Zaph¹, Spyros Stamatelos¹, Paul Bryce² and Panagiota Foteinou¹

¹ Translational Disease Modeling, Digital Data Science, Sanofi, Bridgewater, NJ

² Type 2 Immunology & Fibrosis Cluster, Sanofi, Cambridge, MA

³ Pharmacokinetics, Dynamics and Metabolism US, Sanofi, Bridgewater, NJ

⁴ RES Group, Inc, Needham, MA

Objectives: Immunoglobulin E (IgE) antibodies play a crucial role in the pathogenesis of allergic diseases such as asthma, a disease affecting as many as 339 million people worldwide. Studies on the immunological basis of allergic diseases have indicated that aberrant production of the prototypical type 2 cytokines, interleukin (IL)-4 and IL-13 contribute to enhanced IgE synthesis and the development of clinical atopy. Despite tremendous scientific inquiry, the relative contribution of these cytokines to the production of IgE in allergic patients has remained poorly characterized, partly due to lack of suitable experimental models. Innovative approaches such as Quantitative Systems Pharmacology (QSP) modeling are valuable in deciphering such complexity by quantifying *in vivo* functional interactions within a biological network. On this basis, a human QSP model for type 2-driven IgE regulation was developed. A unique aspect of this modeling framework is that the simulated human (asthmatic) IgE levels emerge as a result of a complex inflammatory network spanning multiple scales (molecular, cellular, tissue).

Methods: The QSP model is multiscale in design, allowing the mechanistic representation of key biological processes underlying the production of human allergic IgE in their appropriate organ compartments (lymph node, blood). At the molecular level, the model represents explicitly the physicochemical interactions between IL-4/IL-13 cytokines and their receptor subunits (γ_c , IL-4R α , IL-13R α_1) located in the lymph node, particularly on the surface of human memory B cells. Serum IgE is, in turn, produced by plasma cells arising from B cell proliferation/differentiation, induced by the upstream cytokine-receptor signaling. During the model development phase, datasets from diverse sources (experimental and clinical) were used to parameterize and validate the model, with most of these data derived exclusively from clinical studies. These include quantitative *in vitro* (e.g. dose-dependent) data derived from human cells, as well as receptor and cytokine expression levels, tissue cell numbers, half-lives, and cytokine-receptor affinities. In terms of clinical validation, the model was benchmarked against its capability to reproduce IgE responses as seen clinically in published lebrikizumab studies.

Results: A mechanistic QSP model for IgE production in allergic asthma has been constructed and clinically calibrated to relevant experimental data. In terms of application, two exploratory case studies were performed to better understand the relative contribution of endogenous IL-4 vs. IL-13 signaling on aberrant IgE secretion. Interestingly, the model predicts greater sensitivity of asthmatic IgE levels to endogenous IL-4 than IL-13 signaling, due to a greater potency of IL-4 signaling in the lymph node (~4-fold difference).

Conclusions: A robust multiscale QSP strategy has been successfully implemented to capture key aspects of type 2 inflammation in IgE production. The proposed model has identified counterintuitive cytokine sensitivities – a novel hypothesis difficult to experimentally dissect – that have the greatest influence on IgE production in asthma.

WED-045

Towards Achieving Regulatory Endorsement of a Disease Progression Model-based Clinical Trial Simulation Tool for Duchenne Muscular Dystrophy– Models of Progression of Timed Motor Function Tests

Karthik Lingineni¹, Juan Francisco Morales¹, Daniela J Conrado², Camille Vong³, Nathan Hanan², Diane Corey², Jackson Burton², Jane Larkindale², Klaus Romero², Stephan Schmidt¹, Sarah Kim^{1,*}, on behalf of the Cooperative International Neuromuscular Research Group (CINRG) investigators and Duchenne Muscular Dystrophy Regulatory Science Consortium (D-RSC) members

¹ Center for Pharmacometrics and Systems Pharmacology, Department of Pharmaceutics, College of Pharmacy, University of Florida, Orlando, FL, USA

² Critical Path Institute, Tucson, AZ, USA

³ Novartis Pharma AG, Basel, Switzerland

* Corresponding author's email: sarahkim@cop.ufl.edu

Objectives: The objective of this research was to optimize the design of clinical trials for Duchenne Muscular Dystrophy (DMD), through quantitative disease progression modeling and simulations, using 3 timed motor function tests, i.e. velocities of the 4 stair climb test, stand from supine test, and 10 meter (or 30 foot) walk/run.

Methods: Disease progression models were built from an aggregation of longitudinal patient-level data comprising 9 studies that include natural history and clinical trials with a total of #patients (#observations): 842 (4797) for velocity climb, 677 (3724) for velocity stand, and 825 (4538) for velocity walk/run. Patients were randomly divided into training and test datasets at a ratio of 4:1 for each endpoint, while maintaining the covariate composition in the composite dataset. Non-linear mixed effects modeling was utilized to describe disease progression. Several mathematical functions were tested to describe the longitudinal dynamics of endpoints in the training dataset, with the test dataset reserved for model validation. Missing observations resulting from the inability to perform tests due to disease severity were censored using the likelihood-based M4 method, conditional on the observation being greater than zero. Modeling was performed in Monolix (2019R2) using the SAEM algorithm and COnditional Sampling use for Stepwise-Approach based on Correlation tests (COSSAC) approach for covariate analysis¹.

Results: The product of the Chapman-Richards growth function and a sigmoid E_{max} model best captured the time course of all endpoints. The estimated DP_{max} (approximate maximum fractional decrease in score) was found to be 1 for all endpoints (**Table**). Age and velocities at first visit were significant covariates for all endpoints on G_{max} (approximate maximum possible score), DP_{50} (approximate age at which score is half of its maximum decrease) and gamma (shape parameter). Mutation (skip-44/del_3-7 or others) was identified as a covariate on DP_{50} for all endpoints, while race (Asian or others) was incorporated on DP_{50} for velocity stand and velocity climb. If a patient is having either skip-44 or del_3-7 mutations, this resulted in delayed onset of decline in endpoint. On the other hand, onset of decline occurred at younger ages in patients of Asian origin. However, this predicted effect of race could be due to differences in standard of care. Visual predictive checks of longitudinal endpoint observations and fraction of missing observations due to inability showed good agreement with observed data.

Conclusions: The final models adequately capture longitudinal changes of all timed motor function tests in DMD patients, including both increase and decline phases. These models may be used in clinical trial simulations to optimize selection of inclusion/exclusion criteria and other trial design parameters. We will extend these models to incorporate time-to-event models for predicting the probability of dropouts in clinical trials.

Reference:

¹Monolix version 2019R2. Antony, France: Lixoft SAS, 2019.

Table: Parameter estimates of models using 3 timed motor function tests

	Velocity climb		Velocity stand		Velocity walk/run	
	Value	R.S.E. (%)	Value	R.S.E. (%)	Value	R.S.E. (%)
Fixed Effects						
G _{MAX} -pop	0.97	1.18	0.363	1.92	2.95	0.923
beta_GMAX_logtBAGEAA	-1.12	2.81	-0.882	5.16	-0.708	2.18
beta_GMAX_logtBSCOREAA	0.909	1.52	0.831	2.97	0.97	1.47
DP _{MAX} -pop	1		1		1	0.006
DP ₅₀ -pop	10.7	1.1	10.1	1.02	11.4	0.971
beta_DP ₅₀ -Mutation	0.178	20.3	0.196	23.1	0.198	18.1
beta_DP ₅₀ -RACE	-0.0939	24	-0.0795	27.3	NE	NE
beta_DP ₅₀ -STUDY_TYPE	-0.0387	36.7	-0.0334	47.1	NE	NE
beta_DP ₅₀ _logtBAGEAA	0.531	4.8	0.612	4.53	0.528	4.81
beta_DP ₅₀ _logtBSCOREAA	0.0536	17.9	0.0927	13.8	0.155	13.2
DPG_pop	0.037	1.04	0.0946	2.2	0.104	1.29
GAMMA_pop	14.3	5.17	18.4	5.42	12.4	4.3
beta_GAMMA_STUDY_TYPE	0.181	42.2	NE	NE	NE	NE
beta_GAMMA_logtBAGEAA	1.39	9.85	1.28	14.4	1.01	11.7
beta_GAMMA_logtBSCOREAA	-0.682	7.72	-0.593	15.8	-1.39	7
Standard Deviation of the Random Effects						
omega_GMAX	0.151	5.03	0.205	4.43	0.0632	7.69
omega_DP50	0.14	4.37	0.126	4.77	0.16	4.38
omega_DPG	0.0692	10.8	0.109	14.1	0.069	12
omega_GAMMA	0.546	6.34	0.666	6.31	0.584	4.91
Correlations						
corr_GAMMA_DP ₅₀	NE	NE	NE	NE	-0.538	8.87
Error Model Parameters						
b	0.207	1.44	0.216	1.66	0.126	1.41

R.S.E. (%): Relative Standard Errors, G_{max}: approximate maximum possible score, g: power constant, DP_{max}: approximate maximum fractional decrease in score, DP₅₀: approximate age at which score is half of its maximum decrease, gamma: Hill coefficient or shape factor, beta_parameter_logtBAGEAA: power coefficient for age at first visit on parameter, beta_parameter_logtBSCOREAA: power coefficient for velocity at first visit on parameter, beta_DP50_Mutation: coefficient for mutation (skip-44/del_3-7 or others) as categorical covariate on DP₅₀, beta_DP50_RACE: coefficient for RACE (Asian or other) as categorical covariate on DP₅₀, beta_DP50_STUDY_TYPE: coefficient for study type (natural history or clinical trial) as categorical covariate on DP₅₀, and NE: Not estimated.

WED-046

Computational analysis of dynamic interactions between soluble shed target and pharmacokinetics of free drug: A case study with Bispecific Tcell engagers for cancer immunotherapy

Authors: Khamir Mehta, Sergey Ermakov, Vijay Upreti and Sandeep Dutta

Institution: Clinical Pharmacology, Modeling and Simulation, Amgen Inc, South San Francisco, CA

Background: Cell surface molecules representing targets for bispecific drugs often can be found circulating in plasma in a soluble form, for example, shed by tumor cells. The presence of shed target can interfere with drug action by preventing it from binding to the target on the surface of the tumor cell and can affect the observed free drug exposures. Additionally, the drug can also impact the levels of the shed target, by either direct effect and/or via the mechanism of action that includes the modulation of shedding rate, target expression, and finally the lysis of tumor cells. The dynamics of these various simultaneously occurring processes can make the characterization of the pharmacokinetics, and therefore, the prediction of an efficacious and safe dosing regimen quite challenging.

Objectives: In this effort, we explore the impact of shed target and its direct and indirect interactions with the bispecific monoclonal antibodies using a computational model. The key objective of the work is to elucidate the impact of this interactions on the pharmacokinetics of the free drug.

Methods: We have developed a mechanistic modeling framework that incorporates the dynamics of the mechanisms (Figure-1) in form of a system of ordinary differential equations. The model explicitly tracks the pharmacokinetics and biodistribution of the drug and the target-based interactions with tumor cells, whereby the tumor cells can potentially alter the target expression, increase the shedding rate or internalization, and undergo lysis owing to the action of the activated immune cells.

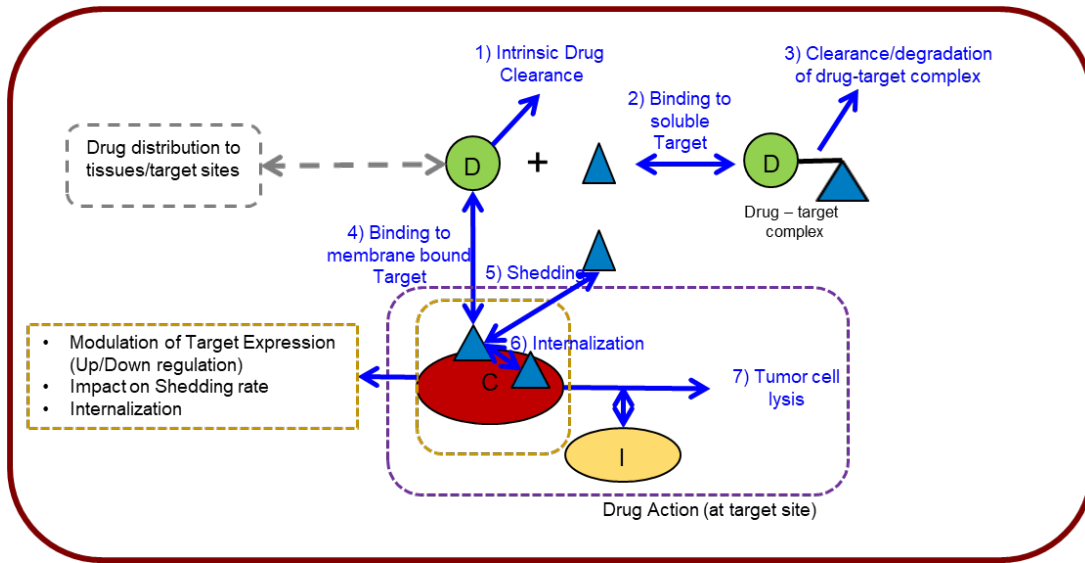
We parameterize the base model with reasonable estimates of parameters based on published clinical data for across different monoclonal antibodies and different shed target levels. Using computational experiments, we systematically explore the impact of the shed target levels on the availability of the free drug as a function of various system and drug related parameters.

Results:

Expectedly, our analysis shows a sharp decline in the free drug exposures when the levels of shed target increase above the dissociation constant of binding (K_d). Furthermore, the impact of the tumor growth, drug induced immune cell mediated lysis of tumor cells, target shedding rate can introduce time dependence on the pharmacokinetics of the drug, which may warrant a time varying drug dosing regimen to ensure optimal efficacy. Finally, we also demonstrate the potential impact of drug induced target shedding/internalization on the pharmacokinetics, which can give rise to several non-intuitive pharmacokinetic profiles.

Conclusions: We have developed a platform to theoretically investigate the complex interplay of tumor growth, immune action, antigen shedding and intrinsic drug pharmacokinetics to understand the potential impact on the drug efficacy and safety. This model can provide valuable insight to facilitate the development of various bispecific drugs across different immunotherapeutic areas for cancer treatment.

Figure 1: Relevant Mechanisms governing pharmacokinetics of free drug in presence of soluble/shed target



	Drug
	Target (shed and membrane bound)
	Immune cells
	Cancer cells

Optimization of dose selection using multiple surrogates of toxicity as a continuous variable in Phase I cancer trial

Se Yoon Lee¹, Shankar Lanke¹, Alain Munafo², Pascal Girard², Kosalaram Goteti¹

¹EMD Serono, Inc., Billerica, MA, USA, a business of Merck KGaA, Darmstadt, Germany;

²Merck Institute of Pharmacometrics, Lausanne, Switzerland, an affiliate of Merck KGaA, Darmstadt, Germany

Objective: Using novel methodology for achieving maximum tolerated dose (MTD) for anti-cancer drugs with narrow therapeutic range during Phase I oncology trials.

Methods: In this paper, we consider a fully sequential design setting where patients are introduced to the trials individually and sequentially, and each patient is assigned with an optimal estimate of MTD based on the accumulated patient's information at interim. To protect patients from being overdosed, a drug is initiated at a very low dose and slowly escalated toward the targeted MTD as the trials go on. Typically, two pioneering Bayesian adaptive designs for the phase I cancer clinical trials are continual reassessment method (CRM) and escalation with overdose control (EWOC). Two drawbacks of CRM and EWOC are that, first, adverse event is recorded with a binary response, DLT (dose limiting toxicity) or non DLT, and second, they cannot accommodate grade information for multiple adverse events (AE). To accommodate grade information from multiple AEs, recently, EWOC using normalized equivalent toxicity score (EWOC-NETS)¹, one of expansion of EWOC, has been developed: however, the results cannot be reproduced by simulation because EWOC-NETS is based on a pseudo-Bernoulli likelihood. In this paper, we upgrade one parameter linear dose-finder (1PLD)² into the two- parameter linear dose-finder (2PLD) to address a continuous toxicity response in the phase I cancer clinical trials. The 2PLD assumes a linear relationship between a toxic reaction and a dosage (or an exposure), and treats the toxicity response as a continuous variable, aimed at utilizing the Common Toxicity Criteria for Adverse Events provided by the National Cancer Institute. The proposed search procedure suggests an optimal exposure to each patient by using accrued patients' information while controlling the posterior probability of overdose.

Results: The simulations show that this novel 2PLD method has good operating characteristics and improved accuracy in achieving MTD. Generally, simulations showed that the 2PLD requires a fewer step to converge to the targeted MTD than using adaptive clinical trial design methods that are based on binary responses such as EWOC or CRM.

Conclusions: This novel 2PLD can be an attractive tool for clinical scientists because of its parsimonious description of a toxicity-dose curve, medically interpretable hyperparameters, and an automated posterior computation.

References:

1. Zhengjia Chen, Mourad Tighiouart, and Jeanne Kowalski. Dose escalation with overdose control using a quasi-continuous toxicity score in cancer phase i clinical trials. *Contemporary Clinical Trials*, 33(5):949–958, 2012.
2. Benjamin H Eichhorn and S Zacks. Sequential search of an optimal dosage, i. *Journal of the American Statistical Association*, 68(343):594–598, 1973.

Pharmacokinetics of betamethasone is not associated with respiratory distress syndrome in preterm birth

Larissa Lachi Silva¹, Hayley Krzych Trussel¹, Andrea R Masters¹, Christine Bach¹, David M. Haas¹, Sara Kay Quinney¹

¹Indiana University School of Medicine, Indianapolis, IN, USA.

Objectives: Antenatal glucocorticoids, including betamethasone (BMZ), are administered to women at risk of preterm birth to accelerate fetal lung maturation. This drug administration is known to protect the neonates from developing respiratory distress syndrome (RDS). However, the association between the pharmacokinetic disposition of maternal BMZ and neonatal outcomes remains unclear. This study will evaluate whether maternal pharmacokinetic (PK) parameters are important in predicting the risk of neonatal RDS after antenatal BMZ administration.

Methods: Pregnant women with singleton 23-34 weeks gestational age (GA) and anticipated preterm birth receiving BMZ were enrolled following informed consent. Two doses of BMZ were administered intramuscularly as 6 mg BMZ sodium phosphate and 6 mg BMZ acetate 24 hours apart. Blood was drawn prior to dosing and at intervals up to 72 h after administration of BMZ. Plasma samples were analyzed by a validated LC-MS/MS method. A population PK model of BMZ was developed using NONMEM 7.4.3. First-order conditional estimation method with interaction (FOCE-I) was used to estimate structural and variance parameters. PsN and Xpose were employed for model evaluation. The effects of GA at dosing, weight, BMI, race, and ethnicity were evaluated as covariates on CL/F and V_d/F. The final model was used to simulate the total exposure from the first dose to delivery time, using the function exposure in the mlxR library for R. Multiple linear regression was used to assess the relationship between neonatal RDS and maternal BMZ PK parameters after accounting for GA at delivery using R 4.0.

Results: A total of 931 concentrations from 211 pregnant women were used for model development. The PK of BMZ in pregnant women was adequately described by a one-compartment model with first-order absorption and elimination, a constant error model and log-normal between-subject variability (BSV) on CL/F and V_d/F. The BSV in V_d/F could be in part (~8%) explained by incorporation of weight as a covariate in the model. No other covariates were found to be significant. The population estimates were absorption rate constant (ka) of $1.45 \pm 0.13 \text{ h}^{-1}$, CL/F of $32.20 \pm 1.08 \text{ L/h}$ and V_d/F of $334 \pm 11 \text{ L}$. Delivery occurred 2.6 hours to >2 weeks after BMZ administration. Simulated maternal AUC from the first dose to delivery ranged from 27.25 to 2583.46 h*μg/L. There was no statistically significant relationship between maternal PK parameters and neonatal RDS after adjusting for GA at delivery.

Conclusions: Overall, there was no statistically significant association between maternal PK parameters and the risk of neonatal RDS after antenatal BMZ administration.

WED-049

Author: Leticia Arrington(1,2), Mats O. Karlsson(1), Sebastian Ueckert(1)

Title: Software Performance Comparison of NONMEM and mirt for the Estimation for Item Response Models

Institution: (1) Uppsala University, Uppsala Sweden (2) Merck& Co., Inc., Kenilworth, NJ, USA,

Objectives

Item response theory is a statistical approach that evaluates the relationship between the underlying hidden trait and item level responses measured by an assessment. Pharmacometric (i.e. longitudinal) IRT modeling acknowledges the change in these responses over time and presents a framework to combine different disease outcomes into a joint disease progression model. NONMEM is the classical software used for longitudinal IRT models. To date there has not been an evaluation of item parameter estimation, recovery and overall model performance in NONMEM compared to the alternative software platforms. The objective of this work was to perform a systematic comparison of two software, NONMEM and the R package mirt (multidimensional item response theory) and evaluate the estimation performance and item parameter recovery for a set of scenarios with varying number of subjects, items and latent variables.

Methods: A simulation study evaluating three sample sizes (N=50,100,500), two assessment lengths (item=5 and 20) and one or two latent variables scenarios at baseline was performed. Ordered categorical items were simulated with 5 categories of responses (0-4). The item parameters were randomly sampled from a lognormal distribution (0,0.5²) for the discrimination parameter or uniform distribution for threshold parameters. Replicate (N=1000) datasets were simulated for each sample size and item scenario using mirt from the simulated item parameters. IRT model estimation was performed using the Laplace estimation method in NONMEM and stochastic EM with fixed Gaussian quadrature in mirt. Item parameter recovery from true parameters was evaluated using estimation error and root mean square error (RMSE). Furthermore, model fit in terms of log-likelihood were considered.

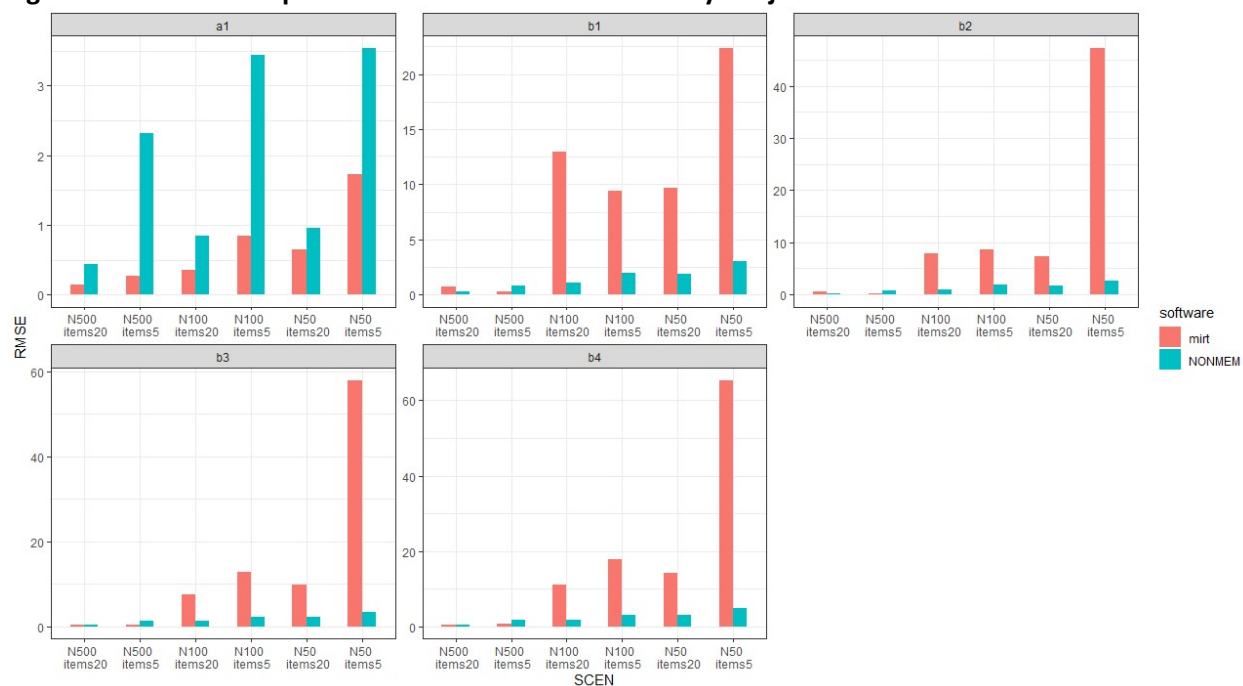
Results: Overall mirt and NONMEM performed similarly with relatively low

estimation error (median near zero) across all scenarios, indicating reasonable item parameter recovery. As the number of subjects and items were reduced the estimation precision decreased. The discrimination (a_1) parameter was more precisely estimated in mirt than NONMEM. However, for the threshold (b) parameters NONMEM appeared to be more precise (Figure 1). Model fit (i.e. log-likelihood) was similar between software for the scenario with 500 subjects. When the number of subjects reduced to 100 or 50 and 5 items, mirt performed better in approximately 10% and 25% of the cases, respectively. Computationally mirt is faster than NONMEM with an average model estimation runtime of approximately 19s seconds compared to approximately 5 minutes in NONMEM for a simulated dataset with 500 subjects and 20 items.

Conclusions:

Item parameter recovery and overall model fit were similar between NONMEM and mirt. The ease of use and speed of estimation in the existing mirt R package make it a well-suited alternative to provide item parameter estimates for a pharmacometric IRT analysis.

Figure 1 Software Comparison of Item Parameter RMSE by Subject and Item Scenario



WED-051

QSP Model Insights into the Role of Energy Demand Dependent Substrate Selection in Myocardial Mitochondria Metabolism

Lyndsey Meyer¹, Daniel A. Beard², CJ Musante¹, Anna Sher¹

¹Quantitative Systems Pharmacology, Early Clinical Development, Pfizer Worldwide Research, Development and Medical, Cambridge, MA, USA

² Department of Molecular and Integrative Physiology, University of Michigan, MI, USA

Background: The metabolic hallmarks of heart failure include diminished ATP hydrolysis potential indicated by a reduced PCr/ATP ratio, alterations in myocardial energy substrate metabolism, such as the switch in substrate utilization from fatty acid (FA) oxidation to carbohydrate oxidation and reduced metabolic flexibility [1]. However, the underlying biological mechanisms and their relative contributions to the impaired mitochondrial oxidative flux are poorly understood.

Objective: The objective of this work is to develop a comprehensive quantitative systems pharmacology (QSP) model of the myocardial mitochondrial metabolism in order to evaluate therapeutic targets modulating FA and glucose substrate selection to improve heart function.

Methods: Published models of oxidative phosphorylation and the TCA cycle [2,3] are combined with a model of β-oxidation [4] and are modified to incorporate an updated representation of the enzyme pyruvate dehydrogenase (PDH) that accounts for the important role PDH plays in substrate selection. β-oxidation enzyme parameters are refit to oxygen consumption data following the addition of acyl-carnitines to isolated cardiac mitochondria from male Wistar rats (400-600 g, n = 5, 12-16 weeks old). The model is then simulated under varying conditions of available pyruvate and palmitoyl-CoA to determine the predominate oxidation pathway contributing to ATP synthesis. In addition, the model is simulated with increasing energy demand to evaluate substrate selection under exercise conditions, and with varying pools of energetic substrates to explore disease state conditions.

Results: The model predicts, as expected, carbohydrate oxidation predominates in the fed state and palmitoyl-CoA oxidation predominates in the fasted state. In the healthy myocardium, changing available substrate does not affect PCr/ATP ratio. Reductions in the pools of total adenine nucleotides, total creatine, and total phosphate that are associated with heart failure result in a reduced PCr/ATP ratio and a 35% increase in carbohydrate oxidation in the resting state compared to healthy conditions.

Conclusions: The newly developed *in silico* model of mitochondria metabolism reproduces key biological experiments including substrate selection (i.e., FA vs. pyruvate) under different levels of workload in healthy conditions. We found the mechanism of substrate dependent switch is the result of increased PDH activity driven by feedback from the products and reactants of PDH in healthy and heart failure conditions. However, under the simulated low adenine nucleotides pools, the increase in PDH flux did not impact cardiac energetics measured by the PCr/ATP ratio.

References:

- [1] Karwi, Q.G. et al. *Fontiers in Cardiovascular Medicine*. 2018; 5: p. 68.
- [2] Wu, F., et al. *Journal of Biological Chemistry*. 2007; 282(34): p. 24525-24537.
- [3] Wu, F., J. Zhang, and D.A. Beard. *Proceedings of the National Academy of Sciences*. 2009; 106(17): p. 7143.
- [4] van Eunen, K., et al. *PLOS Computational Biology*. 2013; 9(8): p. e1003186.

**Pharmacokinetic-Pharmacodynamic Modeling of a Cell-Penetrating Peptide Phosphorodiamidate
Morpholino Oligomer in *mdx* Mice**

Marie Claire Mukashyaka¹, Leslie Wu¹, Jianbo Zang¹, Jenna Wood¹, John R. Hadkock¹, Mohammad Shadid¹

¹Sarepta Therapeutics, Inc., Cambridge, MA, USA

Objectives: Phosphorodiamidate morpholino oligomers (PMO) and cell-penetrating peptide conjugated PMOs (PPMO) have shown promise in treating Duchenne Muscular Dystrophy (DMD) owing to their ability to skip exons in mutated dystrophin genes restoring the reading frame. This technology produces an internally truncated yet functional dystrophin protein in DMD patients. The objective of the current work is to build a semi-mechanistic PK-PD model characterizing the relationship between tissue drug concentrations, exon skipping of mutant dystrophin pre-mRNA and produced dystrophin protein over time. A mouse PPMO (RC1001) that skips exon 23 (which contains a point mutation resulting in a stop codon) to restore the open reading frame in dystrophin gene of *mdx* mice was used in the study.

Methods: MDX (C57BL/10ScSn-DMD^{mdx}/J, Jackson Labs) mice were administered single and once-every four weeks (Q4W) multiple dose of RC1001 at 20, 40 and 80 mg/kg. A PK-PD model was built to characterize plasma and tissue PK, and PD effects (exon skipping and dystrophin protein) in tissue (skeletal muscle). Sequential modeling approach was performed: a 2-compartment plasma PK model was first developed to estimate a set of parameters that were fixed in subsequent models. Tissue PK-PD model was built to characterize tissue PK and PD (skipped and unskipped message and dystrophin protein) and estimate parameters. 2-compartment tissue PK model was used to describe tissue concentration data. Tissue concentration was assumed to be the driver of observed PD, and semi-mechanistic indirect response models were used to characterize PD data. Multiple dose dataset was used to verify the developed model. Monolix 2019R2 software was used to fit data and estimate parameters.

Results: The developed PK-PD model was able to characterize plasma PK and tissue PK-PD data as shown in diagnostic plots, and other assessment of goodness-of-fit tools. Additionally, the model was able to accurately estimate parameters as shown by low relative standard error (R.S.E %) values of each estimated parameter. For model verification, the developed model and estimated parameters were able to predict multiple dose dataset.

Conclusions: This is a first semi mechanistic PK/PD model that describes the exon skipping of antisense oligonucleotide in a DMD disease model. The developed PK-PD model well-characterized single and multiple dose data. The developed model will be helpful to predict and characterize the time-course of PK and PD biomarkers in *mdx* mice. Additionally, the developed model frame has a potential to be extended to other exon skipper molecules and species.

Funding Statement: This study was sponsored by Sarepta Therapeutics, Inc.

Disclosures: all authors are employees of Sarepta Therapeutics, Inc. and may own stocks in the company. Products are investigational only.

Conditional individual weighted residuals for categorical and count data models

Authors: Yasunori Aoki (1), Joakim Nyberg (2), Mats O. Karlsson (2)

Institutions: (1) National Institute of Informatics, 2-1-2. Hitotsubashi, Chiyoda-ku, Tokyo, Japan,

(2) Department of Pharmaceutical Biosciences, Uppsala University, Sweden

Objectives: To implement and investigate the individual conditional weighted residuals for the categorical or count data, where the model is given as a probability mass function. To demonstrate the utility of this quantity for model structure diagnosis and covariate model building is demonstrated using two clinical datasets.

Methods: We define the conditional individual weighted residual for count and categorical models as:

$$\begin{aligned} \text{CIWRESlike}(y; f_x) &= \Phi^{-1}(U(0, f_x(0; \mathbf{b}))), && \text{for } y=0 \\ \text{CIWRESlike}(y; f_x) &= \Phi^{-1}(U(\sum_{i=0..y-1} f_x(i; \mathbf{b}), \sum_{i=1..y} f_x(i; \mathbf{b}))), && \text{for } y=1,2,\dots \end{aligned}$$

where \mathbf{b} is a vector of the empirical Bayes estimates, $f_x(y; \mathbf{b})$ is the probability mass function given the empirical Bayes estimates and $U(m, n)$ is the probability density function of the uniform distribution for a range m to n .

A few examples were used to illustrated the performance of the CIWRESlike quantity, both using a simulated data example where the CIWRESlike was compared to Pearson's weighted residuals (PWRES) and using two published models. The models used were a proportional odds model for Likert pain score data [1] and a Seizure count model [2].

Results: With the seizure count model, when using simulated data, i.e. no model misspecification, CIWRESLike approximately follows the standard normal distribution. On the other hand, PWRES does not follow the standard normal distribution even when there is no model misspecification. Using real data, CIWRESLike correctly identified that including a Markovian element would improve the fit of the model (fig 1). For the Likert pain score model, CIWRESlike was correctly indicating the model fit is improved by including Paracetamol rescue medication by stratification of quantile-quantile- CIWRESLike by the Paracetamol rescue medication covariate.

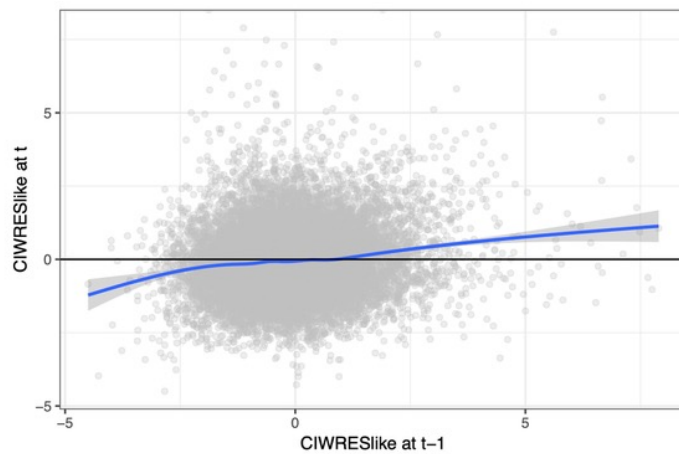


Fig1. CIWRESlike at time t plotted against CIWRESlike at previous time point t-1
(thick blue line with grey shaded areas is the smoothed conditional mean with its uncertainty).

Conclusions: A conditional individual weighted residual like quantity for the statistical model that can be written as a probability mass function is presented. A similar idea, but more comparable to a population residual, has been developed by [3-5] using NPD/NPDEs. However, as we have demonstrated through two pharmacometric models; CIWRESlike can be used for model structure adequacy analysis and covariate model building of nonlinear mixed effect models.

References:

1. Schindler E, Karlsson MO. A minimal continuous-time Markov pharmacometric model. *The AAPS journal* 2017; 19(5):1424–1435.
2. Trocóniz IF, Plan EL, Miller R, Karlsson MO. Modelling overdispersion and Markovian features in count data. *Journal of pharmacokinetics and pharmacodynamics* 2009; 36(5): 461.
3. Nguyen THT, Comets E, Mentré F. Extension of NPDE for evaluation of nonlinear mixedeffect models in presence of data below the quantification limit with applications to HIV dynamic model. *J Pharmacokinet Pharmacodyn* (2012) 39:499–518
4. RJ. Bauer. NONMEM user guide. Introduction to NONMEM 7.4.3, ICON Plc. Gaithersburg, Maryland, 2018.
5. Cerou M, Lavielle M, Brendel K, Chenel M, Comets E. Development and performance of npde for the evaluation of time-to-event models. *Pharmaceutical Research* (2018) 35: 30.

WED-055

Physiologically-based pharmacokinetic modeling of sublingual buprenorphine in newborns with neonatal abstinence syndrome: Implication of biliary clearance ontogeny on pharmacokinetic variability

Matthijs W. van Hoogdalem^{1,5}, Trevor N. Johnson³, Brooks T. McPhail^{1,7}, Suyog Kamatkar^{2,8}, Scott L. Wexelblatt^{2,6}, Laura P. Ward^{2,6}, Uwe Christians⁴, Henry T. Akinbi^{2,6}, Alexander A. Vinks^{1,6}, Tomoyuki Mizuno^{1,6}

¹Division of Clinical Pharmacology, Cincinnati Children's Hospital Medical Center, Cincinnati, OH, USA; ²Perinatal Institute, Division of Neonatology, Cincinnati Children's Hospital Medical Center, Cincinnati, OH, USA; ³Certara UK Limited, Sheffield, UK; ⁴iC42 Clinical Research and Development, University of Colorado, Aurora, CO, USA; ⁵James L. Winkle College of Pharmacy, University of Cincinnati, Cincinnati, OH, USA; ⁶Department of Pediatrics, College of Medicine, University of Cincinnati, Cincinnati, OH, USA; ⁷University of South Carolina, School of Medicine Greenville, Greenville, SC, USA; ⁸Community Hospital East, Indianapolis, IN, USA

Objectives:

Prolonged *in utero* exposure to opioids causes neonatal abstinence syndrome (NAS) in newborns. NAS is a withdrawal syndrome that results in a variety of central nervous system and respiratory disturbances, associated with severe neonatal and early childhood morbidity [1, 2]. Buprenorphine is used in NAS to control symptoms in those infants with severe withdrawal. However, the development of an effective evidence-based dosing protocol is impeded by large variability in buprenorphine pharmacokinetics (PK) and pharmacodynamics. The aims of this study were (1) to develop and assess the predictability of a physiologically-based pharmacokinetic (PBPK) model of buprenorphine in neonates and (2) to identify the sources of variability in buprenorphine PK.

Methods:

A PBPK model for buprenorphine was developed in Simcyp (v18) using physicochemical properties and in vitro enzyme kinetics data for CYP3A4, 2C8, UGT1A1, 1A3, 2B7 and 2B17 with additional biliary clearance [3], as buprenorphine is known to be predominantly excreted in the bile. After model validation with adult data, the prediction in neonates was assessed using 52 blood concentrations obtained from 19 term and preterm infants treated with sublingual buprenorphine solution. Biliary clearance ontogeny was estimated by minimizing concentration residuals as a function of postnatal age (PNA). Performance was evaluated by comparing predicted and observed concentrations and clearance (CL). Predicted CL was determined by simulating a standard buprenorphine dose in 1000 virtual individuals per patient, using Virtual Twin methodology [4]. Observed individual CL was estimated by Bayesian estimation in MwPharm++ (v1.8) using a previously developed population PK model.

Results:

The PBPK model adequately predicted observed concentrations in neonates with 71% and 96% of predictions falling within 2- and 3-fold of the observed values, respectively. In 17 out of 19 neonates (89.5%), predicted CL fell within 2-fold of the observed value. Increasing biliary clearance as a function of PNA increased the model's predictive performance, indicating minimal clearance at birth and reaching full maturation at 4.5 days PNA (Figure).

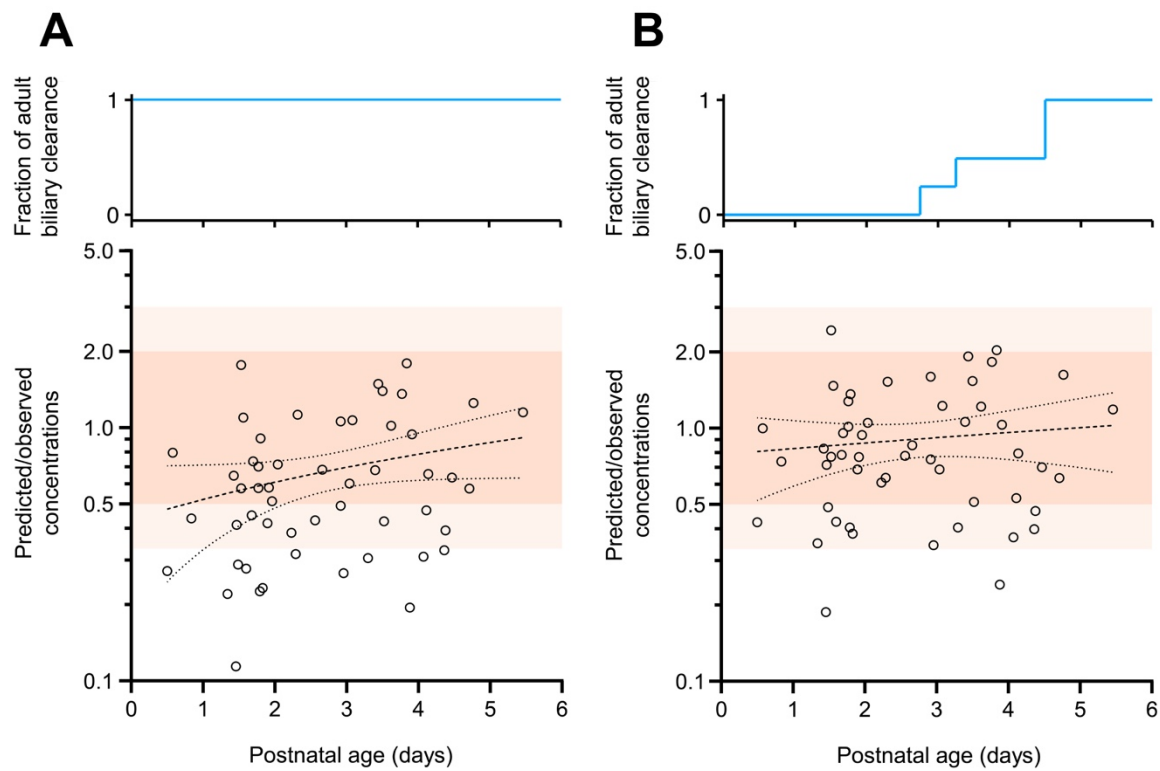
Conclusion:

A minimal PBPK model of sublingual buprenorphine in neonates was successfully developed. This study underscores the importance of establishing biliary clearance ontogeny profiles, since the results indicate that this can be an important determinant of buprenorphine clearance and PK variability in neonates.

References

1. Lisonkova et al. Pediatrics. 2019;144(2):1-11.
2. Witt et al. J Perinatol. 2017;37(10):1124-1129.
3. Johnson et al. Drug Metab Dispos. 2016;44(7):1090-1098.
4. Polasek et al. Br J Clin Pharmacol. 2018;84(3):462-476.

Figure



WED-056

Analysis of continuum and compartmental modeling approaches for intrathecally administered drugs to improve monkey-to-human model scalability

Michael Monine¹ and Ivan Nestorov¹

¹Clinical Pharmacology and Pharmacometrics, Biogen, Cambridge, MA, USA

Objectives:

Complex subarachnoid space geometry and slow cerebrospinal fluid (CSF) turnover limit distribution of intrathecal (IT) drugs within the central nervous system (CNS). Animal data suggests that concentration gradients along the spinal CSF persist over several hours after IT administration to the lumbar area [1,2]. These gradients may become more dramatic in human because of the lengthier spinal column and upright position. The objectives of this work are to 1) describe the spinal column as a continuum one-dimensional (1D) system; 2) explore scaling of the model with the spinal column length.

Methods:

In a physiological-based pharmacokinetic (PBPK) framework, the spinal column is treated as either a continuum or compartmental system (Fig. 1). In a continuum model representation, the spinal CSF is described by an advection-diffusion equation in 1D. Local concentrations in the spinal cord, brain, plasma and peripheral tissues are represented by a system of homogeneous compartments described by ordinary differential equations. The *effective* diffusion coefficient (D) and net flow speed (u) of a drug in the CSF are estimated based on non-human primate (NHP) data generated in imaging studies with a radioactive tracer [2] and PK studies with antisense oligonucleotides (ASOs). The continuum model accounts for actual lengths of the spine segments in cynomolgus monkey. The model is implemented in R with the 1D part discretized using ReacTran package [3].

Results:

Simulations of the continuum model for varied values of D , u and length were compared to time- and space-dependent concentration data from the imaging studies [2]. The analysis suggests that after IT administration, the effective rate of diffusion in the spinal CSF is relatively high (10^{-3} - 10^{-2} cm²/s) due to forcing factors such as IT injection, heartbeat and breathing. The estimated net flow rate is consistent with the literature-reported estimates for slow CSF turnover [4]. The continuum model simulations also agree with the NHP PK data for IT-injected ASOs.

Conclusions:

Intercompartment rate constants are empirical parameters that are hard to scale. The main scalable parameter of the continuum model is the spinal column length. The continuum and compartmental spinal CSF modeling approaches agree when diffusion is fast (close to well-mixing approximation). After benchmarking the compartmental model to the continuum model, we conclude that the number of homogeneous compartments in the former model can be scaled by the same factor as the spinal column length in the latter model.

References:

- [1] Krupp JL and Bernards CM (2004) Anesthesiology, 100:315–22.
- [2] Tangen K et al. (2019) IEEE Trans. Biomed. Eng. 2019 Jul 23. doi: 10.1109/TBME.2019.2930451.
- [3] Soetaert K and Meysman F (2012) Reactive transport in aquatic ecosystems: Rapid model prototyping in the open source software R Environmental Modelling & Software, 32, 49-60.
- [4] Pardridge WM (2016) Expert Opinion On Drug Delivery, 13:963-975.

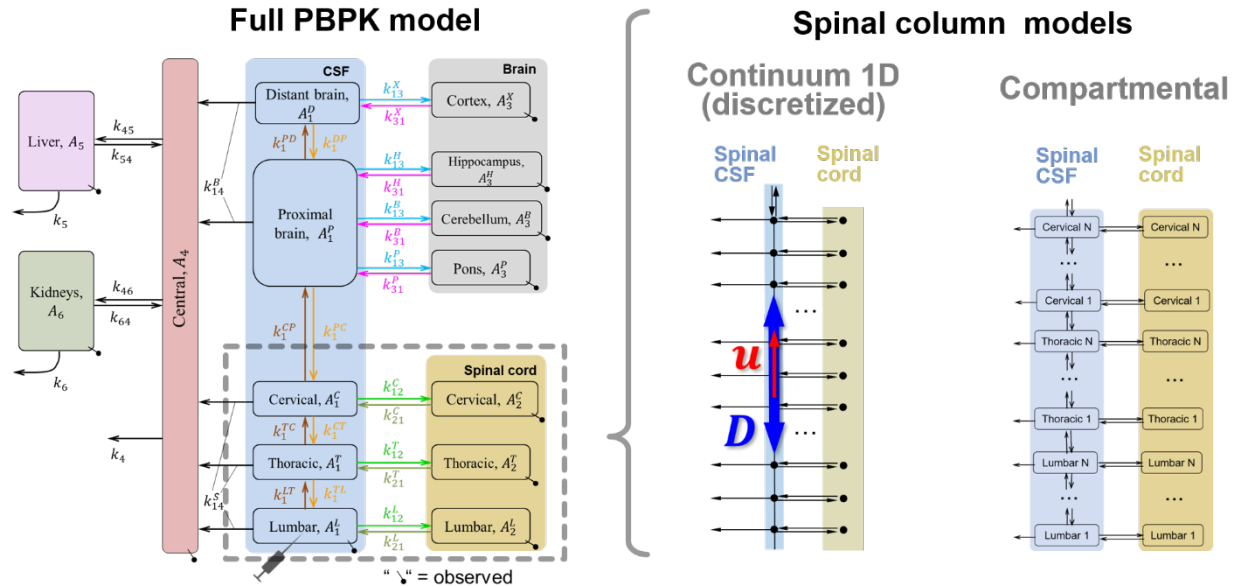


Figure 1. A PBPK modeling framework for IT-injected drugs and different spinal column models.

WED-057

QSP modeling shows efficacy of an NK3R antagonist to reduce treatment-induced vasomotor symptoms

Chris Schelling¹, Rick Ridgewell¹, Christina Friedrich², Katherine Kudrycki², Rebecca Baillie², Douglas Chung², Mike Reed²

¹Acer Therapeutics Newton, MA USA; ²Rosa & Co. LLC, San Carlos, CA USA

Objectives: Vasomotor symptoms (VMS, hot flashes and night sweats) are common among breast and prostate cancer patients resulting from treatment options that induce hormone deprivation. 60%–70% of women treated with antiestrogenic agents (tamoxifen) have hot flashes, while 80% of men on androgen deprivation therapy (leuprolide) will experience hot flashes. NK3 receptor (NK3R) antagonists have been shown clinically to significantly reduce VMS in postmenopausal women without the need for added estrogen. We built a mechanistic model of the hypothalamus-pituitary-gonadal (HPG) axis to evaluate the use of a NK3R antagonist (ACER-801) to reduce the frequency and severity of VMS using representative virtual patients undergoing tamoxifen or leuprolide treatment concomitantly.

Methods: We developed a quantitative systems pharmacology (QSP) neurobiology model of KNDy neurons in the arcuate nucleus based on relevant mechanistic and efficacy data from literature. The model includes detailed NKB, dynorphin and estradiol effects on KNDy neurons, neuroendocrine feedback, and downstream effects on the HPG axis and sex hormones. ACER-801, tamoxifen and leuprolide pharmacokinetics and pharmacodynamics were included. Model parameters such as drug pharmacokinetics, receptor numbers, and hormone production were identified from literature data. Published clinical monotherapy data for other NK3R antagonists, tamoxifen, and leuprolide were used for model calibration and testing. Two Virtual Patients (VPs) were developed based on typical patients included in clinical trials for tamoxifen (postmenopausal female) and leuprolide (male). VMS were estimated based on the level of NKB binding to NK3R.

Results: The Platform was developed and qualified, and drug coadministration simulations conducted for a five-week clinical trial duration. ACER-801 treatment reduced NKB binding and lowered VMS frequency by 80% from baseline in the postmenopausal VP. Tamoxifen treatment in this VP increased VMS by 15%. Coadministration of ACER-801 and tamoxifen in this VP reduced VMS by 75% compared to tamoxifen monotherapy. In the male VP, leuprolide administration induced three episodes of VMS per day, and coadministration of ACER-801 and leuprolide reduced the frequency and severity of VMS to near 0.

Conclusions: Simulations using the HPG Platform demonstrate the efficacy of the NK3R antagonist ACER-801 to reduce NKB binding and vasomotor symptoms due to menopause or tamoxifen- or leuprolide-induced hormone deprivation.

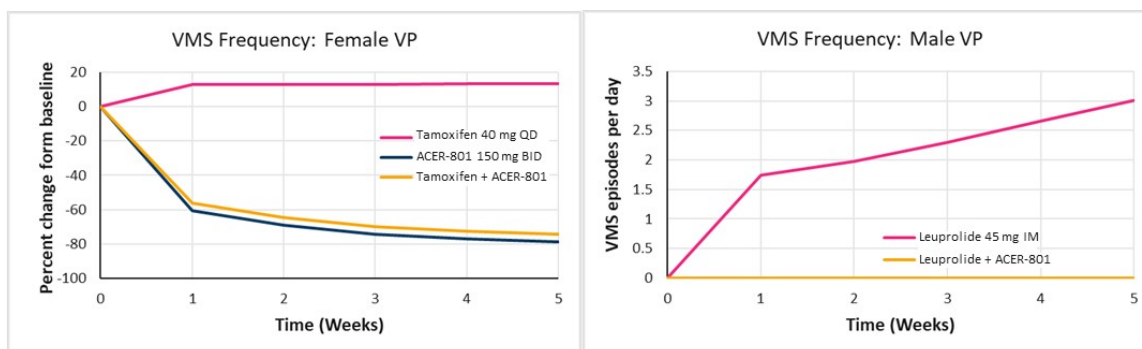


Figure 1. Simulation results showing change in VMS with drug treatment in a female postmenopausal (left) and male (right) virtual patient. Drugs were dosed at time 0.

Application of a Deep Learning Algorithm as a Prescreening Tool to Assign Individualized Absorption Models in a Population Pharmacokinetic Analysis

Mutaz M. Jaber¹, Kyriakie Sarafoglou^{1,2}, Mahmoud Al-Kofahi¹, Richard C. Brundage¹

¹Experimental and Clinical Pharmacology, ²Department of Pediatrics University of Minnesota

Objectives: A specific model for drug absorption is necessarily assumed in pharmacokinetic (PK) analyses. However, with frequent sampling, not only may it become evident that a simple absorption model is inadequate, but also that data from different individuals in a population-based analysis may suggest different absorption processes. An inappropriate absorption model may force other model parameters to be poorly estimated. The aim of this study is to demonstrate that a Deep Neural Network (DNN) algorithm can be used to prescreen data and assign an individualized absorption model consistent with either a first-order, Erlang, or split-peak/shoulder process.

Methods: In a recent cortisol population PK analysis, 12 concentrations were obtained over 6 hours in 48 children with congenital adrenal hyperplasia, a form of adrenal insufficiency. Three distinct absorption shapes were identified and classified visually by two independent researchers as either a first-order, Erlang, or split-peak/shoulder process¹. Using the results from this analysis, 10,000 profiles were simulated for each of the three aforementioned shapes and used for training the DNN algorithm (TensorFlow/Keras engine in R). The DNN algorithm consisted of input, a single hidden, and output layers. Categorical cross-entropy was used as a loss function with an RMSprop optimizer and a 0.01 learning rate. 30% of the 30,000 profiles were randomly selected as validation data during training. Once the training phase was completed, the 48 observed cortisol data sets from the PK study were used to evaluate the algorithm classification performance as a prescreening tool. The percentages of correct classifications were calculated by comparing the algorithm classification to the original visual inspection classification. We compared the accuracy rate with uninformative rate (correct classification due to chance).

Results: No benefit was noted when increasing the number of hidden layers beyond one. A 99% accuracy rate was found using the validation data during the training phase. In testing the algorithm classification performance with observed patient data, a 92% overall accuracy was attained. Table 1 presents the confusion matrix. A comparison between accuracy rate of 92% and the uninformative rate of 45% was significant ($p<0.001$).

Table1. Confusion matrix for classification results.

Algorithm Classification	Reference/Visual Classification		
	First order	Erlang	Shoulder
First order	94.4%	4.0%	11.6%
Erlang	0.0%	96.0%	0.0%
Shoulder	5.6%	0.0%	88.4%

Conclusion: A DNN algorithm was developed to classify absorption shape and was found to have a higher accuracy rate in classifying shape compared to the uninformed rate. This algorithm is envisioned to be used as a prescreening tool to select individualized absorption models prior to a population modeling analysis and has the potential to reduce the time needed to perform a manual visual assignment and eliminate inter-assessor variability and bias in assigning the shapes. This approach may be useful in other situations with multiple sub-models observed.

Reference:

1. Jaber MM, Al-Kofahi M, Sarafoglou K, Brundage RC. Individualized absorption models in population pharmacokinetic analyses. *CPT PSP*. 2020;1-3. DOI:10.1002/psp4.12513

WED-060

Population Pharmacokinetics of Heptanoate in Healthy Volunteers and Patients with Long-Chain Fatty Acid Oxidation Disorders (LC-FAOD) Treated with Triheptanoin

Authors: Nathalie H Gosselin¹, Sun Ku Lee², Claudia Jomphe¹, and Jack Shi²

Institutions: ¹Certara Strategic Consulting, Princeton, NJ, USA, ²Ultragenyx Pharmaceutical Inc., Novato, CA, USA

OBJECTIVE: Long-chain fatty acid oxidation disorders (LC-FAODs) are a group of rare, autosomal recessive genetic disorders that impair the conversion of long-chain fatty acids into energy. Triheptanoin (UX007) is an odd-carbon, medium-chain triglyceride consisting of three 7-carbon fatty acids on a glycerol backbone, and is being investigated for LC-FAOD treatment. Heptanoate is the most abundant and pharmacologically-active metabolite of triheptanoin in human plasma. The objective of this study was to characterize the pharmacokinetics (PK) of heptanoate in patients with LC-FAOD and evaluate covariates that potentially affect the exposure of heptanoate.

METHODS: A non-linear mixed effect model (NLME) in Phoenix™ NLME® v8.1 was developed using the pooled concentration-time data of heptanoate from adult healthy subjects (N = 13) and adult and pediatric subjects with LC-FAOD (N = 30). A total of 528 plasma concentration data points for heptanoate was included in the analysis, with the majority of data from healthy subjects (~83%). Multiple structural models were evaluated to describe the unique PK characteristics of heptanoate such as double peaks, and an apparent accumulation after multiple dosing. The final structural model was selected based on Akaike information criterion, goodness-of-fits plots and visual predictive check plots.

Following visual assessments, selected covariates (i.e., healthy volunteers vs LC-FAOD, creatinine clearance and bilirubin) were further tested in the final structural PK model using a forward inclusion ($p < 0.05$) and backward elimination ($p < 0.01$) approach. The influence of patient characteristics (age, hepatic function, race, weight and sex) was evaluated based on heptanoate exposure derived with the posterior Bayes parameters.

RESULTS:

The observed plasma concentration-time profiles of heptanoate were adequately described by a 1-compartmental, linear-elimination model with the dual first-order absorption across a wide range of dose levels (0.3 – 2.2 g/kg/day) tested in both healthy subjects and subjects with LC-FAOD. Notably, the observed double peaks of heptanoate in human plasma (~45 min and ~4 h) were adequately described by incorporating dual-absorption compartment. The apparent clearance (CL/F) and apparent volume (V/F) were allometrically scaled with body weight to describe PK data across a wide range of body weights in adult and pediatric subjects with LC-FAOD. Time-varying CL/F described the apparent accumulation of heptanoate after multiple doses of triheptanoin. The typical CL/F in adult subjects with LC-FAOD at steady state with a body weight of 58 kg is 236 L/hr, which is ~22% lower in comparison to the one estimated in healthy subjects with the same body weight. No other covariates influenced the absorption and disposition of heptanoate significantly.

CONCLUSION: Population PK analysis successfully described the complex absorption and disposition of heptanoate, and demonstrated that the kinetic nature of heptanoate is similar between healthy subjects and patients with LC-FAOD.

WED-061

Semi-mechanistic PK/RO modeling of anti-CD47 therapeutic agents

Elena Vasileva^{1,2}, Oleg Demin Jr²

¹Lomonosov Moscow State University, Moscow, Russia

²InSysBio, Moscow, Russia

Objectives:

Antibodies and fusion proteins targeting CD47 are the new type of therapy to treat both solid and liquid tumors. Aim of this work is to develop semi-mechanistic PK/RO model of anti-CD47 therapeutic agents and to predict CD47 occupancy in tumor tissues and periphery during treatment with ALX148, a CD47 blocker.

Methods:

A semi-mechanistic PK/RO model was developed. It describes PK of ALX148 in blood plasma, distribution to the lymph nodes, spleen and bone marrow, non-linear clearance of ALX148 due to the binding with CD47 and its further internalization. CD47 occupancy was described on the red blood cells and tumor cells. The model takes into account CD47 expression (molecules per cell) and a number of cells expressing CD47. Parameters were fitted against clinical PK data. Clinical data on RO in the periphery was used for model validation.

Results:

The model successfully described ALX148 clinical data on PK and RO in blood plasma. Concentrations in lymph nodes, spleen and bone marrow were predicted to be similar and in approximately 3 times lower than in blood plasma. Such high concentration in tumor tissues is caused by relatively small size of ALX148 (molecular weight is 78 kDa). High doses (10 mg/kg QW and 30 mg/kg Q2W) of ALX148 resulted in 95% median trough steady-state RO in tumor tissues, whereas even lower 95% confidence band is above 90%. The model predicted that trough steady-state CD47 occupancy in lymph nodes, spleen and bone marrow was around 85- 90% after administration of 3 mg/kg QW.

Conclusions:

Developed semi-mechanistic PK/RO model predicted that at least 10 mg/kg of ALX148 should be administrated weekly to achieve more than 90% of CD47 occupancy in tumor tissues. Similar doses were chosen for further phase 2 clinical trials of ALX148.

WED-063

Prediction of overall survival with atezolizumab-containing treatments in solid tumors using tumor growth inhibition-overall survival (TGI-OS) modeling framework

Phyllis Chan¹, Mathilde Marchand², Kenta Yoshida¹, Benjamin Wu¹, Yachi Chen¹, Kari Morrissey¹, Sandhya Girish¹, Jin Y. Jin¹, René Bruno³

¹Genentech, Inc., South San Francisco, CA, USA; ²Certara, Marseille, France; ³Genentech/Roche, Marseille, France.

Objectives: To utilize multivariate tumor growth inhibition-overall survival (TGI-OS) models to predict the OS distribution and benefit of atezolizumab-containing treatments across 10 clinical studies with different solid tumor types.

Methods: Longitudinal tumor size data from 10 Ph2 and Ph3 studies (Figure 1) were independently fitted to estimate TGI metrics, using a bi-exponential model [1] and implemented as a nonlinear mixed effect model in NONMEM [2]. TGI-evaluable patients had to have at least one post-baseline tumor assessment (N=6699 of 7367 treated patients, 90.9%). The impact of TGI metrics and baseline prognostic factors from a pre-defined list for each study on OS was evaluated using Kaplan-Meier and Cox regression analyses. Parametric survival regression models were developed to describe the OS distribution. Full models were built by including all significant ($p < 0.05$) covariates from the Cox univariate analysis, followed by a backward elimination step ($p < 0.01$). The model performance for each trial was evaluated by simulating 1000 times OS distributions and hazard ratio (HR) of the atezolizumab-containing arms vs. respective controls. Baseline prognostic factors as well as the tumor growth rate constant, KG, were resampled from individual patients for each study.

Results: KG was the most significant predictor of OS across all studies. In the final multivariate models, several baseline prognostic factors were highly significant across multiple studies, such as inflammatory status (C-reactive protein, albumin, and/or neutrophil-to-lymphocyte ratio, all studies), tumor burden (sum of longest diameters, number of metastatic sites, and/or presence of liver metastases, 9 studies), Eastern Cooperative Oncology Group performance status (6 studies), lactate dehydrogenase and race (3 studies). The model predicted HR indicates good model performance across the 10 studies, with observed HR within the 95% prediction intervals for all study arms except for IMpower131 Arm B (atezolizumab+carboplatin+nab-paclitaxel vs. carboplatin+nab-paclitaxel), where the model-predicted HRs were numerically lower than observed (Figure 1). The discrepancy between the model-predicted and observed HR in IMpower131 may be attributed to a high proportion of patients who received 2nd-line therapy with other immunotherapies in the control arm of the study.

Conclusions: TGI-OS models adequately described the Kaplan-Meier OS curves and showed that KG, baseline inflammatory status, and tumor burden were the top predictors of OS. Multivariate TGI-OS models developed for different solid tumor types were able to predict treatment effect with various atezolizumab monotherapy or combination regimens. These models are being used to help support decisions based on early tumor dynamic data for novel combinations in these diseases [3].

Acknowledgements: Xiaobin Li, Shweta Vadhavkar, Alyse Lin, Nina Wang for data preparation.

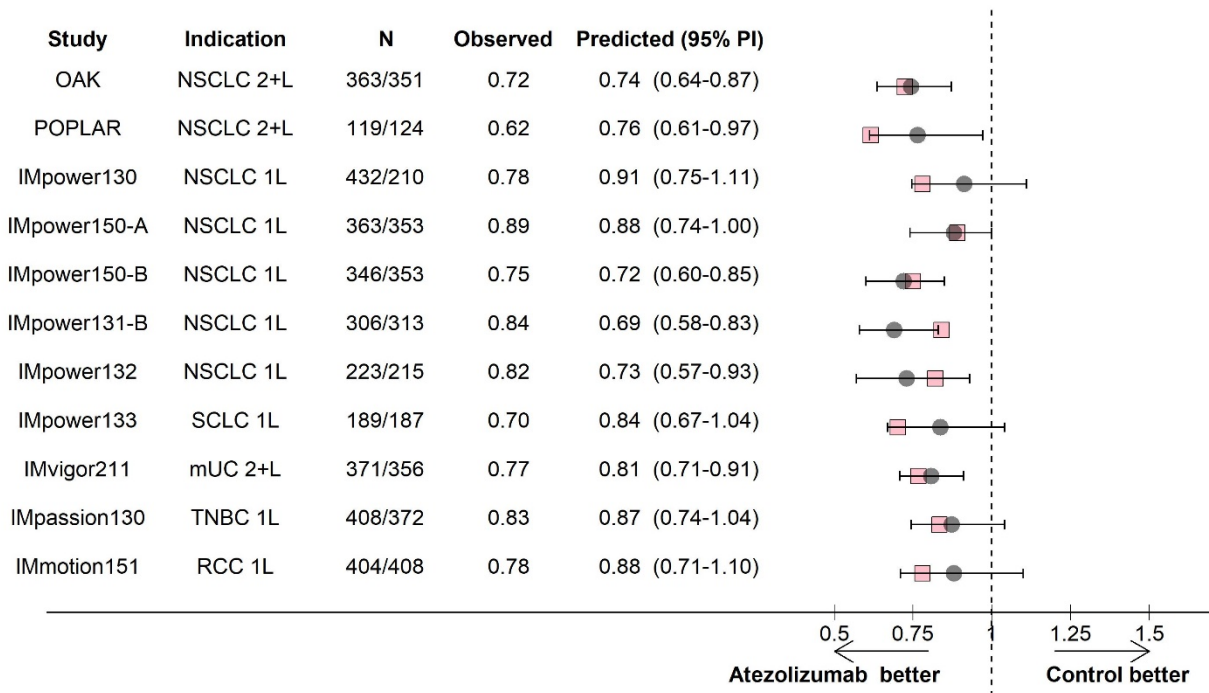
References:

- [1] Stein et al. Clin Cancer Res. 2011;17:907-917.

[2] Claret et al.. Clin Cancer Res. 2018;24:3292-3298.

[3] Bruno et al. Clin Cancer Res. OnlineFirst December 23, 2019; DOI: 10.1158/1078-0432.CCR-19-0287.

Figure 1: Evaluation of overall survival models by hazard ratio (HR) across 10 clinical trials



Note: N=number of TGI-evaluable patients with non-missing covariates in atezolizumab-containing arm/control arm in each trial; Observed=observed HR; Predicted=predicted HR; circles=model-predicted HRs; squares= observed HRs; horizontal bars=95% prediction intervals (1000 replicates); vertical dashed line=HR of 1; 1L=chemotherapy-naïve patients; 2+L= patients who have progressed during or following platinum-containing regimen; NSCLC=non-small cell lung cancer; TNBC=triple negative breast cancer; mUC=metastatic urothelial carcinoma; RCC=renal cell carcinoma. IMpassion130 evaluation performed in the ITT population.

WED-064

Population Pharmacokinetic (PopPK) Modeling of SAR440340 in Asthma Patients and Healthy Volunteers

Pratik Bhagunde¹, Christine Xu¹, Xia Pu², Matthew P. Kosloski², Vanaja Kanamaluru¹, Qiang Lu¹

¹Sanofi, Bridgewater, NJ; USA ²Regeneron Pharmaceuticals, Inc., Tarrytown, NY; USA

Objectives:

SAR440340 (REGN3500), a fully human anti-interleukin (IL)-33 monoclonal antibody, binds to circulating IL-33, inhibiting signaling of IL-33 and potentially attenuating downstream Type-1 and (or) Type-2 inflammatory pathways. This analysis aimed to develop a PopPK model to characterize the SAR440340 PK model structure, variability and identify intrinsic/extrinsic factors significantly contributing to PK variability.

Methods:

The SAR440340 PopPK model was developed using data pooled from two phase 1 studies (phase 1a in healthy volunteers, NCT02958436 and phase 1b in asthma patients, NCT02999711) and one phase 2a study (NCT03387852) in asthma patients. In the phase 1a study, SAR440340 doses were 0.3, 1, 3, or 10 mg/kg as a single intravenous (IV) dose or 150 mg as a single subcutaneous (SC) dose. In the phase 1b study, patients received SAR440340 at doses of 75 or 150 mg SC every week (QW) for 4 weeks. In the phase 2 study, patients received SAR440340 at 300 mg SC every two weeks (Q2W) alone or in combination with 300 mg Q2W SC dupilumab, for 12 weeks. Demographic variables, baseline disease characteristics (e.g. baseline eosinophil level) and disease status (healthy volunteer or patient) were tested as covariates by forward selection and backward elimination. The model was validated with visual predictive check and bootstrap.

Results:

The PopPK dataset included 1426 PK observations from 193 subjects (SAR440340 alone in N = 30 healthy volunteers and N=163 patients; SAR440340 and dupilumab combination in N=74 patients). A 2-compartment PK model with first order absorption and linear elimination was used to characterize SAR440340 PK. SAR440340 PK exhibited linear elimination kinetics. Baseline body weight (WT) on clearance (CL), central (V_C) and peripheral (V_P) volumes, age on V_P and disease status on CL were identified as statistically significant covariates. Typical bioavailability estimate was 56.5%, with 27.1 day terminal half-life in patients. The CL was 29% lower and 51% higher for a 57 kg (5th percentile WT) & 109 kg (95th percentile WT) patient respectively, relative to 76 kg (median WT) patient, and CL was 18% lower in patients relative to healthy volunteers. For 300 mg Q2W dosing regimen, steady state area under the concentration time curve (AUC_{ss}) was 38% higher and 33% lower for a 57 kg and 109 kg patient respectively, relative to a 76 kg patient. The disease status and age did not show clinically relevant impact on AUC_{ss}. Other demographic factors, baseline disease characteristics, and dupilumab co-administration showed no significant influence on SAR440340 PK.

Conclusions:

The SAR440340 PK in healthy volunteers and asthma patients was well characterized by a 2-compartment model with first order absorption and linear elimination. Body weight was determined to be the primary source of SAR440340 PK variability.

WED-065

Vadadustat Population Pharmacokinetic Modeling to Support Dosing Recommendation for the Treatment of Anemia in Japanese Patients with Chronic Kidney Disease

Huub Jan Kleijn¹, Shinsuke Inoue², Megumi Furukawa², Rishikesh Sawant³, Atsuhiro Kawaguchi², Shabnam Sani³, Ajit Chavan³

¹Certara Inc., Oss, the Netherlands; ²Mitsubishi Tanabe Pharma Corp., Tokyo, Japan; ³Akebia Therapeutics, Inc., Cambridge, MA, USA.

Objectives: Vadadustat, an oral hypoxia-inducible factor prolyl hydroxylase inhibitor (HIF-PHI), is in late-stage development for the treatment of anemia in chronic kidney disease (CKD). Vadadustat has been studied in patients with anemia due to CKD at a starting daily dose of 300 mg and dosing was adjusted between 150 and 600 mg daily based on hemoglobin response. A moderate variability in pharmacokinetic (PK) exposures was observed. The aim of population PK (POPPK) modeling was to quantify the impact of intrinsic and extrinsic factors affecting the exposures of vadadustat in the patient population.

Methods: Vadadustat concentration data available from multiple studies with either intensive or sparse blood collection were included in the analysis. A structural model was built with intensive PK data collected from both healthy subjects after multiple dosing and patients after single dosing of vadadustat. The structural model incorporated body weight, estimated glomerular filtration rate (eGFR), and food intake as covariates. Upon inclusion of sparse PK data in CKD patients from Phase 2 and Japanese Phase 3 studies, covariate effects were investigated. Nonlinear mixed-effect modeling (NONMEM 7.3) was applied to the PK data. The post hoc estimations were used to predict the vadadustat exposures in CKD patients in the Phase 2 and Japanese Phase 3 studies and to further characterize and quantify the covariate effects.

Results: The POPPK analysis data set consisted of 678 subjects and was composed of 60 healthy volunteers, 327 non-dialysis-dependent (NDD) CKD patients, and 291 dialysis-dependent (DD) CKD patients. A model with a lag time and first-order oral absorption accurately described the pharmacokinetics of vadadustat. In the NDD-CKD and DD-CKD patient populations, geometric mean oral clearance (CL/F) values were 0.652 L/h (47.1% coefficient of variation [CV]) and 0.505 L/h (42.9% CV), respectively. The apparent steady-state distribution volume was estimated as 11.6 L (13.8% CV). PK parameters were allometrically scaled by body weight. Furthermore, lower eGFR was associated with a decrease in CL/F, and higher bilirubin was associated with decreased CL/F. Food impacted absorption of vadadustat, decreasing the absorption rate constant (k_a) and increasing lag time, but did not affect bioavailability. Concomitant oral iron or non-iron phosphate binder usage marginally reduced the bioavailability of vadadustat. No effects of age, sex, race, ethnicity, liver enzymes (ALT, AST, albumin), or Japanese descent on CL/F were detected.

Conclusions: This is a first reported analysis to characterize the POPPK of the HIF-PHI class of molecules. Vadadustat oral PK were well described by POPPK modeling and estimation of individual exposures following post hoc analyses stratified by covariate subgroups further illustrated that body weight is the most important covariate for vadadustat exposure. No substantial differences were observed in clearance of vadadustat in NDD-CKD and DD-CKD patient populations.

Funding: Akebia Therapeutics, Inc.

WED-066

Population RTTE analysis of exacerbations in asthma patients: a novel approach for predicting asthma exacerbations based on biomarkers, spirometry and diaries/questionnaires

Robin J Svensson^{1*}, Jakob Ribbing^{1*}, Naoki Kotani², Michael Dolton², Shweta Vadhavkar², Dorothy Cheung², Tracy Staton², David F Choy², Wendy Putnam², Jin Jin², Nageshwar Budha², Mats O Karlsson^{1,3}, Angelica Quartino², Rui Zhu²

¹Pharmetheus, Sweden ²Genentech, South San Francisco, USA ³Department of Pharmaceutical Biosciences, Uppsala University, Sweden *Contributed equally

Objectives: Early-stage asthma trials focus on changes in biomarkers, spirometry, or diaries/questionnaires (here referred to as covariates), instead of asthma exacerbations (registration endpoint). Identification of relevant covariates that predict asthma exacerbations could inform decision-making for subsequent clinical trials. Furthermore, if the relationship between relevant predictors and asthma exacerbations were to be quantified, it would allow predictions of asthma exacerbations from early-stage data. The objective of this work was to describe longitudinal asthma exacerbations in patients, as a function of baseline and time-varying covariates.

Methods: A repeated time-to-event (RTTE) model for asthma exacerbations was developed in NONMEM 7.3 assisted by PsN[1], using 502 severe asthma patients randomized to subcutaneous placebo or 70, 210, or 490 mg MSTT1041A (mAb targeting the IL-33 receptor, ST2) every 4 weeks for 52 weeks (NCT02918019). Asthma exacerbations were defined as new or increased asthma symptoms that resulted in treatment a) with systemic corticosteroids for ≥3 days and/or b) requiring hospitalization/emergency department visit. Covariates were based on data collected daily (diary-based) or during scheduled visits, including patient demographics, and MSTT1041A exposure.

Different hazard distributions were explored for the base model. Full random effects modeling (FREM)[2] was used to explore 20 baseline covariates, followed by stepwise covariate modeling (SCM), exploring 9 time-varying covariates. Following SCM, MSTT1041A exposure on hazard was explored. Models were selected based on difference in OFV (dOFV), RSEs and diagnostic plots.

Results: The final model described the observed data well (Figure 1). A Weibull distribution described the baseline hazard. Exacerbation history and symptom score were the most influential baseline covariates. Diary-based symptom score (dOFV=83.7), diary-based short-acting rescue medication use (dOFV=33.5) and forced expiratory volume in 1 second (FEV1, dOFV=14.9) were selected as time-varying covariates. MSTT1041A exposure was not significant at p=0.05 (dOFV=2.1) but was included as a conservative measure. Exposure was not regarded as irrelevant given the effect size (on top of its effect on the time-varying covariates) of 28.3% lower hazard as a step function.

Conclusions: The longitudinal asthma exacerbation data were well described by the final model where relevant covariates for describing asthma exacerbations were identified. An MSTT1041A treatment effect was included, which should be considered when using this model to predict asthma exacerbations for other drugs. This work demonstrated the utility of a population-RTTE approach to characterize exacerbation hazard in severe asthma patients.

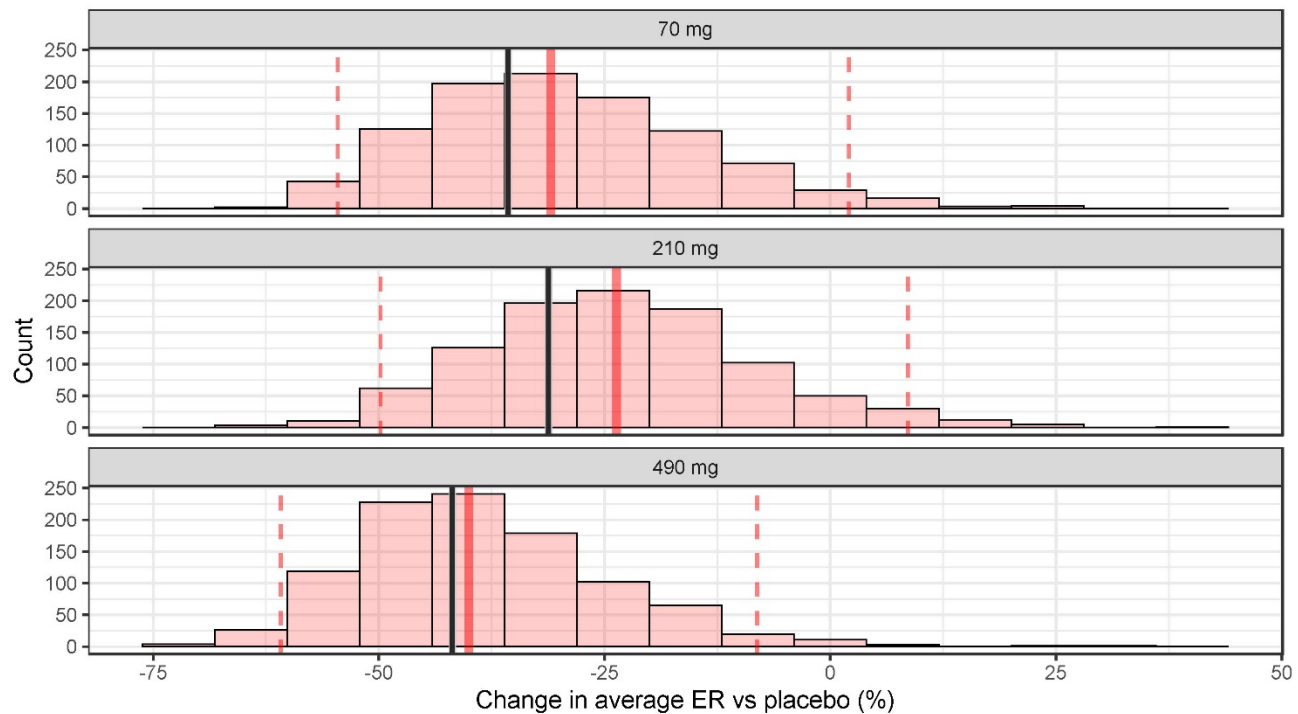


Figure 1 Posterior-predictive check for difference in mean-weighted exacerbation rate (ER) for active arms versus placebo. Black line=observed change in ER. Red bars=distribution of difference in ER for 1000 simulated studies. Dashed, red lines=95% confidence interval of difference in ER (simulations). Solid red line=50th percentile difference in ER (simulations).

References:

- [1] Keizer RJ, Karlsson MO & Hooker A. CPT:PSP 2013;2:e50;doi:10.1038/psp.2013.24
- [2] Karlsson MO. PAGE 21 (2012) Abstr 2455 [www.page-meeting.org/?abstract=2455]

WED-067

Application of Quantitative Systems Pharmacology (QSP) platform for Immuno-Oncology for evaluating OX40 agonist, and anti-PD1+OX40 agonist therapies for advanced NSCLC

Roy Song¹, Loveleena Bansal¹, Niranjan Yanamandra², Herbert Struemper³, Valeriu Damian¹

¹Systems Modeling and Translational Biology, GSK, Collegeville, PA; ²Immuno-Oncology and Combinations Research Unit, GSK, Collegeville, PA; ³Clinical Pharmacology Modeling and Simulation, GSK, Durham, NC

Objective: A comprehensive immuno-oncology (IO) QSP platform was developed using a modular approach for NSCLC (1). A key step prior to application of the QSP platform to novel IO therapies, is to validate against existing therapies. For this purpose, the model results were compared with the clinically observed efficacy of OX40 agonist (OX40a), anti-PD1 and OX40a+anti-PD1 therapies.

Methods: Receptor expression and interaction dynamics of PD1 and OX40 was implemented on immune and tumor cells in the IO platform. The effect of PD1-induced CD8 exhaustion and OX40-induced enhanced proliferation were implemented as the primary effects of receptor engagement. A virtual population of NSCLC patients was generated by varying biological parameters in the model including tumor growth rate, tumor PD-L1 expression, immune cell proliferation rate, cytokine synthesis, and immune cell receptor expression of OX40 and PD1. A final virtual cohort was assembled to match the variability and distribution of surface molecule expression and different immune cell-types measured in real NSCLC patient population. Lastly, model response predictions to anti-PD1 and OX40a were compared against results from clinical trials (2-5).

Results: Model prediction of overall response rates was evaluated for anti-PD1, OX40a and anti-PD1+OX40a. The model exhibited overall response trend consistent to first-line pembrolizumab clinical studies, where the greatest response was observed in patients with high PD-L1 expression (2-4). In addition to PD-L1, the model identified CD8 exhaustion in the tumor microenvironment as potential biomarker for responders to anti-PD1 monotherapy. The model also showed minimal response with OX40a monotherapy for NSCLC and marginal improvement in OX40a+anti-PD1 therapy over anti-PD1 alone. The modeling results based on several virtual patients predicted an inverse relationship between OX40 expression on Tregs to OX40a monotherapy response.

Conclusion: The model correctly identified high PD-L1 virtual patient cohort as best candidate for first-line anti-PD1 monotherapy treatment. The model also correctly predicted OX40a monotherapy clinical outcome for unselected advanced NSCLC in line with clinical trial results (5). Further, the model has provided insights into the mechanism of action and has been used for exploring biomarkers for OX40a and OX40a+anti-PD1 therapies. The QSP model will be further applied for predicting the response distributions in anti-PD1+OX40a clinical trials by calibrating virtual patient prevalence to real patients with a goal of using the fully validated model to assist in the prioritization of novel combinations at GSK.

References:

1. Song et al. (2018) ACoP9 Poster presentation T-095
2. Garon et al. (2015) doi.org/10.1056/NEJMoa1501824 (KEYNOTE-001)
3. Reck et al. (2016) doi:10.1056/NEJMoa1606774 (KEYNOTE-024)
4. Mok et al. (2019) doi.org/10.1016/S0140-6736(18)32409-7 (KEYNOTE-042)
5. Postel-Vinay et al. (2020) AACR Abstract CT150 (ENGAGE-1)

WED-068

Predicting drug efficacy and cytokine release with a versatile Quantitative Systems Pharmacology (QSP) modeling strategy for multispecific T-cell engagers

Abrams, R.E.¹, Pierre, K.¹, El-Murr, N.², Li, A.³, Fretland J.³, Li, J.¹, Wu, L.⁴, Seung, E.⁴, Yang Z-Y.⁴, van de Velde, H.⁵, Pelekanou, V.⁵, Stamatelos, S.K.¹

1 Sanofi, Bridgewater, 55 Corporate Dr., Bridgewater, NJ, 08807 USA

2 Sanofi, 13 quai Jules Guesde 94403 Cedex, VITRY-SUR-SEINE, Vitry/Alforville France

3 Sanofi, 153 Second Avenue, Waltham, MA 02451, USA

4 Sanofi, 270 Albany St., Cambridge, MA 02139, USA

5 Sanofi, 50 Binney St., Cambridge, MA 02142, USA

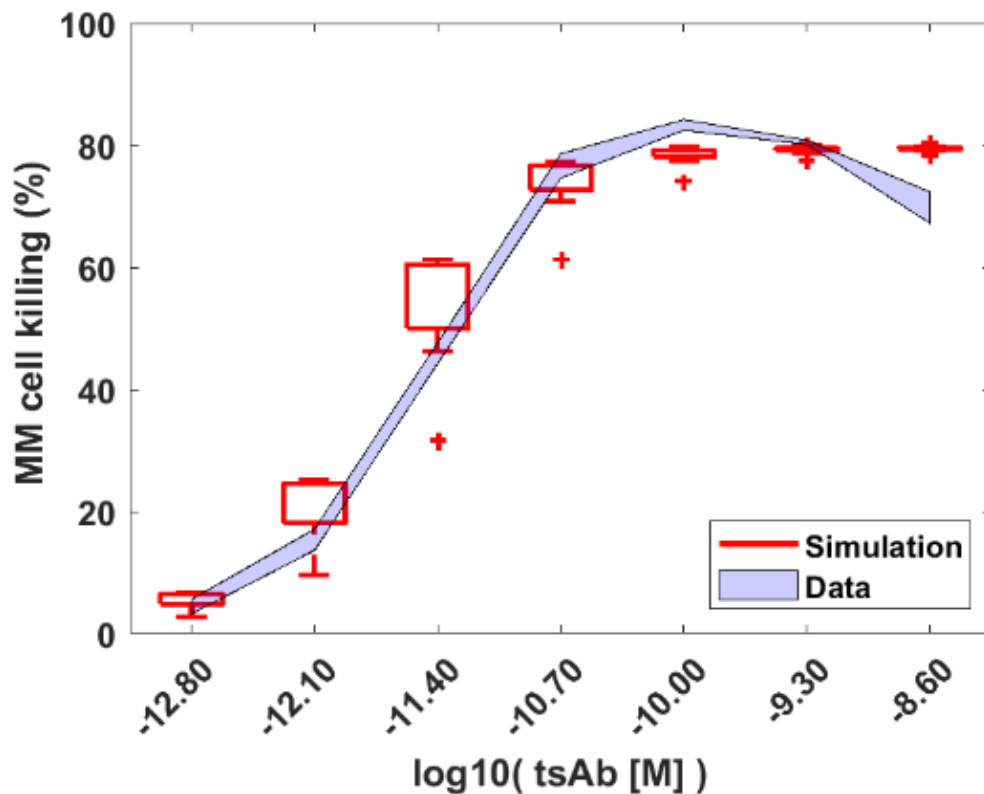
A CD38-CD28-CD3 trispecific antibody targeting tumor cells (e.g. multiple myeloma) by engaging both T-cells and tumor cells is in clinical development. This compound differs from CD3-CD38 T-cell engagers by binding CD28 antigen on either tumor or T-cells, which improves activation, proliferation, and cytolytic activity of T-cells.

In order to increase our understanding of the relevant biology and to support the clinical development program of this trispecific antibody we have established a Quantitative Systems Pharmacology (QSP) that covers CD28+ and CD38+ tumor cells, CD38+ PBMCs, and six T-cell subtypes. The model describes synapse-based T cell activation, cytokine production, and tumor killing. To create variations of the model we developed a rule-based algorithm of cell behavior and synapse formation. We used global optimization to calibrate parameter sets to preclinical data.

The applied code produced several model versions with minimal effort or time. We calibrated these to cytotoxicity (Fig. 1), proliferation, and cytokine release data. Simulations suggest that tumors with a range of CD38 expression can be treated safely and effectively.

The calibrated model captures a complex system involving multiple cells, antigens, interactions, and processes, as shown by its ability to match experimental results. We can easily adapt our model to many settings, by our code building methodology. We use this platform to predict how differences in levels and distribution of antigen, tumor, and T-cells will impact drug safety and response.

Figure 1. Model calibration to tumor cytotoxicity data



The QSP model was optimized to in vitro data on cytotoxicity of multiple myeloma cells (KMS-11 cell line) incubated with pre-activated CD8 T-cells and an E/T ratio of 10. The range of experimental data produced from 3 replicates is plotted here in light blue versus the simulated population distribution in red.

WED-069

Linking Mobile Sensor Technology Measurements to Clinically Meaningful Outcomes: Case Studies in Type-I Diabetes (T1D) and Parkinson's Disease (PD)

Sakshi Sardar¹, Varun Aggarwal¹, Roopal Bhartnagar¹, Diane Stephenson¹, Inish O'Doherty¹, Klaus Romero¹, Jackson Burton¹

¹Critical Path Institute, Tucson, Arizona, USA

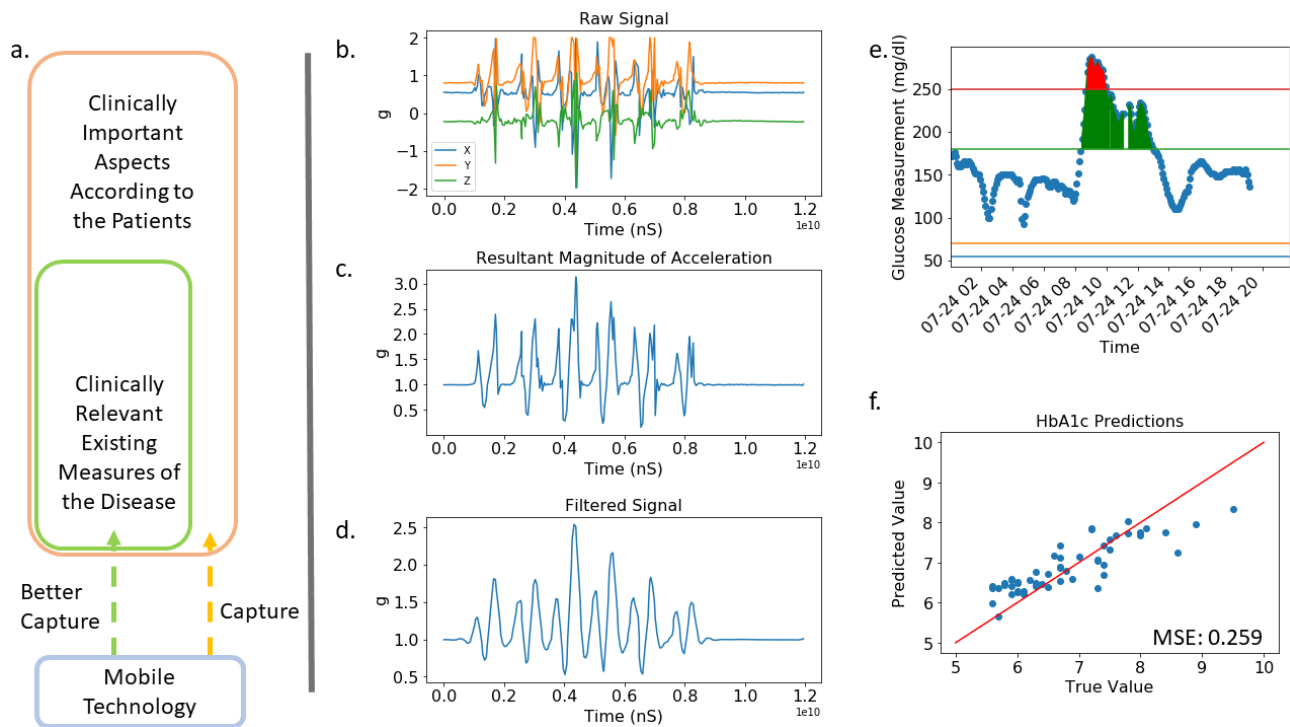
Objectives: The objective of this work is to quantitatively link measurements from mobile sensing technologies to clinically meaningful outcomes in type 1 diabetes (T1D) and Parkinson's disease (PD). In both diseases, Critical Path Institute's public-private partnerships Critical Path for Parkinson's (CPP) and the Type-1 Diabetes Consortium (T1DC) have specific efforts focused on understanding the voice of the patient (VOP) to identify clinically meaningful aspects of the disease as well as established clinical outcome assessments (COAs). The utility of mobile sensing technology has then been reviewed to more sensitively capture existing measures and address gaps in clinically meaningful aspects of the disease not currently being captured (Figure 1a).

Methods: Regarding PD, a comprehensive catalogue of three core areas: VOP, COAs, and existing digital studies in PD was developed. Gait was identified to be one of important aspects of PD and normative digital time-series gait data were analyzed to extract features that can be used to establish reference standards for PD associated gait abnormalities. The data were generated in-house using STEVAL-BCN002V1B for a single subject with three repeats. For T1D, continuous glucose monitoring (CGM) was identified as a technology to sensitively measures blood glucose and identify clinically relevant diabetic events. CGM and HbA1c (an indirect measure of glycemic control) from the JAEB study with 70 patients was used. Daily CGM parameters were extracted from the data, followed by data clean-up leading to usable data from 19 patients. Subsequently, feature engineering was carried out and linear regression machine learning model was trained for HbA1c prediction.

Results: Figure 1 b, c and d show the raw accelerometer data for a walk test, resultant magnitude derived from it and the filtered signal using a low pass filter with a cutoff frequency of 2 Hz, respectively. The filtered signal was used to derive quantitative measures of steps, strides, times associated with different sections of the gait and their variation with time. For T1D, the trained model showed good predictive power with an R² score of 0.69 and mean squared error was 0.259.

Conclusions: These quantitative methodologies can be emulated across different disease areas to provide informed guidance on the use of relevant technologies that provide more frequent and objective measure of aspects of the disease. The case studies highlight the linking of mobile/digital technologies to clinically meaningful outcomes based on the patient's perspective. This process is critical in light of the rapid emergence of mobile sensing technology for engaging in regulatory bodies for advancing such technology in drug development.

Figure 1: a) Strategy for identifying clinically important aspects of the disease based on patient input, COAs and, assessment of aspects of disease being captured or have potential to be captured using technology. b, c and d) Case example from PD showing, raw accelerometer data and subsequent processing to extract quantitative features. e) Daily CGM measurement example from the data, and f) the prediction capability of using CGM data metrics for HbA1c.



Model-Based Assessment of Hemoglobin Response to Treatment with Vadarustat in Patients With Chronic Kidney Disease

Floris Fauchet¹, Huub Jan Kleijn¹, Shinsuke Inoue², Megumi Furukawa², Shabnam Sani³, Atsuhiro Kawaguchi², Rishikesh Sawant³, Ajit Chavan³

¹Certara Inc., Oss, the Netherlands; ²Mitsubishi Tanabe Pharma Corp., Tokyo, Japan; ³Akebia Therapeutics, Inc., Cambridge, MA, USA.

Objectives: Vadarustat is an orally administered hypoxia-inducible factor prolyl hydroxylase inhibitor (HIF-PHI) in the late stages of clinical development for the treatment of anemia due to chronic kidney disease (CKD). This analysis describes the use of an empirical pharmacokinetic/pharmacodynamic (PK/PD) model to explore and quantify the exposure–response relationship for hemoglobin (Hb) modulation after vadarustat treatment in the CKD population based on longitudinal Hb data. The analysis takes into account prior use of erythropoiesis-stimulating agents (ESAs) and other patient characteristics affecting exposure and Hb modulation in CKD patients.

Methods: Long-term Hb concentration data (16–24 weeks) for vadarustat were obtained from 4 completed phase 2 studies (US, 2; Japan, 2) and 2 Japanese phase 3 studies conducted in both dialysis-dependent and non-dialysis-dependent CKD populations. Dose titration based on Hb response was applied, aimed to maintain the desired therapeutic Hb target range in patients. The data set contained longitudinal Hb observations (typically every 2 weeks), actual dosing information, patient demographics, prior ESA status and dose level, disease state, estimated glomerular filtration rate, and concomitant medications. The model included components that described the residual effects of the prior ESA treatment, baseline endogenous Hb, and vadarustat-induced Hb response. Vadarustat exposures were obtained from a previously developed population pharmacokinetics model. The analysis was performed using nonlinear mixed-effects modeling implemented in NONMEM 7.3. The predictive performance of the final model was assessed by conducting a posterior predictive check.

Results: A total of 726 patients (7298 observations) treated with vadarustat (150–600 mg daily) were included in the model-based analysis. Hb versus time profiles were characterized by an initial Hb decline, which reflected the decreasing impact of the prior ESA treatment, followed by a gradual vadarustat-induced Hb increase, with stable Hb levels achieved after approximately 10 weeks of treatment. Structural model components consisted of (1) baseline Hb level, (2) a first-order rate process to account for the washout of residual Hb effects from prior ESA use, and (3) a set of transit compartments to account for the gradual response to vadarustat modulation, with a linear function translating exposure to modulation of the Hb production rate. The baseline Hb level, prior ESA effect, associated washout rate, Hb production rate, and slope of the exposure–response relation were accurately estimated, and predictive checks confirmed the model’s performance.

Conclusions: This is a first-reported analysis to characterize the PK/PD of the HIF-PHI class of molecules. The PK/PD model adequately described the longitudinal Hb–time data in CKD patients. Further understanding of the exposure–response relationship for Hb could be used to optimize vadarustat dosing in CKD patients.

Disclosure: This study was funded by Akebia Therapeutics, Inc.

WED-071

Genotype-Dependent Changes in Warfarin Clearance upon Co-administration of an Inhibitor (fluconazole) and an inducer (rifampin): A Model-based Analysis

Shen Cheng¹, Darcy R. Flora¹, Timothy S. Tracy², Allan E. Rettie³, Richard C. Brundage¹

1. Department of Experimental and Clinical Pharmacology, College of Pharmacy, University of Minnesota, Twin Cities; 2. Tracy Consultants; 3. Department of Medicinal Chemistry, School of Pharmacy, University of Washington, Seattle

Objective: Warfarin is one of the most commonly prescribed oral anticoagulant drugs for preventing long-term thromboembolic events worldwide. Warfarin is administered as a mixture of two enantiomers, S-warfarin and R-warfarin, in a 1:1 molar ratio. CYP2C9 is highly associated with the metabolic clearance of S-warfarin but not R-warfarin. Since S-warfarin is 7-fold more potent, patients' CYP2C9 metabolic status impacts exposure and therapeutic response. CYP2C9 is subject to genetic polymorphisms as well as susceptible to enzyme induction and inhibition, all of which complicate the dose-exposure relationship of warfarin. The objective of this research is to investigate the impact of CYP2C9 genetic polymorphisms on warfarin drug-drug interactions using a nonlinear mixed-effects modeling approach.

Methods: From our pharmacogenomics registry of 1950 subjects, 29 subjects with five CYP2C9 genotypes were recruited and administered single doses of warfarin alone, and together with fluconazole (inhibitor) and rifampin (inducer) in a crossover fashion (Figure 1). S- and R-warfarin were quantitated using LC/MS/MS in plasma and urine collected out to 15 days. A linear compartmental modeling approach was first explored for S-warfarin and R-warfarin but significant model misspecification was noted. A target-mediated drug disposition (TMDD) model was found to adequately describe both S-warfarin and R-warfarin plasma and urine concentrations after administration of warfarin alone as well as when fluconazole and rifampin were co-administered. The TMDD model was implemented within NONMEM using the IMP estimation method.

Results: Our results confirm S-warfarin exhibits CYP2C9 genotype-dependent clearance whereas R-warfarin does not. S-warfarin baseline clearance and the percent of baseline clearance when administered with fluconazole or rifampin are presented in Table 1. R-warfarin clearance decreased to 52% of baseline when warfarin was taken with fluconazole and increased to 270% of baseline when taken with rifampin. No significant differences in R-warfarin clearance were noted among subject genotypes.

Conclusions: S-warfarin is the major active compound in warfarin and patients with different CYP2C9 genotypes will likely require different warfarin doses to attain a similar exposure, and moreover, require different magnitudes of dose adjustments when adding CYP inhibitors and CYP inducers.

Reference:

1. Flora, D. R., Rettie, A. E., Brundage, R. C., & Tracy, T. S. (2017). CYP2C9 Genotype-Dependent Warfarin Pharmacokinetics: Impact of CYP2C9 Genotype on R- and S-Warfarin and Their Oxidative Metabolites. *J Clin Pharmacol*, 57(3), 382-393. doi:10.1002/jcph.813
2. Levy, G., Mager, D. E., Cheung, W. K., & Jusko, W. J. (2003). Comparative pharmacokinetics of coumarin anticoagulants L: Physiologic modeling of S-warfarin in rats and pharmacologic target-mediated warfarin disposition in man. *J Pharm Sci*, 92(5), 985-994. doi:10.1002/jps.10345

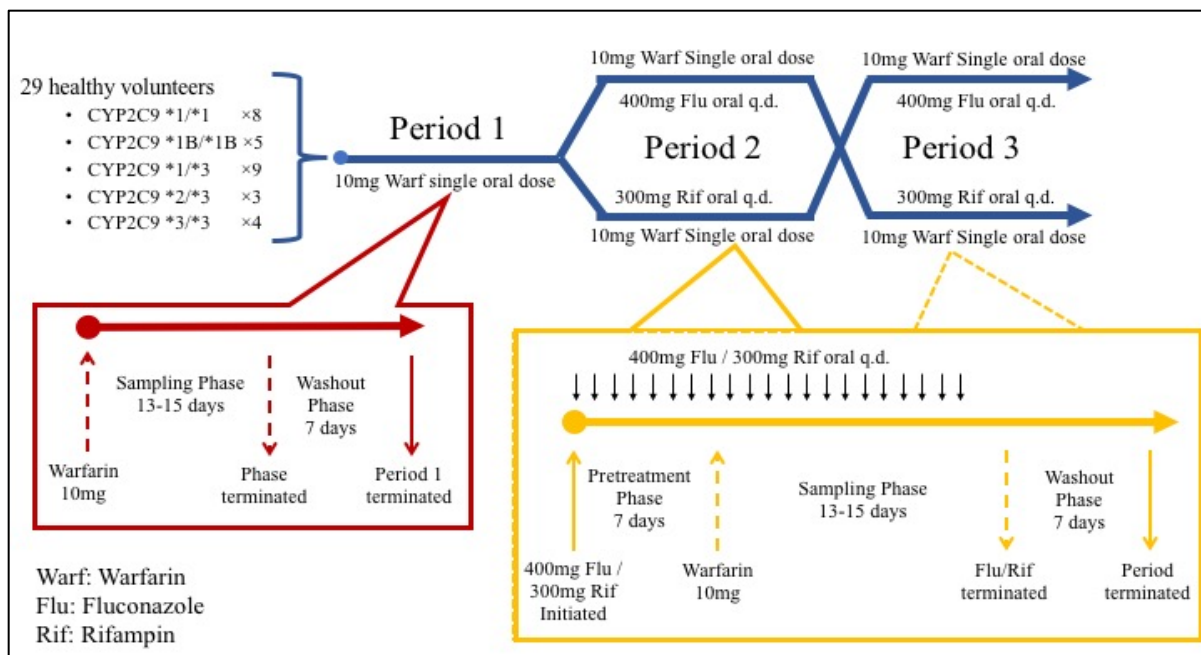


Figure 1. Study Design Diagram. Each subject went through 3 study periods (upper dark-blue section). Period 1 (red box), single 10mg dose of warfarin. Periods 2 and 3 in crossover (yellow box), each subject was pretreated with either 400mg fluconazole or 300mg rifampin once daily for 7 consecutive days, followed by a single 10mg dose of warfarin and continuous treatment with either 400mg fluconazole or 300mg rifampin once daily through the sampling phase.

CYP2C9 Genotypes	Baseline CL (L/hr) (%RSE)	% of baseline clearance when administered with an inhibitor or inducer	
		Fluconazole (%RSE)	Rifampin (%RSE)
*1/*1 (n=8)	0.260 (8%)	30.3% (4%)	211% (4%)
*1B/*1B (n=5)	0.230 (13%)	NA	207% (5%)
*1/*3 (n=9)	0.157 (11%)	34.9% (4%)	215% (4%)
*2/*3 (n=3)	0.071 (16%)	40.5% (7%)	295% (9%)
*3/*3 (n=4)	0.056 (14%)	50.3% (7%)	291% (6%)
BSV	23.2% (36%)	11.8% (85%)	11.4% (55%)

Table 1. Genotype-Dependent Changes in Warfarin Clearance upon Co-administration fluconazole and rifampin. (BSV: Between Subject Variability, expressed as %CV)

WED-073

Population pharmacokinetics and pharmacodynamics of tranexamic acid in women undergoing cesarean delivery

Shuhui Li¹, Homa Ahmadzia², Dong Guo¹, Adam Miszta^{3,4}, Naomi Luban⁵, Jeffrey Berger⁶, Andra H. James⁷, Alisa S. Wolberg³, Johannes Van den Anker^{8,9}, Joga Rao Gobburu¹³.

¹School of Pharmacy, University of Maryland, Baltimore, M.D., USA; ²Division of Maternal-Fetal Medicine, Department of Obstetrics & Gynecology, The George Washington University, Washington D.C., USA; ³Department of Pathology and Laboratory Medicine and UNC Blood Research Center, University of North Carolina, Chapel Hill N.C., USA; ⁴Synapse Research Institute, Maastricht, the Netherlands; ⁵Division of Hematology, Children's National Hospital, Washington D.C., USA; ⁶Department of Anesthesiology and Critical Care Medicine, The George Washington University, Washington D.C., USA; ⁷Division of Maternal-Fetal Medicine, Department of Obstetrics & Gynecology, Duke University, Durham N.C., USA; ⁸Division of Clinical Pharmacology, Children's National Hospital, Washington D.C., USA; ⁹Division of Pediatric Pharmacology and Pharmacometrics, University of Basel Children's Hospital, Basel, Switzerland.

Objectives: Few pharmacokinetics (PK) and pharmacodynamics (PD) studies have been conducted for tranexamic acid (TXA) in preventing postpartum hemorrhage (PPH). As a result, there is a lack of information regarding which dose of TXA to administer for PPH prevention. This study characterized the PK and PD of TXA in pregnant women who underwent cesarean delivery, with a goal of projecting the prophylactic dose for future studies.

Methods: Thirty patients scheduled for cesarean delivery entered a prospective, single-center, open-label, dose-ranging study. Ten patients each were sequentially given 5 mg/kg, 10 mg/kg, or 15 mg/kg of TXA intravenously after the umbilical cord clamping. Seven pre- and postpartum specimens were collected up to 24 hours postpartum. The maximum lysis of tissue plasminogen activator spiked whole blood sample using rotational thromboelastometry served as the PD response. Non-linear mixed effects models were adopted to characterize the 174 observations, using Pumas v0.10.0 (Pumas-AI Inc., Baltimore, MD, USA). The in-vitro PK threshold of 10 mg/L TXA and the normal

³ Gobburu is a co-founder of Pumas-AI that commercializes Pumas software.

reference value of maximum lysis of 17% were selected as the therapeutic targets to come up with the prophylactic dose of TXA. Serial thrombin generation and D-dimer data were evaluated as safety outcomes.

Results: A 2 -compartment model with proportional residual error model best fitted the data with following parameters: 9.6 L/hr (clearance), 23.8 L (central compartment volume), 16.5 L (peripheral compartment volume), and 3.4 L/hr (intercompartmental clearance). Between-subject and residual variability were less than 25% (CV%) and no covariates were found to further explain the variability. A fractional sigmoid Emax model with combined error model best linked the TXA concentration to the effect on the maximum lysis, with the baseline lysis at 98%, maximum inhibition of TXA at 89% of the baseline, 5.7 mg/L as the IC50 and hill factor at 7.7. The variability of the PD model parameters was about 88% (CV%). Simulation results showed that 550 mg and 650 mg of TXA maintained the concentrations and maximum lysis levels above the therapeutic targets for 30 minutes and 1 hour, respectively, for more than 90% of the patients. Currently pregnant women receive 1 gram of TXA. There was no significant difference in thrombin generation data or D-dimer data across different dosing cohorts, supporting the safety of TXA use.

Conclusions: To the best of our knowledge, the PK and PD profiles of TXA in pregnant women who underwent cesarean delivery are described for the first time. The optimal single dose providing sufficient PPH prophylaxis up to 1 hour after delivery was 650 mg.

WED-074

Population Pharmacokinetic Analysis of N-acetylcysteine in Pediatric Patients with Inherited Metabolic Disorders Undergoing Hematopoietic Stem Cell Transplant

Authors: Sahasrabudhe SA^{1,2}, Kartha RV^{1,2}, Ng M³, Cloyd JC^{1,2}, Orchard PJ³, Brundage RC^{1,2}, Coles LD^{1,2}

Affiliations:

¹Center for Orphan Drug Research ²Department of Experimental and Clinical Pharmacology at University of Minnesota ³Department of Pediatric Blood and Marrow Transplantation at University of Minnesota

Objectives

Inherited metabolic disorders (IMDs) include peroxisomal and lysosomal diseases. Adrenoleukodystrophy (ALD) is an X-linked, rare, peroxisomal disorder caused by mutations in the ABCD1 gene, encoding a peroxisomal membrane-bound protein necessary for transport of very long chain fatty acids (VLCFAs) into the peroxisome. In ALD, the VLCFAs accumulate in tissues leading to adrenal insufficiency and, in approximately 40% of cases, a neuroinflammatory condition termed cerebral ALD (cALD). If untreated, cALD is associated with rapid neurological decline and death. Hematopoietic stem cell transplantation (HSCT) is an effective therapy for selected IMDs, particularly when performed early in the disease. The preparatory regimen for HSCT involves myeloablation using radiation and chemotherapeutic drugs. Given the severe neuroinflammation and increased oxidative stress in IMDs, an antioxidant, N-acetylcysteine (NAC), is used in association with HSCT. The objective of this study was to characterize the pharmacokinetics (PK) of NAC in patients with cALD and other IMDs before and after HSCT.

Methods

The 18 boys (median age 8 years) included in this study received NAC (70mg/kg) infused over 1h and repeated every 6h starting approximately 2 weeks before HSCT and until approximately 6 weeks thereafter. Fifteen patients had cALD, while 3 patients were diagnosed with other IMDs. Intensive PK blood sampling was done on up to three occasions (OCC; -7 days, +7 days and +21 days relative to HSCT (day 0)). Plasma NAC was measured using a validated HPLC-MS method. NAC concentrations were modeled in NONMEM v7.4.3 using FOCE-I. Allometric scaling of body size on PK parameters was assumed using standard coefficients. Various structural and pharmacostatistical models were evaluated. OCC was evaluated as a fixed effect and as random effect (BOV) on CL and/or V1. Model selection was based on change in objective function value (dOFV) and diagnostic plots. Significance of covariate additions was set at 0.01 (Chi-square).

Results

NAC PK was best described by a two-compartment model with first order elimination. The estimates for CL, V1, V2 and Q were 13.4 L/h, 16.1 L, 16.1 L, 4.6 L/h, respectively for a 70kg person. HSCT did not change V1 and CL significantly and analysis across OCC did not reveal any trend. The data only supported BSV in CL (19%) and V1 (53%), and BOV in CL (22%). RUV was estimated to be 17% in this setting.

Conclusions

This is the first characterization of NAC PK in children with IMDs undergoing HSCT. A nonlinear mixed-effects model was used to describe concentration-time profiles of NAC before and following HSCT. These results suggest that dosing of NAC does not need to be altered following HSCT. This study has limitations associated with a small sample size that are common with rare diseases.

WED-075**Longitudinal Model Based Meta-Analysis of EASI %Change from Baseline Score, and IGA Responders of Clear (0) or almost Clear (1) for Topical Drugs in Atopic Dermatitis Clinical Trials**

Sima Ahadieh¹, Steve Martin², Ye Tan³, Gerald Fetterly³

¹Global Product Development, Pfizer Inc., Groton CT, ²Global Product Development, Pfizer Inc., Cambridge, MA,

³Worldwide Research, Development and Medical, Pfizer Inc., Cambridge, MA, U.S.A

Objectives: To characterize the efficacy and safety profiles of vehicle/placebo and selected topical comparators in development or marketed treatments for atopic dermatitis (AD). In addition, determining the probability of attaining an EASI and IGA responder target value at specific time points for selected topical agents.

Methods: Meta-Analysis included data obtained from searching Ovid SP and various clinical trials websites. The search targeted mild to moderate AD patients receiving topically administered ruxolitinib, delgocitinib, difamila, crisaborole, pimecrolimus, and tacrolimus in randomized vehicle controlled trials measuring endpoints of EASI (Eczema Area Severity Index) % change from baseline (%CFB), and IGA (Investigator Global Assessment) responders of clear (0) or almost clear (1) score. The literature was reviewed, and the final selection was extracted and modeled using nlme package in R Version 3.6.1. An exponential model for EASI %CFB vs. time for vehicle and drug, with an Emax dose-response function describing drug effects was developed. The final model for IGA responder was a logit scale of exponential versus time for vehicle and drug, with a linear dose response.

Results: A total of 20 studies were included in the analysis. For EASI %CFB, the drugs reached maximal effects at weeks 4 to 6 and for IGA responders of clear or almost clear (0 or 1) this time was 8 weeks. Table 1 summarizes key results.

There was a 90% probability that most drugs could achieve -40 %CFB in EASI score by week 4 and 70% probability that some of these drugs could achieve 30% IGA responder rates at week 8.

Conclusions:

This model was adequate to predict efficacy of topical drugs for atopic dermatitis. Furthermore, the model provides information about the minimum treatment duration needed that would be predictive of the time at which maximum benefit occurs.

Table 1: Predicted EASI %CFB and IGA Responders of 0 or 1

Drug	Predicted EASI %CFB [95% CI] at 6 weeks	Predicted IGA Responders [95% CI] at 8 weeks
ruxolitinib 1.5% BID	-62.9% [-72.1%, -53.8%]	33.5% [21.3%, 42.8%]
delgocitinib 0.5% BID	-63.3% [-74.3%, -45.2%]	30.3% [23.3%, 37.6%]
difamila 1% BID	-42.2% [-49.3%, -35.0%]	33.1% [22.2%, 41.9%]
pimecrolimus 1% BID	-44.3% [-51.6%, -37.0%]	41.1% [34.1%, 48.5%]
tacrolimus 0.1% BID	-57.0% [-65.9%, -46.6%]	51.2% [42.9%, 59.2%]
crisaborole 2% BID	NA	42.9% [20.7%, 56.7%]
vehicle	-10.5% [-16.5%, -4.49%]	18.1% [13.9%, 23.1%]

WED-077

Characterization of Clinical Pharmacokinetics and Exposure-Response Relationships of AMG 330, a CD33 Bispecific T-Cell Engager Antibody Construct, in Patients with Relapsed/Refractory AML

Authors: Agarwal SK¹, Bhagwat S¹, Mehta K¹, Hindoyan A², Stein A³, Ravandi F⁴, Subklewe M⁵, Walter RB⁶, Jongen-Lavrencic M⁷, Ossenkoppele GJ⁸, Paschka P⁹, Khaldoyanidi S¹⁰, Dutta S¹¹, Upreti V¹

¹Clinical Pharmacology, Modeling & Simulation, Amgen, Inc., South San Francisco, CA, USA; ²Clinical Biomarkers & Diagnostics, Amgen, Inc., Thousand Oaks, CA, USA; ³Gehr Family Center for Leukemia Research, City of Hope, Duarte, CA, USA; ⁴Department of Leukemia, The University of Texas MD Anderson Cancer Center, Houston, TX, USA; ⁵Department of Medicine III, University Hospital, LMU Munich, Munich, Germany; ⁶Clinical Research Division, Fred Hutchinson Cancer Research Center, Seattle, WA, USA; ⁷Erasmus University Medical Center, Rotterdam, Netherlands; ⁸VU University Medical Center, Amsterdam, Netherlands; ⁹Ulm University Medical Center, Ulm, Germany; ¹⁰Amgen, Inc., Early Development, Thousand Oaks, CA, USA; ¹¹Clinical Pharmacology, Modeling & Simulation, Amgen, Inc., Thousand Oaks, CA, USA

Objectives: AMG 330 binds both CD33 and CD3 and redirects T cells toward CD33⁺ cells leading to T-cell-mediated cytotoxicity against AML blasts. An ongoing open label phase I dose-escalation study (NCT02520427) has shown preliminary activity and acceptable safety in relapsed or refractory (R/R) acute myeloid leukemia (AML) patients (pts) (Ravandi et al. ASH 2018). To characterize the pharmacokinetics and exposure-response (E-R) relationships of AMG 330 in patients with R/R AML.

Methods: A continuous IV infusion of AMG 330 was evaluated at escalating target doses (range from 0.5 to 720 µg/day) using a 3+3 design with pts receiving step dose/s prior to reaching target doses of ≥ 30 µg/day. Population pharmacokinetics (popPK) using non-linear mixed effects modeling and E-R analyses were conducted to characterize relationships between AMG 330 exposure (steady-state concentration [Css]) at target dose, the baseline tumor burden, clinical response per revised IWG criteria and incidence of cytokine release syndrome (CRS).

Results*: As of Dec 10, 2019, 55 patients (males, 56.4%; median age, 58.0 [18.0–80.0] years) were enrolled in 16 cohorts. AMG 330 PK was best described by a one-compartment linear PK model. Dose dependent increases were observed in AMG 330 Css exposures. Responders typically showed higher AMG 330 Css than non-responders. Preliminary exploratory analysis indicated that higher AMG 330 exposures, lower baseline leukemic burden in bone marrow and CD33+ AML cells in peripheral blood, and higher baseline Effector:Target cell ratio were associated with clinical response. Additionally, a positive relationship was observed for AMG 330 exposures and baseline leukemic burden ($p<0.05$) with probability of CRS occurrence and severity. Based on the model, at a baseline leukemic burden of 20%, a 240 µg/day target dose is predicted to result in 28% and 4% probabilities of developing CRS of grade ≥ 2 and ≥ 3 , respectively.

Conclusions: Clinical pharmacokinetic profile and E-R relationships of AMG 330 were characterized to identify optimal AMG 330 step dosing regimens that minimize the risk for CRS in ongoing and planned clinical investigations.

*The results in this abstract have been previously presented in part at American Society of Clinical Oncology 2020 Virtual Annual Meeting and published in the conference proceedings as abstract 7536".

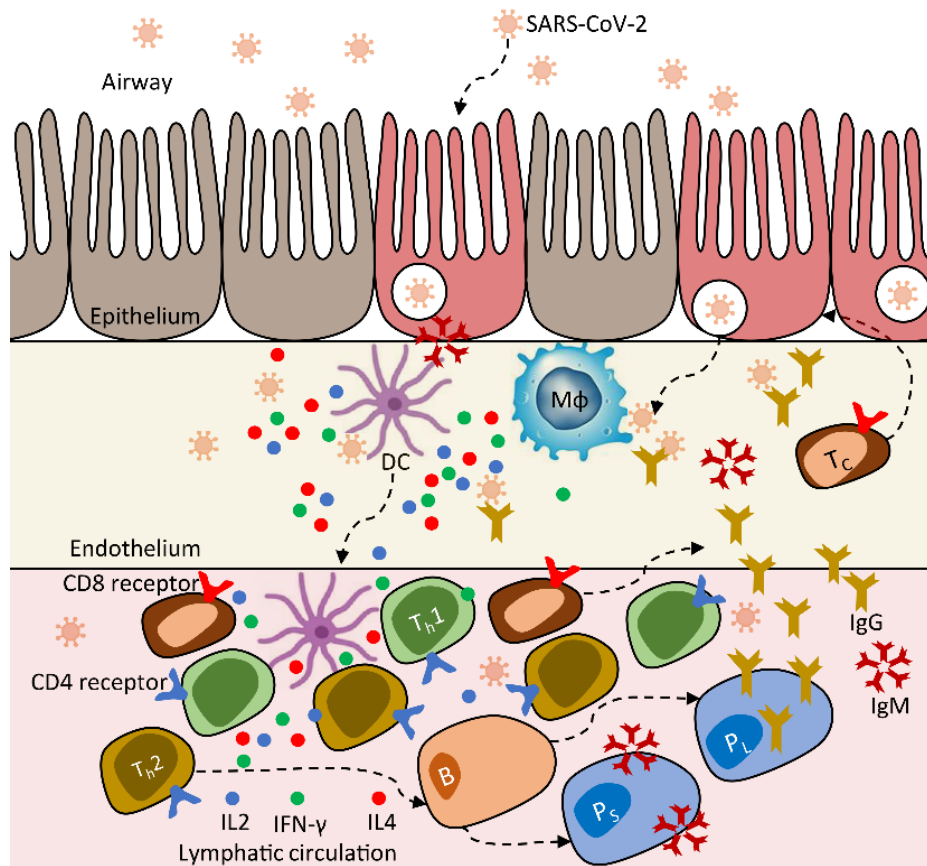
Innate and Adaptive Immune Response to SARS-CoV-2 Infection Play Major Role in Disease Severity

Tarunendu Mapder^{1*}, Sara K. Quinney^{1,2#}, Richard F. Bergstrom^{1§}, Robert E. Stratford^{1¤}

¹Division of Clinical Pharmacology, Department of Medicine, Indiana University School of Medicine, Indianapolis, IN 46202, USA

²Department of Obstetrics and Gynecology, Indiana University School of Medicine, Indianapolis, IN 46202, USA

Objective: The rapid transmission of SARS-CoV-2 in a community is manifested by a wide range of symptoms of coronavirus disease 2019 (COVID-19) including fever, pneumonia, acute respiratory distress syndrome and lymphopenia. The manifestations of CoV-2 infection can be classified into three different timescales: (i) asymptomatic incubation, (ii) mild symptoms and (iii) severe respiratory and immune distress, while the variability between individuals is very high. Unlike other coronaviruses such as SARS-CoV and MERS viruses, SARS-CoV-2 infection exhibits faster virus shedding and a longer incubation period. Hence, community transmission is faster than the disease manifestation and detection of infection. We believe the emergence of a “cytokine storm” as the major regulator of the disease severity. Our aim is to study the role of nonspecific immune response and cytokine release syndrome in disease severity and hence propose different treatments that seek to reduce the symptoms of COVID-19.



Methods: We calibrated a population of models (POMs) with clinical data including viral load, spike protein receptor binding domain (RBD) and nucleoprotein (NP) -specific IgM and IgG antibody levels for 23 patients reported across various days of illness¹. The calibration of the POMs is performed by matching the multivariate distributions of the observed data and model outputs. Optimal distribution matching was used to unlock the underlying variability in the data for the patient population and predict the regime of intervention. We use a computationally less expensive Latin Hypercube Sampling based probability distance (symmetric Kullback-Leibler divergence) minimization in MATLAB 2019b.

Results: Our model indicates that differential feedback regulation among the antigen presenting cells (dendritic cells (DC) and macrophages (MΦ)), helper T-cells (T_{h1} , T_{h2}) and cytokines (IL₂, IL₄, γ -IFN) contribute to the accumulation of cytokine pool and T-cell exhaustion. When the adaptive immune response is triggered, the activated B-cells (B) start to differentiate into short and long living plasma cells (Ps, PL) that produce the IgM and IgG, simultaneously. Although conventional immunopathology of RNA virus infection suggests that the production of IgG is lagged by IgM, the clinical data does not exhibit any delay in the case of CoV-2 infection. A decision switch between the two kinds of plasma cells and their conversion was able to model this phenomenon. The switch is controlled by the concentration of available IgM and IgG levels, viral load and the copies of infected epithelial cells.

Conclusions: We were effectively able to model the time course of viral and immune response following CoV-2 infection. This model may inform development of intervention strategies through monoclonal antibodies, cytotoxic T-cell gene therapy and inhibitors for cytokine receptors.

References:

- [1] To KK, Tsang OT, Leung WS, Tam AR, Wu TC, Lung DC, Yip CC, Cai JP, Chan JM, Chik TS, Lau DP. Temporal profiles of viral load in posterior oropharyngeal saliva samples and serum antibody responses during infection by SARS-CoV-2: an observational cohort study. *The Lancet Infectious Diseases*. 2020 Mar 23.

Population Pharmacokinetic- Pharmacodynamic Model of Eribulin Associated Neutropenia in Children with Refractory or Recurrent Solid Tumors

Thomas R. Larson¹, Eric S. Schafer², Rachel E. Rau², Charles G. Minard², Elizabeth Fox³, Brenda J. Weigel⁴, Joel M. Reid¹

¹Mayo Clinic, Rochester, MN, USA; ²Baylor College of Medicine, Houston, TX, USA; ³Children's Hospital of Philadelphia, Philadelphia, PA, USA; ⁴University of Minnesota, Minneapolis, MN USA

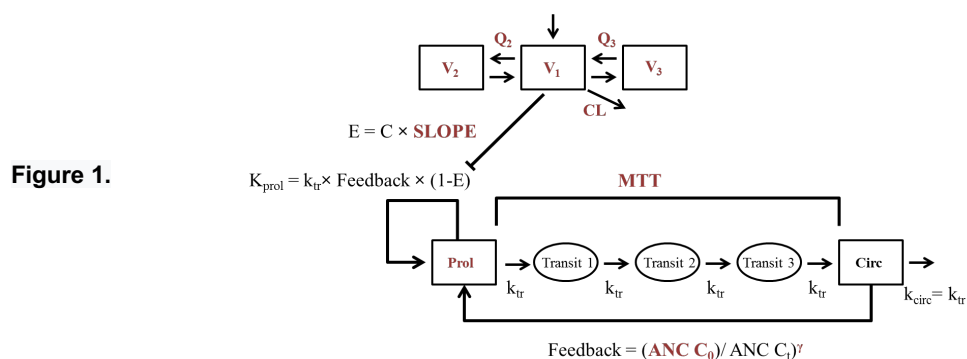
Objectives: Eribulin mesylate, a synthetic analog of halichondrin B, inhibits microtubule growth without effects on microtubule shortening and promotes nonproductive tubulin aggregate formation. It has been approved for the treatment of metastatic breast cancer, for patients who have received at least two prior therapies, and inoperable liposarcoma, for patients who have received a previous therapy. A phase 1 trial of eribulin was conducted in children and adolescents with relapsed or refractory solid tumors¹. In support of this study, a population pharmacokinetic-pharmacodynamic (PK-PD) model for eribulin mesylate associated neutropenia was developed in pediatric patients.

Methods: Eribulin was administered intravenously on days 1 and 8 of a 21 day cycle. Three dose levels (1.1, 1.4, and 1.8 mg/m²) were evaluated using the rolling six design. Additional patients were enrolled into a PK expansion cohort at the maximally tolerated dose. A total of 256 eribulin plasma concentrations and 108 absolute neutrophil counts (ANC) from 22 patients ages 3-17 years and body surface area (BSA) 0.57-2.19 m² were analyzed using nonlinear mixed-effects modeling with NONMEM® v7.4 to develop a semi-mechanistic population PK-PD model of eribulin associated decrease in ANC². No patients received myeloid growth factors during treatment.

Results: A dose-independent three-compartment PK model with BSA scaling adequately described the pharmacokinetic data, and was linked to a semi mechanistic PD model with the proliferating cell compartment (PROL) estimated separately (Figure 1). Population typical values (between subject variability) of CL (AGE<12) 3.64 L/h (0.355), CL (AGE≥12) 1.79 L/h (0.35), V1 3.15 L (0.12), Q2 1.62 L/h (0), V2 1.77 L (0.22), Q3 5.45 L/h (0), V3 95 L (0.16), ANC C₀ 1310 /ml (0), PROL 1570/ ml (0.17), MTT 190 h (0), Gamma 0.237 (1.08), and Slope 0.0099 µg/ml (0). Consistent with our previous report, children less than 12 years of age had a substantially higher CL compared to those 12 years and older and no other covariates were found to be significant¹. The PK and PK-PD models sufficiently describe the data as evaluated by goodness-of-fit plots, visual predictive checks, and bootstrap analysis.

Conclusion: A semi-mechanistic PKPD model was used to describe eribulin mesylate associated neutropenia in children. Body surface area and age of the children were found to be significant covariates in the PK of eribulin, and no pharmacodynamic covariates were identified in the model. This model reports similar results to previous models, but required the addition of separately estimated PROL to capture both trough and rebound ANC in these patients³.

References: [1] Schafer ES, et al. *Pediatr. Blood Cancer*. 2018 Feb; 65:e27066. [2] Friberg, LE, et al. *J. Clin. Oncol.* 2002 Dec;20(24): 4713-4721. [3] Coen van Hasselt JG, et al. *Br. J. Clin. Pharmacol.* 2013 Sep; 76(3):412-24.



WED-080

The platform physiologically-based quantitative computational model for different size of bispecific T cell engagers for cancer immunotherapy

Tomoki Yoneyama, Mi-Sook Kim, Konstantin Piatkov, Haiqing Wang and Andy Z.X. Zhu

Takeda Pharmaceutical International, Cambridge, MA, USA.

Objective: Bispecific T-cell engager (TCE) is an emerging anti-cancer modality which redirects cytotoxic T-cells to tumor expressing tumor-associated antigen (TAA) thereby forming the immune synapses to exerts anti-tumor effects. Considering the complexity of bispecific intercellular bridging and associated challenge in molecular design optimization, a more physiologically relevant computational framework is of crucial importance in TCE discovery and development. In this study, we developed a quantitative, physiologically-based computational framework to predict immune synapse formation in tumor considering the biodistribution of different size of TCEs and shed antigen as well as T-cells extra-vascularization in multiple myeloma.

Methods: The biodistribution of different size of TCEs and shed antigen was estimated using an adapted physiologically-based two-pore theory model. The developed platform model consists of blood, biodistribution to bone marrow (tumor site), lymph nodes and lumped other tissues, and further integrated with extra-vascularization of T cells and tumor cells followed by mechanistic bispecific binding of TCE in the presence of shed antigen. The model was further calibrated using data from clinical stage BCMA-targeting TCEs: AMG420 in BiTE format and PF-06863135 in IgG format. All the physiological and TCE related parameters were collected from public domain except for binding affinities to shed antigen which were estimated against in vitro tumor killing assay in presence of shed BCMA.

Results: The biodistribution of TCE was verified by positron emission tomography (PET) imaging data for [⁸⁹Zr]AMG211 (CEA-targeting BiTE). The developed model reasonably reproduced the observed biodistribution of PET tracer-labelled TCE into bone marrow in patients. The model was further calibrated for AMG420 in terms of binding affinities, membrane-associated and shed BCMA expression. The simulation results suggested the number of immune synapses in tumor site is low (~20/tumor cell) at the clinical efficacious dose of AMG420. The parameter sensitivity analysis indicated that immune synapse formation was highly sensitive to TAA expression, degree of antigen shedding and selectivity to cell surface TAA over shed antigen. Interestingly, the model suggested a “sweet spot” for TCE’s CD3 binding affinity which balanced the trapping of TCE in T cell rich organs. The developed framework was applied to TCE with IgG format in order to determine the dose and dose schedule to achieve the same level of immune synapse formation with AMG420 and critical parameters to maximize efficacy.

Conclusions: A quantitative computational framework for TCEs was developed by integrating the biodistribution of different size proteins based on two-pore theory followed by mechanistic bispecific binding to form immune synapses in presence of shed antigen. This framework can be applied to other targets beyond multiple myeloma to provide a quantitative mean of molecular design and clinical benchmarking in order to facilitate the model-informed best in class TCE discovery and development.

A unifying approach to sampling NLME model parameters

Venelin Mitov¹, Daniel Lill¹, Mohammed Cherkaoui-Rbati², Anne Kümmel¹

¹IntiQuan GmbH, Elisabethenstrasse 23, 4051 Basel, Switzerland

²Medicines for Malaria Venture, Route de Pré-Bois 20, Post Box 1826, CH-1215 Geneva 15, Switzerland

Objectives: Simulation of models is a key element of model diagnostics as well as a popular method for model-based prospective decision making. In the context of NLME models, sampling of the model parameters before simulation is a key prerequisite ensuring that the simulation is consistent with the estimated parameter uncertainty, individual random variability, covariate effects and residual error of the model. Despite its importance, to date there is neither a commonly accepted NLME parameter sampling tool, nor a specification for how NLME parameter sampling should be done. Instead, the parameter sampling is done in a rather *ad hoc* way, differing between modeler and modeling project; the sampling procedures are scarcely reported and hard or impossible to reproduce. We present a unifying software approach for NLME parameter sampling.

Methods: Our proposed solution is based upon the following components:

1. IQRnlmeparamxls: a new Excel file format providing a clear description of the NLME model estimation results and all additional information needed for sampling the parameters. Importantly, this format has been designed to be both, programmable as well as readable by humans.
2. A set of exporter R functions implementing the conversion of model estimation results from existing tools (e.g. NONMEM, MONOLIX) to IQRnlmeparamxls.
3. A set of sampler and calculator R functions implementing all steps from sampling population parameter values from the estimate's uncertainty distribution to obtaining individual parameter values for a user specified dataset of individual covariates.
4. A set of validator R functions checking the consistency of the parameter samples with the IQRnlmeparamxls file.

Results: In this talk, we present the above approach based on real life PKPD modeling examples. For a well behaved NLME example, we show that our implementation provides parameter samples such that the sampled distributions are in line with the distributions defined. Using other examples, we will highlight an important caveat concerning the sampling of positive-definite variance covariance matrix parameters. As the uncertainty of the elements of such matrix-parameters usually is reported as a multivariate normal distribution, there is an inherent risk of sampling invalid parameter sets, namely, negative-definite matrices. We will present our current implemented approach to tackle this problem. Finally, we will show how the validator functions can be used to detect and notify the modeler about mismatches between the sampled and required parameter distributions.

Conclusions: IQRnlmeparamxls is a powerful yet human readable format for specifying NLME model parameters enabling easy sharing of NLME parameter estimation results independent of the used modeling platform. The implementation of a generic and transparent parameter sampling tool presents an important step towards improving the quality and reproducibility of NLME model simulations.

WED-083

A Quantitative Systems Pharmacology Model of Alzheimer's Disease Pathology and Treatment Modalities

Authors: Vidya Ramakrishnan^{1,*}, Christina Friedrich^{2,*}, Colleen Witt², Meghan Pryor², Michael Dolton¹, Jasi Atwal¹, Kristin Wildsmith¹, Katherine Kudrycki², Robert Sheehan², Seung-Hye Lee¹, Hans Peter Grimm³, Roxana Aldea³, Norman Mazer³, Carsten Hofmann³, Ronald Gieschke³, Reina Fuji¹, Jin Yan Jin¹, Saroja Ramanujan¹, Angelica Quartino¹

*VR and CF are co-first authors

Affiliations: ¹Genentech, Inc., South San Francisco, CA, USA; ²Rosa & Co., LLC., San Carlos, CA, USA;

³Hoffmann-La Roche Ltd., Basel, Switzerland.

Objectives:

A quantitative systems pharmacology (QSP) model of Alzheimer's Disease (AD) pathologies was developed and utilized to assess the impact of investigational A β and tau targeting treatments in support of drug development strategies.

Methods:

The inclusion of the mechanisms of the two defining features of AD pathology: A β and tau in the comprehensive QSP model allows for the benchmarking-based evaluation of therapies targeting the A β and tau pathways. The model tracks the production, aggregation, transport dynamics and clearance of soluble biomarkers involved in these mechanisms in the brain, CSF, and peripheral plasma, as well as the impact of investigational treatments on these processes. SimBiology, a MATLAB® based application was used for the implementation of the model. Initial conditions and reaction rate parameters were calibrated based on literature and in-house informed data. The model scope enables scientific hypothesis assessments of biomarker target engagement in brain/CSF, biomarker transport dynamics, patient phenotype evaluation, therapy benchmarking, and treatment strategies.

Results:

The developed model is a comprehensive platform model describing the currently known key disease mechanisms in AD. The detailed mechanisms built into the A β and tau modules, namely: production, aggregation (monomer—oligomer—fibril/plaque), and transport allow assessment of diverse therapeutic agents targeting the two pathways. The model is calibrated to pharmacokinetic and pharmacodynamic/biomarker data in plasma and CSF from published and in-house clinical studies evaluating diverse mechanisms of action targeting different aggregated species. For A β , model simulations allowed quantitative assessment of target engagement in brain and CSF, enabling a comparison between therapies intervening in the A β pathway and the effects of different doses, durations, and dosing regimens (flat/titration doses). The model is adequately equipped for a similar assessment within the tau module. The model is also calibrated to available imaging-based A β PET SUVR data directly assessing disease burden. The calibration provided insights into the possible mechanisms of plaque clearance mediated by plaque targeting antibodies. The overall long duration of disease progression facilitates the model utility to test several patient phenotypes based on stage of disease progression (prodromal/moderate/severe AD) and evaluate effect of investigational therapies on these phenotypes.

Conclusions: A calibrated QSP model incorporating a detailed representation of A β and tau production, aggregation, transport and clearance was developed. The model facilitated a quantitative assessment of target engagement by disease-modifying therapies directed towards A β and tau pathologies in the brain and CSF. The disease platform model is a comprehensive tool to test biomarker and therapy-based strategies and scientific hypothesis.

WED-084

Optimization of FIH (First-in-Human) Starting Dose for an HLE-BiTE® (Half-life Extended Bispecific T-cell Engager Molecule for Patients with Gastric Cancer Using Translational PKPD Modeling

Michael Z. Liao¹, Sergey Ermakov¹, Roman Kischel², Sabine Stienen², Alex Sternjak², Kathrin Locher², Michael Lutteropp², John Harrold³, Julie Bailis³, Benno Rattel², Matthias Friedrich², Khamir Mehta¹, Sandeep Dutta⁴, Vijay V. Upreti¹

¹Clinical Pharmacology Modeling & Simulation, Amgen Inc., South San Francisco, CA, USA; ²Amgen (Munich)

GmbH, Munich, Germany; ³Research, Amgen Inc., South San Francisco, CA, USA; ⁴Clinical Pharmacology Modeling & Simulation, Amgen Inc., Thousand Oaks, CA, USA

Objectives:

HLE BiTE® antibody construct is a targeted immuno-oncology platform designed to engage patients' own T cells to kill cancer cells. This work is to provide an innovative approach for selecting a more rational FIH starting dose. Herein we provide an example of optimizing the starting dose for an HLE BiTE® molecule, integrating preclinical data and the specific BiTE mechanism of action for gastric cancer patients that enabled a 10-fold higher starting dose through translational PK/PD modeling.

Methods:

The selection of starting dose was based on the recommended approach for T cell recruiting constructs using Minimum Anticipated Biological Effect Level (MABEL). MABEL assays with different effector T cell to tumor cell (E:T) ratios were assessed and an assay that is expected to recapitulate patients with solid tumors was selected. Based on human PK modeling and simulation, predicted first dose C_{max} approximated the optimized MABEL. A two compartmental human PK model was derived by allometrically scaling PK parameters of the model developed based on nonhuman primate data. The minimally efficacious exposure range was estimated using both *in vitro* and *in vivo* data. The *in vitro* prediction was based on the EC_{90} of the cytotoxicity assay. The *in vivo* prediction used a mouse xenograft tumor growth inhibition (TGI) translational PK/PD model that incorporated the time course of tumor volume change [$\frac{dV_{tumor}}{dt}$], as below. The model assumed tumor growth as exponential [k_{grow}], drug effect on tumor described by concentration [C], maximal inhibition [I_{max}], tumor volume [V_{tumor}], and half-maximal inhibitory effect [IC_{50}].

$$\frac{dV_{tumor}}{dt} = k_{grow}V_{tumor} - \frac{I_{max}C \cdot V_{tumor}}{IC_{50} + C}$$

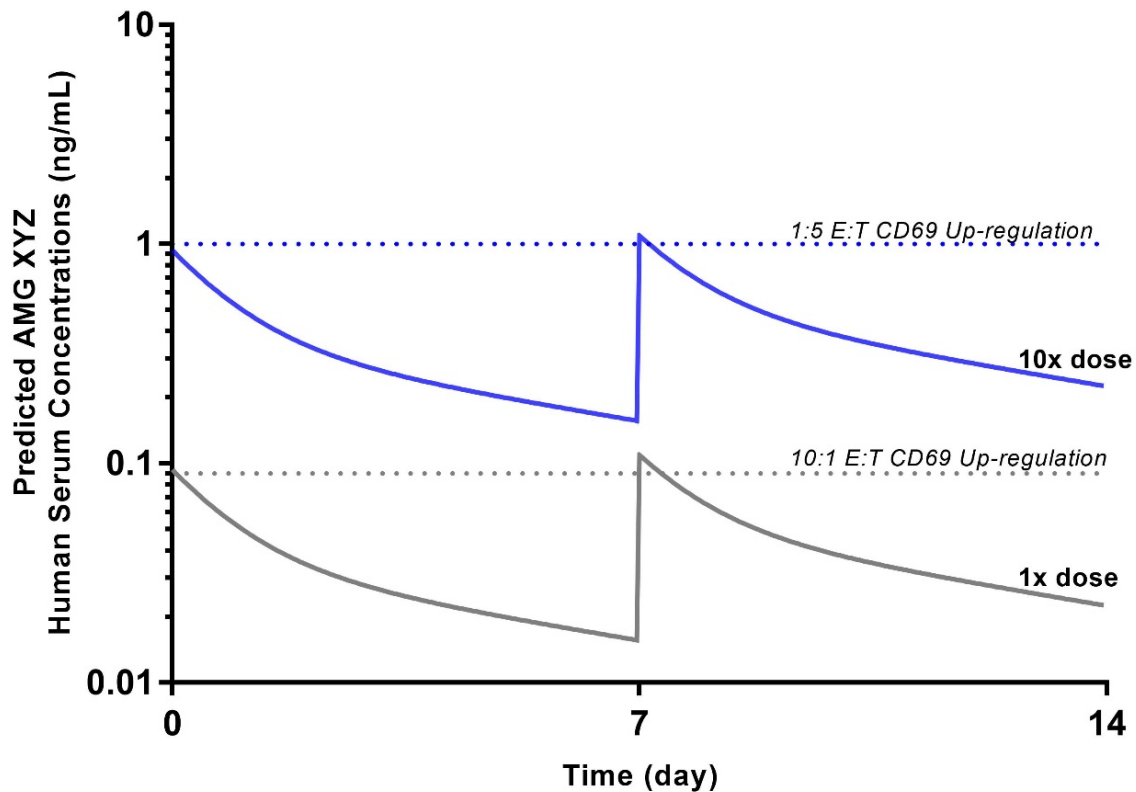
The model estimated the *in vivo* IC_{50} for TGI. Exposure - tumor response curves in patients were simulated to predict the dose range for target trough coverage and tumor tissue distribution.

Results:

The starting dose based on MABEL using typical assay conditions (E:T ratio of 10:1) resulted in a very low dose. Using an E:T ratio of 1:5 to better mimic physiological conditions resulted in a 10-fold higher starting dose for based on PK modeling and simulation. This starting dose was supported by favorable nonclinical safety data. Human PK modeling was used to predict drug concentrations in the tumor tissue, assuming approximately 10% of the serum exposure. Minimal efficacious dose was set to be in the range between the *in vitro* EC_{90} and *in vivo* IC_{50} values estimated using the translational PK/PD mouse tumor xenograft model.

Conclusion:

We present an approach that uses translational PKPD modeling to provide a more rational FIH starting dose for HLE-BiT[®] antibody constructs. It enabled a 10-fold higher starting dose compared to previously used methods in patients with gastric tumors. The clinical starting dose was deemed safe and well tolerated. The current model adequately predicted the drug exposures observed in patients.



**Preclinical-to-clinical translation of GalNAc-siRNA using multiscale PK-PD modeling:
a case study with fitusiran**

Vivaswath S. Ayyar, Dawei Song, Songmao Zheng, Thomas Carpenter, Donald L. Heald

Discovery Translational Research, Biologics Development Sciences, Janssen BioTherapeutics, Janssen Research and Development, Spring House, PA, USA

Objectives: Recent advances in gene therapy for both rare and prevalent diseases are transforming precision medicine. Conjugation of small interfering ribonucleic acid (siRNA) to tris-N-acetylgalactosamine (tris-GalNAc) enable highly selective, potent, and durable knockdown of targeted proteins in liver. However, there is limited mechanistic understanding on how preclinical PK/PD studies using *in vitro* systems, mice, and nonhuman primates can be translated to predict clinical responses apriori as well as guide first-in-human (FIH) dose selection. Many intermediary steps along the PK-PD cascade are nonlinear and time-dependent, complicating dose-exposure-response relationships for these drugs. A multiscale minimal physiologically based pharmacokinetic-pharmacodynamic (mPBPK-PD) model for GalNAc-siRNA was developed using published data for fitusiran (ALN-AT3SC), an investigational compound targeting liver antithrombin (AT) to delineate putative determinants governing their whole-body-to-cellular PK-PD and to facilitate preclinical-to-clinical translation.

Methods: The mPBPK-PD model mathematically linked key PK-PD mechanisms: i) hepatic biodistribution, ii) tris-GalNAc binding to asialoglycoprotein (ASGPR) receptors on hepatocytes, iii) ASGPR endocytosis and recycling, iv) endosomal transport and escape of siRNA, v) cytoplasmic RISC loading, vi) cleavage of target mRNA, and vii) knockdown of protein. Physiological ranges for 38 out of 48 model parameters (including species-dependent volumes and flow rates) were obtained from the literature. Kinetic parameters for GalNAc-ASGPR binding and internalization were obtained by modeling *in vitro* uptake experiments in hepatocytes. The data were extracted from published graphs by computer digitization (WebPlotDigitizer, 4.1). The PK-PD analysis was performed using ADAPT 5 (BMSR). A global sensitivity analysis (GSA) using the Partial Rank Correlation Coefficient-based method was conducted in R to deduce the impact of parameter uncertainty on select model outputs.

Results: The proposed model characterized reported PK, RISC loading, and knockdown of AT mRNA and protein upon ALN-AT3SC dosing in wild-type and *Asgr2^{-/-}* mice reasonably well. Model simulations bridged multiple PK-PD datasets in preclinical species (mice, rat, monkey) and successfully predicted plasma PK and serum AT knockdown in a Phase-I ascending dose study. Estimation of selected model parameters from the mice PK-PD datasets (e.g. liver uptake clearance, cytoplasmic siRNA degradation rate constant, siRNA-RISC association rate constant) were obtained with acceptable precision (< 30% CV) and these estimates were fixed during model scale-up. The estimated *in vivo* drug potency parameters varied within two-fold across species. Subcutaneous drug absorption and serum AT degradation rate constants were identified retrospectively to scale across species by body weight with allometric exponents of 0.3 and 0.2.

Conclusion: The developed platform mPBPK-PD model successfully predicted clinical PK-PD of siRNA based on model-based analyses of preclinical *in vitro* and *in vivo* data. The proposed modeling framework can accelerate the development of future siRNA therapies.

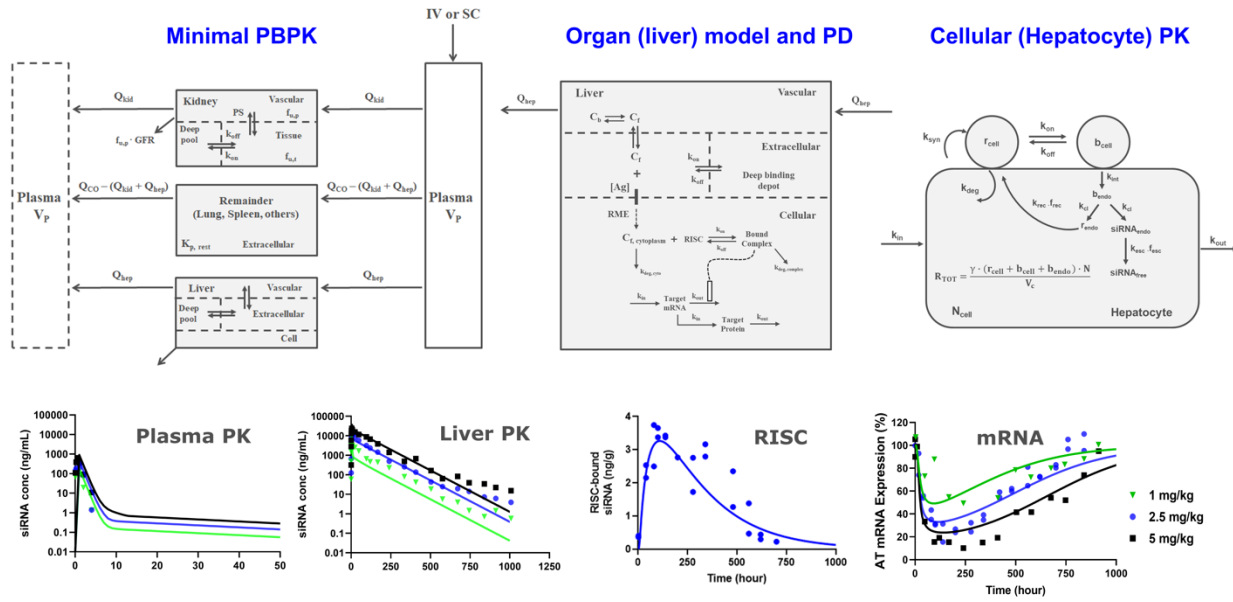


Figure 1. Schematic of the platform mPBPK-PD model for GalNAc-siRNA mediated gene knockdown (top left and right) and model-based characterization of plasma PK, liver biodistribution, RISC occupancy, and mRNA knockdown following a single dose of ALN-AT3SC in mice (serum protein knockdown not shown here).

WED-086

Pharmacokinetic analysis of Ziltivekimab, anti-Interleukin-6 monoclonal antibody in chronic kidney disease patients

Wansu Park¹, Joga Gobburu¹, Larry Lo², Michel Chonchol³ and Matt Devalaraja²

¹Center for Translational Medicine, University of Maryland School of Pharmacy, Baltimore, MD, USA; ²Corvidia Therapeutics, Waltham, MA, USA

2 Corvidia Therapeutics, Waltham, MA 02451

3 Division of Renal Diseases and Hypertension, Anschutz Medical Campus, University of Colorado, Denver CO 80220

Objectives: Ziltivekimab is a human IgG1κ monoclonal antibody directed against interleukin-6 (IL-6) which is being developed for the treatment of inflammatory sequelae in patients with advanced chronic kidney disease (CKD). The objective was to describe the pharmacokinetic (PK) profile of ziltivekimab in a Phase I trial of ziltivekimab in CKD patients using non-compartmental analysis and population PK modeling.

Methods: PK analysis was performed using serum samples from 9 patients following a subcutaneous administration of single dose of 5, 15, and 50 mg of ziltivekimab. Assessment of the PK included the elimination half-life ($t_{1/2}$), area under the curve (AUC), maximum concentration (Cmax), and time to reach Cmax (Tmax) by non-compartmental analysis (NCA). A compartment PK model was tested to describe the data by nonlinear mixed effects (NLME) modeling using first-order conditional estimation with interaction as an estimation method. NCA and NLME modeling were conducted using Pumas version 0.10.0 (www.pumas.ai)¹

Results: A total of 135 ziltivekimab concentrations were used for NCA and model development. Ziltivekimab was slowly absorbed from the injection site reaching the Cmax in approximately 6 days in 5 mg dose group. Mean AUClast was 21.26, 76.93 and 320.82 day*μg/mL for ziltivekimab 5 mg, 15 mg and 50 mg cohorts, respectively. Mean Cmax was 0.34, 0.82 and 3.92 μg/mL for ziltivekimab 5 mg, 15 mg and 50 mg cohorts, respectively. Cmax and AUC of ziltivekimab increased with dose in an approximately dose-proportional manner. Mean apparent clearance was 0.23, 0.18 and 0.19 L/day for ziltivekimab 5 mg, 15 mg and 50 mg groups, respectively. Apparent clearance (CL/F) obtained by NCA were generally similar across the dose groups indicating no evidence of nonlinear PK in the tested dose range. Ziltivekimab PK was adequately characterized by a one-compartment model with first-order absorption. The final population parameters by NLME were CL/F, 0.19 L/day; VC/F, 16.5 L; KA, 0.37 1/day. Exploration of the relationship between covariates interested and empirical Bayesian estimates of individual parameters showed that there was a lack of influence of body weight, body mass index, height, age, serum creatinine, estimated glomerular filtration rate on clearance, volume of distribution and absorption rate constant of ziltivekimab.

Conclusions: The population PK model adequately described the ziltivekimab PK in CKD patients.

Reference:

1. Chris Rackauckas, Andreas Noack, Vaibhav Dixit, Yingbo Ma, Patrick Kofod Mogensen, Shubham Maddhashiya, Simon Byrne, Joga Gobburu, Joakim Nyberg, Vijay Ivaturi. Pumas: High Performance Pharmaceutical Modeling and Simulation. (In preparation)

A Whole-Body Circulatory Model of Neutrophil Dynamics

Wenbo Chen¹, Britton Boras², Mary E. Spilker², David Z. D'Argenio¹

¹Department of Biomedical Engineering, University of Southern California, Los Angeles, CA, USA; ²Pfizer, Inc., San Diego, CA, USA.

Objectives: To develop a physiological circulatory model characterizing the whole-body distribution of neutrophils in humans. The model incorporates our current understanding of neutrophil trafficking in organs, including transendothelial migration and tissue clearance.

Methods: A circulatory neutrophil model was constructed using previously published ¹¹¹Inium (¹¹¹In)-labeled neutrophil tracer kinetic measurements in blood, lung, liver, spleen, and bone marrow (BM) in healthy subjects [1-3]. The circulatory model includes the organs that are primarily responsible for neutrophil hemostasis in health and disease (venous and arterial blood, lung, liver, spleen, lymph node, BM). Each organ is composed of vascular and extravascular spaces, with neutrophils entering the vascular space of each organ through the arterial blood pool, followed by transendothelial migration to the extravascular space, where they are then phagocytosed by macrophages or recycled via the lymphatics to the venous blood pool. The model for the margination process in the blood also includes the kinetics of circulating and marginated neutrophils in the venous blood. As with our previous model [4], the BM subsystem in this circulatory model includes a cell cycle model of the progenitor cells (PC), which allows for a mechanistic representation of the action of relevant anticancer drugs derived from in vitro BM toxicity studies. The model also includes granulocyte-colony stimulating factor (G-CSF) kinetics and its regulation, which allows the action of administered filgrastim or pegfilgrastim support therapies to be modeled [4].

Results: The circulatory neutrophil model adequately described the ¹¹¹In-labeled neutrophil kinetic data in the blood and sampled organs over 48 hours reported in [1-3], with R² ranging between 0.6 and 0.9. The estimated transendothelial migration rates and tissue clearance values were comparable to those reported in humans, which provide confidence in the fitted results. The model was further evaluated by predicting the absolute neutrophil count (ANC), band cell, and segmented neutrophil time course results in healthy volunteers following four dose levels of pegfilgrastim reported in [5], as well as ANC time course responses following both intravenous and subcutaneous administration of filgrastim [6]. Additionally, the model-predicted baseline values of G-CSF and various cell types in the BM (PC, metamyelocyte, band cell, segmented neutrophil) and in the blood (band cell, segmented neutrophil, marginated neutrophil, ANC, G-CSF concentration) are similar to the literature reported values.

Conclusions: The circulatory neutrophil model presented may provide a mechanistic framework for predicting neutrophil homeostasis and neutropenia following drug treatment in patients with cardiovascular, hepatic, or renal impairment.

References:

- [1] Peters et al., *Scand J Haematol* 34:111-120,1985
- [2] Saverymuttu et al., *Br J Haematol* 61:675-685,1985
- [3] Szczepura et al., *Eur J Clin Invest* 41:77-83,2011
- [4] Chen et al., *J Pharmacokinet Pharmacodyn* 47:163-182,2020
- [5] Roskos et al., *J Clin Pharmacol* 46:747-757,2006
- [6] Krzyzanski et al., *J Clin Pharmacol* 50:101S-112S,2010

WED-088**Pharmacometric Evaluation of TAK-954 Effects on Gastric Half-Emptying and Colonic Transit in Patients with Diabetic or Idiopathic Gastroparesis**

Chunlin Chen¹, Victor Chedid², George Dukes¹, William S. Denney³, Jenifer Siegelman¹, Jatinder Muker¹, Cristina Almansa¹, Michael Camilleri²

¹ Takeda Pharmaceuticals International Co., Cambridge, MA, USA

² Mayo Clinic, Rochester, MN, USA

³ Human Predictions Cambridge, MA, USA.

Objectives: TAK-954 is a highly selective and potent 5-HT4 receptor agonist with pharmacologic activity in gastrointestinal tract in vitro and in vivo. The objective of this analysis was to characterize the relationship between TAK-954, gastric half-emptying time, and colonic transit velocity as measured by colonic geometric center (CGC) in patients with diabetic or idiopathic gastroparesis.

Methods: In a single-center, randomized, parallel group, double-blind, placebo-controlled study, 36 participants received placebo (n=10), 0.1 (n=10), 0.3 (n=9), or 1.0 mg (n=7) of TAK-954 as a 60-minute intravenous infusion once a day for 3 days. Enrolment into the 1.0 mg arm was stopped after prespecified interim analysis. At baseline, each participant completed 4-hour gastric emptying scintigraphy test. Following infusion on Day 2, scintigraphic assessment of gastric, small bowel, and colonic transit of solids over 48-hour time period were obtained (same meal plus 111In-charcoal delivered in methacrylate-coated capsule that dissolves in the ileocolonic region) to study effects of TAK-954. Infusion on Day 3 to maintain plasma levels of TAK-954 while assessing colonic transit. CGC is measured on 0 to 5 scale based on the weighted proportion of counts in each of 4 colonic regions (ascending, transverse, descending and rectosigmoid) and stool where 0 is in small bowel and 5 is 100% isotope excreted in stool.

Exposure-gastric half-emptying time models were estimated using 'nlme' package (version 3.1-140) in R (version 3.6.1). Best model was selected by Akaike's Information Criterion. CGC models were estimated using 'Stan' package (version 2.10.0) in R (version 3.6.1). Best model was selected by widely accepted information criterion. Final models were evaluated by visual predictive check (VPC).

Results: TAK-954/gastric half-emptying model was a mixed-effects E_{max} model with baseline effect. Estimated concentration at end of infusion (C_{eoI}) causing half-maximal decrease of gastric half-emptying time (EC_{50}) is 1262 pg/mL

For CGC model, TAK-954 dose rather than exposure was selected based on model parsimony and the fact that exposure metrics did not improve the model. TAK-954/CGC model was a zero-inflated beta-regression model with dose- and time-responsive effect on zero inflation, time effect on the beta distribution shape and scale, and E_{max} effect of dose on beta distribution scale. TAK-954 decreased time in small bowel (decreasing zero inflation metric by a logit function of dose) and increases colonic transit velocity as measured by CGC (by an E_{max} function of dose where ED_{50} was <0.1 mg). In general, the results of the VPC supported predictive ability of the two models.

Conclusions: TAK-954 enhances gastric emptying with an E_{max} trend, suggesting that maximal receptor agonism was achieved over this concentration range. All studied doses are at near-maximal effect for colonic transit. These results support further evaluation of TAK-954 for the treatment of gastric and intestinal motility disorders.

Pharmacodynamic modeling of SOD1 reduction in the cynomolgus monkey following repeat-dose intrathecal injection of antisense oligonucleotide (ASO) tofersen

Xiao Tong¹, Ivan Nestorov¹

1. Biogen, Cambridge, MA, USA.

Objective: Tofersen (BIIB067) is an antisense oligonucleotide (ASO) RNase H1-mediated inhibitor of superoxide dismutase 1 (SOD1) messenger ribonucleic acid (mRNA), in development for the treatment of amyotrophic lateral sclerosis (ALS) with *SOD1* mutations. The therapy has been originally designed by Ionis Pharmaceuticals and is now being developed clinically by Biogen [1, 2]. Tofersen is pharmacologically active in the CNS of cynomolgus monkey following intrathecal injection. The objective of the current analysis was to build a population pharmacodynamic (PD) model to investigate the PD relationship of tofersen in inhibiting SOD1 protein production measured in cerebrospinal fluid (CSF) in nonhuman primates (NHPs).

Method: Data from a 9-month toxicology study with 36 NHPs following intrathecal doses of placebo, 4 mg 12 mg and 35 mg was first used for the model development. An indirect response model was built described by the inhibitory effect of tofersen CSF concentration (C_{trough}) on SOD1 CSF protein production (Kin). Baseline SOD1 CSF protein was tested as covariate on EC₅₀ and Emax. The model was further evaluated by including data from a 13-week toxicology study of the same dosing range (N=42).

Results: SOD1 protein reduction measured in CSF was reasonably described by the indirect response model, where tofersen C_{trough} acted as inhibition on the SOD1 protein production (Kin). The estimated turn-over rate (Kout) based on the 9-month toxicity data was 0.033 day⁻¹ corresponding to a SOD1 protein half-life of 21 days, which was consistent with the previously published value in SILK study[3]. The estimated EC₅₀ and Emax were 7.45 ng/mL and 0.458, respectively, corresponding to approximately 50% maximum reduction of SOD1 protein from baseline in monkey CSF. The estimation of EC₅₀ and Emax are within the observed range from data with reasonable precision,. The baseline SOD1 protein level was not a significant covariate on either EC₅₀ or Emax. The parameter estimates remained consistent when combining the 9-month NHP toxicity data with the 13-week NHP data, with improved precision on Kout.

Conclusion: The indirect response model developed reasonably described the PD relationship between tofersen and SOD1 protein reduction in CSF of NHP. This model can be extended to study the PD relationship in humans and provide guidance to the design of future clinical trials of tofersen.

References

1. Bennett, C.F., A.R. Krainer, and D.W. Cleveland, *Antisense Oligonucleotide Therapies for Neurodegenerative Diseases*. Annu Rev Neurosci, 2019. **42**: p. 385-406.
2. McCampbell, A., et al., *Antisense oligonucleotides extend survival and reverse decrement in muscle response in ALS models*. J Clin Invest, 2018. **128**(8): p. 3558-3567.
3. Crisp, M.J., et al., *In vivo kinetic approach reveals slow SOD1 turnover in the CNS*. J Clin Invest, 2015. **125**(7): p. 2772-80.

WED-090**Lymphatic Distribution of Etanercept Following Intravenous and Subcutaneous Delivery to Rats**

Xizhe Gao¹, Gregory O. Voronin¹, Claudia Generaux², Anne Rose², Alexander Kozhich², Gerard Dalglish², Leonid Kagan¹

¹Ernest Mario School of Pharmacy, Rutgers, The State University of New Jersey, Piscataway, NJ 08854, USA

²Bristol-Myers Squibb, New Brunswick, NJ, USA

Objectives: The goal of this work was to investigate systemic pharmacokinetics and lymphatic recovery of etanercept following intravenous (IV) and subcutaneous (SC) delivery in the thoracic lymph duct cannulated rat model.

Methods: Rats were divided into 4 groups: (1) IV lymph-cannulated group, (2) IV control group, (3) SC lymph-cannulated group, and (4) SC control group (n=3 each). Thoracic lymph duct was cannulated, which allowed for lymph collection for up to 6 days after surgery. Sham operated rats were used as control. Etanercept pharmacokinetics was studied after a single IV or SC (hind leg) dose of 1 mg/kg. Lymph samples were collected continuously (in 30 - 60 minutes intervals) on day 1 and then once daily. Systemic blood was sampled from jugular vein cannula or saphenous vein. Samples were analyzed by a Gyros-based method. Mechanistic pharmacokinetic model with lymph and blood absorption pathways and redistribution of systemically available drug into lymph was developed to capture etanercept disposition.

Results: In lymph-cannulated rats following IV dosing, etanercept concentration in the lymph was consistently lower than in serum (e.g., 4-fold at 24 hours). On the other hand, following SC administration, the concentration in the lymph was significantly higher than in serum (e.g., 11-fold at 24 hours). Lymphatic cannulation reduced the serum AUC (up to 120 hours) by 28% in IV group and by 91% in SC group. SC bioavailability of etanercept in control rats was 65 %. About 53.9% of the dose was absorbed via lymph pathway and 11.3 % of dose was absorbed directly into the blood stream. Pharmacokinetic model successfully captured serum profiles and lymph collection data in all groups and all parameters were estimated with sufficient precision.

Conclusions: Lymphatic system plays a major role in absorption of etanercept after SC administration. Furthermore, a significant redistribution of systemically available etanercept into lymph was observed.

Pharmacokinetics of Buccal versus Vaginal Misoprostol for Labor Induction at Term

Yana Vorontsova¹, David M. Haas¹, Kathleen Flannery¹, Andrea R. Masters¹, David Guise¹, Michael Heathman², Sara Quinney¹

¹Indiana University School of Medicine, Indianapolis, IN, USA; ²Metrum Research Group, Tariffville, CT, USA

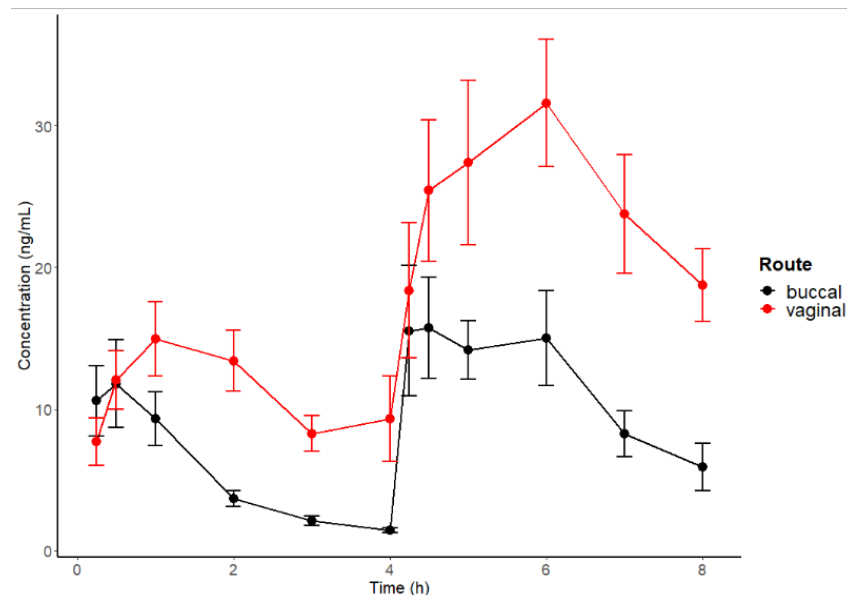
Objectives: The IMPROVE study (NCT02408315) compared the efficacy and safety of vaginal and buccal administration of misoprostol for full-term uncomplicated labor induction. The current study compares the pharmacokinetics (PK) of misoprostol between vaginal and buccal routes.

Methods: Women \geq 14 years of age undergoing induction of labor \geq 37 weeks gestation without significant complications were randomized to vaginal or buccal administration of misoprostol (25 μ g first dose, 50 μ g subsequent) every 4 hrs. Plasma concentrations were collected for the first 8 hours. A population PK model was developed using NONMEM®.

Results: Data included 469 plasma concentrations from 47 subjects. Considerable differences were observed between the two routes of administration. A 1-compartment non-linear CL model with IOV on F, IIV on CL, V, Ka, with the covariates of dose on Ka, and route on F and Ka adequately described the data.

Conclusions: This is the first study to compare PK of buccal versus vaginal misoprostol for labor induction at term using doses recommended in clinical practice. The rate of buccal absorption was 2 times faster for 25mcg and 2.6 times faster for 50 mcg dose than that of vaginal, while bioavailability of vaginal administration was 2.4 times higher than that of buccal. Differences in bioavailability between routes of administration may explain why vaginal administration of misoprostol was more effective than buccal administration.

The results in this abstract have been previously submitted to ASCPT Annual Meeting, Marriott Marquis, Houston, TX, March 18-21, 2020, and published in the conference proceedings as abstract ID:741634.



WED-093

Speed up population Bayesian inference by combining cross-chain warmup and within- chain parallelism

Authors: Yi Zhang(1), William R. Gillespie(2), Ben Bales(2), Aki Vehtari(3)

Institutions: (1) Metrum Research Group, USA (2) Columbia University, USA (3) Aalto University, Finland

Objectives:

The probabilistic programming language and Bayesian inference engine Stan supports general model specification and uses dynamic HMC for Bayesian analysis [1]. Torsten is a Stan functions library that simplifies pharmacometric modeling and extends the range of models that may be implemented [2]. To improve the performance of Bayesian inference of population models, we designed a multilevel parallel scheme combining a cross-chain warmup algorithm with within-chain parallelisation and demonstrated that this approach significantly improves large PKPD model simulation efficiency.

Methods:

Torsten provides ODE integrator functions and pharmacometrics solution functions [2]. For population modeling, these functions solve each ODE system corresponding to each individual in parallel. This is augmented with a cross-chain warmup scheme that performs dynamic warmup adaptation by chain aggregation. During warmup, the joint log posteriors sampled from parallel chains are collected and used to calculate potential scale reduction coefficients (Rhat) and effective sample sizes (ESS) [3]. When they surpass predetermined target values, warmup is terminated to avoid unnecessary computation. We also aggregated samples from chains and used them to calculate and update the HMC stepsize and mass matrix. The proposed algorithm was implemented using MPI for both inter-chain communication during cross-chain warmup and within-chain communication for population model calculations, enabling us to perform large-scale simulations using a cluster and distribute the computation load evenly across chains.

Results:

Models that would benefit most from the proposed scheme are those that involve heavy computation in each HMC leap-frog step. We tested two such models: a hierarchical model with ~400 normally distributed parameters (Model 1) and an ODE-based model that involves long integration times (Model 2). The models are fit using default Stan settings of 4 chains, with 1000 post-warmup samples/chain, using either the proposed or the regular Stan approach (1000 warmup iterations). The proposed scheme gives similar performance in terms of ESS-per-iteration, while reducing the number of warmup iterations and thus wall time significantly (Tables 1).

Table 1: Compare sampling performance of regular run and cross-chain-warmup runs

Performance measure	Model 1 regular run	Model 1 cross-chain run	Model 2 regular run	Model 2 cross-chain run
MIN(ESS bulk /iter)	0.29	0.29	0.23	0.28
MIN(ESS tail /iter)	0.40	0.41	0.30	0.30
MIN(ESS bulk /sec)	83	103	10	18
MIN(ESS bulk /sec)	118	144	13	20
Number Of warmup item	1000	350	1000	350
Warmup wall time(sec)	9.9	6.5	48.0	21.2
Total wall time(sec)	14.1	11.1	91.5	61.9

Conclusions:

Multi-level parallelism using in Stan/Torsten significantly improves computational efficiency and extends the range of models that may be practically implemented.

References:

1. Carpenter et al. Stan: A probabilistic programming language. *Journal of Statistical Software*, 76(1):1–32, 2017.
2. <https://github.com/metrumresearchgroup/Torsten>
3. A. Vehtari et al. Rank-normalization, folding, and localization: An improved Rhat for assessing convergence of MCMC. <http://arxiv.org/abs/1903.08008>.

WED-094

Safety and Pharmacokinetics of Bintrafusp Alfa With Q3W Dosing: Confirmation of the Model-Informed Dose Selection

Yulia Vugmeyster¹, Lena Klopp-Schulze², Peter Rueckert², Akash Khandelwal², Isabell Speit², Motonobu Osada³, Italia Grenga¹

¹EMD Serono Research & Development Institute, Inc., Billerica, MA, USA a; business of Merck KGaA, Darmstadt, Germany; ²Merck KGaA, Darmstadt, Germany; ³Merck Biopharma, Tokyo, Japan; an affiliate of Merck KGaA, Darmstadt, Germany

Objectives: Bintrafusp alfa, a first-in-class bifunctional fusion protein composed of the extracellular domain of the TGF- β RII receptor (a TGF- β “trap”) fused to a human IgG1 mAb blocking PD-L1, showed a manageable safety profile and clinical activity in patients with heavily pretreated advanced solid tumors in phase 1 studies of 1200-mg every-2-weeks dosing. For combination studies with chemotherapies, which follow an every-3-weeks (Q3W) dosing cycle, a 2400-mg Q3W bintrafusp alfa dosing regimen was selected using the previously described, model-informed approach [1]. The objective of this study was to evaluate preliminary safety and pharmacokinetic (PK) data from the 2 ongoing studies with a 2400-mg Q3W dose to confirm the model-informed dose selection.

Methods: First-cycle PK data from studies NCT03840915 (n=23; phase 1b/2, stage IV non-small cell lung cancer) and NCT04066491 (n=6; phase 2/3, first-line biliary tract cancer) with a 2400-mg Q3W regimen were analyzed by noncompartmental analysis (NCA), exploratory statistical data, and graphical analysis. Graphical comparison of observed concentrations/NCA-derived PK parameters vs simulated values from a previously published bintrafusp alfa population PK model [2] was performed. Safety (NCT03840915, n=8; NCT04066491, n=6) was evaluated by the Safety Monitoring Committee.

Results: The safety profile in patients treated at a dose of 2400 mg Q3W to date appears to be consistent with that at lower doses. The observed PK in patients treated with 2400-mg Q3W dosing is in line with the population PK simulation of a 2400-mg Q3W regimen, confirming model-informed dose selection.

Conclusions: Although experience to date is limited, the observed safety and PK profile in patients treated with bintrafusp alfa 2400-mg Q3W supports model-informed dose selection.

References:

1. Vugmeyster Y, et al. *Clin Pharmacol Ther.* 2020 Jan 18. [Epub ahead of print].
2. Wilkins JJ, et al. *Adv Ther.* 2019;36(9):2414-33.

WED-095**A time to event model to predict overall survival in non-human primates with acute radiation syndrome**Zack Jones¹, Per Olsson Gisleskog², Ari Pritchard-Bell¹, Sameer Doshi¹¹Amgen, Inc., Thousand Oaks, CA, USA; ²POG Pharmacometrics, UK.

Objectives: Acute radiation syndrome (ARS) is an acute illness caused by exposure to a high dose of penetrating radiation over a short period of time or by intermediate doses of radiation if the exposure occurs over a longer period. Hematopoietic subsyndrome of ARS (HS-ARS) is characterized by dose dependent bone marrow depression leading to lymphopenia, neutropenia, thrombocytopenia, and anemia. Death due to HS-ARS from infection or excessive bleeding usually occurs within 2 to 3 weeks after exposure. The primary objective of this study was to develop a time to event model that establishes the relationship between hematological response, following acute radiation exposure, and overall survival (OS) in non-human primates (NHP) in the presence and absence of romiplostim treatment while accounting for covariates that may be strong predictors of OS.

Methods: Data used to inform OS model development included both romiplostim and control treated male and female NHPs ($N = 218$) exposed to a range of radiation doses (500-750 cGy). Romiplostim was administered 24 hours post irradiation. Rich sampling provided dense platelet counts over time. Model fitting and development was done using NONMEM 7.4. Decrease in objective function value (OFV) and visual predictive checks (VPC) were used to assess the model's ability to predict OS. Kaplan Meier plots stratified by treatment, radiation dose, and covariates (sex and baseline weight) were used to explore the effect of radiation and romiplostim treatment on OS of irradiated NHPs and guide model development. Commonly used parametric time to event models were evaluated to describe OS in control animals including testing the effect of covariates, radiation, and platelet counts as predictors of OS. The best model for control animals based on objective function and VPC was selected and tested on both control and romiplostim treated animals with reevaluation of covariates.

Results: The best model structure, determined by drop in OFV and VPC, was a log-logistic survival model with a time-varying hazard related to platelet count (Table 1). The addition of covariates did not provide significant improvement with respect to drop in OFV or VPC, suggesting that platelet count alone is sufficient to capture any survival differences due to sex or baseline body weight. Furthermore, the model describes OS over a range of radiation doses in both control and romiplostim treated animals.

Table 1: Parameter estimates for log-logistic OS model, describing survival as a function of platelet count.

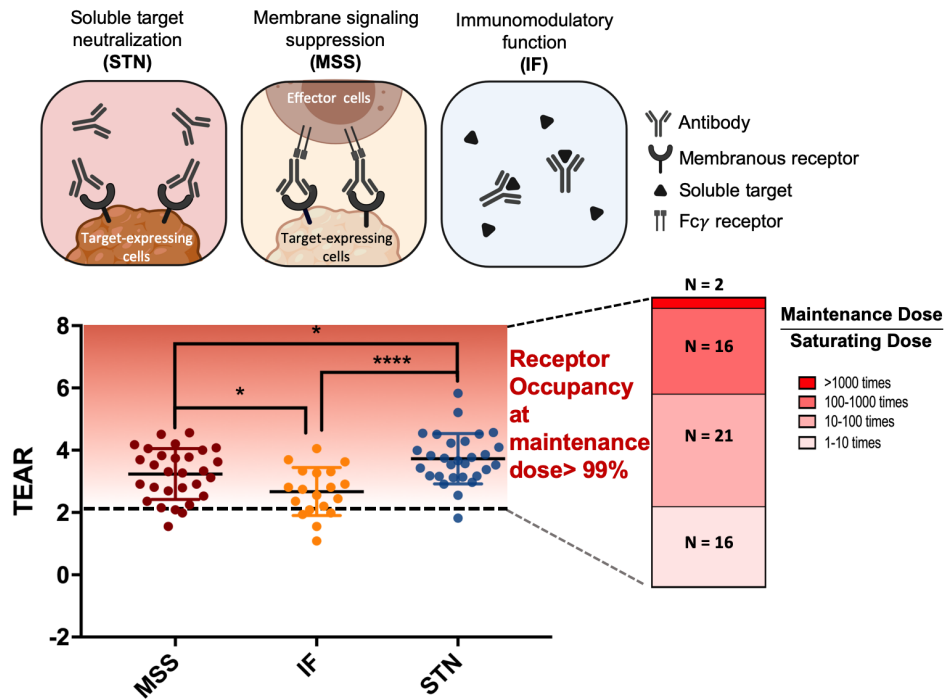
Parameter	Estimate	%RSE	Units
γ (base hazard)	0.057	4.5	day ⁻¹
κ (shape)	6.63	26.8	----
β (slope)	-0.023	28.5	1/10 ⁹ cell/L

Conclusions: A log-logistic survival model with a time-varying hazard related to platelet count was able to accurately capture OS in NHPs with HS-ARS across a wide range of radiation doses, treatment, and sex.

Quantitatively Modeling Factors that Influence the Therapeutic Doses of Antibodies

Yu Tang ¹, Xiaobing Li ^{1,2}, Yanguang Cao ^{1,3 #}

¹Division of Pharmacotherapy and Experimental Therapeutics, UNC Eshelman School of Pharmacy, University of North Carolina at Chapel Hill, Chapel Hill, North Carolina 27599, United States. ²Department of Pharmacy, Shengjing Hospital of China Medical University, Shenyang, China. ³Lineberger Comprehensive Cancer Center, School of Medicine, University of North Carolina at Chapel Hill, Chapel Hill, NC 27599, USA



Objectives:

Dose selection and confirmation are critical tasks in the development of therapeutic antibodies. Although much knowledge has been acquired in the past decade, it remains uncertain which factors are relevant and how to select doses more rationally. In this study, we (1) systematically evaluate the factors that are associated with the doses and dose selections across antibodies, indications, target properties, and stages of development and (2) identify the potentially overlooked factors.

Methods: To evaluate the selected therapeutic doses (TDs) and the influencing factors across diverse classes of antibodies, we developed a quantitative metric, Therapeutic Exposure Affinity Ratio (TEAR), $\text{TEAR} = \log([C_{ss}/K_D])$ to retrospectively evaluate up to 60 antibodies that have been approved by the FDA or the EMA from 1995 to 2019. TEAR reflects the ratio between antibody plasma concentrations at therapeutic doses and the target binding affinity. TEAR has accounted for the variance from antibody bioavailability, systemic clearance, and target affinity, which make the remaining difference in TEARs across antibodies as results of the influence of other factors on TDs, including target properties (target baselines, turnovers, and location), antibody mechanisms of action, and all other factors on the TDs of antibodies.

Results: Most of the surveyed antibodies (55 out of 60) had TEARs > 2 , suggesting that most antibodies had almost completely saturated the target in the plasma at their TDs. Our results challenged the traditional perception that antibodies should have high TDs when the target has a high baseline, rapid turnover, and deep anatomical location. Instead, the mechanisms of action of the therapeutic antibodies were found crucial for the selection of TDs. Among all the antibodies applied in cancer treatment, the ones that trigger immune functions to lyse targeted cells have the lowest TEARs compared with the antibodies with the other modes of action. Mechanism of action also significantly affected the selection of first-in-human doses and the dose selection patterns in Phase I and II trials.

Conclusions: Our study offered a quantitative method to support systematic evaluations of antibody TDs and dose selection patterns, provided some insights into the factors that could have an impact on antibody efficacy and the selections of TDs, and highlighted the importance of the mechanisms of action in the selection of TDs (NIH: GM119661).

THU-001

Practical Lessons in Designing Pediatric PK Studies

Authors: Abhinav Kurumaddali¹, Navin Goyal¹

Institutions: ¹CPMS, GSK, USA

Objectives:

The precise characterization of a drug's PK in pediatrics while critical is challenging owing to the patient, study and resource related considerations. It is thus important that the PK data collected is apt for such analyses. Several open source software (such as PFIM, PopED etc.) based on D-optimal design algorithms are being routinely used to determine the optimal sampling times and sample size required for conducting pediatric PK studies. The objective of this work is to highlight practical issues when employing such approaches and to propose solutions that address them.

Methods:

Trial simulations were conducted for a Drug X that follows two compartment PK model (Q/F and V3/F fixed) with 500mg QD dosing regimen studied in a virtual pediatric population of age 2-18 years and six weight bands. The PK parameters were scaled allometrically and the dose was adjusted by body weight. Both between subject variability (30%CV on KA, CL/F and V2/F) and residual variability (proportional error: 15%CV) were incorporated in the simulations. A virtual population of 30,000 individuals (5000 per weight band) was simulated to represent the true population. A thousand trials were generated by sampling N subjects (N/6 per each weight band) per study followed by the estimation of post-hoc steady-state individual PK parameters including KA, CL/F, V2/F, AUC₀₋₂₄ and C_{max}. Eight study designs (D1-D8) with different sampling times and sample size were evaluated (Table 1) by estimating precision for key PK parameters. These designs ranged from a PK rich sampling scheme (D1) to practically feasible designs (D2-D6) based on study site logistical constraints to D7 and D8 where PFIM suggested PK sample timepoints were included.

Results:

The arbitrarily chosen practically feasible designs (D3 & D4) demonstrated better performance (higher precision, Table 1) compared to the designs (D7 & D8) suggested by the optimal sampling software tool. Six samples (from 36 subjects, D4) or eight samples (from 24 subjects, D3) provide precision that is highly comparable to that observed with an extensive PK design (Table 1) and seem sufficient for precise characterization of the drug's PK in pediatrics. The analysis also demonstrates that increasing the number of subjects or PK samples may not always result in substantial improvement in precision i.e. – *diminishing returns*. In fact, a smaller study with a sparse PK sampling scheme would provide adequate data to characterize exposures.

Conclusions:

The results highlight that there are several approaches that may provide better performance in PK characterization than solely relying on use of optimal design tools to assess and recommend pediatric study designs. The proposed approach allows designing an efficient study that prevents unwarranted drug exposure and minimizes patient burden while adequately characterizing the PK in pediatric population.

Table 1. Relative bias (RB) and root mean square error (RMSE) of AUC_{0-t} and C_{max} for designs D1-D8

Design	Design type	Sample size	Number of sampling timepoints	Sampling timepoints (h post dose)	RB (%)		RMSE (%)	
					Median (90% PI) AUC_{0-24}	Median (90% PI) C_{max}	Median (90% PI) AUC_{0-24}	Median (90% PI) C_{max}
D1	Extensive PK (for comparison)	36	15	0,0.1,0.25,0.5,0.7 5,1,2,3,4,5,6,8, 10,18,24	13.6 (10.6, 16.8)	19.4 (15.4, 24.0)	17.0 (13.3, 21.9)	24.6 (19.3, 31.3)
D2	Practically feasible arbitrarily chosen	36	8	0.5,1,2,3,5,8,10,2 4	14.4 (11.5, 18.3)	20.1 (16.1, 25.2)	18.2 (14.5, 23.1)	25.3 (20.2, 32.4)
D3	Practically feasible arbitrarily chosen	24	8	0.5,1,2,3,5,8,10,2 4	14.5 (10.7, 18.9)	19.9 (15.1, 26.0)	18.0 (13.6, 23.9)	25.1 (19.1, 33.4)
D4	Practically feasible arbitrarily chosen	36	6	1,3,5,8,10,24	15.4 (12.2, 18.6)	21.7 (17.1, 26.8)	19.2 (15.4, 24.0)	27.5 (21.5, 36.1)
D5	Practically feasible arbitrarily chosen	24	6	1,3,5,8,10,24	15.4 (11.4, 20.0)	21.7 (15.8, 28.6)	19.1 (14.2, 25.5)	27.5 (19.8, 37.2)
D6	Practically feasible arbitrarily chosen	36	4	1,3,8,24	17.3 (13.7, 21.5)	22.1 (17.4, 28.0)	21.6 (17.0, 27.5)	27.9 (21.7, 36.8)
D7	PFIM FW algorithm	36	6	0.25,0.5,0.75,6, 7,24	18.1 (14.4, 22.6)	23.9 (18.8, 29.9)	22.6 (18.2, 28.4)	30.3 (23.6, 39.4)
D8	PFIM Simplex algorithm	36	6	0.25,0.27,5.98, 6.23,6.35,23.89	17.9 (14.3, 22.2)	24.1 (19.1, 30.0)	22.6 (17.9, 28.2)	30.7 (24.1, 39.7)

THU-002

A quantitative systems pharmacology (QSP) model to evaluate valproic acid induced hyperammonemia and the benefit of carnitine supplementation

Authors: Alejandra Schiavo (1), Cecilia Maldonado (1), Marta Vázquez (1), Pietro Fagiolino (1), Iñaki F. Trocóniz (2,3), Manuel Ibarra (1)

Institution: (1) Department of Pharmaceutical Sciences. Faculty of Chemistry. *Universidad de la República*. Montevideo, Uruguay. (2) Pharmacometrics and Systems Pharmacology Research Unit, Department of Pharmaceutical Technology and Chemistry, School of Pharmacy and Nutrition, University of Navarra. Pamplona, Spain. (3) IdiSNA; Navarra Institute for Health Research, Pamplona, Spain.

Objective: To develop a QSP model for the understanding of the mechanisms behind the valproic acid (VPA) induced hyperammonemia and the assessment of the benefits related to carnitine supplementation (CS). This adverse effect correlates with VPA dosage and has an overall incidence of ~40%, being associated to CNS damage in symptomatic patients.

Methods: A population pharmacokinetic model for VPA developed in NONMEM 7.4 (Icon plc.) with data from an average bioequivalence study was expanded integrating literature data for the kinetics of VPA metabolites (4-en-VPA, VPA glucuronide, VPA-Carnitine and 2-en-VPA), Carnitine, Ammonia and fatty acids to develop a mechanistic QSP model using mlxR 4.1.0 package (Lixoft) in R 3.5.3 (R-Project). Model validation was performed using reported and clinically available data for different VPA dosage regimens, evaluating model accuracy for VPA, 4-en-VPA, ammonia and carnitine at steady state. For other elements integrating the model for which experimental observations were not available, a baseline of 1 was assumed and relative changes were modeled. A local sensitivity analysis was conducted for critical parameters evaluating the impact of a +/- 10% change on VPA, 4en-VPA, Ammonia and Carnitine mean steady state concentrations. Effect of VPA dosage over ammonia levels and CS antidote efficacy (2g/12h PO) was assessed simulating from the final model.

Results: A QSP model comprising 17 ordinary differential equations relating, through 38 reactions, the eleven elements of the system, was built. The prediction errors were: VPA (-6.6% single dose, -3.0% multiple dose), 4en-VPA (+7.0%), Carnitine (+2.5%) and Ammonia (-12%). The model resulted robust to changes in parameter values. Assuming a normal range of 15-95 uM for Ammonia in plasma, the hyperammonemia predicted incidence for three different VPA dosage regimens was in accordance with previous reports: 14% (500q12), 32% (500q8) and 69% (1000q12). To reproduce clinical observations, a mechanism involving a Carnitine induced Glutamate formation through Acetyl-CoA was included. Secondary to CS, a decrease in VPA and 4-en-VPA levels is predicted, with a subsequent fast decrease in Ammonia and Glutamate levels.

Conclusions: A mechanistic QSP model describing the VPA-Ammonia pathway was developed. Simulations support the use of CS as an antidote for VPA-induced hyperammonemia.

References

- [1] M. Vázquez et al., "Hyperammonemia associated with valproic acid concentrations", BioMed Research International, vol. 2014, Article ID 217269, 7 pages, 2014.
- [2] P. Harper et. al., "Pharmacokinetics of Intravenous and Oral Bolous Doses of L-Carnitine in Healthy Subjects", Eur J Clin Pharmacol., 35:555-562, 1988.
- [3] R. S. Addison et. al., "Steady State dispositions of valproate and diflunisal alone and administrated to healthy volunteers", Eur J Clin Pharmacol., 56:715-721, 2000.

THU-003

Modeling across scales: Application of biophysical, PBPK, and mechanistic models for dose prediction of inhaled anti-infective therapies to inhibit SARS-CoV-2 viral kinetics

Allison Claas, Domenico Bullara, Thomas Dimke, Xiaojun Ren, Monish Jain,
Suzanne Gaudet, Jeff Kearns, Andreas Kuttler, Birgit Schoeberl

Novartis Institutes for BioMedical Research, Cambridge, MA USA

Objectives: In response to the pandemic caused by the SARS-CoV-2 outbreak, there has been a rapid uptick in the number of clinical trials aiming to combat the virus. As viral pneumonia is among the severe responses to SARS-CoV-2 infection, inhaled delivery is an attractive avenue for delivering anti-infective treatments directly to the lung. In the absence of deep biological understanding and clinical experience treating the virus, mathematical modeling becomes critical for ensuring that anticipated safety and efficacy thresholds are met in patients. Here, we develop an integrative modeling framework for predicting anti-viral response after inhaled anti-infective drug delivery.

Methods: To model the delivery to the lung after drug inhalation, we employ a biophysical model describing the underlying architecture and properties of the lung. Combined with a physiologically based pharmacokinetic (PBPK) pulmonary compartment and transit model validated with systemic clinical pharmacokinetic (PK) data, we predict the lung and systemic drug kinetics. To model the anti-infective effect, we combine the pharmacokinetic predictions with models for the in-host viral kinetics of SARS-CoV-2, parameterized by recently published data. To understand the impact of model selection on anti-viral treatment prediction, we employ a family of model structures representing varying complexity and distinct mechanisms of viral kinetics.

Results: Systemic PK reported in the literature was well described by the integrated biophysical and PBPK model. Combined with the family of viral kinetics models, we find that the timing of dose-initiation is critical to reducing viral load to significant levels compared to untreated, while there are subtleties in the predictive behavior of the different model structures. Further, we find concordance between viral inhibition and a PK based time above EC90 metric. Because of this, frequent dosing was predicted to be required to maintain the anti-viral effects.

Conclusion: Through an innovative integration of biophysical, PBPK, and viral kinetics models, we leveraged the multi-scale knowledge about drug and virus behavior to generate highly mechanistic predictions. This enabled a model-based dose-regimen selection optimized for anti-viral effect after inhaled drug delivery.

**Translational modelling of innate immune response following lipopolysaccharide challenge:
from piglets to humans**

Anders Thorsted¹, Elisabet I. Nielsen¹, Sven Benson², Miklos Lipcsey³, Peter Matzneller⁴, Markus Zeitlinger⁴, Matthijs Kox⁵, Peter Pickkers⁵, Lena E. Friberg¹

¹ Department of Pharmaceutical Biosciences, Uppsala University, Uppsala, Sweden

² Institute of Medical Psychology & Behavioural Immunobiology, University Hospital Essen, Essen, Germany

³ Department of Surgical Sciences, Uppsala University Hospital, Uppsala, Sweden

⁴ Department of Clinical Pharmacology, Medical University of Vienna, Vienna, Austria

⁵ Department of Intensive Care Medicine, Radboud University Medical Center, Nijmegen, The Netherlands

Objectives: Lipopolysaccharide (LPS), a component of the plasma-membrane of Gram-negative bacteria, induces the mammalian immune response through toll-like receptor 4 stimulation. Consequently, LPS administration is utilized in studies of innate immune response both *in vitro* and *in vivo*, including in healthy volunteers [1]. The objective was to assess if and how pharmacometric models developed from piglet studies could be translated to predict time-courses observed in human LPS challenge studies.

Methods: A pharmacometric framework [2,3] based on data from 116 piglets, infused with *E. coli* LPS O111:B4 in rates from 63 to 16,000 ng/kg/h for up to 30 hours, was the basis for translation. Human data for tumor necrosis factor alpha (TNF α), interleukin 6 (IL6), heart rate (HR) and mean arterial pressure (MAP) was available from 230 volunteers. Observations were made after intravenous LPS bolus (0.4, 0.8, 1.0 and 2.0 ng/kg) or continuous infusion (1.0 ng/kg bolus followed by 1.0 ng/kg/h for three hours).

Time-related variables (e.g. turn-over rates) were scaled allometrically by weight (fixed exponents) while species-dependent variables, such as cytokine and physiological baselines, were re-estimated. As humans are known to be LPS sensitive, estimation of species-differences in key exposure-response parameters were explored (e.g. the LPS-TNF α relation).

Results: Allometric scaling of time-related variables and refit of baseline parameters adequately predicted MAP, but underpredicted the time-courses of TNF α , IL6 and HR. As refinements, the TNF α potency parameter (EC_{50}) was re-estimated, resulting in a human estimate of 44.3 EU/L (15% of piglet estimate). For prediction of IL6, the stimulation from TNF α was re-parameterized to describe a surge, with the surge amplitude governed by the TNF α increase relative to baseline. For HR and systemic vascular resistance (SVR), EC_{50} 's of 5.27 and 0.598 EU/L (2% of piglet estimates) and an inhibitory Emax for SVR of 0.778 (2.73 times piglet estimate) were estimated. These changes improved the performance of the model to predict the time-courses of TNF α , IL6, HR and MAP across all the doses studied in healthy volunteers.

Conclusions: The experimental model structure worked well to predict the observed median time-courses of TNF α , IL6, HR and MAP following LPS administration in healthy volunteers. LPS was more potent at producing an immune response in humans, compared to piglets, and quantification of differences in exposure-response relationships between species – three potencies, one maximum effect and one slope – were required. The work illustrates how an experimental model can be used to predict human time-courses, exemplified with biomarkers relevant for sepsis and anti-inflammatory research. The developed translational model can potentially be used to inform future study designs and for bridging experimental results to humans.

References

- [1] Suffredini AF. Clin Pharmacol Ther. 2014;96(4):418-422.
- [2] Thorsted A. PLoS ONE. 2019;14(2):e0211981.
- [3] Thorsted A. Uppsala: Acta Universitatis Upsaliensis. 2020.

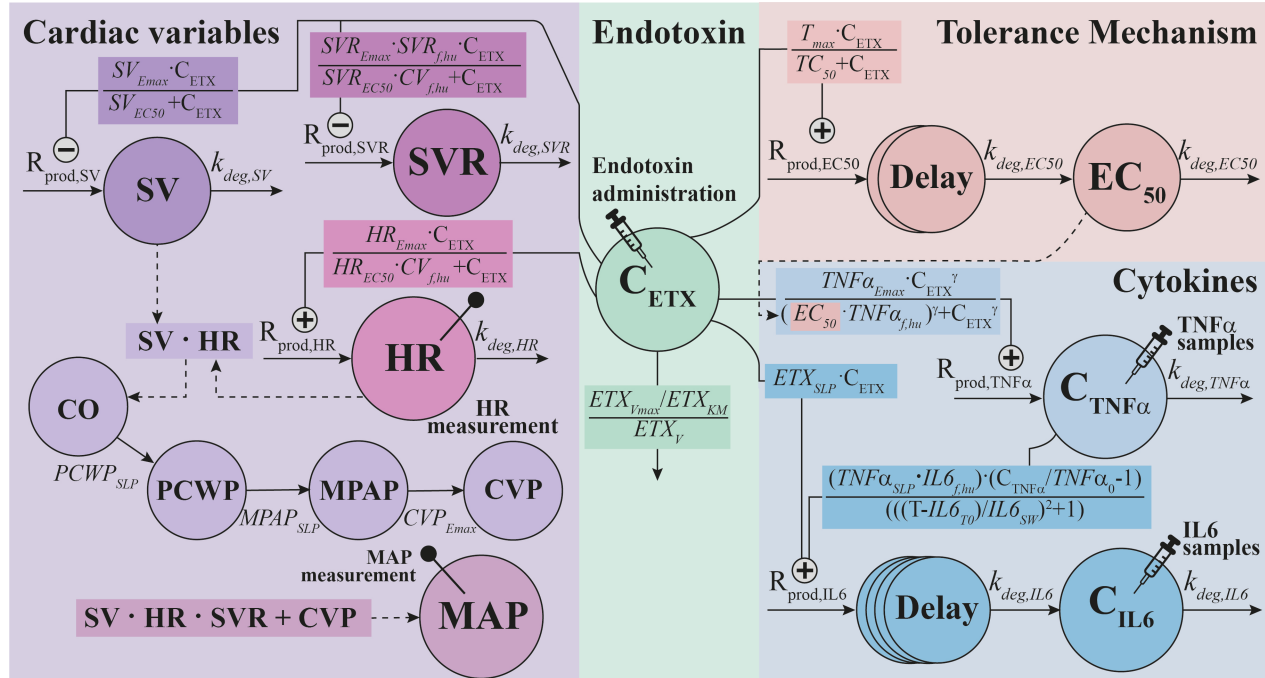


Figure: Final human model schematic, scaled from piglet studies. Administered LPS (C_{ETX}) is linked to predict time-courses of two cytokines (TNF α , IL6) and two cardiovascular variables (HR, MAP), with refinements indicated by parameters: $TNF\alpha_{f,hu}$, $IL6_{f,hu}$, $SVR_{f,hu}$, $CV_{f,hu}$, $IL6_{T0}$, and $IL6_{SW}$.

THU-006

Estimating Impact of Acute Radiation Exposure on PKPD of Romiplostim in Rhesus Monkeys

Ari Pritchard-Bell¹, Zack Jones¹, Sameer Doshi¹

¹Amgen, Inc., Thousand Oaks, CA, USA

Objectives: Acute radiation syndrome (ARS) is caused by exposure to a high dose of penetrating radiation over a short time or by intermediate doses of radiation if the exposure occurs over a longer period. Hematopoietic subsyndrome of ARS (HS-ARS) is characterized by dose dependent bone marrow depression leading to lymphopenia, neutropenia, thrombocytopenia, and anemia. Death due to HS-ARS from infection or excessive bleeding usually occurs within 2 to 3 weeks after exposure. Duration of thrombocytopenia is a predictor of mortality in lethally irradiated animal models, suggesting that a treatment for thrombocytopenia may increase survival in patients with HS-ARS. Our objectives are to integrate time course PK and platelet data from healthy/irradiated nonhuman primates (NHP) dosed with romiplostim and characterize the effects of radiation on the hematopoietic system using a mechanistic PKPD model. This work will be linked with a survival model to predict survival benefit of romiplostim in humans with HS-ARS.

Methods: We use mathematical modeling to bridge romiplostim PK and platelet dynamics from healthy NHP with irradiated NHP with ARS receiving romiplostim rescue. Data from four irradiated NHP studies were combined with data from healthy NHPs who received a single dose of romiplostim. Previously published models of romiplostim PKPD in NHP and humans were adapted to bridge the data. Modifications to the model were made to characterize the effects of acute radiation on romiplostim PKPD.

Results: A mechanistic PKPD model describes the effects of radiation on romiplostim PK and PD in NHP. The effects of acute radiation on platelet dynamics were estimated using data from irradiated NHP across a range of acute radiation exposure from 500 to 750 cGy. Subsequently, the effects of romiplostim dosing on platelet dynamics following radiation exposure were estimated. Age, body weight, and sex were investigated as possible covariates and as potential prognostic or predictive factors for hematopoietic response following irradiation.

Conclusions: The mechanistic PKPD model describing the effects of radiation on romiplostim PK and PD in NHP can be used to predict acute radiation effects on platelets and survival in humans. The typical values of the radiation-specific model parameters obtained from NHP will be scaled to describe the thrombopoiesis and survival effects of acute radiation in humans. Given the lack of human platelet data following acute radiation exposure, the acute radiation model parameters derived from NHP can be calibrated to describe the historical mortality data from humans exposed to acute radiation (in absence of romiplostim) reported in the literature. This work combined with a model linking survival to platelets in NHP (see abstract by Jones et al. for additional detail) can be used to predict overall survival benefit in irradiated humans receiving romiplostim treatment.

THU-007

Nonlinear Dynamics Analysis within the Context of Cancer Combination Therapy

Aymen Balti¹, Didier Zugaj², Frédérique Fenneteau¹, Guillaume Bonnefois², Julie Desrochers², Pierre-Olivier Tremblay², Fahima Nekka^{1,3,4}

¹Faculté de Pharmacie, Université de Montréal, Montréal, Québec, Canada; ²Clinical Pharmacology, Syneos Health;

³Centre de recherches mathématiques, Université de Montréal, Québec, Canada; ⁴Centre for Applied Mathematics in Bioscience and Medicine (CAMBAM), McGill University Montréal, Québec, Canada.

Objectives: Therapies combining immunotherapy with more traditional therapeutic approaches, including chemotherapy and radiation, are increasingly being used. These combinations are purposed to amplify the immune response against the tumor cells and modulate the suppressive tumor microenvironment (1). In order to get the best performance from these combinatorial approaches and derive rational regimen strategies, a better understanding of the interaction of the tumor with the host immune system is needed. Quantitative systems pharmacology (QSP) proved to be a powerful tool to elucidate the underlying pathophysiological complexity that is intensified by biological variability and overlapped by the level of sophistication of dosing regimens in terms of dosing and combinations. The objective of the current work is to provide new insights for the dynamics of immune-mediated tumor environment and its modulation by combination therapy that includes radiation and anti-PD-1/L1 treatment.

Methods: Based on a recent QSP model by Kosinsky et al. (1) to reproduce tumor size dynamics upon administration of radiation therapy and immune-oncology treatment, we here revisit this model in order to perform an in-depth mathematical analysis of its representative components, expressed as ordinary differential equations. A bifurcation analysis of the model is performed and the model stability is analysed.

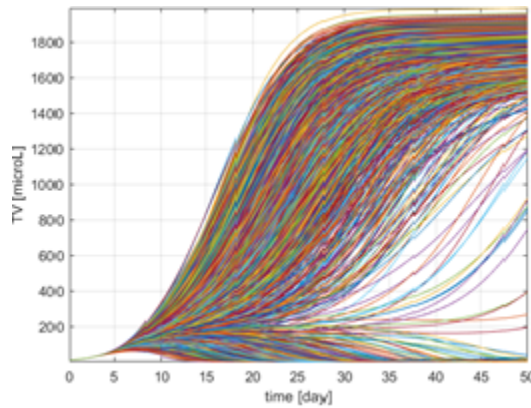
Results: The bifurcation analysis led to the identification of equilibria points, stability properties and basins of attraction. These system characteristics are informative on the fate of therapy in different pathological conditions. The dynamical behavior of model outcomes, including volume growth with time, is investigated with respect to model parameters. The ability of T cells to infiltrate tumor tissue, originally identified by Kosinsky et al. as responsible for individual therapeutic variability, is shown here to be a saddle-node bifurcation point for which the dynamical system oscillates between two states: tumor free, or maximum growth tumor, depending on the initial tumor size (or onset of therapy).

Conclusion: Adopting a dynamical system analysis, we showed that bifurcation theory can bring complementary information to the understanding of complex systems of immunotherapy. The proposed analysis is appealing for its mathematical foundation and interpretation and can be applicable to rationalize therapy combination. The involvement of more traditional biomathematical scientists in quantitative pharmacology will lead to a synergetic collaboration between QSP-based and dynamical systems approaches.

Reference:

- 1- Kosinsky et al. Radiation and PD-(L)1 treatment combinations: immune response and dose optimization via a predictive systems model Journal for ImmunoTherapy of Cancer (2018) 6:17. <https://doi.org/10.1186/s40425-018-0327-9>

Figure: Tumor volume with time, for different values of T cell infiltration **that determine the tumor evolution towards a tumor free or a maximum growth tumor state.**



THU-008

Magrolimab Treatment Does Not Alter Rituximab Pharmacokinetics in Patients with Non-Hodgkin Lymphoma

Bing Wang¹, Denise Jin², Mwe Mwe Chao², Chris Takimoto², Mark Chao², and Balaji Agoram²

¹ Amador Bioscience Inc, Pleasanton, CA

² Forty Seven Inc, Menlo Park, CA

Objectives: Magrolimab is an investigational anti-CD47 antibody in Phase 2 trials for treating relapsed/refractory (R/R) non-Hodgkin lymphoma (NHL) patients in combination with rituximab. The objective of this analysis was to evaluate the population pharmacokinetics (PK) of rituximab in combination with magrolimab and test for presence of drug-drug interaction between magrolimab and rituximab.

Methods: In a Phase 1b/2 study (5F9003; NCT02953509), NHL patients, including diffuse large B-cell and follicular lymphoma, received magrolimab in combination with rituximab. Sparse PK of rituximab were collected before first dose and at pre-designated timepoints during the study. The PK data of rituximab was analyzed using a population approach. Approximately 50% of patients in the study had quantifiable rituximab concentrations at baseline due to prior treatment with rituximab.

A previously published model of rituximab population PK [1] was used to simulate rituximab concentrations in 5F9003 study. In this model, rituximab was eliminated via parallel first-order and nonlinear clearances and the nonlinear clearance decreased after start of rituximab treatment due to loss of CD20-bearing B-cells. To account for time-dependent increase in rituximab clearance after end of previous treatment prior to study 5F9003, a cumulative Weibull function was used to describe recovery of nonlinear rituximab clearance during treatment holiday prior to start of 5F9003. The disposition parameters of rituximab were fixed to values previously reported [1]. The observed rituximab concentrations in study 5F9003 were compared with the model simulations.

Results: The PK dataset contains 518 quantifiable rituximab concentrations from 56 NHL patients. The serum concentrations of rituximab in NHL patients with quantifiable baseline values were underpredicted when prior rituximab treatment was not accounted for. The inclusion of a cumulative Weibull function to describe the underlying recovery of nonlinear clearance during the rituximab holiday substantially improved the overall model fitting. The observed rituximab concentrations during the Phase 1b/2 study of magrolimab were well predicted by a rituximab PK model previously developed for NHL [1].

Conclusions: A novel approach was developed by incorporating prior rituximab treatment history in a model to describe the observed rituximab PK in a Phase 1b/2 study of magrolimab in patients with NHL. The observed rituximab concentrations were well predicted by a model with disposition parameter values fixed to literature values, suggesting the PK of rituximab was unaltered by the concomitantly administered magrolimab.

References:

- [1] Levi, M., et al, Characterization of the time-varying clearance of rituximab in Non-Hodgkin's lymphoma patients using a population pharmacokinetic analysis, ACoP Annual Conference, 2008.

THU-009

Mechanistic PK Modeling to Characterize Relationship of Acetaminophen Exposure Between Blood and Sweat

Authors: Bradley Miyagawa^{1,2}, Tomoyuki Mizuno^{1,3}, Bill Buggele⁴, Gavi Begtrup⁴, Alexander A. Vinks^{1,3}

¹Division of Clinical Pharmacology, Cincinnati Children's Hospital Medical Center, ²Division of Pharmaceutical Sciences, James L. Winkle College of Pharmacy, University of Cincinnati, ³Department of Pediatrics, University of Cincinnati College of Medicine, ⁴Eccrine Systems, Inc., Cincinnati, OH, USA

Objectives: Drug exposure monitoring is an integral part of therapeutic drug monitoring (TDM), but the burden of collecting blood samples is a major hurdle, especially in children. Recently, innovative wearable biosensors have been developed to quantitate substances in sweat that potentially serve as surrogates for circulating analyte concentrations in blood [1]. This technology has the potential to provide clinicians personal PK data for select small molecule drugs via an immediate reading of drug concentration in secreted eccrine sweat. Acetaminophen has been proven as detectable in sweat secretions. The aim of this investigation was to develop a mechanistic PK model to establish a relationship between acetaminophen concentration and exposure in sweat and in blood.

Methods: Time-matched blood and sweat samples were collected from 4 subjects. Each subject took 2 separate single doses (500 mg or 1000 mg) of oral acetaminophen tablets, resulting in 8 profiles for each of blood and sweat concentrations. Blood samples were obtained via a finger prick. Sweat samples were obtained using a sweat collection device developed by Eccrine Systems, Inc. ®. Blood and sweat concentrations were determined by ELISA. Edsim++ software (Mediware, Prague, Czech Republic) was used to develop a structural PK model to describe both blood and sweat concentration profiles and estimate PK parameters.

Results: The structural model that best captured the clinical data had the following properties: two oral absorption routes described by transit compartments reflecting the observed delay and bi-phasic absorption, two compartmental-distribution, and inclusion of a virtual “sweat” bio-compartment linked from the central compartment with a first-order rate constant. Substantial inter-individual variability was observed in each PK parameter estimate. Despite large inter-individual variability in blood and sweat concentration profiles, the acetaminophen concentrations and AUC estimates in sweat were correlated with those in blood, respectively ($R^2=0.65$ and 0.84). The mean AUC ratio of sweat to blood was 20% (range: 16-26%).

Conclusions: A population PK modeling approach was utilized to characterize the relationship between sweat and blood concentration profile of orally-administered acetaminophen. A strong correlation was discovered between the acetaminophen AUC estimates in blood and sweat, indicating a promising future for sweat-monitoring technology in combination with PK model-based prediction as a non-invasive method of drug exposure monitoring for precision dosing.

Reference: 1. Heikenfeld et al. Nat Biotechnol. 2019 Apr;37(4):407-419.

THU-010

Population Pharmacokinetics of Olanzapine and Samidorphan When Administered in Combination in Healthy Subjects and Patients With Schizophrenia

Lei Sun,¹ Richard Mills,² Brian M. Sadler,³ Bhaskar Rege¹

¹Alkermes, Inc., Waltham, MA, USA; ²ICON, Marlow, UK; ³ICON, Gaithersburg, MD, USA

Objectives:

A combination of the antipsychotic olanzapine and opioid receptor antagonist samidorphan (OLZ/SAM) is in development for the treatment of schizophrenia and bipolar I disorder and is intended to provide the established antipsychotic efficacy of olanzapine while mitigating olanzapine-associated weight gain. Population pharmacokinetics (PopPK) analyses were conducted to determine olanzapine and samidorphan PopPK parameters, their associated variability, and covariate effects.

Methods:

PopPK models were developed for olanzapine and samidorphan using nonlinear mixed-effects modeling based on data from 10 studies of OLZ/SAM and 1 study of samidorphan in healthy subjects and patients with schizophrenia.

Results:

PK of both olanzapine and samidorphan were linear across the 5- to 30-mg dose range and best described by a 2-compartment disposition model with first-order absorption and elimination and a lag time for absorption. Population estimates of CL/F and V_c/F were 15.5 L/h and 656 L for olanzapine and 35.4 L/h and 297 L for samidorphan, respectively. Inter-individual variability estimates of CL/F and V_c/F were 43.2% and 35.6% for olanzapine and 29.4% and 23.3% for samidorphan, respectively. The effects of age, sex, race, smoking, and body weight on olanzapine PK based on PopPK analysis were consistent with the reported findings for olanzapine. Samidorphan PK was not affected by age, sex, race, or smoking; the impact of body weight on samidorphan exposure was predicted to be small and not considered clinically meaningful. The effects of hepatic and renal impairment on the PK of olanzapine and samidorphan, estimated by PopPK analyses, were consistent with the findings from clinical studies in subjects with hepatic or renal impairment.

Conclusion:

PopPK for olanzapine and samidorphan was characterized with covariates identified that explain a portion of the inter-subject PK variability.

This abstract was published in *Clin Pharmacol Ther.* 2020;107(Suppl 1):PIII 070 following acceptance to the American Society for Clinical Pharmacology & Therapeutics (ASCPT) 2020 Annual Meeting, but it was not presented at ASCPT 2020 due to a COVID-19-related conference cancellation.

THU-011

Population PK and exposure-response analyses supported the first approval of rituximab in pediatrics with Granulomatosis with Polyangiitis (GPA) and Microscopic Polyangiitis (MPA).

Authors Candice Jamois¹, Jacques Gaudreault², Clarisse Chavanne¹, Melissa Cheu³, and Leonid Gibiansky⁴.

Institution

(1) Clinical Pharmacology, Pharmaceutical Sciences, Pharma Research and Early Development, Roche Innovation Center Basel.

(2) JJG Pharma Consulting, Basel, Switzerland

(3) BioAnalytical Sciences, Genentech Inc., South San Francisco, CA

(4) QuantPharm LLC, North Potomac, MD, United States

Introduction: Rituximab (Rituxan/MabThera®, RTX), an anti-CD20 monoclonal antibody (mAb), is approved for treating adults with GPA and MPA (systemic autoimmune conditions affecting blood vessels) based on the results of RAVE (Induction) and Mainritsan (Maintenance) trials. This work reports the modeling work that supported a full extrapolation strategy from adults to pediatrics¹.

Methods: A population PK model developed in 122 adults from RAVE was updated with data from 25 pediatric patients from Study PePRS who received at least 4 weekly RTX IV doses of 375 mg/m².

Cumulative area under the concentration-time curve over the six-months Induction (AUC₀₋₁₈₀) estimated using actual dosing history and individual PK parameters was used to assess (1) similarity in exposure between children and adults; (2) similarity in exposure, -B-cells response, -probability of Month 6 remission, and - probabilities of occurrence of adverse events relationships.

Finally, simulated exposure was compared between adults and pediatrics to support the extrapolation to children from 2 to < 6 years old (yo), age group not included in PePRS, and a proposal for a standardized maintenance regimen in pediatrics.

Results: A linear 2-compartment model described RTX PK. Model parameters were in the typical range for mAbs (Table 1).

In both adults and pediatrics, RTX induced a rapid and prolonged B-cell depletion across the whole range of exposure with B-cell depletion lasting longer in patients with higher exposure. Similar to adults, no association was found between variability in exposure and clinical efficacy and safety endpoints in pediatrics, suggesting the Induction regimen resulted in exposure at the plateau of the ER relationship.

Known features of FcRn and IgG biology in children, the strong relationship between RTX CL and BSA, with similar AUC₀₋₁₈₀ in children compared to adults across the entire range of BSA and supportive PK simulations suggested that RTX disposition in ≥ 2 to < 6 yo pts is expected to be similar to the one assessed in children ≥ 6 yo. In addition, simulations showed that a 250 mg/m² dosing regimen in children is expected to result in comparable exposure to adults treated with the approved follow-up dose of twice 500 mg administered 2 weeks apart.

Conclusion: In summary, this work supported the regulatory approval of the first pediatric indication for MabThera/Rituxan. An induction regimen of 4 weekly IV infusions of 375 mg/m² is recommended in children ≥ 2 years of age with GPA or MPA; in US and Europe. A follow-up dosing regimen consisting of two 250 mg/m² IV infusions separately by two weeks, followed by a 250 mg/m² IV infusion every 6 months, is also approved in the US.

References

1. Mulugeta Y, Barrett JS, Nelson R, et al. Exposure matching for extrapolation of efficacy in pediatric drug development. J Clin Pharm 2016; 56(11):1326–34.

Table 1: Parameters estimates of the population PK model for a typical patient (BSA=1.9 m² without ADA)

	Estimate	%RSE	95%CI	Variability	Shrinkage (%)
Clearance (CL, mL/day)	258	4.22	236-279		
Inter-compartment clearance (Q, mL/day)	317	9.3	2510-3630		
Central volume (V_c , mL)	3070	3.59	3870-4450		
Peripheral volume (V_p , mL)	4160	4.85	287-347		
CL, $V_c \sim$ BSA	0.952	19.6	0.587-1.32		
CL ~ ADA	1.38	9.9	1.11-1.65		
Q, $V_p \sim$ BSA	1.48	12.7	1.12-1.85		
ω^2_{CL}	0.126	15.4	0.0881-0.164	CV=35.5%	2.1
ω^2_{Vc}	0.0402	50.4	0.000504-0.0799	CV=20.1%	60.7
ω^2_{Vp}	0.0553	18.6	0.0352-0.0754	CV=23.5%	16.4
σ^2	0.0393	2.7	0.0372-0.0414	CV=19.8%	15.8
Terminal half-life (day)	25.6				

RSE: Relative standard error (RSE=100*SE/PE where SE is the standard error and PE a parameter estimate); CI: confidence-interval; CV: coefficient of variation (CV = 100*SD%) where SD is the standard deviation; CL, $V_c \sim$ BSA: body surface area effect (BSA) on CL and V_c ; CL ~ ADA: Anti-drug antibodies effect on CL; Q, $V_p \sim$ BSA: ADA effect on Q and V_p

THU-012

A Bayesian Approach to PK/PD Modeling – A Comparison of NONMEM, Stan, Python, and Julia

Casey Davis, Sandeep Dutta, Khamir Mehta

Clinical Pharmacology, Modeling and Simulation, Amgen Inc, South San Francisco, CA

Objectives:

From the design of clinical trials to the analysis of data, Bayesian methods are becoming more common and more important in the drug-development cycle. They provide an infrastructure to coherently incorporate information from previous experiments and/or expert knowledge and provide a natural probabilistic interpretation of uncertainty. Traditionally, computational difficulties have limited the use of Bayesian methods in PK and PK/PD modeling. However, the increase in computational power and the implementation of the No-U-Turn Sampler (NUTS) to perform Markov Chain Monte Carlo (MCMC) sampling on various software platforms has allowed for estimation with models from simple compartmental PK models to PopPK models to complex TMDD models where Bayesian estimation with older software implementing a Gibbs sampler and Metropolis-Hastings algorithm would have been unreliable or impossible. The goal here is to compare the results and efficiency of the NUTS implementation in Stan¹, NONMEM², Python with PyMC3³, and Julia with Pumas⁴.

Methods:

Population data sets from a two-compartment model with first-order absorption and varying levels of between subject variability and residual variability are simulated, and identical models are fit with each of the software platforms. The accuracy and precision of the estimates are analyzed to compare the ability to recover the true parameters, and analysis of convergence of the MCMC chains is used to compare robustness of each platform.

Results:

Our results show that Stan, Python, and Julia perform similarly and slightly better than NONMEM at recovering the true parameters as measured by root mean squared errors (RMSEs). The robustness of all platforms are similar, with each of them occasionally, but rarely, failing to properly explore the posterior parameter space.

Conclusions:

Stan, NONMEM, Python (with PyMC3) and Julia (with Pumas) are solid platforms to perform Bayesian inference on PopPK models. Stan and Python are more flexible environments, with more distributions available to specify the priors and the ability to write a model and all of its components in any way desired, and both have large user communities, while NONMEM and Julia with Pumas are more tailored to PK/PD-specific modeling.

References:

1. <https://mc-stan.org>
2. NONMEM Users Guides
3. <https://docs.pymc.io/>
4. <https://pumas.ai/>

THU-013

Development of a Minimal Physiologically-Based Pharmacokinetic-Pharmacodynamic Model to Understand Cellular Kinetics of CAR-T Cells following Local Regional Deliveries

Chia-Hung Tsai, Cindy Xia, Haiqing Wang

Takeda Pharmaceutical Company Limited, Cambridge, MA, USA

Objectives:

CAR-T cell therapies have revolutionized the treatment of hematologic malignancies and are striving for solid tumor treatment. To overcome limited distribution of CAR-T cells to solid tumor, local CAR-T deliveries have been tested and shown promising therapeutic outcome in some cases. It is, therefore, of great interest to understand the impact of dosing routes on cellular kinetics, distribution, and subsequent proliferation in a quantitative fashion, which may provide insights into CAR-T efficacy and safety profile, and facilitate design of next generation CAR-T to overcome immunosuppressive tumor microenvironment to improve its efficacy.

Methods:

A minimal physiologically-based pharmacokinetic (mPBPK) model describing CAR-T cell distribution was combined with pharmacodynamic (PD) components to delineate CAR-T cell proliferation, tumor growth, and tumor cell killing after initial distribution. This model was used to investigate the differential responses resulted from systemic intravenous administration, intrapleural delivery and local liver delivery where a pleural tumor and a liver tumor were present, respectively.

Results:

The developed mPBPK-PD model reasonably captured published anti-mesothelin CAR-T cellular profiles in response to intravenous and intrapleural administrations to mice with a pleural tumor, where intrapleural administration led to earlier CAR-T cell proliferation and faster tumor growth inhibition. The established model structure was adapted to describe hepatic artery injection to treat liver metastatic tumor. Local regional delivery to liver tumor resulted in a substantial increase in initial tumor infiltration, followed by an earlier CAR-T cell proliferation phase. Blood flow rate in the tumor was found to be a sensitive parameter for CAR-T cell proliferation and tumor growth inhibition, indicating a potential role of tumor vascularization in the treatment efficacy of CAR-T cell therapies.

Conclusions:

A mPBPK-PD model was established to support local regional deliveries to the tumor site as an effective way to enrich CAR-T cell in the tumor microenvironment in order to improve the efficacy of CAR-T cell therapies.

THU-014

How does mechanistic quantitative systems pharmacology (QSP) modeling reduce R&D risk in data-poor disease areas such as central nervous system (CNS) diseases despite biological uncertainty?

Authors: Christina Friedrich (1), Colleen Witt (1), Meghan Pryor (1), Katherine Kudrycki (1), Rebecca Baillie (1), Robert Sheehan (1), Mike Reed (1)

Institutions: 1. Rosa & Co., LLC, San Carlos, CA

Objectives: Neurodegenerative CNS diseases present unique challenges for drug development, including significant uncertainty about pathophysiology, slow disease progression, and limited data and biomarkers. We examine the conditions under which mechanistic QSP modeling of CNS diseases can be useful when data are sparse, describe methodologies that are most relevant under these conditions, and highlight the impact that QSP modeling can have in this context.

Methods: Mechanistic QSP models were developed in CNS indications with significant biological uncertainty: Parkinson's disease (PD), frontotemporal dementia (FTD), schizophrenia, and Alzheimer's disease (AD). The contexts, methods, and results of these projects were identified and common themes were analyzed. The results of the analysis were summarized and illustrated in case studies from these disease areas.

Results: In a PD example, QSP research contextualized evidence of α -synuclein's role in vesicular trafficking to suggest incisive experiments to resolve uncertainties. In FTD, modeling of progranulin (PGRN) showed a mismatch between data and hypothesized mechanisms and led to recommendations for specific experiments. In schizophrenia, QSP modeling strengthened the rationale for moving a program forward by illustrating likely superiority to an existing compound with related mechanism of action, despite remaining uncertainties. In AD, QSP modeling supported integrated exploration of A β and tau pathologies. In all cases, precise quantitative data about the role of the drug's targets were lacking, and clinical data were of limited utility for extrapolation to novel mechanisms. Despite these challenges, QSP modeling clarified the current state of knowledge, enabled extrapolation, identified key uncertainties, and supported recommendations for incisive experiments to advance the programs. Methods crucial to success included identification and documentation of uncertainties, and systematic exploration of uncertainties using sensitivity analysis, virtual patients, and what-if scenarios. Detailed discussions with all members of the cross-functional project team about biological interpretations, assumptions, and results were also critical. Modeling advanced the state of information about each disease and supported development decisions.

Conclusion: In disease contexts with little data and significant biological uncertainty, QSP modeling supported a range of activities that moved each program forward. Mechanistic QSP modeling in CNS should be undertaken with the understanding that precise quantitative predictions of drug effects may not be possible, but that modeling is valuable to improve understanding, direct research, and mitigate program risk. QSP modeling is valuable for improving biological understanding and reducing uncertainty and risk in disease areas with sparse data.

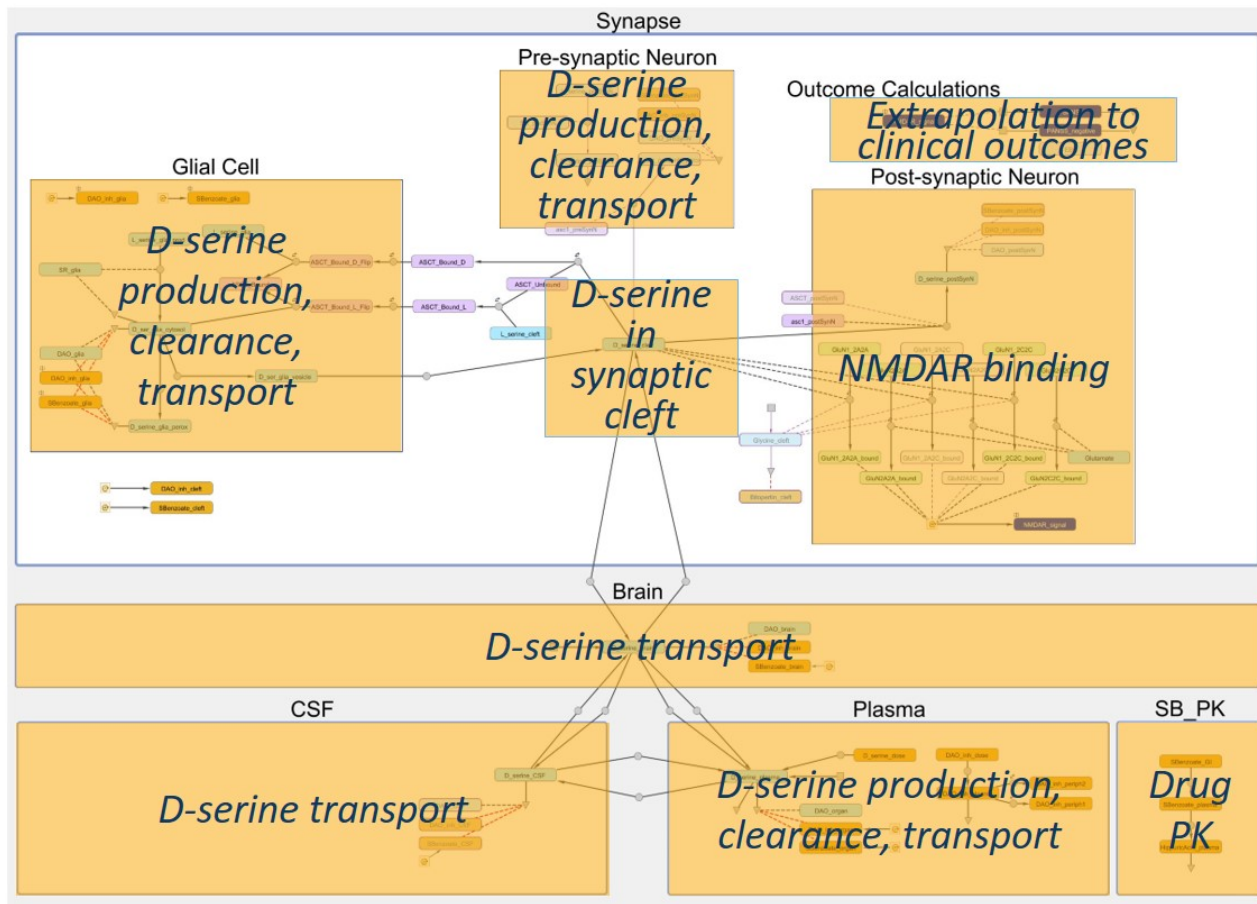


Figure 1. A graphical depiction of the biological scope of a schizophrenia QSP model focused on evaluating D-serine-modulating therapies. Despite significant uncertainties, modeling helped clarify the case for superiority of a new drug and supported dose selection.

THU-015

Extrapolation Strategy in Pediatric Patients with Polyarticular-Course Juvenile Idiopathic Arthritis (pcJIA): Pharmacokinetics-Pharmacodynamics (PK-PD) Modeling and Clinical Trial Simulation

Mei Zhang¹, Tao Sheng¹, Ying Liu¹, Lydie Baret-Cormel², Zhaoling Meng¹, and Christine Xu¹

¹Sanofi, Bridgewater, NJ, USA

²Sanofi, Paris, France

Objectives: Sarilumab blocks interleukin-6 (IL-6) from binding to membrane and soluble IL-6 receptor- α . Sarilumab is approved for adults with rheumatoid arthritis (RA). A 12-week dose-finding study was performed to identify an appropriate sarilumab dose for use in 2–17-year-old patients with polyarticular-course juvenile idiopathic arthritis (pcJIA). Exposure-response (E-R) analyses of selected efficacy and safety endpoints were conducted to evaluate PK-PD relationships.

Methods: Patients were divided by body weight into 2 groups, A (30–60 kg) and B (10–<30 kg), and received sequential ascending doses of sarilumab, Dose 1 (Group A/B): 2.0/2.5 mg/kg q2w; Dose 2 (Group A/B): 3.0/4.0 mg/kg q2w; Dose 3 (Group A/B): 2.0/2.5 mg/kg qw. Treatment effects of different dose regimens were evaluated through the empirical exposure-responses models established for efficacy endpoints (JIA ACR30/50/70 responses) and safety endpoint (percent changes from baseline in absolute neutrophil count [ANC]) at Week 12. For each endpoint, empirical linear, log-linear, and E_{max} PK-PD relationships were evaluated to select the model that best fitted the data. The E-R relationship curve for pediatric patients with pcJIA and adult patients with RA were compared to assess the E-R relationship consistency between pediatric and adult patients. Model-based simulations of 1000 clinical trials were performed to assess the impact of the different sample sizes (n=60 vs. 100 patients) on the precision of efficacy endpoints and robustness of exposure-response relationships of JIA ACR responses.

Results: A log-linear logistic regression model adequately described the E-R relationships between the efficacy endpoints JIA ACR responses and sarilumab trough serum concentration (C_{trough}) at Week 12. JIA ACR30 response rates increased with increasing C_{trough}, but a nearly flat dose-response for concentration range corresponding to Dose 2 and Dose 3. Percent change from baseline in ANC at Week 12 were reasonably well described by a log-linear model, with a trend toward greater ANC reduction with increasing trough concentration. Thus, PK-PD analyses supported the optimal dose selection in pediatric patients with pcJIA. A comparison of empirical models in adult patients with RA and in pediatric patients with pcJIA demonstrated a similar E-R relationship of JIA ACR30. Clinical trial simulations indicated that a total sample size of 60 patients is adequate to assess JIA ACR30 responses.

Conclusions: The E-R relationship of key efficacy and safety endpoints were characterized in pediatric patients with pcJIA. Modeling and simulation supported the extrapolation of efficacy from adults to pediatric patients, streamlining the pcJIA development program and reducing the total number of pediatric patients needed in the trial.

Disclosures: Mei Zhang, Tao Sheng, Ying Liu, Lydie Baret-Cormel, Zhaoling Meng, and Christine Xu are employees of Sanofi and may hold stock and/or stock options in the company.

THU-016

Population Pharmacokinetic, Exposure-Response and Probability of Target Attainment Analyses for Tedizolid in Adolescent Patients with Complicated Skin and Soft Tissue Infection

¹Dan Li, ¹Philip E. Sabato, ¹Hwa-Ping (Ed) Feng, ²Benjamin Guiastrennec, ²Vincent Duval ¹Pamela Sears, ¹Margaret Chou, ¹Catherine Hardalo, ¹Natalya Broyde, ¹Matthew L. Rizk

¹MRL, Merck & Co., Inc., Kenilworth, NJ; ²Certara, Basel, Switzerland

Backgrounds:

Tedizolid phosphate (SIVEXTRO, MK-1986, TZP) 200 mg once daily IV/PO is approved for treatment of acute bacterial skin/skin structure infections (ABSSSI) in adults. A Phase 3 study (MK1986-012) in adolescents with ABSSSI has been completed. This abstract reports the population PK analysis, probability of target attainment (PTA), and exposure-response analyses results for tedizolid, which support selection of a 200 mg once daily IV or Oral dose for adolescent patients.

Methods:

MK-1986-012 is a randomized (3:1 ratio), single-blind, multicenter, global Phase 3 study to assess the safety and efficacy of intravenous (IV) and/or oral (PO) TZP 200 mg once daily for 6 days versus that of comparators, for 10 days, for the treatment of ABSSSI in participants aged 12 to < 18 years of age. Five PK samples were collected for each subject. A previously developed population PK model for tedizolid was updated with additional adolescent data to estimate exposure in patients in this study for comparison with adults and conduct PTA and exposure-response analyses.

Results:

Similar exposure was observed between adolescent and adult patients given the same 200 mg daily dose, with AUC and C_{max} distribution largely overlapping as shown in Table 1. PTA analysis predicted a 100% PK/PD target (fAUC/MIC) attainment at the proposed dose up to the susceptibility breakpoint of 0.5 µg/mL. A high rate of clinical success was observed in adolescents, and no new safety concerns were identified. No exposure-efficacy or exposure-safety relationship was identified at the 200 mg daily dose.

Conclusions:

The proposed 200 mg once daily dose, administered IV or PO, provides sufficient exposure to be efficacious in adolescent patients. There was an exposure-safety profile with 200mg QD in adolescents similar to adults. These results support the selection of a 200 mg dose for the adolescent population.

Table 1 Population PK Model Predicted Exposure After First and Last Dose in Adolescent (MK-1986-012) and Adult ABSSI Subjects (Previous Phase 2 and 3 Studies)

Population	Mean ± SD			
	AUC_{0-24h_day1} (µg·h/mL)	AUC_{0-24h_last} (µg·h/mL)	Cmax_day1 (µg/mL)	Cmax_last (µg/mL)
Adult (N = 830)	23.6 ± 7.03	22.1 ± 6.54	2.11 ± 0.915	2.15 ± 0.737
Adolescent Study P012 (N = 91)	28.0 ± 9.95	30.8 ± 15.5	3.08 ± 1.44	3.37 ± 1.42

Abbreviations: ABSSI = acute bacterial skin and skin structure infection, AUC_{0-24h_day1} = area under the tedizolid concentration-time curve from 0 to 24 h on the first dosing day, AUC_{0-24h_last} = area under the tedizolid concentration-time curve from 0 to 24 h on the last dosing day, Cmax_day1 = maximum tedizolid plasma concentration on the first dosing day, Cmax_last = maximum tedizolid plasma concentration on the last dosing day, N = group size, PK = pharmacokinetic.

Note: The adult population includes ABSSI subjects of age >18 years old from previous Phase 2 and 3 studies receiving 200 mg of tedizolid phosphate.

Practical conclusions from practically unidentifiable models: a case study in semi-mechanistic PK modeling of an enzyme replacement therapy

David Flowers¹, Hoa Q. Nguyen², Diana Marcantonio¹, Helen Moore¹, Fei Hua¹, Shivakumar Patil², Nancy Chen²

¹Applied BioMath, LLC, Concord, MA, USA; ²Takeda Pharmaceutical Company, Cambridge, MA, USA.

Objectives: Mechanistic systems biology models combined with curve-fitting to data can be a useful tool for enabling mechanistic interpretations of data trends. When the data are insufficient to fully inform parameter values, the model predictions can be uncertain and unreliable. In this work, we show how models with practically unidentifiable parameters can still be used to make predictions and identify key sources of uncertainty.

Methods: We built a semi-mechanistic model of the pharmacokinetics of an enzyme replacement therapy (recombinant arylsulfatase A, ASA) for the treatment of metachromatic leukodystrophy (MLD) to predict how the enzyme distributes into the white matter of the brain following intrathecal dosing. The model tracks changes in exposure over time in various central nervous system tissues and the circulation. Nominal values for model parameters were estimated from literature sources and fit to tissue exposure data from cynomolgus monkeys. Based on these nominal parameter values, confidence intervals on the parameters and intracellular white matter exposure were calculated using profile likelihood methods. These methods for investigating identifiability are global but do not depend on expensive sampling procedures.

Results: While many of the model transport rates are not completely identifiable, model predictions of the key output of interest, area under the curve (AUC) of intracellular white matter ASA concentrations, are well-constrained by the data. Ninety-five percent confidence intervals for transport parameters between CNS compartments span two to eight orders of magnitude, but the confidence interval of the intracellular white matter ASA concentration AUC spans no more than a three-fold interval. Additionally, uncertainty in the sensitivity of the AUC to the ASA-M6PR binding affinity is found to result largely from uncertainty in the level of M6PR in the brain.

Conclusions: The results suggest that the significant uncertainty in the model parameters does not propagate to the key model predictions of interest. Specifically, in this case, the model provided predictions of intracellular white matter ASA concentrations with acceptable uncertainty, despite high uncertainty in parameter values. More generally, parameter uncertainty does not imply prediction uncertainty when the prediction is not sensitive to the uncertain parameters. The result of this work was that this model was able to provide mechanistic explanations for data trends, despite practically unidentified parameters.

Acknowledgements: This work was financially supported by Takeda Pharmaceutical Company

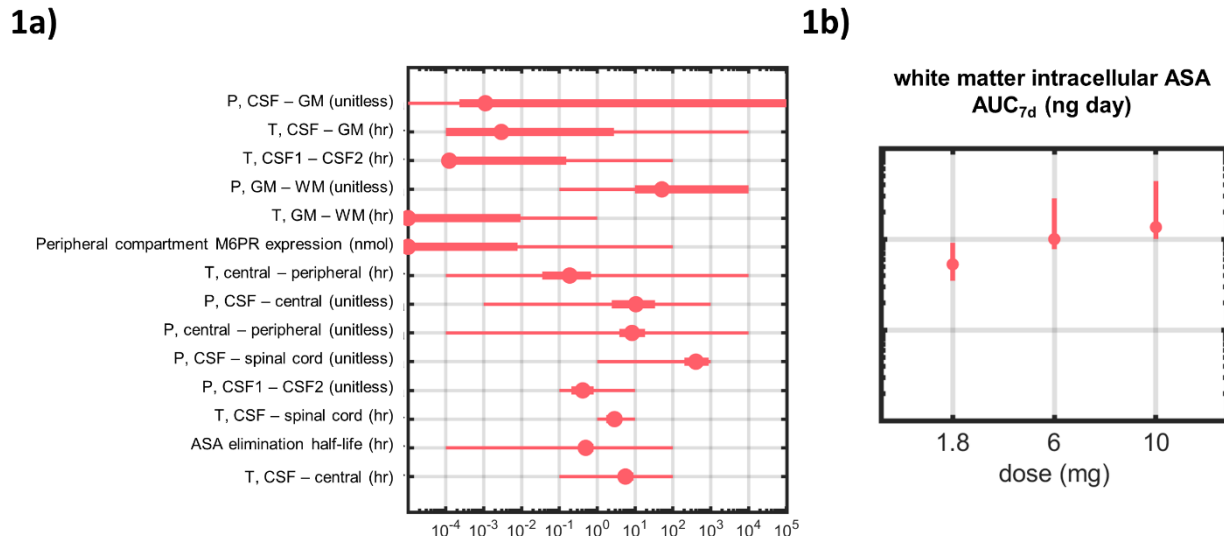


Figure 1. Confidence intervals for model parameters and white matter exposure predictions. (a) 95% confidence intervals on the model parameters. The light shaded lines indicate the lower and upper bounds used for the parameter estimation, and the dark shaded lines indicate the calculated confidence interval. The points indicate the best-fit parameter values. (b) 95% confidence intervals on single-dose intracellular white matter ASA exposure, as represented by the AUC calculated over seven days. The dose is indicated on the x axis. Lines indicates the confidence interval, and the points indicate the best-fit model prediction. Abbreviations: *P*: partition coefficient of transport, *T*: half-time of transport equilibration, *CSF*: cerebrospinal fluid, *CSF1*: injection-site-proximal CSF subcompartment, *CSF2*: brain-proximal CSF subcompartment, *GM*: gray matter, *WM*: white matter, *ASA*: recombinant arylsulfatase A, *AUC*: area under the curve.

THU-020

Semi-Mechanistic Model of Thrombocytopenia Post-Autologous Stem Cell Transplant in Multiple Myeloma

Donald J. Irby¹, Janet Guo¹, Francesca Cottini², Craig C. Hofmeister³, Mitch A. Phelps¹

¹Division of Pharmaceutics and Pharmacology, College of Pharmacy, The Ohio State University, Columbus, OH

²Department of Hematology/Oncology, College of Medicine, The Ohio State University, Columbus, OH

³Department of Hematology and Medical Oncology, Emory University School of Medicine, Atlanta, GA

Objectives: A rapid recovery of platelet counts has been predictive of superior survival following different stem cell transplant regimens in several bone marrow malignancies, including multiple myeloma (MM)^{1,2}. We aimed to characterize the platelet kinetics in MM patients post melphalan conditioning and transplant using novel modifications to the semi-mechanistic myelosuppression model first proposed by Friberg and colleagues.

Methods: Melphalan plasma concentrations (PK) and platelet counts (PD) from 118 MM patients were used to inform the PK/PD model parameters describing post-transplant thrombocytopenia. The FOCEI procedure in NONMEM 7.3³ was used for the parameter estimation, and NONMEM post-processing was completed in R 3.4.3⁴.

Results: A 2-compartment PK model for melphalan combined with a transit PD model for platelets was developed. The final platelet model included several modifications to the Friberg model, including additional empirical feedback functions on megakaryocyte maturation and platelet egress from circulation. The effect of the stem cell transplant was modeled as a linear function on the proliferation rate of progenitor cells in the bone marrow, and it was modified by the stem cell dose. An additional platelet maturation chain was also included in the model to mimic the terminal proplatelet fragmentation that occurs in the peripheral circulation and lung. Platelet transfusions were modeled as bolus IV infusions into circulation. Finally, a published PK model for Granulocyte-colony stimulating factor (G-CSF) was used to incorporate a previously-reported G-CSF induced effect on platelet turnover⁵.

Conclusions: A semi-mechanistic model of melphalan-induced thrombocytopenia was developed on MM patient data in the transplant setting. The final estimates of the model parameters with physiological interpretation were well-aligned with prior expectations. The model also performed well at replicating the observed platelet kinetics in our dataset, and we are currently using the model to discover covariates relevant to platelet recovery in this setting. Ultimately, the model will be explored as a tool to adjust therapy towards more favorable predicted platelet profiles.

References

1. Ninan MJ, Flowers CR, Roback JD, Arellano ML, Waller EK. Posttransplant thrombopoiesis predicts survival in patients undergoing autologous hematopoietic progenitor cell transplantation. *Biology of blood and marrow transplantation : journal of the American Society for Blood and Marrow Transplantation* **13** 895-904. (2007)
2. Ramirez P, Brunstein CG, Miller B, Defor T, Weisdorf D. Delayed platelet recovery after allogeneic transplantation: a predictor of increased treatment-related mortality and poorer survival. *Bone marrow transplantation* **46** 981-986. (2011)
3. Beal SL, Sheiner, L.B., Boeckmann, A.J. & Bauer, R.J. NONMEM 7.4 users guides. (1989–2018).
4. Team RC. R: A language and environment for statistical computing. Vienna, Austria.: R Foundation for Statistical Computing; 2017.
5. Krzyzanski W, et al. Population modeling of filgrastim PK-PD in healthy adults following intravenous and subcutaneous administrations. *Journal of clinical pharmacology* **50** 101S-112S. (2010)

THU-021

**Development of a semi-mechanistic pharmacokinetic model to describe gemcitabine triphosphate formation
in murine peripheral blood mononuclear cells**

Elizabeth G. Gibson¹, Olivia Campagne¹, Abigail Davis¹, Bo Zhong¹, Martine F. Roussel², Clinton F. Stewart¹

¹Pharmaceutical Sciences Department, St. Jude Children's Research Hospital, Memphis, TN

²Department of Tumor Cell Biology, St. Jude Children's Research Hospital, Memphis, TN

Objectives: Gemcitabine (dFdC), a cytosine analog, is currently being evaluated in combination with other chemotherapeutics to treat children and young adults with CNS tumors in institutional clinical trials (NCT01878617, NCT03434262, and NCT04023669). dFdC undergoes a complex and saturable cellular transformation into its primary active metabolite dFdCTP. Our ultimate goal is to determine dFdCTP exposure in pediatric brain tumor tissue and use a translational pharmacokinetic/pharmacodynamic modeling approach to adjust dFdC dosage. As a first step, the objective of this study was to characterize dFdCTP formation in murine peripheral blood mononuclear cells (PBMCs) a surrogate matrix to study the intracellular pharmacokinetics of nucleoside analogs.

Methods: Non-tumor bearing CD-1 nude mice (N=4/ time point) were dosed with 10, 20, 40, 60, and 120 mg/kg dFdC via IV bolus tail vein injection. Each mouse was sacrificed at different time-points (0.25, 1, 2, and 4 h post-dose) via cardiac puncture to collect adequate blood to obtain plasma and process for PBMCs. Plasma dFdC and dFdU, a putatively inactive dFdC metabolite, and PBMC dFdCTP concentrations were measured using validated LC-MS/MS methods. In a stepwise approach, murine plasma dFdC and dFdU, and PBMC dFdCTP data were integrated into a semi-mechanistic pharmacokinetic model using a nonlinear mixed-effects approach with Monolix v2019R2.

Results: The murine plasma dFdC and dFdU and PBMC dFdCTP were adequately described by the pharmacokinetic model depicted in Figure 1. The 10, 20, 40, 60, and 120 mg/kg dosages resulted in plasma dFdC area under the curve (AUC) of 5.8 ± 0.5 , 11 ± 1.1 , 20 ± 2.3 , 35 ± 4.6 and 63 ± 9.6 $\mu\text{M}\cdot\text{h}$, which were within the range of dFdC exposures determined in the institutional clinical trials (14 to 56 $\mu\text{M}\cdot\text{h}$). dFdU formation was best characterized as non-linear and modeled with the Michaelis-Menten equation. dFdU exposure was significantly higher than dFdC exposure at all dosages [$p < 0.001$]. Higher PBMC dFdCTP exposures were observed after 20 mg/kg (143 ± 13 $\mu\text{M}\cdot\text{h}$) and 40 mg/kg (130 ± 31 $\mu\text{M}\cdot\text{h}$) compared with 60 mg/kg (44 ± 13 $\mu\text{M}\cdot\text{h}$) or 120 mg/kg (42 ± 12 $\mu\text{M}\cdot\text{h}$) [$p < 0.0001$], which suggested an inhibition more than a saturation of dFdCTP formation at high dFdC dosages. This phenomenon was best captured by including transit compartments for dFdCTP formation and an inhibitory effect on the dFdCTP formation rate constant driven by dFdU concentrations using a Hill function.

Conclusions: An inhibition of dFdCTP formation in PBMCs at higher dFdC dosages and linked to plasma dFdU concentrations was characterized in mice using pharmacokinetic modeling. To obtain the highest dFdCTP exposure in PBMCs for murine studies with dFdC, dosages between 20-40 mg/kg would be recommended. Future work will evaluate dFdCTP formation in brain tumor tissue in a CNS tumor-bearing murine model and the effect of drug-drug interactions on dFdCTP formation to predict dFdCTP formation in children with CNS tumors.

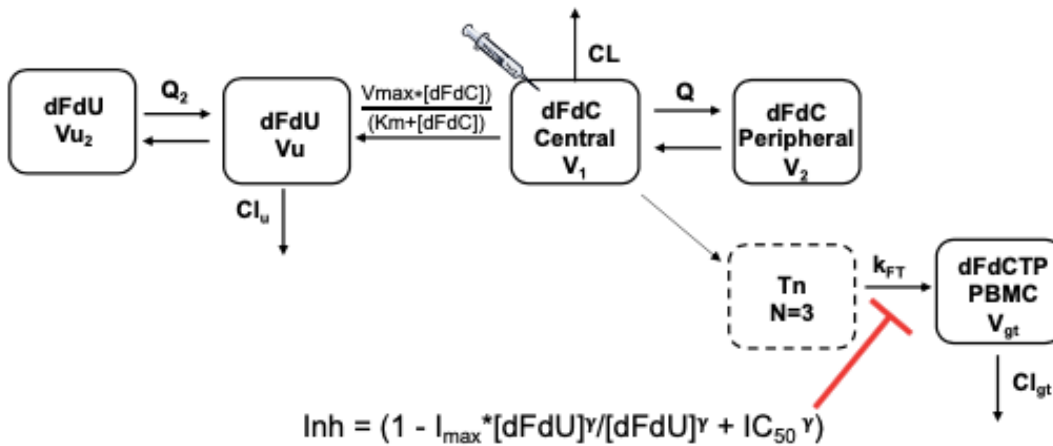


Figure 1. Pharmacokinetic Model Structure:

V₁, V₂, V_u, V_{gt}: Central, peripheral, dFdU (V_u=V₁), and PBMC compartment volumes; CL, Cl_u, Q, Q₂: dFdC central, dFdU central, dFdC peripheral, dFdU peripheral clearance; Tn: Transit compartments, k_{FT}: dFdCTP formation rate; CL_T: dFdCTP clearance; Inh: dFdU inhibition effect on dFdCTP formation

THU-022

A novel physiologically-based pharmacokinetic (PBPK) model to quantify antibody tissue concentration gradients in primary tumors and tumor-draining lymph nodes (TDLNs)

Eric Salgado¹, Yanguang Cao¹

¹Division of Pharmacotherapy and Experimental Therapeutics, UNC Eshelman School of Pharmacy, University of North Carolina at Chapel Hill, NC, USA.

Objectives: Emerging evidence across various cancer-specific clinical trials has demonstrated clear efficacy for antibody immunotherapy prescribed in neoadjuvant (pre-surgical) settings. The primary tumor-TDLN signaling axis has recently been highlighted as a focal point for its effectiveness [1]. Moreover, organ-specific “immunostats,” which includes TDLNs, have recently been observed to contribute to lesion-level heterogeneous responses and the efficacy of antibody immunotherapy in neoadjuvant settings [2]. Thus, the goal of the current work was to construct the first to-date physiologically-based pharmacokinetic (PBPK) model to quantify antibody distribution gradients from organ-specific primary tumors to their tumor-draining lymph nodes (TDLNs). The model would be valuable for predicting antibody concentration gradients in different clinically relevant scenarios, including surgery.

Methods: A PBPK model was constructed to define the micro-anatomical structures of organ-specific primary tumors and their associated TDLNs. Physiologically relevant parameters such as tumor-specific lymph flow were considered. Antibody-antigen binding in both the primary tumor and TDLNs were described by a quasi-steady state target-mediated drug disposition (QSS-TMDD) model. FcRn-mediated antibody salvage in the draining lymphatic vessels was also considered. The model was further calibrated using data from eight immuno-PET mAb-tumor imaging studies in humans (brain, head/neck, breast, lung, esophagogastric, renal, ovarian, pancreatic).

Results: The developed PBPK model was able to adequately capture the antibody PK profiles across all eight cancer types in three anatomical locations (blood, primary tumor, TDLNs) (**Fig. 1**). Antibody concentration gradients from primary tumors to the TDLNs were also well recapitulated, exhibiting high heterogeneity across tumor types and anatomical locations. The model was used to investigate antibody distribution in all primary tumors and TDLNs both pre- and post- tumor resection, as well as in the absence or presence of TDLN metastases, highlighting the importance of the intact lymphatic system (i.e. prior to tumor resection) for antibody distribution and immune activation in TDLNs in neoadjuvant settings.

Conclusions: With this PBPK model, we have provided the first quantitative, proof-of-principle framework that can predict antibody distribution gradients in primary tumors and their TDLNs in various clinical situations (NIH: GM119661).

References:

1. Topalian SL, Taube JM, Pardoll DM (2020) Neoadjuvant checkpoint blockade for cancer immunotherapy. *Science* 367 (6477):eaax0182. doi:10.1126/science.aax0182
2. Osorio JC, Arbour KC, Le DT, Durham JN, Plodkowski AJ, Halpenny DF, Ginsberg MS, Sawan P, Crompton JG, Yu HA, Namakydoust A, Nabet BY, Chaff JE, Riely GJ, Rizvi H, Diaz LA, Jr., Hellmann MD (2019) Lesion-Level Response Dynamics to Programmed Cell Death Protein (PD-1) Blockade. *J Clin Oncol* 37 (36):3546-3555. doi:10.1200/jco.19.00709

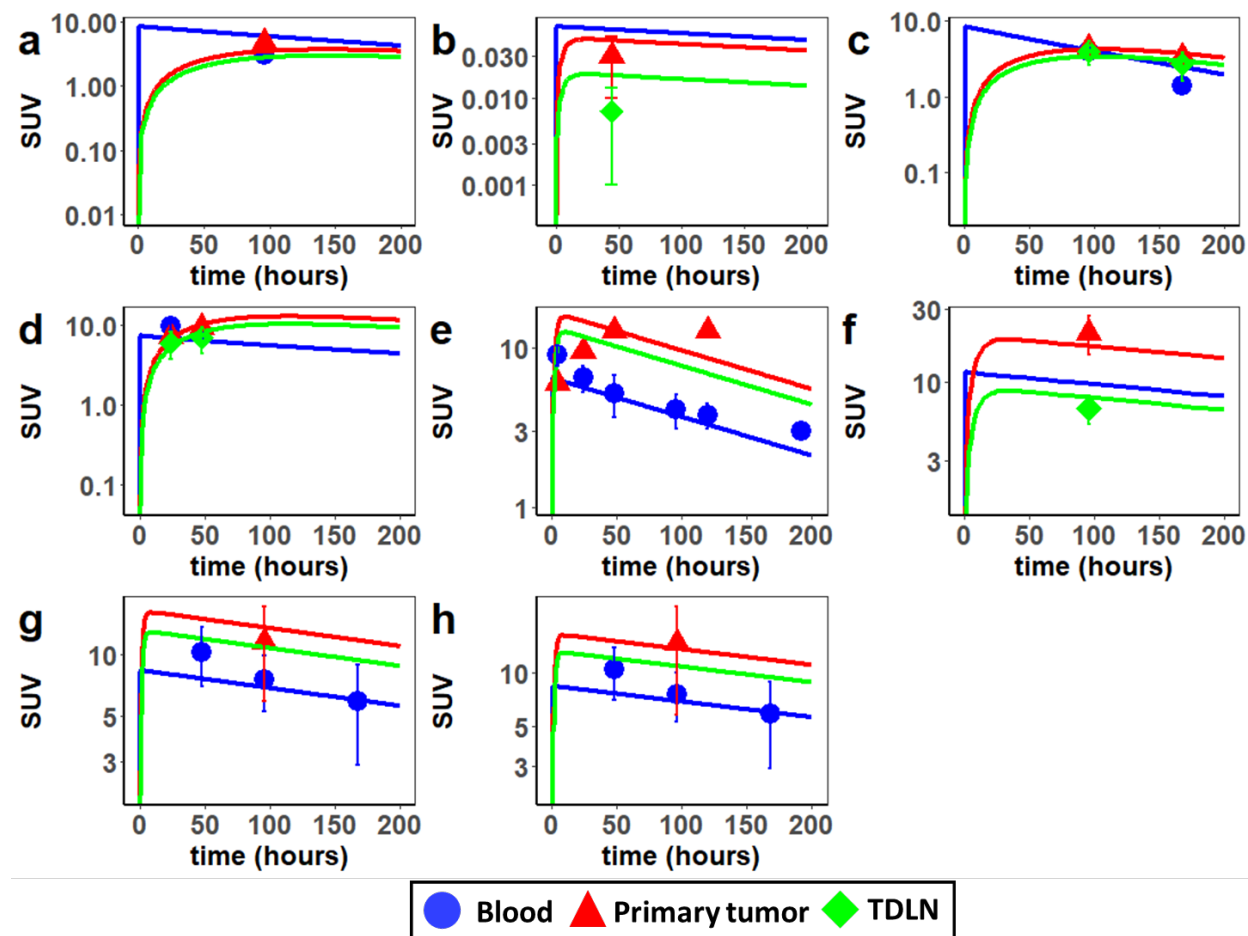


Fig. 1. PBPK model adequately captures antibody concentration gradients from organ-specific primary tumors to the TDLNs. PK data from eight published immuno-PET mAb-tumor biodistribution studies were calibrated into the model. Tissues are color-coded and defined as depicted above; shapes represent observed data. Each plot is a single study and incorporated the following cancer type-immunoPET mAb pairs: **(a)** brain, ^{89}Zr -Fresolimumab; **(b)** head/neck, $^{99\text{m}}\text{Tc}$ -mAb E48 IgG; **(c)** NSCLC, ^{89}Zr -Bevacizumab; **(d)** breast, ^{64}Cu -DOTA-Trastuzumab; **(e)** esophagogastric, ^{89}Zr -Trastuzumab; **(f)** renal, ^{89}Zr -Bevacizumab; **(g)** pancreatic, ^{89}Zr -anti-Mesothelin; **(h)** ovarian, ^{89}Zr -anti-Mesothelin. SUV = unitless standard uptake value of immuno-PET mAb into tissue.

THU-023

“Heta compiler” is a framework for the development and management of Quantitative Systems Pharmacology modeling platforms

Authors: Evgeny Metelkin

Affiliations: InSysBio LLC, Moscow

Objectives

Today the pharmacology modeling is evolving towards complex mechanism-based dynamical modeling and involves a large amount of biological and clinical data [1]. A typical QSP project may include thousands of molecular components, several drugs and usually is done by a research group involving people with different expertise. The data management, workflow and co-operation in such projects are the challenges. In many cases, the critical step also is the translation of the modeling results to other modeling formats and frameworks.

This study is an effort to resolve the typical problems in a QSP project by creating the software infrastructure based on Heta formats and develop a shared and controllable working environment. The pre-formulated requirements are: (i) storing the QSP models and data in integrated infrastructure, (ii) support iterative platform updates, (iii) support of models written in human-readable text and table formats, (iv) export models and data to different popular formats on the fly.

Methods

Heta language is a Domain Specific Language (DSL) designed for the development and annotation of dynamical models in QSP projects. Heta standard of version 0.2 is fully supported in the Heta compiler. The core of the Heta compiler was developed in JavaScript language and can be used in Node environment, can be a part of a web-based application or potentially integrated with simulation software.

Results

Heta compiler is developed and tested based on the series of QSP models and projects. Currently Heta compiler supports the export to the following formats: DBSolve, Simbiology, mrgsolve, Matlab, SBML, etc. It was used in open and commercial QSP projects developed by InSysBio: Alzheimer-consortium platform, Immune Response Template, PK/RO simulator for anti-PD-1 mAbs.

Discussion

Heta compiler will be developing as free open-source software on GitHub and is expected to be a community-driven framework (<https://hetalang.github.io>). A series of additional tools to support Heta and Heta compiler is developed: highlighting syntax in Atom and VSCode, SbmlViewer, slv-utils.

Conclusions

Heta compiler can be used as the framework for a QSP modeling project of any size and complexity. It allows integrate the dynamical models and data as modules and transform the modeling code to different popular formats. It can be easily integrated with existed infrastructure, workflows or used as a part of the CI/CD strategy.

References

1. Knight-Schrijver et al. Computational and Structural Biotechnology Journal (2016) 14, 363-370

THU-024

Mechanistic modeling of Levodopa pharmacodynamics through Parkinson's disease progression

Florence Véronneau-Veilleux¹, Mauro Ursino², Philippe Robaey³, Fahima Nekka^{1,4,5}

¹Faculté de Pharmacie, Université de Montréal, Montréal, Québec, Canada; ²Department of Electrical, Electronic and Information Engineering Guglielmo Marconi, University of Bologna, 40136 Bologna, Italy; ³Faculty of Medicine, University of Ottawa, Ottawa, Ontario, Canada; ⁴Centre de recherches mathématiques, Université de Montréal, Québec, Canada; ⁵Centre for Applied Mathematics in Bioscience and Medicine (CAMBAM), McGill University Montréal, Québec, Canada.

Objectives: Levodopa is one of the most efficient drugs to alleviate Parkinson's disease symptoms. Although very effective in the first years after diagnosis, its effect is altered as the disease progresses³. Indeed, its chronic use combined with the progression of denervation in the substantia nigra leads to motor complications and decrease in effect duration. It results in difficulties to optimize the regimen which calls for a better understanding of the pharmacodynamics through disease progression. The main objective of this project is to understand the role of the different processes involved in the alteration of Levodopa pharmacodynamics as the disease progresses through mathematical mechanistic modeling. To quantify the effect of Levodopa, the frequency in the finger tapping task is used as a measure of bradykinesia.

Methods: We developed an integrative mechanistic model to investigate the modifications of Levodopa's pharmacodynamics. This model is composed of three sub-models that represent respectively levodopa pharmacokinetics¹, dopamine dynamics², interaction with D1 and D2 receptors² and neurotransmission in the basal ganglia with the three main neurotransmission pathways¹. The neurocomputational model of basal ganglia is represented in Figure 1. The impact of denervation on all the mechanisms is included in the model. Each sub-model was built in line with up-to-date knowledge and data of the pathophysiology and pharmacology.

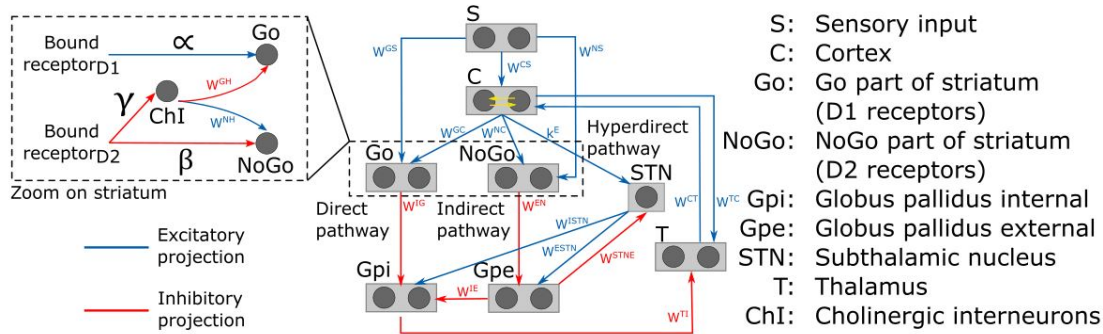


Figure 1 Schematic representation of the neurocomputational model of basal ganglia adapted from [1]

Results: Using our model, we simulated Levodopa plasma concentration, dopamine concentration in the brain, neuronal activity in each nuclei of the basal ganglia as well as frequency of tapping. According to different degrees of denervation and Levodopa intake, we were able to reproduce the tapping frequency across disease progression. A reduction in the effect duration as well as the delay of the effect is reproduced by the model. The model also highlights the role of D2 dopaminergic receptors compared to D1.

Conclusions: This Quantitative Systems Pharmacology approach is a promising step towards regimen optimization and identification and understanding of important mechanisms involved in Parkinson's disease and its therapy.

References

- [1] Baston, C., Contin, M., Buonaura, G.C., Cortelli, P., Ursino, M.: A mathematical model of levodopa medication effect on basal ganglia in parkinson's disease: An application to the alternate finger tapping task. *Frontiers in Human Neuroscience* 10 (2016). DOI10.3389/fnhum.2016.00280
- [2] Dreyer, J.K.: Three mechanisms by which striatal denervation causes breakdown of dopamine signaling. *Journal of Neuroscience* 34(37), 12444-12456 (2014). DOI10.1523/jneurosci.1458-14.2014
- [3] Holford, N., Nutt, J.G.: Disease progression, drug action and parkinson's disease: why time cannot be ignored. *European journal of clinical pharmacology* 64, 207-216 (2008). DOI 10.1007/s00228-007-0427-9

Well-Tempered MCMC Simulations for Population Pharmacokinetic Models

Frederic Y. Bois¹, Nan-Hung Hsieh², Wang Gao³, Weihsueh A. Chiu², Brad Reisfeld⁴.

¹ Certara, Simcyp division, Sheffield, UK.

² Department of Veterinary Integrative Biosciences, College of Veterinary Medicine and Biomedical Sciences, Texas A&M University, USA.

³ INERIS, METO unit, Verneuil en Halatte, France.

⁴ Department Chemical and Biological Engineering and School of Biomedical Engineering, Colorado State University, USA.

Objectives:

A full Bayesian statistical treatment of complex pharmacokinetic or pharmacodynamic models, in particular in a population context, gives access to powerful inference, including on model structure. We present here the results obtained with an improved implementation of the simulated tempering Markov Chain Monte Carlo (TMCMC) algorithm of Geyer and Thompson (1995). TMCMC has a number of advantages over usual MCMC algorithms: it can sample efficiently from sharp multi-modal posteriors; it provides insight into identifiability issues useful for model simplification; it has assured convergence with a single simulated chain if infinite temperature can be reached; it can be used to compute accurate Bayes factors for model comparison and choice.

Methods:

The main challenge to implementing this approach has been setting an adequate scale of auxiliary temperatures, which we solved by stochastically optimizing a grid of inverse-temperatures, or “perks,” through a Robbins-Munro process and adaptive optimization. The resulting grid of perks and associated pseudo-priors was used to perform thermodynamic integration, bridging the joint prior and the posterior distributions, for two stylized case studies and two realistic population pharmacokinetic inference problems: One for theophylline, with a small pharmacokinetic model; the other one for acetaminophen with a large PBPK model.

Results:

In all the cases investigated here, perk zero (infinite temperature) was reached by the automatic perks’ setting algorithm. In the case of a sharply bimodal regression model, the two high posterior density region (in a three dimensional space) were accurately identified, where other algorithms, such as MCMC or Hamiltonian MCMC failed. In the simple case of the identification of a Gaussian mean, we show how to compute a close approximation of the integration constant needed to estimate Bayes factors. The

theophylline population PK modelling case shows that a model with inter- and intra-individual variability is clearly favored compared to a model without intra-individual variability, based on Bayes factors. The posterior parameter estimates are close to those obtained with standard MCMC, except that TMCMC identify a secondary mode of the posterior. The posterior distributions of the most sensitive parameters of the acetaminophen PBPK are closer than those obtained with MCMC, but obtained 20 times faster due to the improved mixing of the chain mixing and assured convergence.

Conclusion:

TMCMC has a number of advantages over other MCMC algorithms, if it is implanted efficiently. Our case studies show a full range of its capabilities, which are useful for pharmacokinetic or pharmacodynamic modeling, but also extend well beyond it.

References:

Geyer CJ and Thompson EA, 1995, Annealing Markov chain Monte Carlo with applications to ancestral inference, Journal of the American Statistical Association. 90:909–920.

Acknowledgements:

Funding for this work was made possible, in part, by the U.S Food and Drug Administration through Grant 1U01FD005838. Views expressed in written materials or publications do not necessarily reflect the official policies of the Department of Health and Human Services; nor does any mention of trade names, commercial practices, or organization imply endorsement by the United States Government.

THU-029

Hereditary angioedema (HAE) prophylaxis with plasma kallikrein inhibitors: Role of target binding kinetics, pharmacokinetics and treatment adherence

Hoa Q. Nguyen¹, Rangaraj Narayanan², Haobin Luo³, Zhiwei Zhang³, Paul Jasper³, Peng Lu¹, Salomé Juethner¹, Dan Sexton¹

¹ Shire, a Takeda company, Cambridge, MA; ² Grünenthal Group, Cambridge, MA; ³ RES Group Inc., Needham, MA

Objectives: Unopposed activation of the contact system leads to excessive production of plasma kallikrein (pKAL) and, subsequently, increased release of bradykinin, a key mediator of HAE attacks pKAL inhibitors block contact system activation; the resulting disease control can be driven by various drug-related factors. We sought to better understand the impact of these factors via a quantitative systems pharmacology (QSP) approach.

Methods: A mechanistic biological model of HAE was developed using QSP modeling that incorporated critical components of the contact system, and a virtual HAE patient population was established. Cleaved high molecular weight kininogen pharmacodynamic biomarker data, and clinical outcomes from lanadelumab clinical studies were used to verify the model. The verified model framework was used to evaluate impact of various drug-related factors on HAE disease outcome, including target binding potency, PK characteristics and treatment adherence in patients (assessed via novel virtual scenarios) of orally available, small molecule pKAL inhibitors.

Results: Target binding potency has a direct correlation with improved disease outcome; however, a critical factor for improved efficacy is that sufficient amounts of “free” drug are available to bind to pKAL. Impact of drug half-life was explored, and simulations showed that drugs with long half-lives (≥ 2 weeks) had ≥ 2 -fold improved efficacy versus those with shorter half-lives (approximately 1–2 days). Simulations showed that with short acting pKAL inhibitors (half-lives < 2 days) 1–2 days of missed doses per week could translate to an approximately 2-fold efficacy decline, thereby increasing risk for HAE attacks.

Conclusions: Results from an in-silico QSP approach were consistent with attributing improved efficacy of lanadelumab in HAE prophylaxis to high availability of “free” pKAL inhibitor and long half-life (≥ 2 weeks).

Disclaimer: The results in this abstract have been previously presented as Poster 327 online at the American Academy of Allergy Asthma and Immunology (AAAAI) Annual Meeting, Philadelphia, PA, March 13–16, 2020, which was cancelled due to COVID-19, and published in the conference proceedings as abstract #327 in *J Allergy Clin Immunology* 2019;145(2):AB105.

THU-030

A Mechanism-based Pharmacokinetic-Pharmacodynamic Model for Hemodynamic Effects of Propofol in Healthy Volunteers

H Su¹, M.M.R.F.Struys^{1,2}, P.J.Colin¹

¹Department of Anesthesiology, University Medical Center Groningen, University of Groningen, Groningen, The Netherlands ²Department of Basic and Applied Medical Sciences, Ghent University, Ghent, Belgium

Objectives:

Propofol, a γ -aminobutyric acid receptor agonist, is used for sedation and anesthesia in clinical practice. One of the adverse effects of propofol is hypotension. Propofol reduces sympathetic tone, leading to vasodilation and potentially decreases blood pressure [1]. This study aims to develop a mechanism-based pharmacokinetic-pharmacodynamic (PKPD) model that can describe the relationship between cardiovascular variables such as mean arterial pressure (MAP), heart rate (HR), pulse pressure (PP) and plasma concentration for propofol.

Methods:

36 healthy volunteers were enrolled in this study and received propofol in a staircase fashion by target-controlled infusion using the Schnider model [2, 3]. PK of propofol was described by a three compartment model developed by Eleveld et al [4]. First, data-driven models for MAP, HR and PP were developed. Then, based on the model by Snelder et al [5], a mechanistic model was explored. PP was used as a surrogate for stroke volume (SV) [6].

Results:

Our data-driven models and the mechanism-based model describe the effect of propofol on MAP, HR and PP. In the data-driven models, changes in MAP, HR and PP were described by indirect response models. The relationship between plasma concentration (C_p) and MAP and PP were described by an Emax model. For HR, a sigmoid Emax model fitted the data best. Age was a covariate on baseline PP. The estimated propofol C₅₀ for MAP, HR and PP were 12.7, 2.32 and 1.34 μ g/ml, respectively. In the mechanistic model, we assume that propofol inhibits total peripheral resistance (TPR) and SV, the resulting change in MAP was calculated from these variables. TPR, HR and SV were regulated by a negative feedback via MAP. In addition, a direct inverse relationship between SV and HR was also included. Higher MAP and HR were found before propofol infusion, this effect was explained by an anxiety term in the HR. Estimated propofol C₅₀ for TPR and SV were 3.37 and 0.52 μ g/ml, respectively. The mechanistic model could describe the propofol-induced cardiovascular side effects. Compare to data-driven models, the goodness of fit plot showed that the mechanistic model was slightly less accurate.

Conclusions:

We developed three data-driven models for propofol effects on MAP, HR and PP as well as a mechanistic model in healthy volunteers. Both data-driven models and mechanistic model could describe the cardiovascular effects well. Further research is focusing on the optimizing and evaluation of the performance the mechanistic model.

References:

1. Sahinovic, M.M., M. Struys, and A.R. Absalom. Clin Pharmacokinet. 2018;57(12):1539-1558.
2. Schnider, T.W., et al. Anesthesiology. 1998;88(5):1170-82.
3. Schnider, T.W., et al. Anesthesiology. 1999;90(6):1502-16.
4. Eleveld, D.J., et al. Br J Anaesth. 2018;120(5):942-959.
5. Snelder, N., et al. Br J Pharmacol. 2014;171(22):5076-92.
6. de Simone, G., et al. Hypertension. 1999;33(3):800-5.

THU-032

Exposure-Response Analysis of Insulin-like Growth Factor-1 (IGF-1) and Bronchopulmonary Dysplasia Following Administration of Recombinant IGF-1 and Binding Protein-3 in Extremely Premature Infants

Authors: Claudia Jomphe¹, Nathalie H Gosselin¹, JF Marier¹, Linda Han² and Indranil Bhattacharya²

Affiliations: ¹Certara Strategic Consulting, Princeton, NJ, USA, ²Takeda, Cambridge, MA, USA

OBJECTIVE: Extremely premature infants are at very high risk of developing morbidities such as bronchopulmonary dysplasia (BPD) and often experience delayed mortality or long-term disabilities. Insulin-like growth factor-1 (IGF-1) promotes organ development and drives growth in extremely preterm infants. A human recombinant form of the naturally occurring protein complex of IGF-1 and insulin-like growth factor binding protein-3 (rhIGF-1/rhIGFBP-3, TAK-607) is being developed for the prevention of complications associated with extreme prematurity. The purpose of this project is to assess the exposure-response relationship between IGF-1 and the prevention of BPD in order to support an optimal dosing regimen in premature infants.

METHODS: A total of 96 premature infants received daily intravenous (IV) infusion of rhIGF-1/rhIGFBP-3 or standard neonatal care (SOC). BPD was assessed by oxygen challenge testing at postmenstrual age (PMA) 36 weeks. Median (range) gestational age (GA) and body weight at birth were 25.9 weeks (23.1 – 27.9) and 0.790 kg (0.425 – 1.22), respectively. Logistic regression models were constructed to assess the relationship between IGF-1 exposure metrics and the probability of BPD (No/Mild vs. Moderate/Severe). Sources of variability in BPD response were explored (GA and birth weight, sex, oxygen saturation on Day 1, APGAR score at 1 min, and study arm). Based on the exposure-response relationship, clinical trial simulations were performed to identify the dosing regimen that would result in IGF-1 levels that optimize BPD response.

RESULTS: A statistically significant exposure-response relationship was observed, whereby higher observed average IGF-1 levels at day 7 (CavD7) were associated with a greater probability of No/Mild BPD. In addition, statistically significant effects of weight at birth and sex were observed, whereby larger females are expected to have a higher probability of No/Mild BPD. Neither oxygen saturation at birth nor APGAR score at 1 min were predictors of No/Mild BPD. A total of 500 trials of 75 subjects treated with 250 and 400 µg/kg/day rhIGF-1/rhIGFBP-3 or no dose (SOC) in a 1:1:1 ratio were simulated based on a population PK model. The probability of No/Mild or Moderate/Severe BPD was determined based on simulated CavD7 in each trial according to the above exposure-response model. Simulations suggested that both rhIGF-1/rhIGFBP-3 treatments are superior to SOC for BPD. In addition, the 400 µg/kg/day regimen was associated with a greater probability of No/Mild BPD relative to the 250 µg/kg/day regimen.

CONCLUSION: A statistically significant exposure-response relationship was observed, whereby higher levels of IGF-1 were associated with a greater probability of No/Mild BPD. Based on simulations, a 400 µg/kg/day dose of rhIGF-1/rhIGFBP-3 is expected to result in a greater probability of No/Mild BPD in extremely premature infants.

Wor

THU-033

Unveiling determinants of nonalcoholic fatty liver disease (NAFLD) activity and nonalcoholic steatohepatitis (NASH) using item response modeling

Iris K. Minichmayr (1), Elodie Plan (1), Benjamin Weber (2), Sebastian Ueckert (1)

(1) Department of Pharmaceutical Biosciences, Uppsala University, Uppsala, Sweden

(2) Translational Medicine and Clinical Pharmacology, Boehringer Ingelheim Pharmaceuticals, Inc., Ridgefield, Connecticut, USA

Objectives: NAFLD—including its progressive subtype NASH—has emerged as a leading indication for liver transplantation and, fueled by the obesity epidemic, an alarmingly increasing threat to public health. There are still no approved drugs for NAFLD/NASH owing to challenges in drug development, e.g. the complex, ‘multi-hit’ pathophysiology of NAFLD or inconsistent diagnostic criteria and treatment endpoints [1,2]. Currently, NASH diagnosis and clinical trial endpoints heavily rely on liver biopsies and histological scoring metrics like the NAFLD activity score (NAS)—considering *steatosis*, *inflammation* and *hepatocellular ballooning*—and *fibrosis* [3]. Our objective was to enhance the understanding of disease processes underlying NAFLD and to assess the role of different histological and non-invasive markers in assessing NAFLD severity by using item response theory (IRT) modeling.

Methods: The study population ($n_{ID}=914$) originated from the public NIDDK NAFLD Adult Database [4] and spanned the full spectrum of NAFLD (NAS 0–8; 52.3% patients with NASH). An IRT model was developed (using R3.6.1/mirt), relating the probability of the outcome of each item (i.e. histological feature) to latent variables, which represent unobserved disease processes underlying the item responses. Biomarkers predicting NAFLD activity were identified using full random effects modeling.

Results: Model development initially focused solely on the NAS items *steatosis*, *inflammation* and *ballooning* and was subsequently extended to 13 histological features, including *fibrosis* [3]. The 13-item model, comprising 5 graded-response and 8 two-parameter logit models, allowed for a better distinction between NASH and Non-NASH patients. The disease processes underlying hepatocellular ballooning and fibrosis appeared to best inform NASH diagnosis, followed by inflammation and steatosis. The IRT model suggested different disease processes (i.e. separate latent variables) for the four cardinal features of NAFLD, i.e. the three *NAS components* and *fibrosis*. Highest correlation (70%) was found between processes reflected by hepatocellular ballooning and fibrosis. Identified non-invasive predictors of NAFLD severity scores inter alia included liver enzymes and partly differed between the NAS score and fibrosis score.

Conclusions: An item response theory model based on hepatic histological scoring allowed to jointly characterize disparate disease processes underlying NAFLD—including more rapidly changing aspects like steatosis and the slowly progressing lesion fibrosis—as well as potential non-invasive biomarkers reflecting NAFLD activity. Our analysis suggests that NASH could be inferred better from a broad panel of histological lesions than from the NAS alone. The model lays the basis for future investigations on the sensitivity of the NAS to changes of different disease processes, e.g. as response to a therapeutic intervention, with the ultimate goal to support model-informed drug development.

References

- [1] Wong et al. Lancet Gastroenterol Hepatol. 2016;1(1):56–67
- [2] Rinella et al. J Hepatol. 2019;71(4):823–833
- [3] Kleiner et al. Hepatology. 2005;41(6):1313–1321
- [4] Neuschwander-Tetri et al. Hepatology. 2010;52(3):913–924

THU-034

Population Pharmacokinetics of Pegilodecakin and Exposure-Safety (Anemia) Assessment in Patients with Solid Tumors

Lisa O'Brien¹, David Ferry¹, Ivelina Gueorguieva²

¹Lilly Research Laboratories, Indianapolis, Indiana, USA; ²Lilly Research Laboratories, Windlesham, Surrey, UK.

Objectives: Clinical benefit of an IL-10 receptor agonist, pegilodecakin (pegylated recombinant human IL-10) was investigated in solid tumors. Aims included evaluation of the pharmacokinetics (PK) of pegilodecakin, identification of patient factors impacting disposition, and understanding mechanisms for hemoglobin decrease from baseline during pegilodecakin treatment.

Methods: A total of 3925 serum concentrations from 579 cancer patients, enrolled in three Phase I/II/III studies were included in the PK analysis. Patients self-administered pegilodecakin subcutaneously at a variety of dose levels (range: 0.02-4 mg) and dosing schedules. Pharmacodynamic (PD) data (~19,000 measurements), including reticulocyte counts, red blood cells, and hemoglobin levels (Hb), were collected weekly from patients enrolled in these studies.

Previously, -unpegylated IL-10 caused anemia with concentration-dependent decrease in Hb in patients with Crohn's disease associated with increased ferritin and no evidence of hemolysis [1]. A novel RBC life span model with pegilodecakin-dependent inhibition on RBC maturation rate was developed using the Phase I/III data. The model evaluated treatment impact on patient RBC life span which resulted in change in hemoglobin and anemia severity grade. Dose modifications for treatment emergent adverse events and blood transfusion information were taken into account. Developmental stages of erythroid cell were modelled related to the hypothesis that pegilodecakin affects erythropoiesis. Simulations were performed to evaluate the impact of various dosing regimens on pegilodecakin exposure and safety.

Results: The pharmacokinetics of pegilodecakin were well characterized by a linear one-compartment model with absorption lag and allometric scaling. Apparent clearance was lower in patients treated with high pegilodecakin doses. Mean (CV%) PK parameters derived from post-hoc parameters were: K_a 0.113 h⁻¹ (64%), CL/F 3.86 L/h (61%), V/F 149 L (84%). Between-patient variability on CL/F was high (58%). No other covariates (patient demographics, disease characteristics) were identified as statistically significant or clinically meaningful. Based on the PK/PD model, RBC life span was decreased by more than half for pegilodecakin-treated patients, compared to literature reported healthy subjects (120 days). Estimates of baseline reticulocytes, RBC count, and mean corpuscular hemoglobin were comparable to those reported for healthy subjects. The mean time for a precursor cell to enter the blood stream for each cell population was reduced in active arm patients (pegilodecakin plus standard of care) with mean concentration 0.6 ng/mL (4.51 %SEE) for half-maximum response. Model predictions demonstrated decreased reticulocyte count and subsequent increased Hb with treatment rest periods. Return to baseline (with no infusions) was only achieved with a prolonged off-treatment period.

Conclusions: A modelling framework was established to quantitatively describe on-target toxicity (anemia) with pegylated IL-10 treatment. Simulations to evaluate appropriate doses and schedules will enable future trial design to optimize exposure-response.

References:

1. Tilg H, H. Ulmer, A. Kaser and G. Weiss. J Immunol 2002, 169: 2204-2209.

THU-036

Leveraging Real-world data for EMA Qualification of a Model-Based Biomarker Tool to Optimize Type-1 Diabetes Prevention Studies

Jagdeep Podichetty¹, Patrick Lang¹, Inish O'Doherty¹, Sarah David¹, Rhoda Muse¹, Laura Song¹, Klaus Romero¹
Jackson Burton¹; on behalf of the Type-1 Diabetes Consortium (T1DC)

¹Critical Path Institute, Tucson, AZ

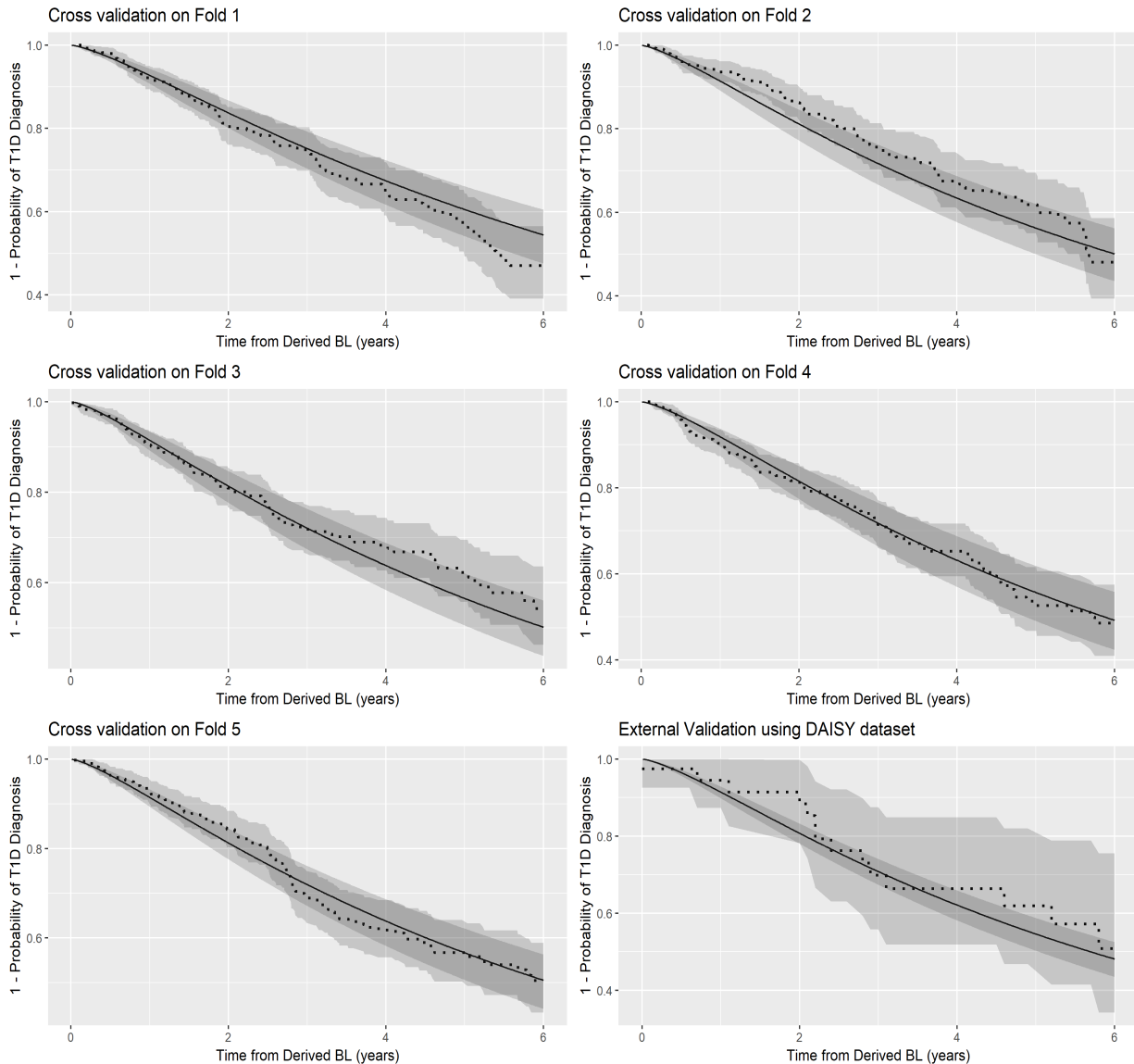
Objectives: Currently, development of therapies to prevent or delay the onset of T1D remains challenging and there is a lack of qualified biomarkers to identify individuals and quantify risk of conversion to a diagnosis of T1D. It is widely accepted that four distinct islet auto-antibodies (AAs) namely GAD65, IAA, ZnT8 and IA-2, are biomarkers associated with risk of T1D diagnosis. The goal of this work was to leverage existing data sources that captured islet AA measurements and glycemic markers in a population likely to participate in T1D prevention trials, and utilize the data to develop a time-to-event model for predicting the time-varying probability of T1D diagnosis. Based on this model, on 25 March 2020, the European Medicines Agency (EMA) released a public Letter of Support for “*Islet autoantibodies as enrichment biomarkers for type 1 diabetes prevention studies, through a quantitative disease progression model*” to address the need for optimized designs of T1D prevention trials. The finalized model will be submitted to EMA for qualification opinion and endorsement of the model-based biomarkers on behalf of the T1D consortium founded by the Critical Path Institute.

Methods: Patient-level data from the TN01, TEDDY and DAISY studies was acquired, curated, and aggregated to conduct analyses. An analysis set was extracted with 2022 individuals and corresponding covariates predictive of T1D, which included the number and type of two or more AAs, blood glucose measurements, HbA1c measurements, HLA subtypes and patient demographics. An Accelerated Failure Time (AFT) model was used to quantify the effect of baseline covariates on the time to T1D diagnosis. Internal validation was performed using K-fold cross validation and external validation using DAISY dataset.

Results: Results from the AFT model analysis indicated that GAD65_IAA and GAD65_ZnT8 combinations have the least relative risk compared to all other combinations, while the IA-2_IAA_ZnT8 has the highest relative risk. The use of 120-minute OGTT and HbA1c values provided significant ability to further stratify risk of T1D diagnosis. A 5-fold cross validation was performed, which showed high overall concordance across all subjects (c-index ≈ 0.81) and external validation with the DAISY study showed a high concordance as well (c-index ≈ 0.85), suggesting that the tool is robust to inform trial design in these islet AA positive populations (**Figure 1**).

Conclusions: We demonstrated that analysis of integrated data from independent observational data sources can be used as evidence for identifying populations for recruitment into T1D prevention studies of reasonable duration. The model-based approach provides a basis to quantitatively link independent sources of risk measured by islet AAs and glycemic measures. The EMA qualification opinion will serve to encourage widespread adoption of the proposed quantitative tool for enrichment strategies and stratification in ongoing and future T1D prevention trials.

Figure 1. Survival plots for k-fold cross validation with 5 folds and external validation with DAISY data. (Dotted curve represents Kaplan–Meier estimate and solid curve represent model prediction)



THU-039

Spatiotemporal Response Heterogeneity across Metastases in Metastatic Colorectal Cancer

Jiawei Zhou¹, Yanguang Cao^{1,2*}

¹School of Pharmacy, University of North Carolina at Chapel Hill, NC, 27599, USA; ²Lineberger Comprehensive Cancer Center, School of Medicine, University of North Carolina at Chapel Hill, Chapel Hill, NC 27599, USA

*corresponding author: yanguang@email.unc.edu

Background

The response pattern of overall tumor burden is broadly used to evaluate patient objective response to interventions. The response patterns of individual lesions and their association with patient survival in metastatic colorectal cancer (mCRC) are still largely uncharacterized. A detailed assessment of the response heterogeneity across metastatic lesions is valuable, but still lacking.

Objectives

The objectives were to evaluate the response dynamics across individual metastases in mCRC, and characterize their associations with treatment types, anatomical sites, and patient survival.

Methods

In this study, we analyzed the lesion-level response dynamics in 2,802 mCRC patients collected in five randomized clinical trials. An algorithm was developed to characterize the response dynamics in individual metastasis by considering three phases: response, stable, and relapse. The response heterogeneity across metastases was quantified by Gower Distances. The association between Gower Distances and patient overall survival was illustrated using an adjusted Cox proportional model. Dunn's multiple comparison test was performed to evaluate the lesion-level response heterogeneity across anatomical sites and treatment types.

Results

High inter-lesion heterogeneity was observed in patient response patterns, and more than 60% of patients have at least one lesion responding differently from the total tumor size. The patient overall survival (OS) is closely associated with the inter-lesion response heterogeneity ($HR=1.145, p < 0.001$). Patients with high inter-lesion heterogeneity had significantly shorter survival (422 days) compared to patients with medium (OS 550 days) or low (OS 630 days) heterogeneity ($p < 0.0001$). Targeted therapies, including bevacizumab or panitumumab in combination with chemotherapy, showed marked reductions in inter-lesion heterogeneity ($p < 0.05$), along with improvements of patient survival compared to chemotherapy alone ($p < 0.001$). The metastatic lesions in the liver have significantly higher shrinkage fractions ($p < 0.05$) and longer response durations ($p < 0.05$) than the lesions in lymph nodes and the lungs in targeted therapies. In contrast, no apparent improvement was observed in the liver lesions under chemotherapy alone.

Conclusions

Due to the high inter-lesion heterogeneity, the response dynamics of total tumor sizes could not fully reflect the individual lesions in mCRC patients. This lesion-level response heterogeneity is associated with patient survival. Targeted therapies showed better effects than chemotherapy on metastatic lesions in the liver. (NIH GM119661)

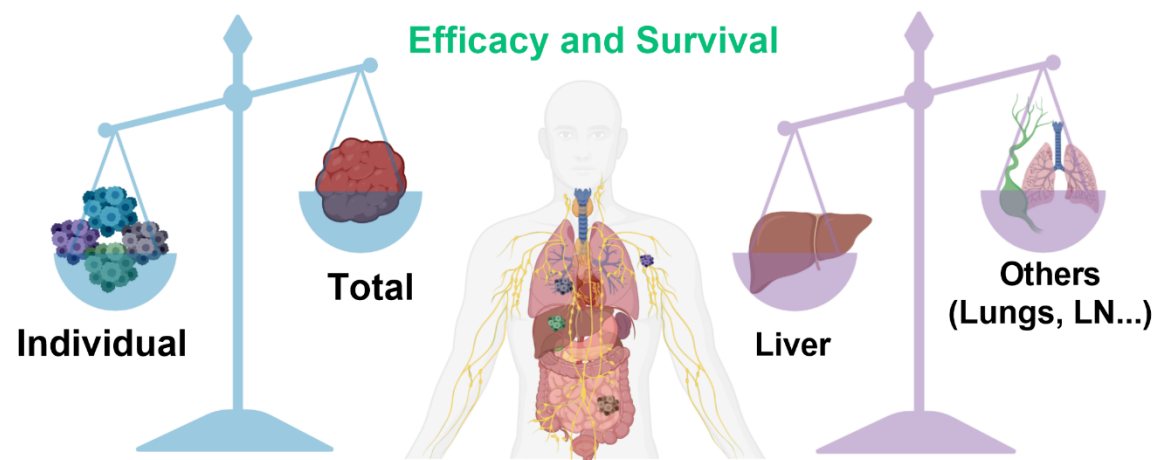


Figure 1. Response heterogeneity across metastases is associated with treatment efficacy and patient survival.

THU-040

Predictions of Systemic, Intracellular, and Lung Concentrations of Azithromycin with Different Dosing Regimens used in COVID-19 Clinical Trials

Jim H. Hughes¹, Kevin Sweeney¹, Sima Ahadieh¹, Daniele Ouellet¹

¹Global Product Development, Pfizer Inc., Groton CT and Collegeville PA, USA

Objectives: Azithromycin (AZ) is currently being investigated for its effectiveness against SARS-CoV-2 in patients with coronavirus disease 2019 (COVID-19). It is hypothesized that the activity of AZ may be linked to its extensive tissue distribution and accumulation in cells. A hybrid of existing published population pharmacokinetic (PK) models was developed to assess AZ exposure in different tissues including lung and intracellularly in alveolar macrophages (AMs).

Methods: A hybrid model utilizing parameters of tissue (1) and systemic PK (2) from two separate models was developed in R using the *mrgsolve* package. This model was extended to predict concentrations in AMs and lung tissue. Model predictions were compared to digitized aggregate tissue data from 8 publications and individual concentrations from two clinical trials ($n = 64$) in plasma/serum, lung tissue, leukocytes and AMs. The model was used to simulate concentrations ($n = 1000$ subjects) based on AZ dosing regimens used in clinical trials of COVID 19 and compared to published in vitro EC90 against SARS-CoV-2 (3). Dosing regimens included: 500 mg QD for 3 days (A); 500 mg single dose followed by 250 mg QD on days 2 through 5 (B); 1000 mg single dose (C); and 500 mg QD for 10 days (D). Finally, a web application for model simulation using additional dosing regimens was developed in R using the *shiny* package.

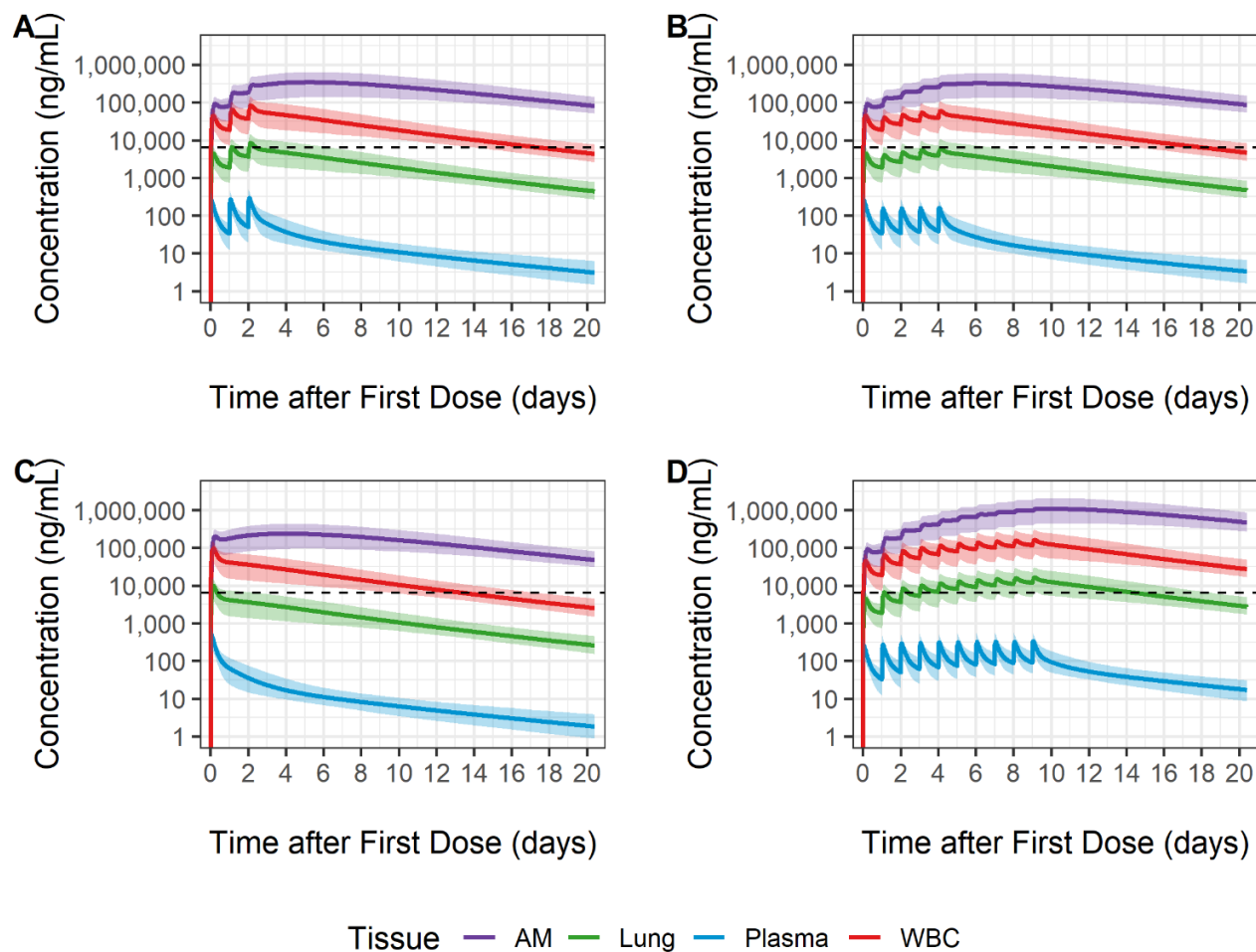
Results: The final model consisted of a base three-compartment PK model with first-order absorption and elimination, three tissue compartments representing subcutis, muscle and lung tissue, and two intracellular compartments for leukocytes (WBCs) and AMs, each associated with a separate deep-tissue compartment. The final model adequately described aggregate and individual concentration data across multiple dosing regimens. Simulated median AZ concentrations and 90% prediction intervals (Figure) showed that concentrations in lung tissue were above the in vitro EC90 (dashed line) when using the highest AZ dosing regimen (D), while AM concentrations were above the in vitro EC90 for an extended period with all tested dosing regimens (A-D).

Conclusions: This model was adequate to predict tissue concentrations and will better inform the evaluation and optimization of dosing regimens used in ongoing and future AZ clinical trials.

References:

1. Zheng, S., et al., Development of a population pharmacokinetic model characterizing the tissue distribution of azithromycin in healthy subjects. *Antimicrob Agents Chemother*, 2014. 58(11): 6675-6684.
2. Zhao, Q., et al., Population pharmacokinetics of azithromycin and chloroquine in healthy adults and paediatric malaria subjects following oral administration of fixed-dose azithromycin and chloroquine combination tablets. *Malar J*, 2014. 13: 36-36.
3. Touret, F., et al., In Vitro Screening of a FDA Approved Chemical Library Reveals Potential Inhibitors of SARS-CoV-2 Replication. *bioRxiv*, 2020. 2020.04.03.2023846.

Figure: AZ Concentration-Time Profiles in Different Tissues after Different Dosing Regimens



THU-041

Population Pharmacokinetic-Pharmacodynamic Analysis of a Complement Factor B Antisense Oligonucleotide in Healthy Volunteers to Support Phase 2 Dose Selection

Authors: Joao A. Abrantes¹, Daniel A. Norris², Jayashree Sahni¹, Michael McCaleb², Yanfeng Wang², Nicolas Frey¹

Institutions: ¹Roche Innovation Center, Basel, Switzerland; ²Ionis Pharmaceuticals, Carlsbad, CA, USA

Objectives:

IONIS-FB-L_{Rx} is a triantennary N-acetyl galactosamine (GalNAc)-conjugated antisense oligonucleotide (ASO) in development as a potential treatment for geographic atrophy associated with age-related macular degeneration (AMD). The ASO portion of IONIS-FB-L_{Rx} targets complement factor B (FB) mRNA thus preventing the production of FB protein, which increased levels are associated with AMD [1,2]. The aim was to characterize the relationship between the PK of IONIS-FB-L_{Rx} and the FB as well as the alternative complement pathway hemolytic activity (AH50) levels using a population model-based approach.

Methods:

Data from 41 healthy volunteers (HV) were available from two Phase 1 clinical studies (single ascending dose (SAD), N=17; multiple ascending dose (MAD), N=24). The drug was administered subcutaneously: 10, 20 and 40 mg single-dose (SAD), or 10 and 20 mg administered in 8 doses during a 6-week treatment period (2x/week during the first 2 weeks and then weekly for 4 weeks; MAD). In total, 796 plasma concentrations, 437 FB observations and 288 AH50 observations (measured with the AH50 hemolytic assay) were included in the analysis. The median subject was a 45-year 84-kg male. The PK-PD model was estimated simultaneously using NONMEM 7.4.1.

Results:

A two-compartment PK model with first-order absorption and linear elimination and two parallel indirect response models were found to describe well the longitudinal PK, FB and AH50 data. Body weight was implemented on the PK disposition parameters. The estimated k_a was 1.3 h⁻¹, and the derived disposition half-lives were $t_{1/2 \alpha}=4.7$ hours and $t_{1/2 \beta}=35$ days (inter-individual variability in estimated primary parameters 15%-50%CV, residual error 27%CV). The post-dose decreases in FB and AH50 levels were described using two structurally independent indirect response models with an Imax drug effect affecting the input. A body weight effect was identified on the estimated baseline FB and AH50 ($p<0.001$; positive relation). For FB, the IC50 was 0.28 ng/mL and the k_{out} 0.0024 h⁻¹, and for AH50 the IC50 was 0.50 ng/mL and the k_{out} 0.0016 h⁻¹. The residual error for FB was 14%CV, and for AH50 was 8.4 IU/mL. All model parameters were estimated with reasonable precision. Simulations using the PK-PD model indicated that to reach an appropriate level of inhibition in FB or AH50 in the median subject (Q2Wx2 + Q4W dosing at steady-state), at least 20 mg or 40 mg, respectively, would have to be administered.

Conclusions:

A population PK-PD model to characterize the PK of IONIS-FB-L_{Rx}, and its inhibitory effect on FB production and AH50 in HV was successfully developed. This model was used to inform the selection of doses and dosing frequency in the clinical development studies of IONIS-FB-L_{Rx} in AMD patients.

References:

- [1] Boyer et al. Retina. 2017 May;37(5):819-835. [2] Reynolds et al. Invest Ophthalmol Vis Sci. 2009 Dec;50(12):5818-27.

THU-042

Simulx-GUI: a flexible, fast and user-friendly application for simulations

Authors: Géraldine Ayral (1), Monika Twarogowska (1), Pauline Traynard (1), Jonathan Chauvin (1)

Affiliations: (1) Lixoft, Antony, France

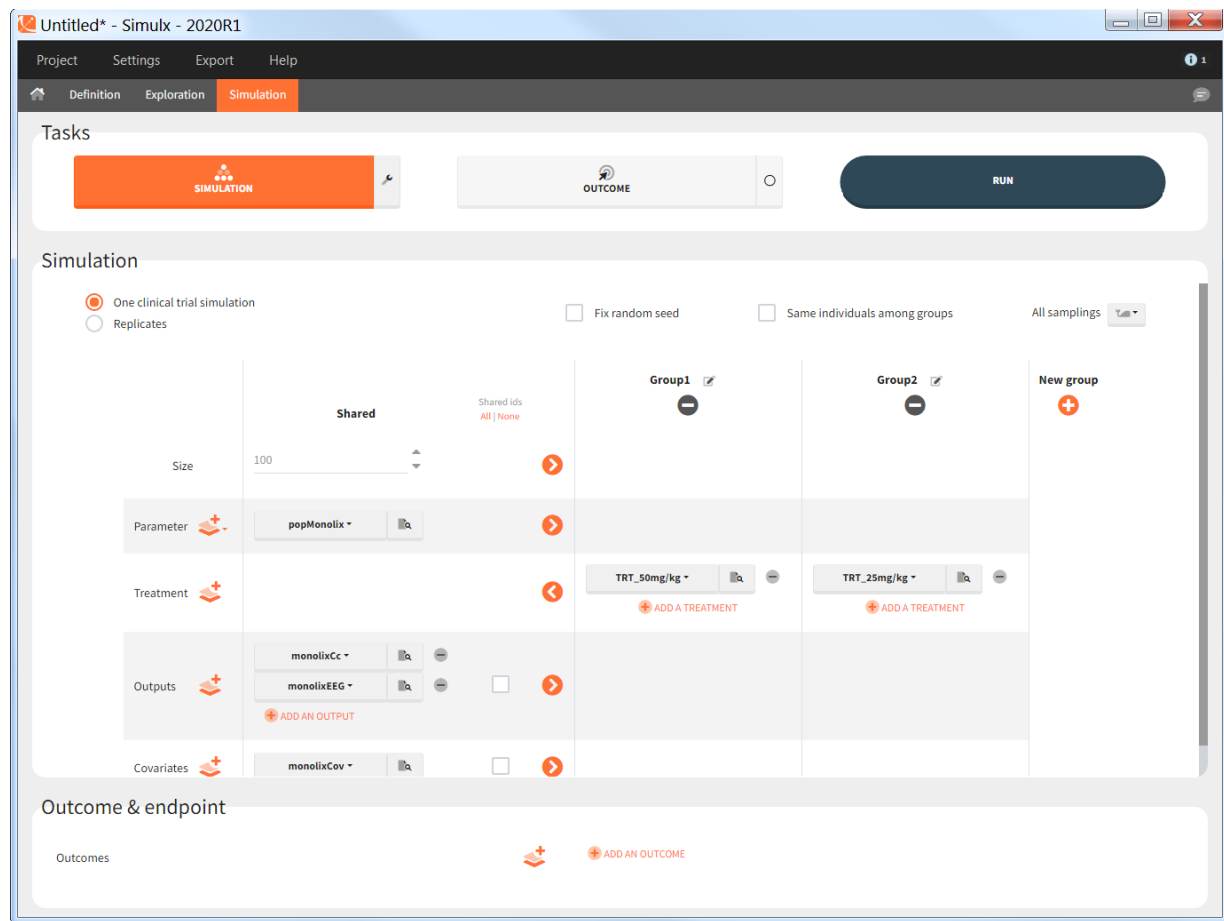
Introduction:

PK/PD models can be used to simulate the expected outcome in new situations such as future clinical trials. We present Simulx-GUI, a tool for advanced simulations integrated within the MonolixSuite. Models estimated with Monolix (population PK/PD) or PKanalix (compartmental analysis) can be exported to Simulx in a single step. Not only will the model itself be exported, but also the estimated population parameters, the EBEs, the treatments and covariates defined in the Monolix data set. These elements can be easily reused for the simulations. The clear interface allows for the definition of new simulations inputs, the setup of the simulation itself and its post-processing. Simulx-GUI uses the same calculation engine in efficient C++ code and same model language as the other applications of the MonolixSuite.

Methods:

The functionalities of Simulx-GUI are illustrated using a PK/PD model for Remifentanil. The goal is to simulate a clinical trial with 2 arms corresponding to two different infusion rates. The Monolix run is first exported to Simulx-GUI. This creates the following elements: the model, the population parameters, the design (treatments and measurement times) of the original data set and the covariates. To setup the simulation, new elements are created. We create two treatment elements by giving the start time, the dose amount and the infusion duration. The model includes covariates, which can be resampled from the original data set, sampled from an external file or defined via a distribution. Two model outputs are defined: the smooth PD prediction over a fine grid and PD measurements (with residual error) at a few time points. The simulation is setup by setting the numbers of arms and individuals and assigning the desired elements to each arm. After running the simulation, plots are automatically generated for all outputs.

We also define an endpoint: the percentage of individuals reaching a target PD interval after 20 minutes. The uncertainty of the endpoint is then assessed via simulation replicates.



Results:

The simulation of the predicted PD shows that 68% of the individuals are within the target interval for the higher infusion rate and 53% for the lower infusion rate.

Conclusion:

Simulx-GUI is a flexible, fast and integrated application for simulations. It can be used to simulate a wide variety of models: population PK/PD (including count, categorical and time-to-event), QSP and PBPK with or without inter-individual and inter-occasion variability. Clinical trial simulations can be easily setup via the definition of arms, outcomes and endpoints. Replicates of the simulations allow to assess the uncertainty of the endpoints and can also incorporate the uncertainty of the population parameters.

THU-043

Modeling Longitudinal Glucose Dynamics to Inform Type 1 Diabetes Prevention Clinical Trial Studies

Juan Francisco Morales¹, Karthik Lingineni¹, Melissa Thomas¹, Patrick Lang², Jagdeep Podichetty², Jackson Burton², Sarah David², Jessica Dunne³, Mark A. Atkinson⁴, Michael J. Haller⁵, Klaus Romero², Inish O'Doherty², Stephan Schmidt¹, Sarah Kim^{1,*}

¹ Center for Pharmacometrics and Systems Pharmacology, Department of Pharmaceutics, College of Pharmacy, University of Florida, Orlando, FL, USA

² Critical Path Institute, Tucson, AZ, USA

³ JDRF, New York, NY, USA

⁴ Department of Pathology and Pediatrics, College of Medicine, University of Florida, Gainesville, FL, USA

⁵ Department of Pediatrics, College of Medicine, University of Florida, Gainesville, FL, USA

* Corresponding author's email: sarahkim@cop.ufl.edu

Objectives: Type 1 Diabetes (T1D) is a chronic autoimmune disease that results from the destruction of insulin-producing beta cells of the pancreas. Currently, there are no approved therapies to prevent or delay the onset of T1D and limitations exist for biomarkers that identify disease progression as well as predict the onset probability of a formal T1D diagnosis. The objective of this analysis is to identify subgroups of the population that differ in disease state and progression through a covariate analysis using longitudinal data following a 2-hour Oral Glucose Tolerance Test (OGTT) value.

Methods: A longitudinal glucose dynamics model was developed based on an extensive individual patient-level data from the NIH TEDDY (0-15 years) and TrialNet TN01 (3-45 years) natural history studies. Following baseline screening, these studies followed volunteers with a high risk of developing T1D by monitoring a series of metabolic, genetic and immunologic tests. After data curation, the final dataset included 2,754 individuals with a total of 15,120 scores. Using a non-linear mixed effects (NLME) modeling approach, the longitudinal progression of the 2-hour OGTT values was quantitatively captured, enabling assessment of inter- and intra-individual variabilities. Candidate factors contributing to the heterogeneity included various quantities and types of autoantibodies, race, family relatives with T1D, ethnicity, C-peptide level, body mass index, age, and the change in glucose level during the 2-hour OGTT test at first visit. The NLME model with stepwise covariate modeling search was developed in Monolix software (version 2019R2).

Results: A linear model structure with a proportional residual error model best captured the time course of the 2-hour OGTT scores. The number of autoantibodies was found to be a significant covariate on the slope parameter which was incorporated using a linear function. The estimated slope parameter was $-0.739 \text{ mg/(dL}\cdot\text{year)}$ with a coefficient of 1.93 for the number of autoantibodies. The slope was steeper as the number of autoantibodies increased. The estimated intercept, i.e. 2-hour OGTT score at time zero, was 112 mg/dL. The 2-hour OGTT value at first visit and the presence of the IA2A autoantibody were incorporated as covariates on intercept using a power function with estimated exponents of 0.673 and 0.0714, respectively. The intercept was higher as the covariates increased.

Conclusions: The number of autoantibodies, in particular IA2A, as well as the 2-hour OGTT values at first visit were identified as clinically relevant covariates for developing T1D. We will now expand this covariate model to a joint model that includes a time-to-event component in order to characterize the transition from healthy to T1D state. Once developed and qualified, this joint model will serve as a tool to optimally design clinical T1D prevention trials.

THU-044

Quantitative Systems Pharmacology (QSP) Model Describing the Local and Systemic Antitumor Response of a Cytokine mRNA Immunotherapy Across Multiple Solid Tumors

Kamau Pierre¹, Lin Lin³, Lore Gruenbaum³, Carissa Young³, Joshua Apgar³, Christian Hotz⁴, Vasiliki Pelekanou², Nicolas Acquavella², Tim Wagenaar², and Spyros K Stamatelos¹

¹Sanofi US Services Inc., Bridgewater, NJ; ² Sanofi US Services Inc., Cambridge, MA; ³Applied BioMath, Concord, MA, ⁴Biopharmaceutical New Technologies Corporation (BioNTech), Mainz, Germany.

Objectives: In contrast to conventional approaches, immunotherapy offers a promising alternative for cancer treatment whereby the therapy engages the immune system instead of directly targeting tumor cells. By various mechanisms of action, immuno-oncology therapies serve to augment the host's immune function and promote effective tumor immune surveillance with various facets of the immune system working in concert to eradicate the tumor. Intratumoral delivery of an mRNA mixture encoding for IL-12sc, IFNa2b, IL-15sushi and GM-CSF cytokines induced pronounced regression in tumor-bearing mice at both local and distal untreated sites. Additionally, in mouse models, the antitumor activity was further enhanced by combining the mixture with anti-PD1 and anti-CTLA4 immune checkpoint inhibitors. Utilizing available data, we have developed a multiscale murine quantitative systems pharmacology (QSP) model that captures the observed preclinical responses for mono- and combo-therapy settings.

Methods: A 7-compartment model was developed to characterize the pharmacokinetic and pharmacodynamic drug responses of treated and untreated tumors, and their corresponding draining lymph nodes. The model simulates local administration of the mRNA therapy at the primary site followed by internalization, translation, and secretion of pro-inflammatory cytokines within the tumor microenvironment. By binding to their corresponding receptors, the released cytokines subsequently promote activation and amplification of tumor-infiltrating lymphocytes (TILs), including CD8+, CD4+ T cells, and natural killer (NK) cells. Primary and abscopal tumor cell killing is modeled to be influenced either directly or indirectly by these mobilized cellular mediators.

Results: Model simulation findings are in alignment with murine preclinical data as they predict enhanced tumor growth suppression with increased doses of the mRNA monotherapy. Furthermore, simulations show an augmented efficacy when combining the mRNA treatment with an anti-PD1 immune checkpoint inhibitor; as observed in the preclinical mouse model.

Conclusions: Our preclinical QSP modeling efforts provide insights into the complex pathophysiology of solid tumors and the dynamic interplay between cancer and immune system components following immunotherapy drug administration. As such, the developed model provides a fundamental platform for probing the therapeutic effects of a variety of cytokine-based immuno-oncology assets.

THU-045

First in Human (FIH) Pharmacokinetic (PK) Prediction of NKTR-255, an IL-15 Receptor Agonist, Based on a Target Mediated Drug Disposition (TMDD) Model

Kavitha Bhasi¹, Palakshi Obalapur¹, Janet Cetz¹, Muhammad Baluom², Xue Snow Ge², Yinyan Tang³, Thomas Chang³, Peiwen Kuo⁴, Brian R. Vuillemenot⁵, Takahiro Miyazaki⁴, Jacqueline A. Gibbons^{1,2}, and Werner Rubas¹

¹Non-Clinical PK, ²Clin Pharm and Quant. Sciences, ³Protein Chemistry, ⁴Research Biology, ⁵Safety Assessment, Nektar Therapeutics, San Francisco, CA

Background: IL-15 is a cytokine that activates and provides expansion benefit to NK and CD8+ T cells and is under clinical evaluation for cancer treatment. Exploiting the therapeutic value of IL-15 has been challenging due to its unfavorable PK properties requiring high daily doses or continuous IV infusion which result in poor tolerability. NKTR-255 is an IL-15 receptor agonist exhibiting improved PK vs recombinant IL-15 in animals, thereby providing sustained pharmacodynamic responses without daily or continuous dosing. A FIH clinical study (NCT04136756) was initiated to evaluate safety and tolerability of NKTR-255 in patients with select hematologic malignancies. Previously we presented a TMDD model designed to predict human drug disposition¹. Here, we compare the predictions from that model to available human PK from Cohort 1.

Methods: NKTR-255 exhibited 2-compartmental TMDD in mice, 2-compartmental linear PK in rats, and 1-compartmental TMDD in monkeys. In the absence of 2-compartmental disposition in monkeys, allometric scaling was confined to central volume (V) and clearance (CL). Allometric scaling exponents across species were 0.973 for V and 1.13 for CL; additionally, a fixed exponent of 0.7 on monkey CL was also explored. For receptor binding parameters (k_{on} , k_{off}) both monkey in vivo and human in vitro estimates were evaluated. Model-derived monkey in vivo internalization rate (k_{int}) was utilized, as human in vitro estimates were not available. Free receptor concentration R_{max} estimates were obtained from monkey PK/PD studies and were also derived from modeling rhIL-15 PK². Modeling was conducted in NONMEM® 7.4.

Results: As of May 14, 2020, PK data were available from the first patient after receiving the first two doses of 1.5 $\mu\text{g}/\text{kg}$ NKTR-255 (intravenous, Q21D). Preliminary modeling showed that human parameter estimates were within or close to the simulation estimates. The human receptor binding k_{on} and k_{off} were comparable to human in vitro estimates of $3.54 \text{ nM}^{-1}\text{hr}^{-1}$ and 0.256 hr^{-1} , respectively. R_{max} was comparable to model derived value from rhIL-15 human PK of 0.0933 nmol/kg . Internalization rate was comparable to k_{int} derived from monkey studies of 0.0112 hr^{-1} . CL was within the range considered for simulations, $0.874\text{--}2.90 \text{ mL/kg/hr}$. V was fixed at the projected estimate of 32.1 mL/kg , due to slight underprediction of V. The observed C_{max} and AUC of 27.5 ng/mL and $398 \text{ ng}\cdot\text{hr/mL}$ were comparable to the predicted estimates of 37.3 ng/mL and $443 \text{ ng}\cdot\text{hr/mL}$, respectively.

Conclusion: The pharmacokinetics of NKTR-255 in an initial cancer patient was adequately predicted by a TMDD model which incorporated in vitro and in vivo animal data. Forthcoming data will further inform the human parameter estimates.

References:

- 1) Bhasi K, et al. ACoP 2018.
- 2) Conlon KC, et al. J Clin Oncol. 2015.

THU-046

Population Pharmacokinetic Modeling of Midazolam to Estimate Efavirenz Induction of CYP3A4/5 in Healthy Individuals

Authors: Kimberly S. Collins¹, Jessica Lu¹, Michael Heathman², Zeruesenay Desta¹

Affiliations: ¹Indiana University School of Medicine, Indianapolis, IN, ²Metrum Research Group, Tariffville, CT

Objectives: Efavirenz has been shown to interact with many drug metabolizing enzymes, impacting the pharmacokinetics of numerous drugs. The aim of this study was to develop a population pharmacokinetic model to determine the extent of efavirenz induction of CYP3A4/5 and the contribution of genetic and non-genetic factors on midazolam pharmacokinetics.

Methods: This study was conducted at the Indiana University School of Medicine Clinical Research Center. Adult men and women volunteers were given 1 mg oral midazolam after single dose efavirenz (600 mg) and steady-state efavirenz (600 mg/day for 17 days). Plasma samples were collected after midazolam dosing. A population pharmacokinetic model was developed using 1149 midazolam concentrations and 1149 1'-hydroxymidazolam concentrations from 70 individuals in NONMEM v7.4 using the SAEM estimation method followed by IMP for calculation of the objective function. Model performance was based on IMP objective function value, evaluation of diagnostic plots and visual predictive checks. Bootstrapping will be performed to determine precision of parameter estimates.

Results: A two-compartment model described both midazolam (with first order absorption) and 1'-hydroxymidazolam concentration data. Covariates included in the final model were CYP3A4/5 genotype, sex, and single dose/steady-state efavirenz dosing on the CL/F of midazolam and weight on the CL/F of 1'-hydroxymidazolam. Steady-state efavirenz induction in CYP3A4/5 metabolism of midazolam was observed. For example, in individuals who were CYP3A5 nonexpressors, CYP3A4 normal metabolizers and male, population predicted apparent oral clearance of midazolam was 32.5 L/hr after single dose efavirenz and 50.9 L/hr after steady-state efavirenz.

Conclusions: The final pharmacokinetic model including CYP3A4/5 genotype, single/steady-state efavirenz, sex, and weight are consistent with known mechanisms of midazolam pharmacokinetics. Further analysis is necessary to determine the impact of CYP2B6 and CYP3A4/5 genotype on efavirenz-mediated induction of CYP3A4/5.

References (if applicable): NA

THU-047

PK and PD modeling and simulation of GX-H9 in the adult patients with growth hormone deficiency

Kwan Cheol Pak¹, Yun Jung Choi², Su Jin Heo³, Hyeong-Seok Lim¹

¹Department of Clinical Pharmacology and Therapeutics, Asan Medical Institute of Convergence Science and Technology, Asan Medical Center, University of Ulsan College of Medicine, Seoul, Republic of Korea; ²Genexine Inc., Seongnam, Republic of Korea; ³Handok Inc., Seoul, Republic of Korea.

Objective:

GX-H9, as long-acting preparation for improved compliance of patients with adult growth hormone deficiency (AGHD), was developed. The major purposes of this study were followed as: 1) To describe the pharmacokinetic (PK) and pharmacodynamic (PD) profile of GX-H9; 2) To explore appropriate starting dose of GX-H9 and the criteria of dose increase/decrease of GX-H9 adopted in the simulation; 3) To predict the sampling time for IGF-1 SDS (Standardized Insulin-like Growth Factor 1 Score) close to average IGF-1 SDS after dosing of GX-H9 at steady state for the purpose of design of phase 3 clinical trial.

Methods:

The serum GX-H9 and IGF-1 concentration data used in this modeling analysis were from the phase 1b/2 study [1]. PK-PD modeling and simulation analyses were conducted using NONMEM® (version 7.4.3) [2]. IGF-1 SDS was simulated by two groups (Group 1 : older male, Group 2 : female who did not take estrogen and younger male) according to the PK-PD model based on the predicted serum IGF-1 level. The starting dose and the degree of dose adjustment were determined by simulations (1,000 replicates) where the IGF-1 SDS is expected to be within the target range (-0.5 SDS ~ 1.5 SDS) [3] in majority of patients. In another simulation study (1,000 replicates), we decided a single sampling time point for IGF-1 SDS which is possible to predict the average IGF-1 SDS at steady state.

Results:

Two-compartmental linear model with mixture of structural model where majority of the parameters were described by mixture models described the PK data well. The PD model was implemented using an indirect response model. The simulation suggests that the appropriate starting dose was 9.547 mg for group I and 16.46 mg for group II. The appropriate doses for increase and decrease during dose adjustment were respective 12.412 mg and 4.966 mg for group I and 14.322 mg and 5.730 mg for group II. The proper sampling times after the last dosing for the prediction of average IGF-1 SDS at steady state was 112 hour (90% PI, 58 - 169 hour) for group I and 116 hour (90% PI, 47 - 169 hour) for group II, respectively.

Conclusions:

We successfully constructed the PK-PD model for GX-H9 and IGF-1 using phase 1b/2 study. The sampling time for IGF-1 SDS will help predict the average IGF-1 SDS to adjust doses, and provide a lot of useful information for designing the future phase 3 clinical trial for GX-H9.

References

- [1] Ku CR, Brue T, Schilbach K, et al. Long-acting FC-fusion rhGH (GX-H9) shows potential for up to twice-monthly administration in GH-deficient adults. Eur J Endocrinol. 2018 Sep;179(3):169-179.
- [2] Beal SL et al. 1989-2011. NONMEM Users Guides. Icon Development Solutions, Ellicott City, Maryland, USA.
- [3] <https://clinicaltrials.gov/ct2/show/NCT01225666>

THU-048

Pharmacokinetics of buprenorphine in pregnant women with opioid use disorder

Larissa Lachi Silva¹, Misty L McDowell¹, Mary P Abernathy¹, Andrea R Masters¹, Christine Bach¹, Sara K Quinney¹

¹Indiana University School of Medicine, Indianapolis, IN, USA.

Objectives: Buprenorphine (BUP) is approved by US Food and Drug Administration to treat opioid addiction. BUP is preferred to methadone for opioid maintenance therapy in pregnancy because it has been shown to result in less severe neonatal abstinence syndrome. There is a lack of studies about BUP pharmacokinetics in pregnancy. The current dose recommendation of BUP for pregnant women is based on posology designed for the nonpregnant subject. However, some pieces of evidence suggest a decrease in BUP exposure due to high clearance induced by pregnancy. The objective of this study was to assess the population pharmacokinetics of BUP in pregnant women.

Methods: Pregnant women ($n = 34$) in the third trimester of singleton gestation, using BUP for opioid use disorder, with total daily doses ranging from 2 to 24 mg, were enrolled following informed consent. Blood was withdrawn prior to dosing and at 0.25, 0.5, 1, 2 and 4 hours after the morning dose of BUP. Plasma samples were analyzed by LC-MS/MS to quantify BUP. Plasma concentration profile data were analyzed using Stochastic Approximation Expectation Maximization (SAEM) followed by importance sampling methods implemented on Monolix 2019R2. The effects of estimated gestational age (EGA) and body mass index (BMI) were evaluated as covariates. The model selection was based on goodness-of-fit plots, precision of estimations and by changes in Bayesian information Criteria (BIC) and log-likelihood ratio (LRT).

Results: The model with one-compartment, first-order absorption, proportional error and exponential inter-individual variability on clearance (CL/F) and apparent volume of distribution (Vd/F) was the most suitable for this dataset. Population estimates were absorption rate constant (ka) of $2.77 \pm 0.823 \text{ h}^{-1}$, CL/F of $201 \pm 32.2 \text{ L/h}$ and Vd/F of $8820 \pm 1760 \text{ L}$. No correlations were identified between CL/F or Vd/F and EGA or BMI.

Conclusions: A better understanding of BUP exposure in pregnancy is a requirement to optimize the treatment of opioid use disorder in this population to avoid withdrawal symptoms and decrease the frequency of neonatal syndrome disorder. Studies using NCA have already shown that pregnant women had lower AUC compared with non-pregnant. The population model showed an increase of BUP clearance in pregnant women and, consequently, lower exposure. Corroborating with NCA analysis, this population pharmacokinetics model also indicates that doses adjustment of BUP may be required during pregnancy

Population Pharmacokinetic analysis of the next generation oral SERD AZD9833 in women with ER-positive, HER-2 negative advanced breast cancer

Li Zhang¹, Tim Brier², Richard Mather², Justin P O Lindemann², Teresa Klinowska², Andy Sykes³

¹CPQP, Clinical Pharmacology and Safety Sciences, R&D, AstraZeneca, Boston, USA; ²Research and Early Development, Oncology R&D, AstraZeneca, Cambridge, UK; ³CPQP, Clinical Pharmacology and Safety Sciences, R&D, AstraZeneca, Cambridge, UK

Objectives : AZD9833 is a next generation oral selective estrogen receptor (ER) antagonist and degrader (SERD)¹ that has shown antitumor efficacy in a range of preclinical xenograft models of breast cancer. The first-in-human study (SERENA-1; NCT03616587) evaluating AZD9833 as monotherapy and in combination with CDK4/6 inhibitor palbociclib in pre-menopausal and post-menopausal women with advanced ER-positive HER2-negative breast cancer is ongoing². This analysis aimed to develop a population pharmacokinetic (Pop PK) model for AZD9833 and assess the influences of intrinsic and extrinsic factors on AZD9833 PK in patients with ER-positive, HER2-negative advanced breast cancer (ABC).

Methods : The Pop PK model was developed using plasma concentrations of AZD9833 in ABC patients after receiving once daily (QD) oral administration of AZD9833 monotherapy across doses ranging from 25 to 450 mg in the ongoing Phase 1 study. Forward selection and backward elimination were used to evaluate the following covariates: demographic (weight, age), lab (renal/hepatic function), disease severity (ECOG) and concomitant medication (i.e. proton pump inhibitors (PPIs)). Model development was conducted in NONMEM® (version 7.3.0) and the final model was validated by visual predictive checks and bootstrap.

Results : The final Pop PK model development dataset included 57 ABC patients with 1126 concentrations of AZD9833. The longitudinal PK profile of AZD9833 after multiple oral QD dosing was adequately described by a two-compartment model with linear elimination plus first order absorption in ABC patients. The population estimates of the key PK parameters were precisely estimated and were : mean apparent clearance of 79.4 L/hr (8.11 %RSE) with moderate inter-individual variability of 41.3 %CV (%22.9% RSE). None of the covariates are statistically significant. Model-derived Bayesian exposure at steady-state (Day 15) was not correlated with demographic (weight [ranged 44 – 108 kg], age [ranged 39 – 79 years]), lab (renal [eGFR ranged 45 – 120 mL/min/1.73 m²] / hepatic function [mild hepatic impairment plus normal hepatic function]), disease severity (ECOG) or concomitant medication (PPIs).

Conclusion : The Pop PK model adequately described AZD9833 PK in ABC patients and enabled robust prediction of individual patient exposure in support of potential dose justification decisions for special populations.

References :

1. Jamie Scott. Small-molecule estrogen receptor degraders (SERDs): Chemical exploration and optimisation at AstraZeneca. ACS National Meeting, *San Diego*, USA, 2019
2. Hamilton E, Oliveira M, Banerji U, et al. A Phase 1 Dose Escalation and Expansion Study of the Next Generation Oral SERD AZD9833 in Women With ER-Positive, HER2-Negative Advanced Breast Cancer. 2020 ASCO Annual meeting, Chicago, USA.

THU-050

A QSP model of neurofilament trafficking in SOD1 Amyotrophic Lateral Sclerosis

Alessio Paris¹, Pranami Bora¹, Silvia Parolo¹, Michael Monine², Xiao Tong², Satish Eraly², Alex McCampbell², Danielle Graham², Toby Ferguson², Stephanie Fradette², Enrico Domenici^{1,3}, Ivan Nestorov², Luca Marchetti¹

¹Fondazione The Microsoft Research - University of Trento Centre for Computational and Systems Biology (COSBI);

²Biogen, Inc., Cambridge, Massachusetts, USA; ³University of Trento, Department of Cellular, Computational and Integrative Biology - CIBIO

Objectives: Amyotrophic Lateral Sclerosis (ALS) is a neurodegenerative disease characterized by elevated levels of neurofilament light (NFL) and heavy (NFH) chains in blood and cerebrospinal fluid (CSF) [1]. Mutations in the *SOD1* gene are the second most common genetic cause of ALS, with high variability in the rate of disease progression depending on the causative mutation. The study aims to develop a Quantitative System Pharmacology (QSP) model of SOD1-ALS for evaluating the potential of NFs as early biomarkers of disease onset and treatment effect.

Methods: The model was implemented as a set of Ordinary Differential Equations (ODEs) describing the trafficking of NFs from the nervous system to the periphery (see Figure). In addition to literature data, NF concentrations in CSF and blood from a randomized, placebo-controlled single and multiple ascending dose Phase I/II study of tofersen (BII067), an antisense oligonucleotide (ASO) being investigated for the treatment of SOD1-ALS, were used to calibrate the model. To consider the difference in rates of disease progression in patients with SOD1-ALS mutations typically associated with slower or faster disease progression, two patient groups were defined *post hoc* for the purposes of analysis. The model was then validated by assessing its capability to simulate a set of treatment scenarios previously excluded from the calibration. NF concentrations in CSF and blood from longitudinal natural history and biomarker studies on ALS mutation carriers [1,2] were also used to define and parametrize a function reproducing NF time-series data of disease progression.

Results: The model was calibrated to fit the experimental data of NFL and NFH from healthy subjects and SOD1-ALS patients with different disease progression rates in both untreated and treated conditions. The computed parameter estimates indicate a 10-fold higher rate of NF release from diseased neurons in patients with faster rates of disease progression. Moreover, the model accurately predicts the reduction of NF concentration in the periphery after a multiple dose administration of tofersen (100 mg) in subjects with faster disease progression. Average peripheral NF concentration in healthy subjects was used as a threshold that may potentially be exceeded in SOD1-ALS patients.

The model enables to predict the time from the moment of exceeding this threshold to the onset of symptoms, thus suggesting NFs as a possible biomarker for pre-symptomatic diagnosis of ALS.

Conclusions: We present a QSP model of NFL and NFH trafficking in untreated and treated SOD1-ALS patients. The predictive model performance makes it a valuable tool for investigating NFs as biomarkers of disease progression and treatment response in SOD1-ALS and for *in silico* evaluation of novel treatment protocols.

References

- 1 Benatar et al. Amyotrophic Lateral Sclerosis and Frontotemporal Degeneration 20:538–548, 2019.
- 2 Benatar et al. Annals of Neurology 84:130–139, 2018.

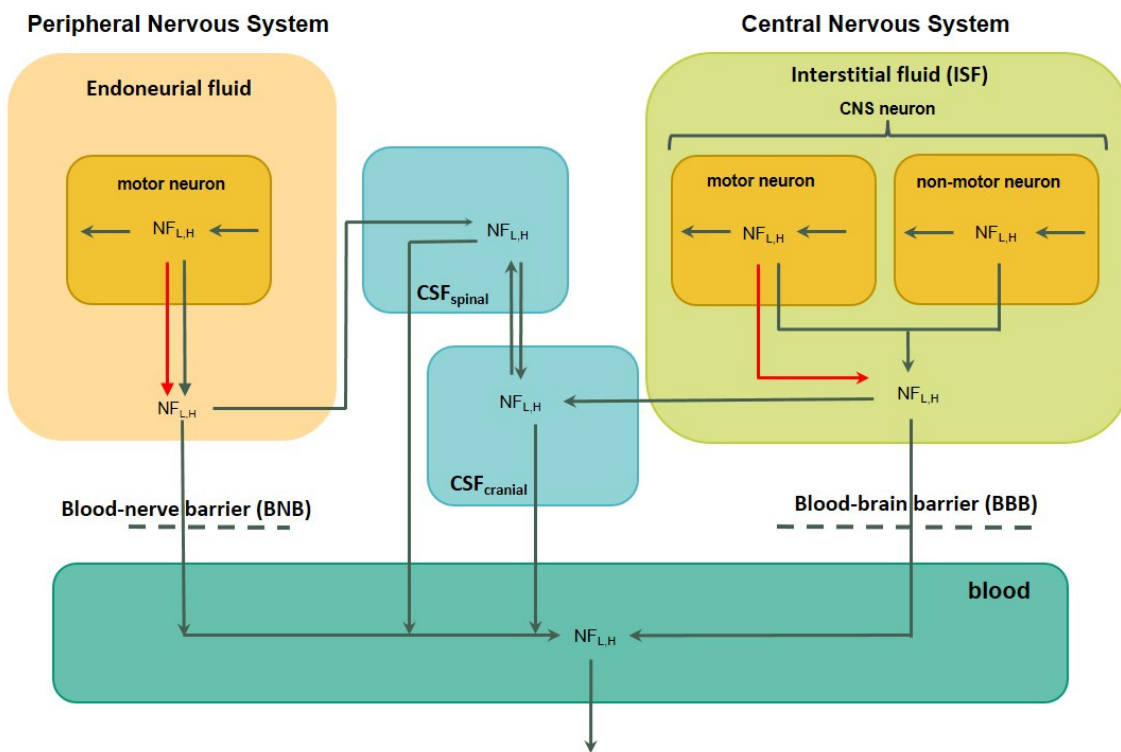


Figure 1: Model scheme of NF trafficking in SOD1 Amyotrophic Lateral Sclerosis. Red arrows indicate the NF additional release from neurons due to the disease.

THU-051

A multivariate hybrid approach for exposure-response analysis of oncology treatments using machine learning classifiers and population pharmacokinetic modeling

Maitreyee Bose¹, Alicia Kaestli², Sandeep Dutta³, Khamir Mehta¹

¹Clinical Pharmacology Modeling and Simulation, Amgen Inc., South San Francisco, CA

²Digital Health and Innovation, Amgen Inc., Thousand Oaks, CA

³Clinical Pharmacology Modeling and Simulation, Amgen Inc., Thousand Oaks, CA

Background:

Multivariate machine learning approaches offer a powerful way to model and predict discrete pharmacodynamic (PD) events, for example, the use of tree-based classification methods can be used for modeling discrete adverse events or efficacy of cancer treatments as a function of pharmacokinetics (PK) and specific patient attributes. These exposure-response analyses are critical to the selection of the optimal dosing regimen of oncology drugs. However, direct use of PK exposure metrics can be plagued by the limitations of the study design and may be sparse, noisy, or missing.

Objectives:

In this poster, we develop and demonstrate the utility of a hybrid multivariate analysis methodology incorporating PK model driven inputs into machine learning models to improve the accuracy of exposure-response relationships

Methods:

The workflow associated with our proposed method is outlined in Figure 1. By inclusion of a population PK model as the source of the PK predictors, we anticipate significant improvement in the predictive capability of the exposure-response models.

We demonstrate the performance of our method using several simulated examples and comparing the performance of our approach (hybrid), traditional approach, and the ground truth. Specifically, we use both binary and ordinal outcome variables to simulate the PD. For the underlying model governing the PD outcomes, we assume models with increasing complexity, for example, linear logistic to non-linear and non-monotonic models with correlated patient specific predictors. The PK model is assumed to be compartmental, while the study design is assumed to reflect a typical phase 3 design. We employ random forest-based methods to model the PD; random forests are powerful tools when there are multiple interacting predictors whose relationship with the outcome is not explicitly known. The PK model is developed using a population approach with NLME modeling in NONMEM.

We systematically evaluate the performance of each of the above scenarios by varying the PK properties, i.e., the between subject variability, the model residual variability and finally the resolution of the observed data.

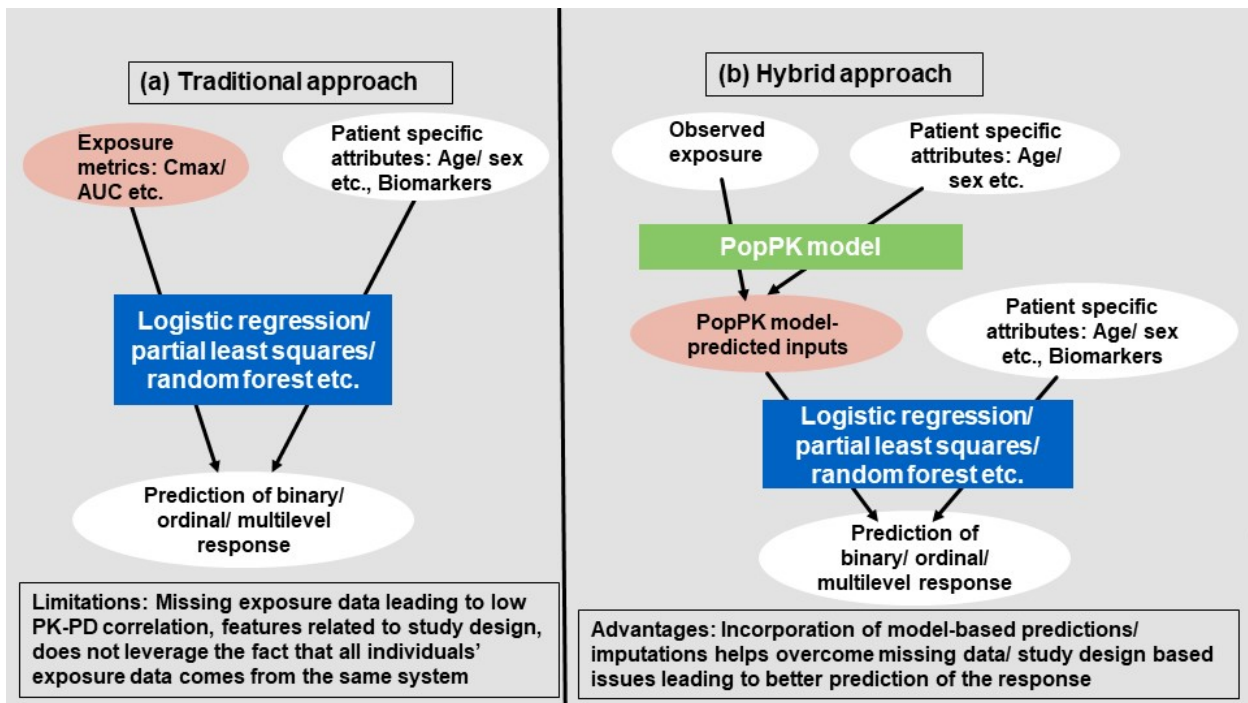
Results:

Preliminary results indicate that the hybrid method outperforms the traditional approach in scenarios with moderate to high between subject variability ($> 40\%$). Situations with sparse data and complexity of the exposure-response relationship also warrant the hybrid approach. We showcase the robustness of the approach by exploring the prediction accuracy across the scenarios mentioned above.

Conclusions:

We have developed a novel multivariate hybrid approach for improved characterization of exposure-response analysis of oncology treatments, that leverages information across the individuals and efficiently integrates diverse predictor variables.

Figure 1: (a) Traditional PD prediction using observed PK. (b) Hybrid PD prediction using model-predicted PK.



THU-052

A Method to Estimate TTP from Summary Level OS and PFS Data: An Example of Use of TTP to Compare Treatments Based on Published Literature for NSCLC Patients Receiving Immune Checkpoint Inhibitors

Mario Nagase¹, Sameer Doshi¹, Sandeep Dutta¹, Chih-Wei Lin¹

¹Clinical Pharmacology Modeling and Simulation, Amgen, Thousand Oaks, CA, USA

Objectives: Summary measures such as progression-free survival (PFS), and overall survival (OS) are commonly reported in literatures for oncology trials, while time to progression (TTP), another key surrogate endpoint, is not usually reported. Since PFS events include not only disease progression but death, it is difficult to separate TTP from PFS and PFS is not interchangeable with TTP. Capturing TTP, a direct measure of treatment effects on cancer growth, would be helpful for researchers to better understand how drugs delay tumor growth. A time-variant transition hazard model was developed to estimate TTP from summary level PFS and OS and applied to published immune checkpoint inhibitor trials for non-small cell lung cancer (NSCLC).

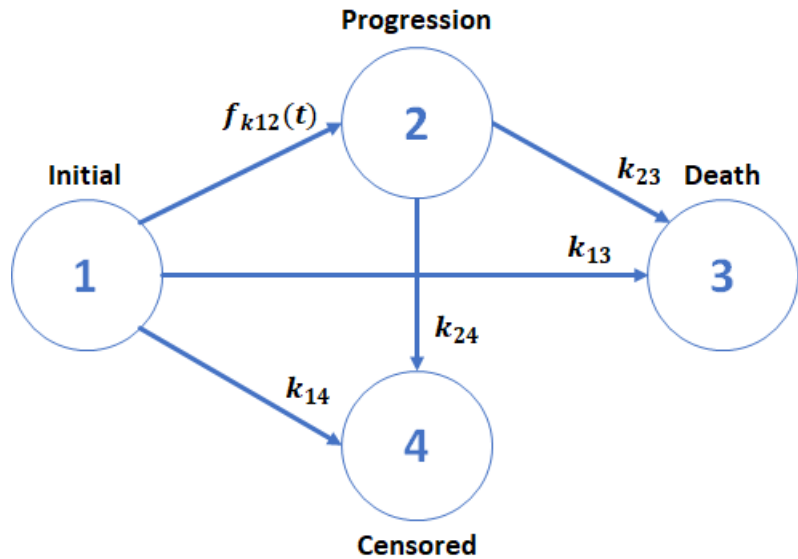
Methods: Publications on immune checkpoint inhibitors for NSCLC were extracted from PubMed, www.clinicaltrials.gov, company registries, conference abstracts/posters/presentations, and regulatory reviews from FDA. The analysis dataset comprised of 19 studies consisting of 32 arms with a total of 6,676 patients, and included PD-1 (pembrolizumab, nivolumab), PD-L1 (atezolizumab, durvalumab), and CTLA-4 (ipilimumab) inhibitors as monotherapies or combination therapies. Kaplan-Meier plots from publications were digitized by month, and the number of patients at risk over time was compiled. A time-variant transition hazard model assuming the states 1) INITIAL, 2) PROGRESSION, 3) DEATH, and 4) CENSORED was developed (Figure). Progression hazard (k_{12}), death hazard due to progression (k_{23}), death hazard without progression (k_{13}), censor hazard (k_{14}), and censor hazard after progression (k_{24}) were estimated. Time-variant rate was set to progression rate, and random effects (between study and arm) were evaluated. All the parameters and the latent variables for the number of patients at risk at each month were estimated.

Results: The time-variant transition hazard model optimally characterized the survival probability and number of patients at risk for both PFS and OS. PD-1 monotherapy provides better OS and PFS, and longer TTP than chemotherapy alone. The estimated TTP for PD-1 ranges from 4.9 to 11 months, longer than the estimated 3.4-8.2

months for chemotherapy. Within PD-1 monotherapies, nivolumab yielded similar to slightly shorter TTP compared to pembrolizumab. PD-1 combined with chemotherapy or other targeted therapy generally had longer TTP than PD-1 monotherapy .

Conclusions: OS and PFS implicitly conveys information about TTP. This model-based method was able to estimate TTP from summary level OS and PFS data and provided a quantitative approach for understanding the patterns of disease progression across treatments through the time-variant disease progression rate function and summarize how different immune checkpoint inhibitor treatments delay TTP. The method can be applied to the other therapeutic areas in oncology.

Figure: Model Schematics



$f_{k12}(t)$: time-variant piecewise hazard function to progression

THU-053

**A Quantitative Systems Pharmacology Modeling Platform for Evaluating Triglyceride Profiles
in Patients with High Triglyceride under Evinacumab Therapy**

Jim Bosley¹, Lyn Powell^{1,3}, Feng Yang², Xia Pu², Nidal Huniti², John D. Davis², Yi Zhang² and
Masood Khaksar Toroghi²

¹Clermont, Bosley LLC, Kennett Square, PA, ²Regeneron Pharmaceuticals, Tarrytown, NY,

³Lynx Bioconsulting, Monmouth, OR

Objectives: The objective of this work is to evaluate lipid trafficking, specifically to understand the mechanism of action and predict the transient responses of different TG-rich particles to modulation of lipoprotein lipase (LPL) activity by Evinacumab, a mAB whose cognate ligand is ANGPTL3 using a quantitative systems pharmacology (QSP) modeling approach.

Methods: A QSP lipid modeling platform was created, based on a previously published lipid model ¹ containing only two plasma triglyceride (TG) compartments: meal-derived chylomicrons and hepatically derived very low-density lipoproteins (VLDL). The published model was augmented and changed to address specific questions relevant to the development of Evinacumab. Intermediate and low-density lipoprotein (IDL and LDL) TG compartments were added to account for TG uptake and particle progression. The effects on LPL activity of modulating ApoCIII activity with siRNA therapy, and a target mediated drug disposition (TMDD) model were included in the model. In addition, ANGPTL3 biosynthesis, clearance, and wall bound compartments were also included.

The particle mass balance approach captured the time profiles of fitted clinical plasma TG data well and predicted the TG profiles for other trials not used in fitting. Initial attempts to use LDL-TG to estimate LDL-cholesterol were less satisfactory, as these simpler models did not account for known mechanisms of particle update. Biological insight lead to improved LDL-cholesterol estimation, by adding receptors to

peripheral tissue to represent whole particle TG-rich particle uptake to the model's existing incremental TG uptake via LPL. Virtual patients were created to represent several classes of subject phenotypes. The model was developed using SimBiology® with Matlab scripting.

Results: The developed QSP model allows stable (>1 year) and accurate representation of plasma TG, glucose and insulin, both in the absence and presence of anti-ANGPTL3 mAB. Model results agreed well with the clinical data that were published in the original article describing the base model¹, as well as with other published and in-house clinical data. Explicit treatment of multiple receptors and LPL action supported facile generation of different virtual patients. Anti-ApoCIII siRNA simulation results agreed with published data.

Conclusions: Simulations from a TG-driven QSP model with novel accounting for TG accurately matched TG profiles for a variety of subject types, both for placebo and evinacumab-treated subjects. Appropriate representation of LPL-driven and particle uptake-related TG uptake allowed estimation of therapy effects on cholesterol from this TG model. A physiologically based TMDD model allowed representation of and prediction of trial mAb, ANGPTL3, and TG. The TMDD approach also allowed inference of unmeasured quantities of interest (e.g., free ANGPTL3). Adding alternate therapies (ApoCIII siRNA) replicated clinical trial data, further enhancing confidence in the model. Finally, a modeling platform was developed that represented TG physiology and drug effect in a range of patient populations with varying levels of TG and/or cholesterol, allowing testing of different hypotheses.

References:

- (1) Pratt, A. C.; Wattis, J. A. D.; Salter, A. M. Mathematical Modelling of Hepatic Lipid Metabolism. *Math. Biosci.* **2015**, 262, 167–181. <https://doi.org/10.1016/j.mbs.2014.12.012>.

THU-054

Individual Risk Prediction Using Machine Learning Approaches in Cardiovascular Outcomes Trials

Matthew C. Pharris¹, Lindsay E. Clegg², Robert J. Mentz³, Rury R. Holman⁴, William R. Hiatt⁵, Manesh Patel⁶, Robert C. Penland¹, David W. Boulton²

¹Clinical Pharmacology & Safety Sciences, R&D, AstraZeneca, Boston, USA;

²Clinical Pharmacology & Safety Sciences, R&D, AstraZeneca, Gaithersburg, USA;

³Duke University and Duke Clinical Research Institute, Duke University School of Medicine, Durham, NC, USA;

⁴Diabetes Trials Unit, University of Oxford, Oxford, UK;

⁵University of Colorado School of Medicine, Division of Cardiology and CPC Clinical Research, Aurora, CO, USA;

⁶Division of Cardiology, Duke University Health System, USA

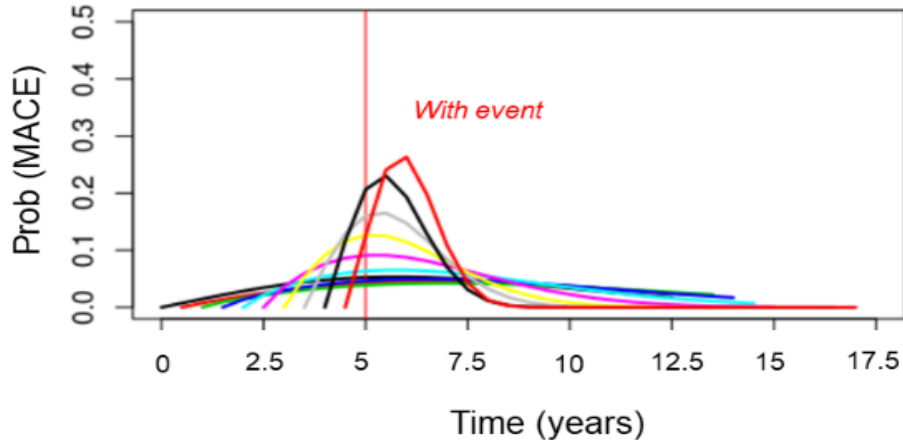
Objectives: A risk calculator for predicting cardiovascular (CV) events in individual patients may aid in personalizing treatments and optimizing patient cohorts for clinical trials. However, existing CV risk calculators are built routinely on data from less diverse patients and many perform poorly for particular patient subgroups such as people with type 2 diabetes (T2DM). Machine learning (ML) may improve on existing CV risk calculators, but it requires extensive training data and predicts risk poorly for low frequency outcomes of interest, such as major cardiovascular events (MACE). To compile sufficient training data, we pooled two CV outcomes trials that included nearly 20,000 multinational T2DM patients. We used these data to train an ML model to generate event time distributions that predict n-year MACE risk for individual patients.

Methods: Model development involved covariate selection, trial dataset pooling, data pre-processing, and model training using data from the large-scale EXSCEL (NCT01144338) and EUCLID (NCT01732822) CV outcomes trials. Covariate selection was based on characteristics broadly categorized as baseline, medical history, biomarker, concomitant medication, or adverse event covariates. Covariates selected from the two trials were identical wherever feasible. Thus, for trial dataset pooling, if a covariate appeared in only one study, then in the other we introduced placeholder values. Placeholder and missing values were imputed, and complemented with binary, indicator covariates. We pre-processed by regularizing patient-observations to the nearest three-month time-point; standardizing each covariate; and balancing patients with and without observed MACE, fulfilling the requirements our neural network-based ML algorithm.

We used the pooled data to train a recurrent neural network (RNN) to predict Weibull distributions of time-to-event (WTTE). Specifically, because ML predictions of discrete event times are error-prone, our model instead generates event time *distributions* estimating an individual patient's future risk of MACE.

Results: The model generated individual MACE probabilities over time. The figure shows how successive observations for the same patient (each trace) yielded sharpening distributions about their true MACE event time of 5 years (vertical red line). With such predictions, we estimated all patients' event times and then constructed population survival curves. Indeed, for a preliminary model trained on EXSCEL data alone, comparing predicted and true survival curves using the log-rank test (given five observations of each patient) yields a p-value of 0.21, suggesting agreement. Moreover, the preliminary model distinguishes between low and high risk of MACE, predicting 5-year MACE occurrence with a C-index of 90.9%, again suggesting strong model performance.

Figure 1: Predicting Individual Risk



Conclusions: Our methods for pooling datasets and predicting event time distributions shows how ML can be used to predict individual MACE risk from longitudinal clinical covariates. In the future, it may be possible to use this model to support individualized treatments, optimize clinical trial cohorts, or quantitatively explore alternative disease treatment strategies.

THU-055

Model-Informed Benefit Risk Assessment of Nivolumab 480 mg Every 4 Weeks across Multiple Tumor Types in Japanese Patients

Mayu Osawa¹, Vijay D. Ivaturi², Shinji Uemura³, Kazuyuki Yamada³, Mathangi Gopalakrishnan², Joga V.S. Gobburu², Takayo Ueno¹, Amit Roy⁴, Xiaochen Zhao⁴

¹Bristol-Myers Squibb K.K., Tokyo, Japan; ²University of Maryland, Baltimore, MD, USA; ³Ono Pharmaceutical, Osaka, Japan; ⁴Bristol-Myers Squibb, Princeton, NJ, USA

Objectives: Flat dosing regimens of nivolumab 240 mg every 2 weeks (Q2W) and 480 mg every 4 weeks (Q4W) are approved in the US, EU and several other markets to provide more flexible options than the initially approved 3 mg/kg Q2W regimen utilizing upon model-based assessment [1,2]. In Japan, nivolumab 3 mg/kg Q2W and 240 mg Q2W are approved for multiple tumor types. To assess the benefit-risk of nivolumab 480 mg Q4W in Japanese patients, model-based approach was used by leveraging robust characterization of nivolumab pharmacokinetics and exposure-response (E-R) relationships for efficacy and safety.

Methods: Nivolumab exposures for 3 mg/kg Q2W, 240 mg Q2W, and 480 mg Q4W were simulated for 420 Japanese patients across tumor types using a previously established population pharmacokinetic model of nivolumab [3]. The qualified E-R models for efficacy and safety [4] were used to predict the responses for the 3 dosing regimens for Japanese patients across tumor types. The time-averaged concentration over the first 28-days of treatment (Cavgd28) was selected for the primary analyses of E-R. Sensitivity analyses were conducted using trough concentration at Day-28 (Cmind28) for efficacy, and the peak concentration after the first dose (Cmax1) for safety. E-R relationships were characterized using a Cox proportional hazard model for efficacy, and a logistic regression model for safety.

Results: Predicted nivolumab Cavgd28 with 480 mg Q4W in Japanese patients was higher than that with 3 mg/kg Q2W (~72%) and 240 mg Q2W (~21%). Predicted Cmax1 for 480 mg Q4W was higher than 3 mg/kg Q2W (~185%) and 240 mg Q2W (~100%), while Cmind28 was comparable with 3 mg/kg Q2W (~6%) and lower than 240 mg Q2W (~25%). The predicted safety profiles with the 3 dosing regimens differed by ≤4% across tumor types for adverse events leading to discontinuation/death, adverse events of Grade 3 or higher, or immune-mediated adverse events of Grade 2 or higher. The predicted probability of survival and achieving a response for nivolumab 480 mg Q4W were similar to those for 3 mg/kg Q2W or 240 mg Q2W. Results of sensitivity analyses were consistent with the E-R analyses with Cavgd28.

Conclusions: Given the established flat E-R relationships for nivolumab, safety and efficacy outcomes achieved with 480 mg Q4W are predicted to be similar to 3 mg/kg Q2W and 240 mg Q2W. Based on the quantitative clinical pharmacology approach, the less frequent dosing regimen of nivolumab Q4W is expected to produce similar benefit-risk profile compared to the approved Q2W regimens, and to be an alternative treatment option for Japanese patients.

References: [1] Zhao et al., *Ann Oncol.* 2017;28(8):2002-2008. [2] Zhao et al., *Ann Oncol.* 2020;31(2): 302-309. [3] Bajaj et al., *CPT Pharmacometrics Syst Pharmacol.* 2017;6(1):58-66. [4] Bei et al., *Cancer Sci.* 2020;111(2):528-35.

Sensitivity analysis framework for assessing drug target probability of success in early drug discovery

Michael Vilkovoy¹, Jangir Selimkhanov¹, Erica L. Bradshaw¹

¹Quantitative Solutions, Quantitative Translational Sciences, Takeda Pharmaceuticals Inc., San Diego, CA, USA

Objectives: Identifying a biological target that can modulate a pathway that results in a therapeutic effect is the foundation for a successful drug discovery program. However, biological pathways are highly interconnected and complex. Thus, successfully identifying the appropriate therapeutic target in a pathway is often unintuitive and difficult to predict. Approaches such as genetics, proteomics, bioinformatics, etc., are often used to identify targets but, these methods often lack mechanistic descriptions of the pathway [1]. Here, we provide a sensitivity analysis framework to enable target prioritization and guide future experiments to increase our confidence in target selection.

Methods: A mechanistic model of a prototypical inflammatory pathway was built as a proof-of-concept. The model structure consisted of 17 parameters and 4 potential targets. We then generated an ensemble of parameter sets using Sobol sequencing. The ensemble was used to assess the modulation of the inflammatory signal with the inhibition or activation of each potential target. The magnitude of reduction in the inflammatory signal relative to no treatment was defined as the therapeutic effect of each target. The targets were scored by their probability of success compared to the other targets across the ensemble and ranked according to their therapeutic effect. In parallel, the framework identified the most significant parameter towards target selection by examining the variance of reduction in the inflammatory signal across targets. A large variance would yield a more conclusive target choice, whereas a small variance would yield an inconclusive choice (Fig. 1).

Results: The sensitivity analysis framework was used to rank the targets and to determine their theoretical probability of success. Thus, we showed that the number of potential targets can be narrowed down to a select few, even with a poorly parameterized system. Furthermore, the framework identified the parameters that need to be determined experimentally to increase confidence in target selection. Once the identified parameter is measured experimentally,

it can be fixed in the model and the process can then be repeated. With a new ensemble of parameters generated, the framework can reassess the target selection with lower uncertainty compared to the first ensemble.

Conclusions: We present a sensitivity framework that can be used in early drug discovery programs to prioritize biological targets based on a model-predicted therapeutic effect. The framework can be further leveraged to identify the most critical parameter value necessary to achieve the greatest improvement in target selection confidence. This process can be applied iteratively to effectively support drug discovery programs.

References:

1. Paanamen, J. & Fortino, V. *Briefings in Bioinformatics*. (2019).

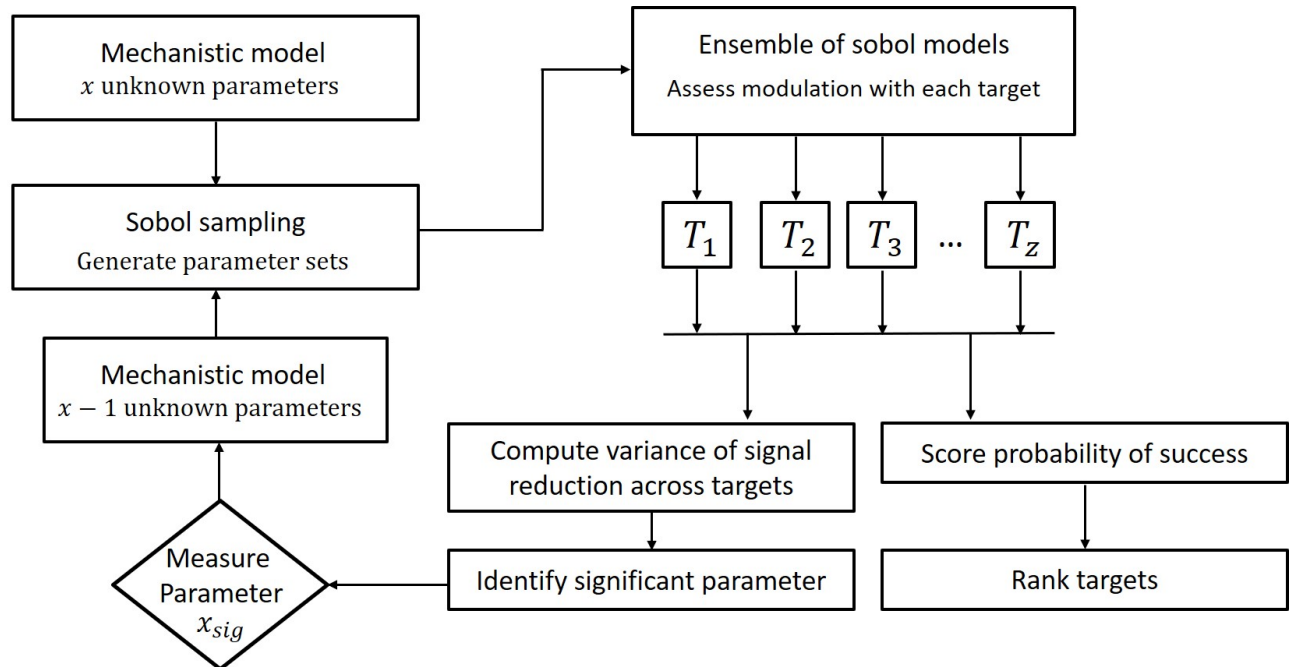


Figure 1: Sensitivity analysis framework for assessing drug target probability of success for early drug discovery.

**QSP modeling predicts higher naloxone doses will safely reverse
more opioid overdoses and save lives.**

Ronald B. Moss¹, Dennis J. Carlo¹, Christina Friedrich², Katherine Kudrycki², Rebecca Baillie², Meghan Pryor², Mike Reed²

¹Adamis Pharmaceuticals Co., San Diego, CA, USA; ²Rosa & Co. LLC, San Carlos CA, USA

Objectives:

The number of deaths due to synthetic opioids has increased dramatically in the last 5 years [1]. Current recommended doses of naloxone for overdose reversal may be inadequate, and redosing is often required. Because of naloxone's use in opioid overdose in a community setting, clinical trials are not possible. The FDA recommended modelling of displacement of potent opioids with naloxone, as one possible avenue for providing justification to support approval of a higher clinical dose to address an unmet medical need.

Methods:

We developed a Mu Opioid Receptor Binding quantitative systems pharmacology (QSP) model with competing drug treatments (naloxone, fentanyl) based on relevant mechanistic data. The model includes detailed mu opioid receptor dynamics, drug pharmacokinetics, drug effect site concentration, and competitive ligand binding. Model parameters such as drug pharmacokinetics, receptor numbers, ligand binding kinetics, and receptor trafficking were identified from literature data.

Results:

The model was developed and qualified, and competitive binding simulations conducted for the synthetic opioid fentanyl and naloxone. At a fentanyl level consistent with a 10 mg trans-dermal dose, naloxone treatment at the current approved dose of 2 mg (intra-muscular) reduces mu receptor occupancy (RO) by fentanyl to just below 50% at 10 minutes post dose. Simulated naloxone treatment at higher doses (5 mg or 10 mg) reduced fentanyl RO to 29% and 17%, respectively, at 10 minutes past treatment. Higher doses of naloxone resulted in a faster fentanyl RO drop. Naloxone treatment of 2, 5, and 10 mg reduced RO below 50% in 10, 4, and 3 min, respectively, after naloxone is dosed. A similar pattern was observed at varying levels of fentanyl concentrations. In all cases, higher-dose naloxone led to greater displacement in a shorter amount of time, strongly suggesting that lives could be saved by the availability of higher-dose naloxone devices.

Conclusions:

Simulations using the Opioid Receptor Binding Platform demonstrate the added utility of higher naloxone doses in displacing fentanyl from the mu receptor. Since a clinical trial is not feasible in this indication, QSP modeling increases confidence in the added utility of the higher-dose naloxone product.

1. Moss, R.B. and D.J. Carlo, Higher doses of naloxone are needed in the synthetic opioid era. *Subst Abuse Treat Prev Policy*, 2019. 14(1): p. 6.

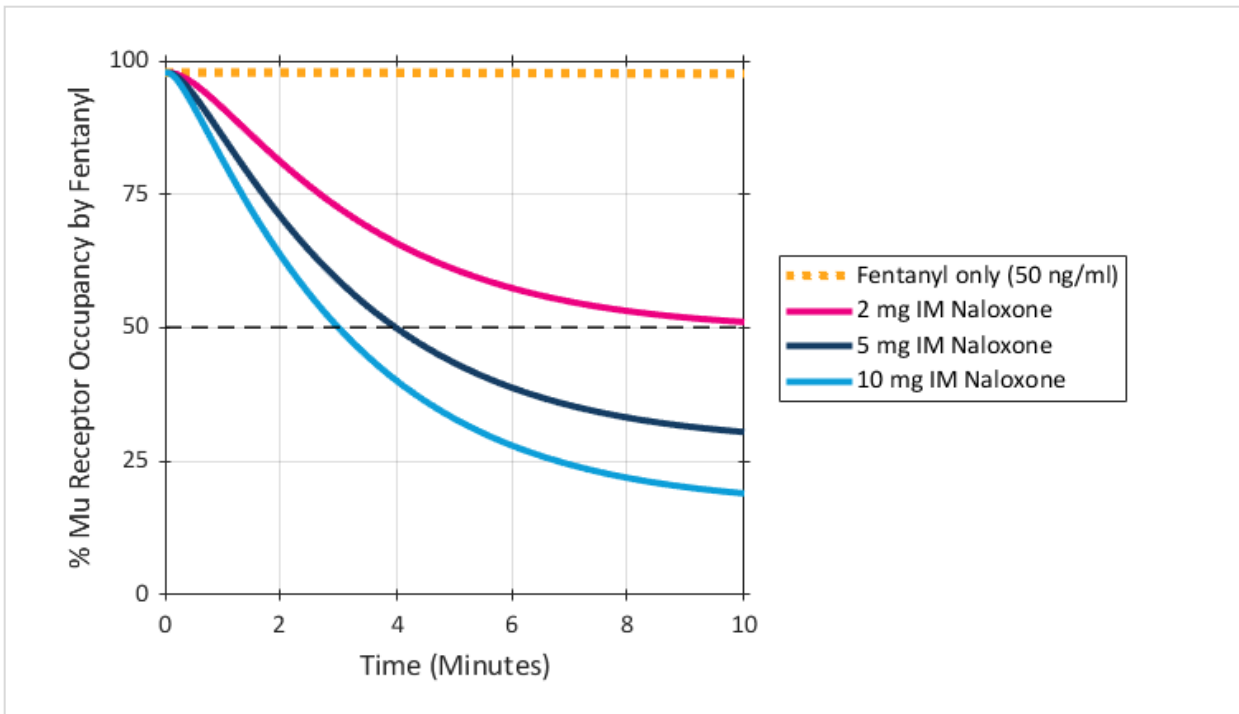


Figure 1. Simulated changes in mu receptor occupancy with fentanyl only or fentanyl with different doses of naloxone treatment. Dashed line in graph shows 50% receptor occupancy (RO).

THU-058

Incorporating pharmacological target-mediated drug disposition (TMDD) in a whole-body physiologically based pharmacokinetic (PBPK) model of linagliptin in rat and scale up to human

Nan Wu¹, Guohua An¹

¹ Division of Pharmaceutics and Translational Therapeutics, College of Pharmacy, University of Iowa, Iowa city, Iowa.

Objectives: Linagliptin is a potent small molecule dipeptidyl peptide 4 (DPP-4) inhibitor for the treatment of type 2 diabetes mellitus (T2DM). Linagliptin demonstrated substantial and complex nonlinear pharmacokinetics due to its saturable binding to DPP-4 in plasma and various tissues, a phenomenon known as target-mediated drug disposition (TMDD). Our objective was to build a mechanistic whole-body PBPK-TMDD model characterizing linagliptin nonlinear pharmacokinetics in rats, scaling up to human and providing a potential modeling framework for other small-molecule compounds exhibiting TMDD.

Methods: The data used for model development came from literature reports. All pharmacokinetics and tissue distribution data for linagliptin following different doses in both wildtype and DPP-4 deficient rats were analyzed simultaneously using the nonlinear mixed effect modeling approach with NONMEM interfaced with Pirana. A whole-body PBPK-TMDD model containing plasma and 14 tissue compartments with a total of 26 differential equations was developed. Among 14 tissue compartments, TMDD binding process was incorporated in 9 of them, namely plasma, kidney, liver, spleen, lung, skin, salivary gland, thymus, and reproductive system. The PBPK-TMDD model developed in rats was extrapolated to human by taking into account the interspecies physiology differences, and the scale up potential of this model was evaluated by comparing model simulated vs literature reported human pharmacokinetic profiles.

Results: Our final model adequately captured the concentration-time profiles of linagliptin in both plasma and various tissues in both wildtype rats and DPP4-deficient rats following different dose regimens. The association rate constant (k_{on}) in plasma and tissues were estimated to be 1.53 and 0.0056 nM⁻¹h⁻¹, respectively, and dissociation rate constant (k_{off}), in plasma and tissues were estimated to be 0.0814 and 0.0098 h⁻¹, respectively. The predicted DPP-4 concentration in plasma for a 0.25 kg rat is 1.11 nmol/L, which is close to the experimental value (3.84 nmol/L). The binding affinity of linagliptin to DPP-4 (K_d) was predicted to be higher in plasma (0.053 nM) than that in tissue (1.75 nM). When scaled up to human, this model accurately predicted the substantial and complex nonlinear pharmacokinetic behavior of linagliptin in human adults that is characterized by less-than dose proportional increase in plasma exposure, dose-dependent clearance and volume of distribution, as well as long terminal half-life with minimal accumulation after repeated doses.

Conclusions: Our PBPK-TMDD model not only captures linagliptin tissue and plasma concentration data in all rats but also has excellent scale-up capability. Our modeling work is not only novel but also of high significance as the whole-body PBPK-TMDD model platform developed using linagliptin as the model compound could be applied to other small-molecule compounds exhibiting TMDD to facilitate their optimal dose selection.

THU-059

Using Population Pharmacokinetics to capture the binding of a Novel Bispecific Fibroblast Activation Protein (FAP) to its 4-1BB Ligand (4-1BBL) and support Phase 2 dose selection in oncology patients

Authors: Sandrine Micallef¹; Peter N Morcos²; Christine McIntyre³; Nicolas Frey¹; Vincent Buchheit¹; Jasna Canadi²; Christina Claus⁴; Ernesto Guarin¹; Jon Chick³; Oliver Krieter⁵; Nassim Djebli¹

Institutions: All authors worked for Roche Pharmaceutical Research and Early Development, Roche Innovation Center at the following locations – 1 Basel, Switzerland; 2 New York City, USA; 3 Welwyn, UK; 4 Zurich, Switzerland; 5 Munich, Germany.

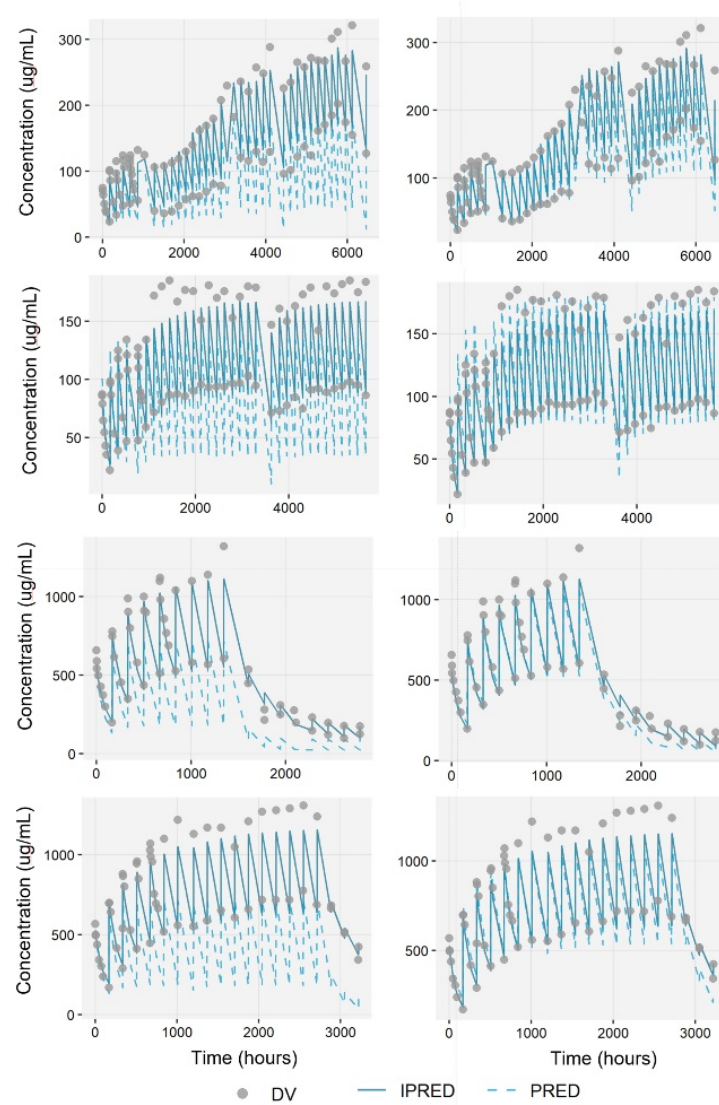
Objectives: Bispecific modalities show promise in cancer immunotherapy. RO7122290, induces potent 4-1BB mediated T cell co-stimulation when cross-linked to FAP expressed on tumor stroma [Claus et al 2019]. The objective of this analysis was to characterize the PK of RO7122290 administered either alone or in combination with atezolizumab in patients with solid tumours through population pharmacokinetic modeling to inform dose recommendation for Phase 2.

Methods: The ongoing study consists of 3 parts: Part A - RO7122290 single agent dose escalation; Part B – RO7122290 dose escalation in combination with atezolizumab; Part C – tumor specific expansion cohort(s), RO7122290 in combination with atezolizumab. RO7122290 was administered via intravenous infusions of 5 to 2000 mg QW as a single agent, and at doses of 45 to 2000 mg in combination with atezolizumab. Serial and sparse PK were used for Population Pharmacokinetic model development with NONMEM v7.4.1. Covariate analysis was performed exploring age, gender, body weight. Impact of atezolizumab on the RO7122290 PK was also investigated. Model selection was confirmed by diagnostic plots, visual prediction-corrected predictive check, parameter precision and bootstrapping techniques.

Results: 3400 PK samples from 108 patients were included in the analysis. RO7122290 was described by a 2-compartment model with linear and non-linear (Michaelis-Menten) clearance (Figure 1). Inter-individual variability was included on the following parameters: Linear clearance (CL), central and peripheral volume of distribution (V1, V2), Michaelis-Menten constant (KM) and maximum elimination rate (VM). Covariance between CL and V1, and between VM and KM random effects improved the model. Residual variability was described by combined proportional and additive error. Linear CL appeared slightly higher than typical for IgG1 [Bai et. al. 2012]; however this is also reported for other bispecific antibodies [Chen, 2017]. V1 and V2 approximated plasma volume. Nonlinear CL likely reflects FAP-binding, as ascribed in nonclinical species [Driessen et al 2019].

Conclusions: A popPK model capturing FAP-binding is established for RO7122290 and is being used to derive exposures for PK/PD investigations in support of the recommended Phase 2 dose selection.

Figure 1: Fitting using linear CL only (left) vs. parallel Michaelis-Menten non-linear and linear clearances (right). Individual (continuous) and population (dashed) predicted concentrations versus time.



References:

- Bai, Shuang, et al. "A guide to rational dosing of monoclonal antibodies." Clinical pharmacokinetics 51.2 (2012): 119-135.
- Chen, Y., and Yan X. "Pharmacokinetics of bispecific antibody." Current Pharmacology Reports 3.3 (2017): 126-137.
- Claus, C., et al. "Tumor-targeted 4-1BB agonists for combination with T cell bispecific antibodies as off-the-shelf therapy." Science translational medicine 11.496 (2019): eaav5989.
- Driessens et al. Integrated PK/PD Approach to Derive the First-In-Human Starting Dose of RG7827, a Novel Tumor Targeted Co-Stimulatory Bispecific Fusion Protein Cancer Immunotherapy. Clin Pharmacol Ther 2019; 105(Suppl S1): Abstract PII-045:S55.

THU-060

Progress Towards Regulatory Endorsement of a Clinical Trial Simulation Tool for Early Motor Parkinson Disease

Nathan J. Hanan¹, Varun Aggarwal¹, Diane Stephenson¹, Klaus Romero¹, Babak Boroojerdi², David Dexter³, Tanya Simuni⁴, Donald Grosset⁵, Kenneth Marek⁶, Rachael Lawson⁷, Michelle Hu⁸, Caroline Williams-Gray⁹ Jackson Burton¹ on behalf of Critical Path for Parkinson's Modeling team

¹ Critical Path Institute, Tucson, AZ, USA; ² UCB S.A., Brussels, Belgium; ³ Parkinson's UK, London, UK; ⁴ Northwestern University, Chicago, IL, USA; ⁵ University of Glasgow, UK; ⁶ Institute for Neurodegenerative Disorders, New Haven, CT, USA ⁷ New Castle University, UK; ⁸ Department of Clinical Neurology, John Radcliffe Hospital, Oxford, UK, ⁹ Department of Clinical Neurosciences, University of Cambridge, UK.

Objectives: Development of disease-modifying therapeutics targeting early Parkinson's disease (PD) is a primary focus in PD drug development. Critical Path Institute's Critical Path for Parkinson's (CPP) Consortium houses a comprehensive database containing early PD patient-level observations from 12 clinical trials and five observational cohorts. A primary objective of CPP is to leverage the database to develop clinical trial simulation tools for both motor and non-motor aspects of disease using the Movement Disorder Society's revised Unified Parkinson's Disease Rating Scale (MDS-UPDRS). To optimize trial design, simulation tools are being built with disease progression, placebo response, patient dropout, and drug effect models. Here, we describe preliminary results of a disease progression model that will serve as the backbone for clinical trial simulation using the MDS-UPDRS Part II endpoint.

Methods: Four observational studies (PPMI, OPDC, ICICLE-PD, Tracking) and one randomized clinical trial (STEADY-PD3, control arm) comprising 3,339 patients (PD diagnosis < five years at baseline) and 13,534 MDS-UPDRS Part II observations were utilized in a nonlinear mixed-effects model to describe early PD progression with three levels of random effects: beta-distributed residual variability, inter-individual variability (IIV) and inter-study variability (ISV). A preliminary covariate model was developed using a stepwise approach, with significance set at 0.01 for forward addition and 0.001 for backward selection. Model performance was evaluated using goodness-of-fit criteria and visual predictive plots.

Results: MDS-UPDRS Part II progression was best described by the generalized Gompertz function, a 3-parameter logistic model that allows for a non-symmetric inflection point (estimated at Part II score ~ 23). Baseline severity and progression for a typical patient aged 67 years with a PD duration of 11 months were 6.70 points and 0.080 points/month (0.96 points/year), respectively (**Table 1**). The identified covariates for baseline MDS-UPDRS part II

were sex, age, and PD duration. Baseline MDS-UPDRS part II was about 15 % lower in females than males and increased with age (0.04 points/year) and PD duration (0.08 points/month). Age was also identified as a covariate on progression rate, with older patients progressing faster. Both base and covariate models were stable upon perturbation of the initial estimates and had low condition numbers (11.62 and 12.8, respectively).

Conclusions: This preliminary work, which quantifies the effect of patient characteristics on MDS-UPDRS Part II progression, is under regulatory review with FDA and EMA. Covariate modeling will be extended to assess the effects of genetics and longitudinal PD medication use. The execution of the final model will also include MDS UPDRS Part III and will quantify placebo response, patient dropout, and drug effect models. Upon final endorsement from FDA and EMA, the tool will be publicly available for sponsors to help optimize clinical trial design in early motor PD.

Table 1: Parameter estimates from MDS-UPDRS Part II disease progression model

Parameter	Base Model Estimate (% RSE)	Final Model Estimate (% RSE)	Non-parametric Bootstrap Mean (95% CI) n=1000
MDS-UPDRS ₂ Baseline	6.48 (1.2)	6.70 (1.5)	6.71 (6.50, 6.91)
• PD Duration at Baseline (centered at 11 months)	NE	0.0118 (10.5)	0.0118 (0.00945, 0.0143)
• Female	NE	-0.143 (14.3)	
• Age (centered at 67 years)	NE	0.00638 (19.6)	0.006413 (0.00374, 0.009012)
Intrinsic Progression Rate (per month)	0.00732 (3.6)	0.00721 (3.6)	0.00720 (0.00654, 0.00788)
• Age (centered at 67 years)	NE	0.0135 (15.9)	0.0135 (0.00811, 0.0189)
Dispersion factor of Beta Distribution	38.6 (1.7)	38.6 (1.7)	38.6 (36.6, 40.7)
Shape (γ)	0.659 (8.3)	0.723 (7.8)	0.727 (0.551, 0.895)
IV			
• MDS-UPDRS ₂ Baseline	0.388 (3.1)	0.366 (3.1)	0.365 (0.342, 0.390)
• Intrinsic Progression Rate (per month)	0.918 (8.5)	0.905 (8.5)	0.906 (0.759, 1.07)
ISV			
• MDS-UPDRS ₂ Baseline	0.0344 (60.8)	0.0286 (60.5)	0.0288 (0.0215, 0.0358)
• Intrinsic Progression Rate (per month)	0.0165 (71.5)	0.0134 (74.0)	0.0150 (0.00163, 0.0289)

RSE: relative standard error. NE: not evaluated. MDS-UPDRS₂ Baseline and the typical progression rate in MDS-UPDRS₂ score is estimated by: MDS-UPDRS₂ Baseline = 6.70*(1 + 0.0118*(Disease duration - 11.01))*exp(0.00638*(age - 67))*(1 -0.143, if female); Intrinsic Progression Rate=0.00721 *exp(0.0135*(age - 67)). The typical progression rate (points/month) in MDS-UPDRS₂ score is estimated by dScorei/dt = ri*Scorei *[[ln(max(Scorei)/Scorei)] ^γ.

Mechanistic Modeling of Cyclosporine A-induced Acute Kidney Injury with RENAsym®

Pallavi Bhargava^a, Christina Battista^a, Viera Lukacova^b, Jeff Woodhead^a

^aDILIsym Services, Inc., Research Triangle Park, NC; ^bSimulations Plus Inc., Lancaster, CA

Objectives:

The use of Cyclosporine A (CsA) can cause tubular damage leading to a decline in renal function as determined by decreases in serum creatinine levels and glomerular filtration rate (GFR)¹. This work uses RENAsym®, a quantitative systems toxicology (QST) model of acute kidney injury (AKI), to recapitulate clinical outcomes following long-term CsA administration in humans.

Methods:

The effects of CsA on mitochondrial function and reactive oxygen species (ROS) production were assessed to define the potential for CsA-induced kidney injury. Human renal proximal tubule epithelial cells (RPTECs) were treated with CsA and its effects on mitochondrial respiration as well as ROS production were measured. Seahorse XFe96 Analyzer was used to measure mitochondrial respiration. High content screening was used to measure ROS production after RPTECs were exposed to dihydroethidium staining. These *in vitro* data were used to define kidney toxicity parameters, and together with PBPK simulations of clinical CsA exposure created in Gastroplus®, kidney injury was predicted in RENAsym.

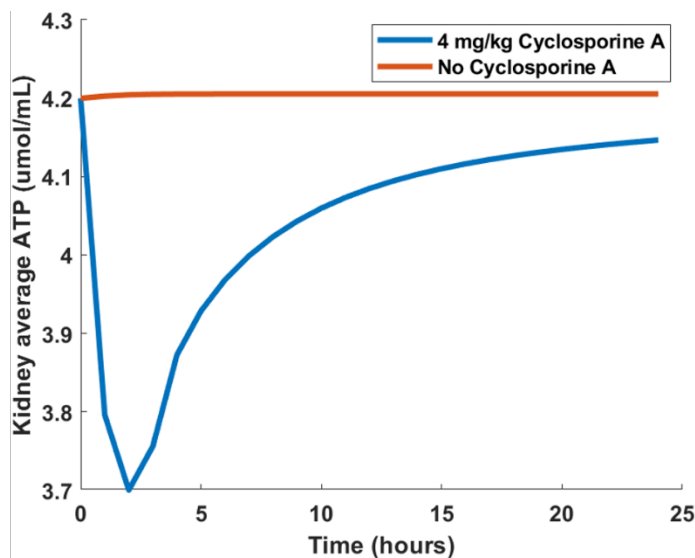


Figure 1: Simulations in baseline human dosed with and without a single dose of 4mg/kg Cyclosporine A for 24 hours predict a decrease in kidney average ATP, indicative of renal injury.

Results:

CsA inhibited the mitochondrial electron transport chain flux (ETC inhibition coefficient=1458.33 µmol/L) and induced ROS production ($V_{max}=0.049$ 1/hr, $K_m =13.075$ µmol/L). RENAsym predicted CsA-induced kidney injury such as a decrease in kidney average ATP as shown in Figure 1. RENAsym was further utilized to perform a mechanistic analysis to determine the main driver in simulated CsA nephrotoxicity. The mechanistic analysis indicated that CsA-induced kidney injury is primarily driven by inhibiting mitochondrial function via inhibition of the electron transport chain.

Conclusions:

Using *in vitro* data to determine toxicity parameters, RENAsym accurately predicted CsA-induced nephrotoxicity in humans, consistent with observed in clinical studies.

References:

1. Schaft, J., Zuilen, A., Deinum, J., Bruijnzeel-Koomen, C. & Bruin-Weller, M. Serum Creatinine Levels During and After Long-term Treatment with Cyclosporine A in Patients with Severe Atopic Dermatitis. *Acta Derm. Venereol.* **95**, 963–967 (2015).

THU-062

Population Pharmacokinetics and Simulation to Support CC-93538 Dosing in Pediatric Subjects

Peijin Zhang¹, Nastya Kassir², Jonathan Q. Tran¹

¹Bristol-Myers Squibb, Summit, NJ, USA; ²Certara, Princeton, NJ, USA

Objectives: CC-93538 (previously known as RPC4046 or ABT-308) is a humanized immunoglobulin G1 monoclonal antibody (mAb) that binds to human IL-13 and blocks its binding to IL13Ra1 and IL13Ra2. CC-93538 has completed Phase 1 and 2 studies and is being developed for treatment of eosinophilic esophagitis (EoE). Subjects eligible for enrollment in the Phase 2 study had body weight (WT) ≥ 40 kg. The current analysis was performed to determine (1) a population pharmacokinetic (PPK) model of CC-93538; (2) if adolescents participating in the adult Phase 3 study with WT <40 kg can receive the same adult dose; and (3) initial CC-93538 doses for pediatric EoE subjects based on simulation of systemic exposure.

Methods: Pharmacokinetic samples from 118 subjects including Phase 1 (24 healthy subjects) and Phase 2 (94 EoE subjects) studies were used for the PPK analysis. Several models were examined. A formal covariate analysis was performed using stepwise covariate analysis. The final model was qualified using goodness-of-fit criteria, bootstrap resampling, and visual predictive check. CC-93538 exposure (area under the curve at steady state [AUC_{ss}]) was determined for adolescent and pediatric subjects with WT 10 to 40 kg using empirical individual Bayesian estimates of pharmacokinetic parameters from the final PPK model. Appropriate CC-93538 dose levels for pediatrics by WT range were determined by matching simulated adult AUC_{ss} at 360 mg SC QW (<25% difference). In addition, the percentage of subjects with simulated AUC_{ss} above the 95th percentile of adult exposure was determined with attempts to make it less than 20%.

Results: A two-compartmental model with first-order absorption and first-order elimination was selected. WT and baseline albumin were identified as statistically significant covariates for clearance (CL). WT was identified as a statistically significant covariate of volume of distribution in the central compartment (Vc). Both CL and Vc increased with increasing WT. CL decreased with increasing albumin. Sex and age were not significant covariates. Pharmacokinetic simulation suggested that the use of the adult CC-93538 dose in subjects 30 to <40 kg would result in at least 58% of AUC_{ss} above the adult 95th percentile. For pediatric subjects with WT 10 to 25 kg and 25 to 40 kg, CC-93538 doses of 150 mg and 200 mg QW SC, respectively, resulted in simulated AUC_{ss} similar to adults at 360 mg SC QW.

Conclusion: CC-93538 exhibits pharmacokinetic properties typical of mAbs without target-mediated clearance. The WT threshold for pediatric subjects to receive the adult dose of CC-93538 is 40 kg. For pediatric subjects with WT 10 to 25 kg and 25 to 40 kg, the anticipated CC-93538 dose to achieve the adult exposure is 150 mg and 200 mg SC QW, respectively.

Comparison of Joint Tumor Dynamic-Overall Survival Models with a Long-Term Surviving Fraction

Ramon I Garcia¹, Seth Robey², Pavan Vaddady², Lokesh Jain², and, Jonathan L French¹

¹Metrum Research Group, Tariffville, CT, USA; ²Quantitative Pharmacology and Pharmacometrics, Merck, Kenilworth, NJ, USA

Objectives:

In certain disease and treatment settings, some patients achieve long-term survival. In these cases, the survival function for the time to event can appear to have a non-zero asymptote. Two approaches which accommodate such a “cure fraction” are the mixture cure rate model [1] and the promotion time cure rate model [2]. It is of interest to compare and contrast the assumptions, model fit, and long-term survival predictions of these two models.

Methods:

A joint model for tumor size and survival using a promotion time cure rate framework was developed using data from three clinical trials of first- and second-line pembrolizumab monotherapy in non-small cell lung cancer. In this model the hazard function is given by:

$$h_i(t) = \lambda \times \alpha_i \text{RTS}(t)^\beta \times \exp(-\lambda t)$$

where RTS(t) is the predicted tumor size relative to the baseline value and α_i is a scale parameter which includes effects of subject-specific covariates. A key feature of this model is that when RTS(t) is bounded or RTS(t) is substituted by a tumor metric g(t) which is $O(\exp(-\lambda t))$ then the limit of the cumulative hazard function is finite which is a property required of a cure rate model.

The promotion time cure model was compared to a mixture cure rate model:

$$S_i(t) = p_i + (1 - p_i) \times S_{1i}(t),$$

where p_i is the probability of achieving long-term survival and $S_{1i}(t)$ is a proper survival function.

Results:

The mixture cure rate model directly expresses the cure fraction as a function of baseline covariates but not time-varying predictors. In contrast, the promotion time cure rate model estimates fewer parameters and allows for baseline and time-varying predictors to influence the cure fraction, but the cure fraction has to be derived using numerical methods.

Objective function values and visual predictive check plots indicate both models fit the observed data equally well. However, the models yield different extrapolations to 5-year survival. For example, for patients with PDL1 expression > 50%, the promotion cure rate model estimates a 5-year survival of 0.03 (.01, .06) and .30 (.22,.38) for chemotherapy and pembrolizumab, respectively, while the mixture cure rate model estimates are 0.09 (.04,.19) and .26 (.18,.34) respectively.

Conclusions:

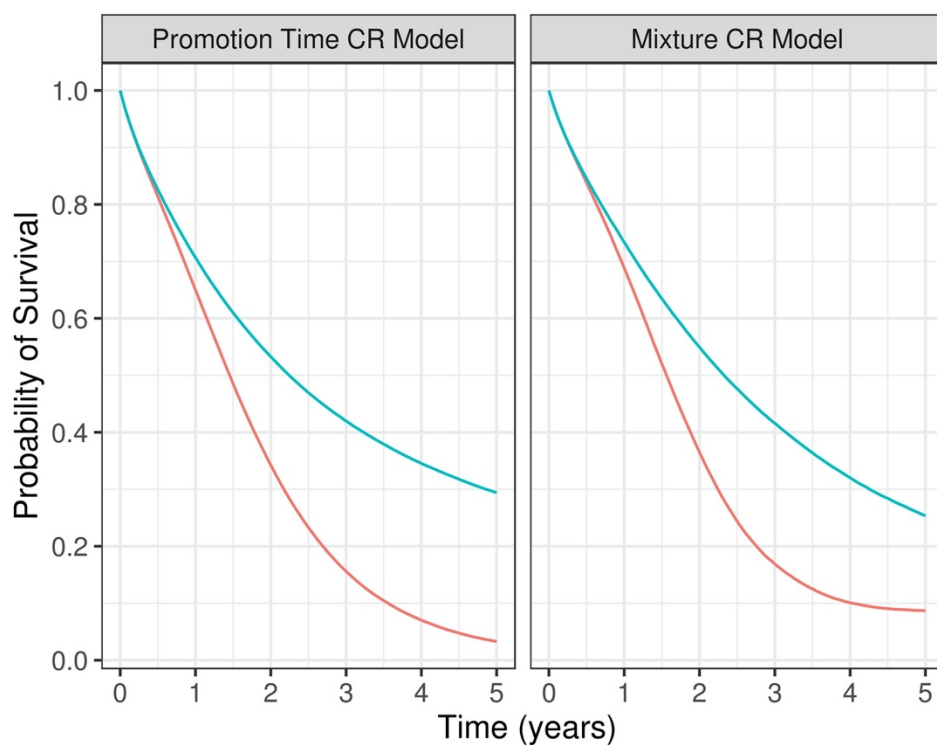
Mixture and promotion time cure rate models produce similar results over the observed time span yet yield different predictions of long-term survival. The promotion time cure rate model allows more flexibility in the key drivers of long-term survival.

References:

- [1] Law NJ, Taylor JM, Sandler H. The joint modeling of a longitudinal disease progression marker and the failure time process in the presence of cure. *Biostatistics*. 2002;3(4):547–563. doi:10.1093/biostatistics/3.4.547
- [2] Chen M-H, Ibrahim JG, Sinha D. A new Bayesian model for survival data with a surviving fraction. *J Am Stat Assoc*. 1999 Sep;94(447):746.

Survival Predictions by Treatment Arm for Promotion Time and Mixture Cure Rate Models

Treatment Arm — Chemo — Pembro



THU-066

A QSP model of B-cell depletion in RA and SLE

Authors: Rohit Rao, Sarita Koride, C.J. Musante, Richard Allen

Affiliations: Pfizer Early Clinical Development Worldwide Research, Development & Medical
Cambridge, MA 02139, USA

Objective

B-cell depletion is a promising therapeutic strategy for the treatment of rheumatoid arthritis (RA) and systemic lupus erythematosus (SLE). However, the factors determining the extent of B-cell depletion and repopulation are not well understood leading to concerns around excessive immunosuppression. B-cell subsets exhibit differential susceptibility to depletion. For example, naïve B-cells exhibit greatest susceptibility to depletion by anti-CD20 targeting rituximab (RTX), whereas auto-antibody producing plasma cells are relatively resistant to depletion (1). Moreover, multiple approaches for B-cell depletion have been proposed with recent evidence suggesting that additional targeting of T-follicular helper (T_{FH}) cells in the germinal center may be a viable therapeutic strategy (2). A QSP model of the B-cell activation cascade was built to assess potential downstream effects of such therapeutic strategies on B-cell subpopulations.

Methods

The model accounts for interactions between multiple B-cell subpopulations including naïve, activated and memory B-cells, plasmablasts, and T_{FH} cell-dependent germinal center reactions [Figure 1]. Redistribution of B-cells between plasma and lymph compartments was implemented to account for the effects of differential drug exposure between these compartments (3). As an initial step, we focused on simulating B-cell depletion by RTX. The prospective model response was validated against published data that quantified the effect of two 1000mg RTX doses on naïve B-cells, memory B-cells and plasmablasts (4). A simplified pharmacokinetic model for RTX was implemented using published data (5). Parameter estimates determining B-cell dynamics were obtained from prior *in vitro* and modeling studies (6).

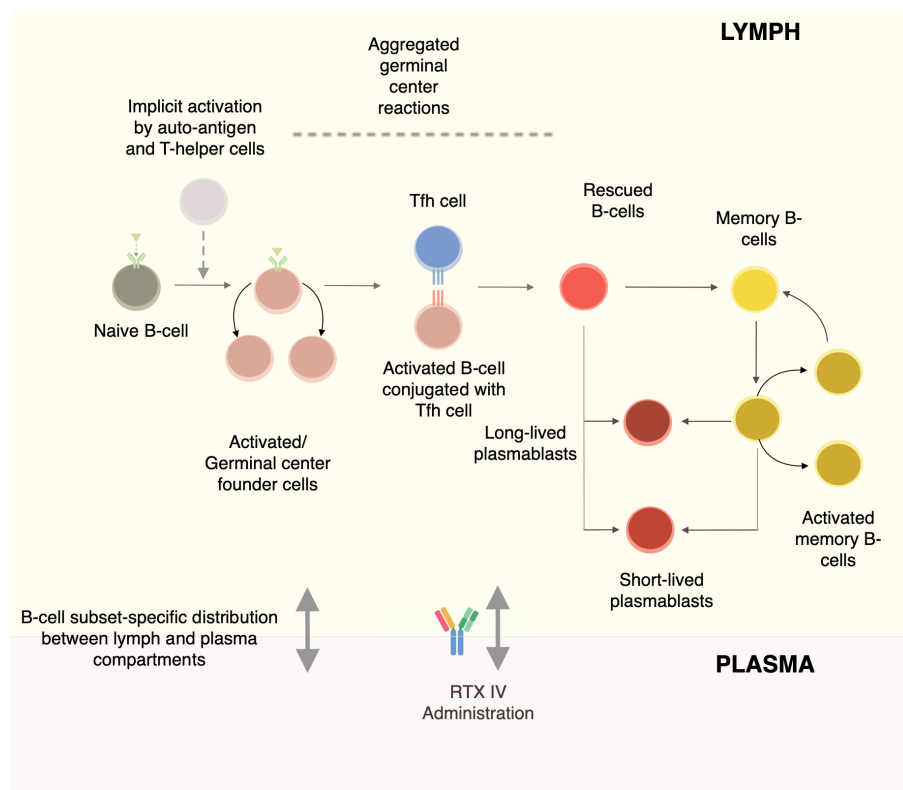


Figure 1: Schematic of model of B-cell activation cascade

Results

Model simulations predicted a near total depletion of naïve and memory B-cell subpopulations in both plasma and lymph compartments in agreement with the clinically reported time-course of B-cell dynamics. Plasmablasts exhibited >70% depletion; however, were less susceptible to depletion by RTX than naïve and memory B-cells. In agreement with clinical data, B-cell repopulation occurred within 52 weeks.

Conclusion

The model accurately captured clinically reported measurements on the time-course of depletion and repopulation for plasma B-cell sub-populations in response to RTX administration. Moreover, it provides insight into B-cell subpopulations at the site of action (lymph) that are not readily amenable to clinical measurement. The model will be used as a platform to optimize dosing schedules and assess the efficacy of strategies that target additional cell populations in the B-cell activation cascade including the germinal center-localized T_{FH} cells.

1. M. J. Leandro *Arthritis Res Ther* **15 Suppl 1**, S3 (2013).
2. L. Yan *et al. Front Immunol* **8**, 1510 (2017).
3. P. M. Glassman *et al. MAbs* **9**, 297-306 (2017).
4. E. M. Vital *et al. Arthritis Rheum* **63**, 3038-3047 (2011).
5. S. Rozman *et al. Br J Clin Pharmacol* **83**, 1782-1790 (2017).
6. X. Chen *et al. CPT Pharmacometrics Syst Pharmacol* **3**, e133 (2014).

THU-067

Using an IO QSP Model to Re-Define Efficacy, Discontinuation Criteria, and Biomarker Analysis.

Authors: Madhav Channavazzala* (1), Kannan Thiagarajan* (1), Tamara Ray (1), Rukmini Kumar (1), Kapil Mayawala (2), Dinesh De Alwis (2), Alex Snyder (2), Brian Topp (2)

Institutions: Vantage Research, India (1) Merck & Co., Inc., Kenilworth, NJ, USA (2)

*Co-first authors

Objectives: First generation immuno-oncology (IO) therapies have generated unprecedented success in treating cancer. Several companies are developing IO QSP models to facilitate development of second-generation IO combination therapies. These models generally focus on immune-mediated tumor killing within a single lesion. Here we develop an IO QSP model that includes the full complexity of patients with multiple target, non-target, and new metastatic lesions.

Methods: We developed a basic tumor dynamics model with replication (k_1) and death (k_2) rates. This model was expanded to include inter- and intra-patient variability for each parameter. Virtual patients were created with multiple tumors, randomly assigned as Target and Non-Target. Next the probability of developing a new metastatic lesion during any given time interval was assumed to be driven by overall tumor burden. The model was calibrated to lesion-level and patient-level data using a pembrolizumab melanoma study (Keynote-001).

Results: Intra-Patient (tumor-to-tumor) heterogeneity was significant (%CV = 70%) and clinically meaningful in that the same patient can have shrinking and growing lesions. While 308 patients developed progressive disease (PD), only 113 displayed a net increase in tumor burden. Most patients displayed stable (n = 125) or reduced (n = 70) tumor burden at the time of progression. PD in these patients is defined by growth of a non-target or new metastatic lesions. Only 6% of patients displayed a loss of efficacy (rebound).

Conclusions: Disease progression is generally considered a surrogate for drug failure. However, this analysis clearly shows that most melanoma patients with progressive disease display continuing response to pembrolizumab in the majority, but not all, of their lesions. This suggests that depth of response may be a better index of drug efficacy than RECIST v1.1. Furthermore, patients with disease progression are often switched to a new therapy. However, patients who are showing continuing efficacy at the time of progression, may benefit from continued pembrolizumab (for responding lesions) and a new therapy (for the non-responding lesions). Finally, the large degree of heterogeneity observed in patients suggests that biomarkers sampled from a patient with PD could have come from a growing or a shrinking lesion.

THU-069

Trapezoid bioequivalence: the exchange rate between mean and variance of bioavailability

Authors:

Sara Soufsaf, B.Sc.¹, Fahima Nekka, Ph.D.¹, Jun Li, Ph.D.¹

¹ Université de Montréal, Montréal, Québec, Canada

Abstract:

Objectives:

In the statistical analysis of bioequivalence, the FDA defines three levels of bioequivalence: average bioequivalence (ABE), population bioequivalence (PBE) and individual bioequivalence [1]. To establish bioequivalence, PBE adds a statistical comparison of the bioavailability metrics' variance for the reference and generic drug (σ_R^2 and σ_T^2). Since PBE was defined in FDA's 2001 Guide *Statistical Approaches to Establishing Bioequivalence* [1], it has been criticized for its overly permissive results [3]. Thus, the objective of our work is to propose an alternate bioequivalence criterion which overcomes the limitations of PBE and incorporates parameters dependent on therapeutic properties of a drug.

Methods:

In the assessment of therapeutic equivalence, we define an alternative trapezoid bioequivalence (TBE) which considers the variability of the drugs' PK and allows a drug-specific trade-off in the comparison of its average and variance. In other words, the TBE criterion establishes bioequivalence by balancing a similarity in both drugs' average (μ) AND variance (σ^2) of bioavailability. The TBE is translated in the equation below, defining the graphical trapezoid in Figure 1.

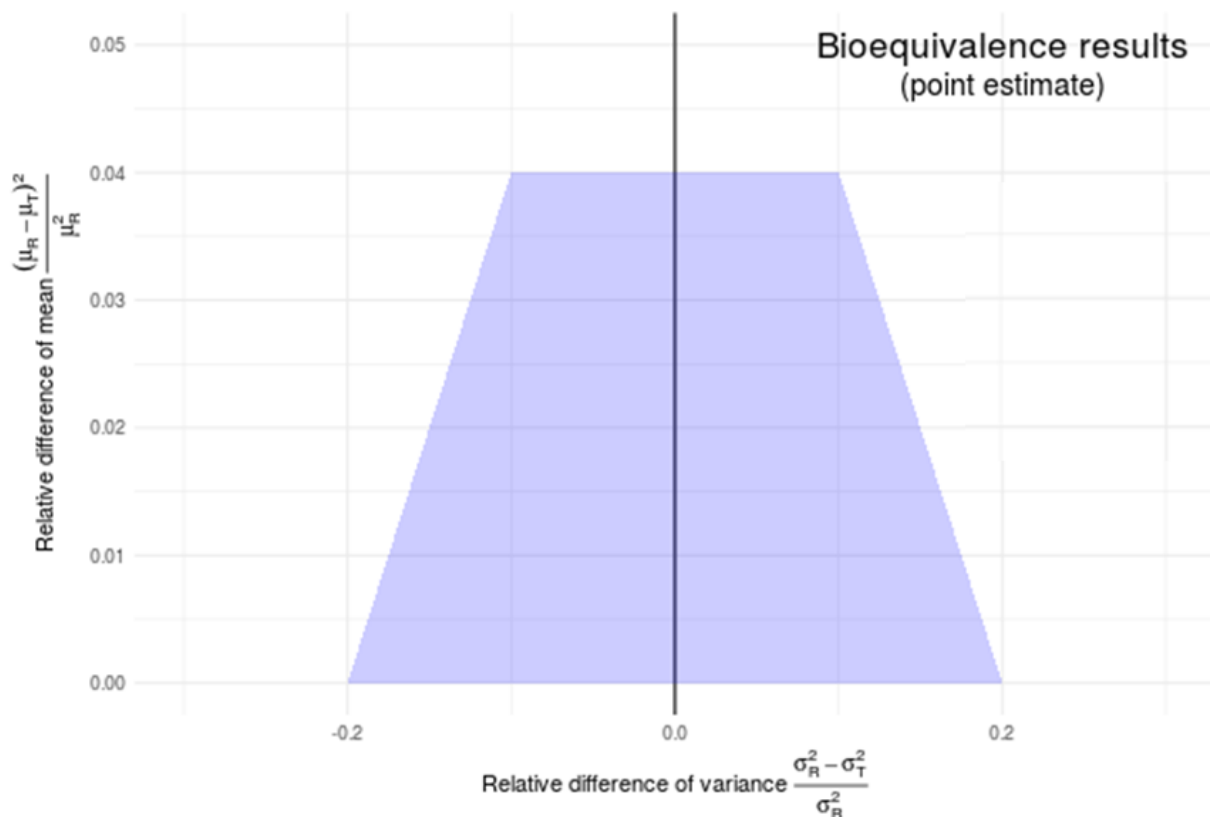
$$\left(\frac{\mu_T - \mu_R}{\mu_R}\right)^2 \leq \begin{cases} \lambda_1 * \left(\frac{\sigma_T^2 - \sigma_R^2}{\sigma_R^2}\right) + \lambda_2, & \frac{\sigma_T^2 - \sigma_R^2}{\sigma_R^2} < \alpha_{threshold} \\ \theta_{tolerance}, & \alpha_{threshold} \leq \frac{\sigma_T^2 - \sigma_R^2}{\sigma_R^2} \leq \alpha_{threshold} \\ -\lambda_1 * \left(\frac{\sigma_T^2 - \sigma_R^2}{\sigma_R^2}\right) + \lambda_2, & \frac{\sigma_T^2 - \sigma_R^2}{\sigma_R^2} > \alpha_{threshold} \end{cases}$$

Where $\theta_{tolerance}$ is the maximal relative difference of μ ; λ_1 and λ_2 are a flexible trade-off between μ and σ^2 ; and $\alpha_{threshold}$ is the therapeutically acceptable relative difference of σ^2 .

Our methodology is applied to the treatment of Attention Deficit Hyperactivity Disorder with methylphenidate (MPH) since the individualization of doses is especially difficult [4]. Using a two-linear absorption (immediate-release and extended-release) population pharmacokinetic model with different ranges of absorption parameters, we simulated plasma concentrations of MPH. We then applied ABE, PBE and TBE to these datasets. In concordance with MPH literature, we fixed $\lambda_1 = 0.4$, $\lambda_2 = 0.08$, $\theta_{tolerance} = 0.04$, and $\alpha_{threshold} = 0.1$.

Results: As expected, TBE slightly more strict than PBE. In fact, 20% of simulations where the absorption constant was changed between the test and reference formulations did not pass TBE but passed PBE. This number climbs up to 30% when evaluating changes to the fraction of MPH that is formulated as an extended release.

Conclusion: TBE, contrary to PBE, allows a balance between μ and σ^2 to be adapted according to desirable pharmaceutical characteristics. This is particularly interesting for drugs with high variability between individuals, where the variance's importance may be higher to ensure best interchangeability for a patient.



References:

1. Food and Drug Administration, *Guidance for Industry. Statistical Approaches to Establishing Bioequivalence*, H.a.H. Services, Editor. 2001.
2. Sheiner, L.B., *Bioequivalence revisited*. Stat Med, 1992. **11**(13): p. 1777-88.
3. Zariffa, N.M. and S.D. Patterson, *Population and individual bioequivalence: lessons from real data and simulation studies*. J Clin Pharmacol, 2001. **41**(8): p. 811-22.
4. Soufsaf, S., et al., *A Quantitative Comparison Approach for Methylphenidate Drug Regimens in Attention-Deficit/Hyperactivity Disorder Treatment*. J Child Adolesc Psychopharmacol, 2019.

THU-070

**Development of Quantitative Systems Toxicology Model to Predict Drug Induced Acute Kidney Injury
via mtDNA Depletion Pathway**

Shailendra B. Tallapaka, Nader Hamzavi, Yeshitila Gebremichael, Scott Q. Siler, Jeffrey L. Woodhead

DILIsym Services, Inc., a Simulations Plus company, Research Triangle Park, NC, USA

Objective: Treatment of chronic viral infections like HIV, Hepatitis B etc., necessitates long-term administration of powerful antivirals like nucleoside/nucleotide reverse transcriptase inhibitors (NRTIs). Several NRTI's are primarily excreted renally and have been reported to cause nephrotoxicity. The observed toxicity is partially attributed to mitochondrial dysfunction caused by inhibition of mitochondrial DNA (mtDNA) synthesis[1]. We are developing a quantitative systems toxicology (QST) model called RENAsym® that can potentially predict drug-induced acute kidney injury (AKI) in humans and pre-clinical species by leveraging *in vitro* mechanistic toxicity data. The objective of this work is to develop a mechanistic model to represent drug-induced mtDNA depletion in proximal tubular cells and subsequent downstream toxic effects in the kidney.

Methods: The mtDNA depletion model was built within the mitochondrial dysfunction sub-model of RENAsym®. The current representation of kidney bioenergetics includes equations that describe mtDNA and electron transport chain (ETC) protein turnover, and substrate uptake and utilization by mitochondria to produce ATP. The model was parameterized based on human and rodent kidney bioenergetics data reported in literature. A physiologically based pharmacokinetic (PBPK) model including kidney exposure of IV administered adefovir was developed in GastroPlus™ 9.7 as an input for RENAsym. Toxicity parameter inputs into RENAsym for adefovir were derived from *in vitro* studies where changes in mtDNA content in primary human renal proximal tubule cells exposed to adefovir were measured using RT-PCR[2].

Results: Simulations in human at 3 mg/kg QD dosing for 40 weeks predicted a ~10% decrease in ATP level and minimal reduction in the fraction of viable PTCs. Sensitivity analysis indicated that a ~10-25% increase in either mtDNA destruction rate or kidney concentration of adefovir would predict significant nephrotoxicity (Fig. 1), which is well within the expected variability in pharmacokinetic and toxicological parameters. This qualitatively agrees with clinical observation of elevated serum creatinine in ~60% of patients treated with 120mg QD adefovir for 24 weeks[3].

Conclusions: A QST model of drug-induced mtDNA depletion and subsequent AKI has been constructed within RENAsym®. The model reasonably predicts adefovir-induced nephrotoxicity and shows promise in being a predictive tool for drug-induced AKI.

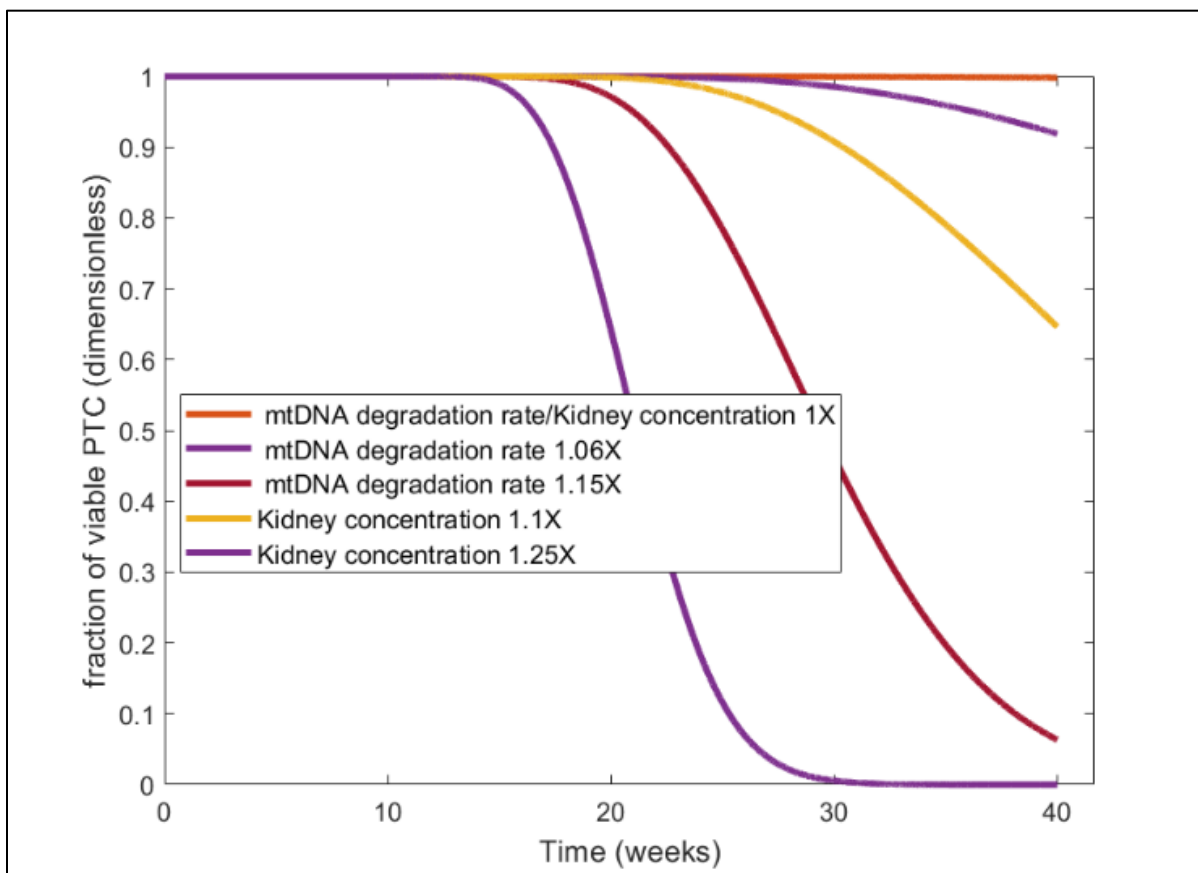


Figure 1. Sensitivity analysis of toxic and PK parameters demonstrating adefovir induced AKI

References:

1. Lewis, W., Day, B. & Copeland, W. Mitochondrial toxicity of nrti antiviral drugs: an integrated cellular perspective. *Nat Rev Drug Discov* 2, 812–822 (2003).
2. Faye Wang, Oliver P. Flint. BMS-986001, an HIV Nucleoside Reverse Transcriptase Inhibitor, Does Not Degrade Mitochondrial DNA in Long-Term Primary Cultures of Cells Isolated from Human Kidney, Muscle, and Adipose Tissue. *Antimicrobial Agents and Chemotherapy* Nov 2013, 57 (12) 6205-6212
3. Kahn J, Lagakos S, Wulfsohn M, et al. Efficacy and Safety of Adefovir Dipivoxil With Antiretroviral Therapy: A Randomized Controlled Trial. *JAMA*. 1999;282(24):2305–2312.

THU-071

Whole-body physiologically-based modeling to predict monoclonal antibody pharmacokinetics in multiple species with different administration routes

Shihao Hu and David Z. D'Argenio

Department of Biomedical Engineering, University of Southern California, Los Angeles, CA, USA

Objectives: Monoclonal antibodies (mAbs) are used to treat a broad range of diseases, including cancers, immunological disorders and infectious diseases. Various methods have been investigated to improve mAb PK, including Fc engineering and co-formulation strategies [1-4]. Previously, we developed a whole-body physiologically-based PK (PBPK) model to predict mAb PK after intravenous (IV) and subcutaneous (SC) administration in humans [5]. The goal of this work was to extend the previous model and apply it to investigate the complex relationship between observed mAb PK and underlying properties governing mAb absorption, distribution, metabolism, and excretion (ADME).

Methods: In this work, we extended the model in [5] as follows. The endosomal space in each organ now includes vascular membrane and interstitial membrane compartments, where IgG is released from FcRn binding at neutral pH after processing and recycling in early endosomes. The overall PBPK model includes all major organs, with versions that incorporate physiological parameter values for different species (mouse, monkey, human). The model was used with mAb PK data digitized from published studies [1-4] to investigate the role of model-based ADME properties related to absorption, transendothelial migration and FcRn-mediated processing.

Results: The resulting PBPK model simulations are consistent with the observed complex relationship between plasma concentration and FcRn-IgG binding kinetics reported in several mouse studies [1-3]. For example, compared to the wildtype antibody, the variant with increased binding affinities at both pH 6.0 and pH 7.4 was predicted by the model to have no significant change in plasma concentration, as reported in [2]. Also, model simulations identified the FcRn binding affinity threshold at neutral pH that controls IgG recycling, in agreement with [3]. Using the human version of the PBPK model with a mechanistic SC site sub-model, hyaluronidase's influence on the SC absorption of Tocilizumab reported in [4] could be described. Specifically, a two-fold increase in the model-based parameter representing interstitial transport and lymphatic uptake described the difference observed in Tocilizumab PK alone and after coadministration with hyaluronidase [4] (pre-systemic catabolism rate constant unchanged in the model). Thus, the model provides a basis for mechanistically representing the effects of hyaluronidase to digest extracellular matrix, enhance the interstitial permeation and facilitate SC absorption of biomolecules.

Conclusions: Our study presents a mechanistic, whole-body PBPK model for different species that can be applied to investigate the role of ADME properties on observed mAb plasma concentrations.

References:

- [1] Brian Mackness et al, mAbs (2019)
- [2] Rong Deng et al, Drug Metabolism and Disposition (2010)
- [3] Jack Borrok et al, Journal of Biological Chemistry (2015)
- [4] Peter Morcos et al., Int. Journal of Clinical Pharmacology and Therapeutics (2013)
- [5] Shihao Hu et al, J Pharmacokinet Pharmacodyn (in press)

THU-072

Implementation of gamma distributed delays through a fast ODE approach

Authors: Shuhua Hu¹, Michael Tomashevskiy¹, and Wojciech Krzyzanski²

Institutions: ¹Certara; ²Department of Pharmaceutical Sciences, University at Buffalo

Objectives: The gamma distributed delay is a natural extension of the widely used transit compartment model (TCM). It was implemented in Phoenix Modeling Language (PML) through the delay function, which allows users to estimate the shape parameter instead of manually finding a proper one as required by the TCM [1]. However, the delay function involves direct numerical calculation of the integral with the values of the signal to be delayed recorded in a table upon every derivative evaluation, and hence it may become very expensive or even prohibitive for complex population analysis. In Phoenix NLME 8.3, an alternative function, gammaDelay, was implemented based on the ODE approximation method proposed in [3] wherein it was shown that this approach is much faster than the delay function. The goal is to demonstrate the gammaDelay function through an example.

Methods: The example is a gamma distributed delay model in [1], which is a generalization of the TCM in [2] for describing the delay process in the platelet production following Lusutrombopag dosing with feedback mechanism. The data was simulated using the original TCM approach with number of platelets simulated for 78 subjects every 24 hours during the timeframe of 648 hours. To compare the performance of gammaDelay and delay functions, the gamma distributed delay model was implemented using both functions. They were then fitted to the data in Phoenix NLME 8.3 using the FOCE-ELS engine, where the values of all PK and some PD parameters are fixed to the ones used to generate the data. To see if the shape parameter can be recovered from the data, the initial value for all the estimated parameters are chosen away from their true values.

Results: The models using gammaDelay and delay functions gave very similar estimation results, and both well described the simulated data. However, the total running time for the model using the gammaDelay function is 9.4 minutes while the one for the delay is 25.5 hours with the same setup running in a Windows desktop machine with 1.8 GHz Intel Core i7-8565U CPU. Table 1 lists the estimation results obtained using the gammaDelay function, and it indicates that the shape parameter can be reliably estimated along with other parameters with its estimate very close to its true value.

Table 1: The true values for fixed effects as well as their corresponding estimates, standard errors (SE), and coefficients of variation in percentage (CV%) obtained using the gammaDelay function with 61 ODEs, where the mean delay time in the gammaDelay function is parameterized in terms of its shape parameter and the transition rate in the TCM model. The values for all the other parameters were fixed to the ones that were used to generate the simulation data.

Parameter	Definition	True value	Estimate	SE	CV%
ν	Shape parameter	3	2.987	0.054	1.811
EC_{50}	Drug concentration which produces 50% of maximum drug effect	80.9	77.094	3.760	4.878
β	Exponent to describe the feedback based on platelets	0.286	0.301	0.013	4.257
γ	Hill coefficient	1.61	1.487	0.072	4.826
σ	Standard deviation of additive error	1	0.961	0.014	1.440

Conclusions: The gammaDelay function in PML provides a flexible and powerful way to model delayed outcomes without compromising the performance. Even though the ODE approximation approach [3] can be manually implemented in any PKPD software, the gammaDelay function allows single line code specification, and hence is more efficient and less error-prone.

References

- [1] Hu et al (2018) J Pharmacokinet Pharmacodyn 45:285-308.
- [2] Katsume et al (2016) Clin Pharmacokinet 55:1423-1433.
- [3] Krzyzanski (2019) J Pharmacokinet Pharmacodyn, 46:53-63.

Combining Elementary Effects and Sobol Global Sensitivity Analysis to reduce computational expense for complex models

Authors: Sietse Braakman, Florian Augustin, Ricardo Paxson

Affiliations: The MathWorks, Natick, MA, USA

Objectives: Decision making in pharmacological development relies increasingly on complex, mechanistic models, such as Quantitative Systems Pharmacology (QSP) and Physiologically-based Pharmacokinetic (PBPK) models. These models often have more parameters than available data can reasonably constrain. Sensitivity analyses can elucidate which parameters most affect the model output. Local sensitivity analysis (LSA) is generally inadequate to characterize sensitivities in non-linear models with uncertainty in parameters and global sensitivity analysis (GSA) is preferred instead. However, GSA methods are generally computationally expensive and scale exponentially with increasing model complexity. To address this problem, we present a systematic and scalable workflow to perform GSA on larger, mechanistic models using SimBiology®.

Methods: A mechanistic lesinurad/febuxostat model¹ with 14 independent input parameters was used to illustrate the workflow. Physiologically meaningful bounds on each input parameter were determined and used to span the input-space. An Elementary Effects GSA² (multi-point, one-at-a-time LSA) was performed on all input parameters to prioritize 8 parameters that most affect serum uric acid. The EEGSA was performed to reduce the dimensionality and make the computational load of the subsequent Sobol GSA³ manageable. A Sobol GSA (all-at-a-time, Sobol sampling) with 10,000 samples was then performed to rank the remaining parameters. A multiparametric GSA⁴ (MPGSA) was used to investigate whether input effects were significant with respect to serum uric acid nadir. All methods were implemented using SimBiology and MATLAB® using built-in function for LSA, Sobol GSA and MPGSA.

Results: The EEGSA was able to reduce the dimensionality of the problem to the 8 most important parameters. The remaining parameters were ranked using a Sobol GSA with first-order indices. Total-order Sobol indices were used to identify interactions between input parameters. The MPGSA showed that 6 out of 8 parameters had a significant effect ($p<0.05$) on reaching serum uric acid nadir $<68\text{mg/L}$ by comparing empirical cumulative distribution functions of accepted and rejected samples using a Kolmogorov-Smirnov test.

Conclusions: The workflow described above enables the systematic exploration of global input parameter sensitivities on model outputs of interest using SimBiology. Sobol GSA does not have the underlying assumptions of monotonicity and linearity that EEGSA has and is therefore preferred for ranking most important parameters. Meanwhile, the EEGSA step reduces the computational expense of GSA by reducing the number of input parameters whose input space can be sufficiently sampled for a Sobol GSA or MPGSA analysis. This allows the workflow to scale better with increasing model size.

References:

- [1] Aksenov S et al., *Physiol Rep.* 2018, 6(5): e13614.
- [2] Saltelli A et al., *Global Sensitivity Analysis, The Primer*, Wiley 2007
- [2] Saltelli A et al., *Computer Physics Communications* 2010, 181(2): 259–70.
- [4] Tiemann C et al., *PLoS Computational Biology* 2013, 9(8): e1003166.

THU-075

Longitudinal Placebo Response Modeling in Patients with Ulcerative Colitis

Authors: Sonoko Kawakatsu, Rui Zhu, Wenhui Zhang, Meina T. Tang, Tong Lu, Angelica Quartino, Matts Kågedal

Affiliations: Genentech, Inc., South San Francisco, CA, USA

Objectives: Clinical trial design in the ulcerative colitis (UC) population faces the challenge of historically high placebo response rates. A better understanding of placebo response rates and factors that influence response may allow for more informed clinical trial design. A placebo response model was developed to describe the combined stool frequency and rectal bleeding (SF+RB) subscore of the Mayo Clinical Score over time in placebo arm patients with UC, and to evaluate the impact of baseline characteristics on placebo response.

Methods: Placebo arm individual level clinical trial data from the TransCelerate Database were pooled for analysis. A proportional odds (PO) model and two logistic regression models were developed using nonlinear mixed effects modeling. The PO model was used to describe the time course of the SF+RB subscore, and the two logistic regression models were used to correlate SF+RB subscore with discontinuation from placebo arm at the end of induction phase and during the maintenance phase (drop-out model). The combined model was evaluated by visual predictive check.

Results: Data from 755 adult, placebo arm patients with moderate to severe active UC were available from five Phase 2/3 trials. Three trials were induction and maintenance studies, and two were induction only studies. A PO model with linear placebo effect, logistic regression model correlating discontinuation with SF+RB subscore at end of induction phase, and logistic regression model correlating discontinuation during maintenance phase with the last observed SF+RB subscore adequately described the time course of the SF+RB subscore (Figure 1). Baseline SF+RB subscore and TNF status were included as covariates on α_1 (intercept parameter). Patients with higher baseline SF+RB subscore and prior anti-TNF therapy had higher SF+RB subscore, and patients with higher SF+RB subscore at the end of induction phase and during maintenance phase were more likely to discontinue from the placebo arm.

Conclusions: A placebo response model was developed using an ordered categorical approach to describe the longitudinal SF+RB subscore in placebo arm patients with moderate to severe active UC. Expected placebo

response can be simulated to inform clinical trial design, and simulations can potentially be used as “virtual placebo arms” for trials in which a placebo arm is not feasible to enroll. Future work will include the use of Markov models to describe the SF+RB subscore.

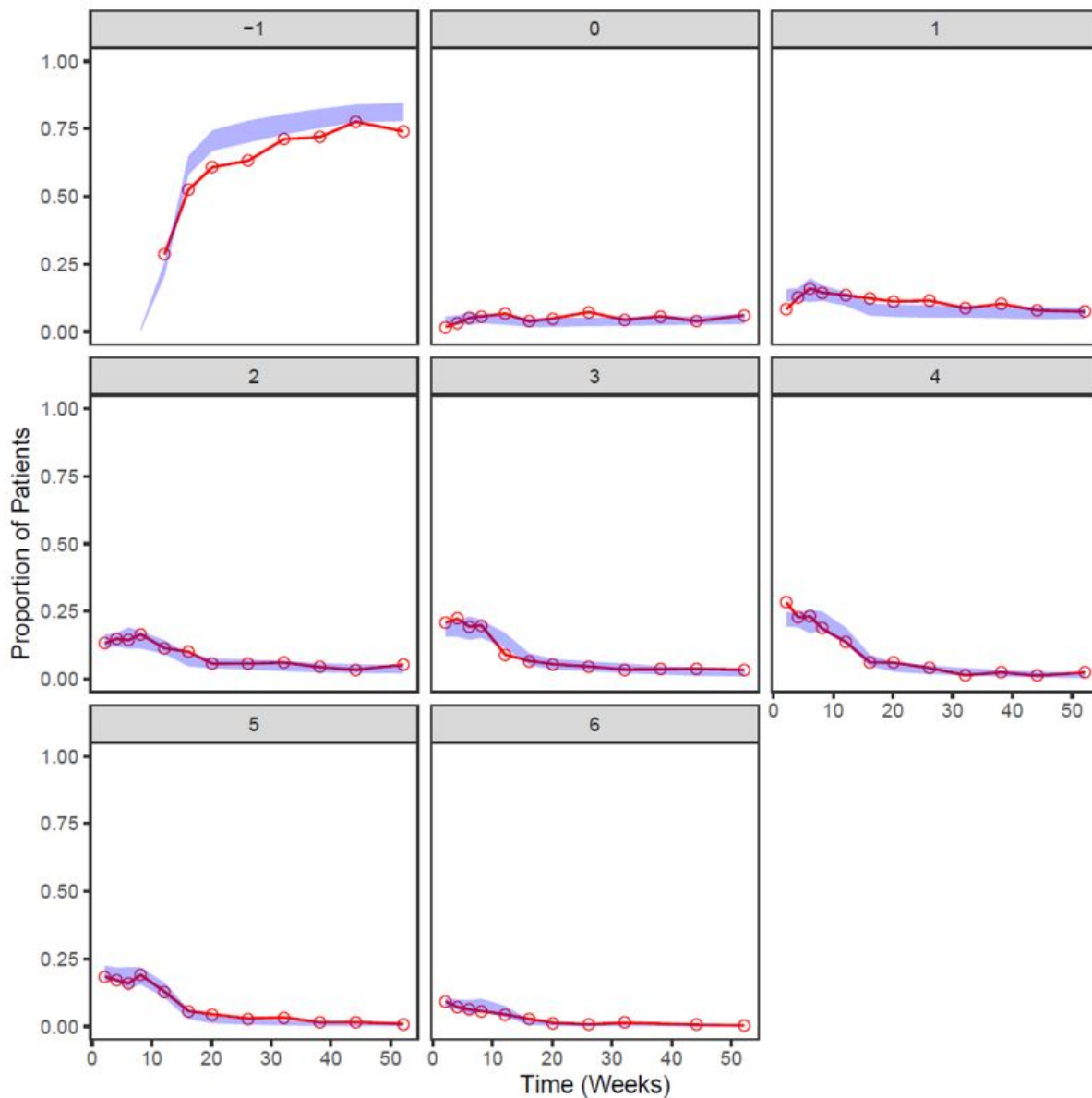


Figure 1 Categorical visual predictive check applied to combined SF+RB subscore data. Proportion of patients for each SF+RB subscore category ranging from 0 to 6 are plotted over time. The category is -1 for patients who have discontinued from the placebo arm at end of induction phase or during maintenance phase. Observed data are plotted in red, and model simulation based 95% confidence interval is represented by the blue fields.

THU-076

Mechanistic PK/PD Modeling of Canakinumab to evaluate the exposure and target engagement requirements for Interleukin (IL)-1 β antagonists in atherosclerotic patients

Authors: Sumit Basu, Gayathri Swaminath, Paul Rearden, Harish Shankaran

Affiliations: Merck & Co., Inc., Kenilworth, NJ, USA

Objectives:

Interleukin (IL)-1 β , an inflammatory cytokine is one of the significant pathogenic mediators of autoimmune, autoinflammatory, infectious and degenerative diseases. Inflammation in the arterial walls, driven in part by IL-1 β , is a key risk factor for cardiovascular events. In 2017, the CANTOS trial demonstrated canakinumab, a neutralizing anti-IL 1 β antibody, can significantly lower the rates of cardiovascular events, independent of lipid levels. Importantly, cardiovascular benefits were observed in patients who achieved on-treatment high sensitivity C-Reactive protein (hs-CRP; a downstream biomarker) levels of less than 2 mg/L. Our objective was to develop a mechanistic PK/PD model for canakinumab to understand the exposure and target engagement requirements to achieve meaningful reductions in hs-CRP for driving efficacy in the atherosclerotic patient population.

Methods:

An extensive literature review was performed and two population PK/PD models of canakinumab were found that described the temporal changes in total canakinumab, IL-1 β and hsCRP concentrations in cryopyrin-associated periodic syndromes (CAPS)¹ and rheumatoid arthritis (RA)² patients. Further, clinical PK data was available in the literature from a dose-escalation study of single intravenous doses of canakinumab (0.03, 0.1, 0.3, 1.5 or 10 mg/kg) in type 2 diabetes mellitus (T2DM) patients (n=222)³, and this dataset was used to calibrate the model to this population. Model development, evaluation and simulations were performed in Berkeley Madonna version 8.3.18.

Results:

A standard two compartment PK model with linear clearance from the central compartment described the PK of total canakinumab and a quasi-equilibrium model was used to describe the binding of canakinumab to IL-1 β . Simulations of drug exposure and total IL-1 β were consistent with data in T2DM patients. The model was adapted to describe the relationship between canakinumab exposure and hs-CRP kinetics in T2DM patients. Additional models were built to link free IL-1 β levels to hs-CRP kinetics. Our analysis revealed a closer temporal link between reductions in free IL-1 β in the interstitium and serum hs-CRP levels.

Conclusions:

This mechanistic PK/PD model can be utilized to understand the PK/PD requirements for IL-1 β antagonists in the atherosclerotic patient population.

References

1. Lachmann et al., 2009,
2. Ait-Oudhia et al., 2012,
3. Noe et al., 2014.

THU-077

Physiologically-based Pharmacokinetic (PBPK) Modeling to Assess the Impact of Cytochrome P450 2D6 Activity on Tramadol and O-Desmethyltramadol Exposure

Tao Long¹, Rodrigo Cristofoletti¹, Jacques Turgeon², Veronique Michaud², Lismaury Galiano¹, Nashid Farhan¹, Stephan Schmidt^{1*}

¹ Center for Pharmacometrics and Systems Pharmacology, Department of Pharmaceutics, College of Pharmacy, University of Florida, Orlando, FL, USA

² Tabula Rasa HealthCare, Precision Pharmacotherapy Research and Development Institute, Orlando, FL, USA.

Objectives: Tramadol is a μ -opioid receptor agonist and a serotonin–norepinephrine reuptake inhibitor, used to treat moderate to severe pain. O-desmethyltramadol (M1), the major active metabolite, is mainly produced by CYP2D6. It has a much stronger μ -opioid receptor binding affinity and higher potency for analgesic effects compared to those of Tramadol. Hence, the variability in CYP2D6 activity due to intrinsic and extrinsic factors is expected to modulate analgesic effects of the drug. The objective of this research was to develop and verify of a PBPK model to evaluate the impact of CYP2D6 activity on Tramadol and M1 exposure in healthy Caucasian subjects.

Methods: A combination of bottom-up and top-down approaches, leveraging published clinical studies on Tramadol and M1 biotransformation, were used to derive a comprehensive mass balance analysis, mapping out the contribution of different metabolic pathways. PK-Sim V8 was used for model development. A PBPK model was first developed using the physicochemical properties and total clearance data of Tramadol and M1 as the initial parameters inputs as reported in the literature. Based on the relative contribution of individual clearance pathways, the model was further refined by optimizing parameters, e.g. renal clearance and retrograding the corresponding unbound intrinsic clearance for each involved CYP450 isoforms, using well-stirred liver model and *in vitro/in vivo* extrapolation approaches. The developed PBPK model was verified by comparing the predicted (PRED) *vs.* observed (OBS) clinical data from subjects receiving a single dose of 100mg Tramadol by i.v. (infusion) and p.o., and from subjects classified as CYP2D6 normal (NMs) and poor metabolizers (PMs).

Results: About 26% of the administered dose of Tramadol is excreted in urine in the unchanged form; CYP3A4 and CYP2B6 contribute 21% to its metabolic clearance forming N-desmethyltramadol, while 53% is transformed to M1 (38% by CYP2D6 and 15% by an unknown enzyme). For M1, 20% of the administered dose is excreted in urine while 33% undergoes phase 1&2 metabolism. The ratios of PRED *vs.* OBS $AUC_{0-\infty}$ and C_{max} are 0.82 and 0.99 for Tramadol; 1.20 and 1.16 for M1. The PRED PM/EM $AUC_{0-\infty}$ ratios are 1.52 and 0.44 for Tramadol and M1, respectively, which are consistent with the OBS. These results suggest that our model adequately captured the concentration–time profiles of Tramadol and M1 from multiple clinical studies.

Conclusions: A PBPK model was developed and verified using existing clinical pharmacokinetic and gene-drug interaction data. The final model can be prospectively applied to estimate the effects of concomitant administration of CYP2D6 inhibitors or higher affinity substrates on the PK of Tramadol and M1 and further to determine the optimized time delay associated with minimized DDI between Tramadol and perpetrator drugs.

THU-078

Monoclonal antibody therapy efficacy can be boosted by combinations with other treatments: predictions from integrated Alzheimer's disease platform

Tatiana Karelina, Stepan Lerner
InsysBio, Moscow, Russia

Objectives:

Clearance of pathological accumulations of amyloid beta (A β) and tau protein are still considered as important requirement for the treatment of Alzheimer's disease. It is known that pathologies interact, but the efficacy of amyloid targeting therapies on tau pathology is questionable and pharmacodynamics of CSF tau markers differ from amyloid markers. Improvement of efficacy could be achieved by combinations of treatments. Quantitative systems pharmacology model allows for integration of available information from multiple preclinical studies to simulate clinical studies. The goal was to apply the translational systems pharmacology model of key AD markers to simulate efficacy of potential combinations of known treatments with perspective immunotherapy.

Methods:

A β [1] and tau pathology submodels are merged through the model of intracellular protein degradation systems (proteasome, autophagy) which govern protein accumulation and can be disrupted progressively in AD. Literature data (concentration baselines and dynamics, SUVR) from mice and human, in vitro perturbations of cellular pathways (rapamycin, proteasome inhibitors, vinblastine, ACAT inhibitors, calpain inhibitors) have been used for calibration. Simplified pharmacokinetic model of antibodies describes distribution to the brain and target binding, preventing seeding and growth of aggregates; it was calibrated on the data for non-specific IgG [2], and partially verified of BAN2401 CSF data. Data from clinical studies for aducanumab and BACE inhibitor (verubecestat) have been used for model validation, together with mouse data for treatment by rapamycin, calpain inhibitors, proteasome activation as well as tau targeting antibodies, DC8E8 (tau) [3] and GW-23B7 (anti- β -sheet), in Tau and APP/Tau mouse AD models.

Result:

Model correctly describes progression and interaction the A β and tau pathologies. It correctly predicts effect of rapamycin, calpain inhibitors, proteasome activation on tau or amyloid in transgenic mouse models, as well as efficacy of antibodies. Predictions for aducanumab efficacy in Tg2576 mouse [4]

correspond to the data (about 40-50% for soluble and insoluble amyloid). Translation to clinical trial predicts correctly amyloid SUVR decrease by 0.2 from baseline within 54 weeks [4]. Tau in cortex and hippocampus is predicted to change by 10-15%. Similar prediction was derived for verubecestat low efficacy towards tau in CSF. Simulated addition of rapamycin to aducanumab therapy increase efficacy tremendously, leading to 80% brain tau reduction within one year and acceleration of amyloid clearance.

Conclusion:

QSP modeling allows for choice of combinations of newly emerging biologics combined with targeting cell metabolism, to lead optimization and increase of treatment efficacy.

References

1. Karelina, T. et al. CPT: Pharmacometrics & Systems Pharmacology (2017) 6(10), 676–685.
2. Chang, H.-Y. (2019). Journal of Pharmacokinetics and Pharmacodynamics (2019) 46(4), 319–338
3. Kontsekova, E. et al. Alzheimers Res Ther (2014) 6(4), 45.
4. Sevigny, J. The antibody aducanumab reduces A β plaques in Alzheimer's disease. Nature, (2016). 537(7618), 50–56.

THU-079

Identifying a coherent target modulation of ion channel conductances to rescue striatal neuronal excitability in Huntington's Disease phenotypes

Sushmita Allam¹, Tim Rumbell¹, Jaimit Parikh¹, Viatcheslav Gurev¹, James R. Kozloski¹

¹IBM T.J. Watson Research Center., Yorktown Heights, NY, USA

Objective: Huntington's Disease, an autosomal dominant neurodegenerative disorder mainly affects striatal neurons by making them hyperexcitable, a biomarker for appearance of first motor symptoms [1]. Prior evidence points to dysfunctional potassium channels that cause these changes in neuronal excitability [2]. Population-based modeling is widely used to represent intrinsic variability of electrophysiological features of healthy, disease and drug treated phenotypes. The objective of this work is to identify a single coherent direction of ion channel target modulation for phenotypic recovery, represented by a modulation of neuronal excitability that transforms the heterogeneous Huntington's disease (HD) phenotype towards the Wild-Type (WT) phenotype.

Methods: Our approaches are based on quantitative systems pharmacology principles combining mechanistic simulations, generation of populations of models using evolutionary algorithms [3] and hybrid statistical/mechanistic modeling approaches grounded in theoretical frameworks described in related reports of this method. We built a large population of neuron models representing both healthy, disease, and drug-treated phenotypes. We describe several approaches using heuristic and applied machine learning methods to perform phenotypic screening and design single target and multiple target perturbations of ionic currents for rescuing a heterogenous disease population to the healthy phenotype. We introduce distance metrics to compare the performance of the virtual drug perturbations with a known candidate pharmacotherapy, PDE10i in HD.

Results: Using robust linear regression models, we were able to provide mechanistic insights into how the ionic conductance parameters influenced the varied electrophysiological properties that gave rise to distinct clusters of phenotypes. We found that coherent modulation of fast inactivating potassium, persistent potassium, and transient sodium conductances identified using heuristic approaches performed better than the single target modulators and PDE10i to rescue the healthy population in terms of divergence of various excitability features. Using similar population-based modeling approaches, we also found populations of models adhering to *in vivo*

electrophysiological recordings of striatal neurons under modulation of the drug papaverine, and similarly identified underlying coherent parametric changes to ion channels capable of altering the membrane excitability to represent that context.

Conclusions: We show how our population of models approaches both identify multiple target perturbations to rescue HD phenotypes, and represent pharmacological perturbations to single neurons, by identifying ion channel parameter combinations that recreate alterations of membrane excitability. Combining these insights, we introduce a potential program for ‘reverse phenotypic screening’, in which coherently modeled drug-induced membrane activity changes are mapped to desired recovery vectors in parameter space for disease states.

References:

1. Cao Y, Bartolomé-Martín D, Rotem N, Rozas C, Dellal SS, Chacon MA, et al. Rescue of homeostatic regulation of striatal excitability and locomotor activity in a mouse model of huntington’s disease. *Proc Natl Acad Sci U S A*. 2015 Feb 17;112[7]:2239–44.
2. Ariano MA, Cepeda C, Calvert CR, Flores-Hernández J, Hernández-Echeagaray E, Klapstein GJ, et al. Striatal potassium channel dysfunction in Huntington’s disease transgenic mice. *J Neurophysiol*. 2005 May;93[5]:2565–74.
3. Rumbell T, Kozloski J. Dimensions of control for subthreshold oscillations and spontaneous firing in dopamine neurons. *PLoS Comput Biol*. 2019;15[9].

THU-080

Physiologic indirect response model to describe buprenorphine pharmacodynamics in newborns with neonatal abstinence syndrome

Tomoyuki Mizuno^{1,4}, Brooks T. McPhail^{1,5}, Suyog Kamatkar^{2,6}, Scott L. Wexelblatt^{2,4}, Laura P. Ward^{2,4}, Uwe Christians³, Henry T. Akinbi^{2,4}, Alexander A. Vinks^{1,4}

¹Division of Clinical Pharmacology, Cincinnati Children's Hospital Medical Center, Cincinnati, OH, USA

²Perinatal Institute, Division of Neonatology, Cincinnati Children's Hospital Medical Center, Cincinnati, OH, USA, ³iC42 Clinical Research and Development, University of Colorado, Aurora, CO, USA,

⁴Department of Pediatrics, University of Cincinnati College of Medicine, Cincinnati, OH, USA,

⁵University of South Carolina School of Medicine, Greenville, SC, USA, ⁶Community Hospital East, Indianapolis, IN, USA

Objectives: Neonatal abstinence syndrome (NAS) is caused by disruption of fetal exposure to opioids or psychotropic drugs used by the mother during pregnancy. Buprenorphine has been shown to be effective in treating infants with NAS. However, providing individualized buprenorphine dosing to newborns is challenging as the buprenorphine exposure-response relationship has not been well characterized. The aim of this study was to develop an integrated pharmacokinetic and pharmacodynamic (PK/PD) model to facilitate prediction of buprenorphine treatment outcomes in newborns with NAS.

Methods: Clinical data were obtained from 19 newborns who were enrolled in a pilot PK study of buprenorphine in patients with NAS. Sparse blood sampling was performed using heel sticks with dried blood spot technology. Samples were taken prior to the second buprenorphine dose, 1-2 hours post-second dose and prior to the third or fourth dose. Finnegan scores were evaluated every 2-5 hours based on symptoms by nursing staff. Mean Finnegan scores were calculated every 12 hours and used as a PD marker in the modeling. The concentration-Finnegan score relationship was described using a physiologic indirect response model with the inclusion of natural disease remission. PK/PD modeling was performed using NONMEM.

Results: A total of 52 buprenorphine blood concentrations and 780 Finnegan scores were available for the PK/PD modeling. A one-compartment model with first order absorption adequately described the PK data. The buprenorphine IC₅₀ for the inhibition of disease progression was 0.77 ng/mL (95%CI: 0.32-1.2). The inclusion of natural disease remission described as a function of postnatal age significantly improved the model fit. The R² for individual prediction of PK and PD were 0.53 and 0.47, respectively.

Conclusions: A buprenorphine PK/PD model was successfully developed. The developed PK/PD model could facilitate model-informed optimization of the buprenorphine dosing regimen in the treatment of NAS. The results in this abstract have been published in the conference proceedings of American Society for Clinical Pharmacology and Therapeutics (ASCPT) 2020 as abstract [abstract# PIII-116]¹, but have not been presented due to cancellation of the meeting.

Reference: 1. Mizuno et al. Clin Pharmacol Ther. 2020; 107(S1). S110.

THU-081

Item Level Analysis of the MDS-UPDRS clinical outcome measure in Parkinson's Disease (PD)

Varun Aggarwal¹, Nathan Hanan¹, Robert Stafford¹, Mussie Akalu¹, Glenn Stebbins², Tanya Simuni³, Jesse Cedarbaum⁴, Donald Grosset⁵, Kenneth Marek⁶, Rachael Lawson⁷, Michele T. Hu⁸, Caroline Williams-Gray⁹, Diane Stephenson¹, Klaus Romero¹, Jackson Burton¹ on behalf of the CPP Modeling team.

¹ Critical Path Institute, Tucson, AZ USA; ² Rush University Medical Center, Chicago, IL USA; ³ Northwestern University, Chicago, IL, USA; ⁴ Coeruleus Clinical Sciences LLC, USA; ⁵ University of Glasgow, UK; ⁶ Institute for Neurodegenerative Disorders, New Haven, CT, USA; ⁷ New Castle University, UK; ⁸ Nuffield Department of Clinical Neurosciences, Oxford University, John Radcliffe Hospital, Oxford, UK; ⁹ University of Cambridge, Cambridge UK.

Objective: This effort is intended to provide a framework to analyze the individual items of the Movement Disorder Society's Unified Parkinson's Disease Rating Scale (MDS-UPDRS), based on an item response theory (IRT) modeling approach. The MDS-UPDRS is a composite scale consisting of four parts- each made up of several items related to different aspects of PD. It is imperative to understand the behavior of individual items to best assess their ability to measure underlying disease state for use in drug development. The Critical Path for Parkinson's (CPP) is a public-private partnership that has enabled significant data sharing of observational studies and clinical trials, which this analysis utilizes.

Methods: The standardized patient-level data at baseline from the CPP database was integrated with item-level MDS-UPDRS scores across 5 studies (n=5380, for MDS UPDRS Part II, results shown here). To assess assumptions required for latent modeling, exploratory factor analysis (EFA) followed by confirmatory factor analysis (CFA) was used. Modeling of item-level data was conducted using the *mirt* program implemented in R. A graded response model was fitted to the responses to derive discrimination and location parameters and construct item characteristic curves (ICC). Location parameters and ICC provided estimates of sampling adequacy.

Results(Shown here for MDS UPDRS Part II): The CFA confirmed the unidimensionality of Part II. Discrimination parameters were adequate for all items except Tremor. Location parameters suggested the 5-point Likert scaling

was adequate for all items (see Table 1). Location and discrimination parameters were estimated for other parts as well and were found adequate (results not shown). On/Off state was not distinguished for part III and needs further exploration.

Conclusion: This analysis demonstrates that the individual items of Part II provide adequate discrimination of underlying motor functional impairment, with the exception of the item measuring tremor. Additionally, the use of a 5-point Likert scaling appears appropriate for these items. The indication that tremor provides the least discriminative input may suggest further examination for its use in the composite MDS-UPDRS part II score could be considered.

Table 1: Discrimination (a) and location (b_{0-3}) parameters of MDSUPDRS Part II.

Items	a	b_0	b_1	b_2	b_3
Chewing and Swallowing	1.41	1.35	3.16	3.77	6.78
Doing Hobbies Other Activities	2.42	0.10	1.13	2.04	2.59
Dressing	3.33	0.23	1.27	2.41	3.15
Eating Tasks	2.32	0.60	1.77	3.32	4.92
Freezing	2.18	1.36	2.17	2.70	3.49
Get Out of Bed Car Deep Chair	2.77	-0.02	1.28	2.16	2.93
Handwriting	1.49	-0.24	1.09	2.21	3.48
Hygiene	3.01	0.67	1.96	2.81	3.41
Saliva and Drooling	1.18	0.44	1.03	2.07	4.04
Speech	1.49	0.55	1.55	3.04	5.53
Tremor	0.98	-0.94	1.58	3.73	5.53
Turning in Bed	2.28	0.34	2.00	2.74	3.26
Walking and Balance	2.28	0.06	1.39	1.90	3.00

THU-082

Unified approach for parameters estimation based on *in vitro* data

Authors: Veronika Musatova (1), Oleg Demin (1), Svetlana Rubina (1)

Affiliations: (1) InSysBio, Moscow, Russian Federation

Objectives:

The main aim of this study is to develop a unified approach to parameters estimation from the *in vitro* data and its implementation in an upgrade of the Immune Response Template (IRT) - platform describing the interaction of different types of immune cells, cytokines and facilitating the development new immunotherapies and their combinations.

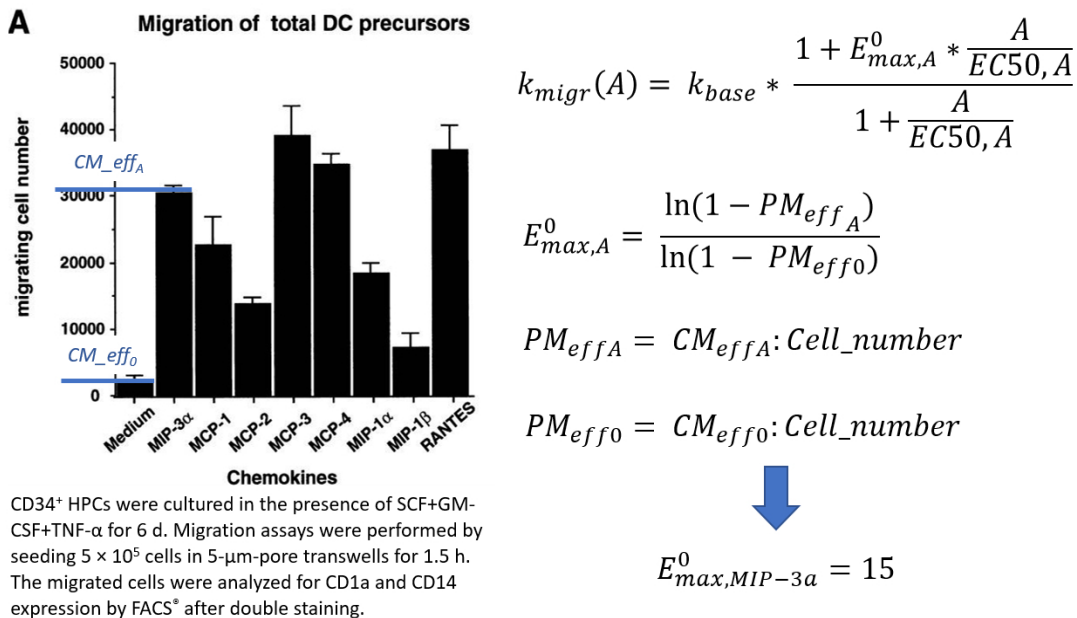
Methods:

Immune Response Template (IRT) is QSP platform of the immune system and a tool for the development of QSP and mechanistic models related to immune response. The core of IRT is an ordinary differential equations-based model, which includes a description of immune cells cycle processes, cytokines secretion and surface molecules interaction. Model parameters may be assessed from the *in vitro* data, obtained in experiments with typical design for cells survival, proliferation, migration or secretion studies. We developed 6 mathematical models describing typical *in vitro* experiments to derive formulas allowing direct parameters calculation from the *in vitro* data assessing apoptosis, proliferation, migration, differentiation and cytokine synthesis by immune cells.

Results:

Typical *in vitro* experiments were modeled, and processes were described using a mathematical approach to account for multiple cytokines regulatory impact on cell processes [1]. Derived formulas allow direct calculation of parameters from the *in vitro* data, resulting in a reduction of a model development time. The example of parameter calculation is shown on the figure 1. Developed formulas were used in parameter identification for IRT version 3 and 3.1, allowing the calculation of nearly 950 parameters directly from the *in vitro* data without additional models development and fitting.

Figure 1. Example of the migration parameter calculation performed for the *in vitro* data from Figure 1A [2]



Conclusions:

An approach to processes description, accounting multiple regulators impact [1], together with developed derivations for typical *in vitro* experiments studying cell proliferation apoptosis, migration and cytokines secretion allowed the significant increase of identified parameters number in the IRT platform version 3.1 as compared to the IRT version 2.1.

References:

1. Mechanistic approach to describe multiple effects of regulatory molecules on cell dynamics process in immune response. Oleg Demin, Evgeny Metelkin, Galina Lebedeva, Sergey Smirnov, ACoP7, Bellevue, WA, US.
2. Dieu-Nosjean MC, Massacrier C, Homey B, et al. Macrophage inflammatory protein 3alpha is expressed at inflamed epithelial surfaces and is the most potent chemokine known in attracting Langerhans cell precursors. *J Exp Med.* 2000;192(5):705-718. doi:10.1084/jem.192.5.705

THU-084

Model-informed target selection and validation through combining quantitative systems pharmacology (QSP) with network-based analysis (NBA)

Viji Chelliah¹ & Piet H van der Graaf^{1,2}

¹Certara UK Limited, Canterbury Innovation Centre, University Road, Canterbury, CT2 7FG, United Kingdom; ²University of Leiden, The Netherlands

Background/Objectives

The majority of drug development projects fail in Phase 2 and Phase 3 clinical trials, mainly due to the lack of efficacy and unacceptable safety profiles . It has been suggested that poor target selection and validation is a main underlying reason for this attrition. Indeed, AstraZeneca reported that the implementation of their revised R & D strategy to focus decision-making based on the so called 5R framework (which includes “the right target”) increased the trial success rate from 4% to 19% (1).

It has been proposed that target selection/validation is one of the main areas where quantitative systems pharmacology (QSP) can impact drug discovery and development (2). However, due to the multi-scale nature and complexity of typical QSP models and the resource it takes to develop them, the target space that can be explored in a timely manner is still significantly constrained. Therefore, we propose to combine QSP with network-based analysis (NBA) to increase the efficiency and effectiveness of *in silico* (model-informed) target selection and validation. In this paradigm, the initial target selection step is driven by NBA and the subsequent target validation by QSP, arguably in the spirit of the original NIH White Paper where QSP was defined as Quantitative AND Systems Pharmacology(3). Here, we present a workflow of NBA-QSP integration with a case study of its application to Covid-19.

Methods

We developed a NBA method that integrates differentially expressed genes from individual-specific transcriptomic data with disease-specific genes and drug targets mapped on to the large-scale protein-protein interaction network in order to explore potential targets and treatment scenarios.

Results

The gene expression data of SARS-CoV-2 infected patients was obtained from GEO datasets. The NBA of disease network generated using gene expression data of virus infected individuals and host-virus interaction identified key molecular signatures and pathways. This followed by the identification of the

likelihood of response to drugs having effect on the predicted pathways using NBA scores formed the basis for novel QSP models.

Conclusions

Currently, the biological scope of QSP is largely driven by expert opinion and traditional literature survey. We propose that the impact and efficiency of QSP in target selection and validation can be significantly improved through integration with NBA.

References

- (1) Morgan, P. *et al.* Impact of a five-dimensional framework on R&D productivity at AstraZeneca. *Nat Rev Drug Discov* **17**, 167-81 (2018).
- (2) Bradshaw, E.L. *et al.* Applications of Quantitative Systems Pharmacology in Model-Informed Drug Discovery: Perspective on Impact and Opportunities. *CPT Pharmacometrics Syst Pharmacol* **8**, 777-91 (2019).
- (3) Sorger, P.K. *et al.* Quantitative and Systems Pharmacology in the Post-genomic Era: New Approaches to Discovering Drugs and Understanding Therapeutic Mechanisms: An NIH White Paper by the QSP Workshop Group. NIH, Bethesda. 1-48 (2011).

THU-085

CYTOCON as a tool to collect, compare and visualize available data on cells and cytokine concentrations in humans

Vlad Leonov¹, Ekaterina Mogilevskaia¹, Elita Gerasimuk¹, Nail Gizzatkulov¹, Oleg Demin¹

¹INSYSBIO, Moscow, Russia

Objectives:

Calibration of QSP models may require comparison of model simulations with *in vivo* baseline data measured in different tissues of patients. The data is often available in scientific literature and represents cytokine and cell concentrations measured in patients. The data is typically measured in different units and for different patient groups with various demographic and disease associated characteristics. These features make it difficult direct use of the baseline *in vivo* data for calibration of a QSP model. To cope with the difficulties and facilitate access of QSP modelers to such type of *in vivo* data we have developed an online database and started to collect baseline *in vivo* data available in public domain [<http://cytocon.insysbio.com/>]. The aim of the poster is to describe the database and demonstrate its application for the comparison of baseline values of cells and cytokines.

Methods:

CYTOCON DB (Cell and cYTOkine CONcentrations database) is developed as a web application based on the ASP.NET MVC framework, Microsoft IIS web server, Microsoft SQL Server database, Telerik Kendo UI and Bootstrap.

Most part of baseline values found in papers were converted from original units (i.e., mg/ml, number of cells per mm² of biopsy surface section) to unified units: “pM” for cytokine and “kcell/l” for cell concentration. Formulas for the conversion were implemented in the database.

Workflow for papers annotation was designed in such a way to provide satisfactory level of quality control. A group of annotators add information from papers to the DB and a group of reviewers verify the accuracy and completeness of the data. Cytocon DB is continuously extended with new data.

Results: Key features implemented in CYTOCON DB:

- Search query may include both patient group attributes (age, gender, patient number, etc) and disease-specific clinically measured characteristics (asthma – FEV1 range, dermatitis – SCORAD range, etc)
- Both table and graphic representation of search results
- Export of search results in csv format

CYTOCON DB can be applied for comparison of baseline values of cells and cytokines measured in tissues of different patient groups. For example, aggregating data from multiple sources on IL6 concentration in serum of healthy subjects and patients with diseases allows us to see the variability of the measured data. Similar analysis for blood level of eosinophils revealed substantial differences between healthy controls and patients suffering from different immune and inflammatory diseases (Fig.1).

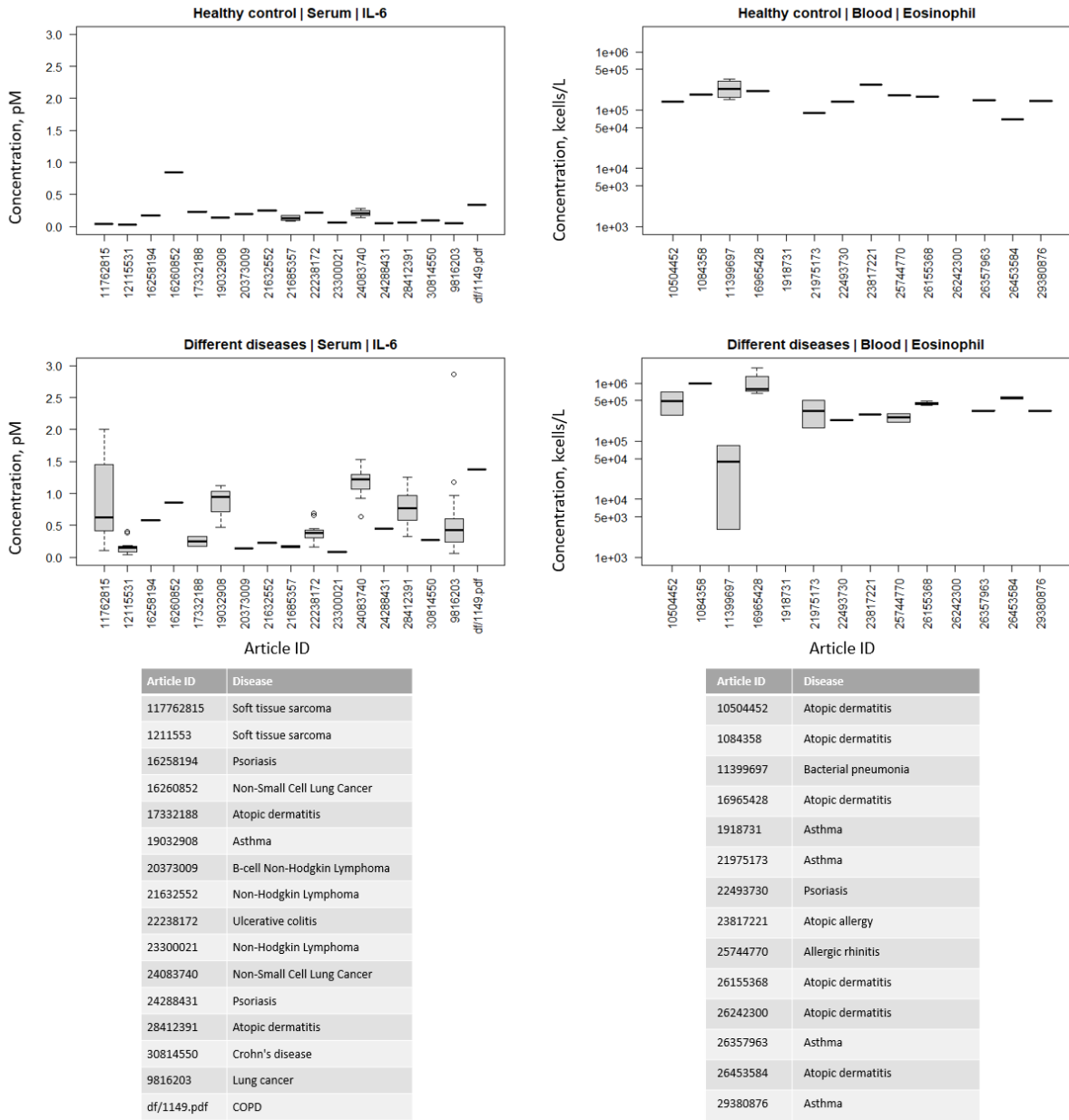


Fig. 1. Comparison of baseline values of eosinophils and IL6 measured in blood of different patient groups collected in CYTOCON DB and converted to unified units.

Conclusions:

CYTOCON DB is a database of human baseline concentrations of cytokines and cells can be applied to facilitate calibration of QSP models and to compare baseline data measured in different tissues of patients suffering from various pathologies.

THU-087

A modeling and simulation framework to help rationalize the design of BCMA-CD3 bispecific therapeutics

Wenlian Qiao¹, Małgorzata Nocula-Lugowska¹, Chao-Pei Betty Chang², Divya Mathur², Frank Barletta¹

¹ Department of BioMedicine Design, Pfizer Inc.

² Department of Oncology Research, Pfizer Inc.

Objectives: The selective expression profile of B-cell maturation antigen (BCMA) prompted the research of BCMA-CD3 T cell engagers for treating multiple myeloma. As of March 2020, seven BCMA-CD3 T cell engagers of various formats are being evaluated in the clinic (clinicaltrials.gov). Herein, we established mechanistic models of BCMA-CD3 T cell engagers for both in vitro and in vivo systems in an effort to understand the potencies of BCMA antibody-CD3 tri-molecular complexes (trimers) formed by different antibody formats, and focus their design to maximize T cell and myeloma cell engagement in the bone marrow for efficacy. Furthermore, the models were used to investigate possible effects of shed BCMA (sBCMA) on unbound drug molecules that distribute to the site of action in myeloma patients.

Methods: Parameters such as BCMA shedding rate were measured in vitro. Drug elimination and distribution rates are functions of their molecular sizes. The concentration of trimers was used as a surrogate for efficacy (1,2), which was then used to investigate the impact of target biology and drug properties on trimer formation and consequential efficacy in vitro and in vivo.

Results: Membrane BCMA exhibits rapid shedding in vitro. Utilizing the model, binding of antibodies to sBCMA explained an observed difference between the dissociation constant measured by Surface Plasmon Resonance and the EC50 of flow cytometry-based on-cell binding data. The model was then used to compare the potency of trimers formed by different antibody formats within the context of in vitro cytotoxicity. Finally, using a mechanistic model of the human system, the impact of sBCMA, drug affinities, molecular weight and corresponding PK / distribution on trimer formation in the bone marrow were all investigated. We found that tighter target affinity does not necessarily lead to more trimer formation given the presence of sBCMA. For each antibody format, a window of BCMA antibody KD was determined to minimize sBCMA sink effect while maximizing T cell and myeloma cell engagement.

Conclusions: In summary, mechanistic models of BCMA-CD3 T cell engager were established to capture the interplay between the antibody, sBCMA and membrane BCMA to form trimers that drive target pharmacology. The in vitro model revealed the cause of the difference between Surface Plasmon Resonance measured BCMA KD and the EC50 of on-cell binding and allowed us to compare potencies of trimers formed by different T cell engager formats. The in vivo model enabled us to rationalize the design of BCMA-CD3 T cell engagers to maximize clinical response.

References:

1. Chen et al. (2016) Clin Pharmacol Ther 100(3):232
2. Betts et al. (2019) AAPS J 21(4):66

THU-088

A mechanistic in vitro model of Antibody-Dependent Cellular Cytotoxicity (ADCC) and translation into a minimal PBPK framework

William Rittase, Katharine Rogers, Songmao Zheng

Biologics Development Sciences, Janssen Biotherapeutics, Janssen Research & Development, LLC.

Objectives: Despite significant interest in developing antibody therapeutics with Antibody-Dependent Cellular Cytotoxicity (ADCC) function, the quantitative metrics behind ADCC remain elusive. Recent advances in antibody engineering have found that production of antibodies in a low fucose (LF) environment improves the Fc:CD16a binding affinity ~10 fold over production in a natural fucose (NF) environment, and significantly increases ADCC activity. A unifying mechanistic model of the ADCC killing process for both LF and NF antibodies was utilized to quantify relevant biophysical aspects of the ADCC cytotoxic process *in vitro and in vivo*.

Methods: *In vitro* data from published internal studies as well as literature sources with varying receptor densities and different targets were fit to a mechanistic ADCC model, which expanded upon a previously published ADCC model¹ to include aspects of 2-dimensional binding after cell-cell contact, to determine relationships between receptor density, antibody affinity, killing potency, and killing rate. The *in vitro* model and parameters combined with a minimal PBPK model and patient specific parameters (eg., receptor density and NK cell distribution) were utilized to predict ADCC activity in humans.

Results: The average number of Fc:CD16a bonds spanning NK cells and target cells required for 50% maximum killing rate was estimated to be 1.38 (R.S.E. = 21.0%), 1.59 (R.S.E. = 0.1%), and 1.31 (R.S.E. = 17.6%) for trastuzumab (anti-HER2), JNJ-61186372(anti-EGFR/cMET), and rituximab(anti-CD20), respectively, regardless of fucosylation status. The maximum rate of cell killing was determined to vary significantly in each assay, from 3.2×10^{-5} to $1.7 \times 10^{-4} \text{ s}^{-1}$, and appeared to be dependent largely on the target cell lines and not on the quality of the antibody itself. Utilizing *in vitro* data from mogamulizumab, an Anti-CCR4 antibody with enhanced ADCC targeting T cells, clinical published PK data, and patient-specific parameters, the *in vivo* model predicted complete killing of all CCR4+ T cells in the peripheral blood at doses of 0.01 mg/kg – 1 mg/kg within 2.5 days in Adult T Cell Lymphoma patients, consistent with the clinical observations.

Conclusions: A mechanism-based *in vitro* PD model was developed and fit to data with comparable estimated parameters across various targets and receptor densities. The model can be used to guide target selection and human dose projections for molecules that utilize an ADCC mechanism as a key mechanism of action.

¹Hoffman, F., et al., *A mathematical model of antibody-dependent cellular cytotoxicity (ADCC)*. J Theor Biol, 2018. 436: p. 39-50.

THU-089

Physiologically-Based Pharmacokinetic Analysis of Prednisolone in Rats

Xiaonan Li, Debra C. DuBois, Richard R. Almon, and William J. Jusko

Department of Pharmaceutical Sciences, School of Pharmacy and Pharmaceutical Sciences (X.L., D.C.D., R.R.A., W.J.J.); and Department of Biological Sciences (D.C.D., R.R.A.), State University of New York at Buffalo, Buffalo, New York

Objectives:

The pharmacokinetics of prednisolone in humans and animals exhibit nonlinearity, which is complicated by nonlinear plasma protein binding, nonlinear tissue binding, metabolic interconversion with prednisone, and nonlinear renal elimination. The aim of this work was to characterize these diverse complexities in disposition of prednisolone in rats using physiologically-based pharmacokinetic (PBPK) modeling.

Methods:

Blood and 11 tissue samples were collected from 27 healthy male Wistar rats over 24 hr after a subcutaneous (SC) bolus of 50 mg/kg of prednisolone. Concentrations of prednisolone and its major metabolite prednisone in blood, plasma, plasma ultrafiltrates and tissues were measured by liquid chromatography-tandem mass spectrometry (LC-MS/MS). The observed plasma and tissue profiles were described by a PBPK model with prednisone and prednisolone concentrations found to be in rapid equilibrium in plasma and most tissues. The apparent tissue partition coefficients (K_p) of prednisolone and prednisone calculated from the ratio of area under the curve (AUC) of the PBPK model-predicted tissue and plasma curves were compared to those obtained from a steady-state (SS) infusion study and published in silico methods (GastroPlus).

Results:

The blood-to-plasma ratio of prednisolone in rats was about 0.71; calculated red blood cell concentrations of prednisolone were close to the unbound plasma concentrations, as also found in humans and rabbits. Nonlinear plasma protein binding (fraction bound of 60 to 90%) was observed owing to known corticosteroid-binding globulin (CBG) saturation. The tissue-to-unbound plasma concentration ratios decreased in all tissues with unbound plasma

concentrations, indicating nonlinear tissue distribution. The PBPK model-estimated tissue binding equilibrium dissociation constant (K_D) of prednisolone shared by all tissues was about 0.56 ng/mL with highest binding (B_{max}) observed in liver, heart, intestine, fat, and bone, followed by muscle, skin and spleen, with the lowest in kidney, lung and brain. Clearances of CBG-free prednisolone (CL_{int}) was 3051 mL/hr from liver and (CL_k) 589 mL/hr from kidney. Low brain prednisolone concentrations ($K_p=0.06$) in contrast to its expected high permeability ($\log P=1.62$) were well captured by a presumed P-glycoprotein (P-gp) mediated efflux process. The PK profiles of prednisolone in fat and bone were reasonably characterized by assuming only the interstitial space was available for distribution. The apparent K_p values of prednisolone obtained from the PBPK model fittings were similar to values obtained from the SS infusion study and in silico methods. The metabolite/drug ratio of prednisone/prednisolone was 0.02 for bone and 0.05 for all other tissues except for kidney where the ratio was 0.19 at high prednisolone concentrations.

Conclusions:

A PBPK model incorporating nonlinear plasma and tissue binding reasonably characterized the observed prednisolone and prednisone PK profiles in plasma, and 11 tissues of rats. As steroids have similar PK properties in various species, receptors in most tissues, and multiple therapeutic and adverse actions, this PBPK model may provide greater insights into the pharmacodynamic complexities of corticosteroids.

THU-090

The Impact of *SLC22A12* Genotype on Pharmacokinetics and Pharmacodynamics of Allopurinol in Hmong with Gout and/or Hyperuricemia

Authors: Ya-Feng Wen, Pharm.D.¹, Richard Brundage, Pharm.D., Ph.D.¹, Robert J. Straka, Pharm.D., FCCP¹

Affiliations: ¹Department of Experimental and Clinical Pharmacology, College of Pharmacy, University of Minnesota, Minneapolis, USA

Objectives:

Allopurinol is the most widely used urate-lowering therapy. Genome-wide association studies identified an association between several key renal transporter genes and urate-lowering (PD) response to allopurinol [1]. However, these genotypes did not significantly impact the PK and PD parameters of oxypurinol, the active metabolite of allopurinol, in a patient cohort of Caucasian, Maori, and Pacific Island decent [2]. Hmong have a higher prevalence of gout and the gout treatment in this population is often suboptimal. The goal of this project was to identify and quantify the sources of variability, including key genotypes in oxypurinol PK and their effect on plasma urate in Hmong population.

Methods:

Hmong patients (n=34) received 100 mg allopurinol twice daily for 7 days followed by 150 mg allopurinol twice daily for 7 days. On the last day of therapy, plasma oxypurinol concentrations were obtained at times 0, 2, 4, and 6 hours. Plasma urates were obtained at baseline, and before and after the last dose of allopurinol. Using a sequential PKPD analysis, non-linear mixed-effects modeling (NONMEM v7.4.2) was used to evaluate model parameters. The impact of anthropometrics, concomitant medications (9 categories of drugs), and key renal transporter genotype information (17 genotypes) on oxypurinol PKPD parameters was evaluated using a centered power model. Goodness of fit diagnostics and visual predictive checks were used to evaluate the predictive performance of the PKPD model.

Results:

A one-compartment pharmacokinetic model with first order absorption and elimination best described the oxypurinol concentration-time data. Inhibitory of plasma urate by oxypurinol was described with an inhibitory Emax model using the steady-state oxypurinol concentration. Weight, renal function measured by creatinine clearance (CrCL) using ideal body weight and genotype of *SLC22A12* rs505802 were found to predict differences in the clearance of oxypurinol. Oxypurinol demonstrated a clear exposure-response relationship on urate reduction. None of covariates tested were found to predict differences in baseline plasma urate, Imax and IC₅₀. The population estimates and between-subject variability of the PK and PD parameters are listed in **Table 1**. The final models apparent oxypurinol clearance and plasma urate concentration are described in the end of **Table 1**.

Conclusions:

In addition to body weight and renal function, *SLC22A12* rs505802 genotype significantly influences the apparent clearance of oxypurinol in Hmong patients with gout. An inhibitory Emax model can describe the urate-lowering response of oxypurinol.

References:

- [1] Brackman DJ et al. Clin Pharmacol Ther. 2019;106(3):623-31 [2] Wright DFB et al. Br J Clin Pharmacol. 2018;84(5):937-43

Table 1. Parameter estimates of the covariate model and the 1000 bootstrap runs (median and 95th percentiles)

Parameter	Covariate (final) model (RSE%)	1000 Bootstrap replicates median (95%CI)
Fixed parameters		
CL/f_m (L/h)	1.4 (11)	1.4 (1.1, 1.8)
V/f_m (L)	47.7 (10)	47.5 (40.0, 57.9)
K_{fm}	1.1 (fixed)	1.1 (fixed)
BL_{urate} (mg/dL)	9.3 (3)	9.3 (8.8-9.8)
I_{max}	0.6 (fixed)	0.6 (fixed)
IC_{50} (mg/L)	6.5 (14)	6.4 (5-8.4)
Exponents of covariates on CL/f_m		
Weight	1.34 (26)	0.51 (0.08, 1.26)
rs505802 CT or TT within <i>SLC22A12</i>	1.30 (55)	1.29 (0.98, 1.67)
Random parameters		
BSV CL/f_m (CV%) [shrinkage]	34.6 (13) [0%]	32.7 (23.9, 40.8)
BSV V/f_m (CV%) [shrinkage]	39.1 (19) [25%]	37.5 (21.6, 52.9)
BSV K_{fm} (CV%) [shrinkage]	36.1 (fixed)	36.1 (fixed)
BSV BL_{urate} (CV%) [shrinkage]	9.3 (3) [8%]	13.5 (9.5-17.9)
BSV I_{max} (CV%) [shrinkage]	16.0 (fixed)	16.0 (fixed)
BSV IC_{50} (CV%) [shrinkage]	6.5 (14) [70%]	33.8 (6.9-62.3)
Residual error		
Plasma oxypurinol, proportional (CV%) [shrinkage]	5.20 (18) [23%]	5.16 (4.17, 6.09)
Plasma urate, additive (mg/dL) [shrinkage]	0.76 (37) [18%]	0.60 (0.27-1.19)
Final Model		
$CL/f_m \text{ (L/h)} = 1.4 \times \left(\frac{CrCL \text{ (mL/min)}}{100 \text{ (mL/min)}} \right) \times \left(\frac{Wt \text{ (kg)}}{80 \text{ (kg)}} \right)^{1.34}$ $\times (\mathbf{1} \text{ for } SLC22A12 \text{ rs505802 CC, 1.3 for CT or TT})$ $Plasma\ urate(mg/dL) = BL_{urate} \times \left(1 - \frac{I_{max} * Css_{oxy}}{IC_{50} + Css_{oxy}} \right)$		

f_m , fraction of the allopurinol systematically available as oxypurinol; CL/f_m , apparent clearance of oxypurinol; V/f_m , apparent volume of distribution of oxypurinol; K_{fm} , combined absorption and formation rate constant; BL_{urate} , baseline urate; I_{max} , maximum oxypurinol inhibitory effect; IC_{50} , oxypurinol concentration at ½ maximum inhibitory effect; $CrCL$, creatinine clearance calculated using ideal body weight; Wt , actual body weight; Css_{oxy} , steady-state plasma oxypurinol concentration

THU-091

Application and validation of a whole body PBPK modeling approach to predict OATP transporter mediated drug-drug interaction with Rifampicin—case study of Asunaprevir

Authors: Yang Song^{1,*}, Hamed Ghaffari^{2,*}, Sietse Braakman^{3,*}, Xiaomin Liang¹, Bernard Murray¹, Yurong Lai^{1**}

Institutions: 1. Gilead Sciences, Foster City, CA, USA

2. Department of Mechanical Engineering, University of California Santa Barbara, Santa Barbara, CA, 93106, USA.

3. Application Engineering, MathWorks, Natick, MA.

* Authors have equivalently contribution to the publication

Objective: Application of a whole body PBPK modeling approach to predict human pharmacokinetics profiles and OATP transporter mediated drug-drug interaction between rifampicin and asunaprevir, an OATP transporter substrate.

Methods: A whole-body PBPK model of asunaprevir was first established using human pharmacokinetic data of asunaprevir from Single and Multiple Ascending Dose (SAD, MAD) studies^{1,2}. in MATLAB SimBiology. Based on the mechanism known from in vitro assays, the in vivo parameters including hepatic active uptake, metabolism³, and passive permeability clearance in the model were estimated using a particle swarm optimization (PSO) method. Global sensitivity analysis and practical identifiability methods were used to guide the optimization process. The calibrated PBPK model of asunaprevir was then coupled with a established PBPK model of rifampicin⁴ to predict clinical drug-drug interactions between the two drugs.

Results: Single and multiple ascending dose human clinical pharmacokinetic profiles of asunaprevir were reasonably captured by the model in a dose range of 10 mg to 1200 mg (in all cases satisfying two-fold criteria and GMFE for AUC prediction). The nonlinear pharmacokinetics of asunaprevir at high doses was explained by the saturable OATP uptake ($K_{m,u,uptake} = 0.015 \text{ mg/L}$). The model was externally validated by performing simulation of drug-drug interaction between rifampicin and asunaprevir for the mechanism of OATP inhibition: the predicted AUC and C_{max} change of asunaprevir was within 1.5-fold of clinical observations.

Conclusions: A full PBPK modeling approach can be applied in drug discovery to predict nonlinear human pharmacokinetic profiles and drug-drug interaction for drugs that are cleared by active OATP uptake with saturable processes. A modular platform to simulate dynamic and complex drug-drug interactions can be implemented in SimBiology, and can be extended to other types of drug-drug interactions and/or to predict interactions between multiple (>2) drugs.

References:

1. T Eley, 2013. Pharmacokinetics of the NS3 Protease Inhibitor, Asunaprevir (ASV, BMS-650032), in Phase I Studies in Subjects With or Without Chronic Hepatitis C. *Clin Pharmacol Drug Dev.* 2013 Oct;2(4):316-27.
2. T Shinozaki, 2015. Single- and multiple-ascending dose studies to evaluate the safety, tolerability, and pharmacokinetics of daclatasvir and asunaprevir in healthy male Japanese subjects. *Int J Clin Pharmacol Ther.* 2015 Apr;53(4):292-302.
3. T Eley, 2014. Organic anion transporting polypeptide-mediated transport of, and inhibition by, asunaprevir, an inhibitor of hepatitis C virus NS3 protease. *Clin Pharmacol Ther.* 2015 Feb;97(2):159-66.
4. Asaumi R, 2018. Comprehensive PBPK Model of Rifampicin for Quantitative Prediction of Complex Drug-Drug Interactions: CYP3A/2C9 Induction and OATP Inhibition Effects. *CPT Pharmacometrics Syst Pharmacol.* 2018 Mar;7(3):186-196.

THU-092

Population pharmacokinetics (PopPK) and concentration-QTc (C-QTc) analysis of DS-1062, an anti-TROP2 antibody drug conjugate (ADC), in patients with non-small cell lung cancer (NSCLC)

Yasong Lu¹, Kashyap Patel², Helen Kastrissios², Stefanie Hennig², Bill Poland², Tajima Naoyuki³, Ophelia Yin¹

1. Quantitative Clinical Pharmacology, Daiichi Sankyo, Inc., Basking Ridge, NJ; 2. Certara Strategic Consulting; 3. Quantitative Clinical Pharmacology, Daiichi Sankyo Co., Ltd., Tokyo, Japan

Objectives:

DS-1062, an anti-TROP2 ADC with a payload DXd (an exatecan derivative), is being investigated in a Ph1 dose escalation and expansion study in NSCLC¹. The objectives of the current analyses were to characterize the PopPK of DS-1062 and to evaluate the QT prolongation potential based on the Ph1 interim data.

Methods:

PK and standard 12-lead ECG data were collected over the DS-1062 dose range of 0.27 to 10 mg/kg, administered via intravenous infusion every 3 weeks. A 2-step sequential approach was used for PopPK model development: a model for DS-1062 was first developed, then with the DS-1062-related population parameters fixed to the estimates, a model for DXd was developed. Model structures were selected based on data exploration and model performance. Candidate covariates were predefined based on pharmacological plausibility and clinical interest, and evaluated using stepwise forward selection ($p<0.01$) and backward elimination ($p<0.001$). For C-QTc analysis, mean values of triplicate QT measures were matched with observed concentrations of DS-1062 and DXd within ± 30 minutes from the ECG time. QT was corrected using both the Fridericia formula (QTcF) and population-based correction (QTcP). The baseline-subtracted QTc (ΔQTc , $\Delta QTcF$ and/or $\Delta QTcP$) was analyzed using linear mixed-effects modeling.

Results:

The PopPK dataset included 1316 observations for DS-1062 and 1313 observations for DXd from 83 subjects. DS-1062 PopPK was described using a 2-compartment model with parallel linear and nonlinear (Michaelis-Menten) clearance. Body weight was a significant covariate on linear clearance and central volume, and baseline albumin level was a significant covariate on linear clearance. The PopPK of DXd was described using a 1-compartment model with linear clearance, and no covariate was identified. Adequate performance of both models was confirmed with diagnostic plots and prediction-corrected visual predictive check. The C-QTc dataset contained 965 pairs of time-matched observed records from 92 subjects. The RR interval appeared independent of concentrations, and no hysteresis was evident for the C- ΔQTc relationship. Slopes of the four linear mixed-effects models ($\Delta QTcF$ or $\Delta QTcP$ vs DS-1062 or DXd concentration) were not significant at the 0.01 level. Across the four models, the mean ΔQTc at the geometric mean Cmax of DS-1062 or DXd at 8 mg/kg, the maximum tolerated dose, was predicted to be from -0.03 to 1.89 ms with 90% CI upper bounds from 2.28 to 3.96 ms.

Conclusions:

PopPK models were developed for DS-1062 and DXd. Identified significant covariates (body weight and baseline albumin level) are consistent with current knowledge of the PK of DS-1062. DS-1062 did not demonstrate a clinically meaningful QTc prolongation effect based on the Ph1 interim data.

References:

- Heist et al. 2019. Oral presentation at IASLC 2019 World Conference on Lung Cancer (Abstract #3854). Barcelona, Spain.

THU-093

A virtual population (VPop) development workflow with improved efficiency and scale applied to immuno-oncology quantitative systems pharmacology models (I-O QSP platforms)

Authors: Yougan Cheng¹, Md Shahinuzzaman¹, Ronny Straube¹, Abed Alnaif¹, Radha Konduri², Amirmahdi Ghasemi³, Eric Sison², Tarek Leil¹, Brian J. Schmidt¹

Institution:

¹Clinical Pharmacology and Pharmacometrics, Bristol Myers Squibb

²Scientific Computing, Bristol Myers Squibb

³Data Capability Management, Bristol Myers Squibb

Objectives: VPop development is an essential component of QSP platform application to a clinical setting, as it is often anticipated that a QSP model quantitatively reproduces observed biomarker and response variations from patients before it should be applied to provide predictions. We previously reported an algorithm to calibrate a VPop to multiple therapies and clinical trials, and applied it to an I-O QSP platform [1]. We noted potential improvements, including: eliminating the manual step to find missing clinical phenotypes not returned from initial sampling of the parameter space; ensuring the algorithm can weight and resample virtual patients (VPs) for agreement with clinical data across a broader range of fitting scenarios automatically; and directly calibrating important joint relationships between endpoints. Our goal was to improve the previous VPop workflow to address these considerations and successfully scale it to run on a cluster, not just a single server.

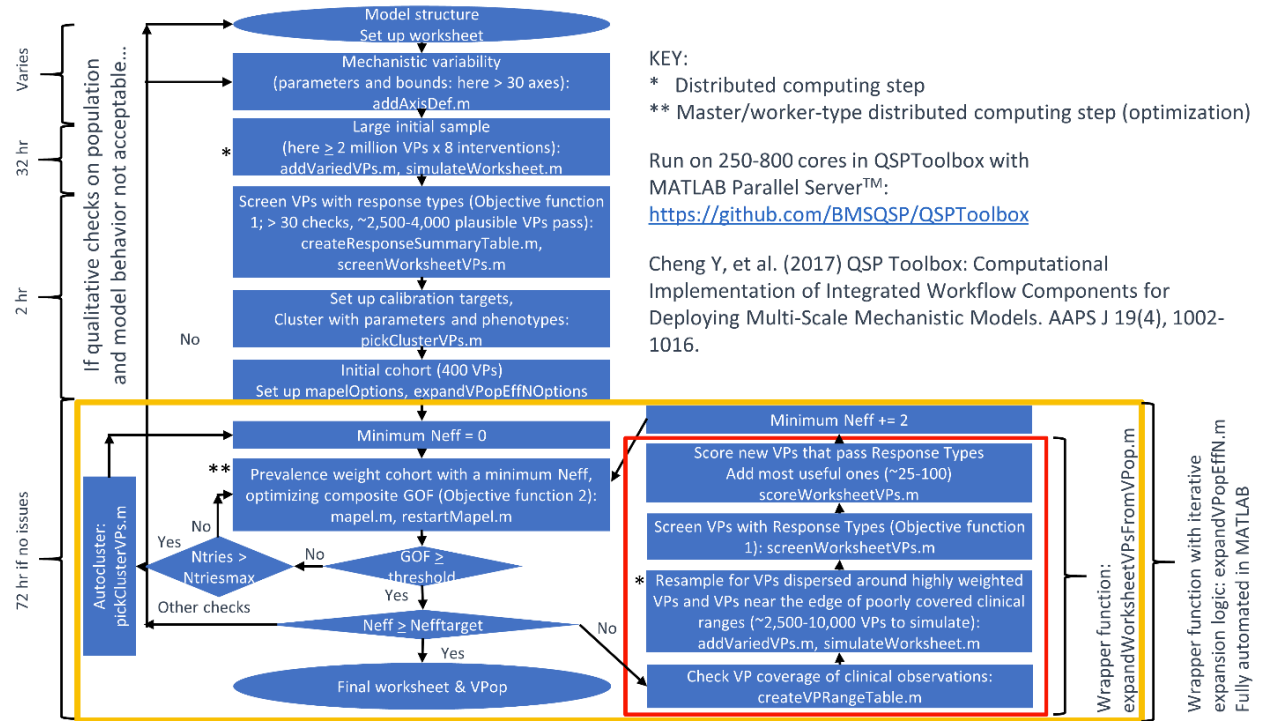
Methods: The updated I-O QSP platform includes type 1 conventional dendritic cells in the tumor microenvironment to reflect additional contributions to immunotherapy responses. The workflow and algorithm were updated to: automate detection of where VPs do not fill ranges in observed data and direct resampling for missing clinical phenotypes, inform initial points of a prevalence weight optimization step with averaged ensemble solutions from a linearized version of the prevalence weight calibration problem [2]; use modifications of Fisher's r-to-z transformation and a two-dimensional version of the Kolmogorov-Smirnov test for comparing relationships between endpoints; and automate clustering of VPs to further expedite prevalence weight optimization in the expanding VP cohort while maintaining diversity in parameter and phenotype space (Figure 1).

Results: We developed a VPop that captures population variability of clinical biomarkers and response at multiple time points. In addition to previous results [1], the new calibration includes additional therapies that target CTLA4, additional doses and endpoints, including changes in absolute lymphocyte counts, and joint relationships that include tumor immune cell content and relative lesion changes. The resulting VPop had a composite goodness-of-fit (GOF) to data of greater than 0.9 for calibrated endpoints, accurately predicted response for second line anti-CTLA4 therapy after progression on anti-PD1 therapy (withheld from training data), and predicted an anti CTLA4 and anti-PD1 therapy combination response. The algorithm runs on a cluster using MATLAB Parallel Server™. The updated code is available (<https://github.com/BMSQSP/QSPToolbox>).

Conclusions: As new targets, interventions, and biology are added to QSP platforms, increasingly efficient and scaled workflows are needed for model recalibration while maintaining fit and predictive performance. We integrated an updated I-O QSP platform into an even more automated, iterative VPop development workflow and developed a predictive, recalibrated VPop.

References: [1] Cheng Y, et al. ACoP10 [2] Alnaif A, et al. ACoP10

Figure 1. Updated workflow



Avelumab dose selection for clinical studies in pediatric patients with solid tumors

Yulia Vugmeyster¹, Ana-Marija Grišić², Brigitte Brockhaus², Peter Rueckert², Mary Ruisi¹, Haiqing Dai¹, Akash Khandelwal²

¹EMD Serono Research & Development Institute, Inc., Billerica, Massachusetts, USA; a business of Merck KGaA, Darmstadt, Germany; ²Merck KGaA, Darmstadt, Germany

Objectives: Avelumab is an anti-PD-L1 IgG1 antibody approved in the United States and other countries as monotherapy for the treatment of adults and children aged ≥ 12 years with metastatic Merkel cell carcinoma and adults with advanced platinum-treated urothelial carcinoma, and in combination with axitinib for advanced renal cell carcinoma. The approved dose is 800 mg every 2 weeks (q2w). Avelumab has been administered to children with refractory or relapsed malignant solid tumors (NCT03451825). The objective of this study was to select the dose for further clinical evaluation of avelumab in children.

Methods: Pharmacokinetics (PK) data from children aged 3-17 years and with body weight (BW) of 13.4-78.7 kg who received either avelumab 10 (n=6) or 20 mg/kg (n=15) q2w were analyzed by noncompartmental (NCA) and pharmacometric analyses. Safety was evaluated by the Safety Monitoring Committee. A population (pop)PK model was developed in NONMEM using frequentist prior approach. A pediatric population was simulated using US Centers for Disease Control weight-for-age tables. Simulated exposure distributions for 10 mg/kg, 15 mg/kg, 20 mg/kg, and 800 mg q2w in 2 pediatric subgroups (≥ 12 years and ≥ 40 kg, and < 12 years or < 40 kg) were compared to popPK-simulated adult exposures at the approved dose [1].

Results: Similar to its safety profile in adults, avelumab up to 20 mg/kg was considered safe in children, since only 1 pediatric patient (in the 20 mg/kg group) had dose-limiting toxicities (DLTs). 20 mg/kg, but not 10 mg/kg, dosing in children achieved adult exposures associated with the 800 mg dose regardless of BW. A trend of lower exposure in children with BW of ≤ 40 kg was observed at both the 10 and 20 mg/kg doses compared with those with higher BW. A 2-compartment model with time-varying linear clearance and BW as a covariate described the data best. The optimal exposure overlap between simulated adult and pediatric subgroups was achieved with the 800 mg q2w dose for children ≥ 12 years and ≥ 40 kg and with 15 mg/kg q2w for children < 12 years or < 40 kg, with geometric mean exposures of $\geq 90\%$ of adult ones. The pediatric geometric mean exposures for the selected dose are predicted to be below both the pediatric and adult exposures achieved with the 20 mg/kg dose.

Conclusions: The recommended doses for further clinical evaluation of avelumab in pediatric patients are 15 mg/kg q2w for children < 12 years or < 40 kg and the adult dose of 800 mg q2w for children ≥ 12 years and ≥ 40 kg; these are expected to provide exposures similar to those in adults.

References:

1. Novakovic AM, et al. *Clin Pharmacol Ther.* 2020 ;107(3):588-96.

THU-095

Modeling Insights on Species Differences in Response to CD8+ T cell-mediated Liver Injury

Zackary R. Kenz^a, Christina Battista^a, Lisl K.M. Shoda^a

^aDILIsym Services, Inc., a Simulations Plus company, Research Triangle Park, NC

Objectives: Idiosyncratic drug-induced liver injury (iDILI), which is typically rare and often severe, has led to black box warnings or drug withdrawals from the market, with adverse effects on patients and drug development¹. T cell-mediated immune responses have been implicated for many iDILI drugs¹. Previous work has expanded an existing quantitative systems toxicology (QST) model (DILIsym[®]) to include mouse CD8+ T cell responses to hepatocyte-expressed OVA² and mouse CD8+ T cell responses to hepatocyte-expressed amodiaquine (AQ) antigen³. This work aims to reproduce human CD8+ T cell responses to hepatocyte-expressed AQ antigen and explore putative mechanisms underlying cross-species differences.

Methods: Simulating human responses involved human AQ dosing protocols and species differences in the represented biology, including numbers of human naïve antigen-specific CD8+ T cells^{4,5}. The simulated mouse was treated with 250mg/kg/day AQ⁶. The simulated human was treated with 600mg AQ per week⁷.

Results: AQ exposure in a simulated mouse resulted in delayed, mild hepatotoxicity, illustrated by alanine aminotransferase (ALT) elevations >100U/L after two weeks of treatment. There was no progression to severe liver injury on continued drug treatment through 10 weeks, consistent with published data⁶. In a simulated human, AQ exposure resulted in delayed hepatotoxicity, illustrated by ALT elevations 120U/L after roughly 4.5 weeks of simulated AQ treatment. With continuing AQ treatment, the simulated human progressed to severe liver injury, evidenced by ALT >1000U/L and TB >2mg/dL, consistent with AQ DILI⁷. Relative expansion of CD8+ T cells was similar between species, as was their cytotoxic potential. A surprising variable that differentiated the severity of injury was the relative recovery potential of mouse vs. human hepatocytes. Simulations include hepatocyte proliferation with subsequent liver regeneration. Hepatocyte proliferation rates were previously optimized to available acetaminophen recovery data^{8,9} and were unaltered for these simulations. The parameterization is permissive for balanced injury and recovery in the simulated mouse but generates progressive injury with insufficient recovery in the simulated human. These abstract results have been previously presented in part at Immunology2020, Honolulu, HI, 5/2020 and published in the conference proceedings as abstract 2352.

Conclusions: The results provide proof-of-concept that leveraging data from mouse studies of CD8+ T cell responses in the liver can translate to a human representation consistent with published data. The results illuminate a potential mechanism for cross-species differences in susceptibility to T cell-mediated injury. Further simulations and experimental follow-up will be conducted to confirm or refute the model findings.

References:

1. Kullak-Ublick. Gut 66:1154-1164 (2017)
2. Kenz. ACoP9 Poster W-076 (2018)
3. Kenz. Immunology2020 2395 (2020)
4. Alanio. Blood 115:3718-3725 (2010)
5. Bechara. Front. Immunol. 10:1331 (2019)
6. Mak. Chem Res Toxicol. 28:1567-1573 (2015)
7. Larrey. Ann. Intern. Med. 104:801-803 (1986)
8. DeAngelis. Hepatol. 42:1148-1157 (2005)
9. Portmann. J Pathol. 117:169-181 (1975)